



S-NPP VIIRS Thermal Emissive Bands Performance and Calibration Improvements

**Boryana Efremova, Xiaoxiong (Jack) Xiong, Jeff McIntire, Aisheng
Wu, Vincent Chiang, Samuel Anderson**

VCST, NASA/GSFC

**Acknowledgements: VIIRS SDR Team Members
VCST Members**



Outline



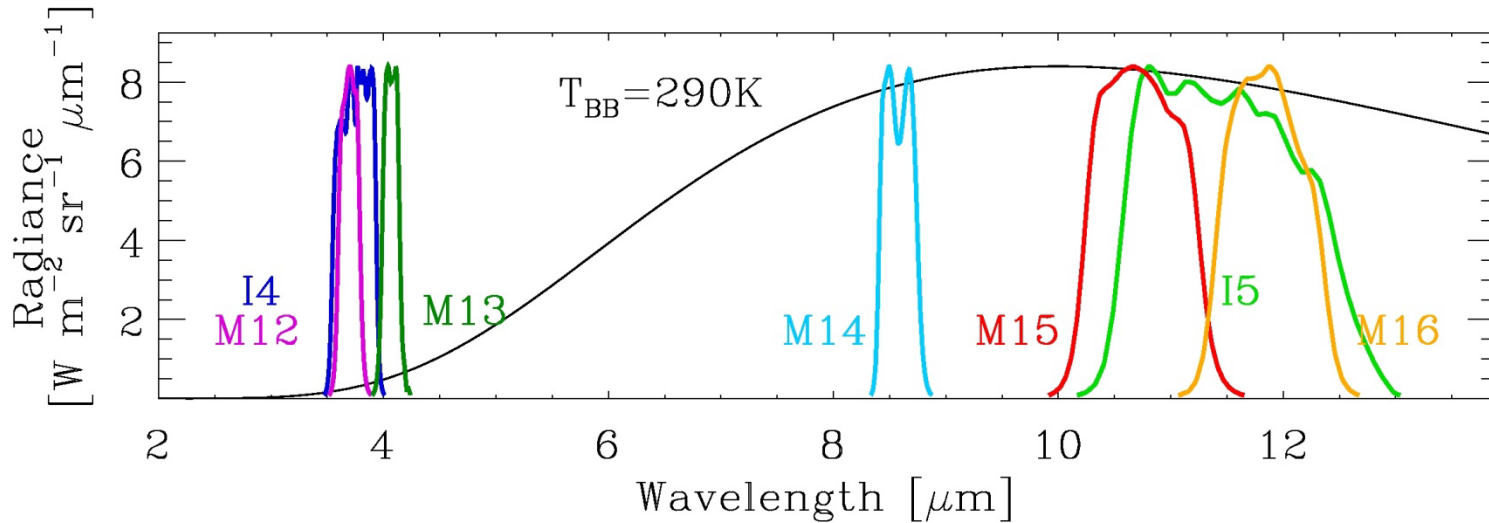
- **TEB Calibration**
- **On-orbit Performance**
 - ✓ BB performance
 - ✓ Detector short-term stability and long-term response (F-factors)
 - ✓ Detector noise characterization (NEdT)
 - ✓ Trending during WUCD
- **Potential Improvements and Uncertainty Estimates**
 - ✓ Uncertainty assessment
 - ✓ Improving M13LG calibration
 - ✓ Average vs per-scan F-factor
 - ✓ Moon in SV processing
- **Conclusions**



Thermal Emissive Bands (TEB)



5 M-bands and 2 I-bands, covering wavelengths from 3.7 to 12 μm



Band	I4	I5	M12	M13	M14	M15	M16
Wavelength $[\mu\text{m}]$	3.74	11.45	3.70	4.05	8.55	10.76	12.01

Calibrated using an on-board blackbody (BB):

- ✓ Scaling factor “F-factor” is derived and applied each scan.
- ✓ Warm-up and cool-down (WUCD) cycles are performed quarterly to fully characterize TEB detector response, including offset and nonlinear terms.



TEB Calibration Methodology



VIIRS Earth View radiance is retrieved following ATBD Eq.(116)

$$L_{EV}(B, \theta) = \frac{F(B) \sum_{i=0}^2 c_i(B) dn^i(B) - \Delta L_{bg}(B, \theta)}{RVS(B, \theta)},$$

dn: detector response
 c_i: calibration coefficients
 RVS: response versus scan-angle

where the $\Delta L_{bg}(B, \theta)$ is the background difference between the EV and SV path:

$$\Delta L_{bg}(B, \theta) = (RVS(B, \theta) - RVS_{SV}(B)) \left[\frac{(1 - \rho_{RTA}(B))}{\rho_{RTA}(B)} L_{RTA} - \frac{1}{\rho_{RTA}(B)} L_{HAM} \right],$$

the F-factor is derived each scan for each band, detector, and HAM-side:

$$F(B) = \frac{RVS_{BB}(B) L_{ap}(B) + \Delta L_{bg}(B, \theta_{BB})}{\sum_{i=0}^2 c_i dn_{BB}^i},$$

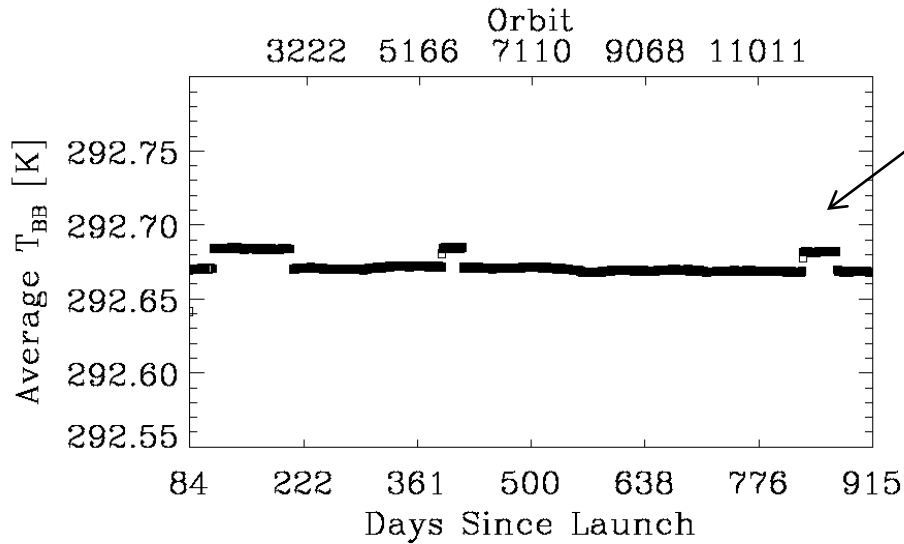
Estimated BB radiance
 Retrieved BB radiance

and the aperture radiance from the BB is:

$$L_{ap}(B) = \varepsilon L_{BB} + (1 - \varepsilon)(F_{RTA} L_{RTA} + F_{SH} L_{SH} + F_{CAV} L_{CAV})$$

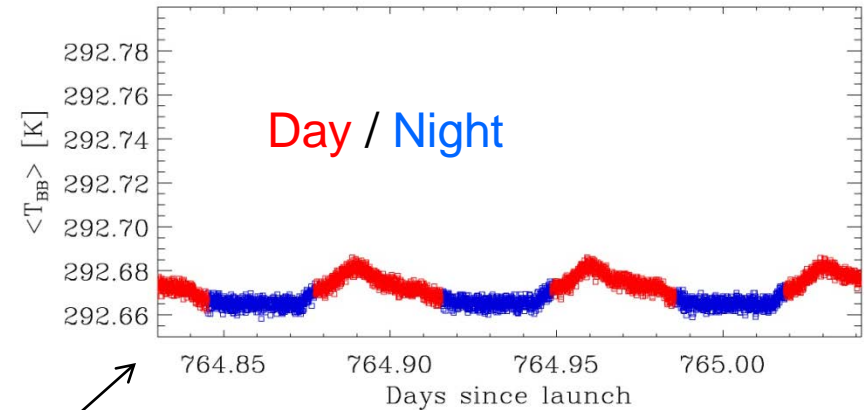


BB Performance



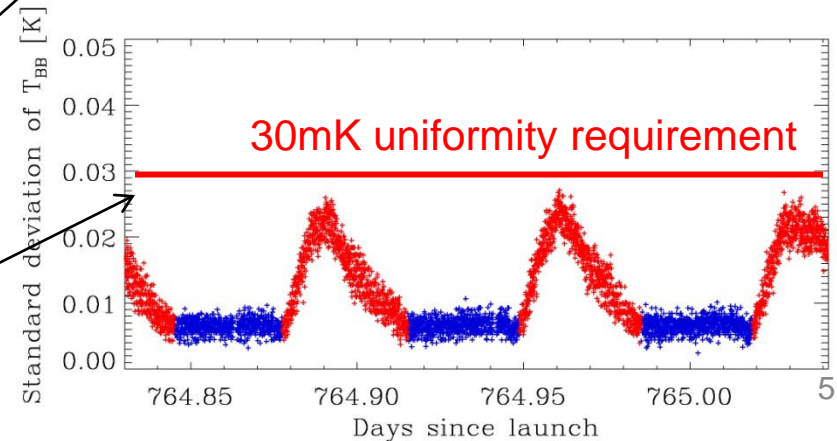
Long-term trend of daily-averaged T_{BB}

- Stable to within a few mK.
- ~15mK offsets were due to the use of two different T_{BB} settings.



Short-term stability (scan-by-scan T_{BB}):

- Orbital variations of individual thermistors up to 40mK
- Variations in average temperature ~ 20mK
- Temperature difference between individual thermistors up to 60mK
- **BB uniformity meets the requirement with standard deviation less than 30mK**





Detector Short-term Stability



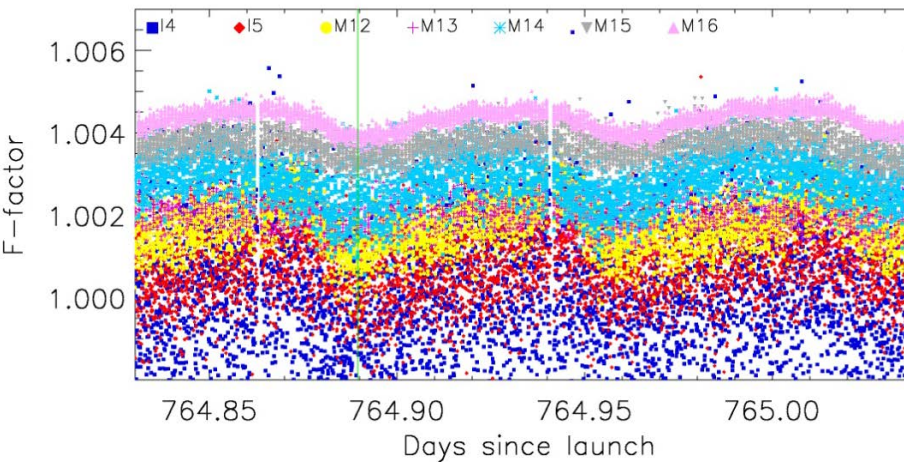
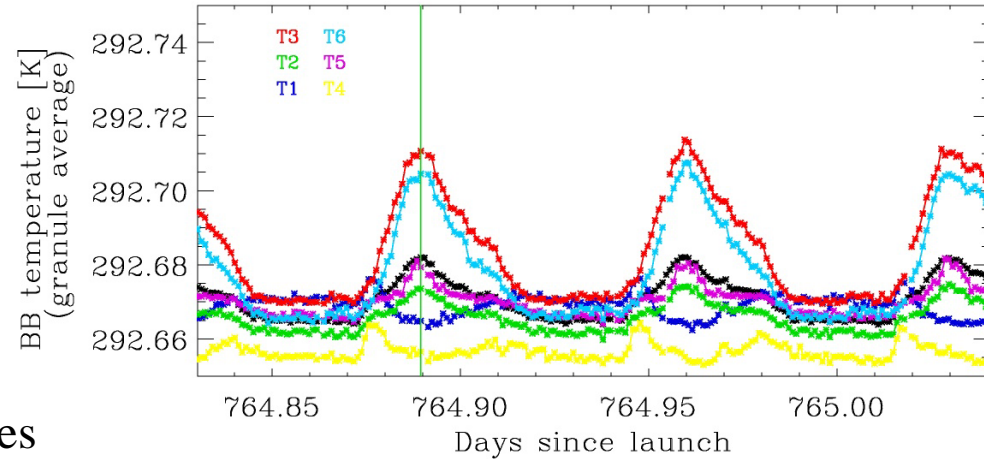
Detector responses (F-factors) show small orbital variations:

- ±0.2% or less for scan-by-scan
- ±0.1% or less for granule average

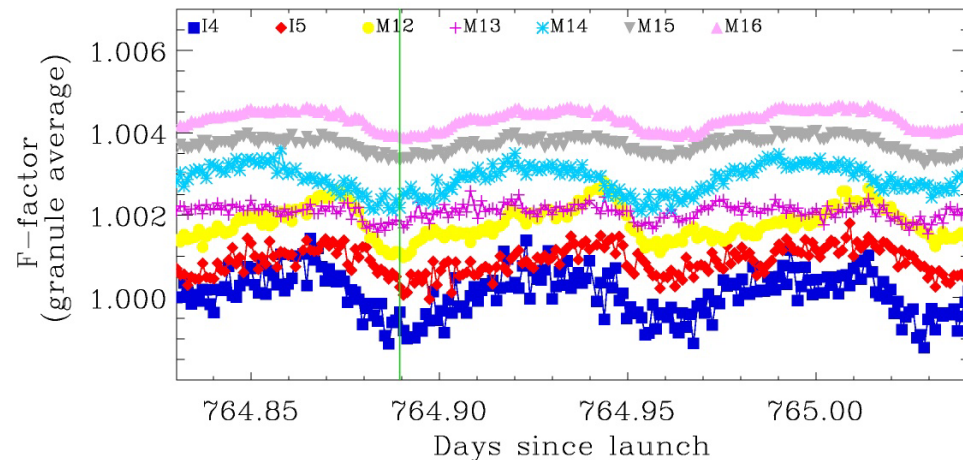
Would using averaged F-factors improve SDR product?

F-factor orbital variations correlate with T_{BB} variations and instrument temperatures variations.

Orbits: 10853, 10854, 10855



Scan-by-scan (HAM-A)



Granule average (HAM-A)

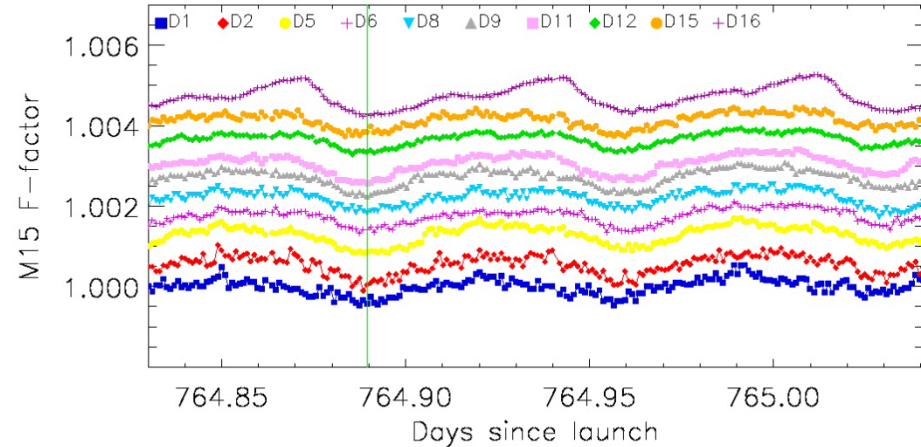
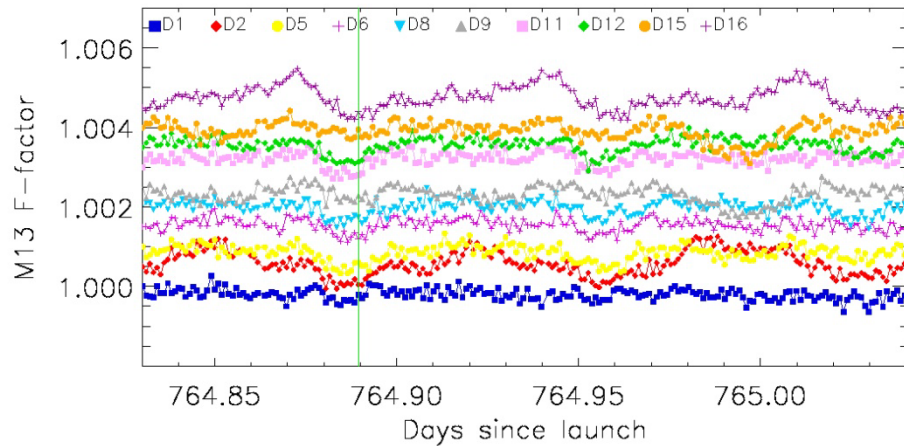
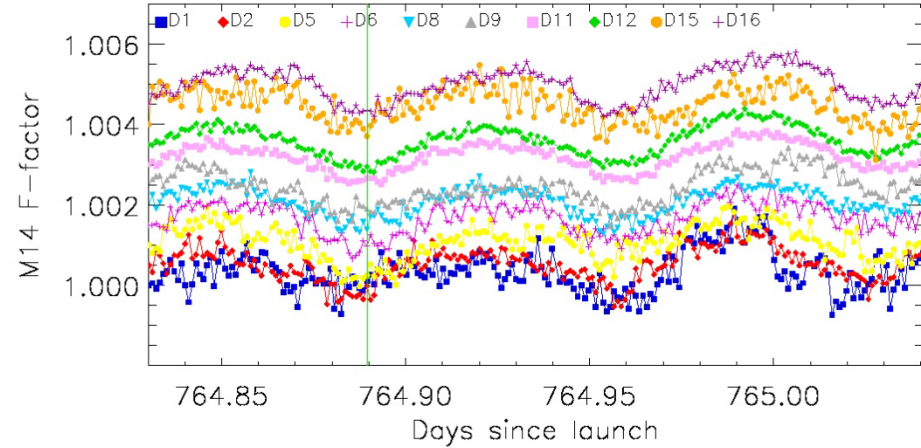
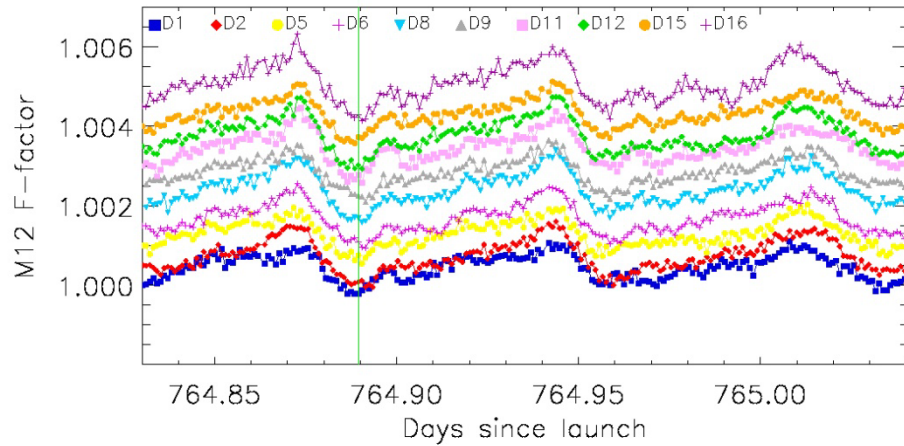
* For clarity the F-factors are shifted.



Short-term Stability- Individual Detectors



Orbits: 10853, 10854, 10855



Granule average (HAM-A)

M16 (not shown) similar to M15; same D16 out of family behavior₇

* For clarity the F-factors are shifted.

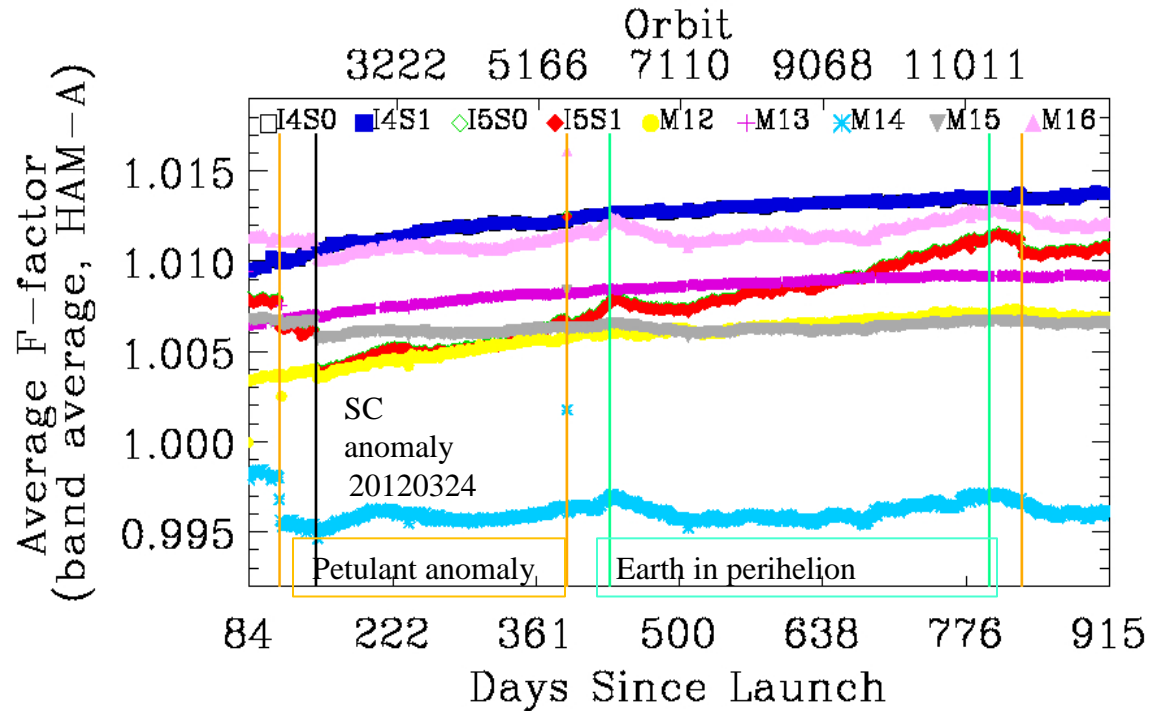


Detector Long-term Response



Daily average F-factor trend:

- From 1/20/2012 (orbit 1200) to 4/30/2014 (orbit 12983)
- I5 shows the most noticeable trend of 0.68%, followed by M12 and I4 of 0.33% and 0.32%, respectively
- Discontinuities in the trend are coincident with S/C anomalies during which the CFPA and/or instrument temperatures changed.
- Features in LWIR bands F-trend appear to coincide with the passage of the Earth through perihelion.



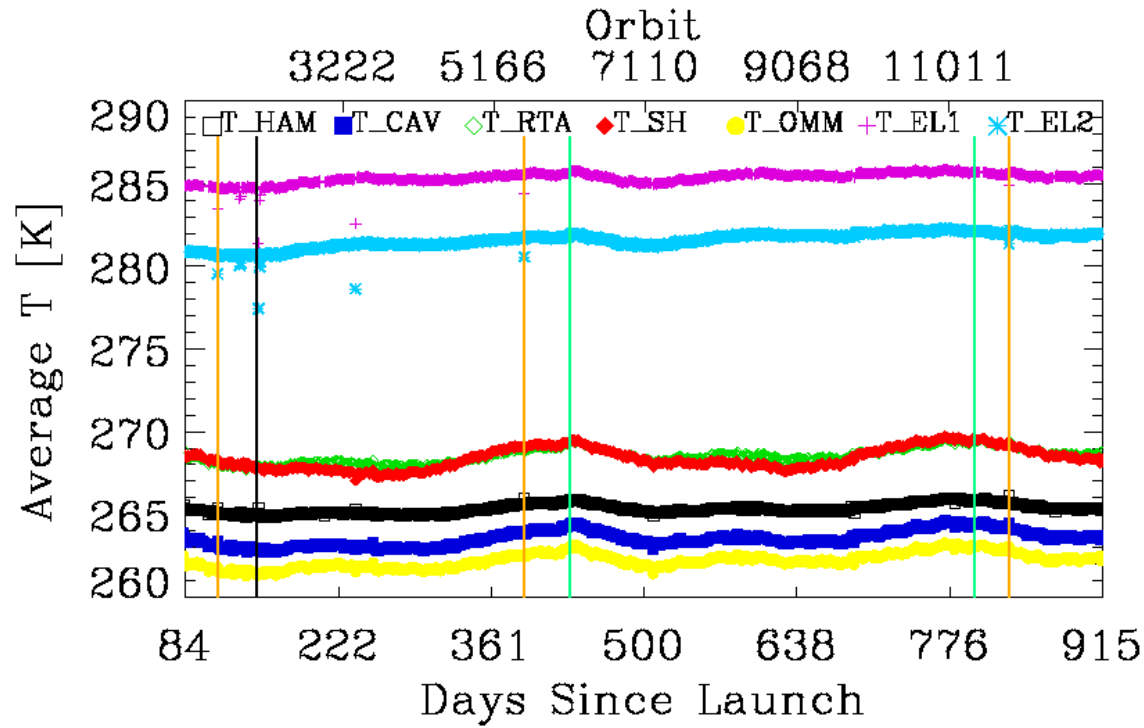
Band	I4	I5	M12	M13	M14	M15	M16
Average F-factor: 03 26 2012	1.0105	1.0040	1.0035	1.0070	0.9946	1.0056	1.0101
Average F-factor: 04 30 2014	1.0137	1.0109	1.0068	1.0092	0.9961	1.0066	1.0121
Trend [%]	0.32	0.68	0.33	0.22	0.15	0.09	0.19



Instrument Temperatures Trend



- Discontinuities in the instrument temperatures trends coincident with discontinuities in the F-factor trends shown on previous slide.
- Features in instrument temperature trends appears to coincide with the passage of the Earth through perihelion. The F-factor for LWIR bands shows features at the same time.



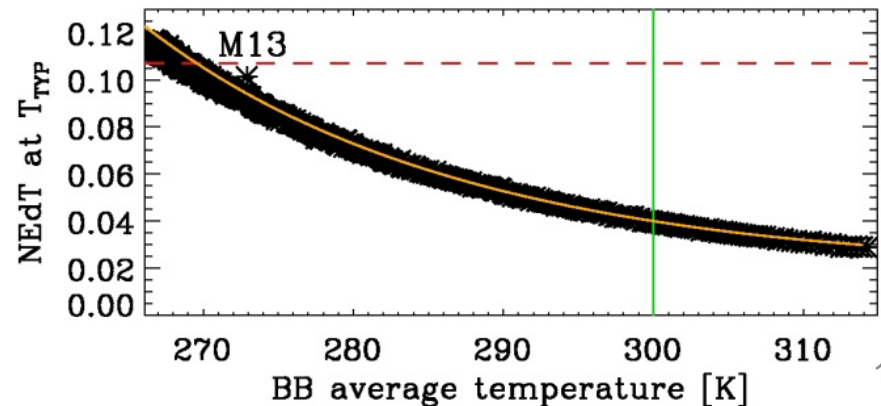
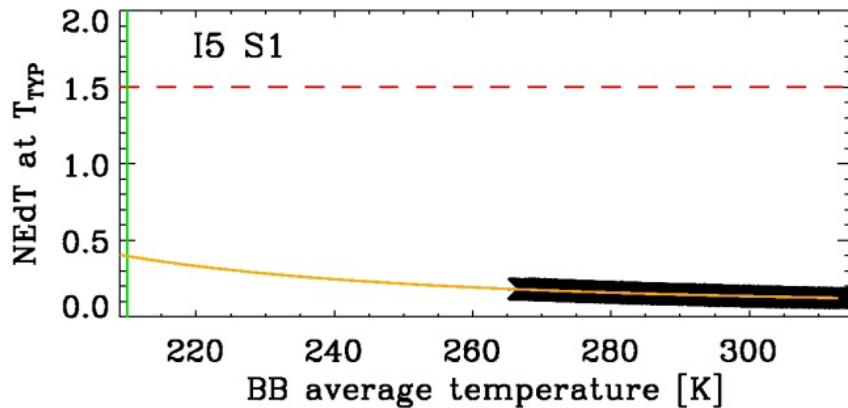
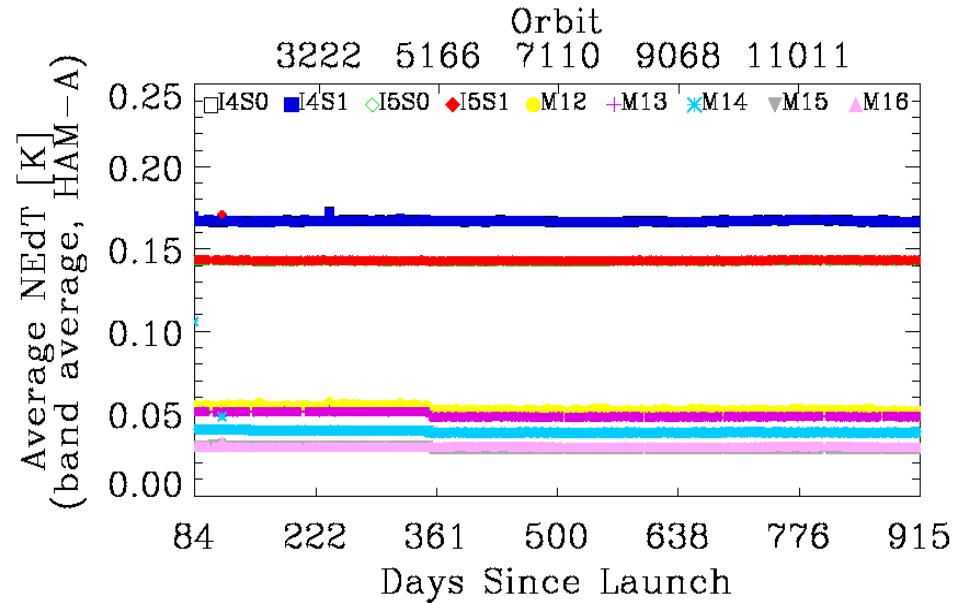


Detector Noise Characterization (NEdT)



$$NEdT = \frac{NEdL}{\partial L / \partial T} = \frac{L}{SNR \partial L / \partial T}$$

- NEdT routinely trended at 292.5K: stable since the CFPA temperatures reached ~80K (orbit 1200). Band averaged values are within 0.2 K for I bands and 0.07 K for M bands
- NEdT at T_{TYP} derived periodically from BB WUCD data: stable and meeting the sensor design requirements by a wide margin:





Detector Noise Characterization (NEdT)



NEdT at T_{TYP} (derived from BB cool-down data)

Band	T_{TYP} [K]	NEdT at T_{typ} [K]									
		Requirement	02/12	05/12	09/12	12/12	03/13	06/13	09/13	12/13	03/14
I4	270	2.5	0.4	0.4	0.4	0.4	0.4	0.4	0.4	0.4	0.4
I5	210	1.5	0.4	0.4	0.4	0.4	0.4	0.4	0.4	0.4	0.4
M12	270	0.396	0.13	0.13	0.13	0.11	0.12	0.12	0.12	0.12	0.12
M13	300	0.107	0.04	0.04	0.04	0.04	0.04	0.04	0.04	0.04	0.04
M14	270	0.091	0.05	0.06	0.06	0.06	0.06	0.06	0.06	0.06	0.06
M15	300	0.070	0.03	0.03	0.03	0.03	0.03	0.03	0.03	0.03	0.03
M16	300	0.072	0.03	0.03	0.03	0.03	0.03	0.03	0.03	0.03	0.03

Continue to meet the sensor design requirements

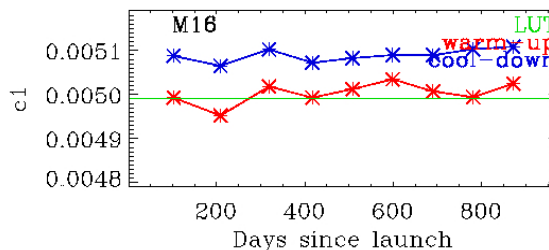
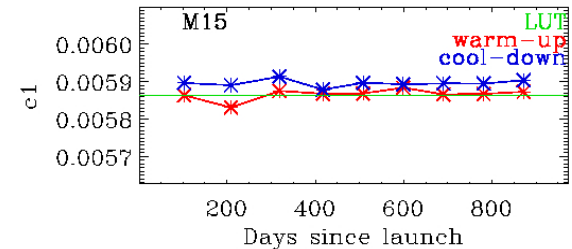
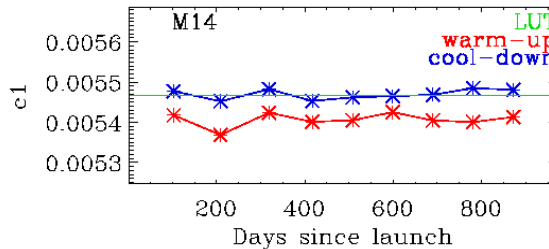
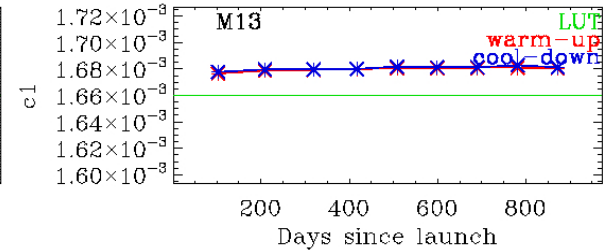
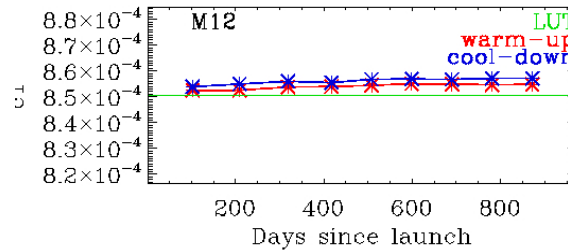
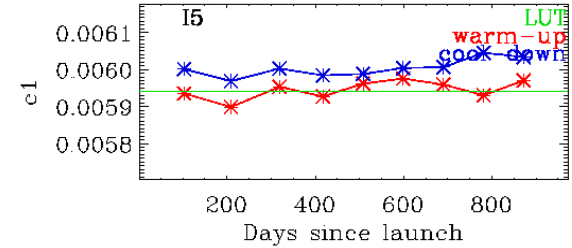
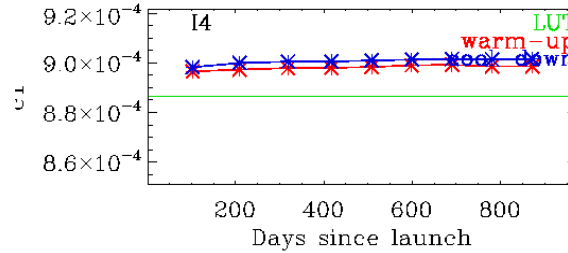


Calibration Coefficients – Band-average c_1

- Band-average c_1 coefficients, as derived from the nine WUCD cycles performed till Mar 2014, are shown in red (WU data), and blue (CD data) in comparison with pre-launch (green) values.

- Band-average c_1 coefficients derived during WUCD cycles are within 1.9% on average (at M16 CD) from pre-launch values.

- An offset between WU and CD results is present through the nine WUCDs, especially for LWIR bands.



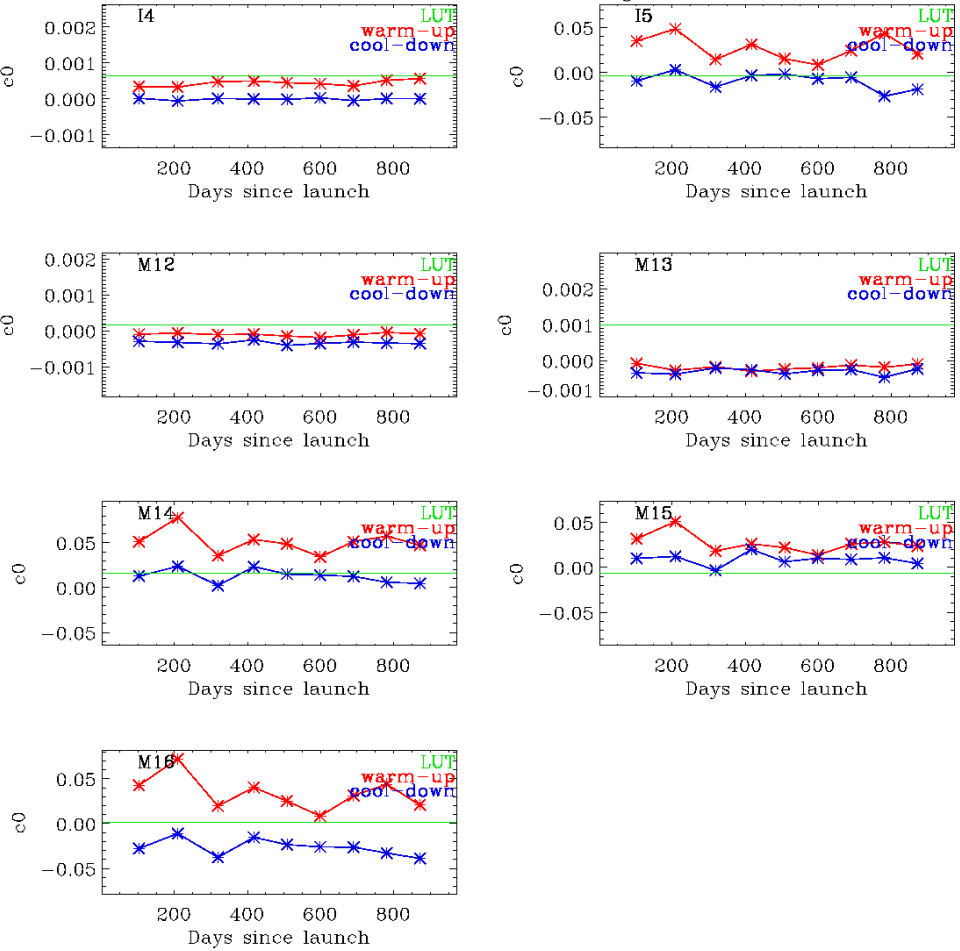
Y-range spans $c_{ILUT} \pm 4\%$ c_{ILUT}



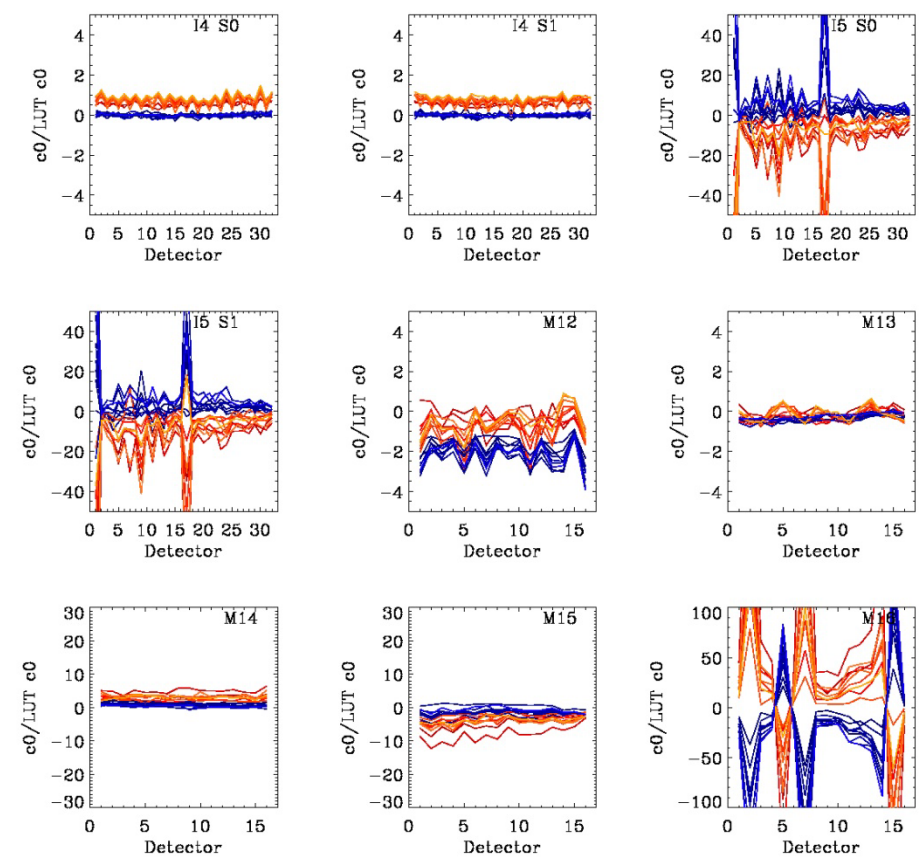
C₀ Coefficients



Band average c₀



Detector specific c₀/c_{0LUT}



Y-range spans: $c_{0LUT} \pm 0.002$ (MWIR),
 $c_{0LUT} \pm 0.1$ (LWIR)

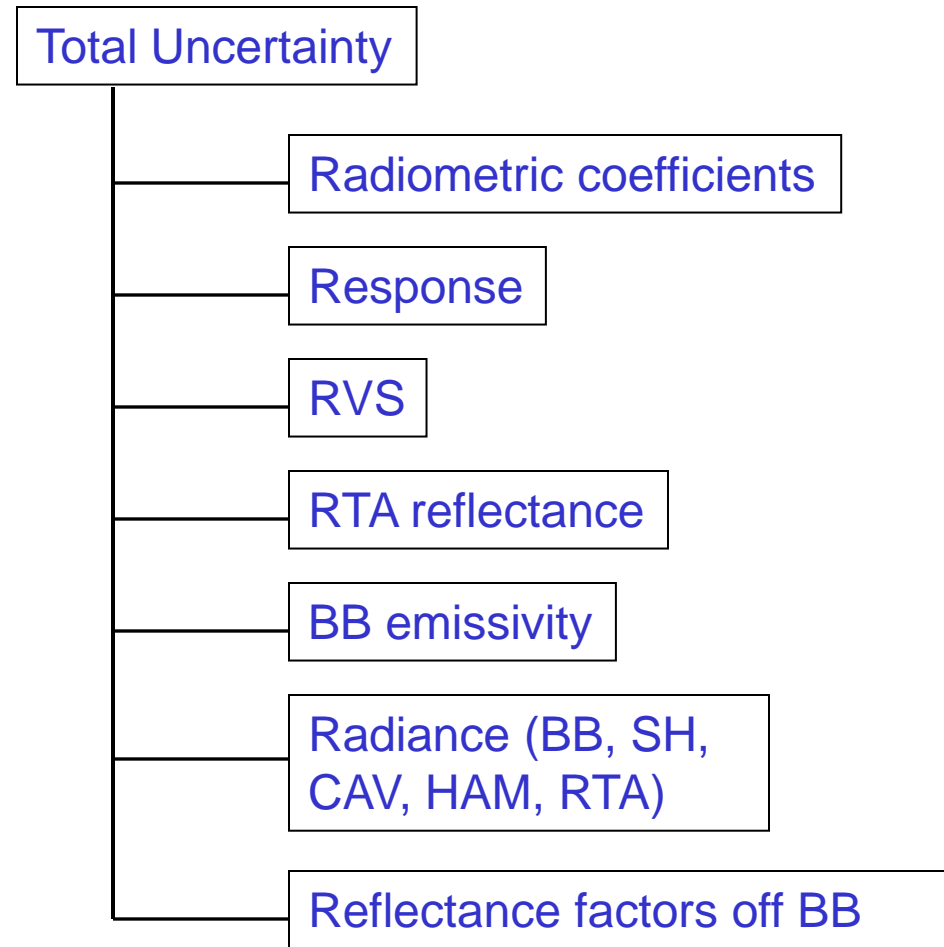
- | | |
|-----------------------|-------------------------|
| Warm-up 02/2012 HAM-A | Cool-down 02/2012 HAM-A |
| Warm-up 05/2012 HAM-A | Cool-down 05/2012 HAM-A |
| Warm-up 09/2012 HAM-A | Cool-down 09/2012 HAM-A |
| Warm-up 12/2012 HAM-A | Cool-down 12/2012 HAM-A |
| Warm-up 03/2013 HAM-A | Cool-down 03/2013 HAM-A |
| Warm-up 06/2013 HAM-A | Cool-down 06/2013 HAM-A |
| Warm-up 09/2013 HAM-A | Cool-down 09/2013 HAM-A |
| Warm-up 12/2013 HAM-A | Cool-down 12/2013 HAM-A |
| Warm-up 03/2014 HAM-A | Cool-down 03/2014 HAM-A |



Uncertainty Estimates



- EV retrieved radiance uncertainty propagated using standard NIST formulation ($k=1$)
- Some uncertainty contributors determined pre-launch by the instrument vendor: RTA reflectance BB emissivity
- Radiometric coefficient and RVS uncertainties determined from NASA pre-launch analysis
- Uncertainties investigated for a range of input signal levels and scan angles





Comparison to Requirement [K]



Uncertainty specifications

Defined in terms of %, at particular uniform scene temperatures, converted to K

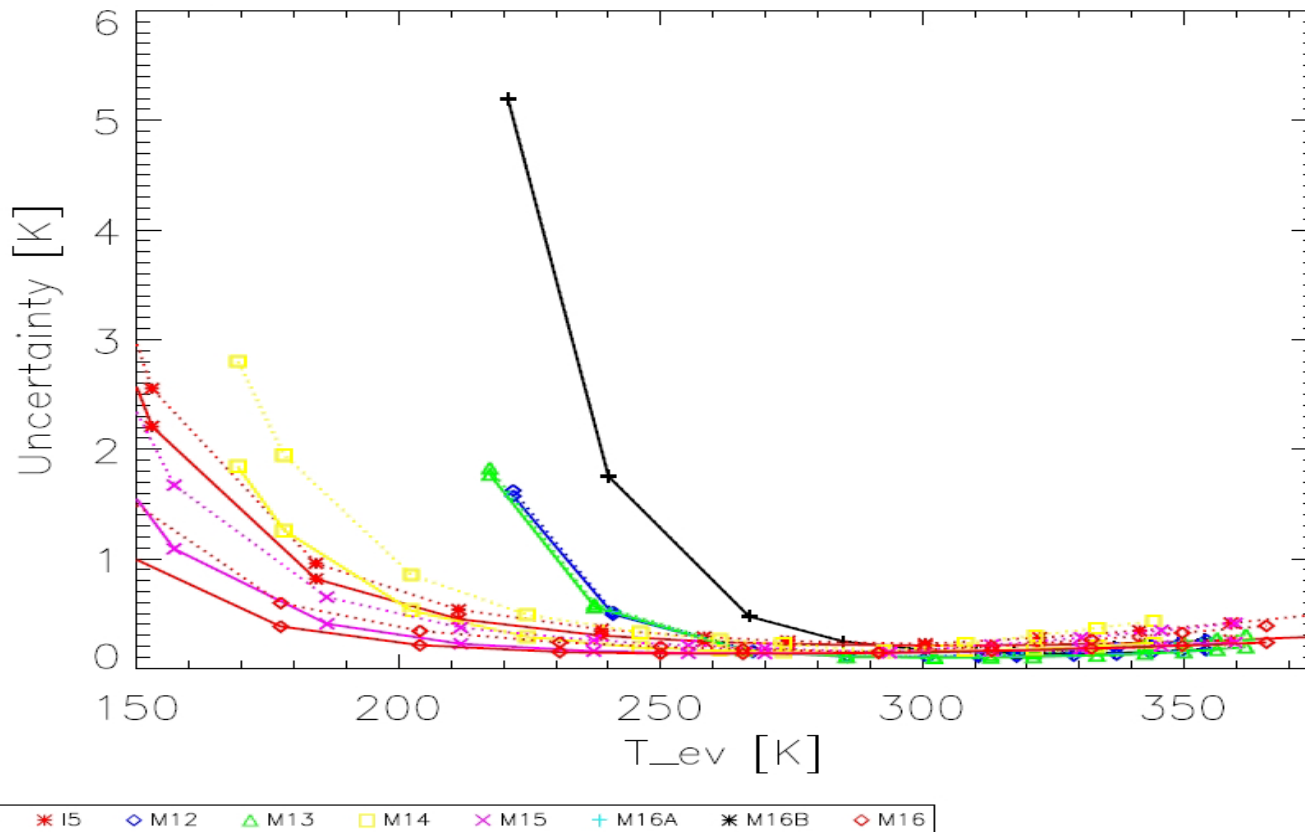
Estimates exceed the specification at lower scene temperatures for bands M12 and M13

Band	267 K
I4 spec	0.91
I4 estimate	0.468
I5 spec	1.4
I5 estimate	0.226

Band	190 K	230 K	270 K	310 K	340 K
M12 spec	---	0.92	0.13	0.17	0.21
M12 estimate	---	1.11	0.13	0.07	0.09
M13 spec	---	0.85	0.14	0.19	0.23
M13 estimate	---	1.01	0.14	0.07	0.10
M14 spec	2.60	0.75	0.26	0.23	0.34
M14 estimate	0.95	0.26	0.12	0.12	0.20
M15 spec	0.56	0.24	0.22	0.28	0.34
M15 estimate	0.42	0.18	0.12	0.13	0.19
M16 spec	0.48	0.26	0.24	0.31	0.37
M16 estimate	0.35	0.16	0.12	0.14	0.19

Uncertainty contributors:

- Dominant for MWIR bands are the relative BB radiance uncertainty and the relative EV dn uncertainty (increasing rapidly with decreasing scene temperature).
- The LWIR bands uncertainties are dominated by the c_0 , RVS, and EV dn relative uncertainties, which increase with decreasing scene temperatures.





M13 LG Calibration



M13 low gain: No scan by scan F factor correction

Prelaunch analysis differs between Government team (Aerospace and VCST) and sensor subcontractor – current LUT. Government team results are:

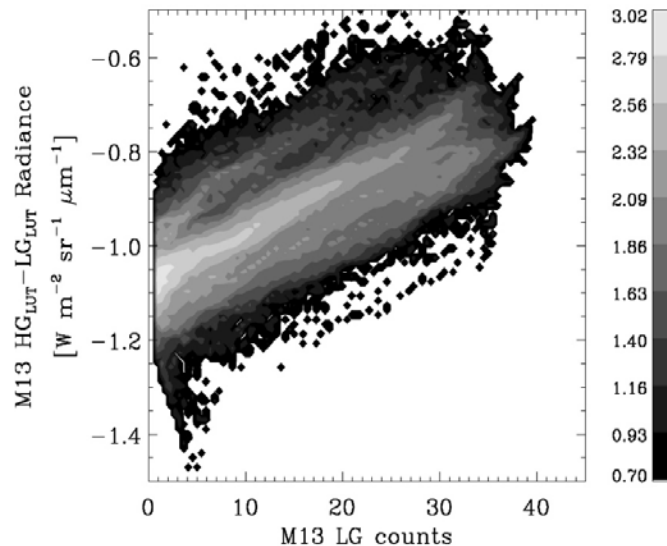
- ✓ $c_1 = 0.142$ - 7% higher than LUT value $c_{1LUT} = 0.132$;
- ✓ $c_0 = 0$ - inconsistent with $c_{0LUT} = 1.15$

Proposal:

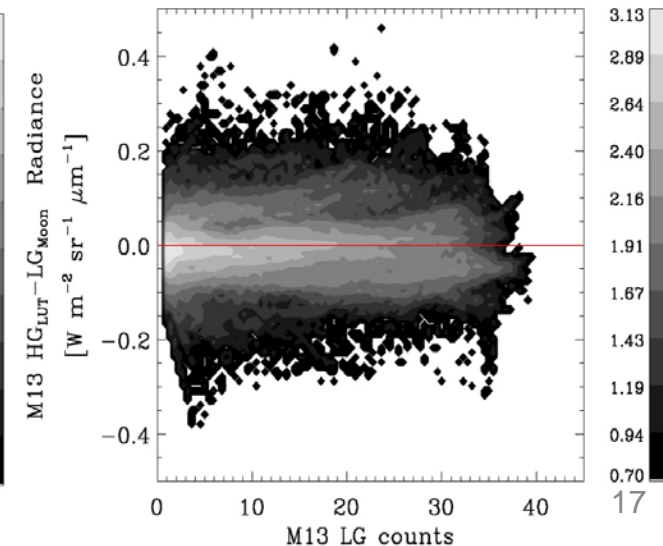
Update M13 low gain coefficients based on Government team pre-launch analysis, which is consistent with results from on-orbit calibration

On-orbit comparison of lunar images in M13 LG and M13 HG - supports Government team pre-launch results:

M13 LG c_{1LUT}, c_{0LUT}



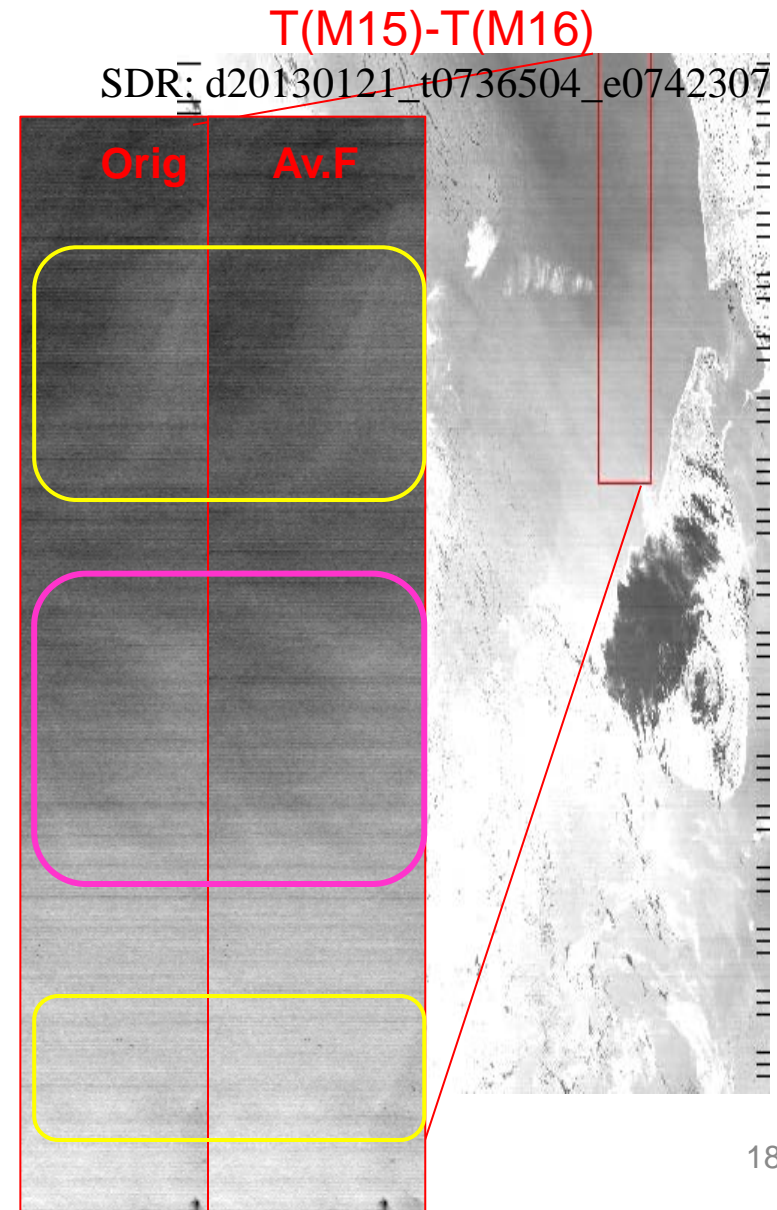
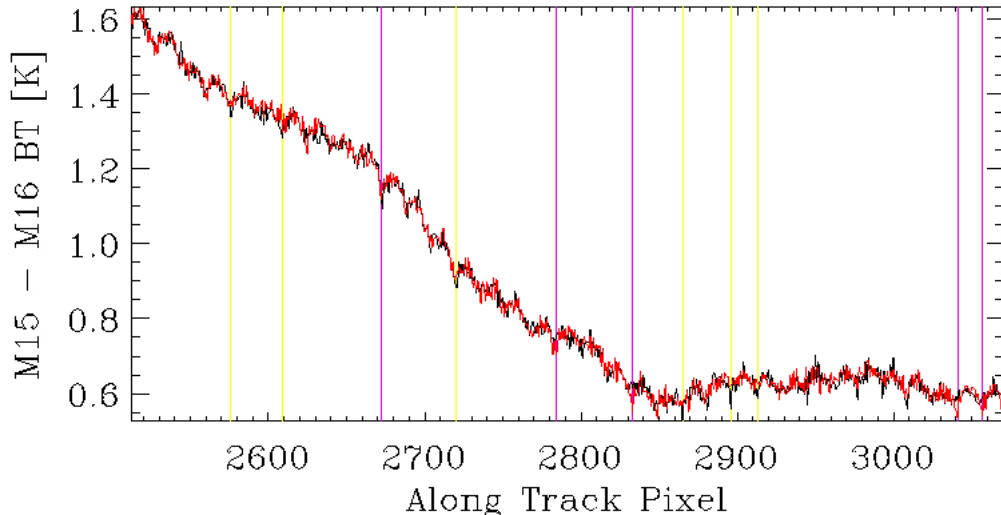
M13 LG $c_1=0.142, c_0=0$



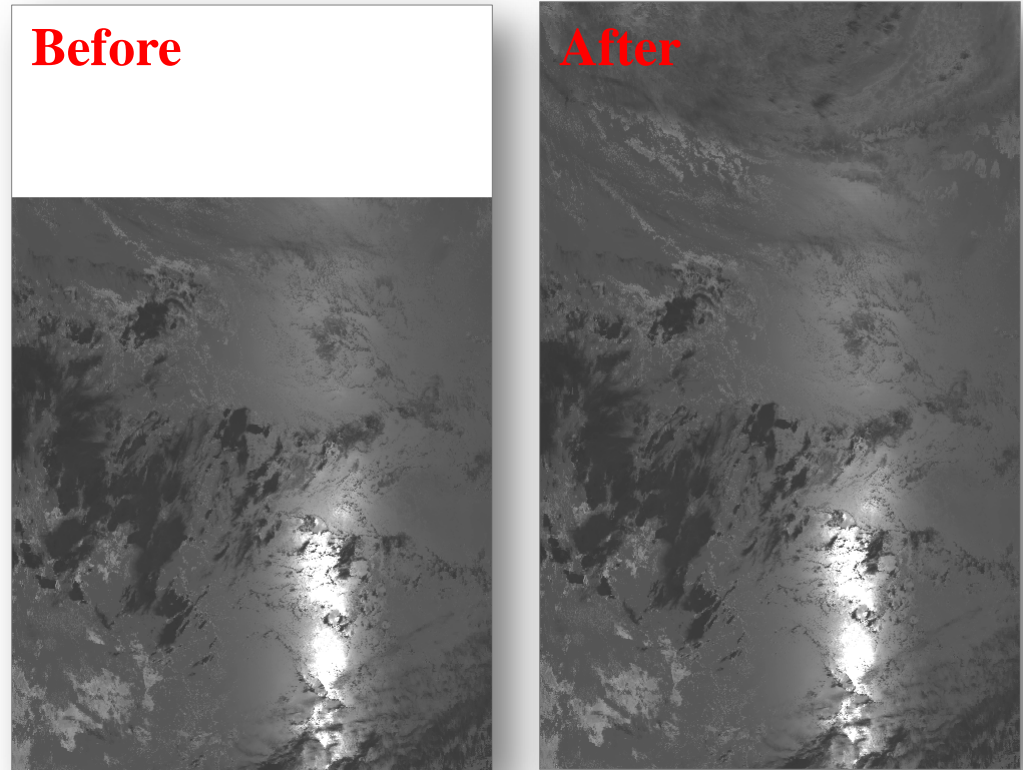
- ✓ $c_1 = 0.142$; 7% higher than c_{1LUT} -consistent with Gov. team pre-launch
- ✓ $c_0 = 0$ consistent with Gov. team pre-launch

Evaluating the effect of using average F-factors

- The VCST VIIRS SDR code was modified to apply average F-factors instead of per-scan F-factors for TEB calibration.
- The F-factors for each band, detector, HAM are averaged over 24 scans.
- Using average F-factors does not significantly impact the SDR product.
- Striping on the noise level affects SST products based on M15 and M16 brightness temperatures.



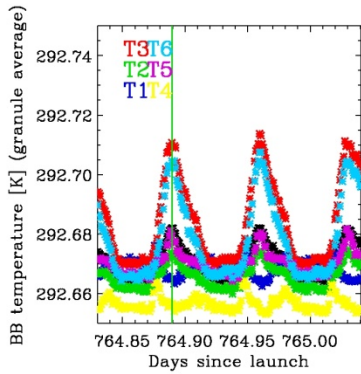
- Currently for TEB, Fill values are assigned in EV SDR when the Moon is in the SV.
- Improved algorithm computes the mean and standard deviation of a 48-frame sample each scan. Then the outlier samples (Moon intrusion) with selected rejection scheme are identified and excluded from the SV average for background subtraction.



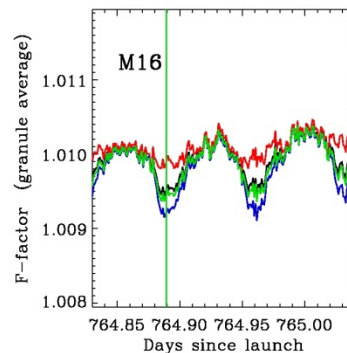
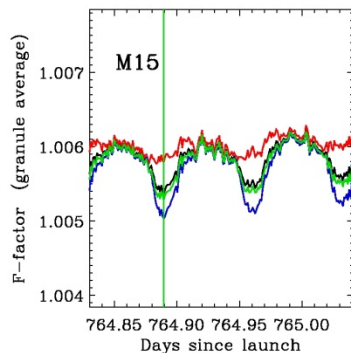
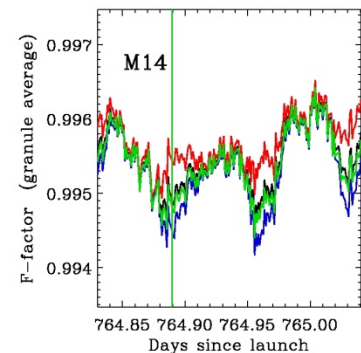
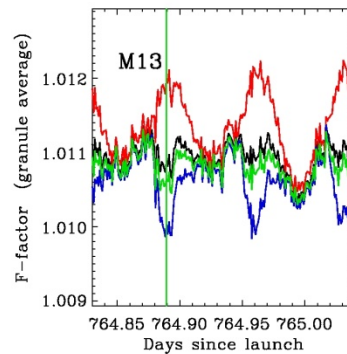
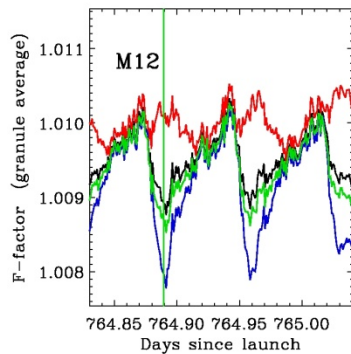
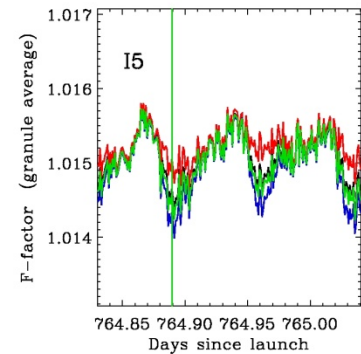
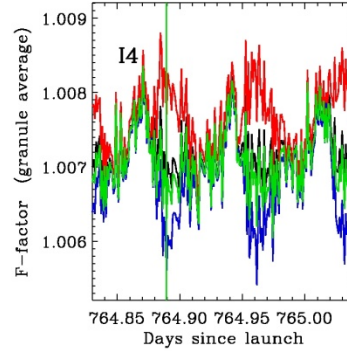
Images of calibrated radiance from 4 consecutive Band **M12** SDRs, generated with current SDR code (left) and modified (right) calibration algorithms (Data: Jan 22, 2013; Time 22:24:02). [Reference SPIE 2013, 8866-72]



F-factors Orbital Variation Reduction



T3 & T6
T2 & T5
T1 & T4
average T1-T6



- F-factor orbital variations are present, on the order of 0.05-0.1 %.
- Changing the BB thermistor weighting can reduce the F-factor orbital variations. Using T3 and T6 yield less variation for most bands (except M13).
- Improving the background model which would also reduce the F-factor orbital variations.



Conclusions



- **S-NPP VIIRS on-orbit BB long-term (2+ yr) performance is very stable. Short-term (orbital) temperature variations are present but within the uniformity requirement of 30mK**
- **Detector response (F-factor) trending is stable, with I5 showing maximum band-average trend of 0.68% followed by M12 and I4. Small orbital variations are present (0.05-0.1%)**
- **No change is observed for TEB detector noise characteristics. NEdT at Ttyp is in compliance with the requirements**
- **Uncertainty estimates: TEB meet calibration requirements for most scene temperatures; M12 and M13 have slightly larger than specified UC at low scene temperatures; Larger uncertainties in M13 low gain (above 350 K)**
- **Improvements: Updates to M13 LG offset and linear coefficients to improve calibration; Modifications to the SDR code/algorithm to allow TEB calibration to be performed when the Moon is in SV; Modifications to SDR code to apply average F-factor do not have significant impact.**



Back Up

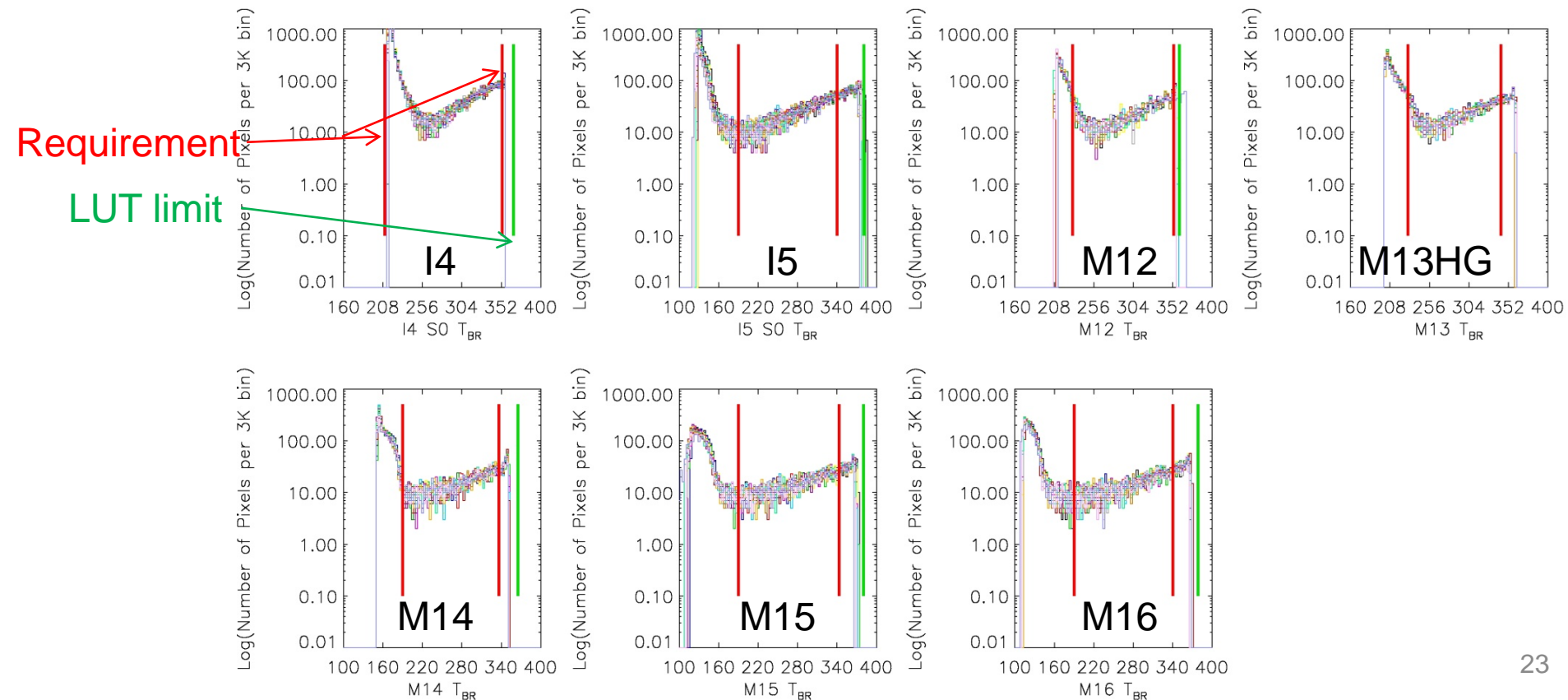


Dynamic Range Verification

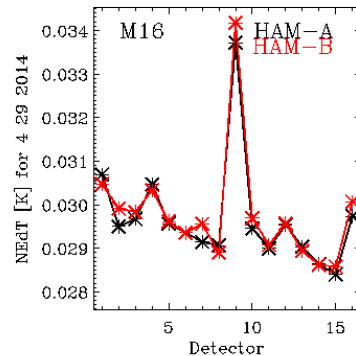
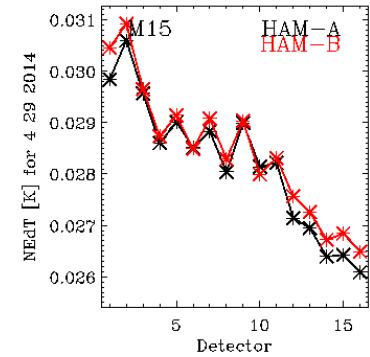
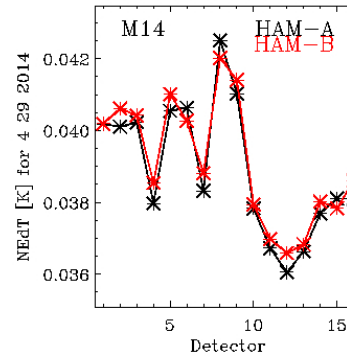
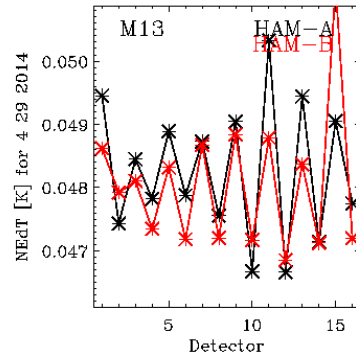
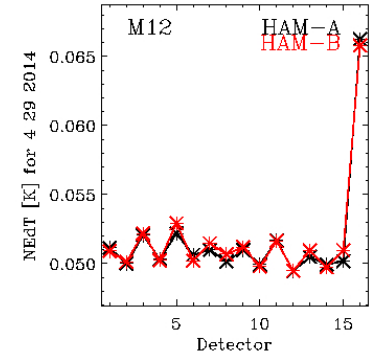
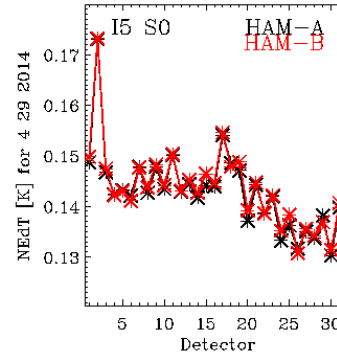
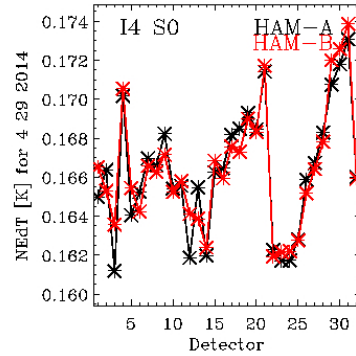


Dynamic range verified using scheduled Lunar observations

- All detectors of all TEB bands meet the T_{min} (marginal non-compliance at I4) and T_{max} requirements
- For some detectors of some bands the radiance limits in the Radiance-to-Temperature LUT do not extend to the largest possible unsaturated radiance



- Detector specific NEdT is stable through the mission.

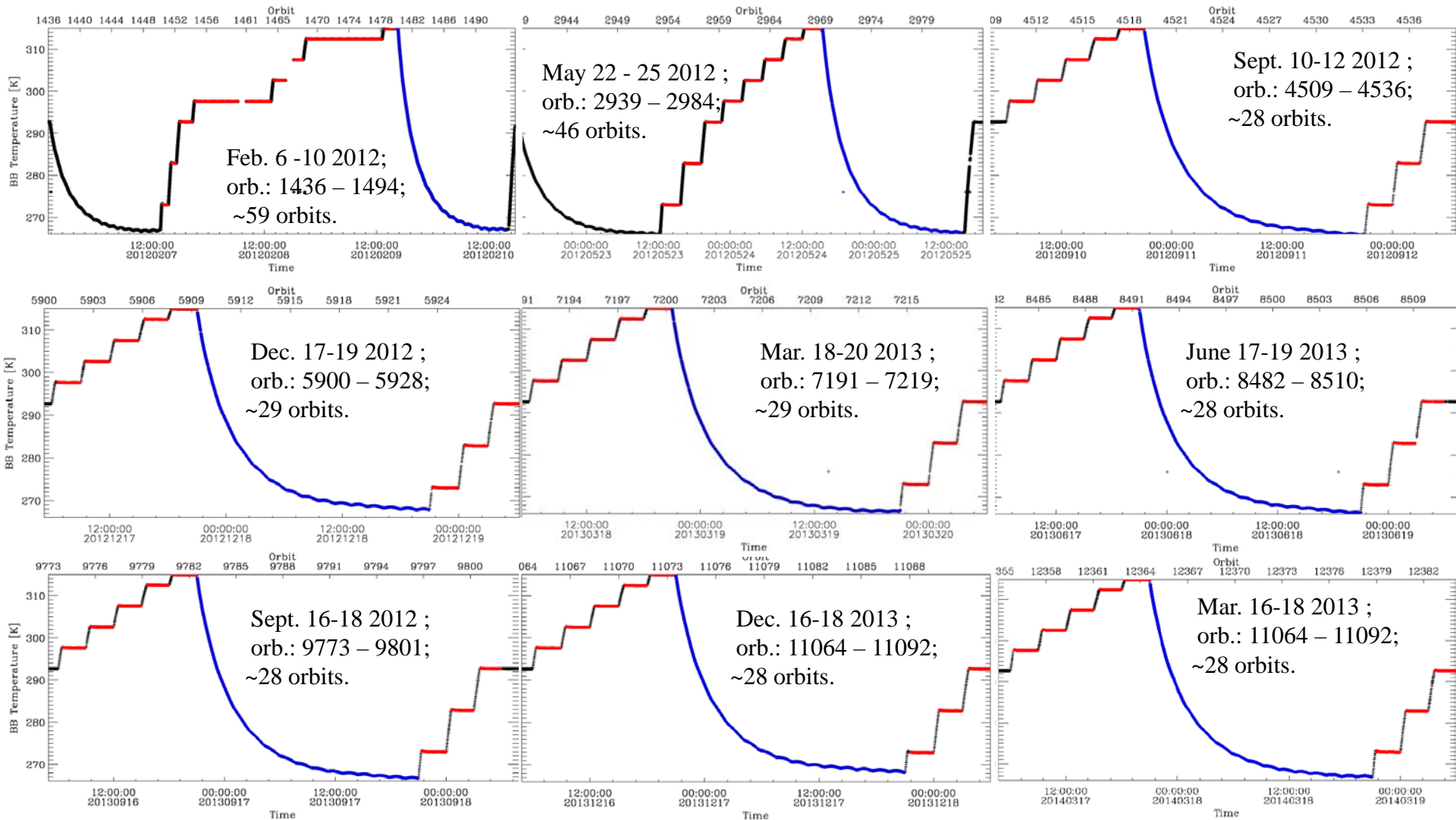




Warm-up Cool-down (WUCD) Cycles



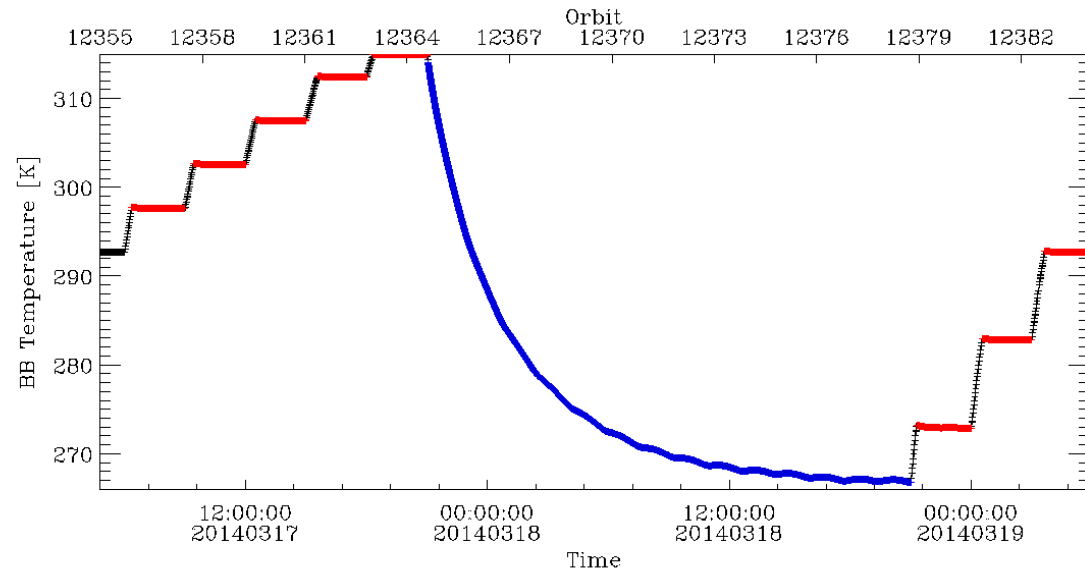
WUCD cycles performed: Feb, May, Sep, Dec 2012; Mar, Jun, Sep, Dec 2013, Mar 2014





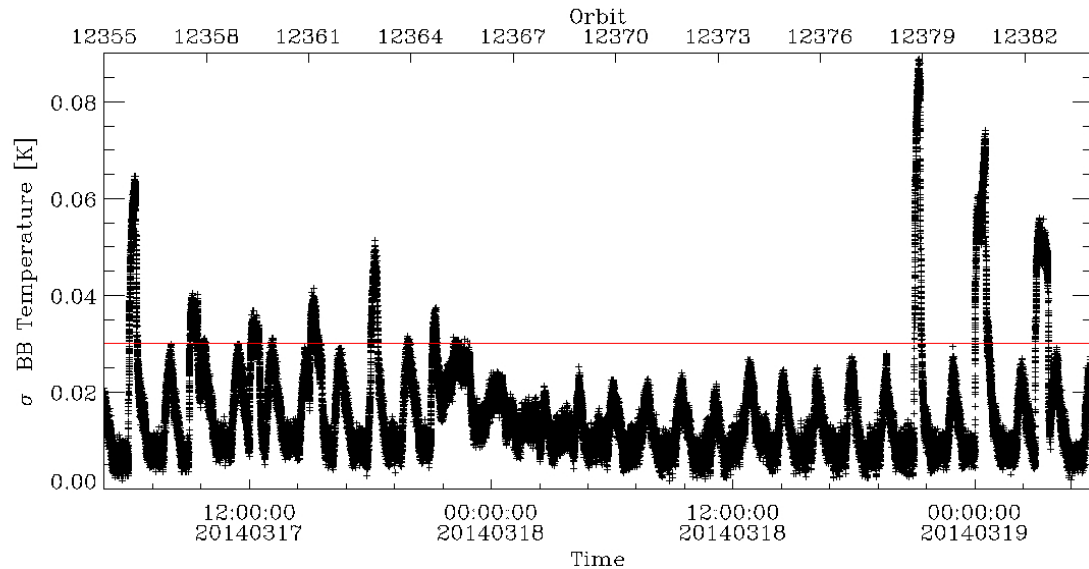
Warm-up:

- Orbits: 12355 – 12364; 12378 – 12383
- T_{BB} set to: 297.5K, 302.5K, 307.5K, 312.5K, 315.0K and 272.5K, 282.5K, 292.5K,
- The scans used (~40700) are highlighted in red.



Cool-down:

- Orbits: 12364 – 12378.
- T_{BB} range: 266.8K to 315K;
- The scans used (~47700) are shown in blue.





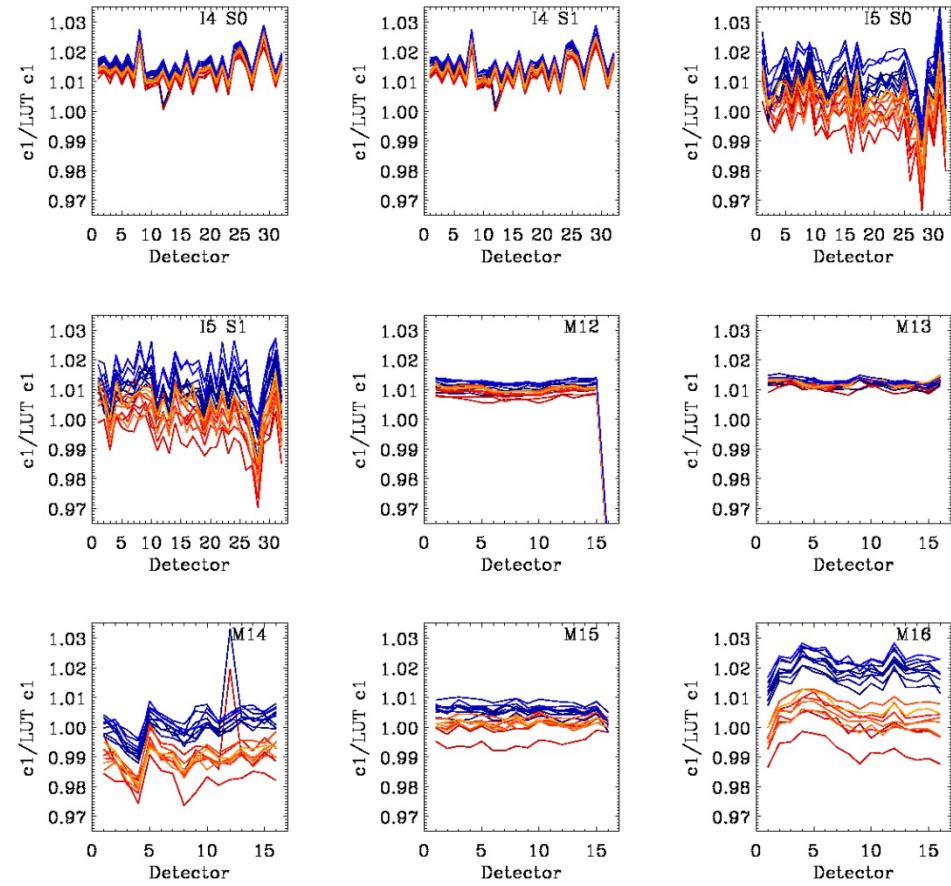
Calibration Coefficients – c1/LUT



Band average c1 difference

$$100 * (c1_{on-orbit} - c1_{LUT}) / c1_{LUT}$$

	I4	I5	M12	M13	M14	M15	M16
WU 02/12 [%]	1.2	-0.8	0.4	1	-1.1	-0.2	-0.3
CD 02/12 [%]	1.5	0.6	0.6	1.2	0.2	0.4	1.6
WU 05/12 [%]	1.2	-0.6	0.4	0.9	-1.7	-0.6	-0.8
CD 05/12 [%]	1.6	0.5	0.7	1.3	-0.6	0.3	1.1
WU 09/12 [%]	1.3	0.2	0.6	1.2	-0.8	0.2	0.5
CD 09/12 [%]	1.6	1	0.8	1.7	0.3	0.9	2.2
WU 12/12 [%]	1.3	-0.2	0.6	1.2	-1.2	0.1	0.03
CD 12/12 [%]	1.6	0.7	0.8	1.2	-0.2	0.3	1.6
WU 03/13 [%]	1.4	0.4	0.6	1.2	-1.1	0.1	0.4
CD 03/13 [%]	1.7	0.8	0.9	1.3	-0.1	0.6	1.8
WU 06/13 [%]	1.4	0.6	0.7	1.2	-0.7	0.4	0.9
CD 06/13 [%]	1.7	1.1	0.9	1.3	-0.01	0.5	2
WU 09/13 [%]	1.5	0.3	0.7	1.2	-1.1	0.1	0.3
CD 09/13 [%]	1.7	1.1	0.9	1.3	0.05	0.6	2
WU 12/13 [%]	1.4	-0.18	0.7	1.2	-1.2	0.1	0.05
CD 12/13 [%]	1.7	1.7	0.9	1.4	0.4	0.6	2.2
WU 03/14 [%]	1.4	0.5	0.7	1.2	-1.0	0.2	0.7
CD 03/14 [%]	1.7	1.6	0.9	1.3	0.3	0.7	2.4



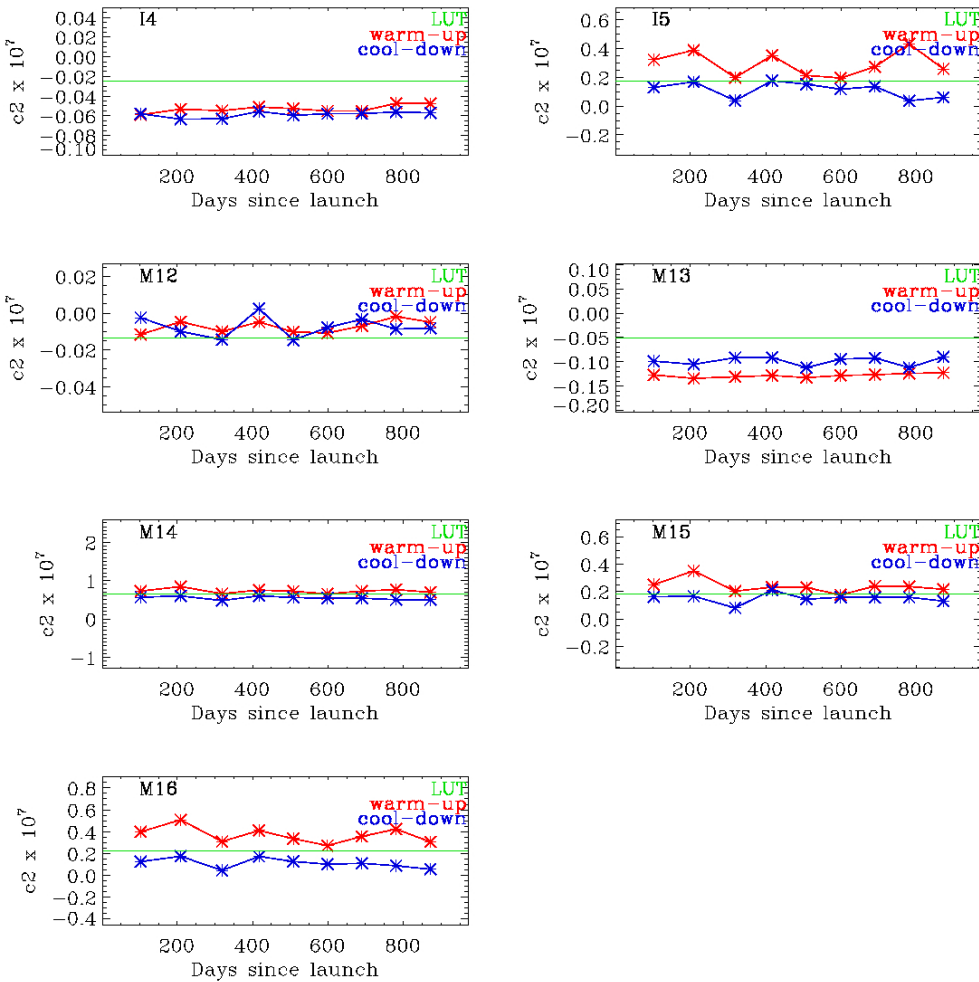
- Warm-up 02/2012 HAM-A
- Warm-up 05/2012 HAM-A
- Warm-up 09/2012 HAM-A
- Warm-up 12/2012 HAM-A
- Warm-up 03/2013 HAM-A
- Warm-up 06/2013 HAM-A
- Warm-up 09/2013 HAM-A
- Warm-up 12/2013 HAM-A
- Warm-up 03/2014 HAM-A
- Cool-down 02/2012 HAM-A
- Cool-down 05/2012 HAM-A
- Cool-down 09/2012 HAM-A
- Cool-down 12/2012 HAM-A
- Cool-down 03/2013 HAM-A
- Cool-down 06/2013 HAM-A
- Cool-down 09/2013 HAM-A
- Cool-down 12/2013 HAM-A
- Cool-down 03/2014 HAM-A



C2 Coefficients

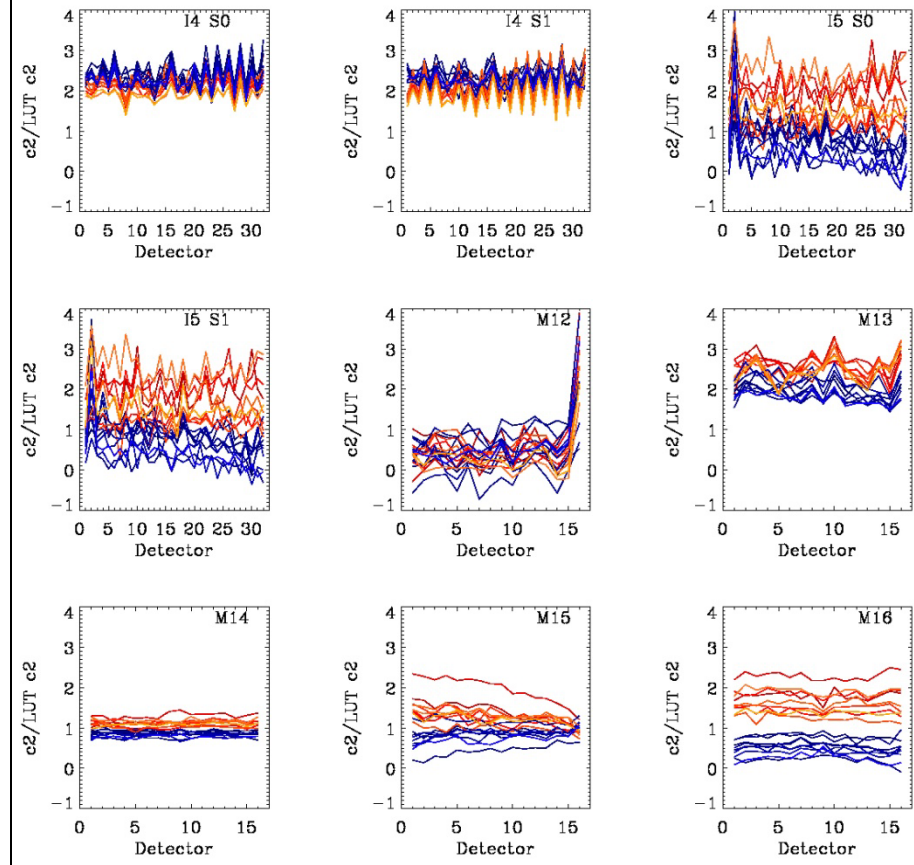


Band average c_2



Y-range spans $c_{2LUT} \pm 3 \times c_{2LUT}$

Detector specific c_2/c_{2LUT}



- | | |
|-----------------------|-------------------------|
| Warm-up 02/2012 HAM-A | Cool-down 02/2012 HAM-A |
| Warm-up 05/2012 HAM-A | Cool-down 05/2012 HAM-A |
| Warm-up 09/2012 HAM-A | Cool-down 09/2012 HAM-A |
| Warm-up 12/2012 HAM-A | Cool-down 12/2012 HAM-A |
| Warm-up 03/2013 HAM-A | Cool-down 03/2013 HAM-A |
| Warm-up 06/2013 HAM-A | Cool-down 06/2013 HAM-A |
| Warm-up 09/2013 HAM-A | Cool-down 09/2013 HAM-A |
| Warm-up 12/2013 HAM-A | Cool-down 12/2013 HAM-A |
| Warm-up 03/2014 HAM-A | Cool-down 03/2014 HAM-A |



Comparison to Requirement [%]



Uncertainty specifications

Defined in terms of %, at particular uniform scene temperatures

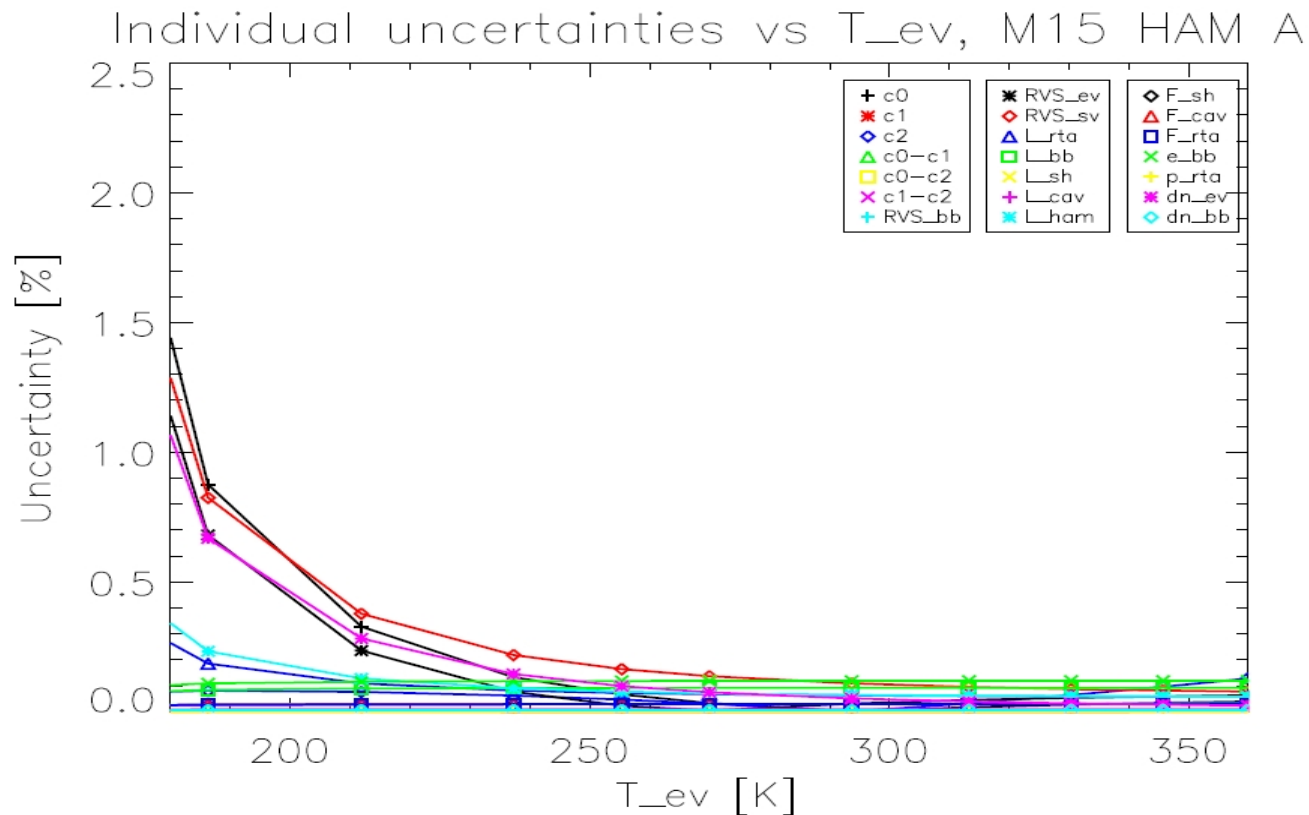
Estimates exceed the specification at lower scene temperatures for bands M12 and M13

Band	267 K
I4 spec	5.00
I4 estimate	2.55
I5 spec	2.50
I5 estimate	0.41

Band	190 K	230 K	270 K	310 K	340 K
M12 spec	---	7.00	0.70	0.70	0.70
M12 estimate	---	8.98	0.71	0.27	0.32
M13 spec	---	5.70	0.70	0.70	0.70
M13 estimate	---	7.50	0.69	0.26	0.31
M14 spec	12.30	2.40	0.60	0.40	0.50
M14 estimate	4.82	0.84	0.28	0.21	0.29
M15 spec	2.10	0.60	0.40	0.40	0.40
M15 estimate	1.59	0.47	0.22	0.19	0.22
M16 spec	1.60	0.60	0.40	0.40	0.40
M16 estimate	1.24	0.37	0.21	0.18	0.20

Uncertainty contributors:

- Dominant for MWIR bands are the relative BB radiance uncertainty and the relative EV dn uncertainty (increasing rapidly with decreasing scene temperature).
- The LWIR bands uncertainties are dominated by the c_0 , RVS, and EV dn relative uncertainties, which increase with decreasing scene temperature.





Resolving S-NPP VIIRS Thermal Emissive Band Performance Issues

Chris Moeller, Univ Wisconsin
David Moyer (Aerospace Corp.)

with contributions from

Dave Tobin, Greg Quinn (Univ. Wisconsin)

Thanks to all VIIRS SDR team partners in this work

2014 STAR JPSS Science Teams Annual Mtg

May 12-16, 2014

College Park, MD

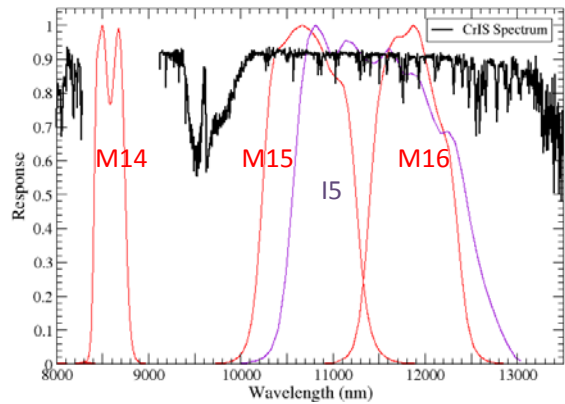
Outline

- VIIRS TEB Performance Status and Issues
 - Radiometric Comparisons
 - Trending
 - Scene Temperature Dependence (C0)
 - OBC Dependence Consistency
 - Mirror Side Dependence
 - Detector Dependence
- Summary

Objective: understand TEB SDR performance
“On-orbit sensor performance characterized and
calibration parameters adjusted accordingly”.

VIIRS-CrIS SDR Comparisons

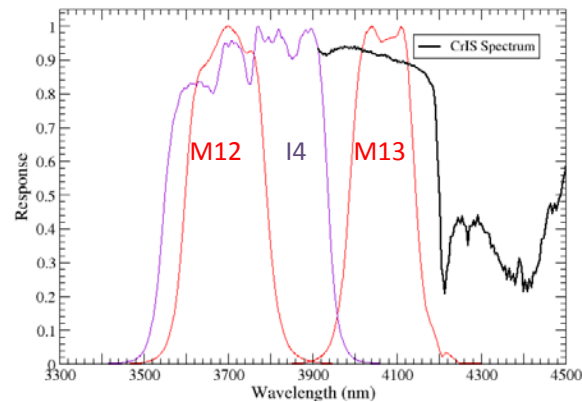
- VIIRS SDR accuracy/stability plus RVS performance
- Global; 2.9 million matchups daily from SNPP platform
- Cross Track coverage
- In-band spectral radiance for M13, M15, M16 and I5
- Long term high quality data record to assess stability



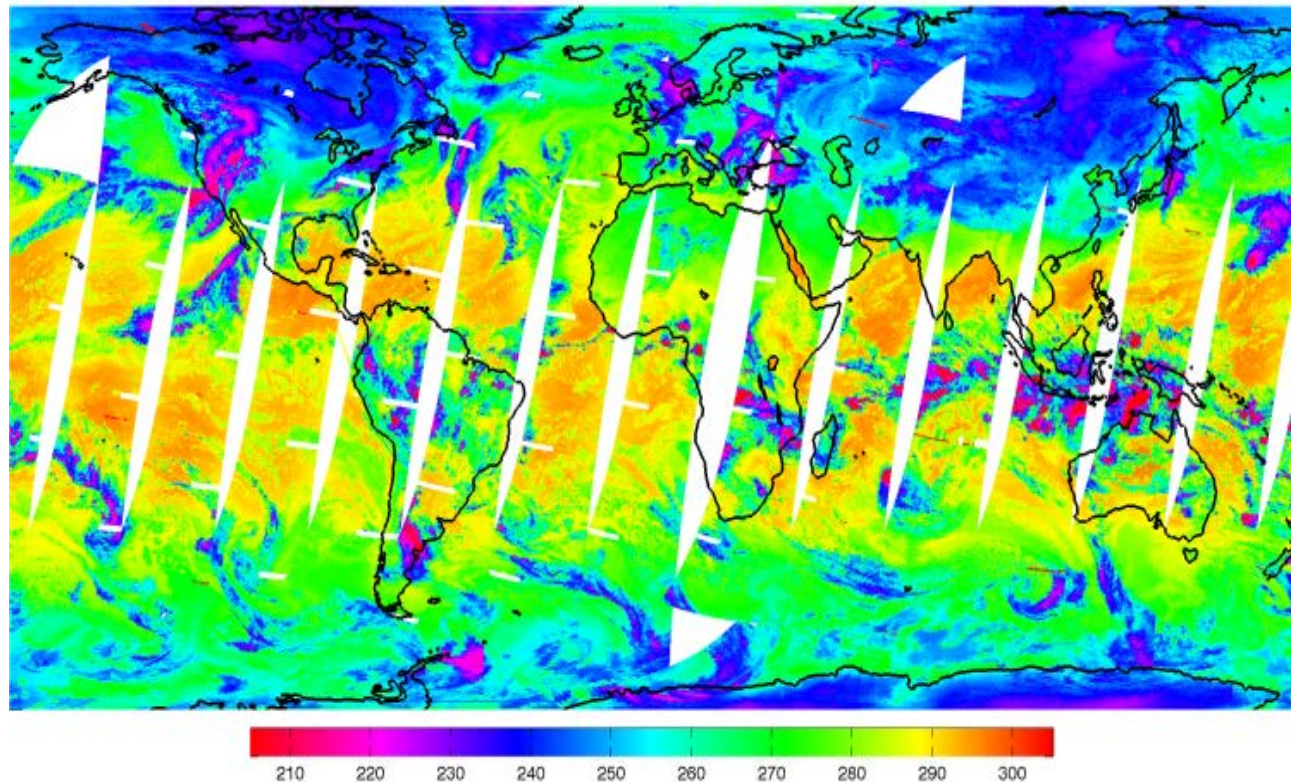
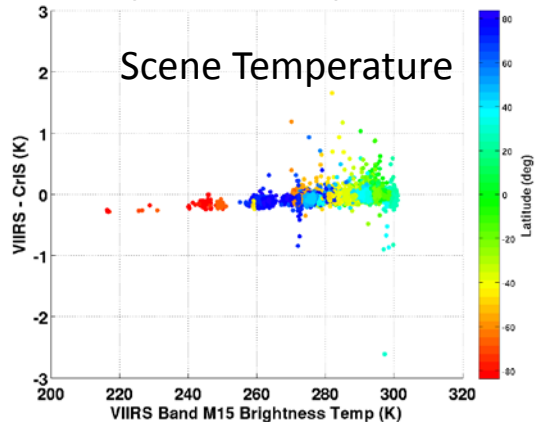
CrIS spectrum covers VIIRS M13, M15, M16, and I5 but does not include OOB response in M15 and M16

CrIS convolved with VIIRS SRF

VIIRS mean within CrIS FOVs



Jul 01, 2013 : SNPP VIIRS - CrIS; Band M15

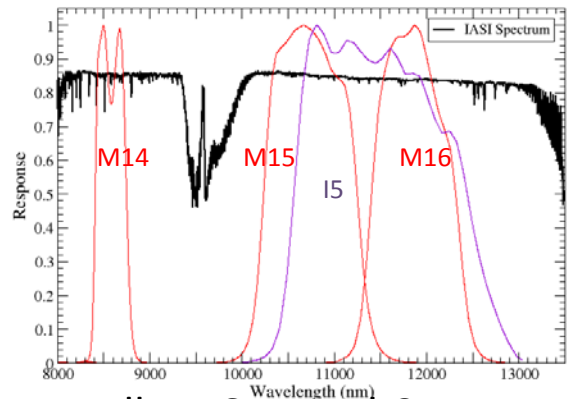


VIIRS-IASI SDR Comparisons

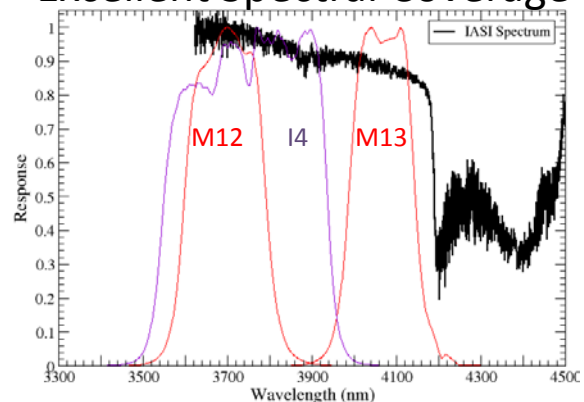
- Evaluate VIIRS SDR accuracy and OOB impact
- High latitude SNOs; limited data sample
- All FOVs inside 50 km radius around each SNO are retained: 14-16 IASI FOVs and >10,000 VIIRS 750m FOVs
- 10 minute tolerance on SNO occurrence
- IASI spectral coverage of VIIRS M13-M16, I5; nearly complete spectral coverage of M12 (85%) and I4 (81%)

+/-10 minute tolerance on overpass of SNO point

S-NPP/MetOp-A SNOs occur exclusively at polar latitudes



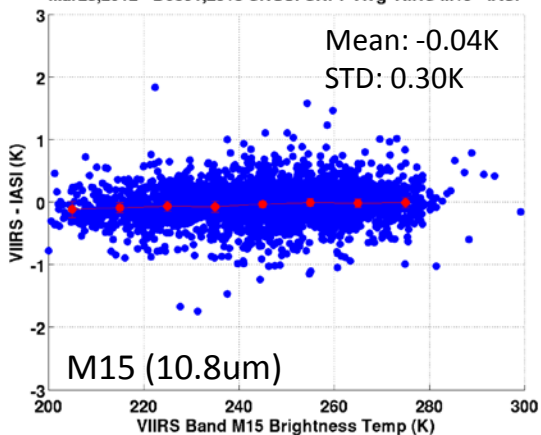
Excellent Spectral Coverage



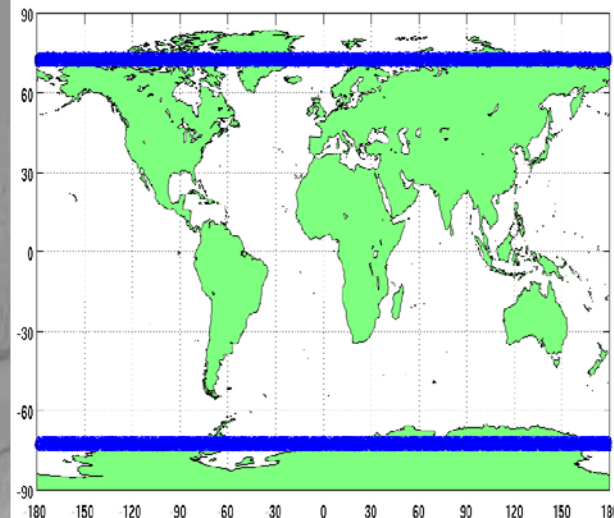
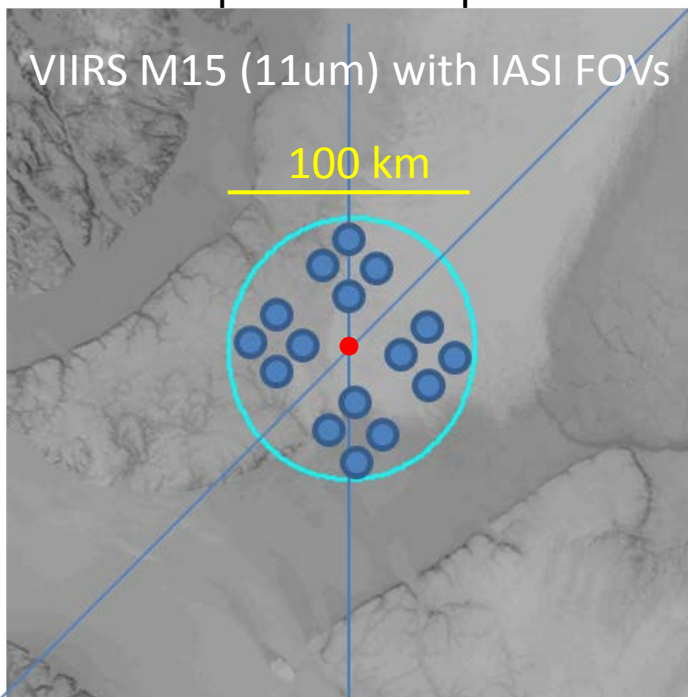
Difference as a function of scene temperature

Mar28,2012 - Dec01,2013 SNOs: SNPP Avg VIIRS M15 - IASI

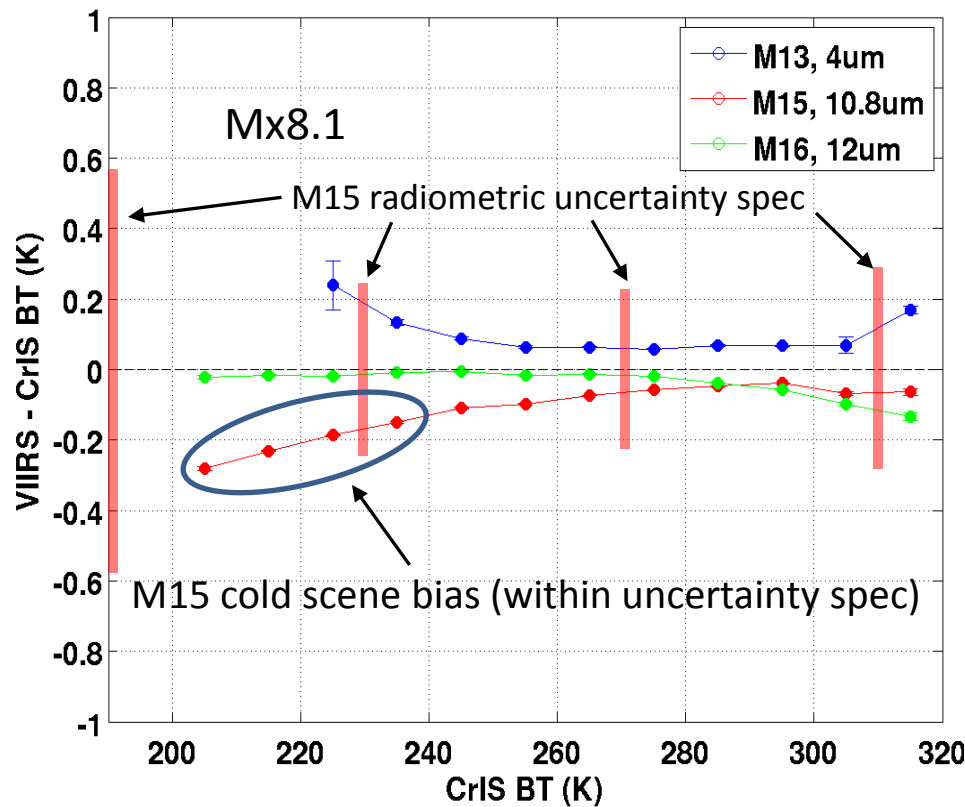
Mean: -0.04K
STD: 0.30K



M15 (10.8um)



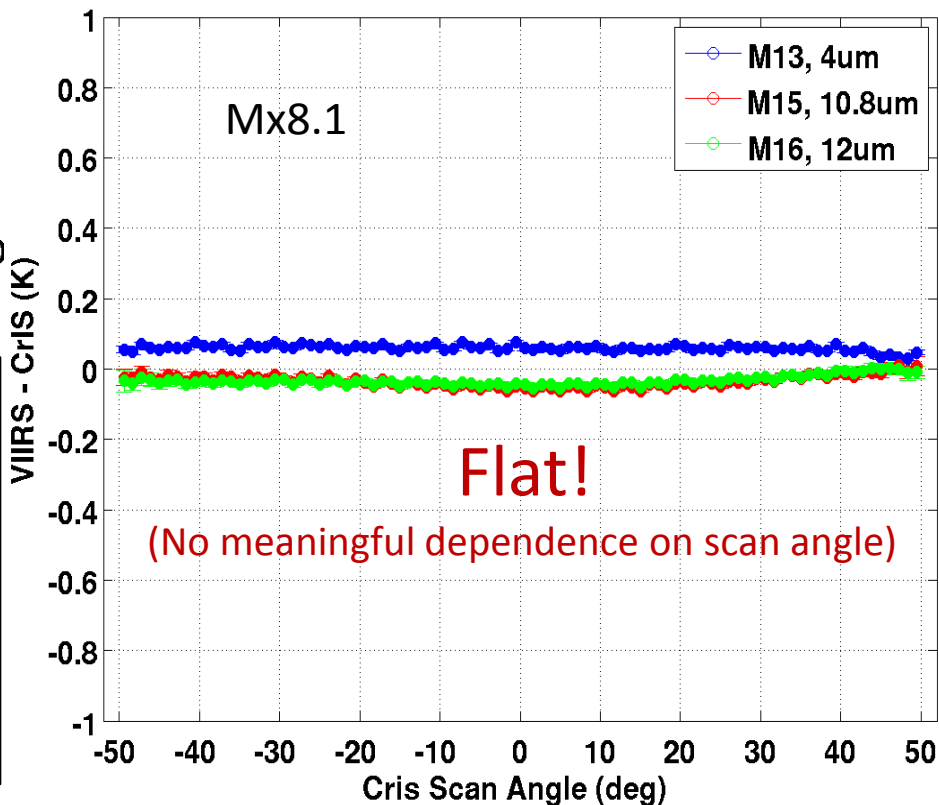
Jul 01, 2013 : Mean SNPP VIIRS - CrIS:v33a



VIIRS-CrIS (Mx8.1)

- Scene temperature provides insight on calibration coefficient performance.
- Scan angle provides insight on HAM RVS characterization quality.
- Data shown for July 1, 2013 is typical of all days. CrIS calibration Mx8.1.

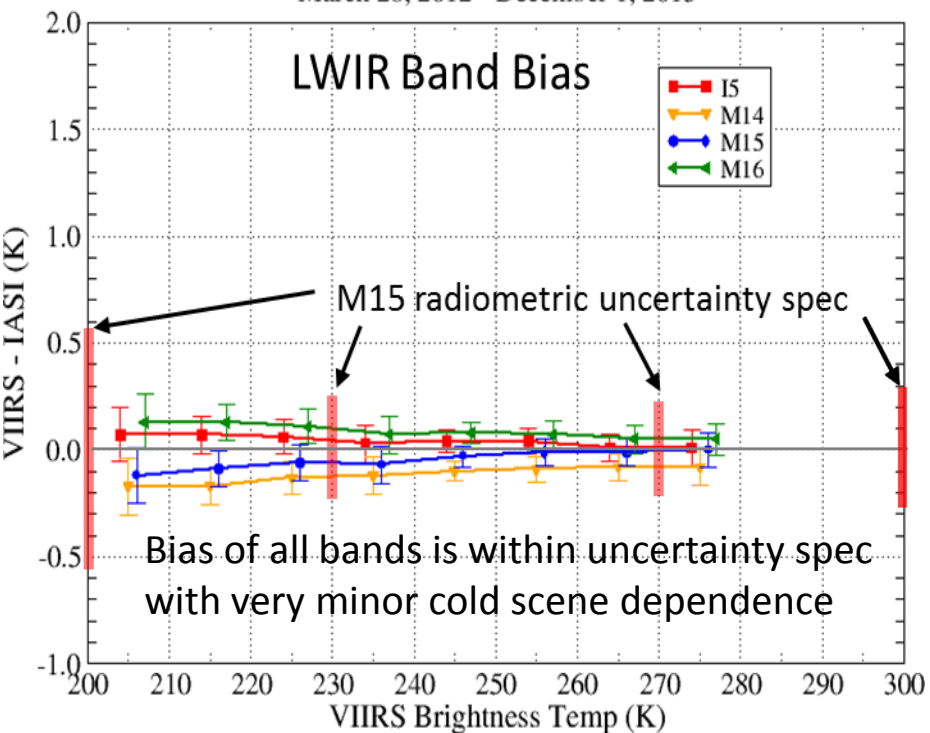
Jul 01, 2013 : Mean SNPP VIIRS - CrIS:v33a



- M15 bias (above) has minor cold scene dependence, less so for M13. Suggests that C_0 coefficient may not be optimally set. Note: this dependence has been reduced by Mx8.1 CrIS calibration.
- Minimal dependence of bias on scan angle (right). TEB RVS well characterized.

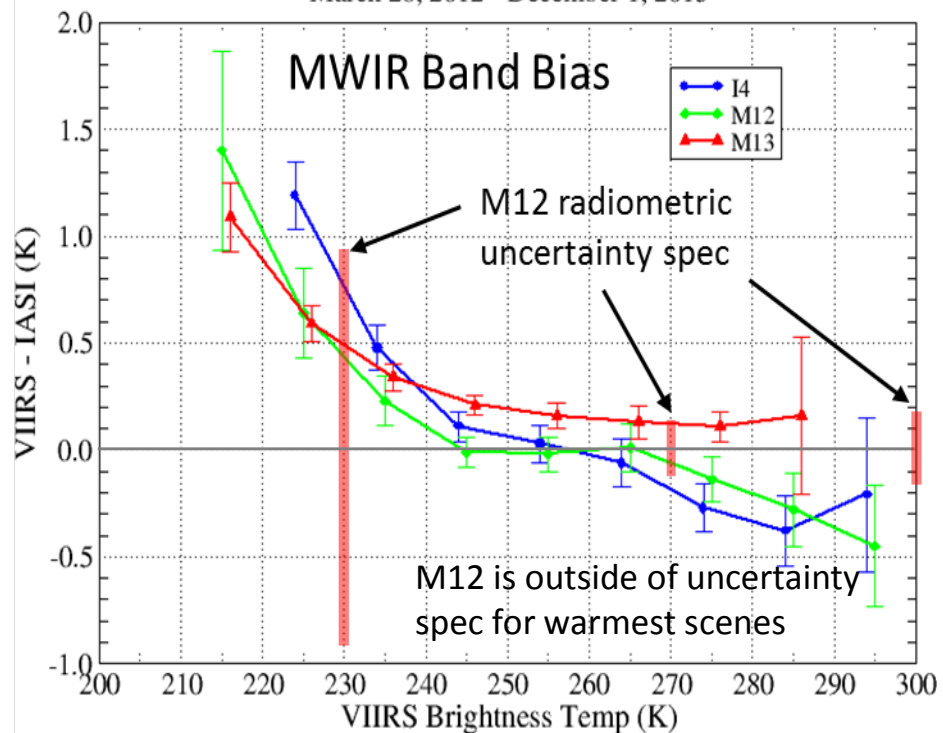
SNPP VIIRS - IASI SNO Comparisons

March 28, 2012 - December 1, 2013



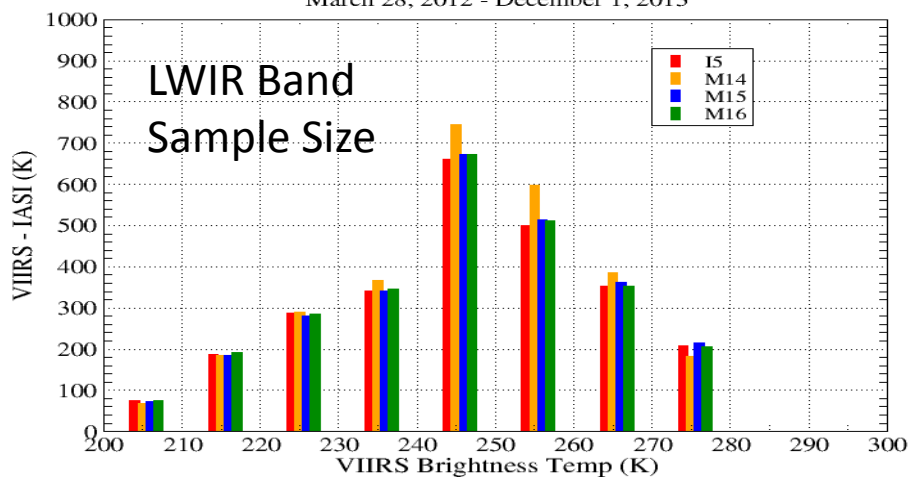
SNPP VIIRS - IASI SNO Comparisons

March 28, 2012 - December 1, 2013



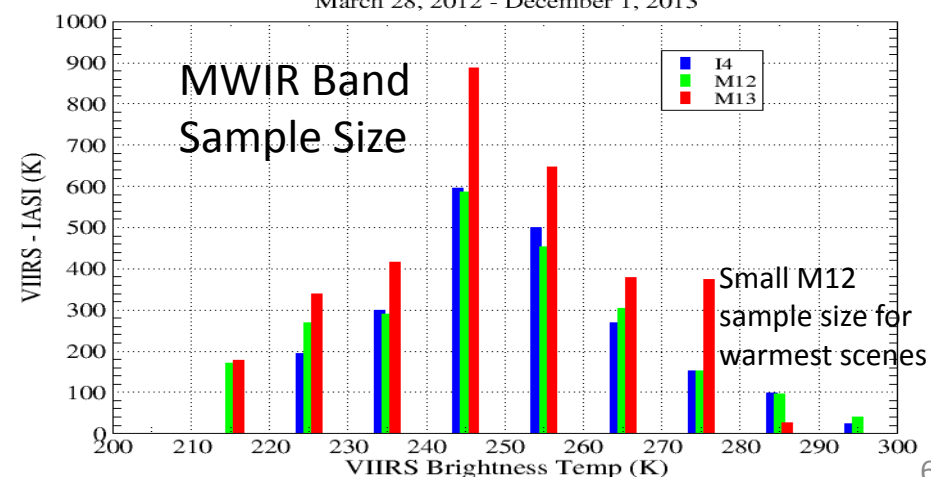
SNPP VIIRS - IASI SNO Sample Size

March 28, 2012 - December 1, 2013



SNPP VIIRS - IASI SNO Sample Size

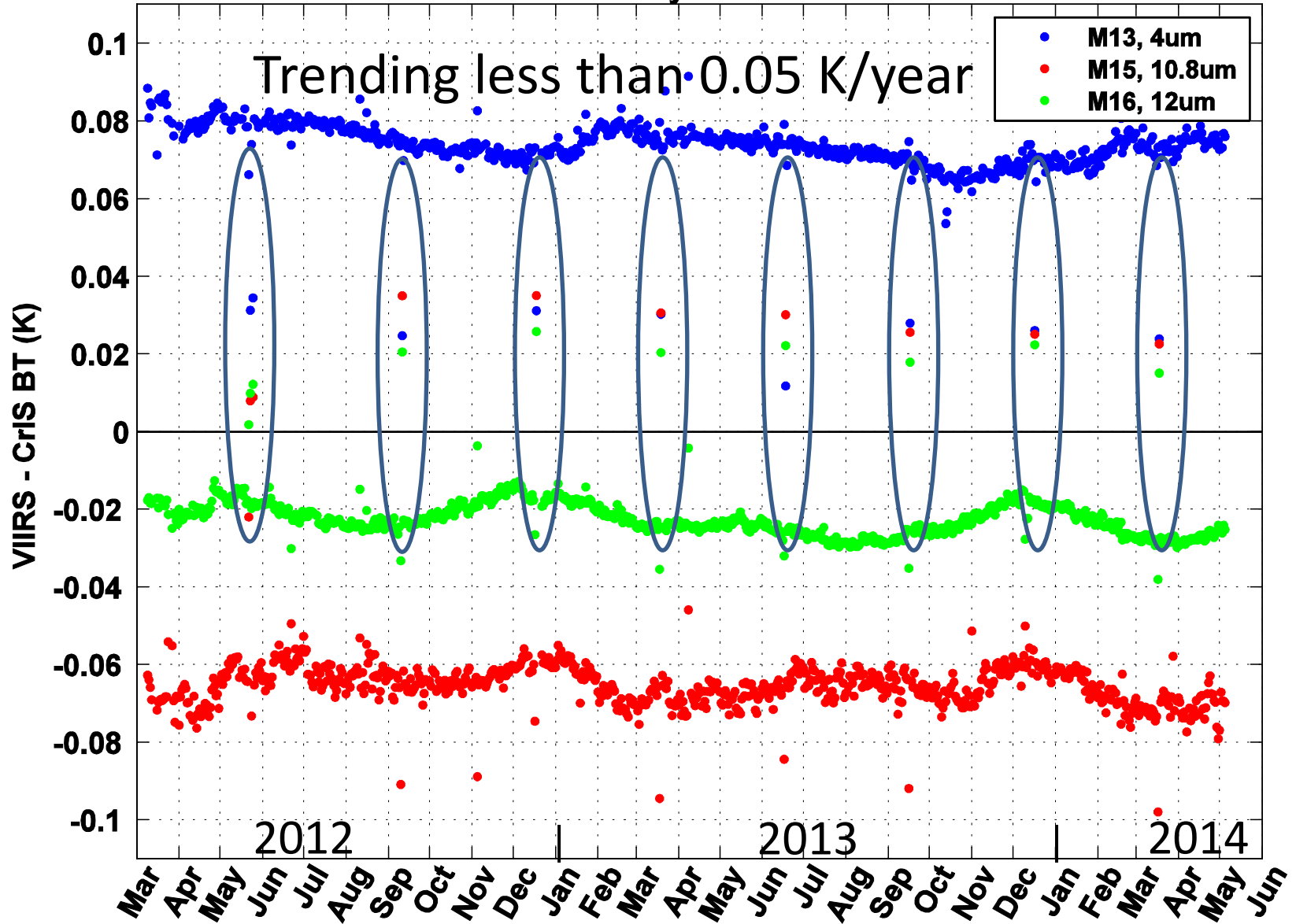
March 28, 2012 - December 1, 2013



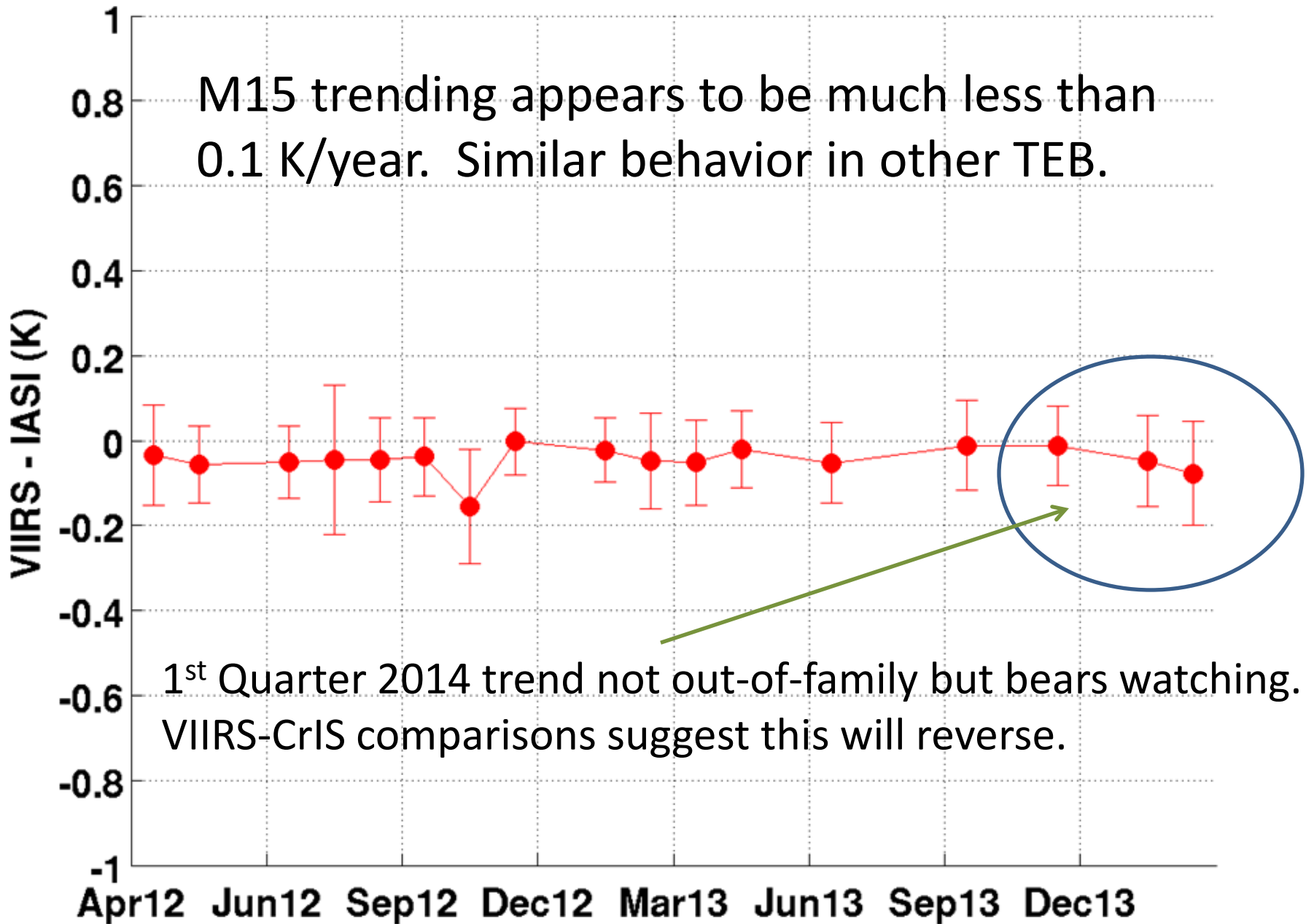
VIIRS-CrIS SDR Comparisons

VIIRS WUCD Event

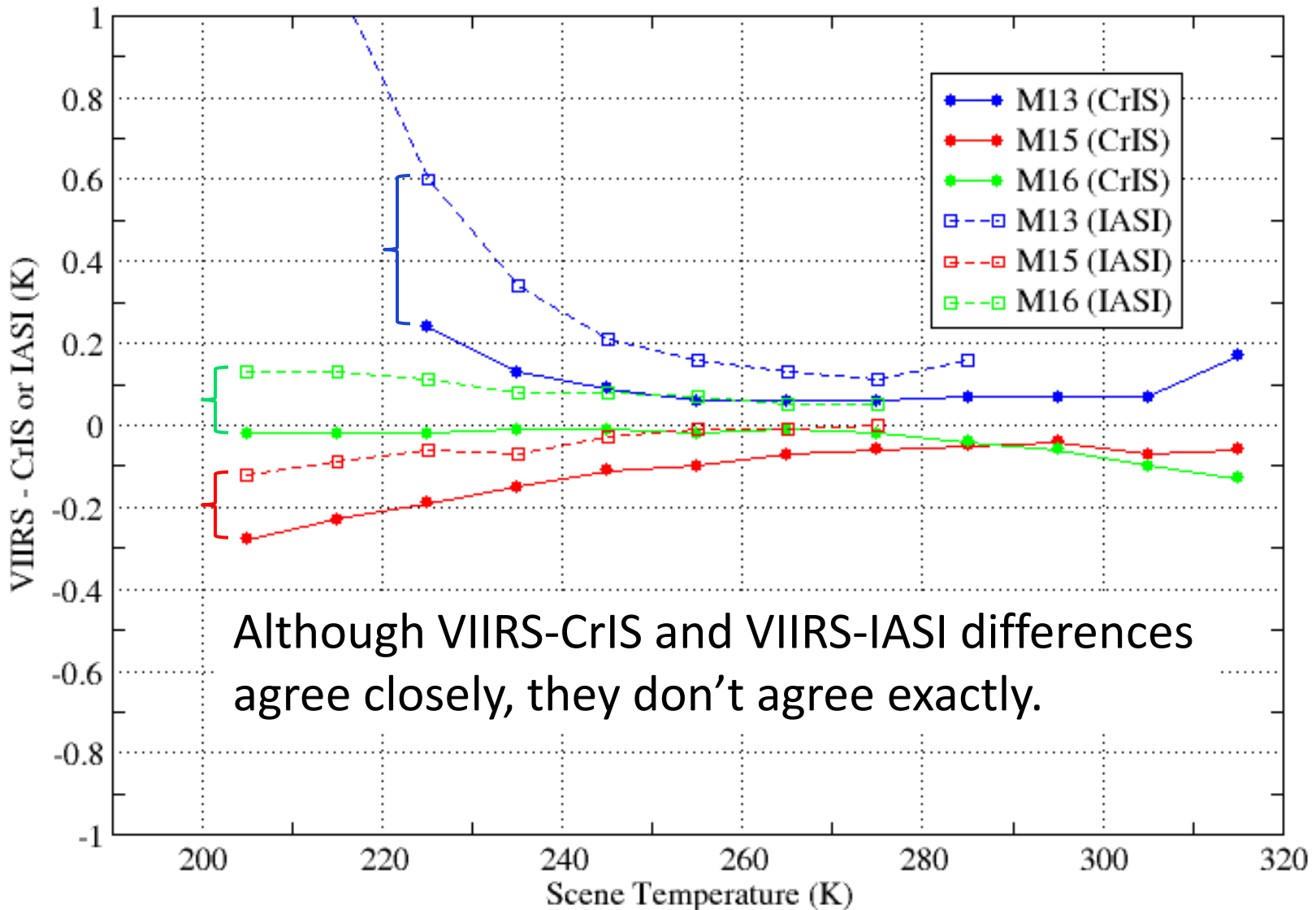
CrIS/VIIRS Daily Mean Differences



Mar28,2012 - Mar31,2014 SNOs: SNPP Avg VIIRS M15 - IASI



SNPP VIIRS SDR Comparisons to CrIS and IASI



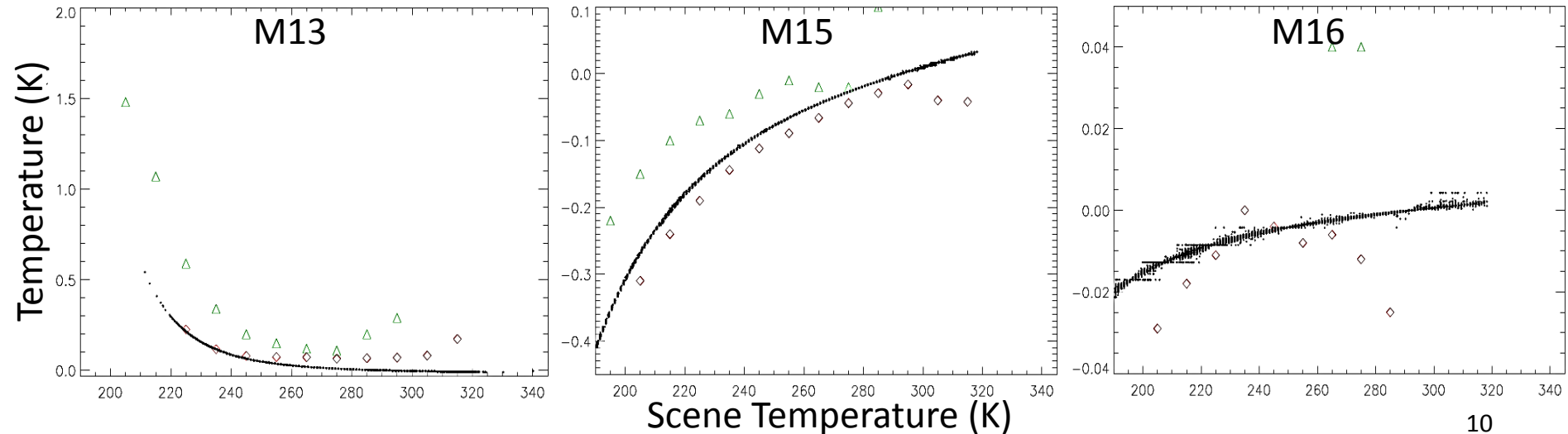
VIIRS C₀ Calibration Coefficient Modification

- Modify the VIIRS TEB delta C LUT to change the VIIRS cold brightness temperatures to better match CrIS and IASI on-orbit cold scene performance (brightness temperature).
- Preserves VIIRS detector-to-detector, HAM side and temperature relative “shape” in prelaunch tables.
- Latest testing uses CrIS calibration planned for Mx8.1.
- ADR-7414: TEB calibration coefficient C₀ requires modification to ... improve radiometric accuracy.

Residual Background Emission

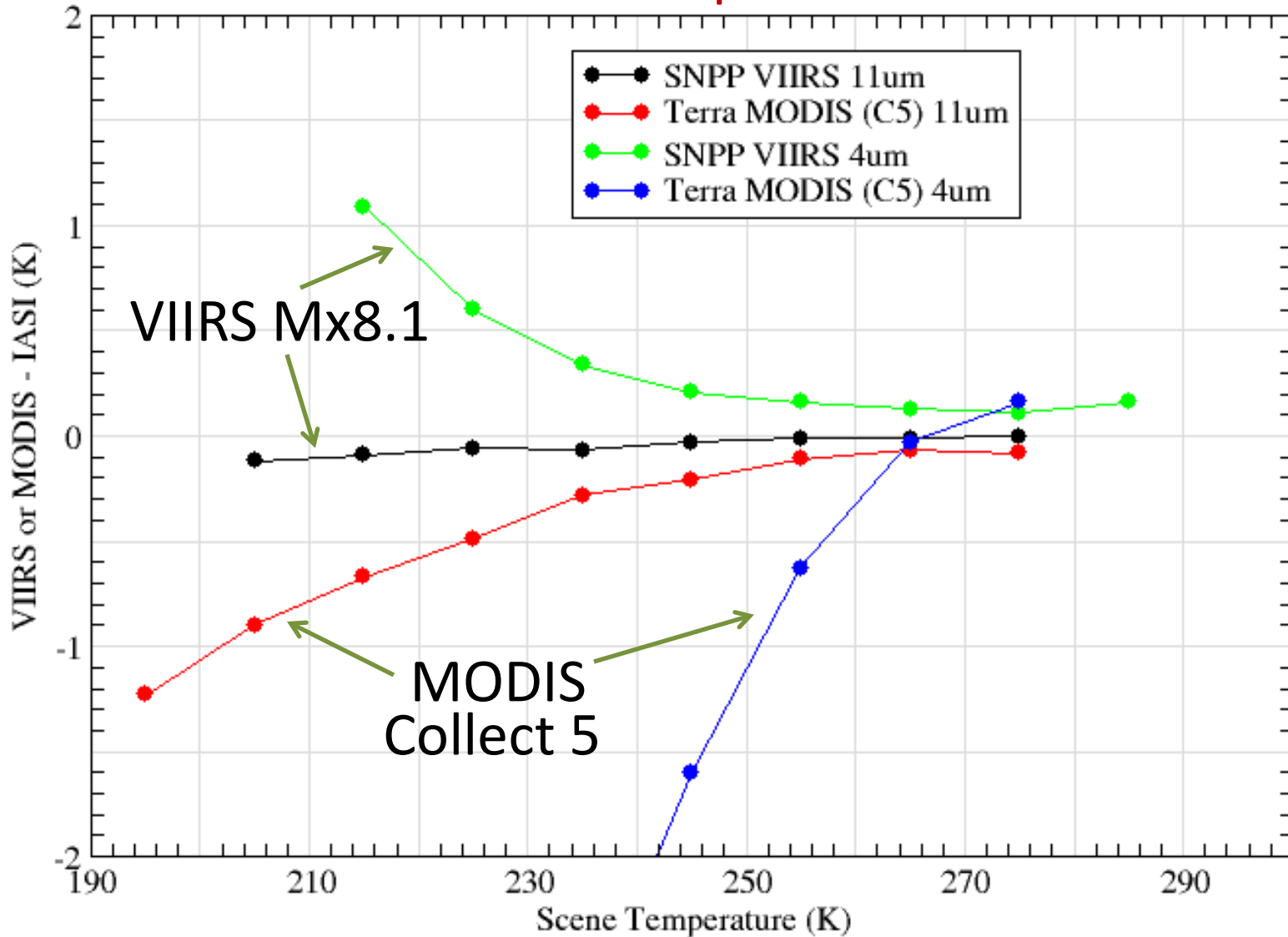
Calculated Radiance

$$L_{ap}(RVS_{EV}) = \frac{(RVS_{SV} - RVS_{EV}) \cdot \left[\frac{(1 - \rho_{rta}) \cdot L(T_{rta}) - L(T_{ham})}{\rho_{rta}} \right] + F \cdot (c_0 + c_1 \cdot dn_{EV} + c_2 \cdot dn_{EV}^2)}{RVS_{EV}}$$



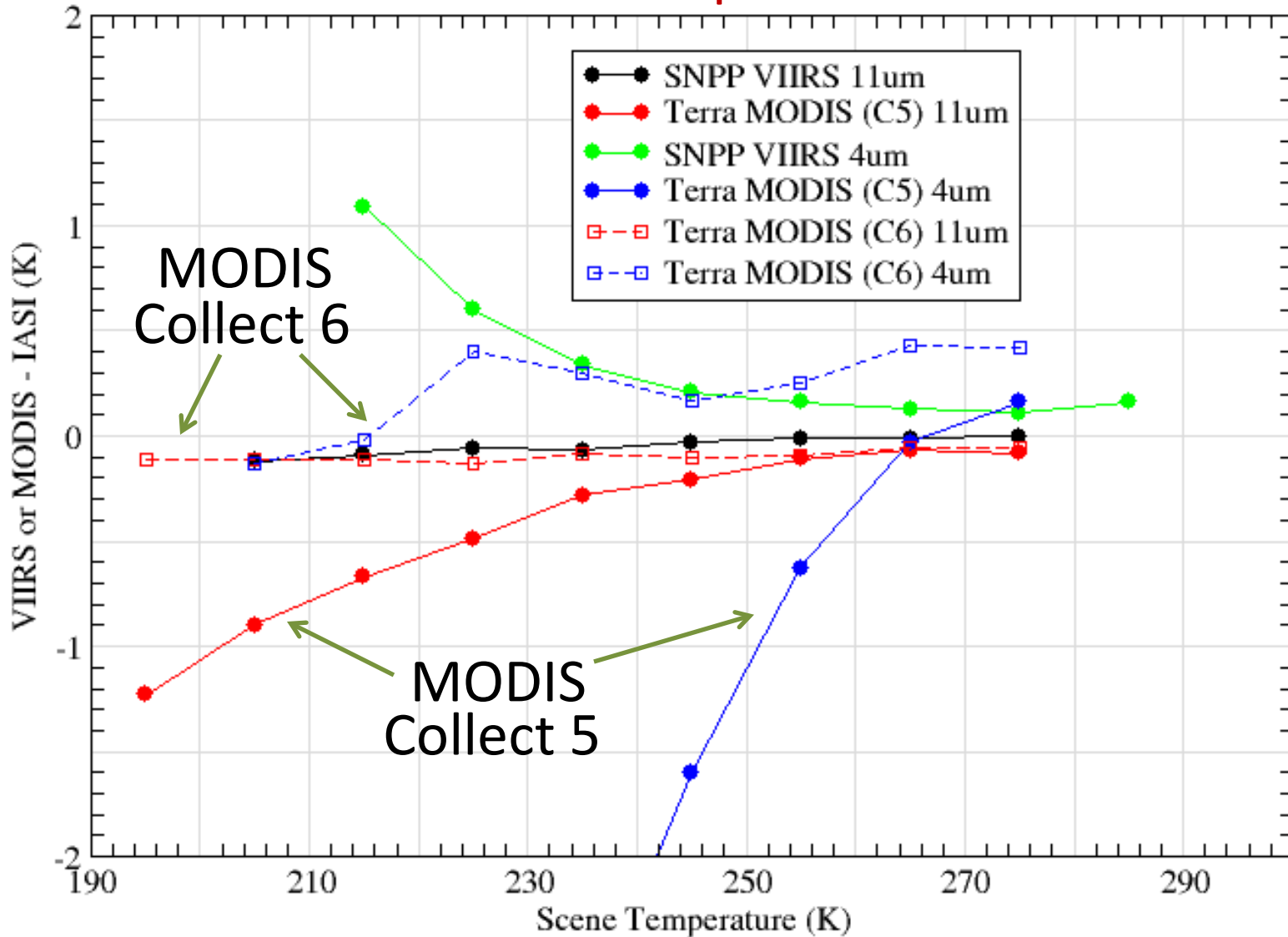
MODIS and VIIRS TEB Comparisons to IASI

Some Perspective!



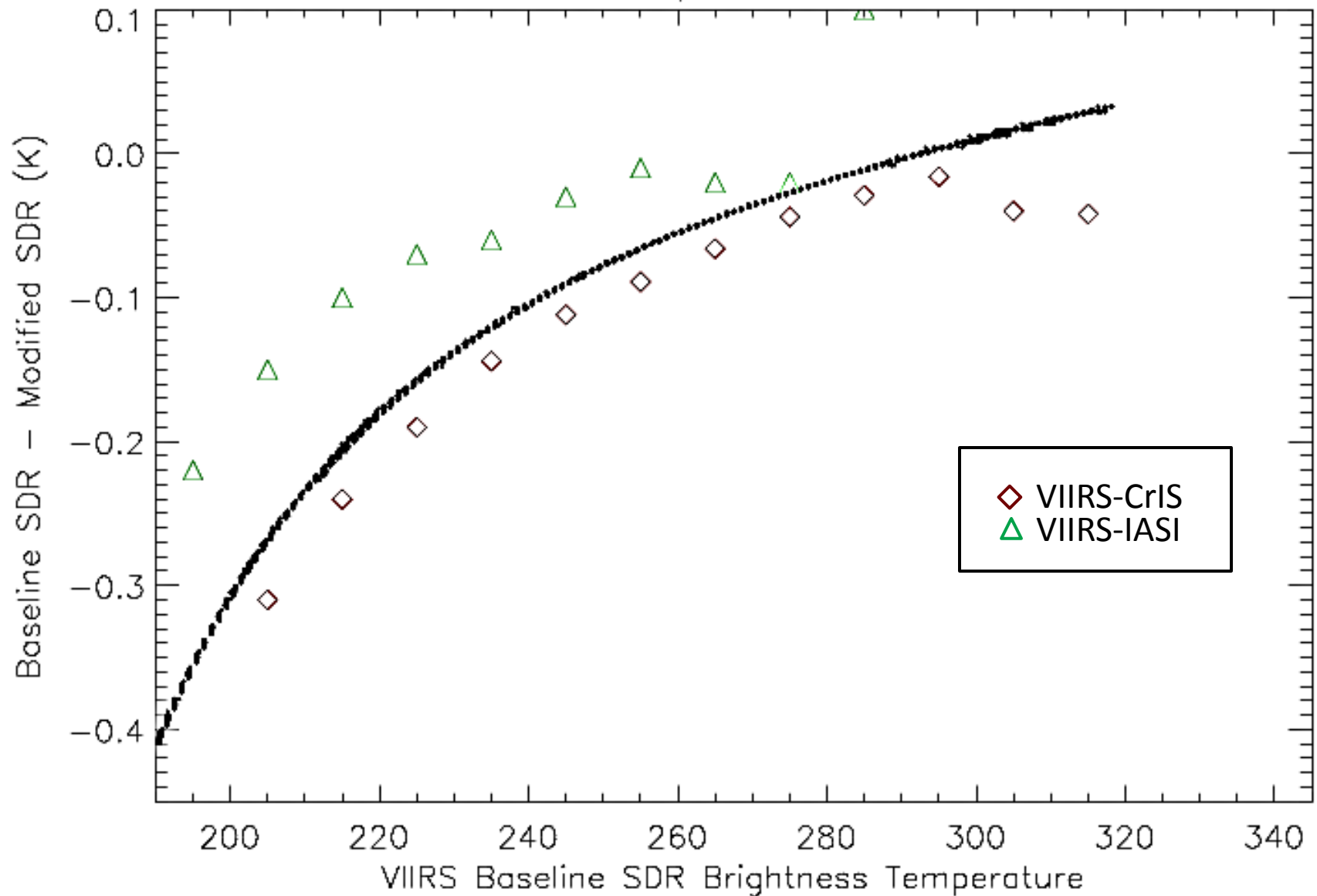
MODIS and VIIRS TEB Comparisons to IASI

Some Perspective!



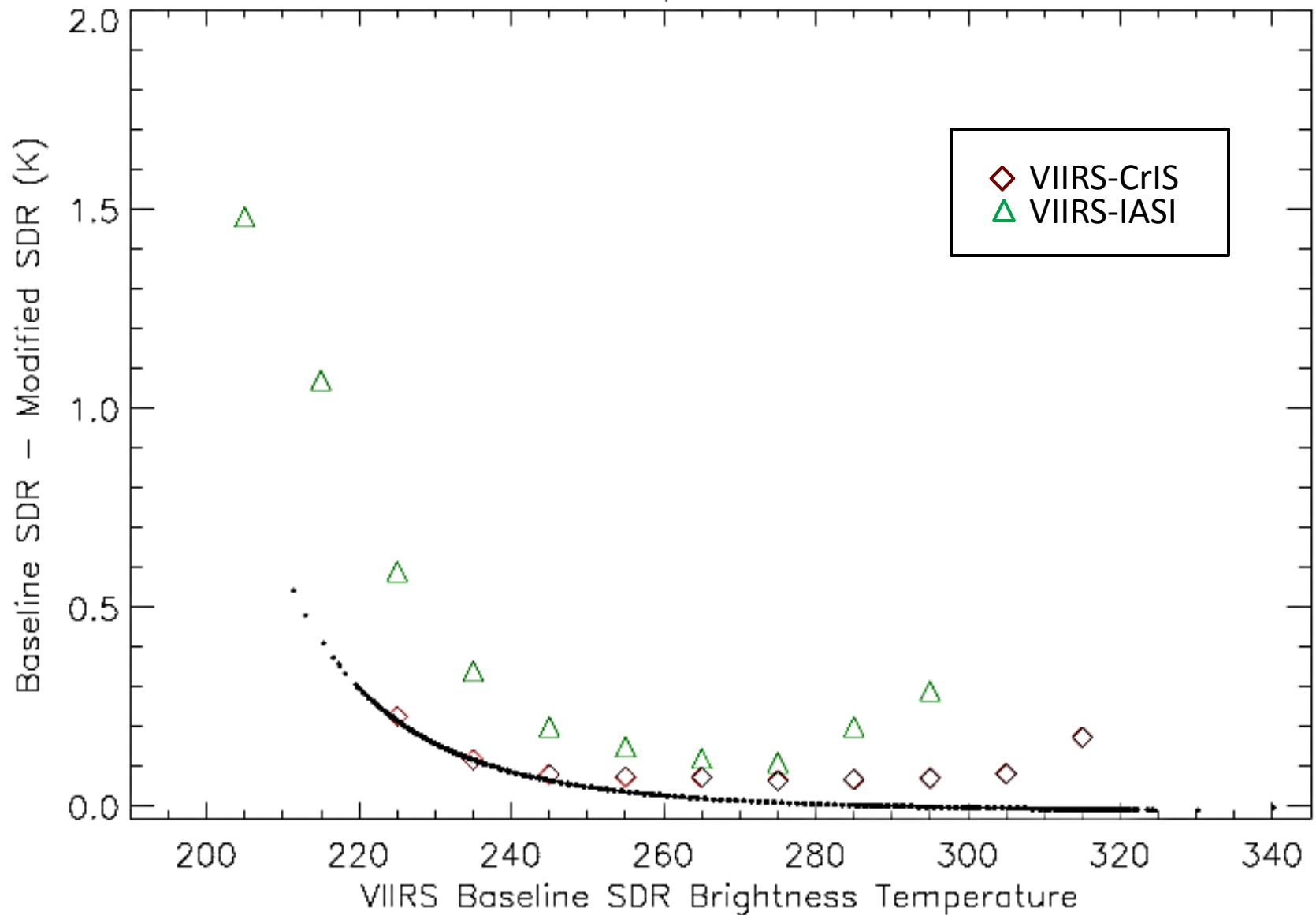
VIIRS C_0 Calibration Coefficient Modification

NPP VIIRS F1 SDR Comparison for Band M15 HAM A



VIIRS C_0 Calibration Coefficient Modification

NPP VIIRS F1 SDR Comparison for Band M13 HAM A



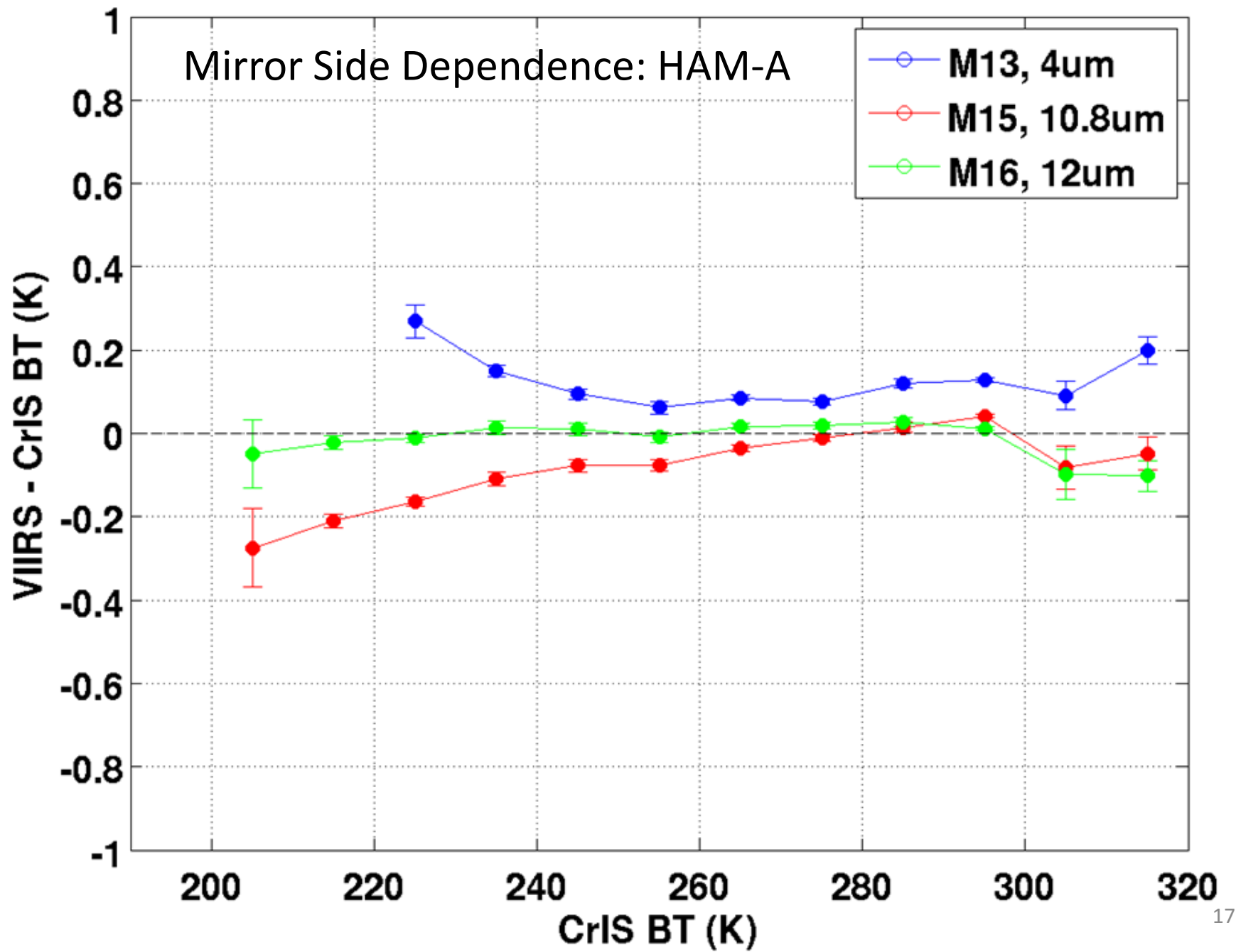
Considerations on CO Adjustment

- CrIS, AIRS, Metop-A IASI and Metop-B IASI are all well calibrated systems. But they disagree at cold scenes by $\sim 0.1 - 0.2$ K in LWIR and more so in MWIR. Which is “truth”?
- VIIRS currently about as good as C6 MODIS 11 μ m
- 0.25 K accuracy is well within VIIRS specification for LWIR cold scenes.
- On the other hand.....
 - M15 and M16 are commonly used together in science algorithms; consistent relative performance between M15 and M16 would seem beneficial.

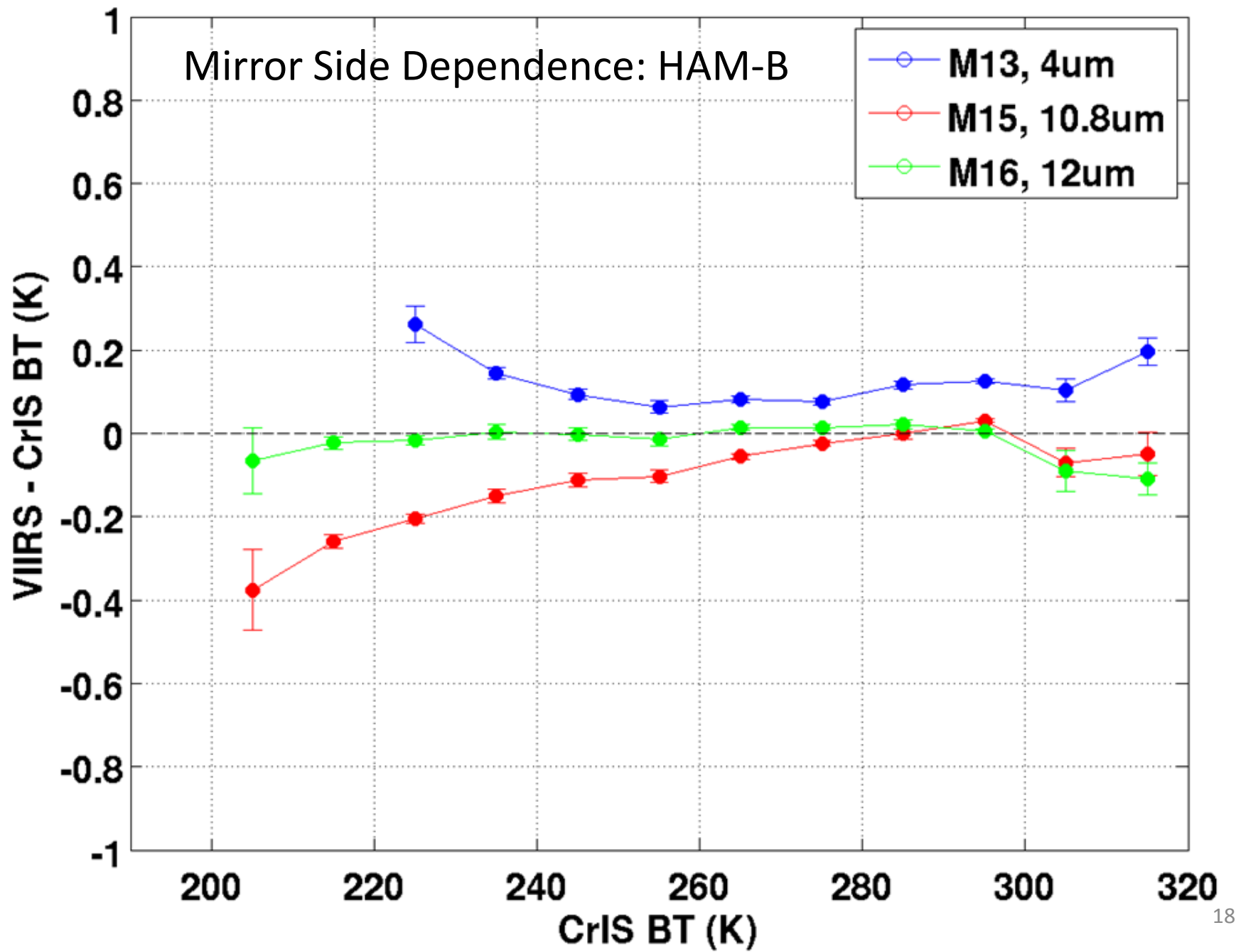
Mirror Side and Detector Striping

- Using VIIRS-CrIS global day comparisons, stratify the data by mirror side and detector.
- Reveals information on striping in SDR that may be masked by natural variability.
- M13, M15, and M16 examined (insufficient spectral coverage for M12, M14 by CrIS).
- 4 global days tested; similar result each day:
 - Suggestion of small mirror side effect in M15.
 - M13 has distinct even-odd detector pattern.

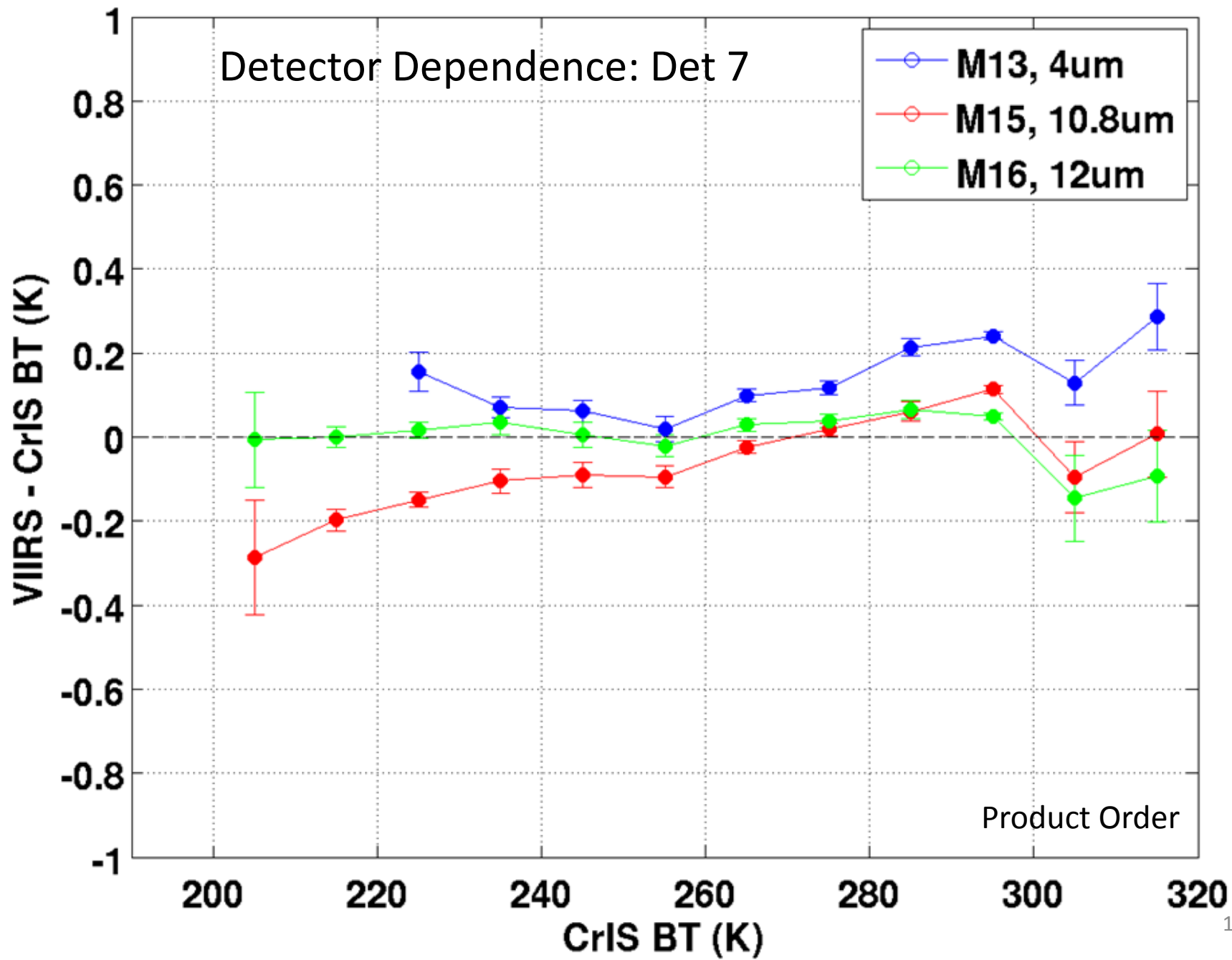
2013172 : MS1 AD Mean SNPP VIIRS - CrIS:v33a



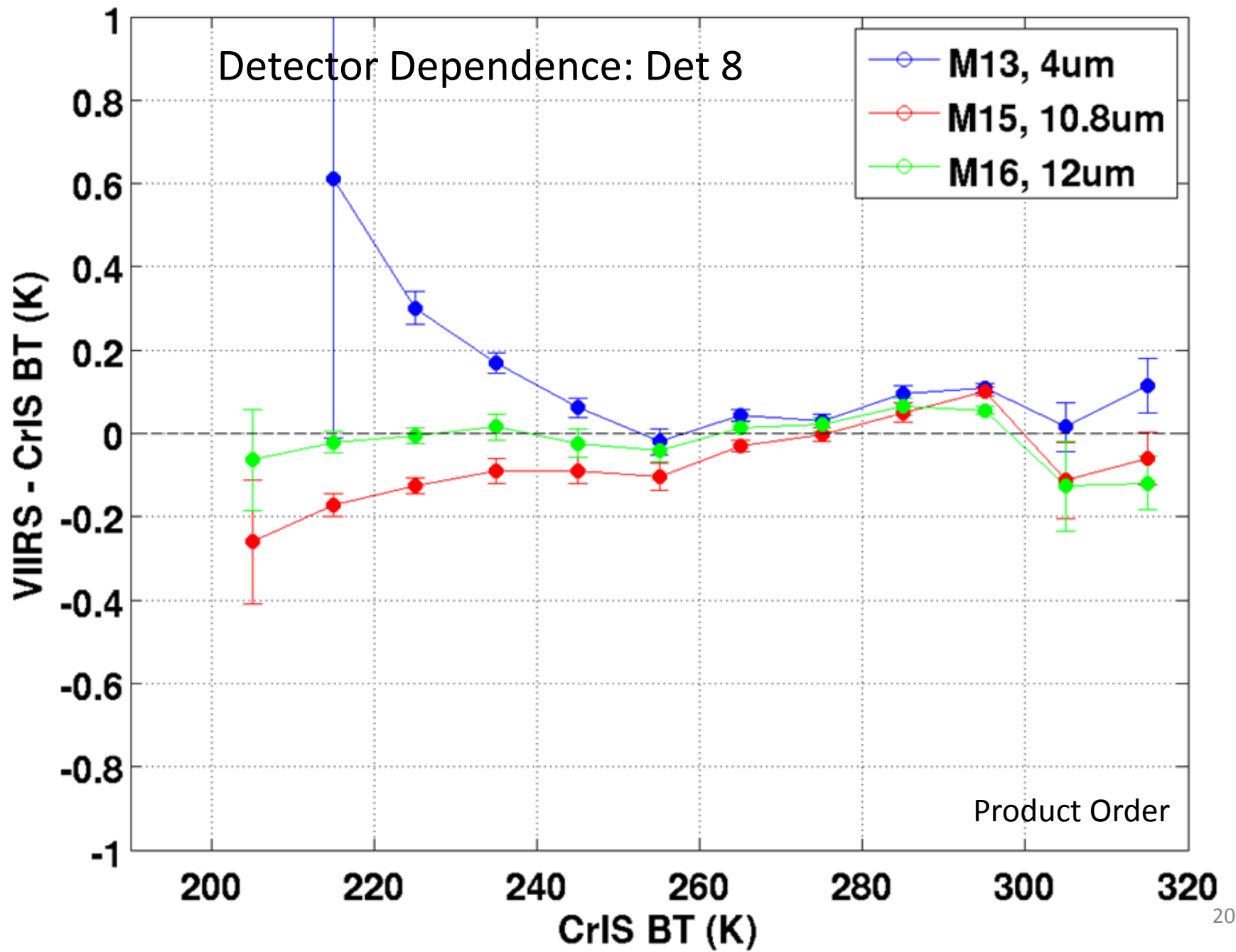
2013172 : MS2 AD Mean SNPP VIIRS - CrIS:v33a



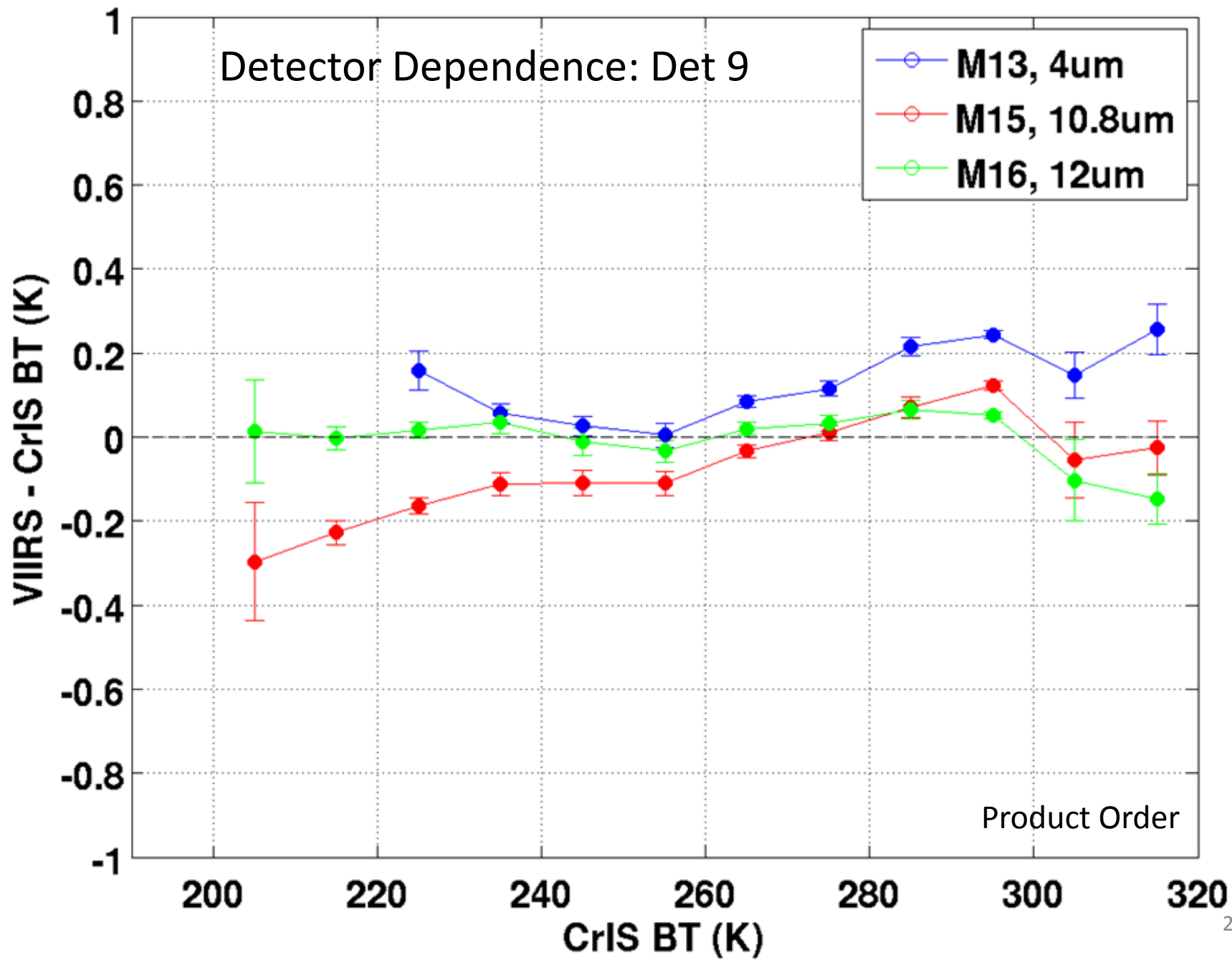
2013172 : MS1 Det7 Mean SNPP VIIRS - CrIS:v33a



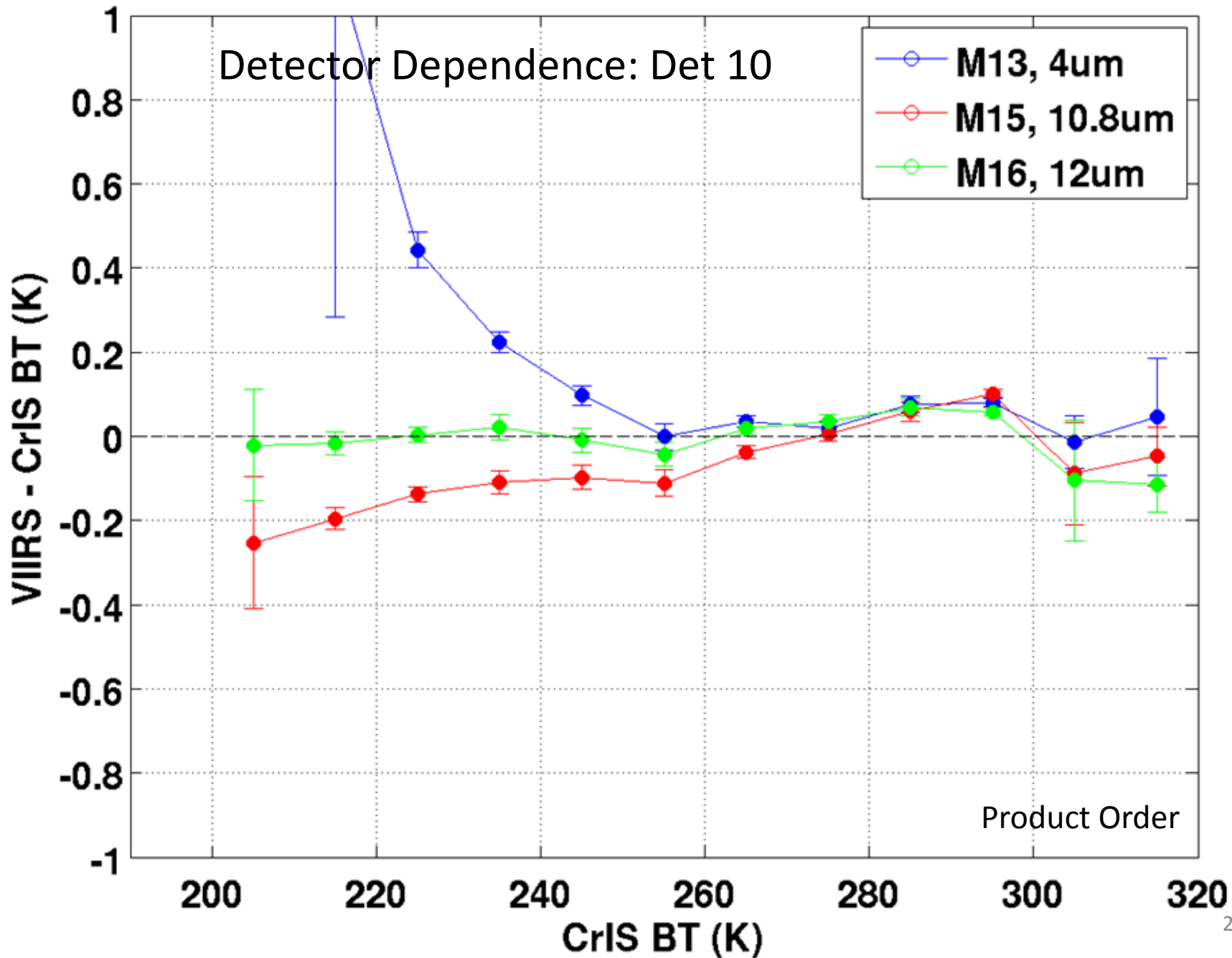
2013172 : MS1 Det8 Mean SNPP VIIRS - CrIS:v33a



2013172 : MS1 Det9 Mean SNPP VIIRS - CrIS:v33a

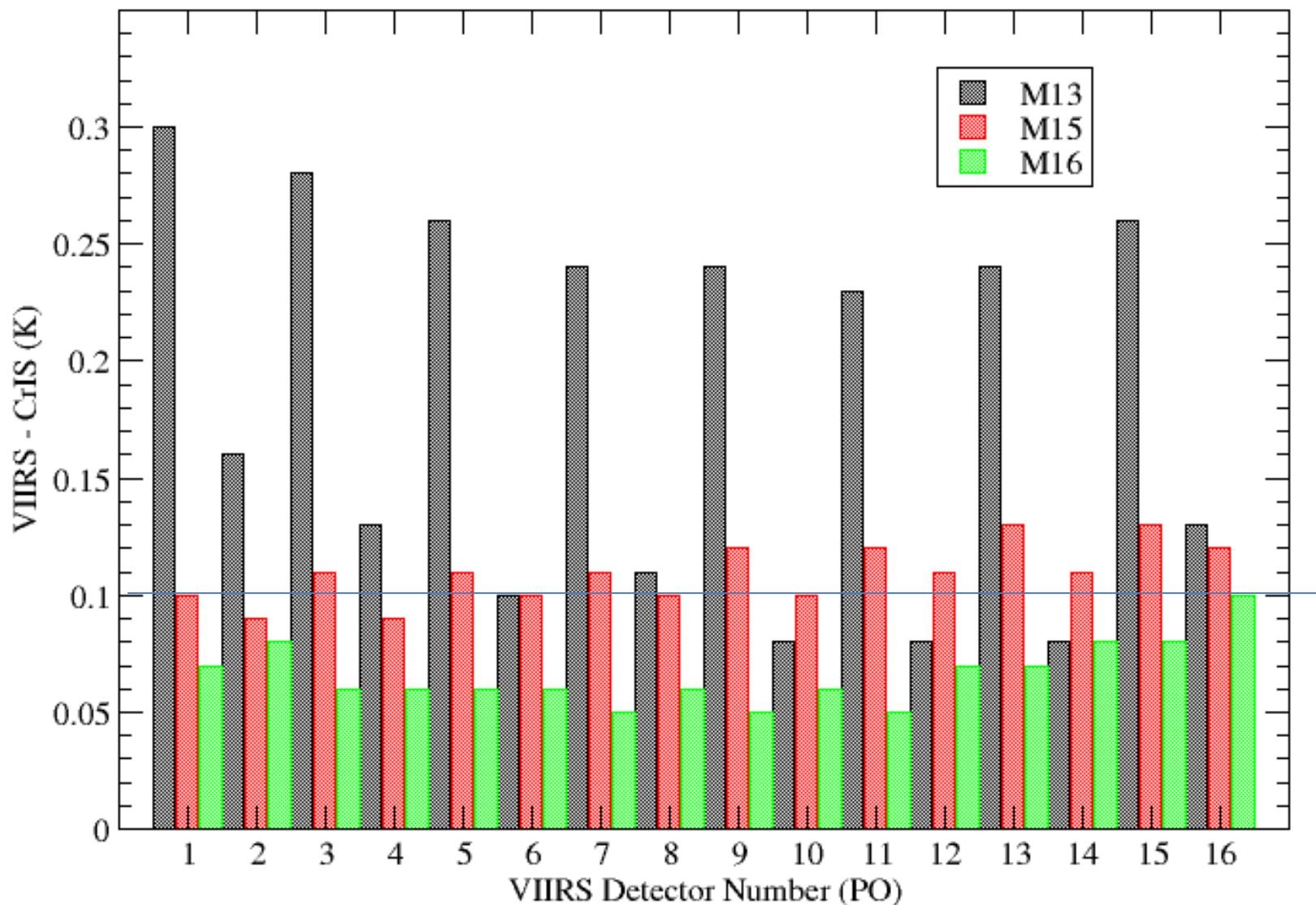


2013172 : MS1 Det10 Mean SNPP VIIRS - CrIS:v33a



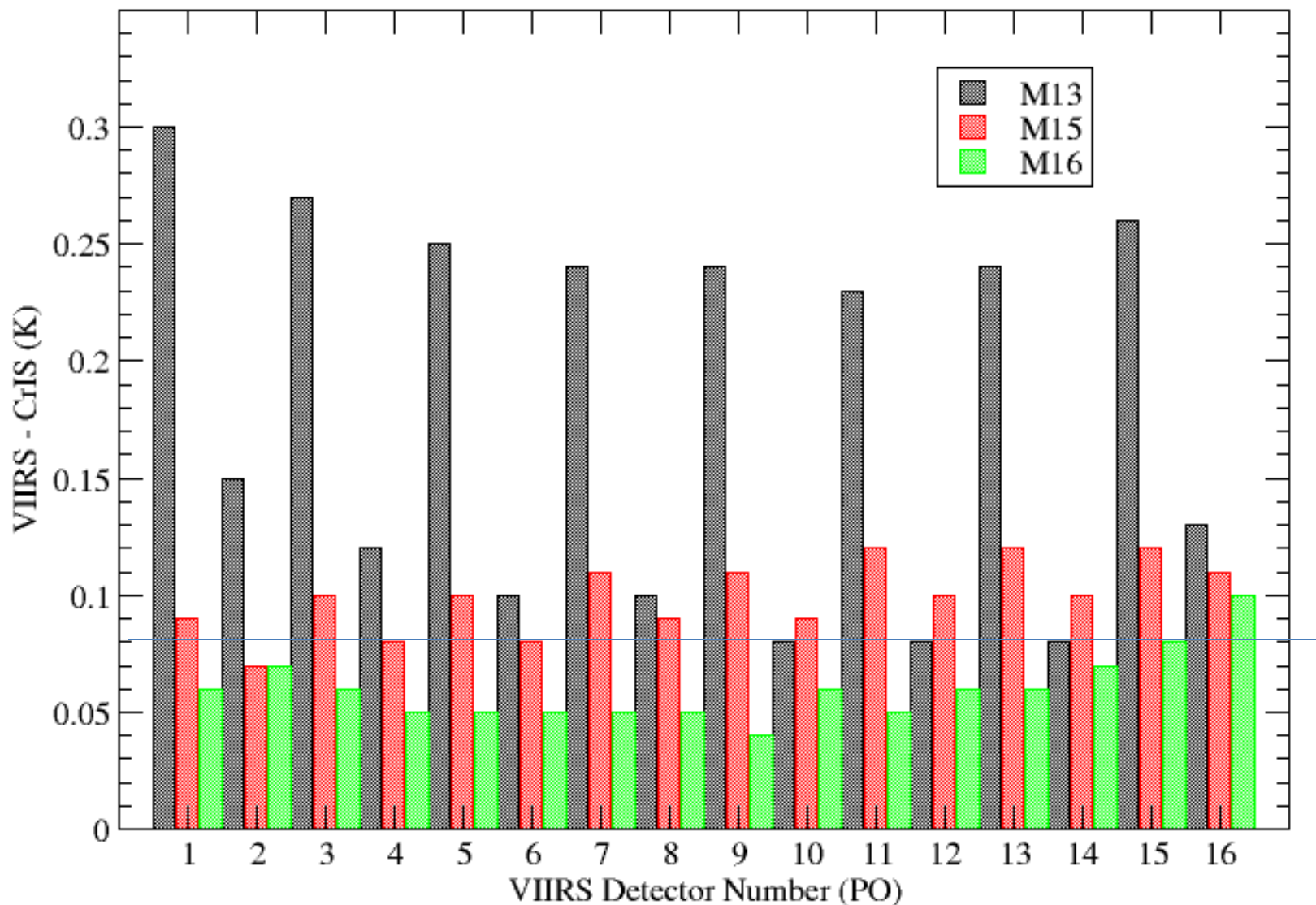
SNPP VIIRS - CrIS Biases

Global Day 2013172; 290 - 300 K Earth Scene Temperatures; HAM A



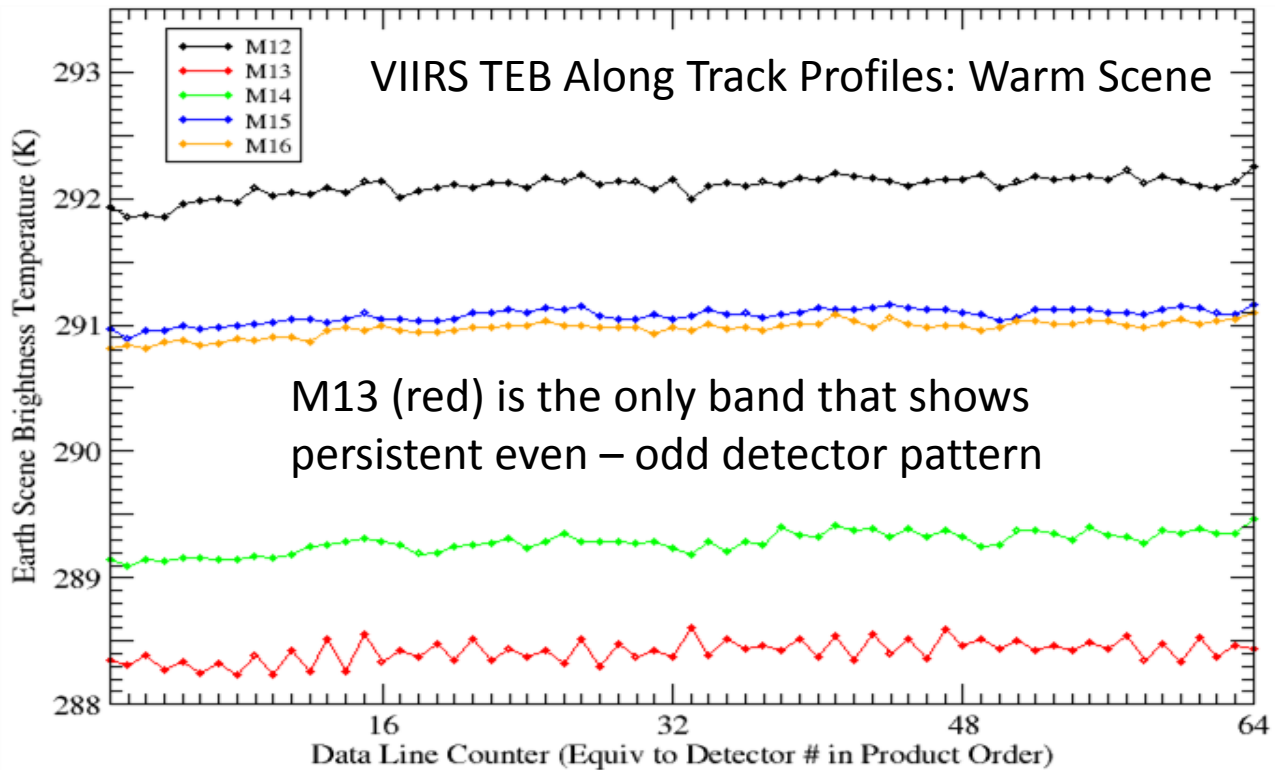
SNPP VIIRS - CrIS Biases

Global Day 2013172; 290 - 300 K Earth Scene Temperatures; HAM B



SNPP VIIRS
Band M13
April 30, 2014
21:25:47 UTC

SNPP VIIRS
Band M15
April 30, 2014
21:25:47 UTC



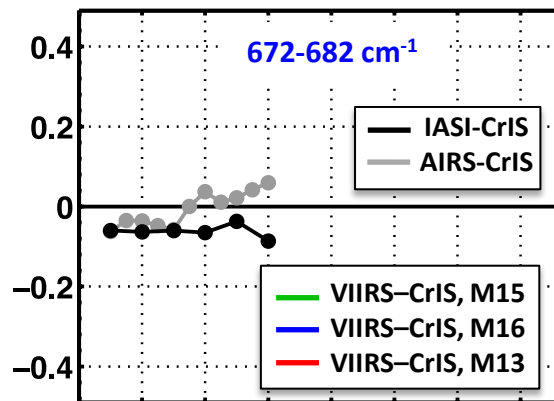
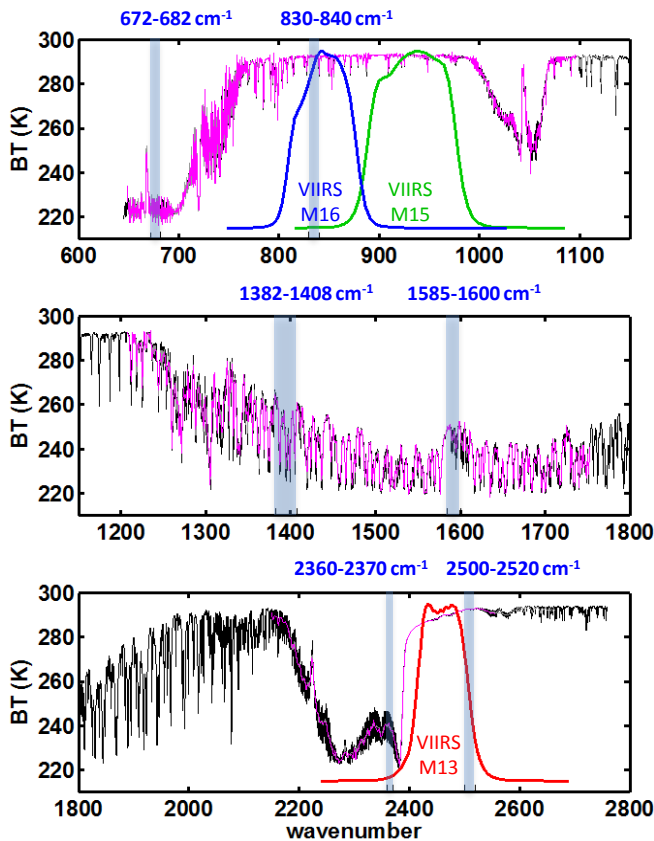
Summary

- SNPP VIIRS TEB SDR performing within uncertainty requirements; minimal trends
- Minor adjustment to M15 C0 calibration coefficient will bring M15 and M16 performance closer together, but question on which sensor (AIRS, IASI, CrIS) is “truth”
- Evidence of mirror side striping in M15
- Detector level striping evident in M13 and seems to exist at a very small level in M15 and M16

Backup

Summary of SNO results

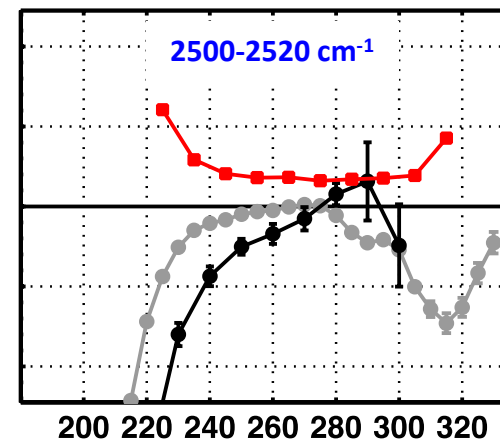
for 6 representative spectral regions,
and VIIRS/CrIS comparisons:



1382-1408 cm^{-1}

1585-1600 cm^{-1}

2360-2370 cm^{-1}



- LW differences display only small dependence on scene BT for both IASI and AIRS SNOs.
- MW differences are relatively independent of scene BT for IASI and for AIRS at 1382-1408 cm^{-1} ; Differences for AIRS at 1585-1600 cm^{-1} range from $\sim +0.3\text{K}$ at 200K to -0.1K at 265K.
- SW differences are relatively flat above $\sim 240\text{K}$; Below $\sim 230\text{K}$ larger differences between all three sensors are observed.
- Consistent with SNO results shown in L. Strow presentation, and reported by L. Wang et al. at NOAA STAR.

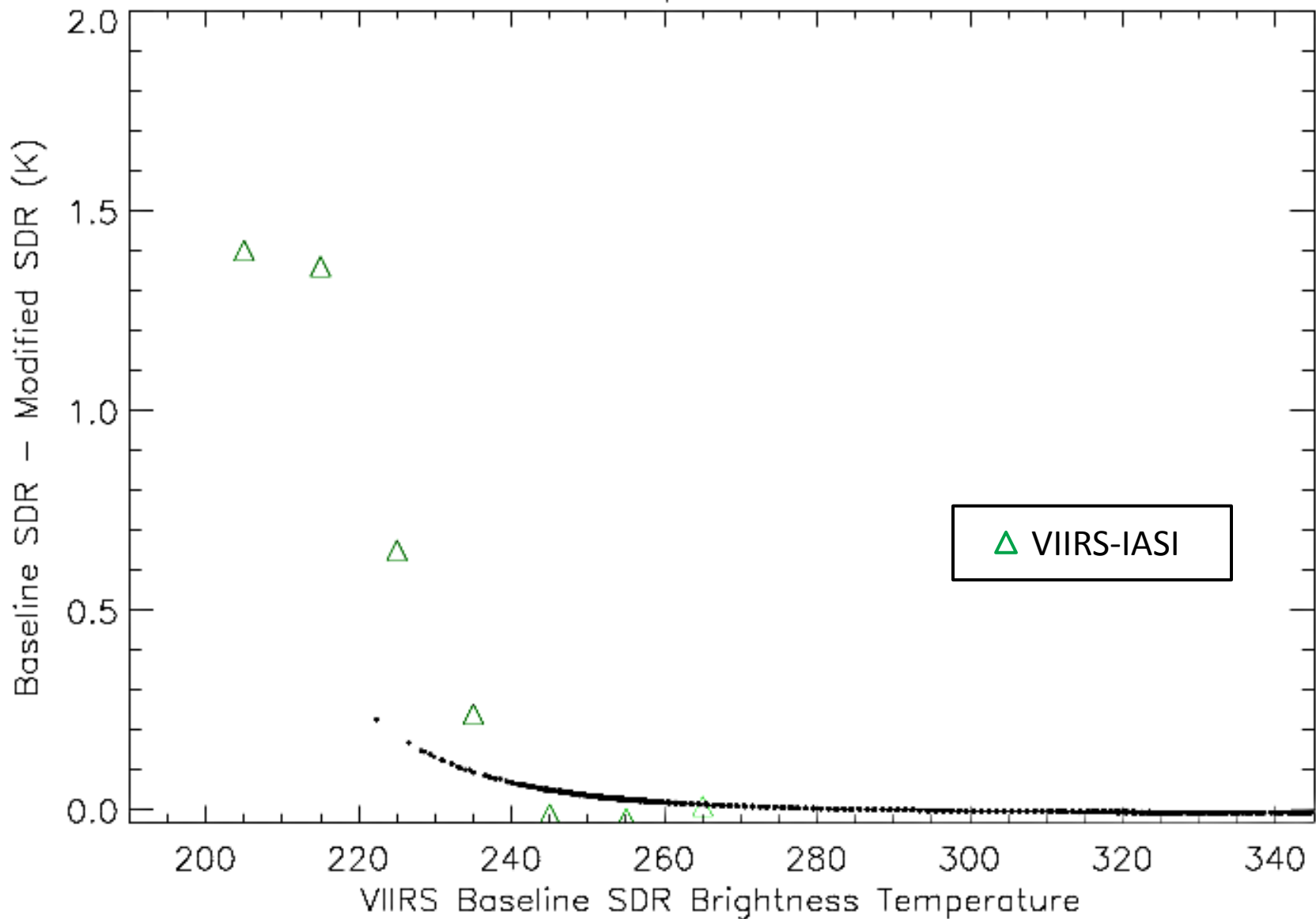


VIIRS C_0 Calibration Coefficient Modification

- ADR7414: TEB calibration coefficient c_0 requires modification to reduce striping and improve radiometric accuracy at low scene temperatures
- The zero-th order calibration coefficient c_0
 - introduced as an ad hoc parameter...compensating for errors in other retrieval equation parameters or...in the radiometric model.
 - can reduce discrepancies between VIIRS and CrIS and between VIIRS and IASI at low scene temperatures..., and reduce striping in the TEB SDR that is evident in cold uniform scenes.

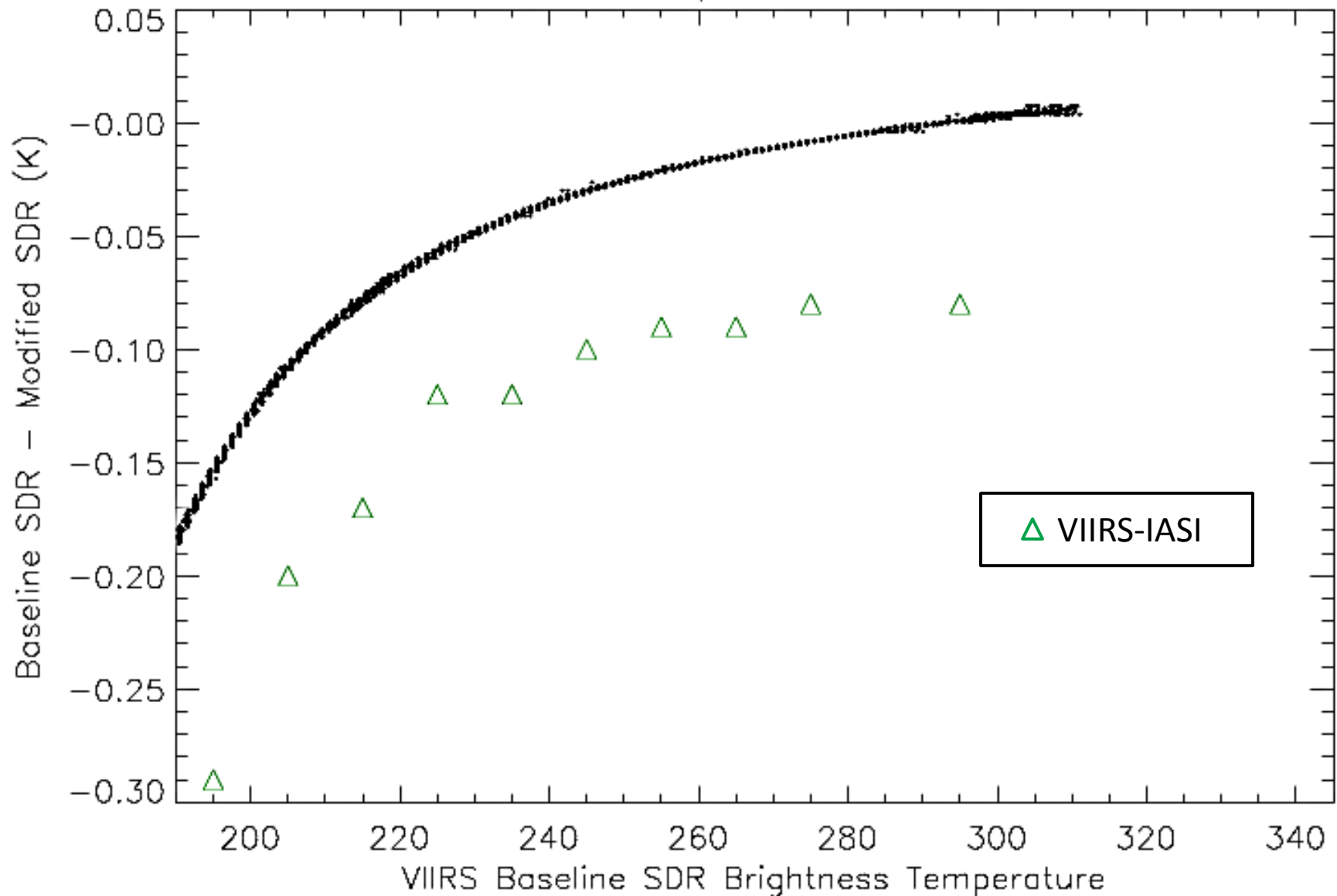
VIIRS C_0 Calibration Coefficient Modification

NPP VIIRS F1 SDR Comparison for Band M12 HAM A



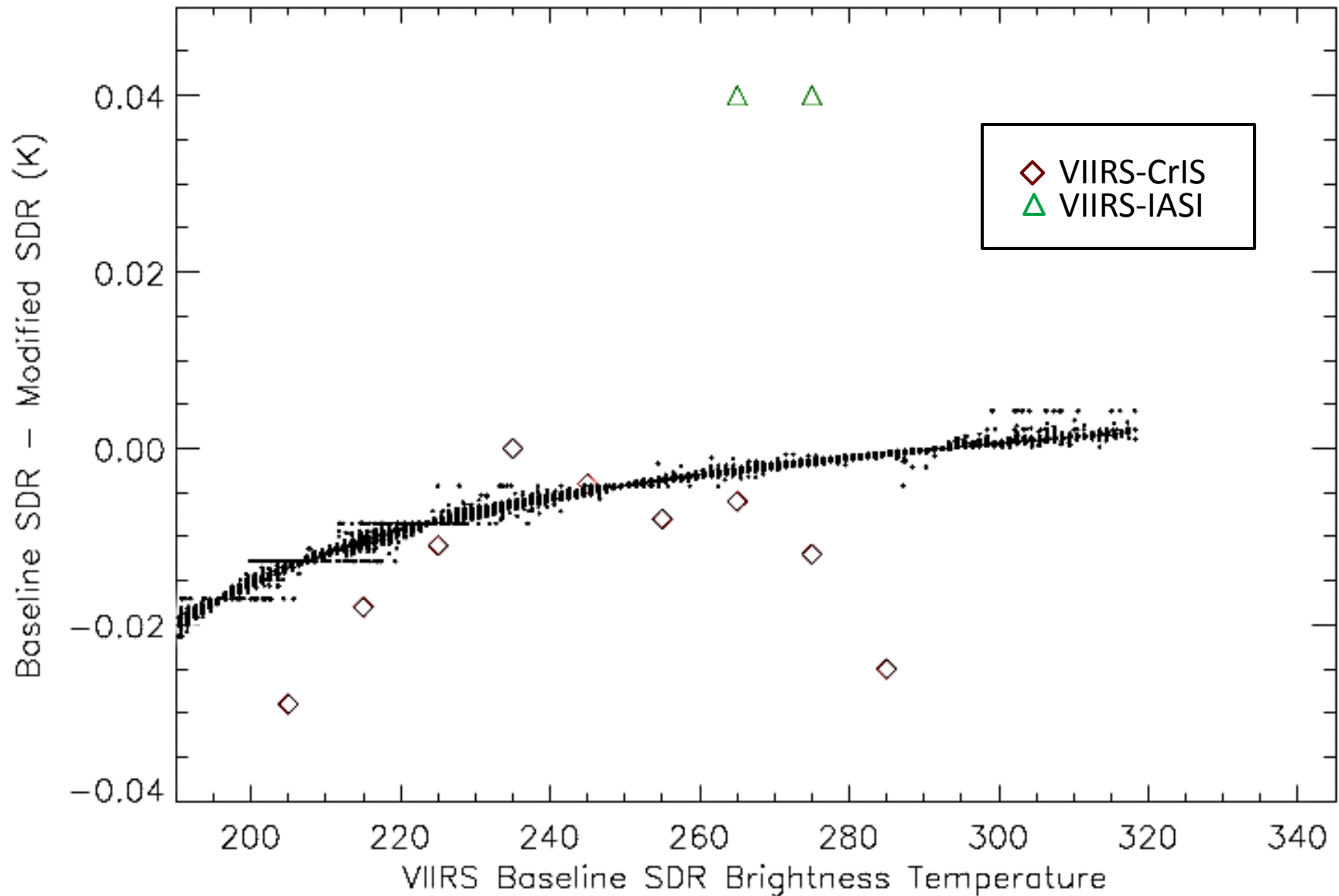
VIIRS C_0 Calibration Coefficient Modification

NPP VIIRS F1 SDR Comparison for Band M14 HAM A



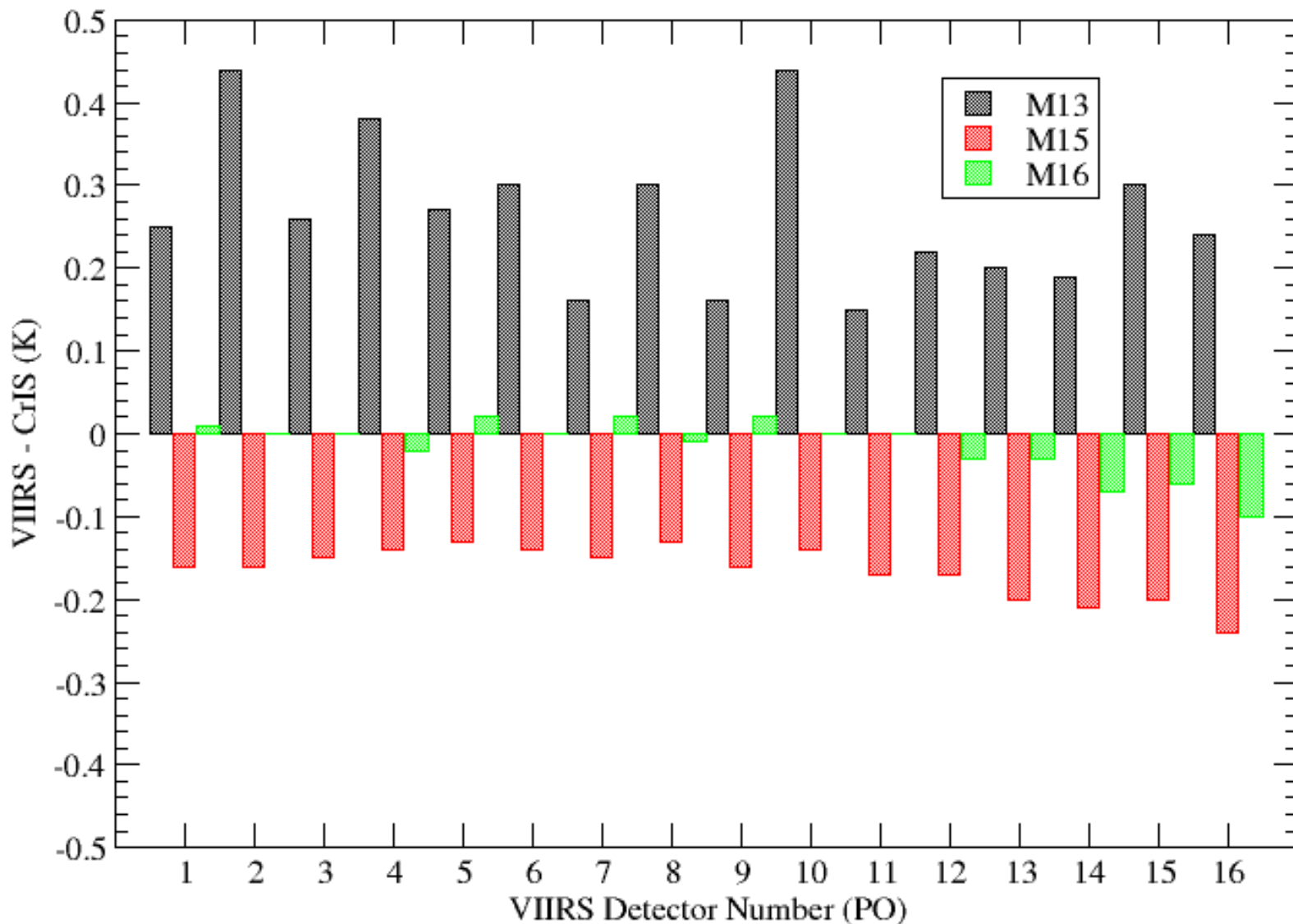
VIIRS C_0 Calibration Coefficient Modification

NPP VIIRS F1 SDR Comparison for Band M16 HAM A



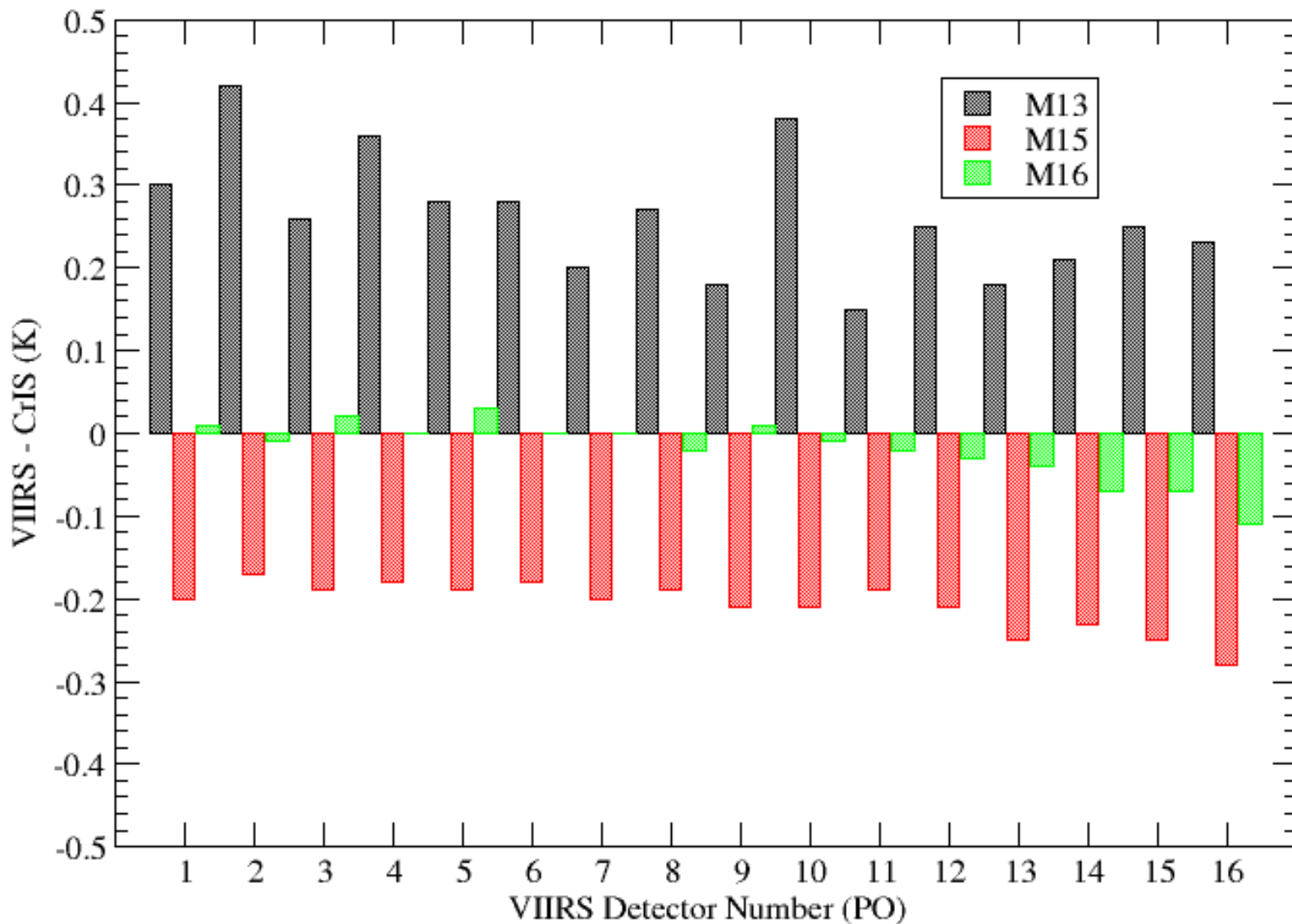
SNPP VIIRS - CrIS Biases

Global Day 2013172; 220 - 230 K Earth Scene Temperatures; HAM A

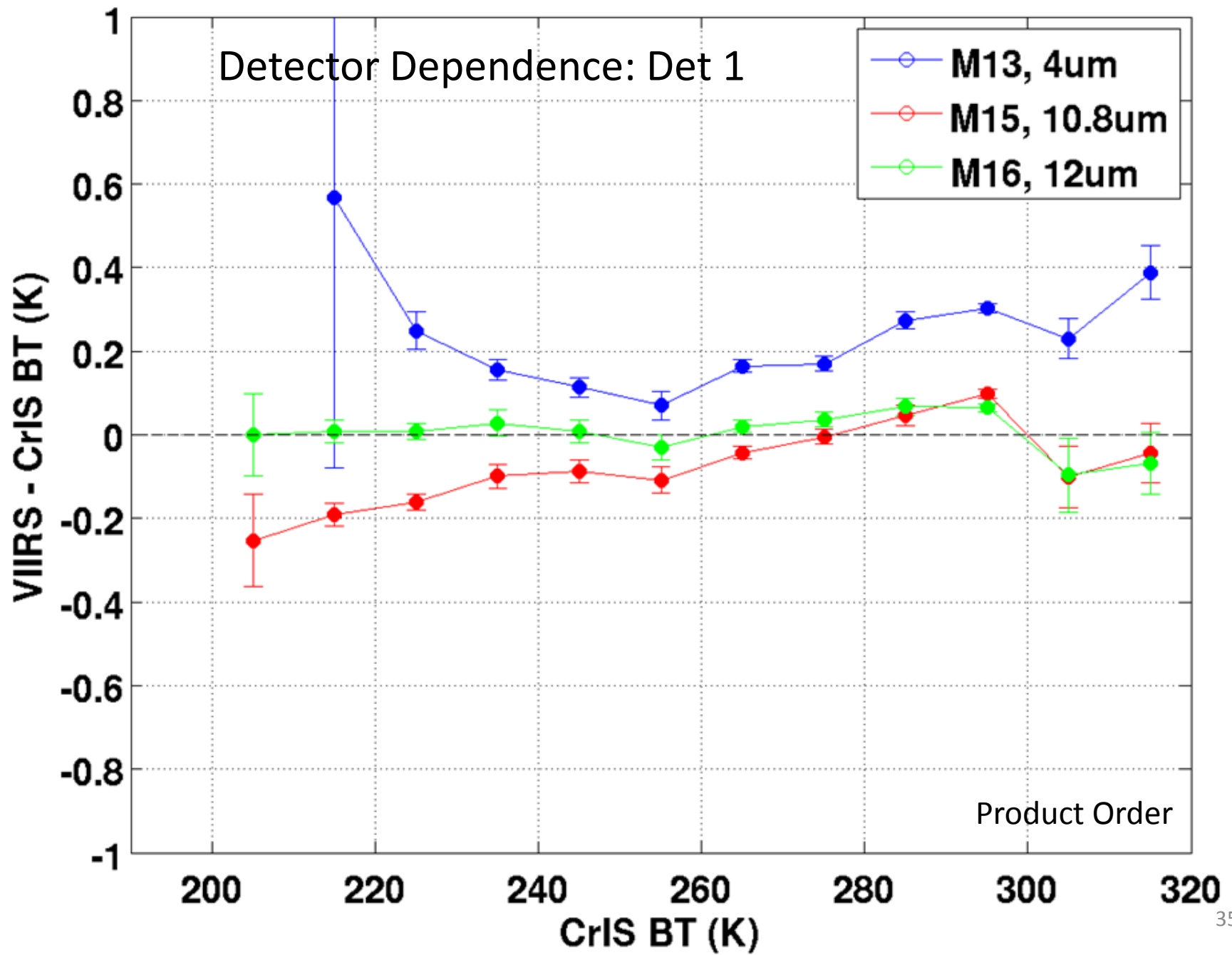


SNPP VIIRS - CrIS Biases

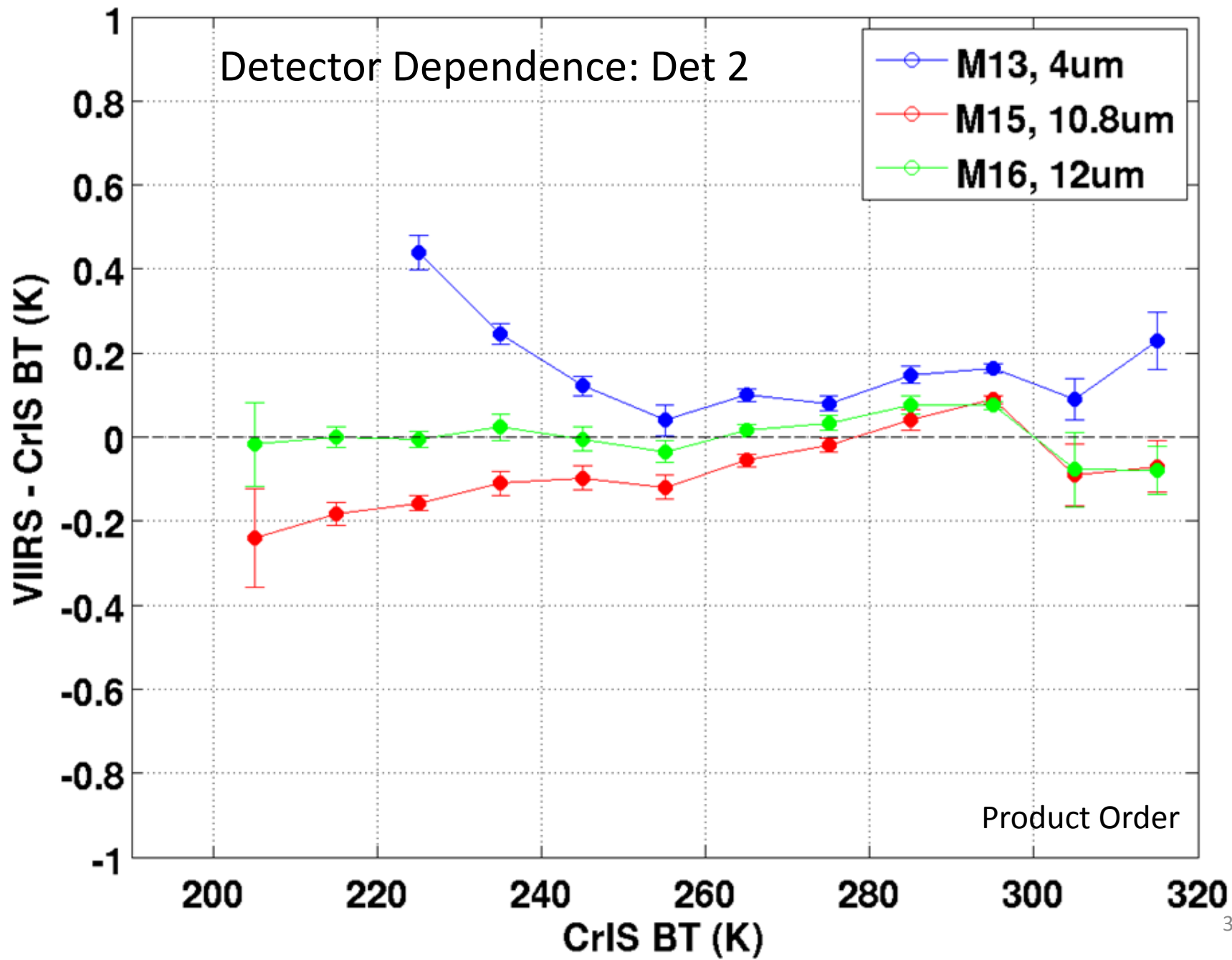
Global Day 2013172; 220 - 230 K Earth Scene Temperatures; HAM B



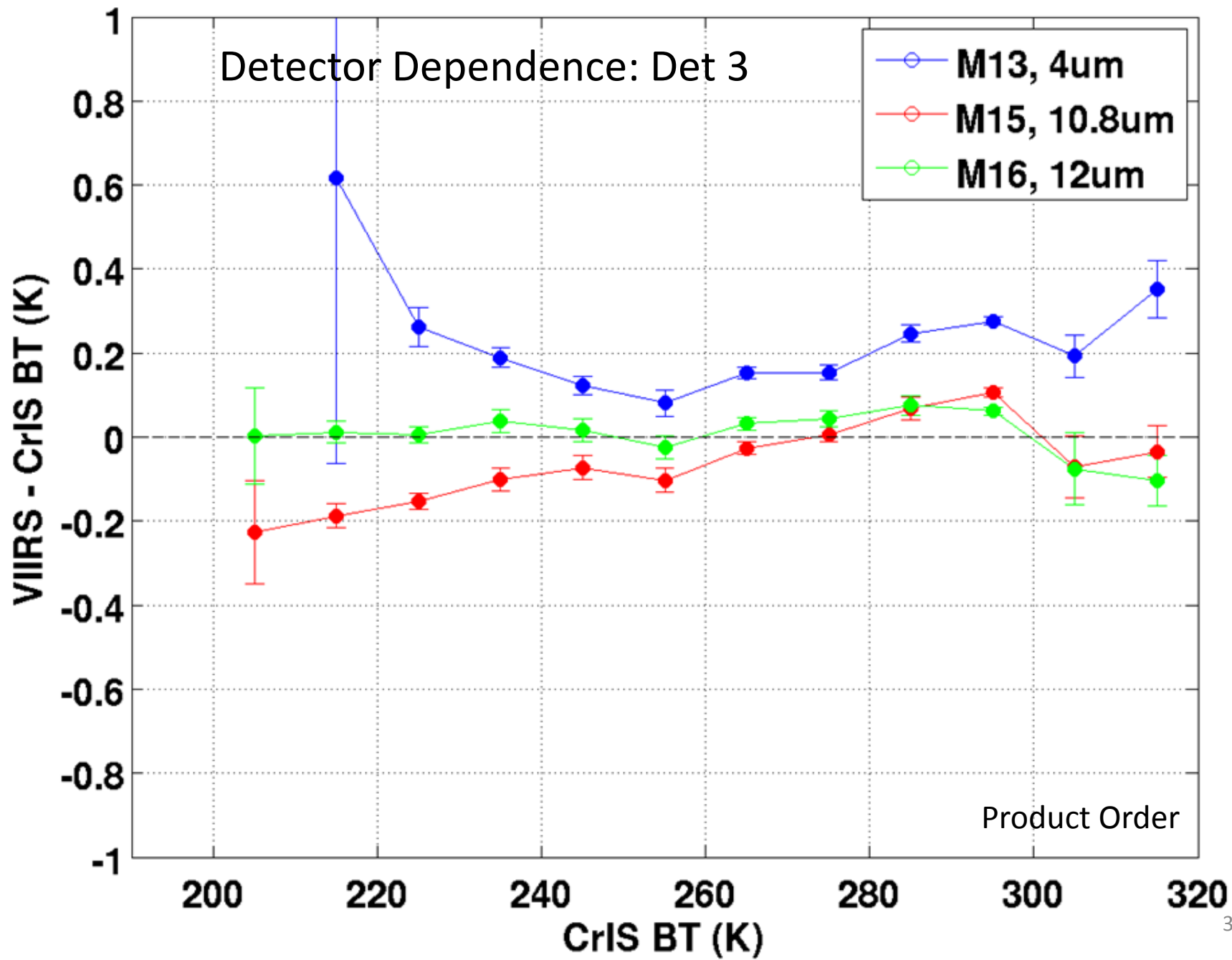
2013172 : MS1 Det1 Mean SNPP VIIRS - CrIS:v33a



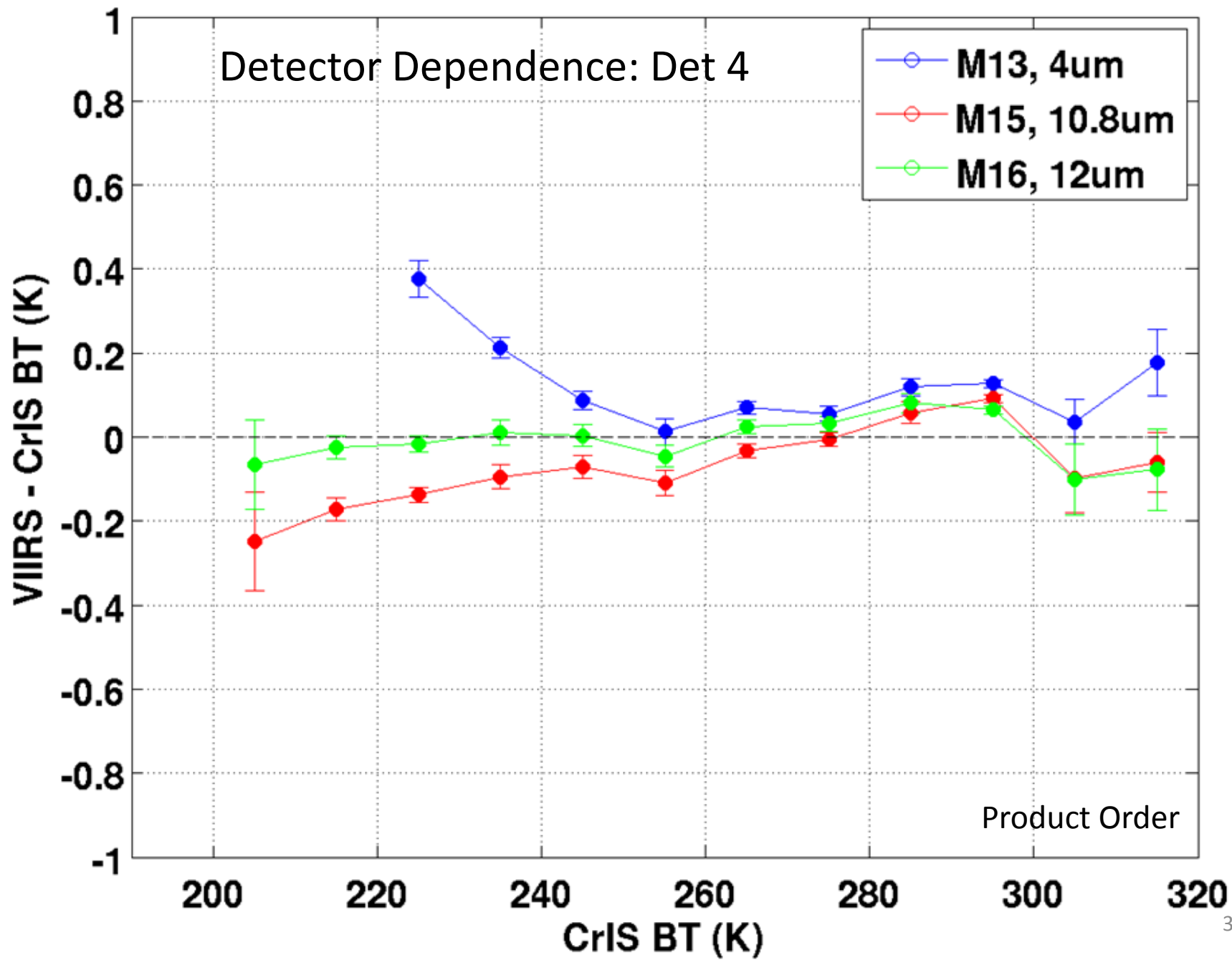
2013172 : MS1 Det2 Mean SNPP VIIRS - CrIS:v33a



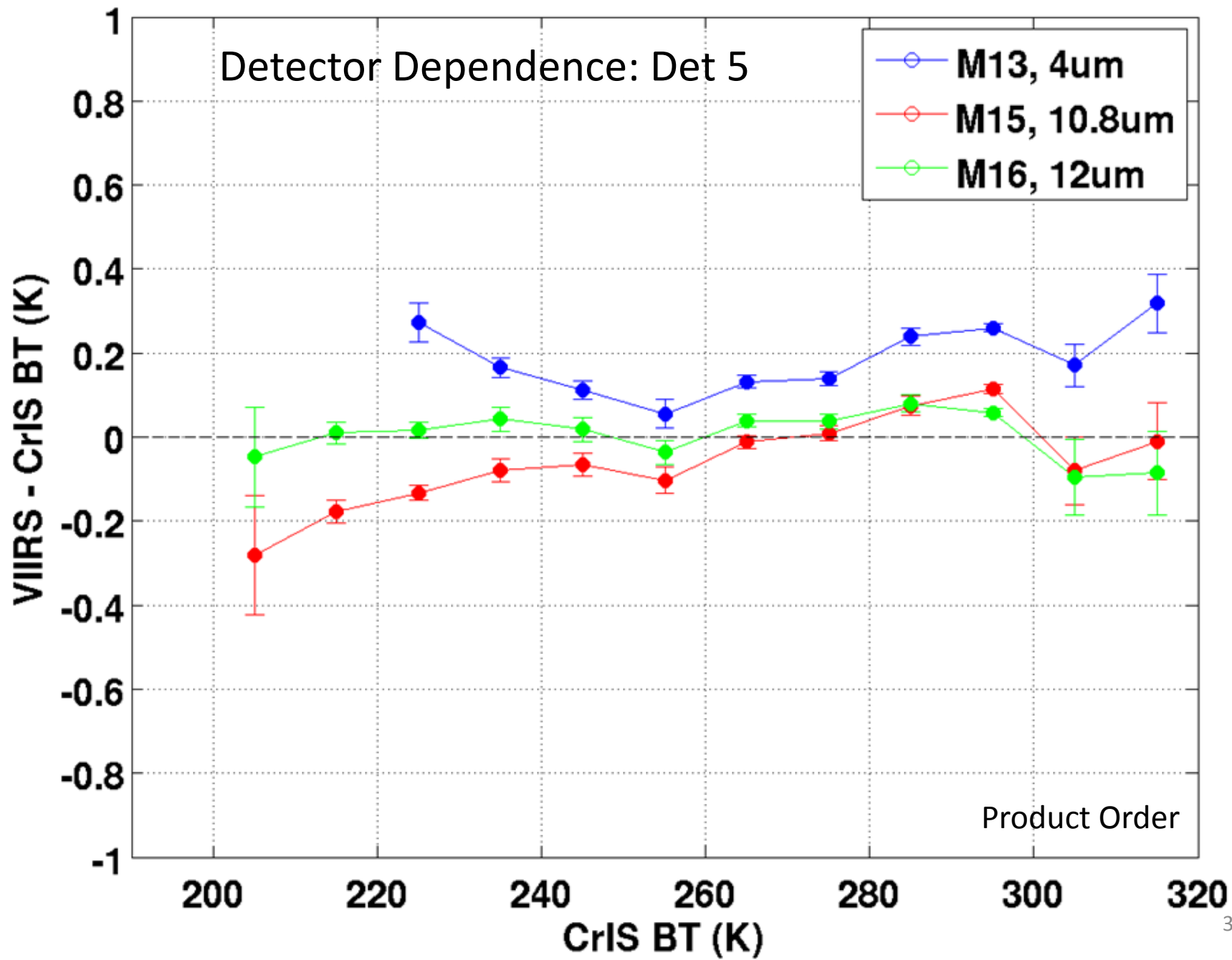
2013172 : MS1 Det3 Mean SNPP VIIRS - CrIS:v33a



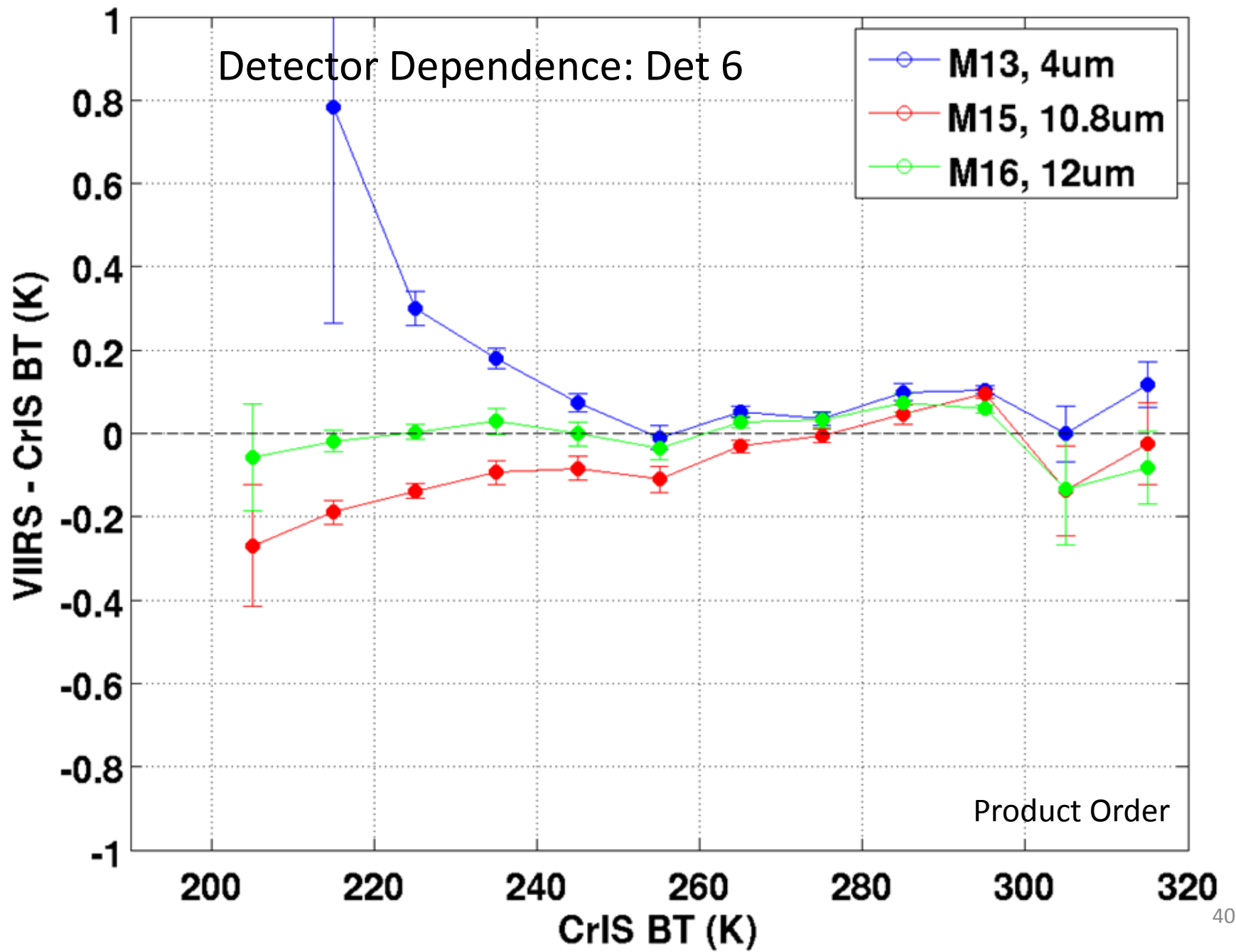
2013172 : MS1 Det4 Mean SNPP VIIRS - CrIS:v33a



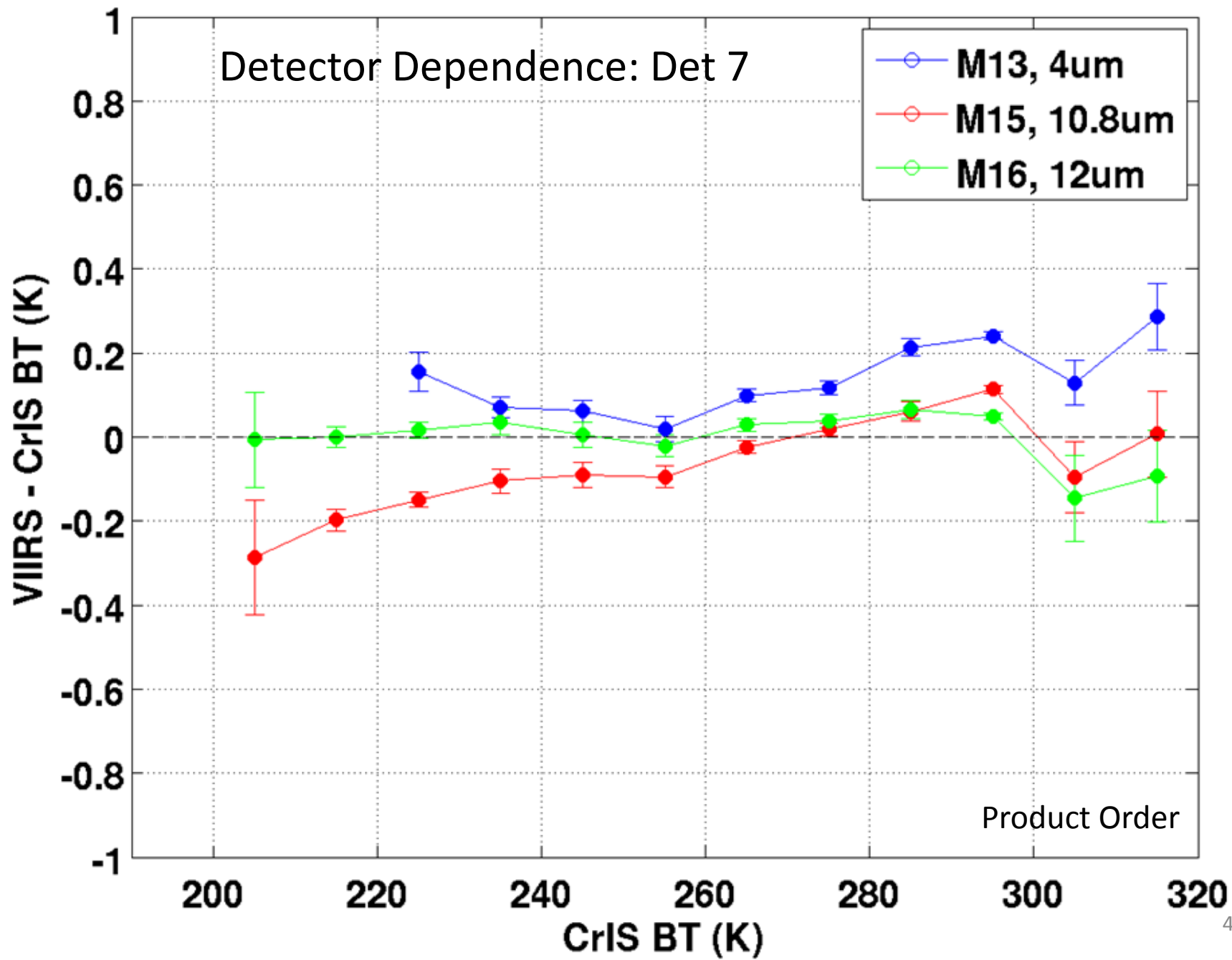
2013172 : MS1 Det5 Mean SNPP VIIRS - CrIS:v33a



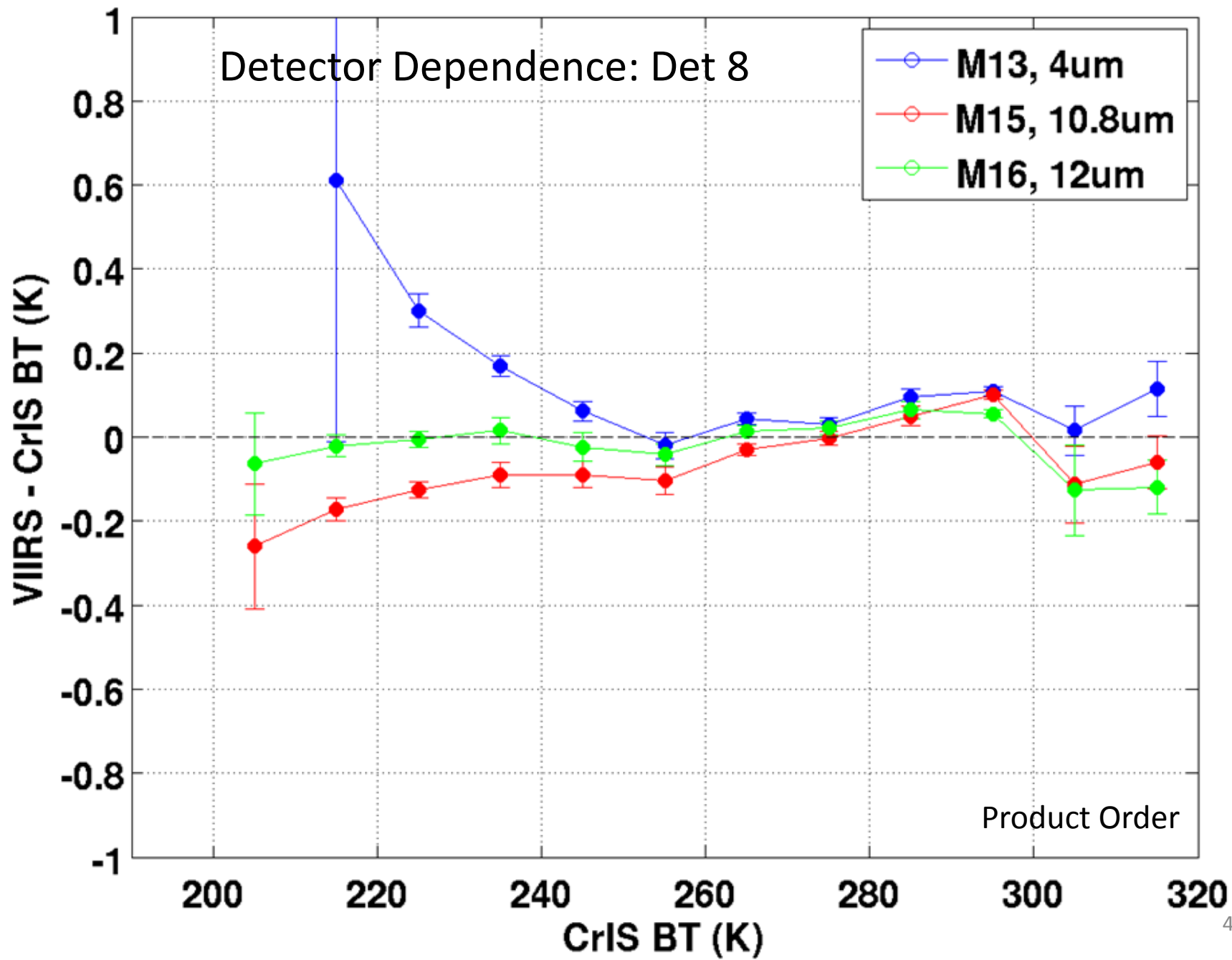
2013172 : MS1 Det6 Mean SNPP VIIRS - CrIS:v33a



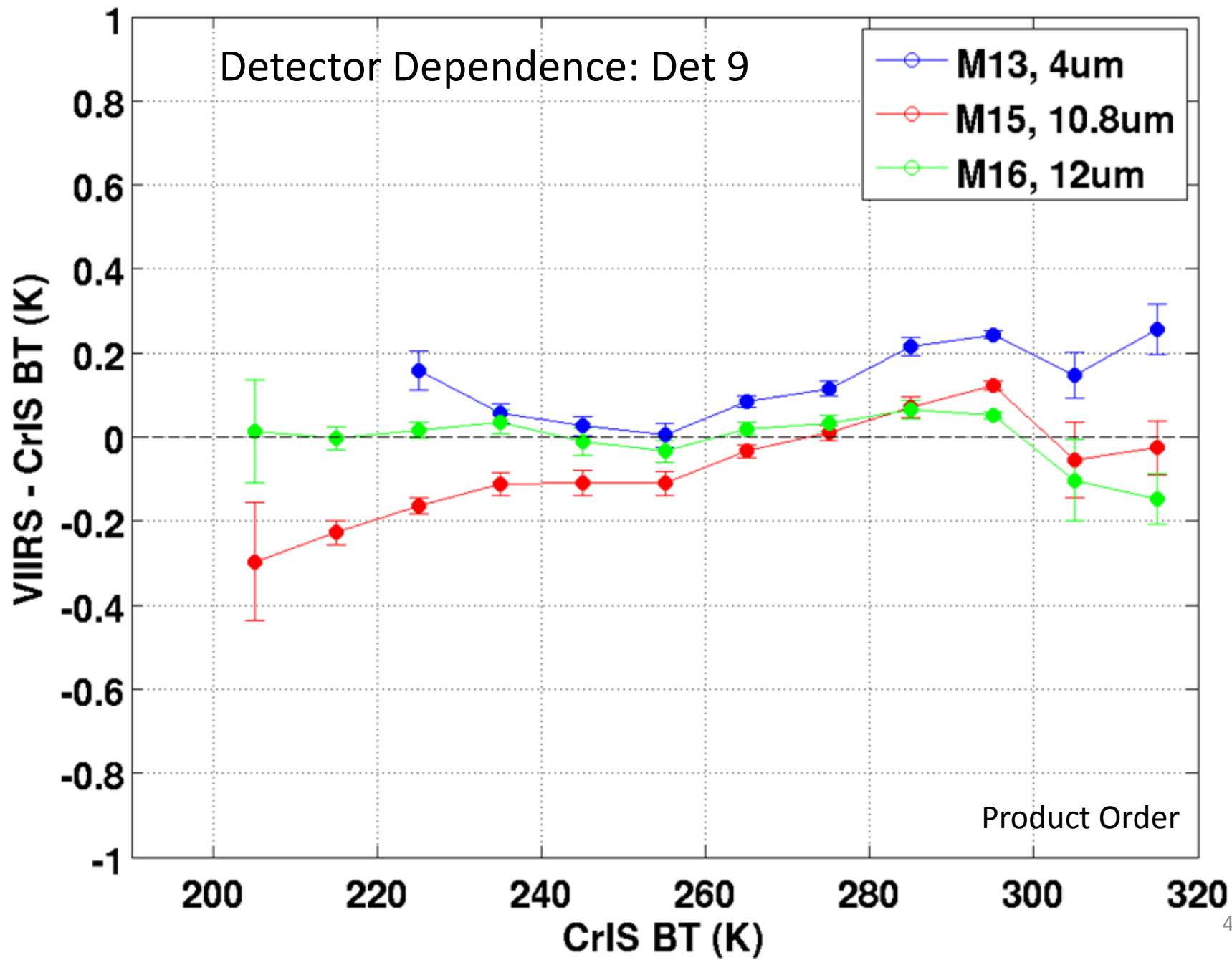
2013172 : MS1 Det7 Mean SNPP VIIRS - CrIS:v33a



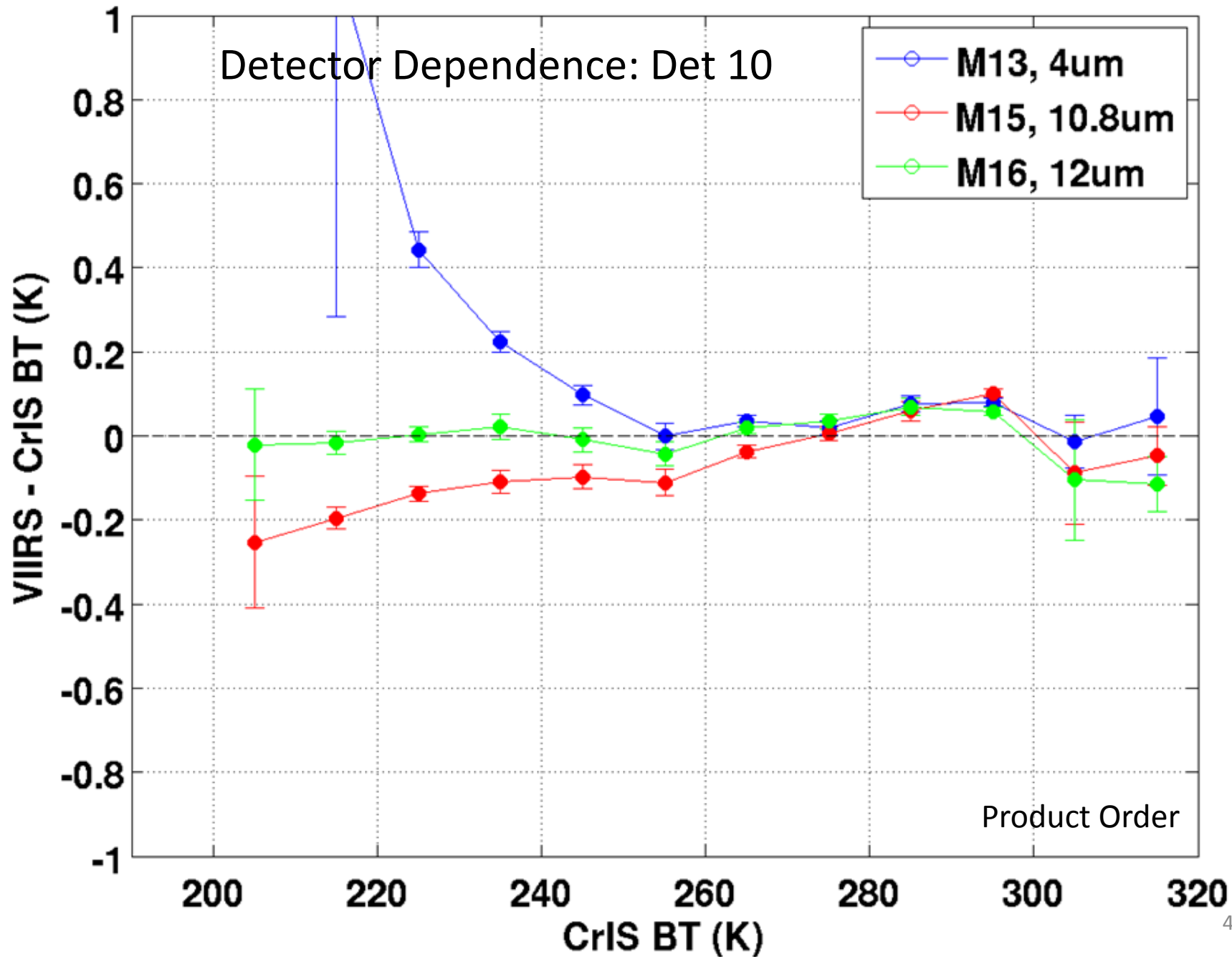
2013172 : MS1 Det8 Mean SNPP VIIRS - CrIS:v33a



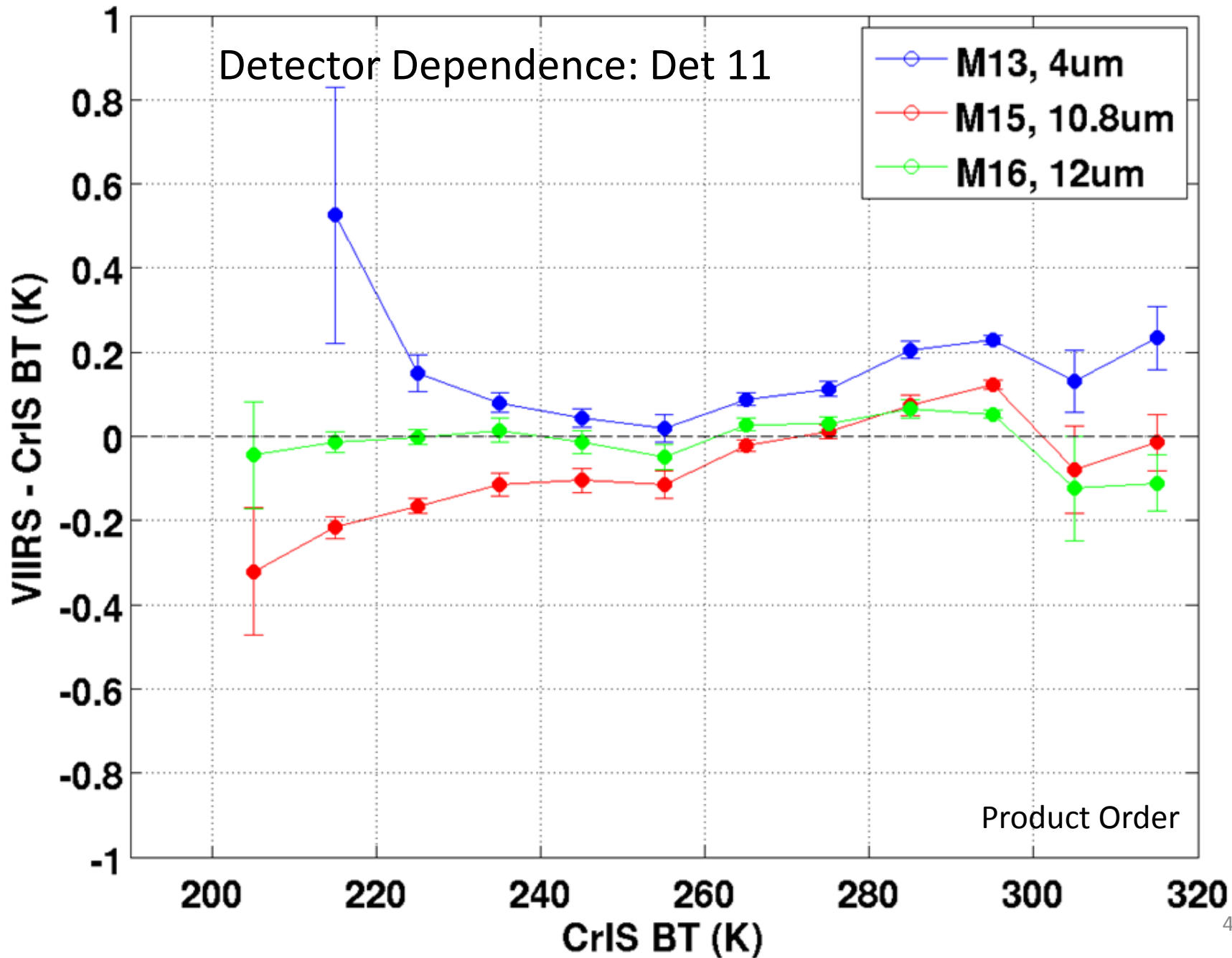
2013172 : MS1 Det9 Mean SNPP VIIRS - CrIS:v33a



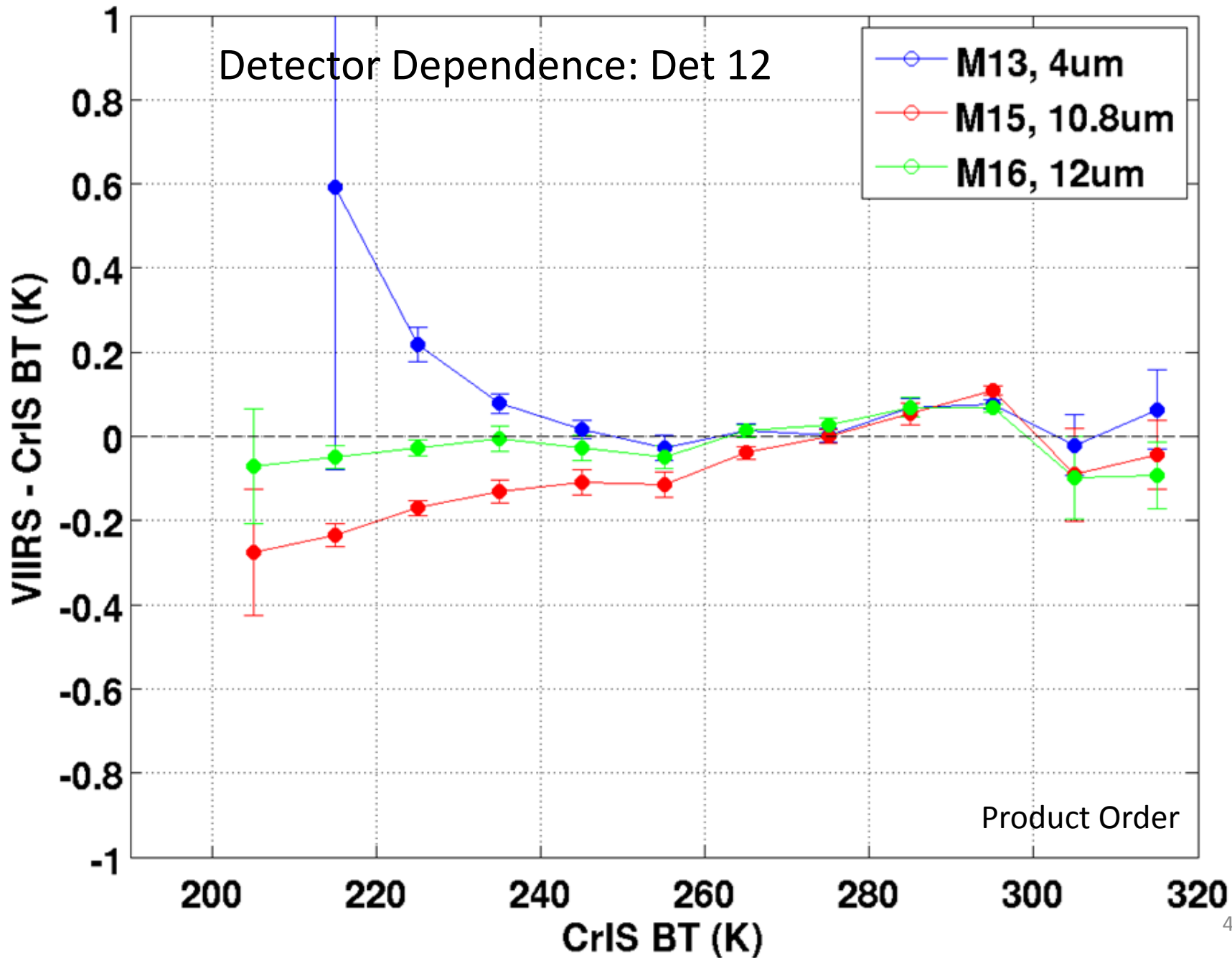
2013172 : MS1 Det10 Mean SNPP VIIRS - CrIS:v33a



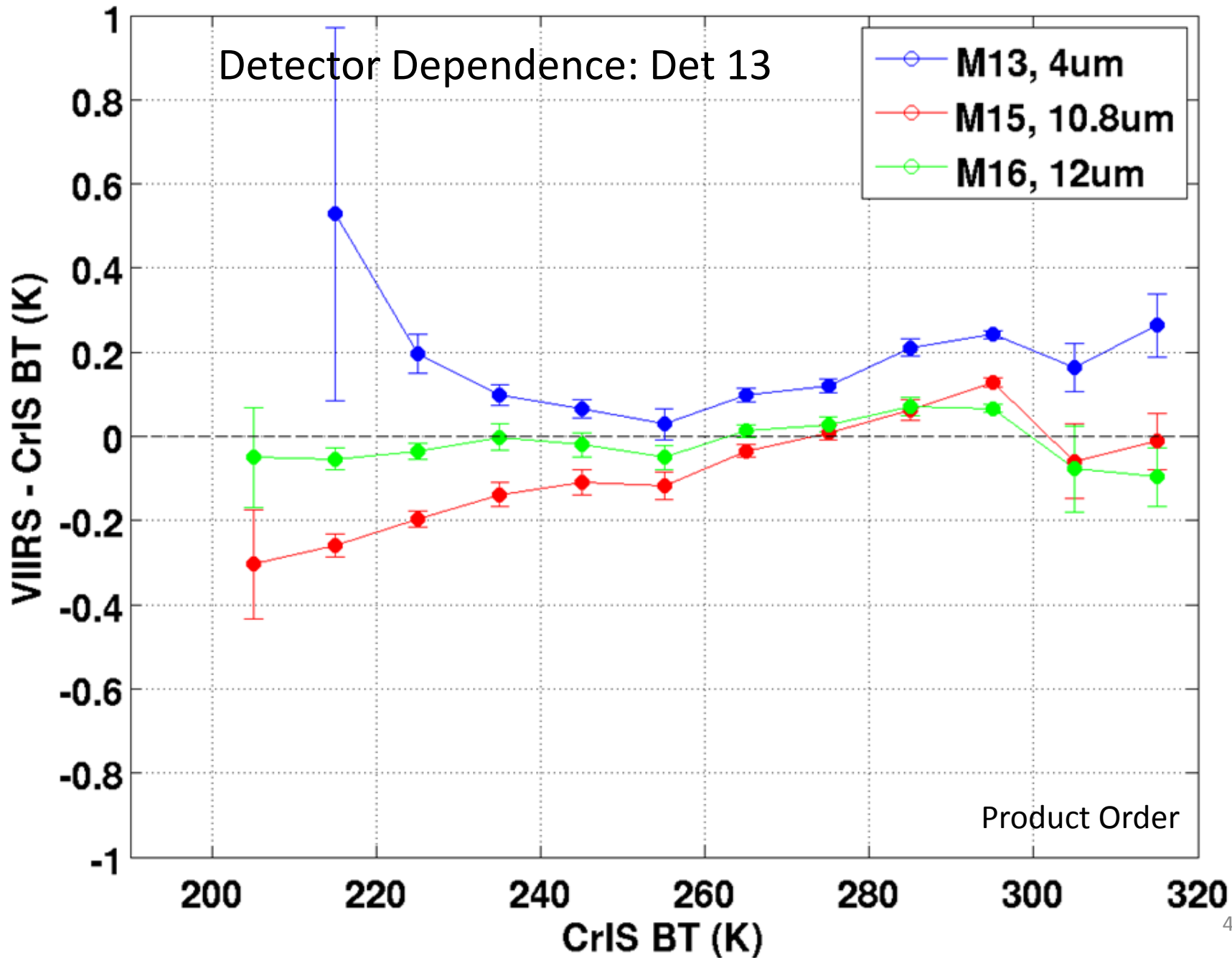
2013172 : MS1 Det11 Mean SNPP VIIRS - CrIS:v33a



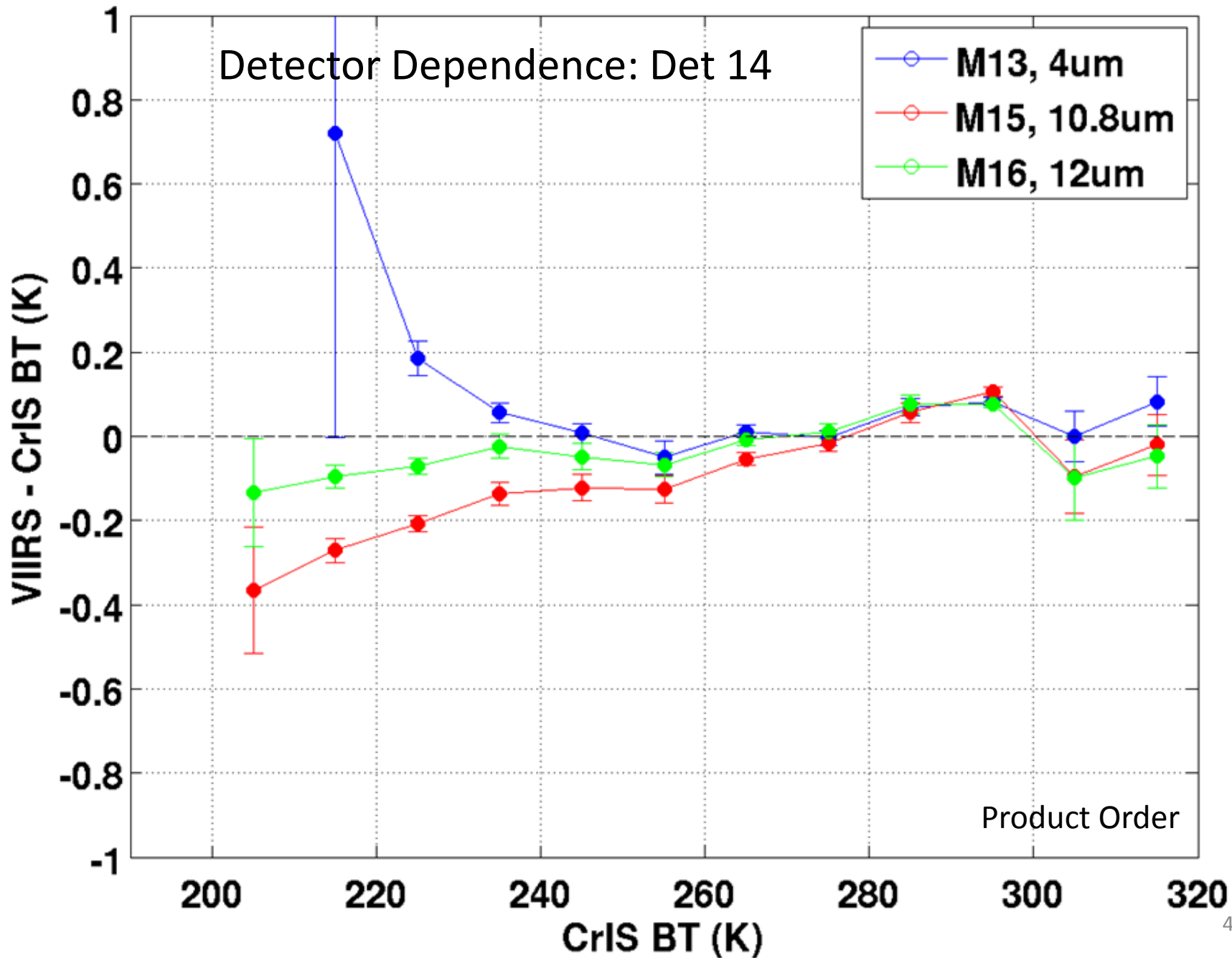
2013172 : MS1 Det12 Mean SNPP VIIRS - CrIS:v33a



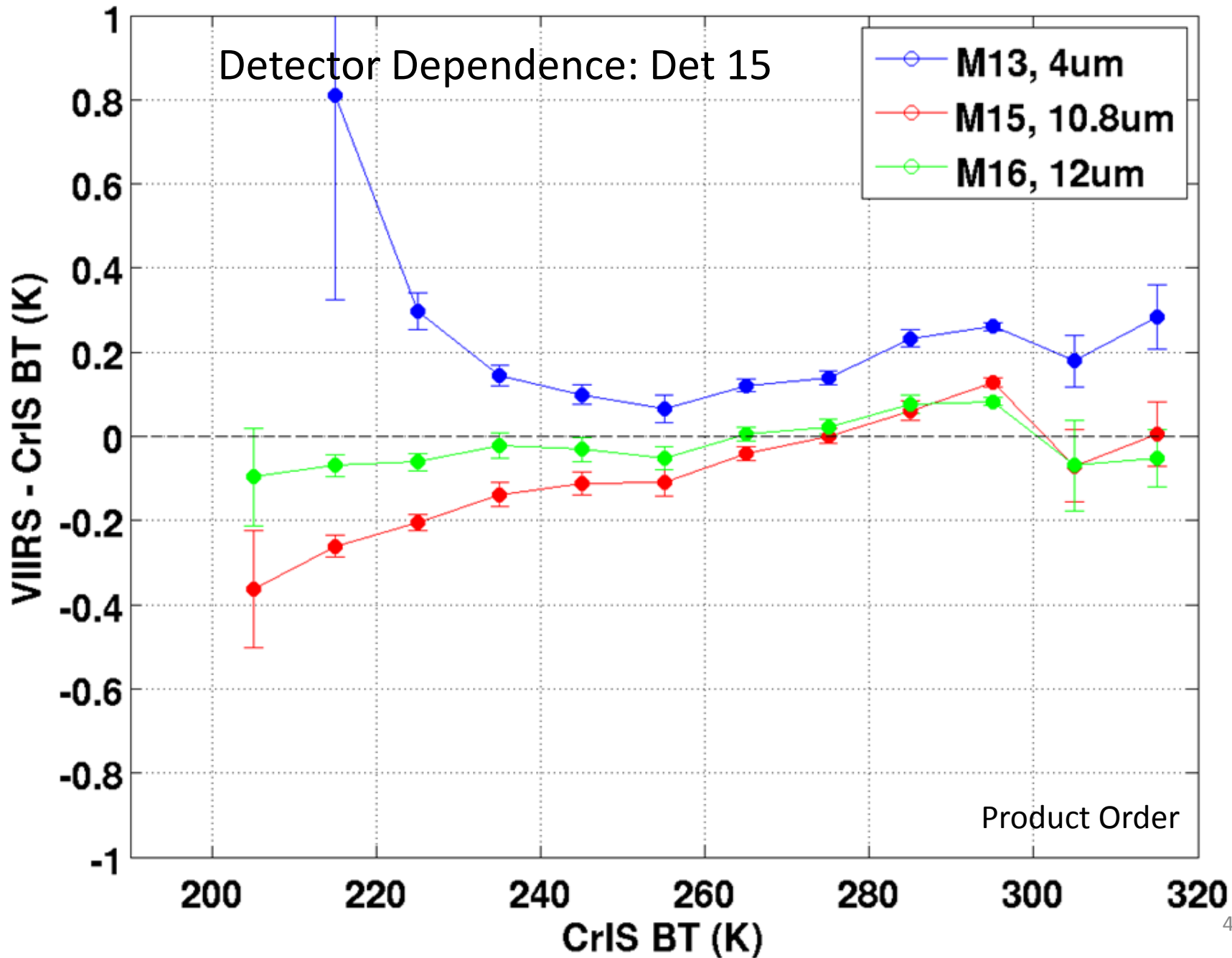
2013172 : MS1 Det13 Mean SNPP VIIRS - CrIS:v33a



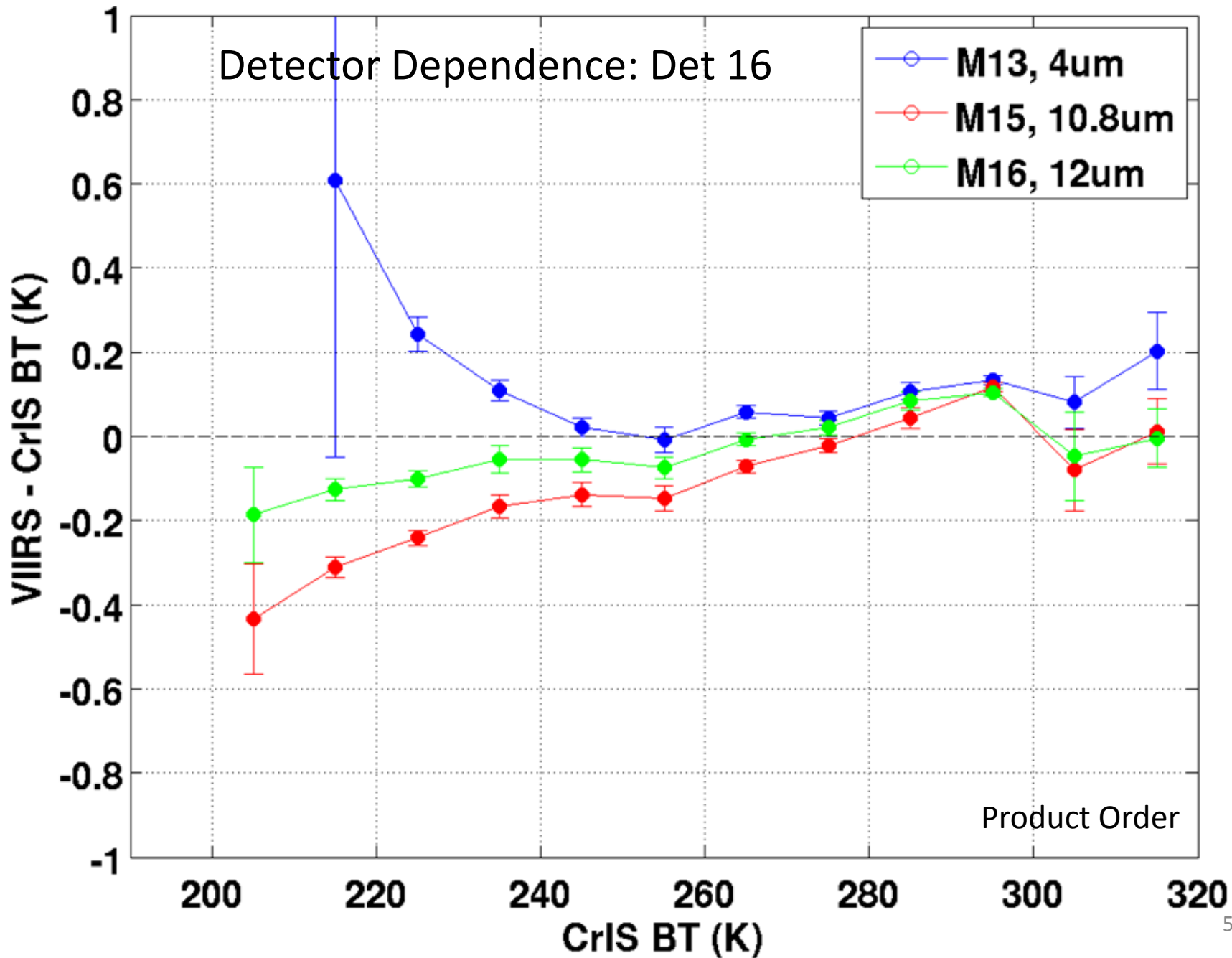
2013172 : MS1 Det14 Mean SNPP VIIRS - CrIS:v33a



2013172 : MS1 Det15 Mean SNPP VIIRS - CrIS:v33a

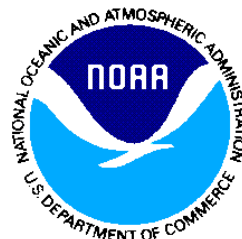


2013172 : MS1 Det16 Mean SNPP VIIRS - CrIS:v33a





JPSS Annual Meeting
12-16 May 2014, College Park, MD



SST Feedback to VIIRS SDR

Sasha Ignatov, Xingming Liang, Irina Gladkova,
Karlis Mikelsons, Marouan Bouali

with inputs from STAR SST Team

J. Stroup, Y. Kihai, B. Petrenko, P. Dash, J. Sapper

NOAA/NESDIS, CSU/CIRA, GST Inc, CUNY

Summary: VIIRS Performance for SST

Overall, VIIRS is a very good, state of the art sensor for SST

- ✓ Radiances are stable (critical for regression SST)
- ✓ Radiances consistent w/AVHRR/MODIS (critical for physical SST)
- ✓ VIIRS imagery comparable or better than Aqua MODIS
- ✓ VIIRS striping comparable or better than Aqua MODIS

Striping affects SST

- ✓ Striping in VIIRS BTs is within specs. However, it
 - Affects the VIIRS cloud mask and prevents improvements
 - Gets amplified in SST
 - Affects downstream SST products (SST gradients)
- ✓ SST Team works with SDR to reduce striping based on 1st principles
- ✓ Also, SST Team explores destriping in BTs to improve SST EDR

Suggested Improvements

- ✓ Small navigation misalignments are corrected for, for cloud mask
- ✓ Fill in radiances in bow-tie areas. (Currently, filled in with NaNs – suggest put real numbers, while keeping the “bow-tie” flag on)

VIIRS, MODIS, and AVHRR Radiance Monitoring in MICROS

www.star.nesdis.noaa.gov/sod/sst/micros/

Liang, Ignatov: Stability & Radiometric Consistency between AVHRR, MODIS, & VIIRS in SST bands. JGR, Jun 2013.

M-O Biases and Double Differences (“DD”)

Model minus Observation (“M-O”) Biases

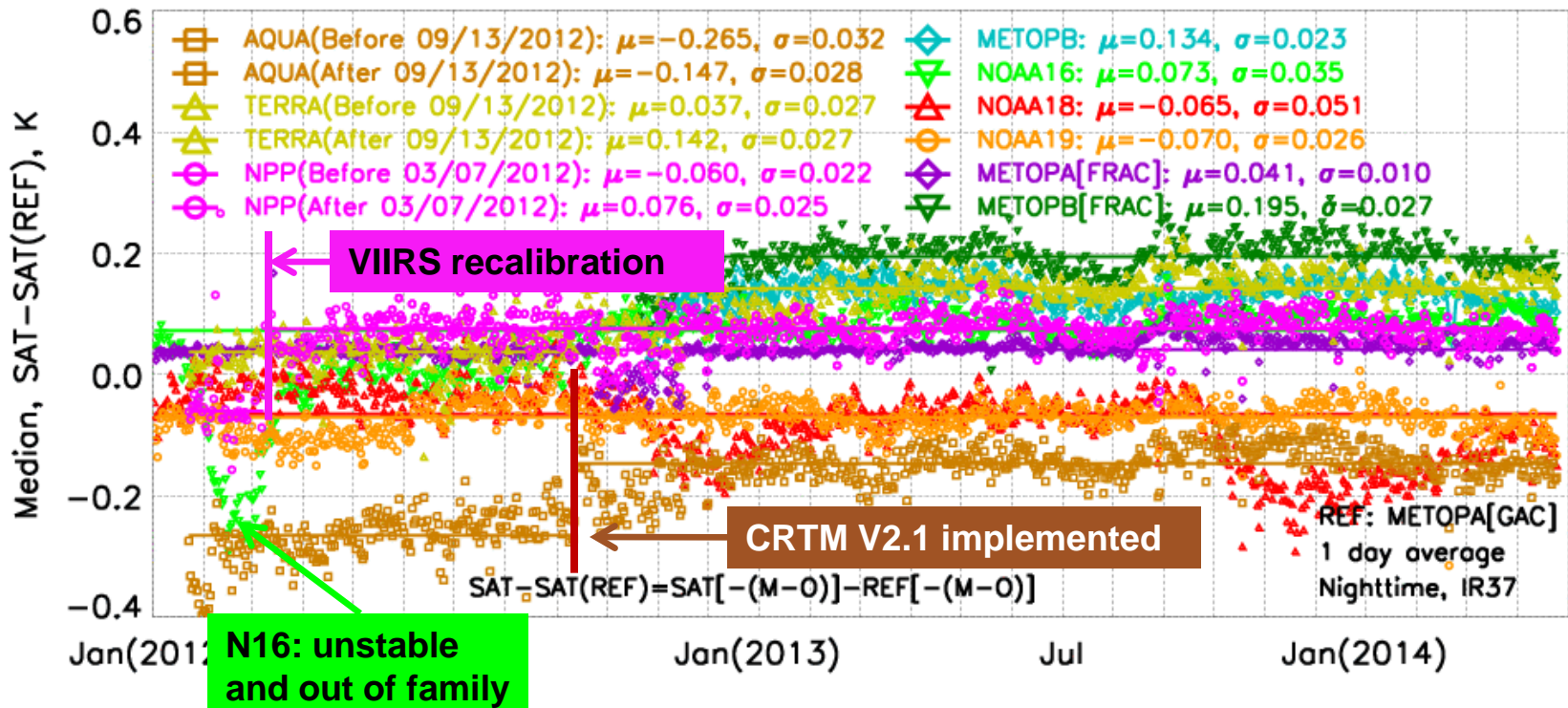
- **M (Model)** = Community Radiative Transfer Model (CRTM) simulated TOA Brightness Temperatures (w/ Reynolds SST, GFS profiles as input)
- **O (Observation)** = Clear-Sky sensor (AVHRR, MODIS, VIIRS) BTs

Double Differences (“DD”) for Cross-Platform Consistency

$$SAT - REF = SAT[-(M - O)] - REF[-(M - O)]$$

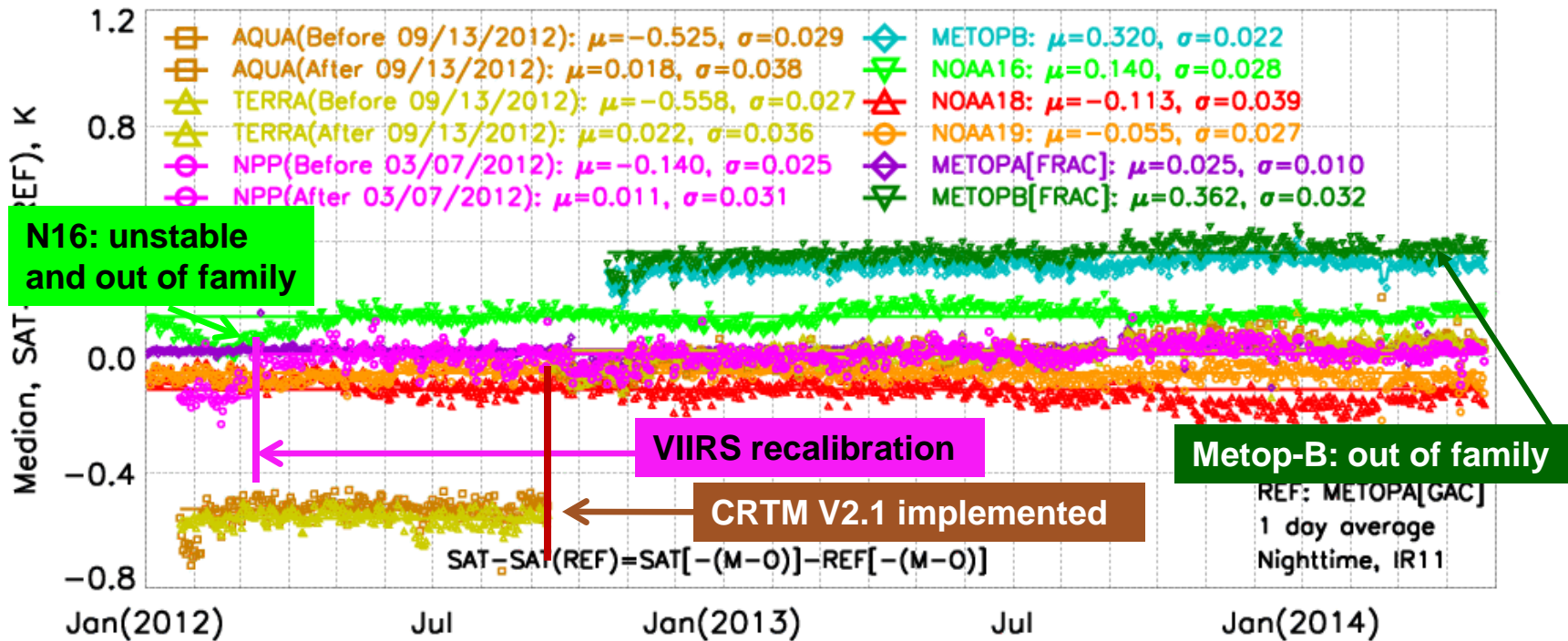
- “M” used as a “Transfer Standard”
- DDs cancel out/minimize effect of systematic errors & instabilities in BTs arising from e.g.
 - Errors/Instabilities in Reynolds SST & GFS
 - Missing aerosol
 - Possible systemic biases in CRTM
 - Updates to ACSPO algorithm

Double Differences in IR37 (VIIRS M12)



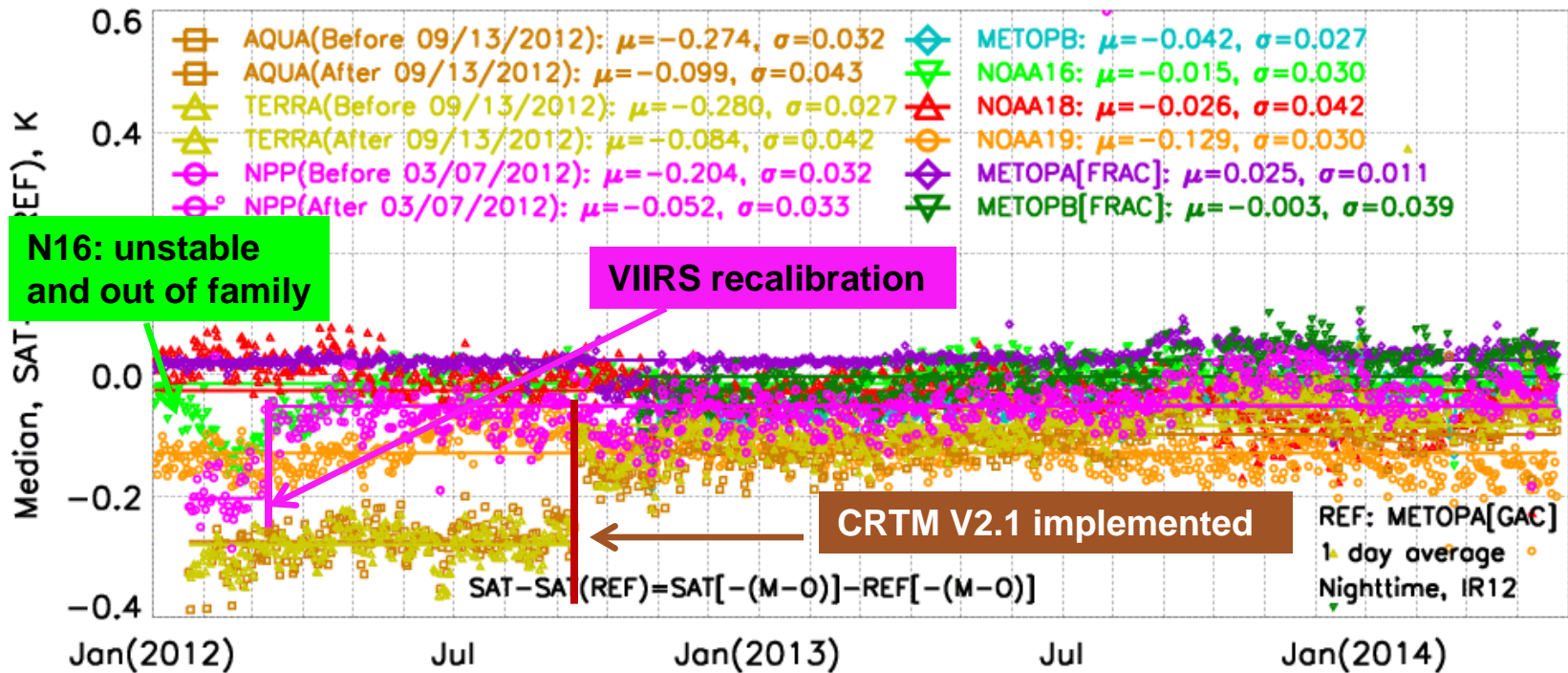
- All sensors are typically within $\pm 0.1K$ (except Metop-B and Terra/Aqua MODIS)
- VIIRS Cal change 7 Mar 2012 reset BT@M12 by +0.14K – now better in family
- In Sep 2012, CRTM changed from V2.02 to v2.10 – affected DDs (N.B.: No change to sensors BTs)
- CRTM V2.1 implemented 13 Sep 2012: Two MODISs shifted up by 0.1K, better bracket family now
- Metop-B out of family by $\sim +0.15 K$ (likely due to suboptimal CRTM coefficients used in CRTM V2.1)

Double Differences in IR11 (VIIRS M15)



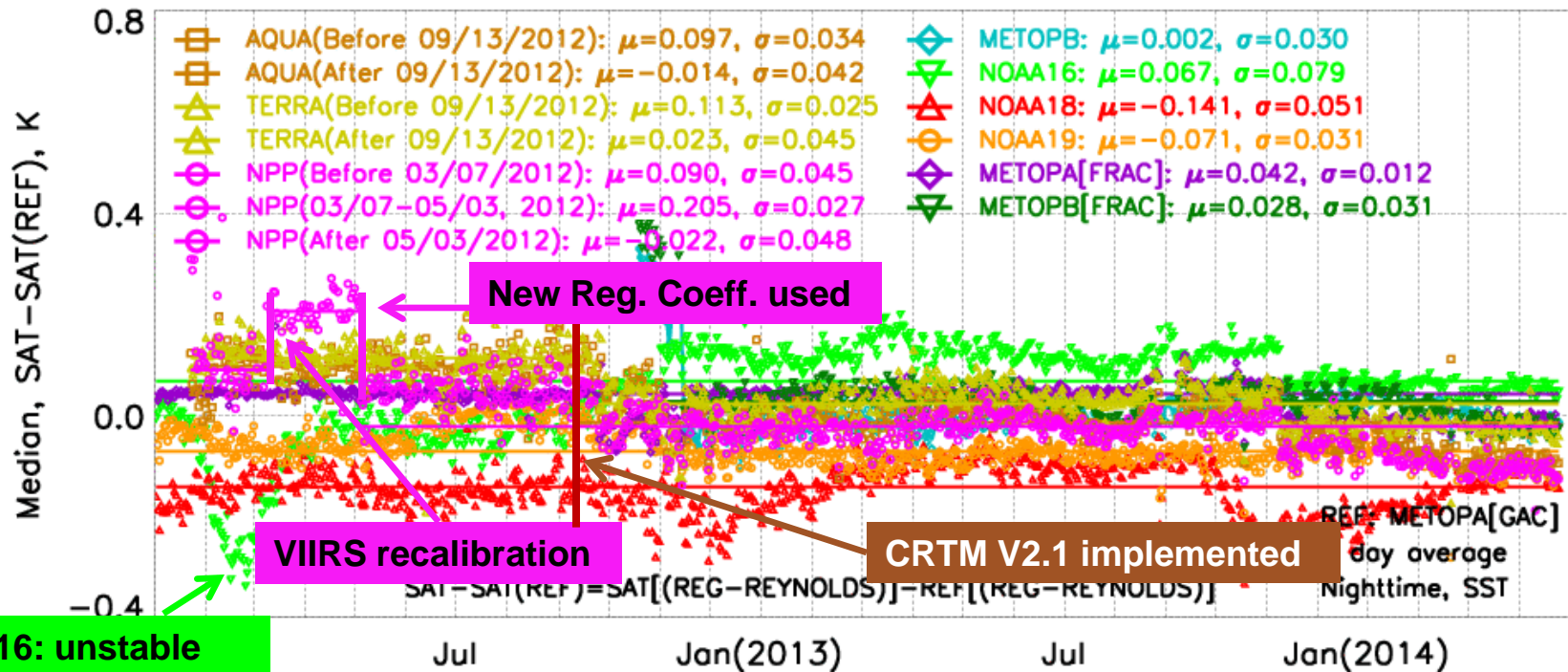
- All AVHRRs (except N16 and Metop-B), MODISs, and VIIRS are now consistent to within $\pm 0.1K$
- VIIRS Cal change 7 Mar 2012 reset BT@M15 by +0.14K – now better in family
- Before 13 Sep 2012: Terra & Aqua/MODIS were biased by -0.6K (suboptimal CRTM coeffs in v2.02)
- Both are back in family now, after CRTM V2.1 implemented on 13 Sep 2012
- Metop-B out of family by $\sim +0.3 K$ (likely due to suboptimal CRTM coefficients in CRTM V2.1)

Double Differences in IR12 (VIIRS M16)



- All AVHRRs, MODISs, and VIIRS are now consistent to within $\pm 0.1K$
- VIIRS Cal change 7 Mar 2012 reset BT@M16 by +0.14K – now better in family
- Terra and Aqua/MODIS were out of family by -0.3K, due to suboptimal CRTM coefficients in V2.02
- Both are back in family now, after CRTM V2.1 implemented on Sep. 13, 2012
- Metop–B in family, but this may change once CRTM coefficients used in CRTM V2.1 are updated

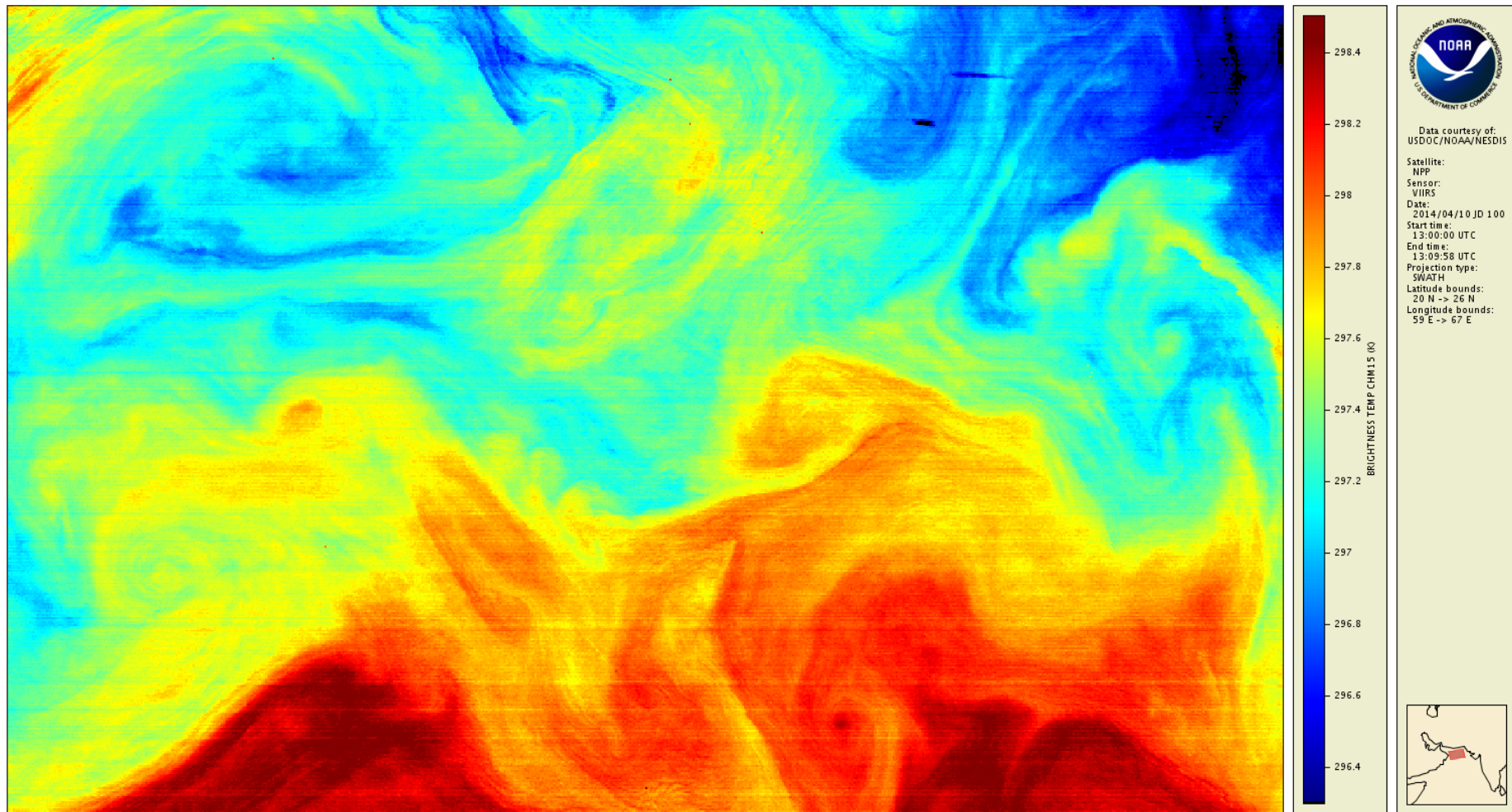
Double Differences in SST



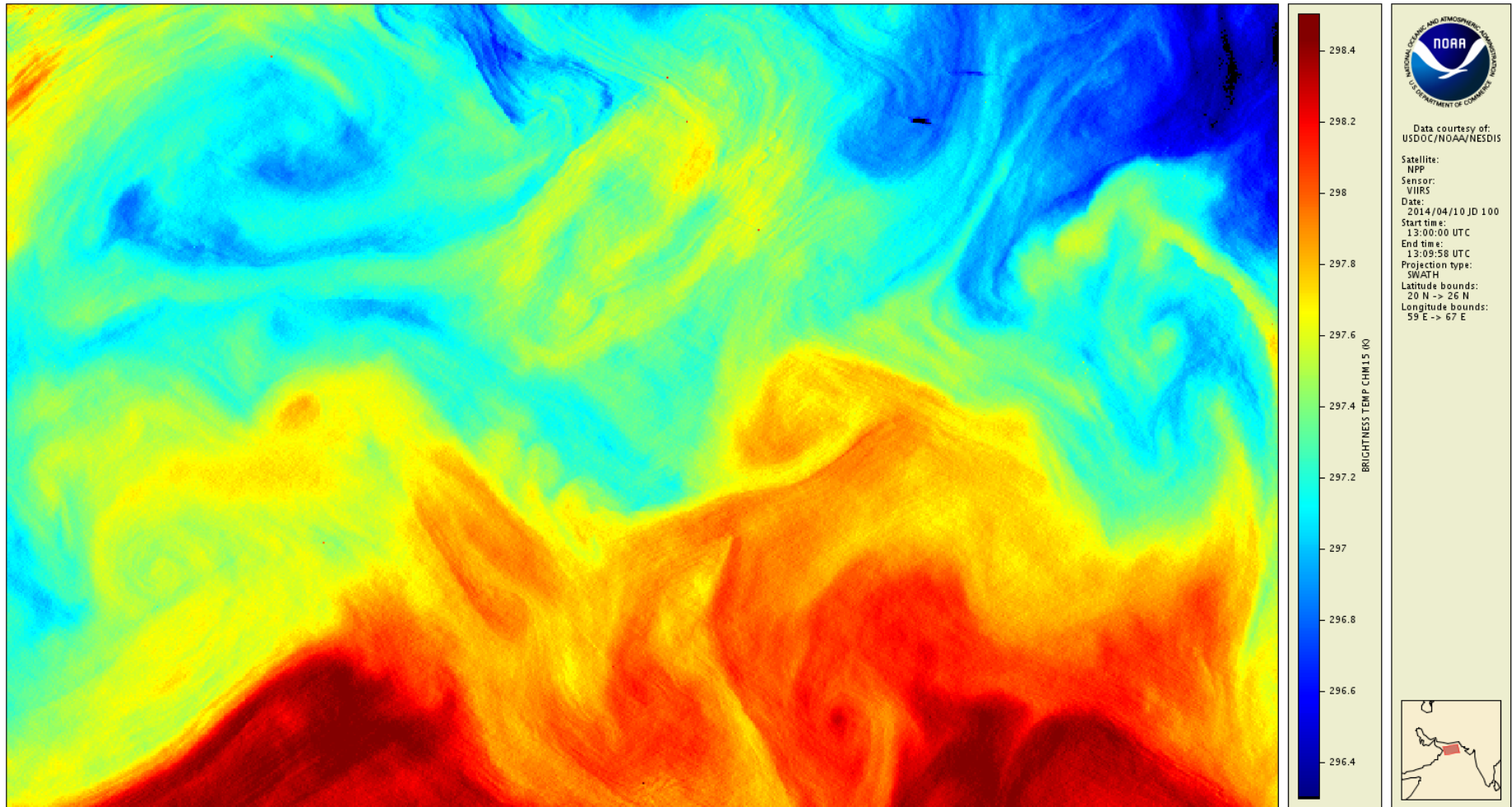
- All AVHRRs, MODISs and NPP/VIIRS SSTs are consistent to within $\pm 0.1K$
- As a result of VIIRS Cal Change on 7 Mar 2012, VIIRS SST went out of family
- Was brought back in family when new SST coefficients implemented 3 May 2012
- CRTM update resulted regression SSTs more noise, and the new coefficients have been implemented since Dec. 2012. More data is needed to understand their performance

Effect of VIIRS Striping on SST

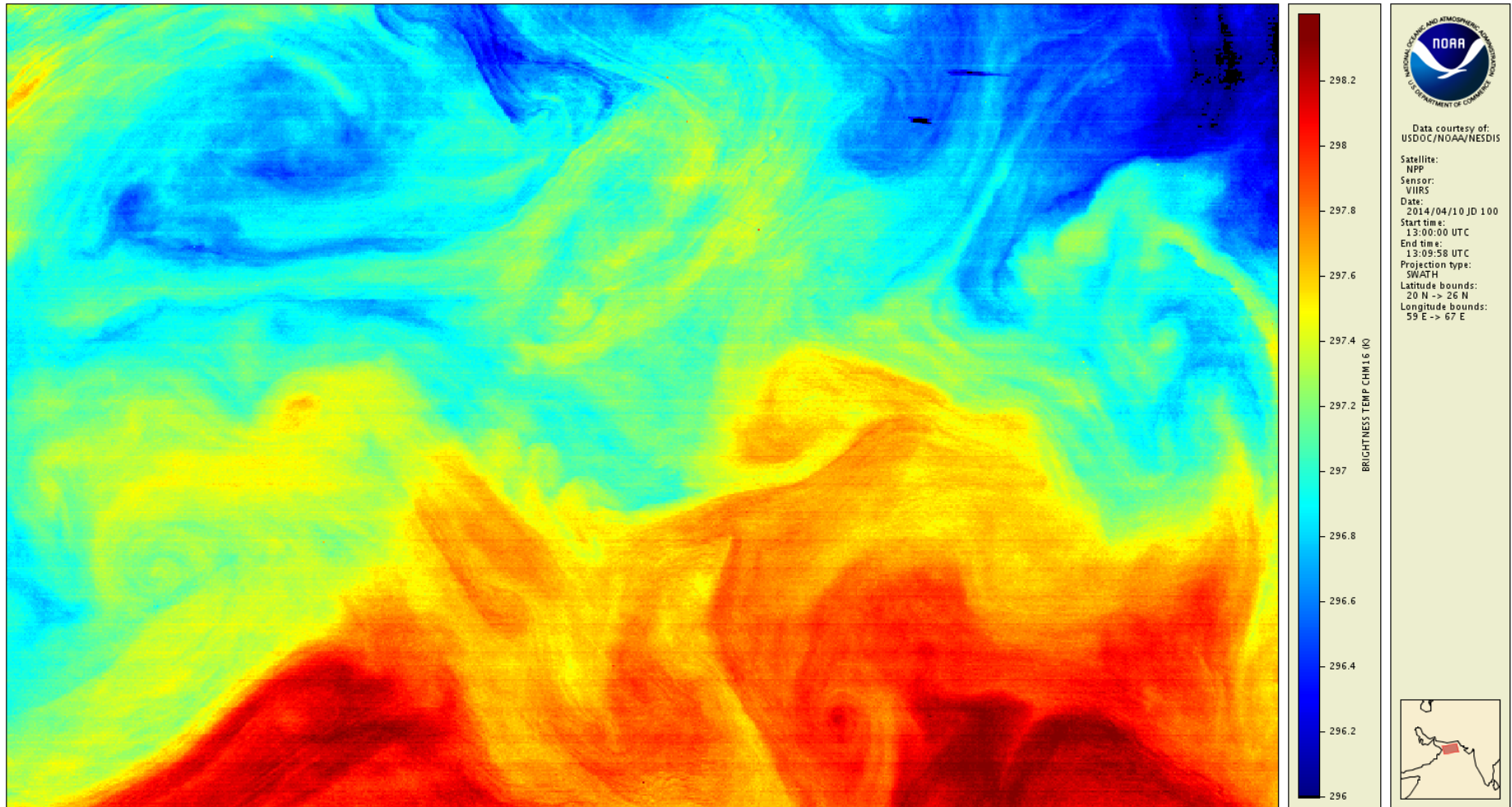
DAY – Original BT in VIIRS band M15 (10.8 μ m)



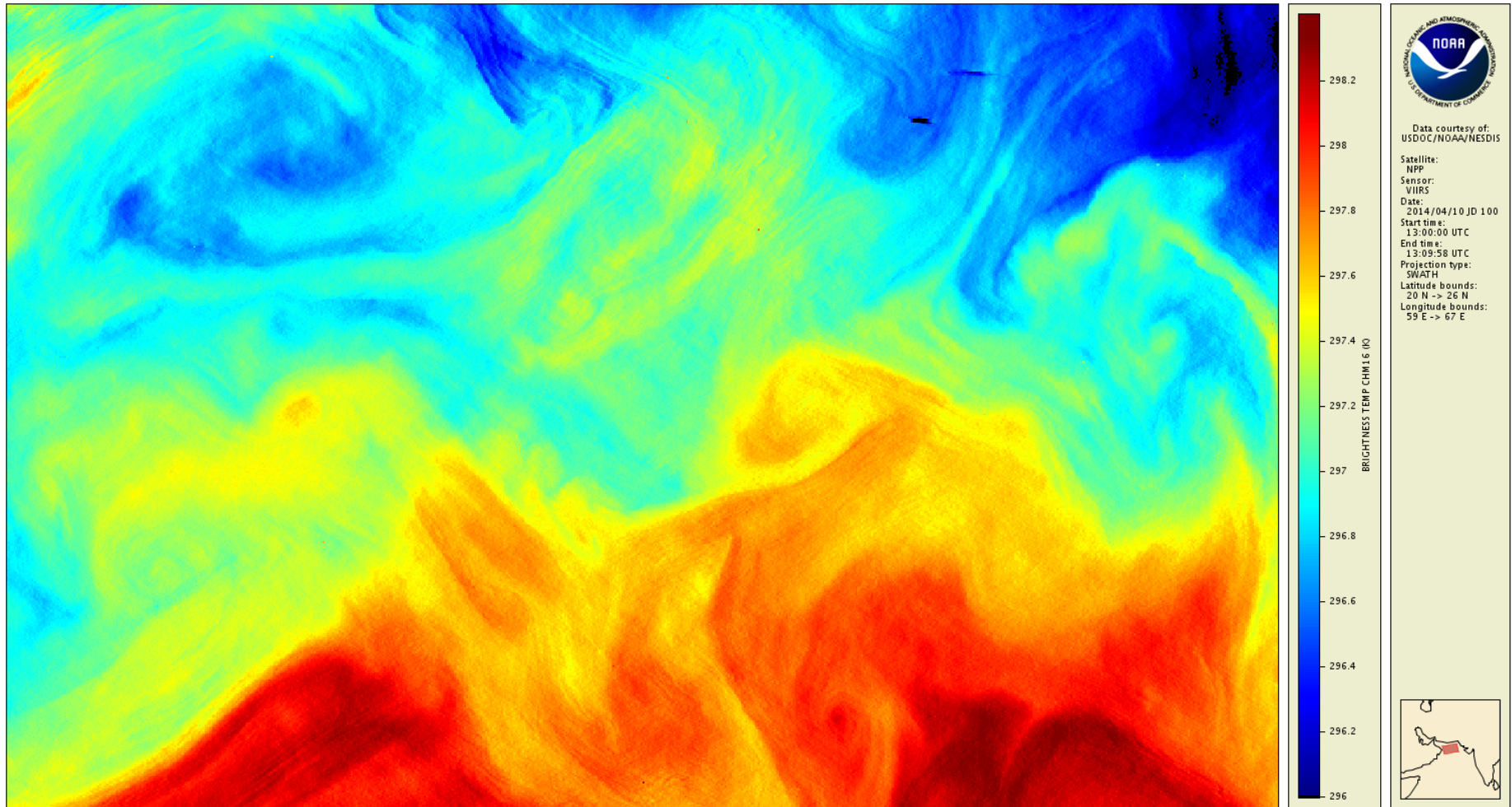
DAY – Destriped BT in VIIRS band M15 (10.8 μ m)



DAY – Original BT in VIIRS band M16 (12 μ m)



DAY – Destriped BT in VIIRS band M16 (12 μ m)



Daytime

$$T_S = a_0 + (a_1 + a_2 S_\theta) T_{11} + [a_3 + a_4 T_S^0 + a_5 S_\theta] (T_{11} - T_{12}) + a_6 S_\theta$$

T_{11}, T_{12}

observed BTs in M15, M16

$S_\theta = 1/\cos(\theta)$

θ is view zenith angle

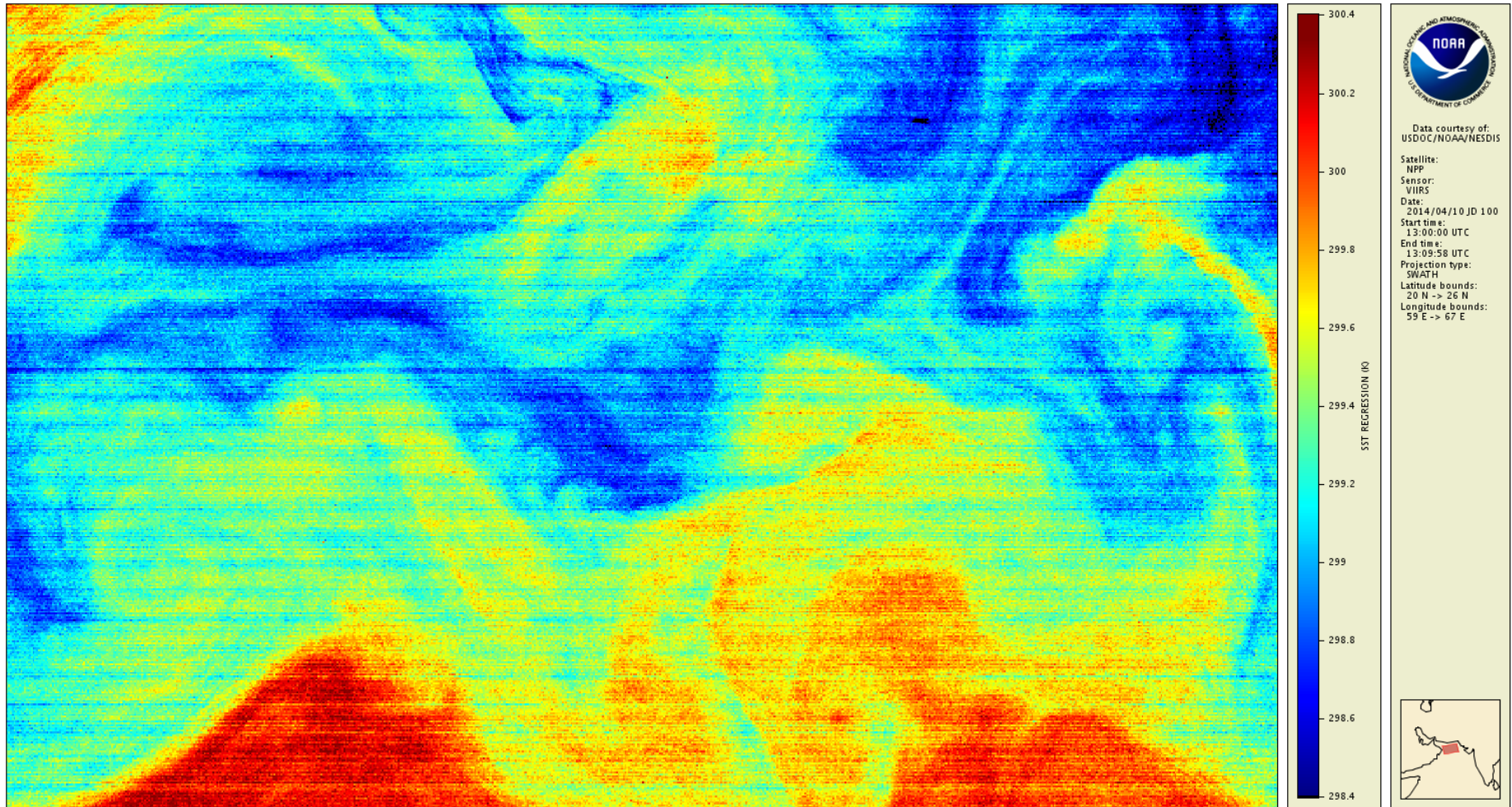
T_S^0

first guess SST (in ° C)

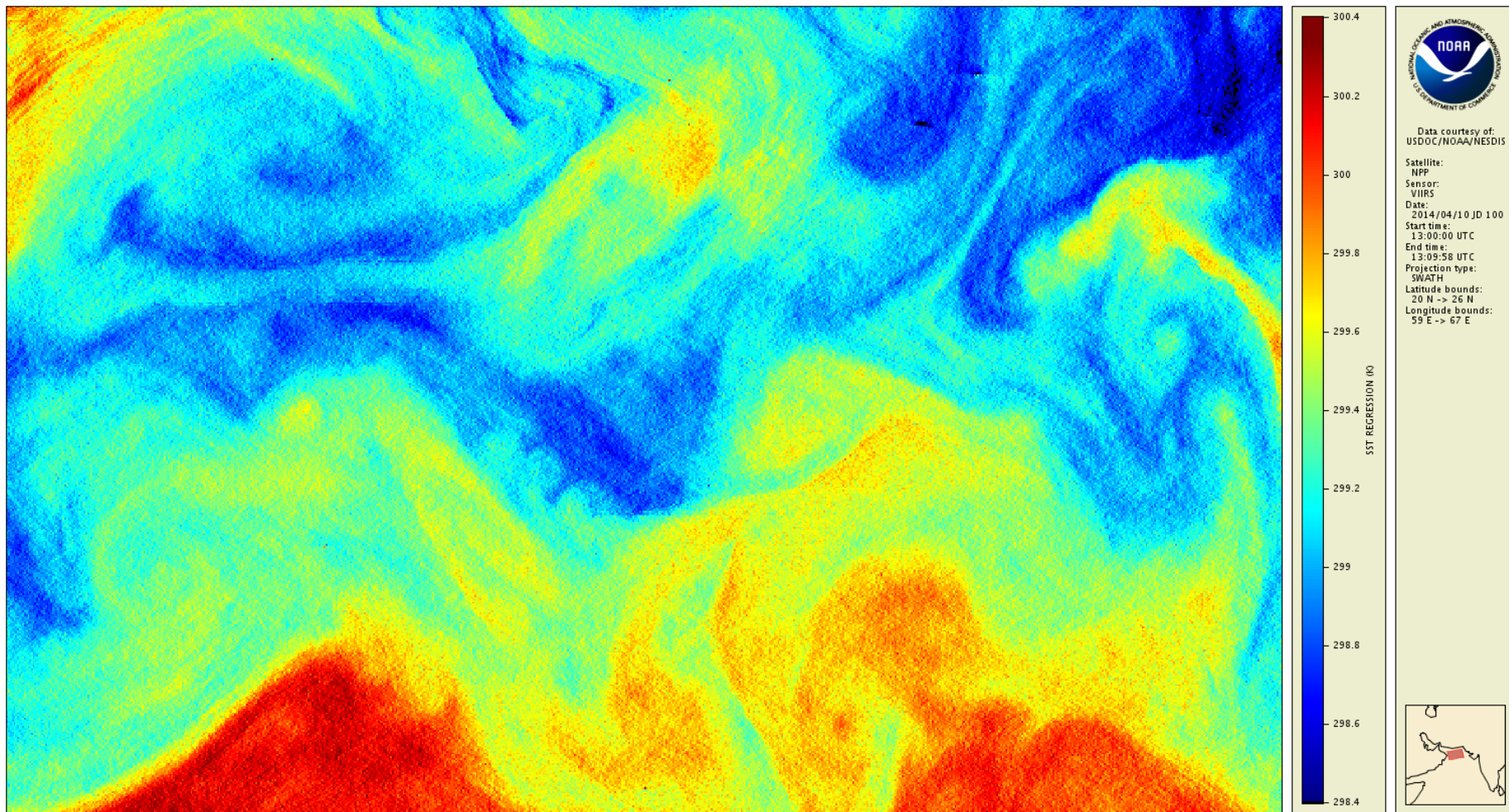
a 's

regression coefficients

DAY – SST from original BTs in M15 and M16

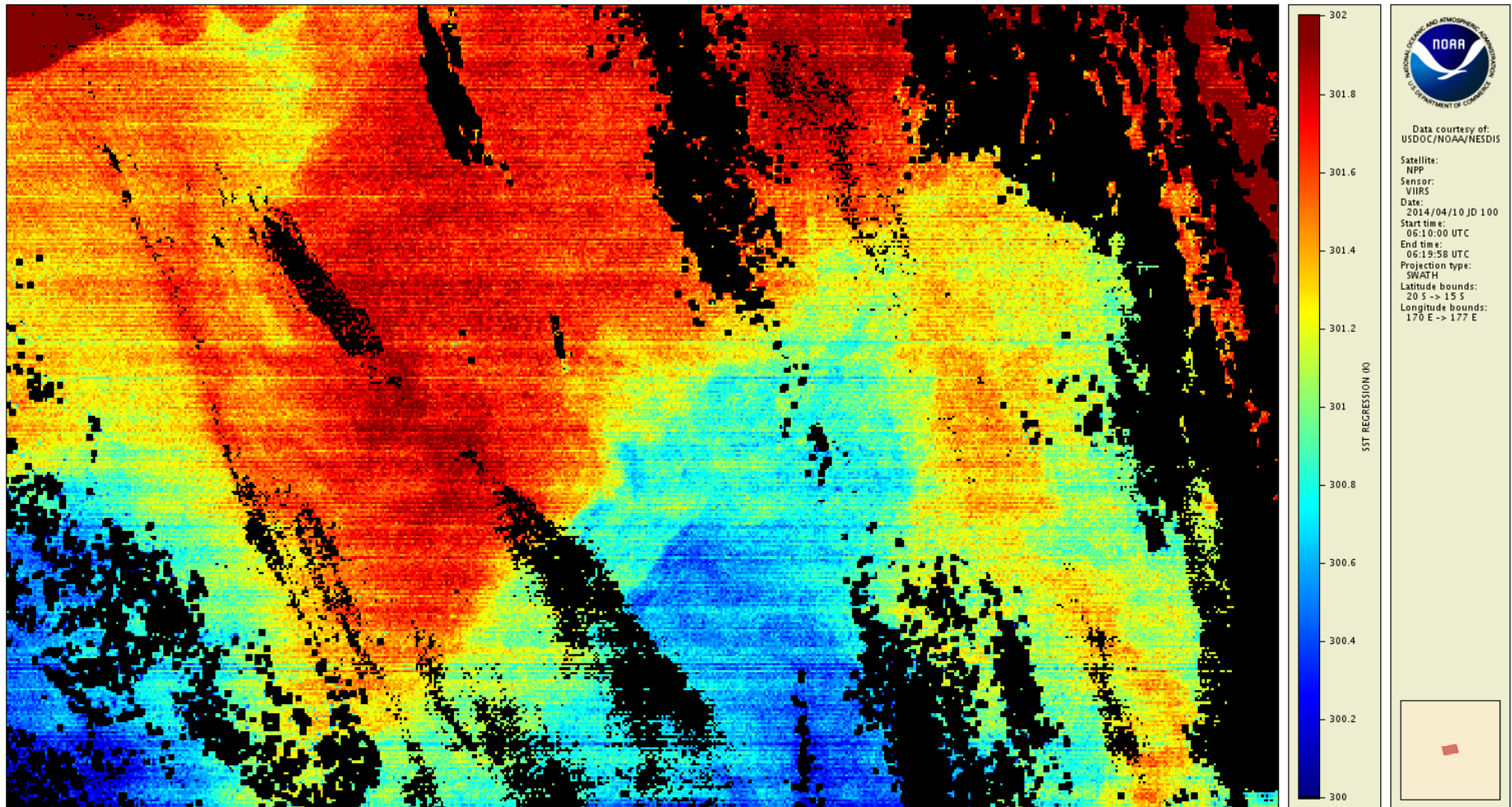


DAY – SST from destriped BTs in M15 and M16

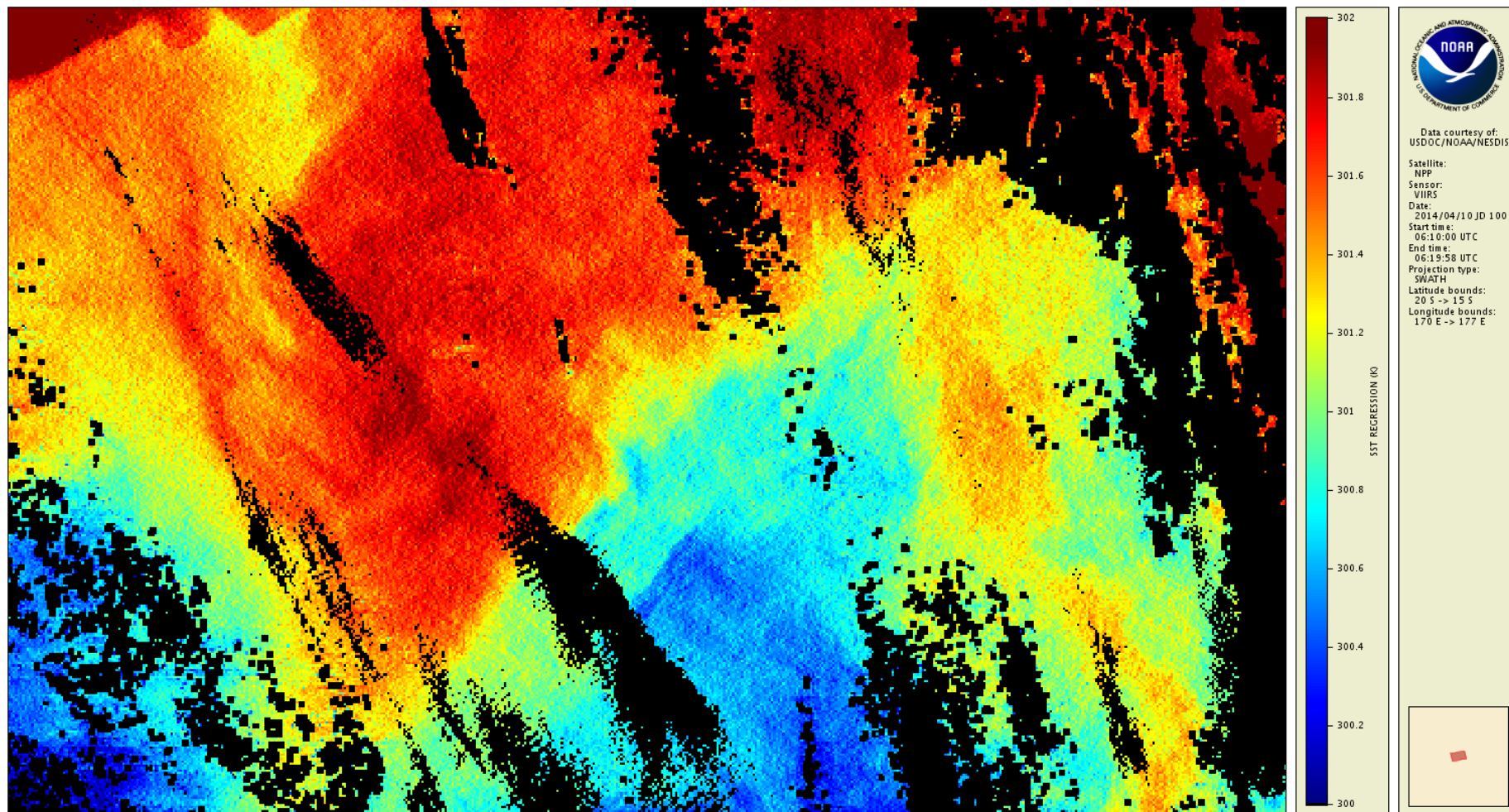


Effect of striping on ACSPO Clear-Sky Mask

DAY – SST from original BTs – effect on cloud mask



DAY – SST from destriped BTs – effect on cloud mask

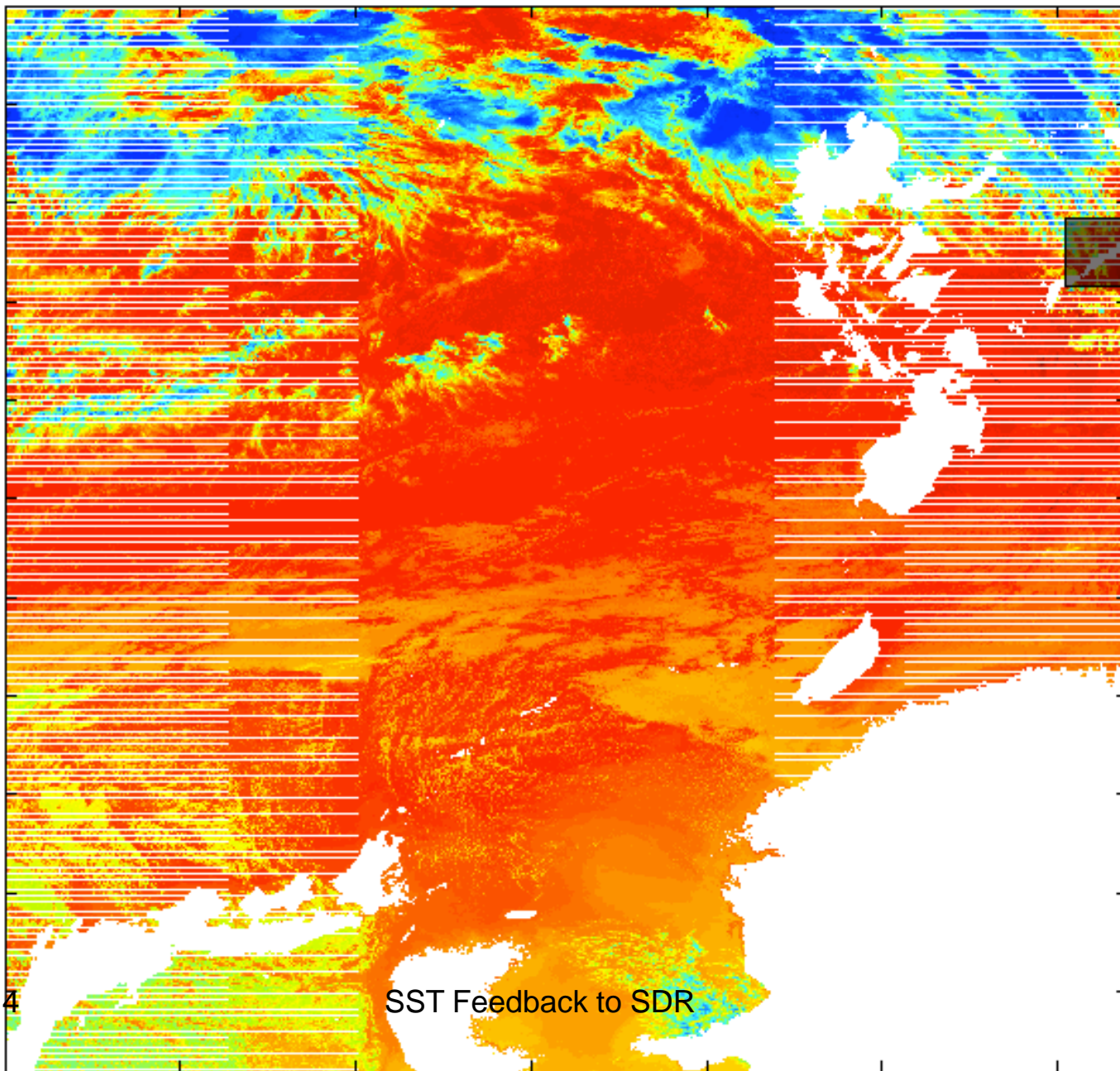


Performance – IDL vs C

	IDL	C
Test environment	Intel Xeon 3.5 GHz NVIDIA Tesla M2070 GPU gpulib, cuda libraries	Intel Xeon 3.5 GHz 8 threads fftw3, openmp libraries
Running times		
One day of VIIRS (M12, M15, M16)	6 hours	37 min
One day of MODIS (Aqua + Terra) Bands 20, 31, 32	6 hours	83 min
One day of VIIRS (M12, M15, M16) + MODIS (Aqua + Terra) Bands 20, 31, 32	12 hours	2 hours

- overall, C code is about 6 times faster
- I/O is a significant factor for C version: $\approx 25\%$ time (VIIRS) and $\approx 40\%$ time (MODIS)

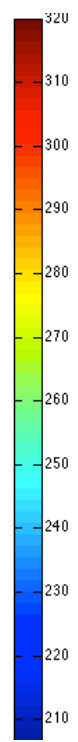
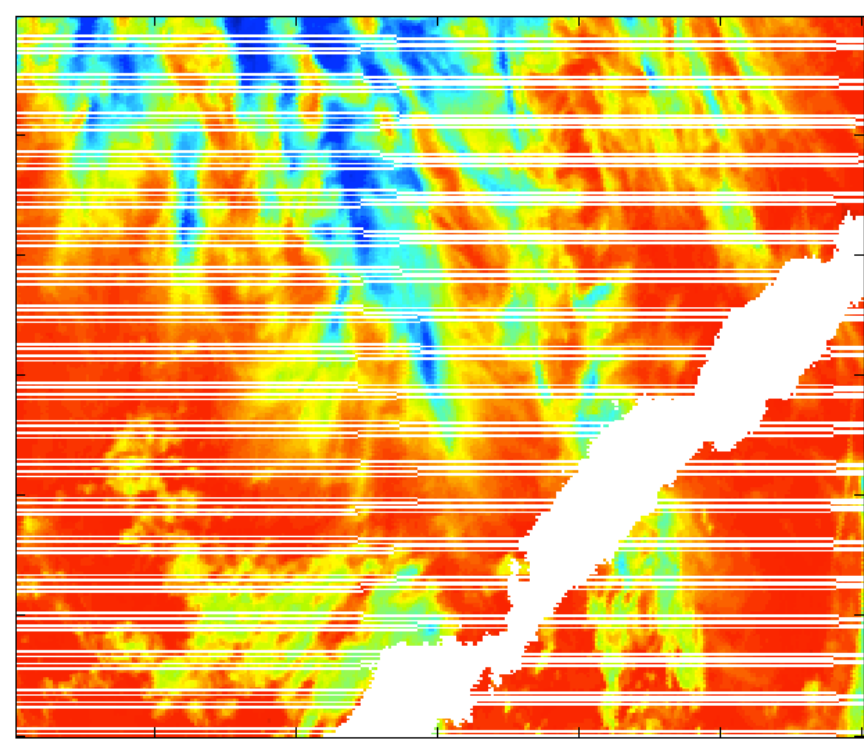
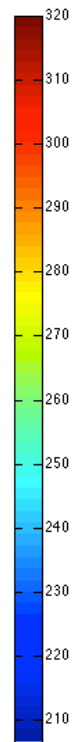
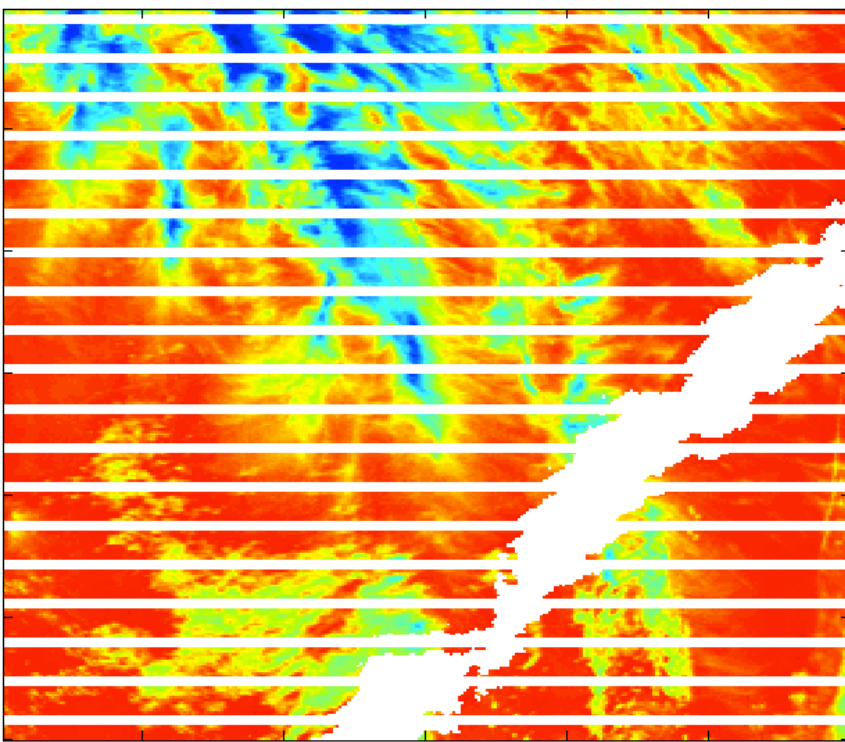
Swath imagery affected by bow-tie & small navigation misalignments



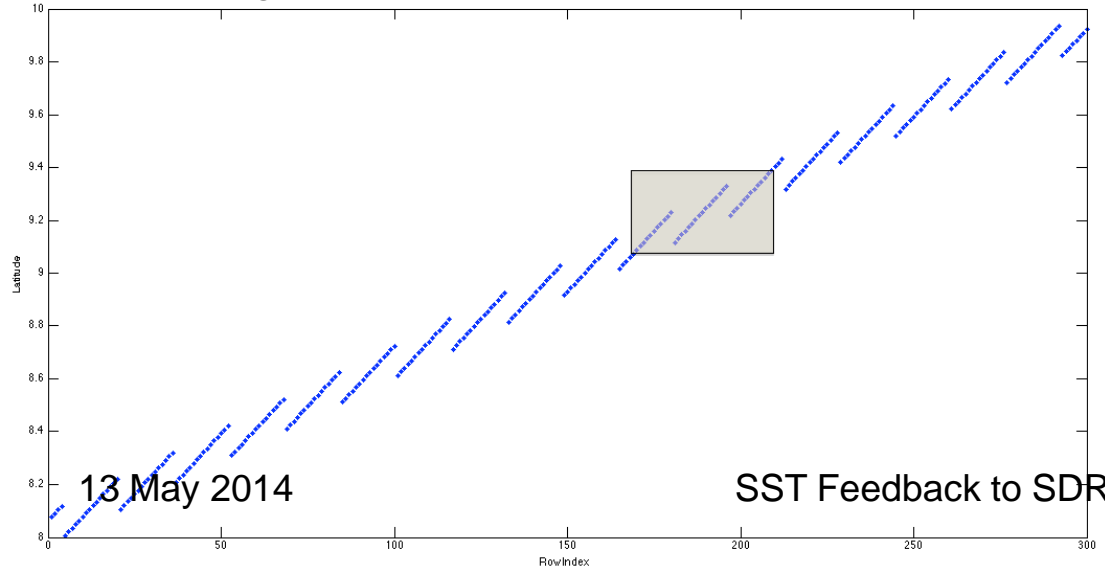
13 May 2014

SST Feedback to SDR

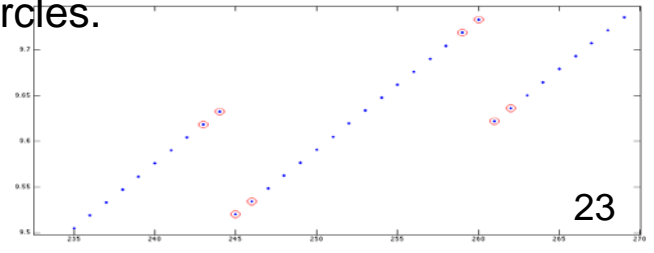
22



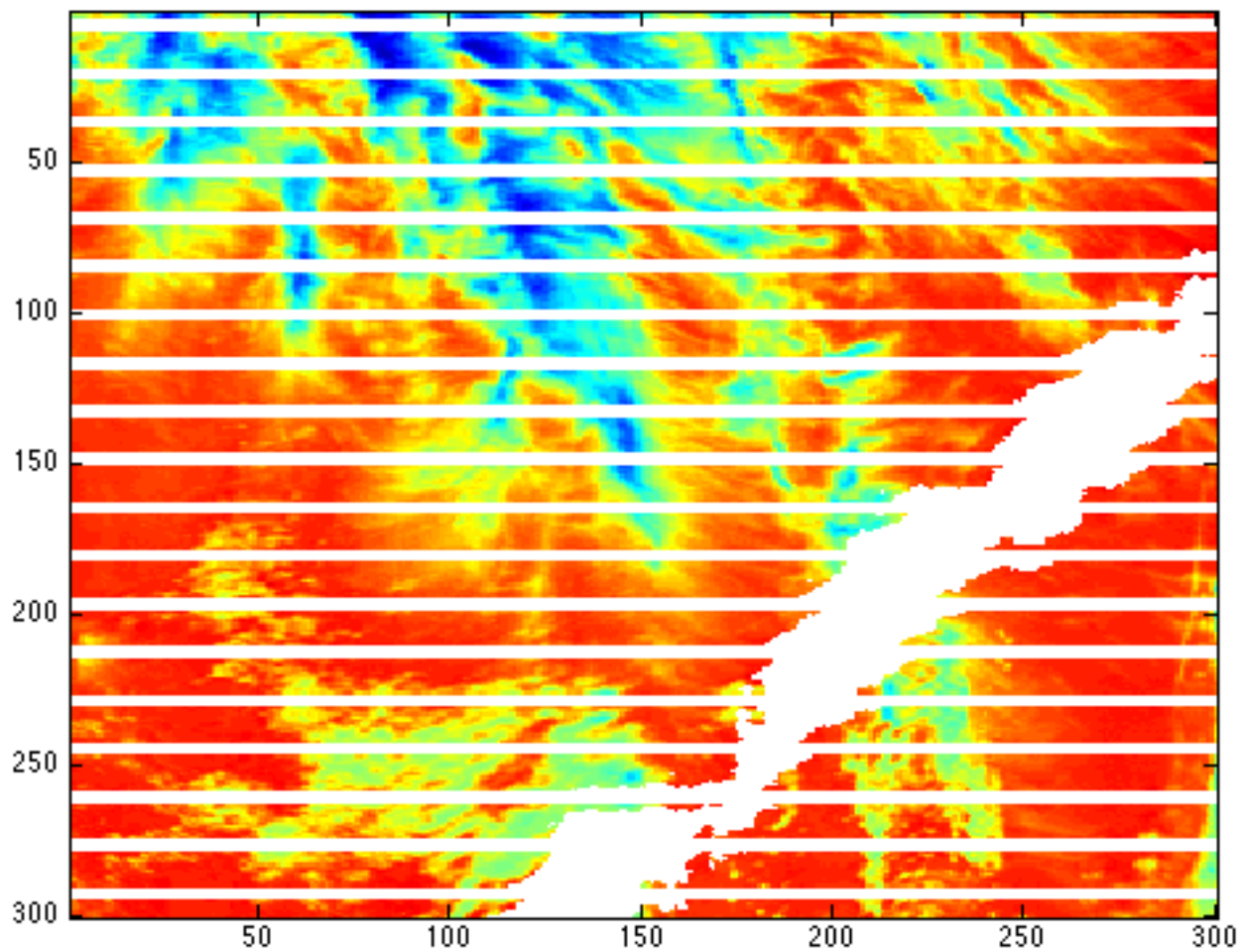
Left: Original SST Regression from ACSCO product. Right: Resampled Version corresponding to non-decreasing latitude values. The total number of “masked out rows” is the same as in original.



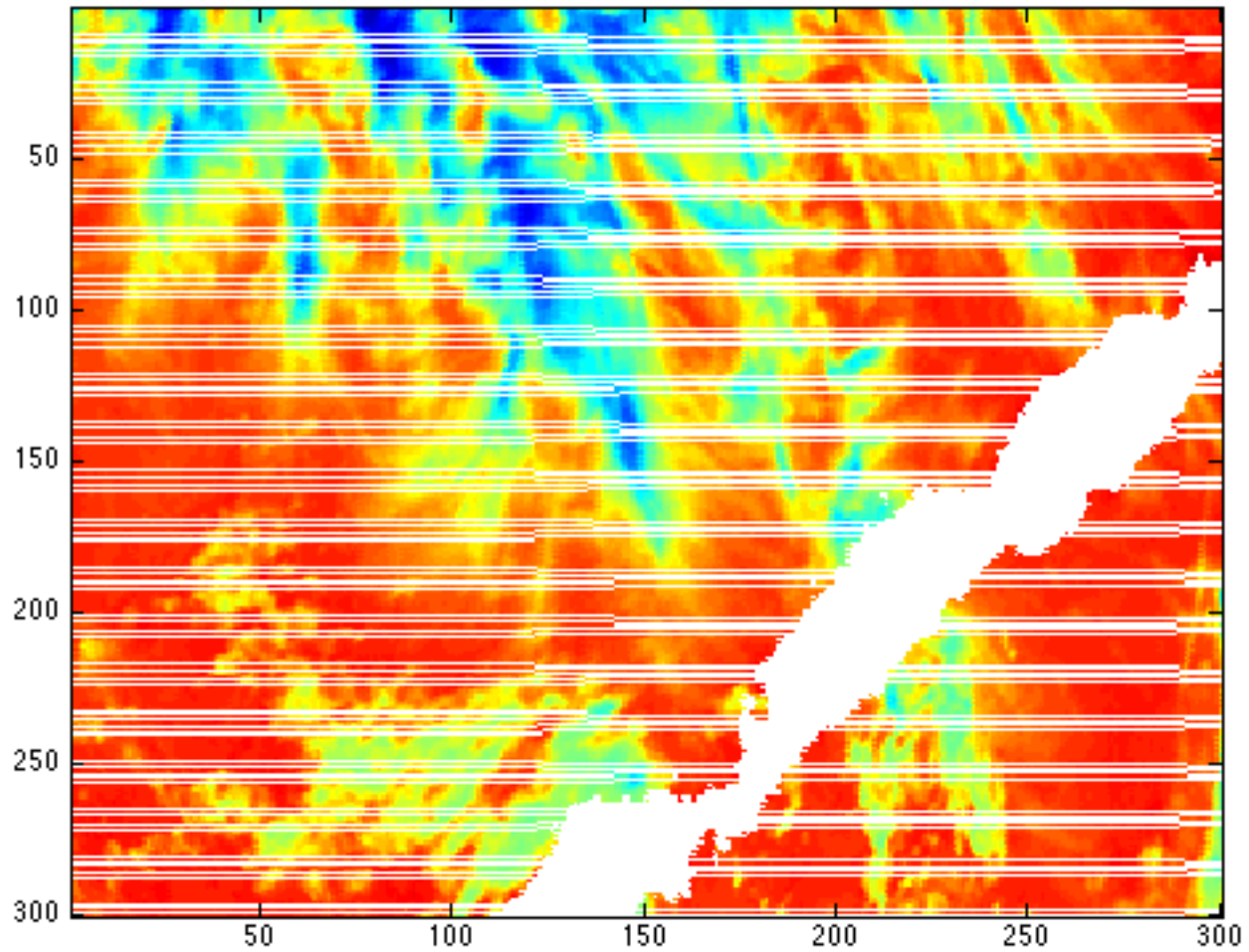
Overlapping pattern of latitude values for a fixed column. NaNs in SST correspond to locations marked by red circles.



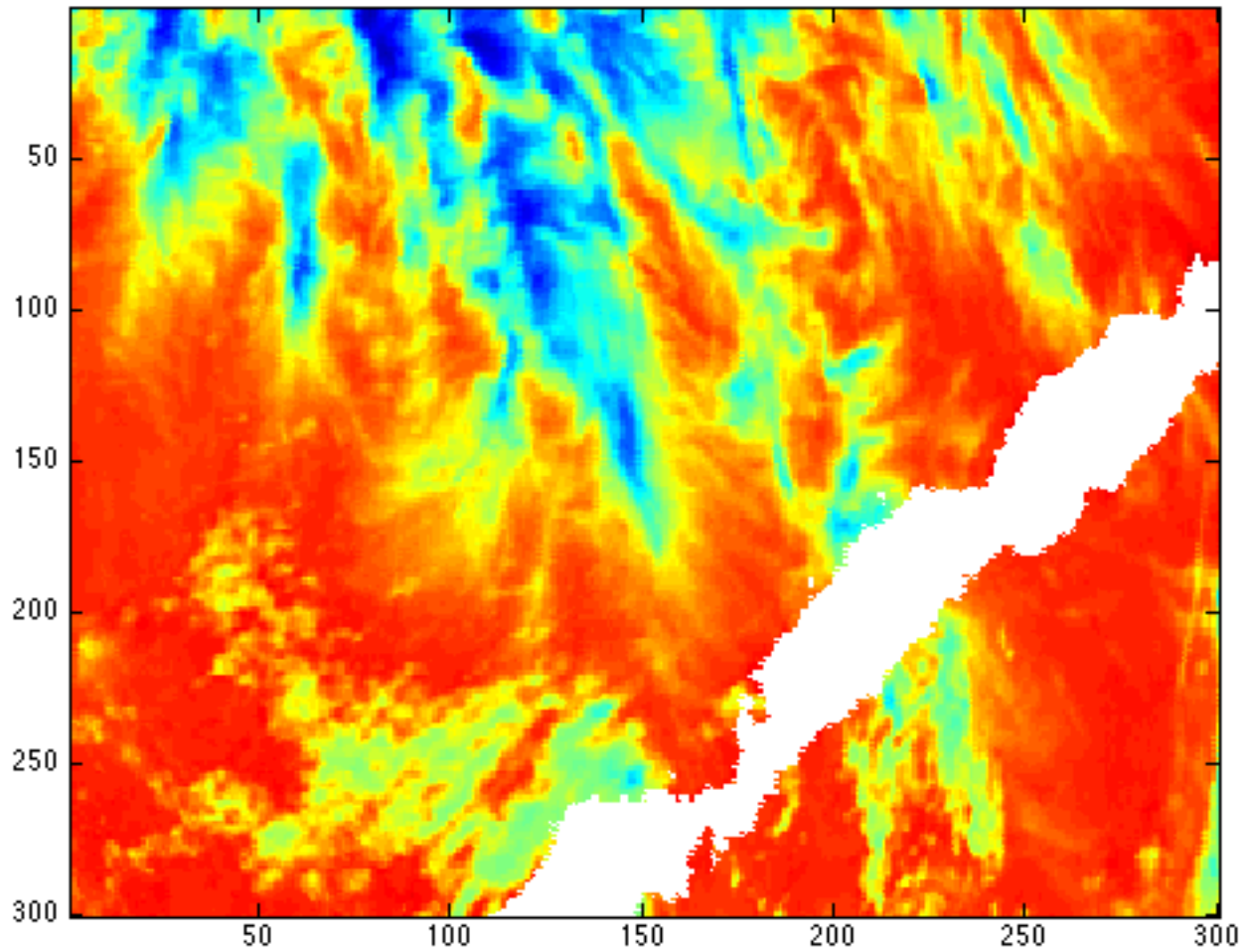
Original SST Regression Values at the bow tie region

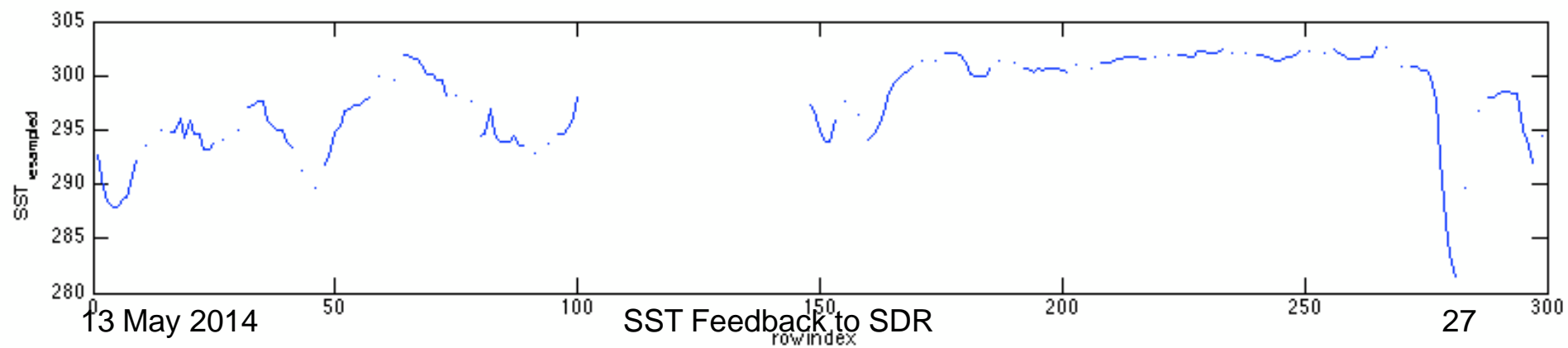
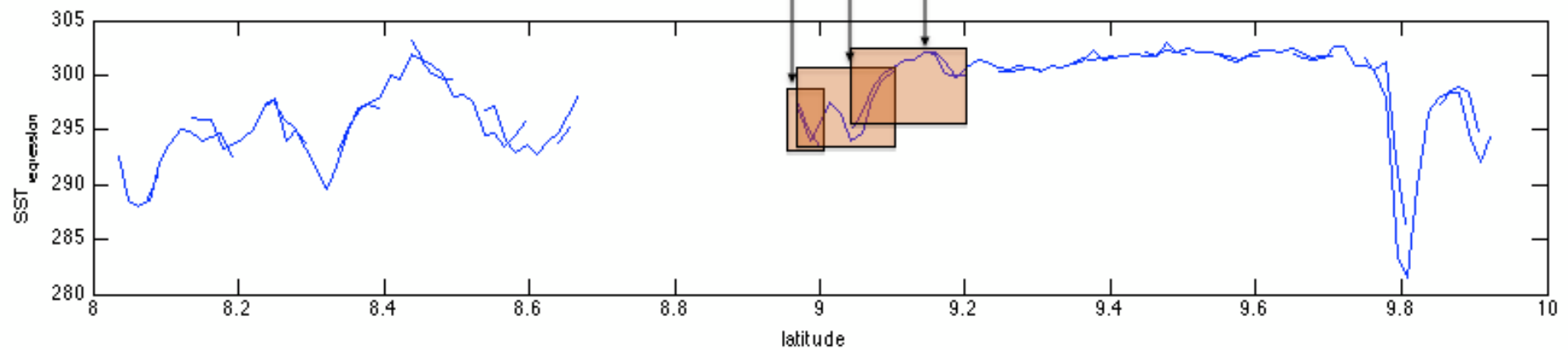
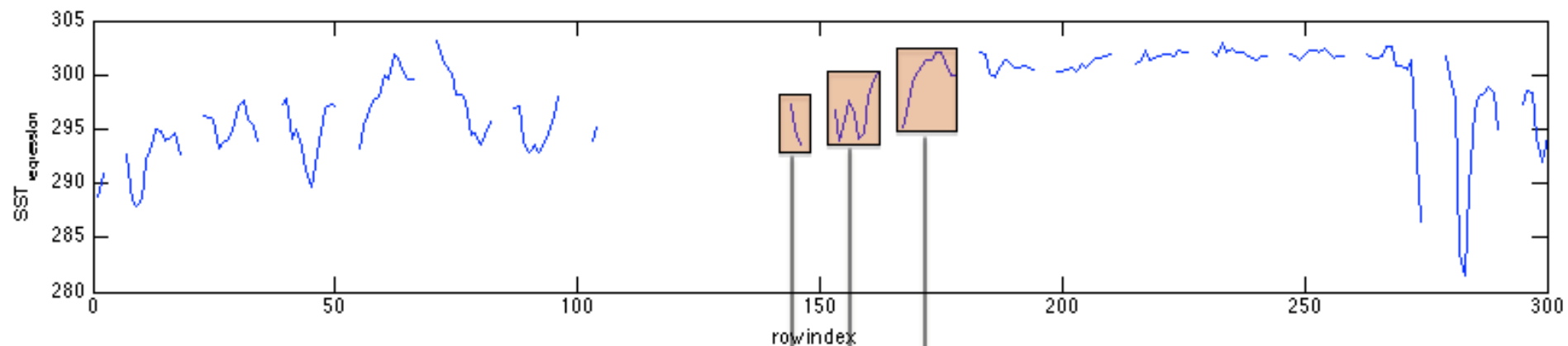


Resampled SST Values with monotonic Latitude values. No Interpolation

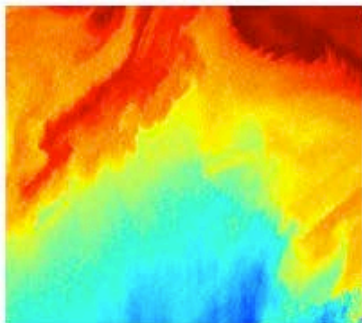


Resampled using 1D median filter over bow tie areas.

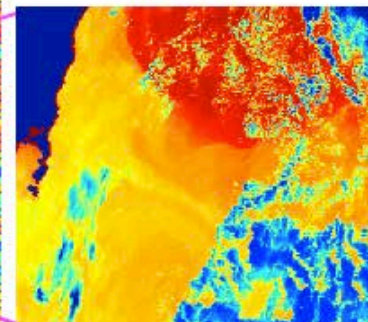




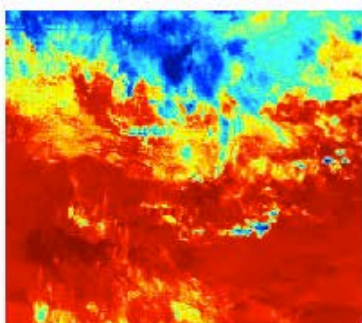
Crop 5



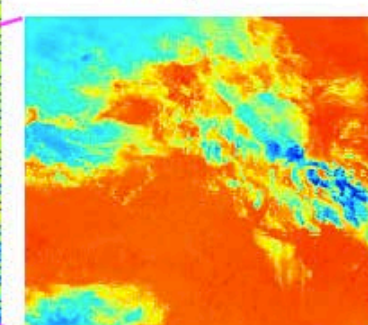
Crop 1



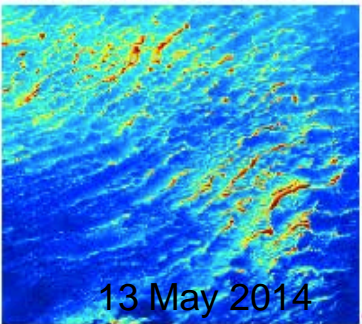
Crop 4



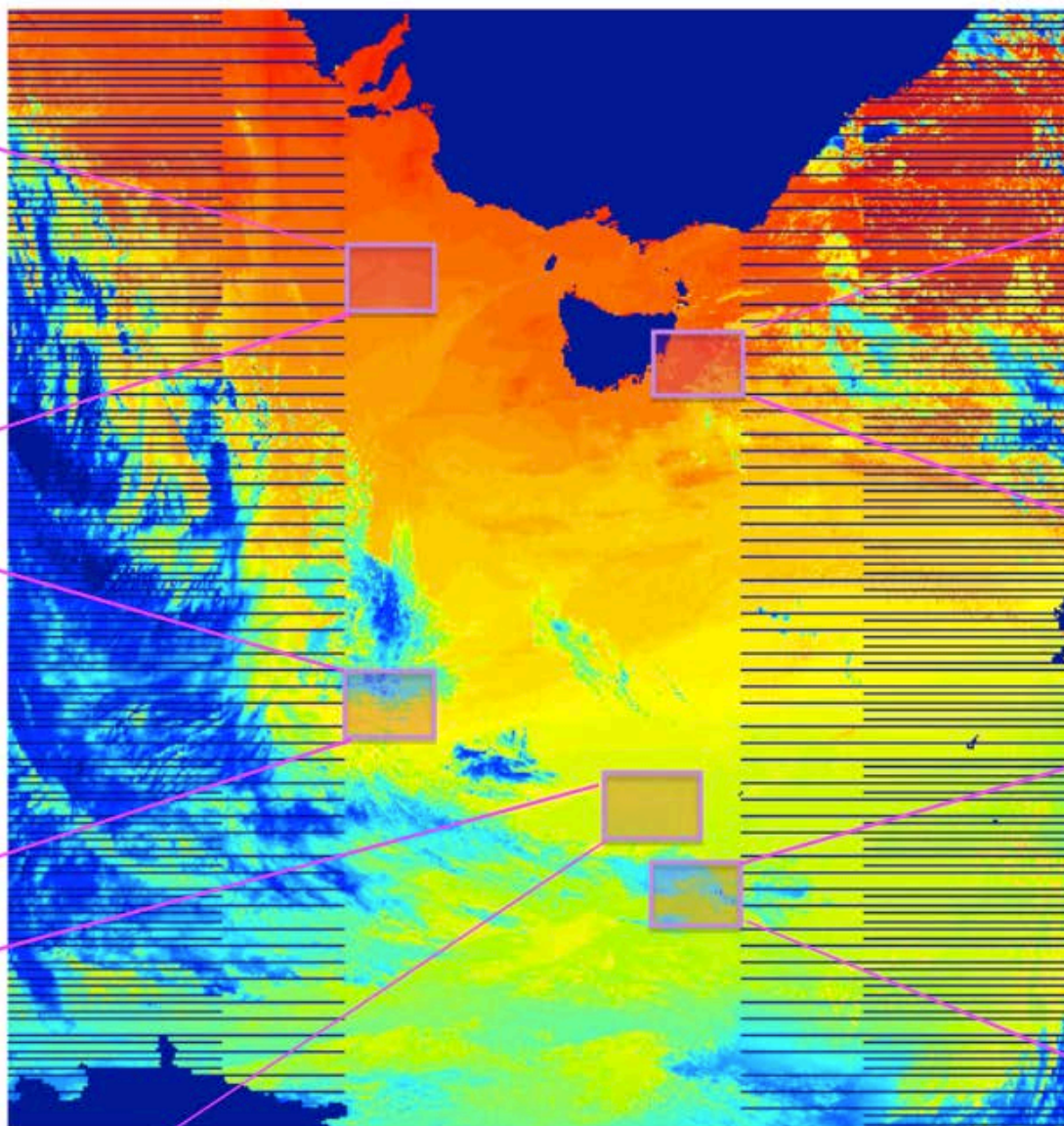
Crop 2



Crop 3



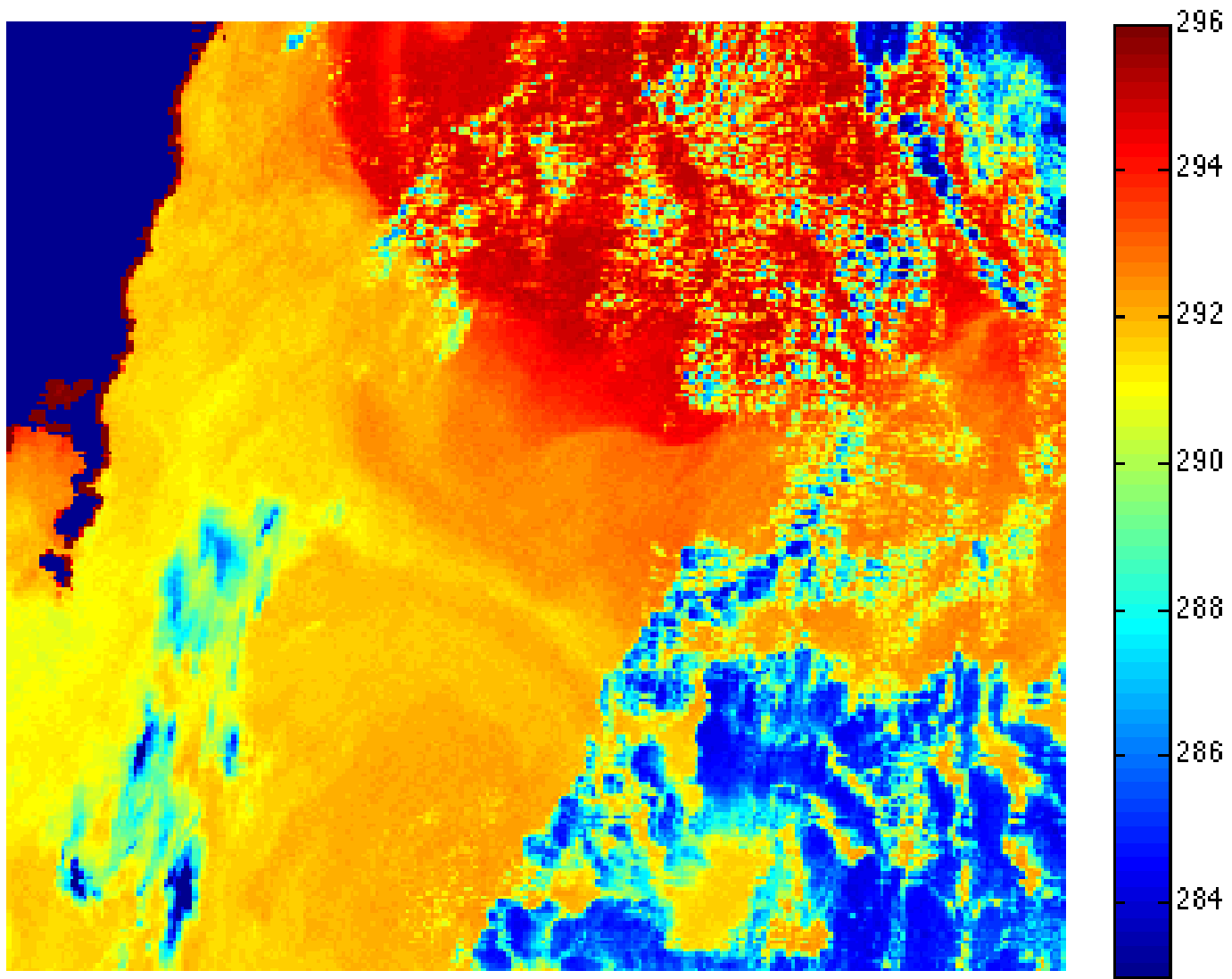
13 May 2014



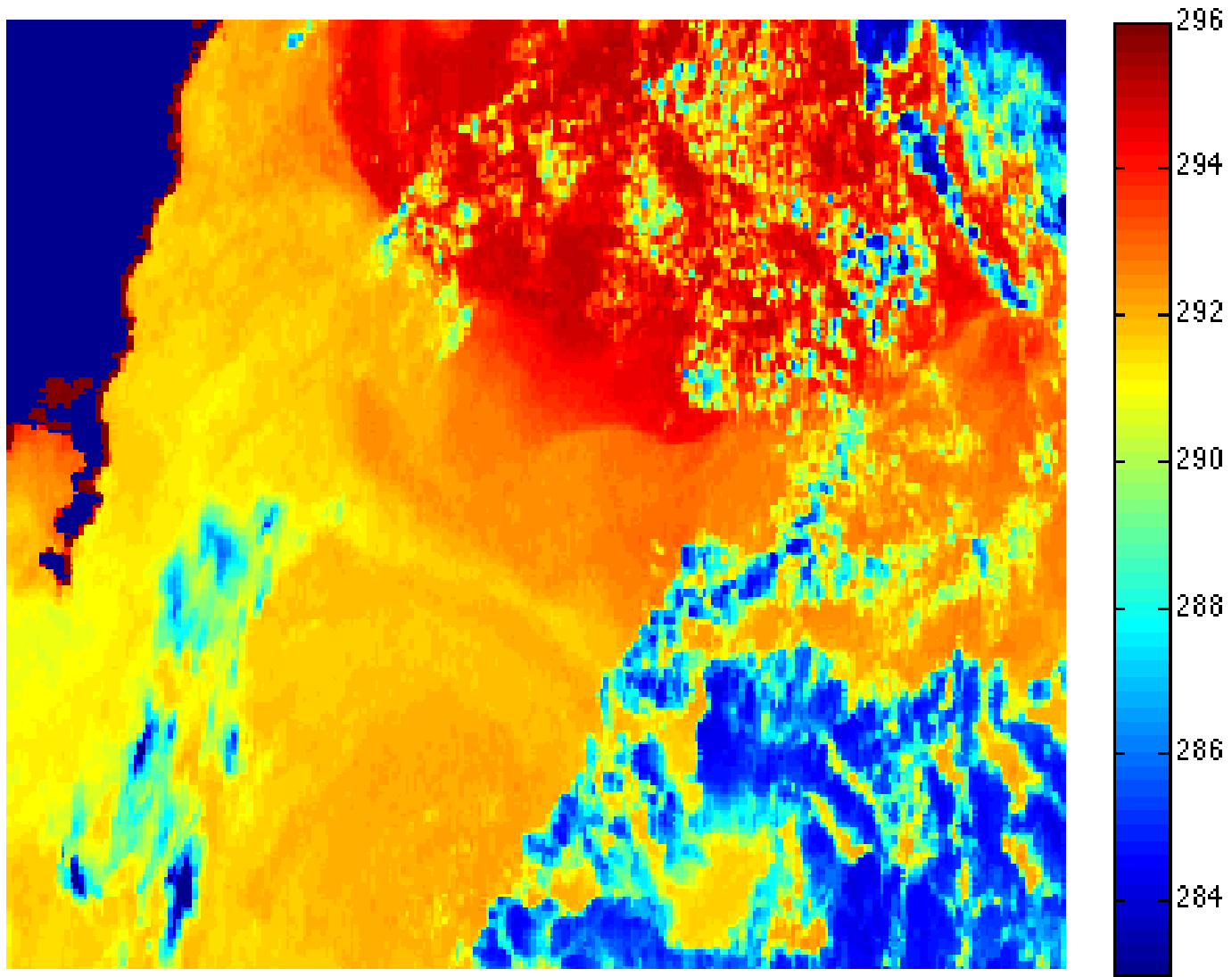
SST Feedback to SDR

ACSPO_V2.20_NPP_VIIRS_2013-02-16_0410-0419_20130219.232350.nc

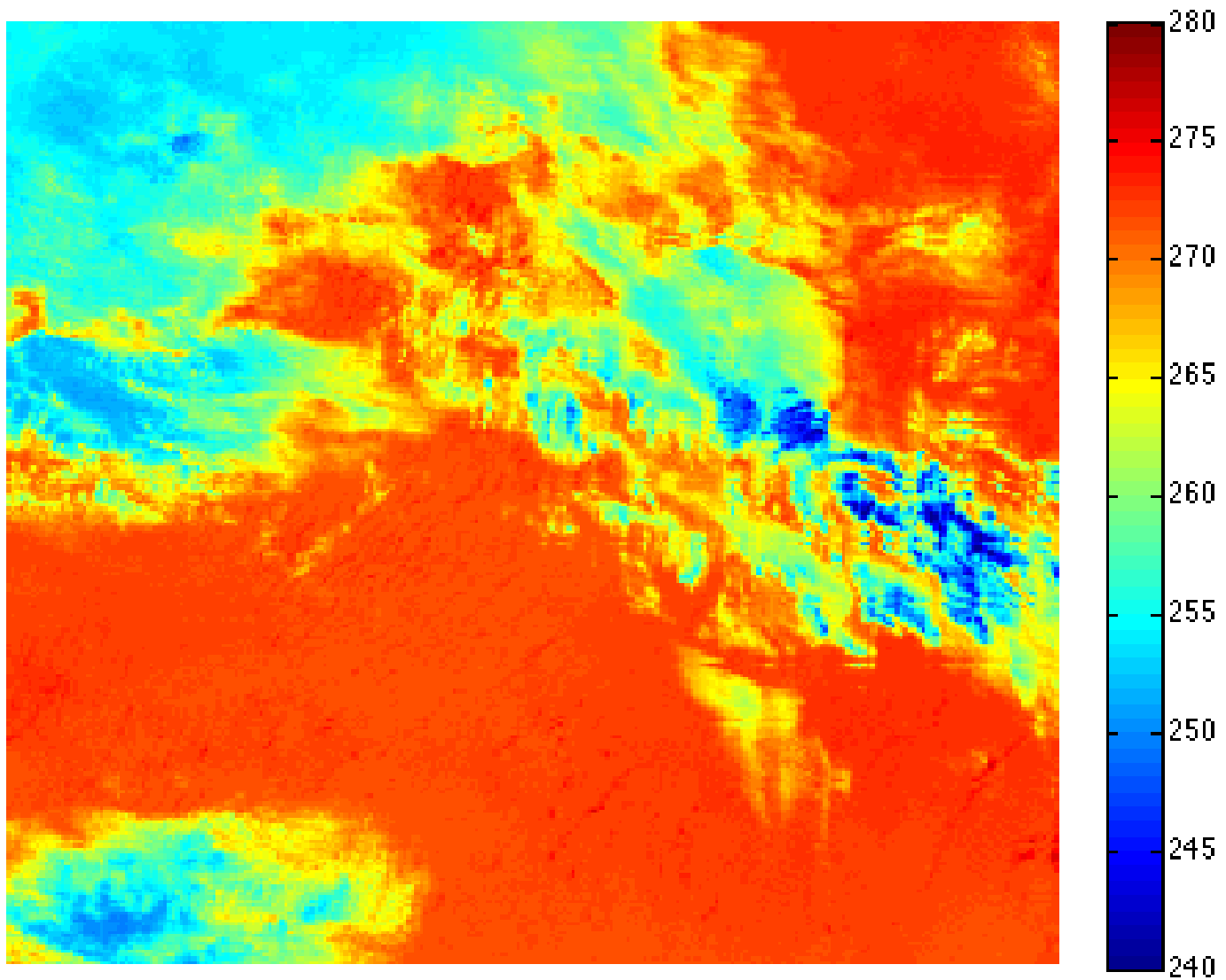
Retrieved SST: Crop 1



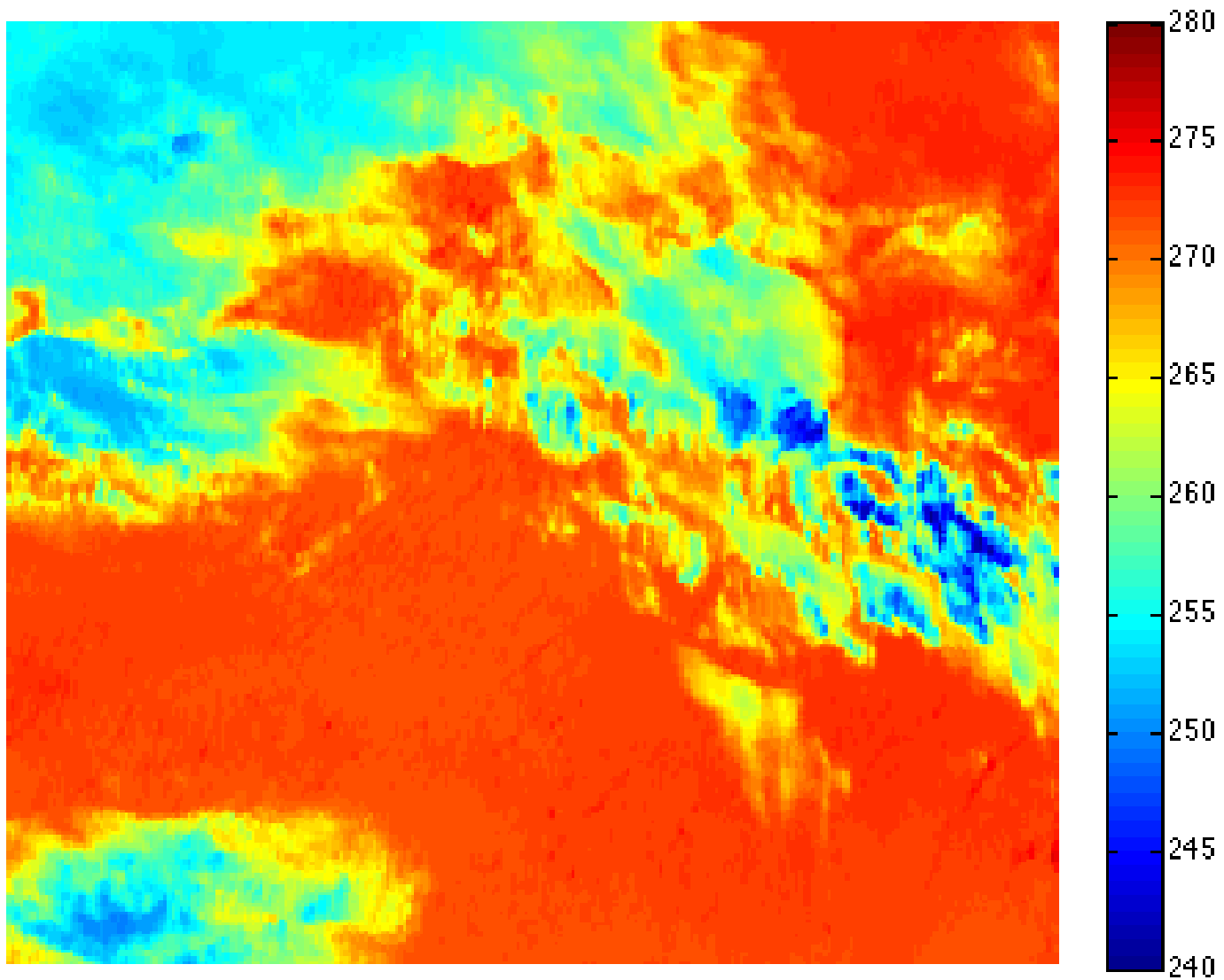
Resampled SST: Crop 1



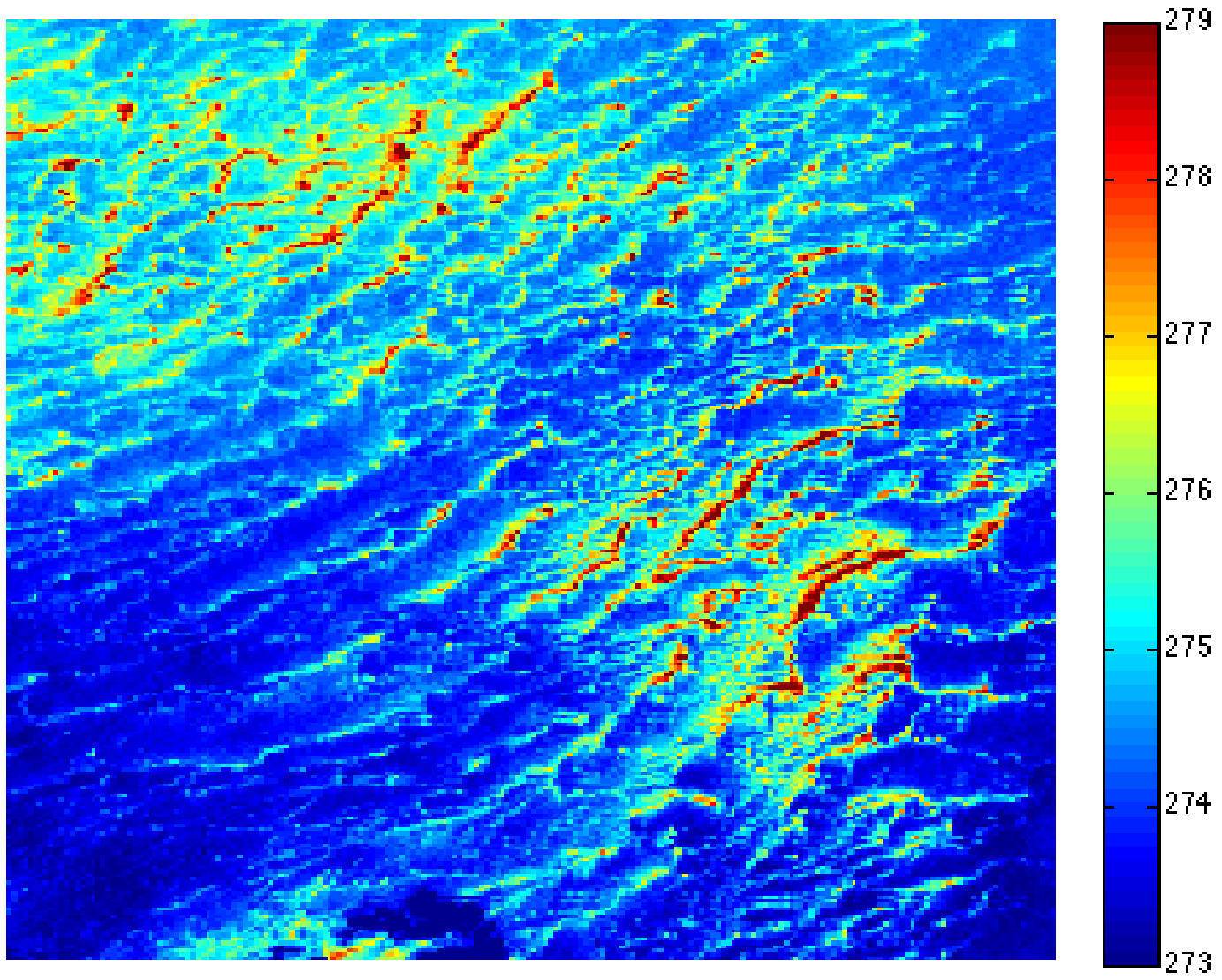
Retrieved SST: Crop 2



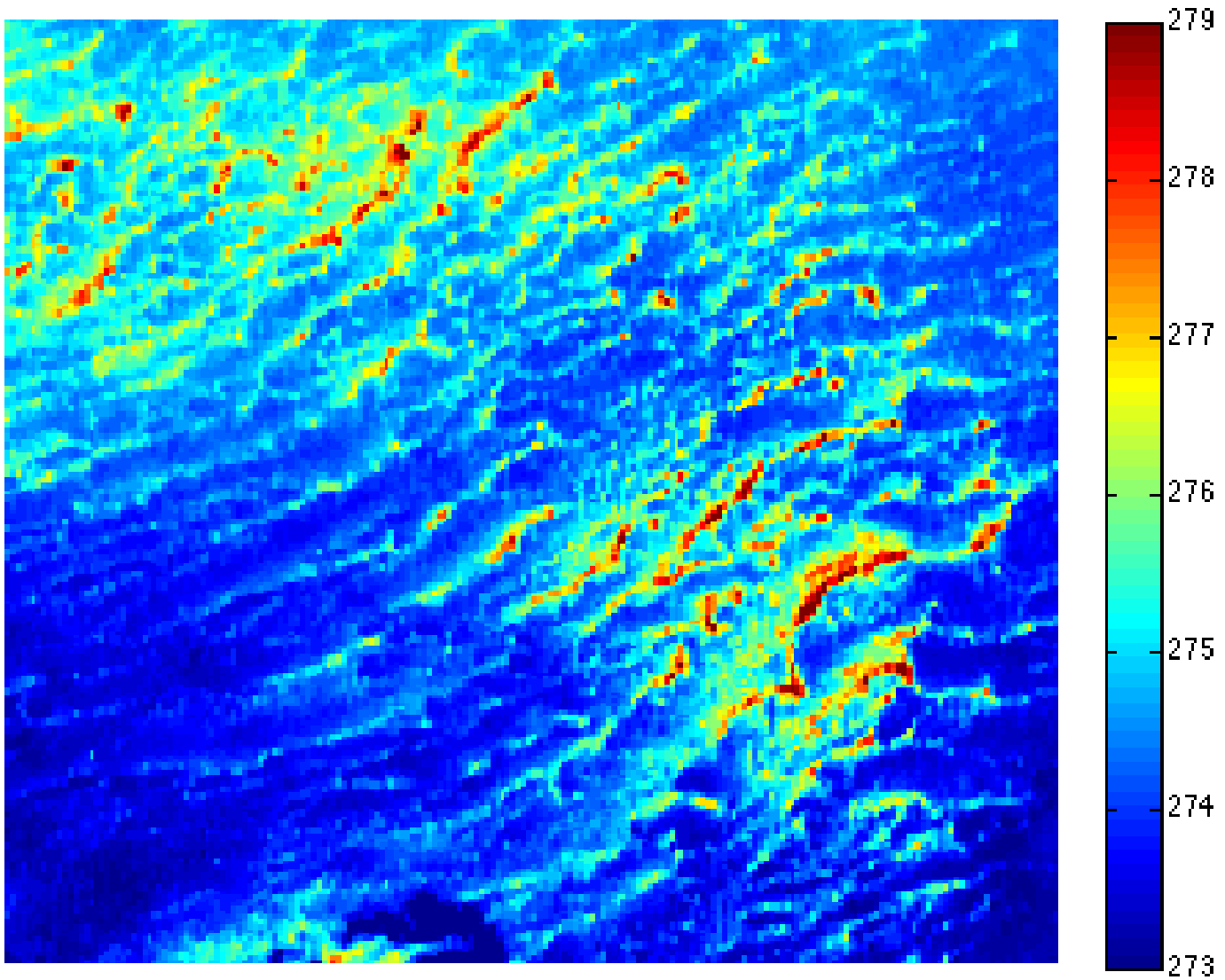
Resampled SST: Crop 2



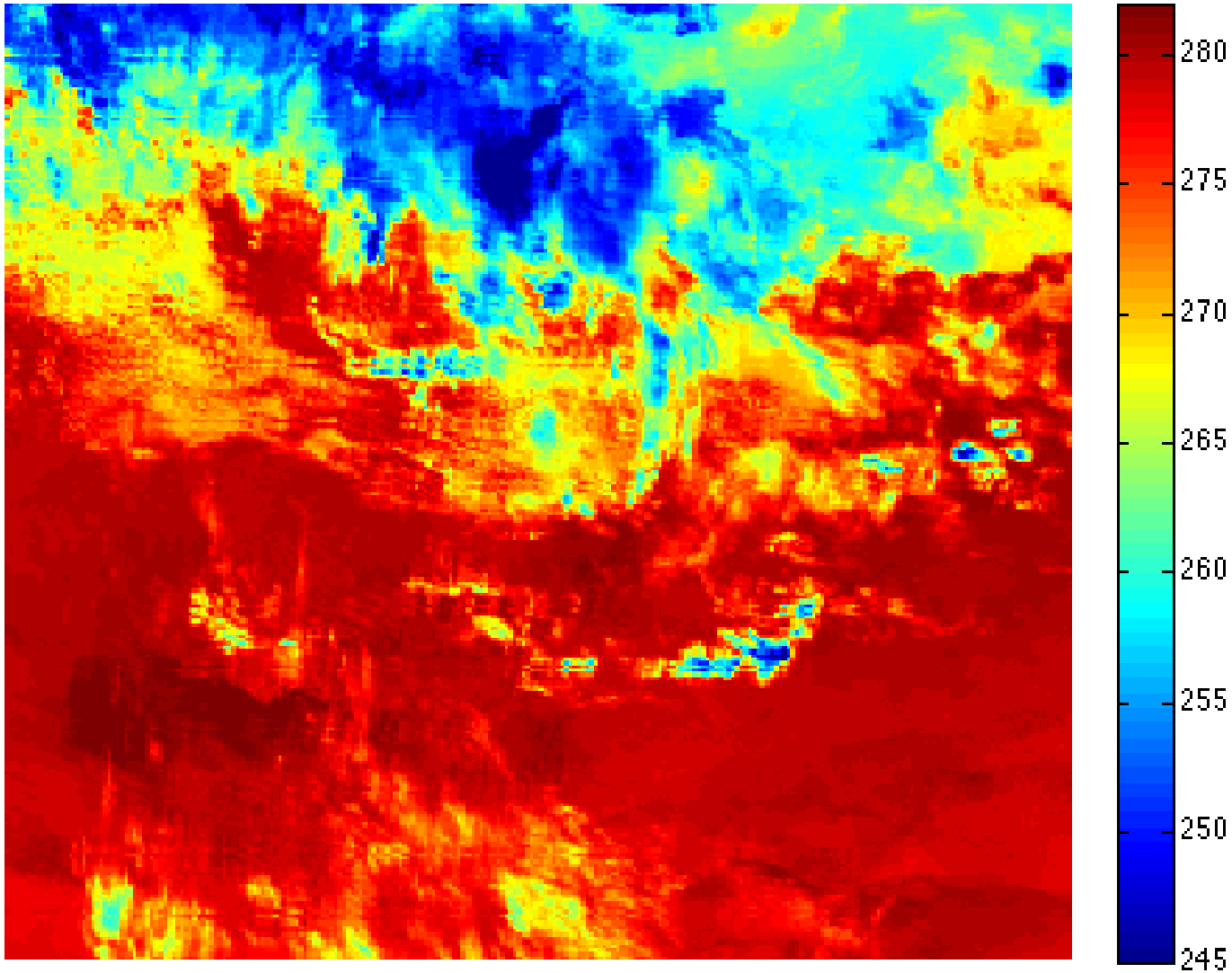
Retrieved SST: Crop 3



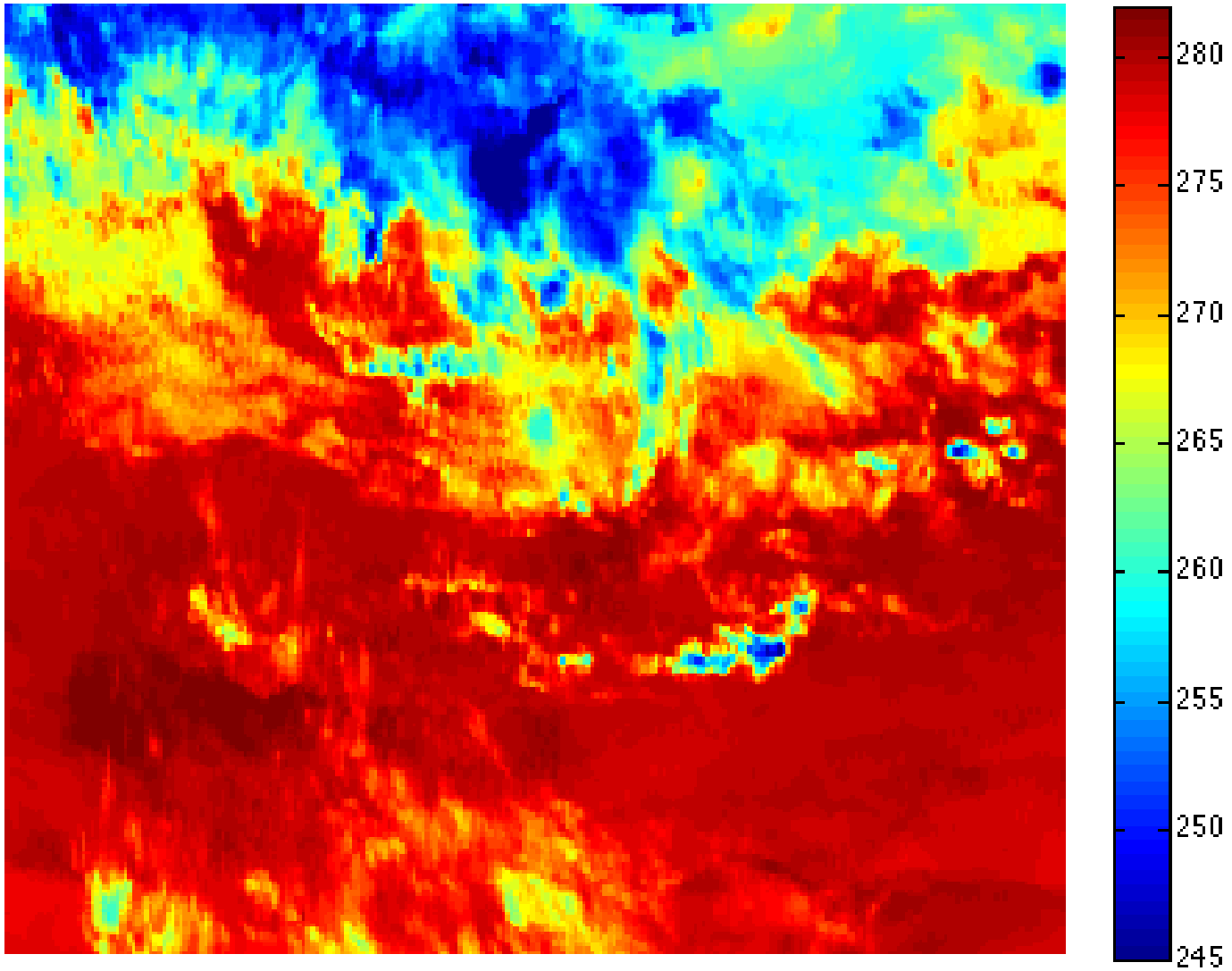
Resampled SST: Crop 3



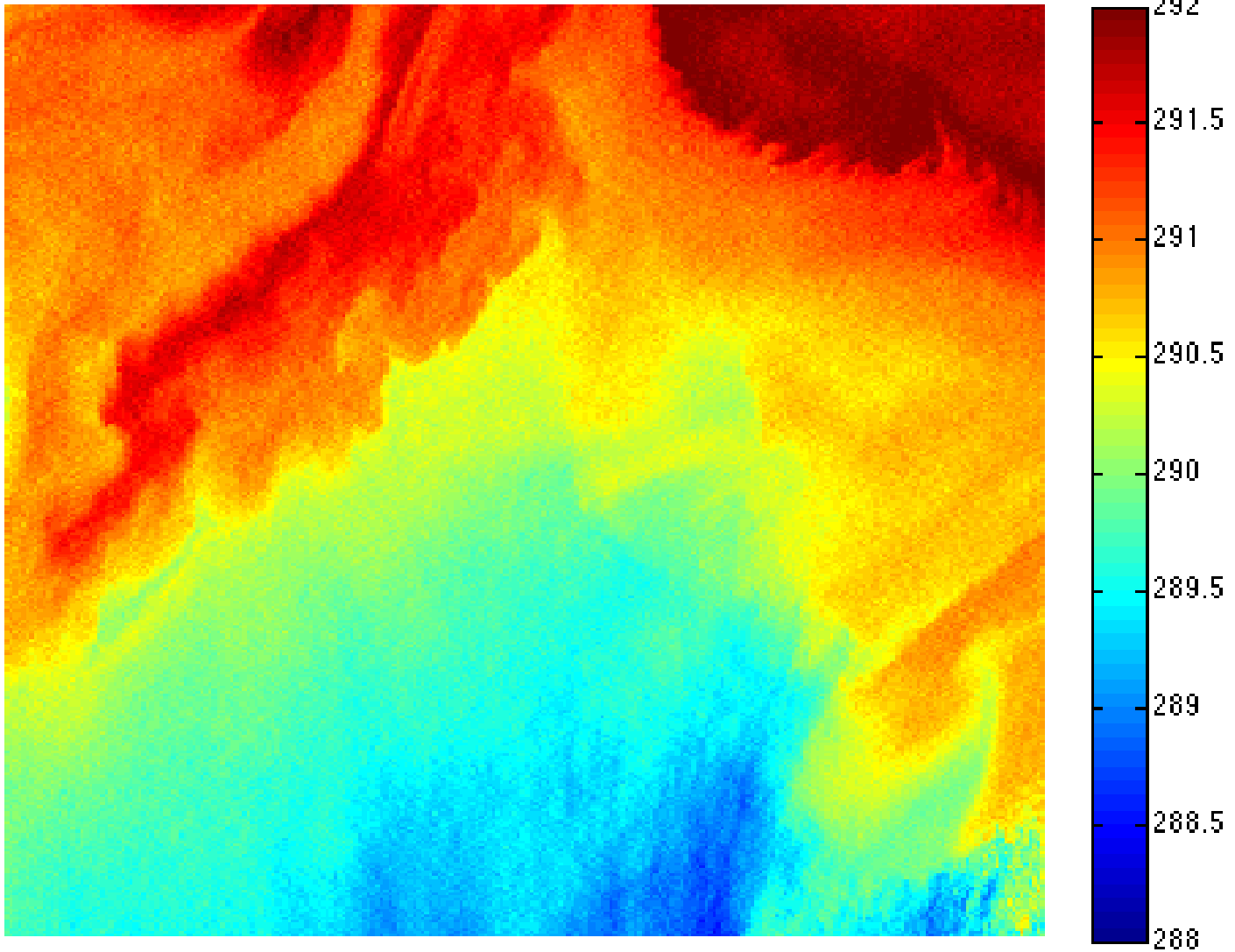
Retrieved SST: Crop 4



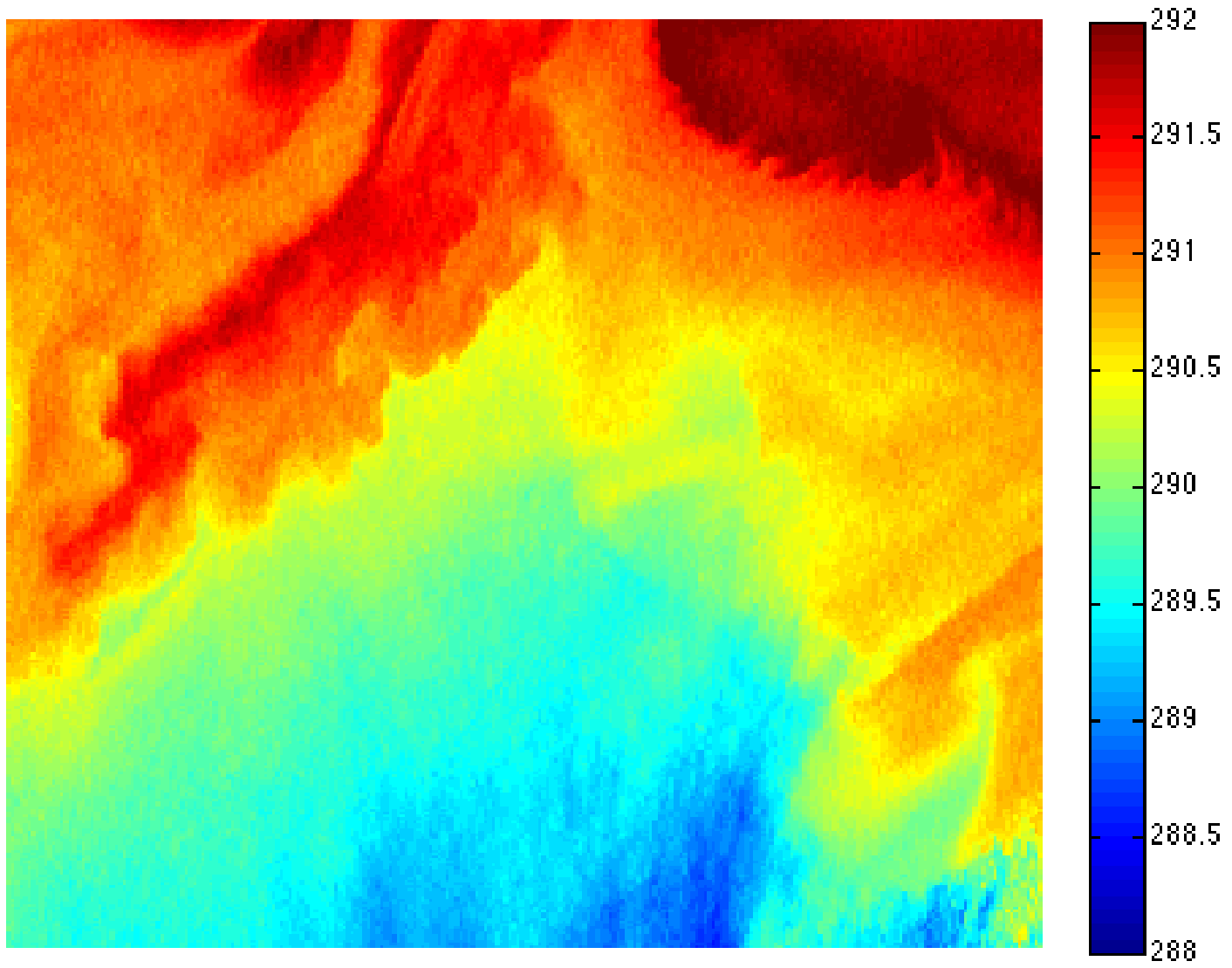
Resampled SST: Crop 4



Retrieved SST: Crop 5



Resampled SST: Crop 5



Conclusion

Overall, VIIRS is a very good, state of the art sensor for SST

- ✓ Radiances are stable (critical for regression SST)
- ✓ Radiances consistent w/AVHRR/MODIS (critical for physical SST)
- ✓ VIIRS imagery comparable or better than Aqua MODIS
- ✓ VIIRS striping comparable or better than Aqua MODIS

Striping affects SST

- ✓ Striping in VIIRS BTs is within specs. However, it
 - Affects the VIIRS cloud mask and prevents improvements
 - Gets amplified in SST
 - Affects downstream SST products (SST gradients)
- ✓ SST Team works with SDR to reduce striping based on 1st principles
- ✓ Also, SST Team explores destriping in BTs to improve SST EDR

Suggested Improvements

- ✓ Small navigation misalignments are corrected for, for cloud mask
- ✓ Fill in radiances in bow-tie areas. (Currently, filled in with NaNs – suggest put real numbers, while keeping the “bow-tie” flag on)

Visible Infrared Imaging Radiometer Suite

VIIRS TEB Detector-Level RSR Performance Effects

Francis Padula & Changyong Cao

NOAA/STAR

Suomi NPP SDR Product Review

With Contributions from:

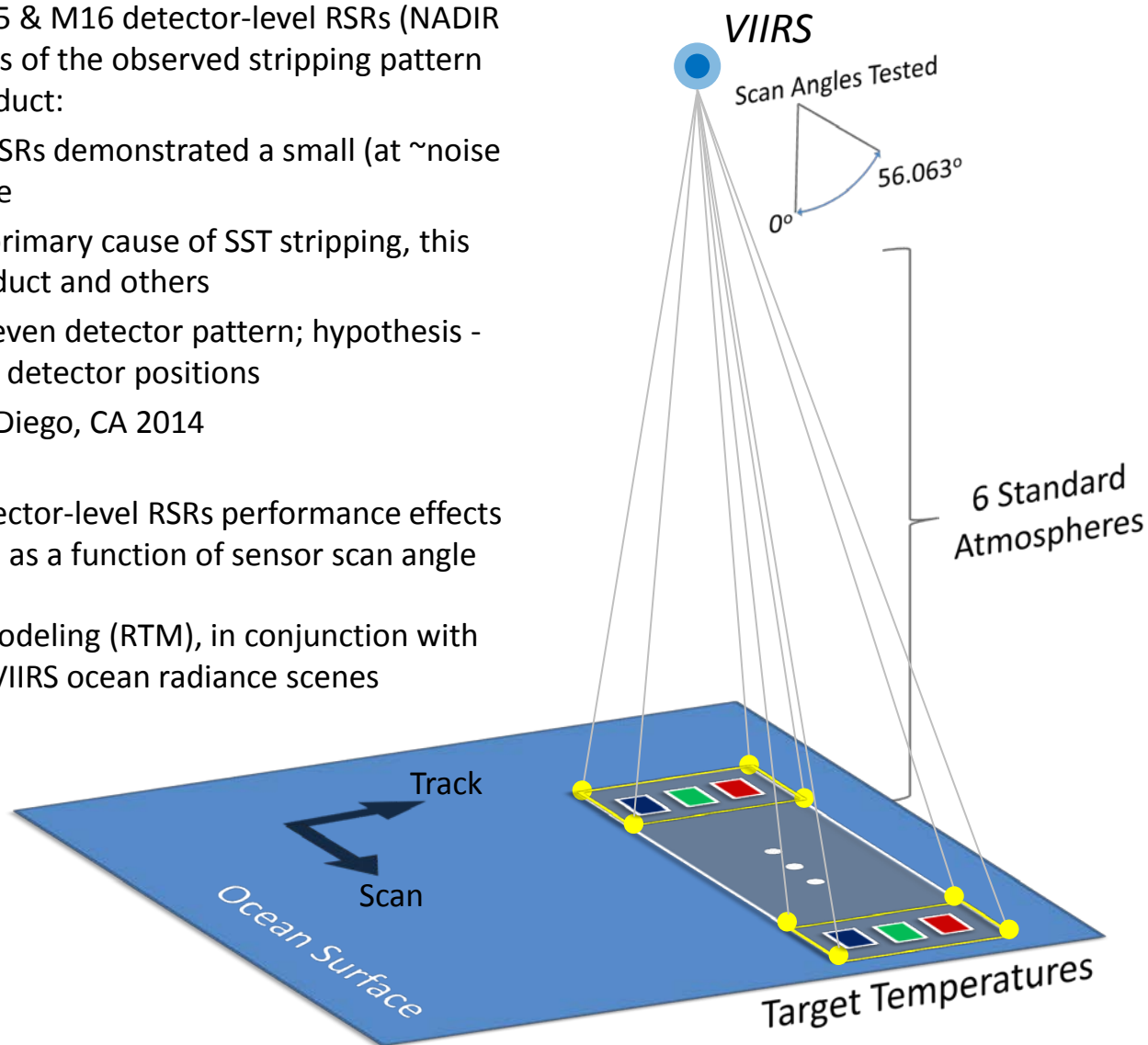
Aaron Pearlman, Slawomir Blonksi & Wenhui Wang

Background: Previously studied M15 & M16 detector-level RSRs (NADIR only) in support of root cause analysis of the observed stripping pattern in the daytime clear-sky SST EDR product:

- » M15 & M16 detector-level RSRs demonstrated a small (at ~noise level) atmospheric dependence
- » Though not likely to be the primary cause of SST stripping, this effect may impact the SST product and others
- » Observed a systematic odd/even detector pattern; hypothesis - this is likely due to the relative detector positions
- » To be presented at SPIE San Diego, CA 2014

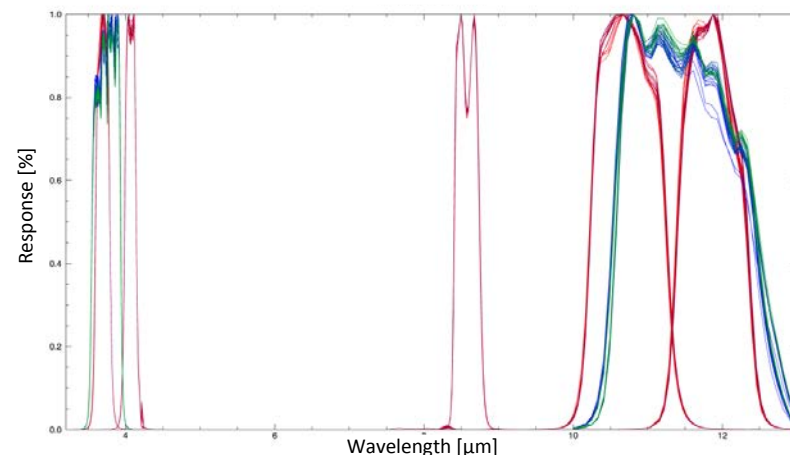
Objective: Investigate VIIRS TEB detector-level RSRs performance effects in response to different atmospheres as a function of sensor scan angle

Approach: Use Radiative Transfer Modeling (RTM), in conjunction with VIIRS RSR data, to simulate on-orbit VIIRS ocean radiance scenes

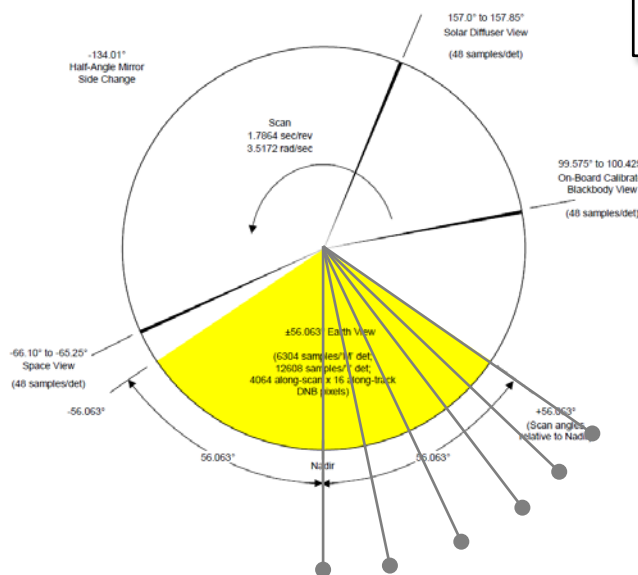


- » **Detector-Level VIIRS M & I TEB RSR Data:**
 - ng-viirs-npp-rsr-filtered-oct2011-ba-det
(<https://cs.star.nesdis.noaa.gov/NCC/SpectralResponseVIIRS>)
 - Provided by NG: system-level measurements performed in TVAC [IDPS Operational RSRs]
- » Six VIIRS scan angles tested:
[0.0°, 10.744°, 21.566°, 32.568°, 43.932°, 56.063°]
- » Sensor altitude of 829 km (at equator)

VIIRS Detector-Level RSRs

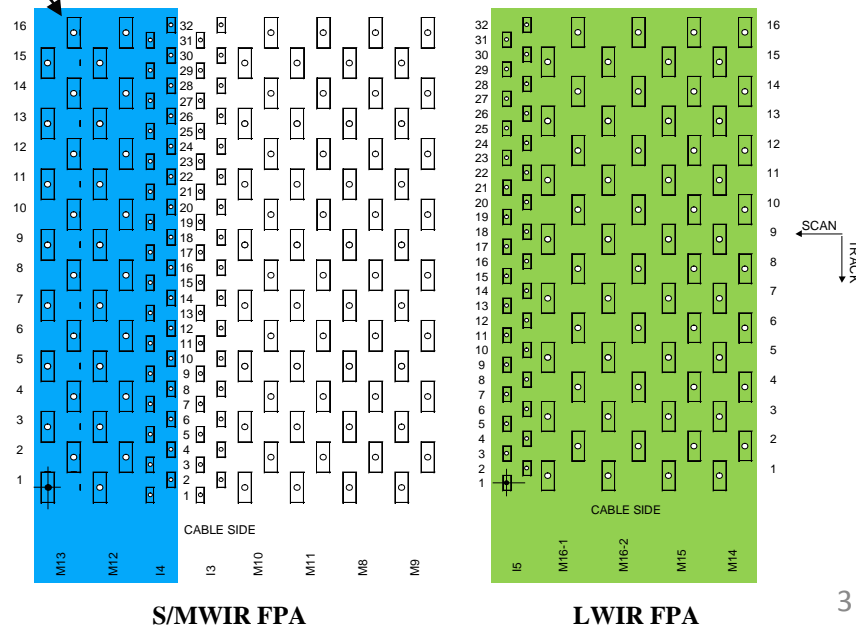


VIIRS Scan Pattern¹



Note the Odd/Even Layout of Detectors

VIIRS Detector Layout¹

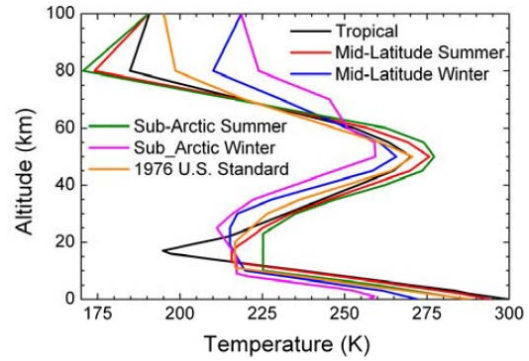


¹Images Courtesy of JPSS VIIRS SDR Radiometric Calibration ATBD

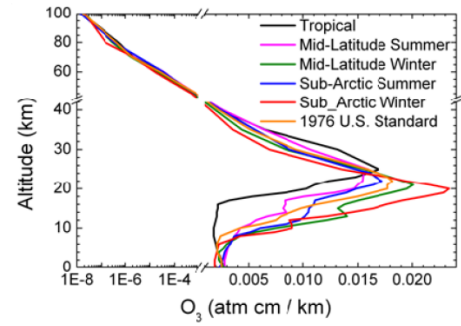
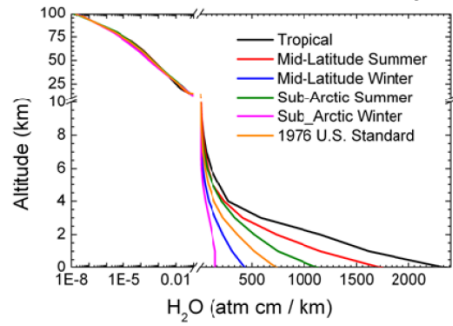
Simulated Radiance Data:

- » **RTM:** MODTRAN (v5.3.2)
- » **Spectral Range:** 3333 to 741 wn (3 to 13.5 μm)
- » **Spectral Resolution:** 1 wn
- » **Time of Day:** Nighttime
- » **Atmospheric profiles:** (6 Atmospheres) Tropical, Mid Latitude Summer (MLS), Mid Latitude Winter (MLW), U.S. Standard (USS), Sub-Arctic Summer(SAS), Sub-Arctic Winter (SAW)
- » **Boundary Layer Aerosol:** Maritime - VIS = 23 km
- » **Surface Target:** Water
- » **Surface Emissivity:** 0.985
- » **Surface Temperature:** 3 SST temperatures used for each atmosphere (T_{min} , T_{nominal} , T_{max})

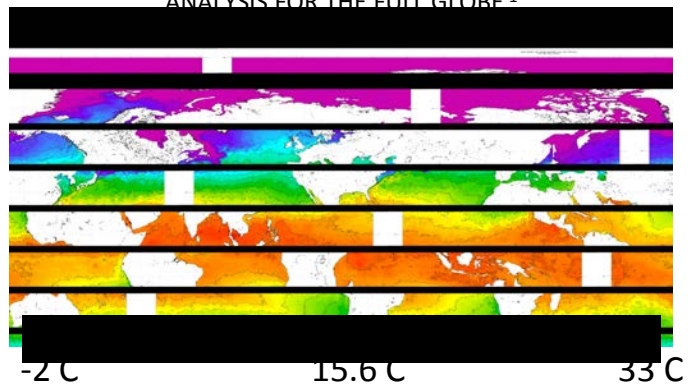
6 MODTRAN Standard Atmospheres²



H₂O & O₃ Density Profiles



NOAA/NESDIS GEO-POLAR BLENDED 5 km SST ANALYSIS FOR THE FULL GLOBE¹



	Tropical [K]	MLS/MLW/USS [K]	SAS/SAW [K]
T_{min}	290.15 (17 C)	273.70 (0.6 C)	271.71 (-1.4 C)
T_{nominal}	297.75 (24.6 C)	287.15 (14 C)	277.75 (4.6 C)
T_{max}	306.15 (33 C)	299.15 (26 C)	283.15 (10 C)

Temperature Range: 271.71 to 306.15 K

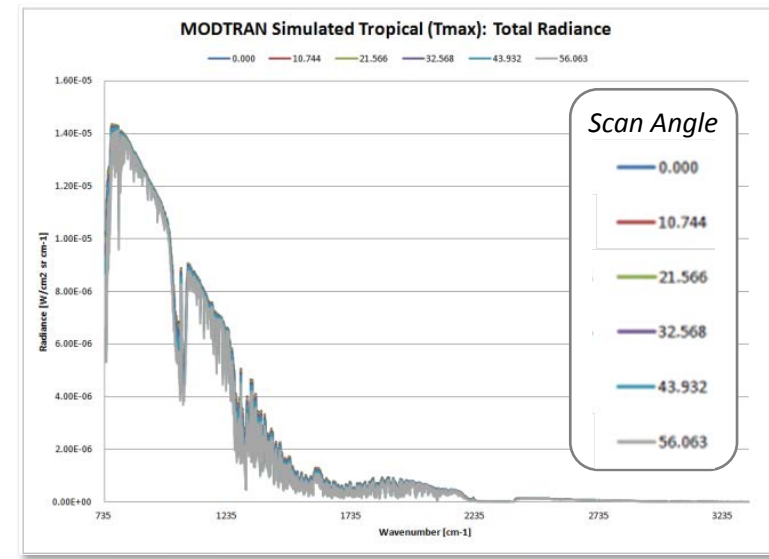
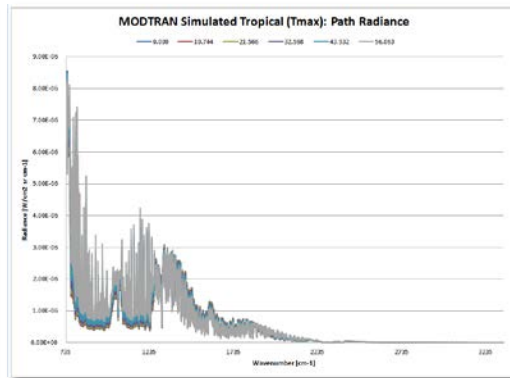
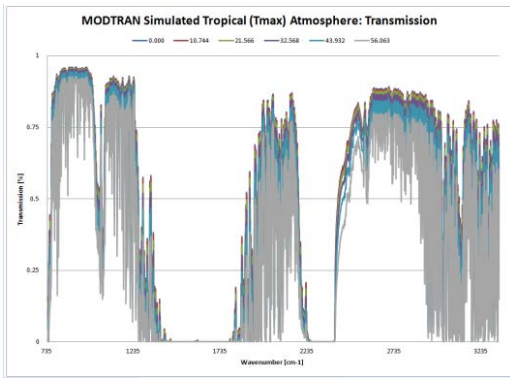
¹<http://www.ospo.noaa.gov/Products/ocean/sst/contour/index.html>

²Atmospheric graphics courtesy of MODTRAN Users Manual (5.3)

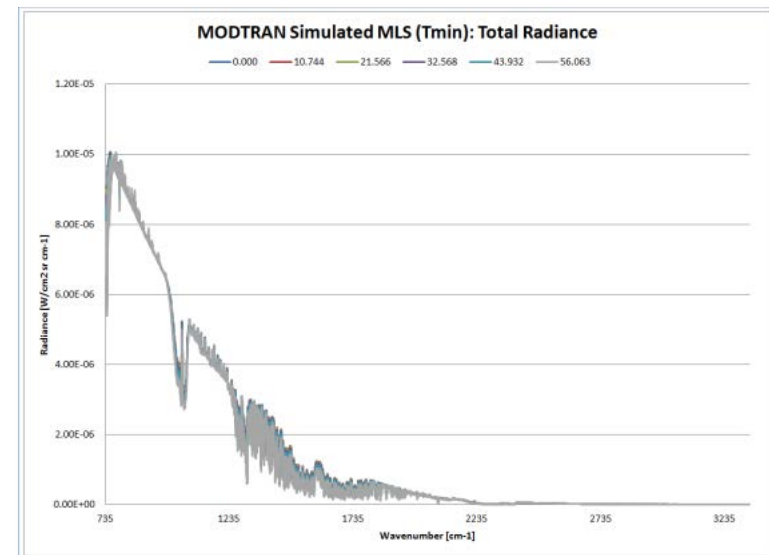
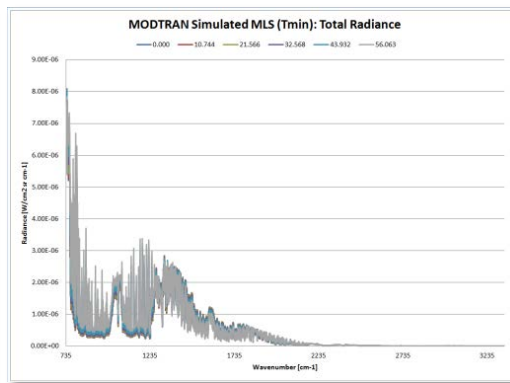
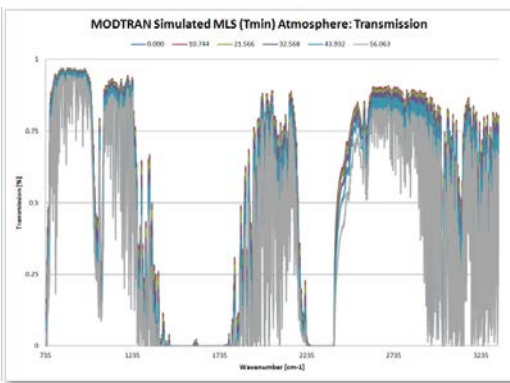
Example of Competing Atmospheric Effects

Primary Atmospheric Contributors

Total Radiance



Tropical Atm @ T_{max} - **atmospheric Transmission term dominates** ➡

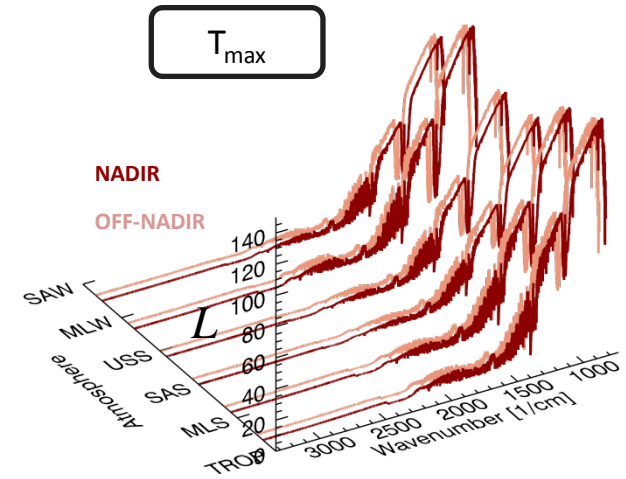
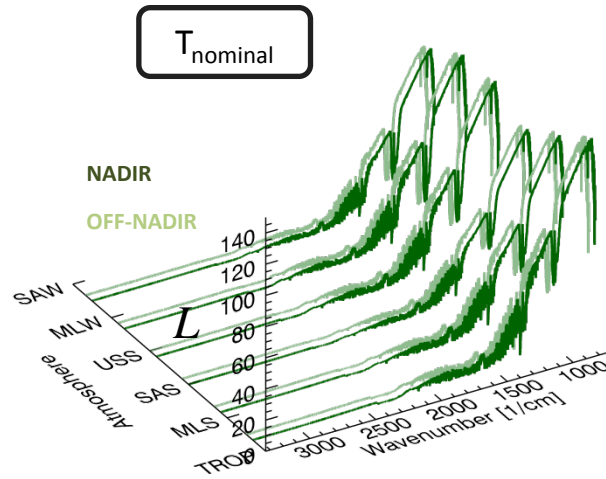
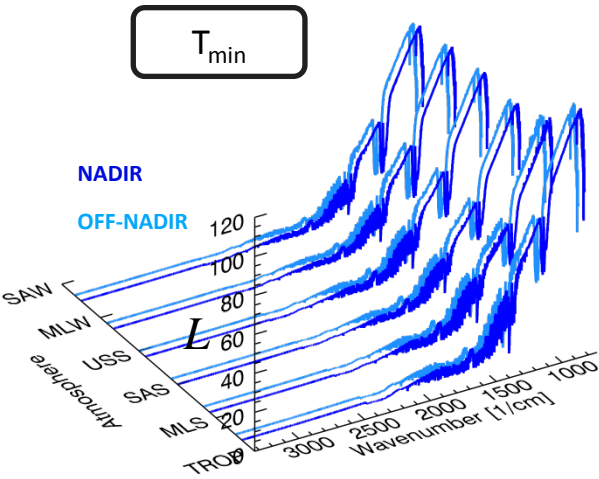


MLS Atm @ T_{min} - **atmospheric Upwelling radiance term dominates** ➡

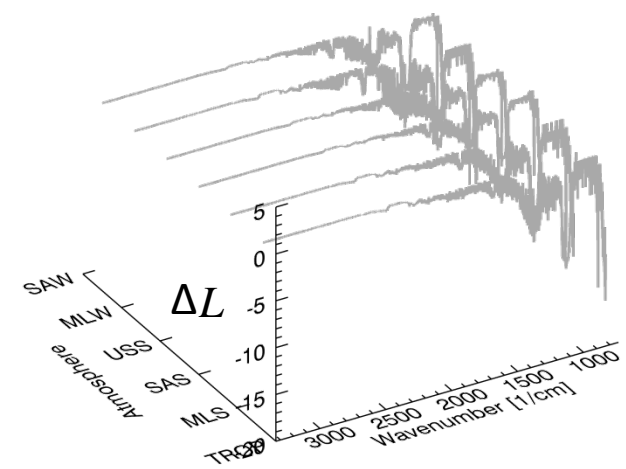
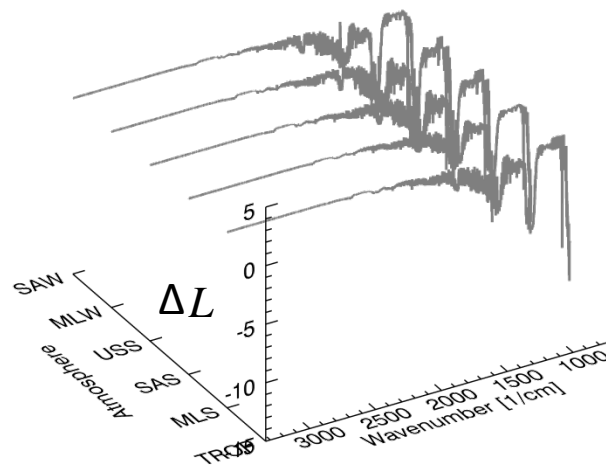
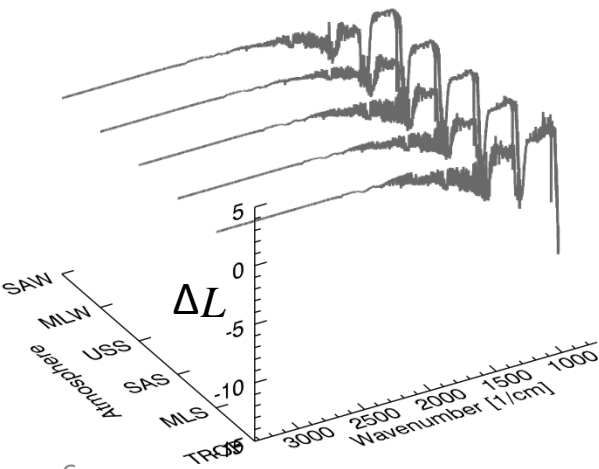
MODTRAN Derived Radiance:

NADIR (0°) & OFF-NADIR (56.063°)

Simulated Radiance (L) [$\text{mW}/\text{m}^2 \text{sr cm}^{-1}$]



$\Delta L = \text{OFF-NADIR}(L) - \text{NADIR}(L)$ [$\text{mW}/\text{m}^2 \text{sr cm}^{-1}$]



- » Calculated channel effective spectral radiance (L_{eff}) for each VIIRS TEB:
 - Using the detector-level & band averaged RSR data and the MODTRAN simulated radiances [Eq 1]
- » Converted radiance to effective temperature (T_{eff}) using a LUT of radiance and temperature pairs approach

Analysis:

- » Qualitative & quantitative analysis conducted

Metric of comparison:

$$\Delta T_{eff} = T_{eff \text{ detector RSR}} - T_{eff \text{ band avg. RSR}}$$

Interpreted as:

$$\Delta T_{eff} = (T_{eff \text{ band avg. RSR}} - \text{Operational [IDPS]})$$

Note:

- 1) Radiometric differences between the band average & detector level RSRs, when viewing a calibration source, are small relative to system requirements
- 2) Radiometric differences between the band average & detector level RSRs, when viewing earth scenes, can be larger due to earth & atm. spectral phenomenology

Goal: determine if any atmospheric dependencies exist between VIIRS TEB band average and detector-level RSRs

L sensor reaching radiance
MODTRAN Results

$$L_{eff} = \frac{\int_{\lambda_1}^{\lambda_2} L R'_\lambda d\lambda}{\int_{\lambda_1}^{\lambda_2} R'_\lambda d\lambda} \quad \text{Eq. 1}$$

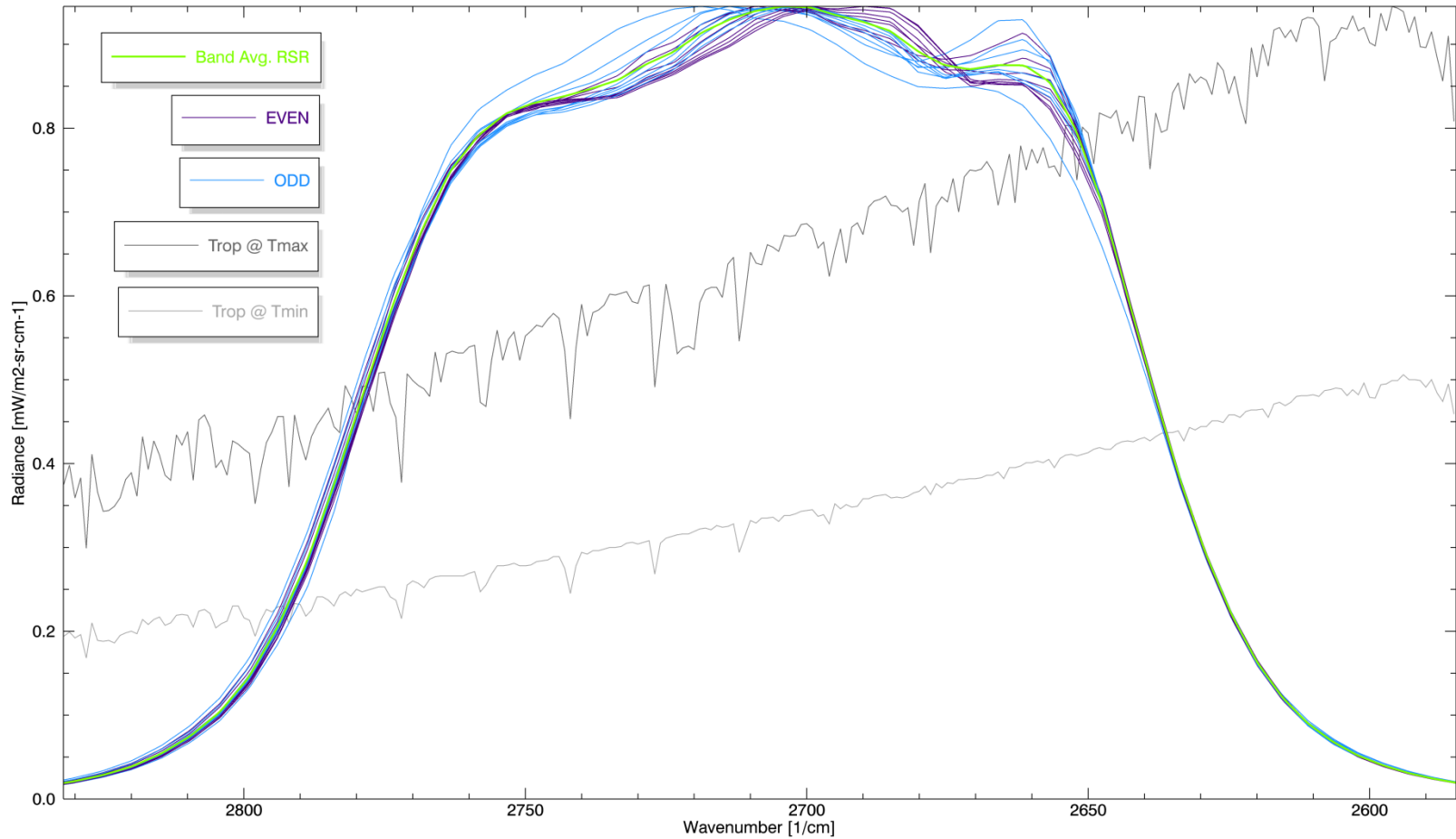
R'_λ peak normalized RSRs for a given band

Assumptions:

- Target is water
- Considered only global SST temperature ranges for this study
- Clear Sky Scenes
- Nighttime conditions only
- Restricted study to only consider system spectral response effects

M12 Detector-Level RSRs

M12 Detector-Level and Band Avg. RSRs

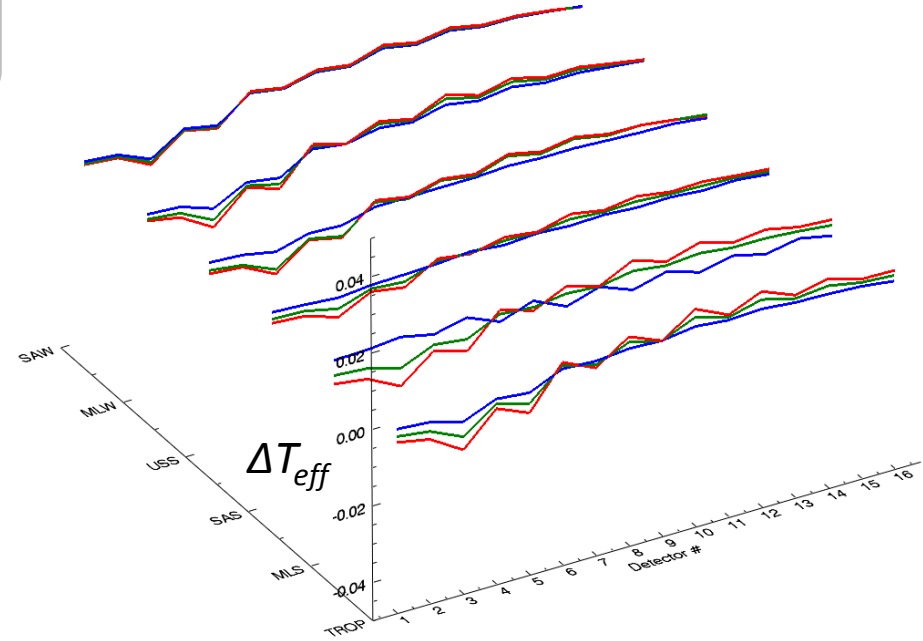
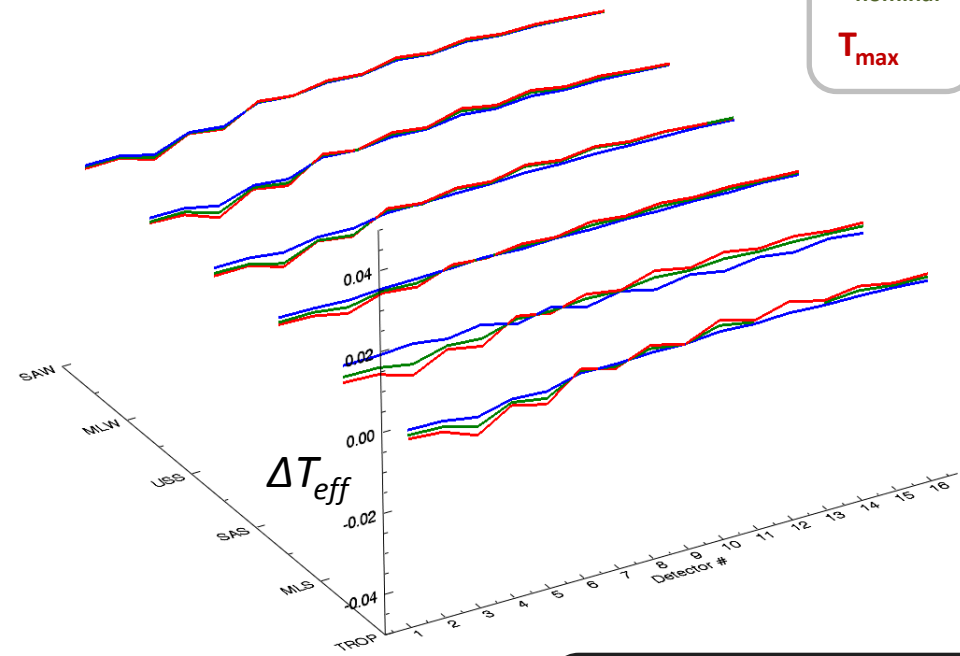


$$M12 (\Delta T_{eff} = T_{eff \text{ detector RSR}} - T_{eff \text{ band avg. RSR}})$$

NADIR

OFF-NADIR

T_{min}
 $T_{nominal}$
 T_{max}



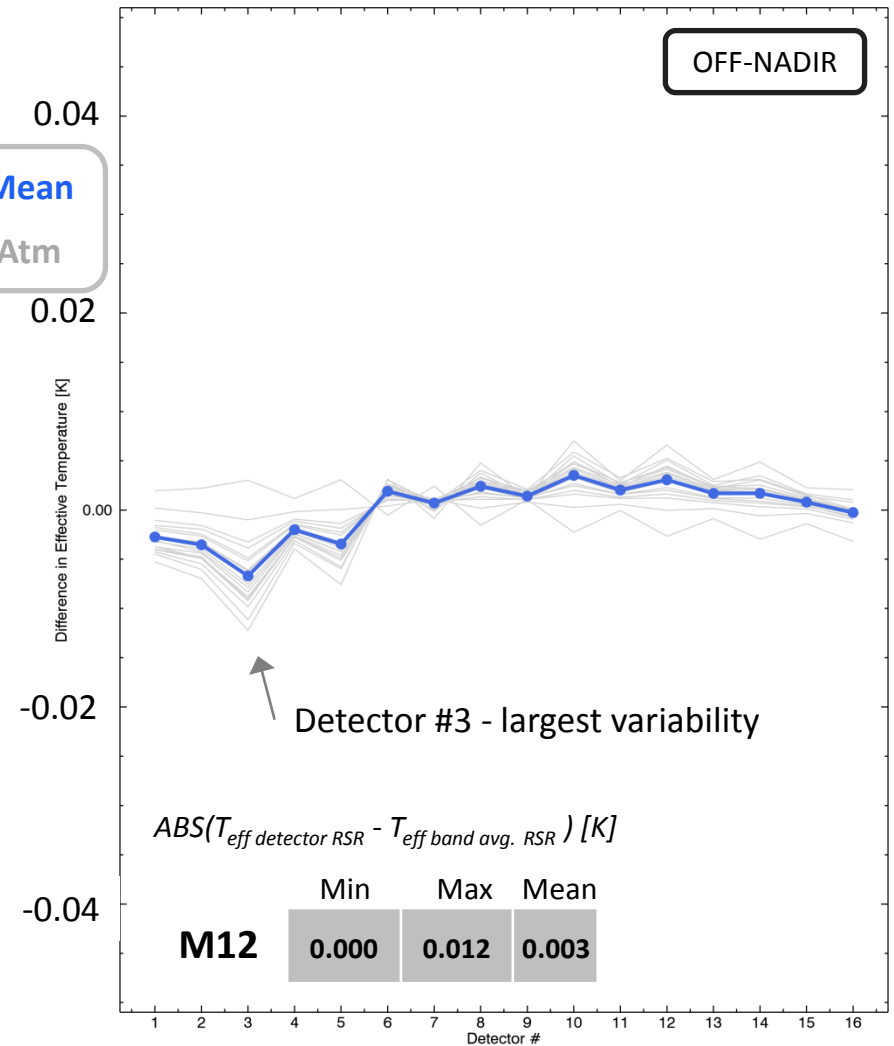
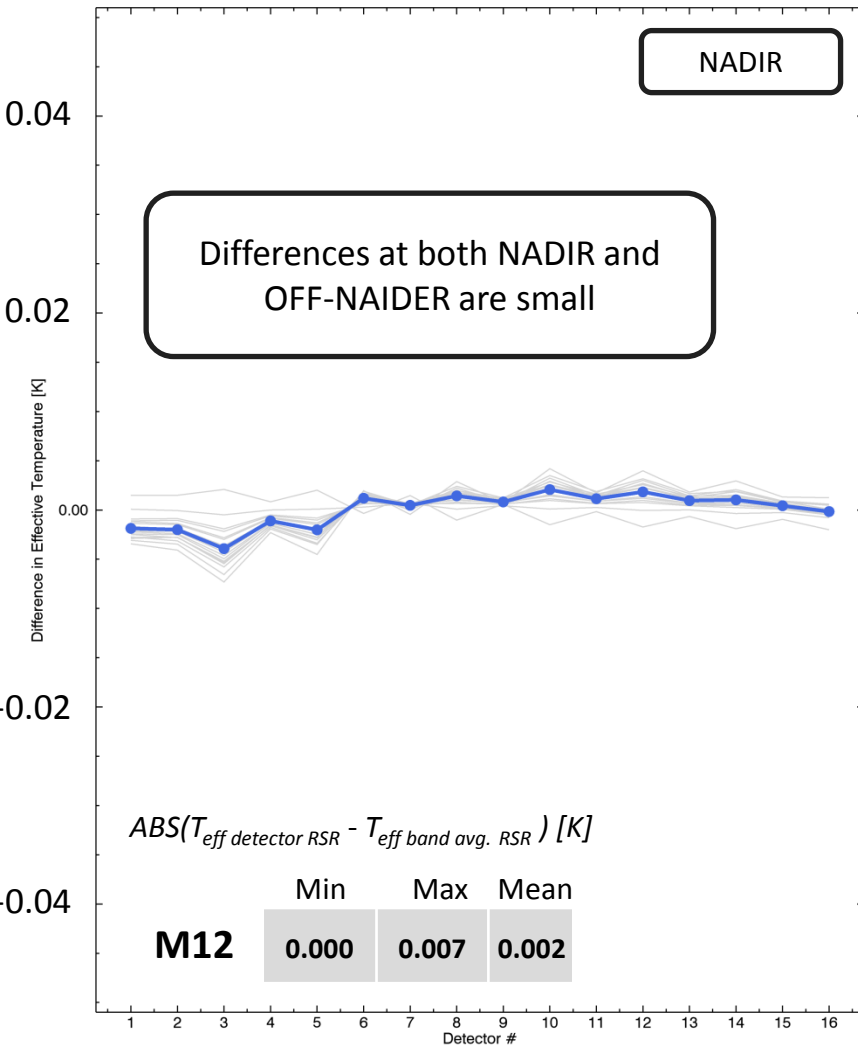
ΔT_{eff} larger for warm moist atmospheres;
smaller for cold dry atmospheres

$$M12 (\Delta T_{eff} = T_{eff \text{ detector RSR}} - T_{eff \text{ band avg. RSR}})$$

$NE\Delta T$ (270 to 300 K) = ~ 0.2 to $0.1 K^1$

Detector-Level RSR - Band Avg. RSR (All Atms) at NADIR

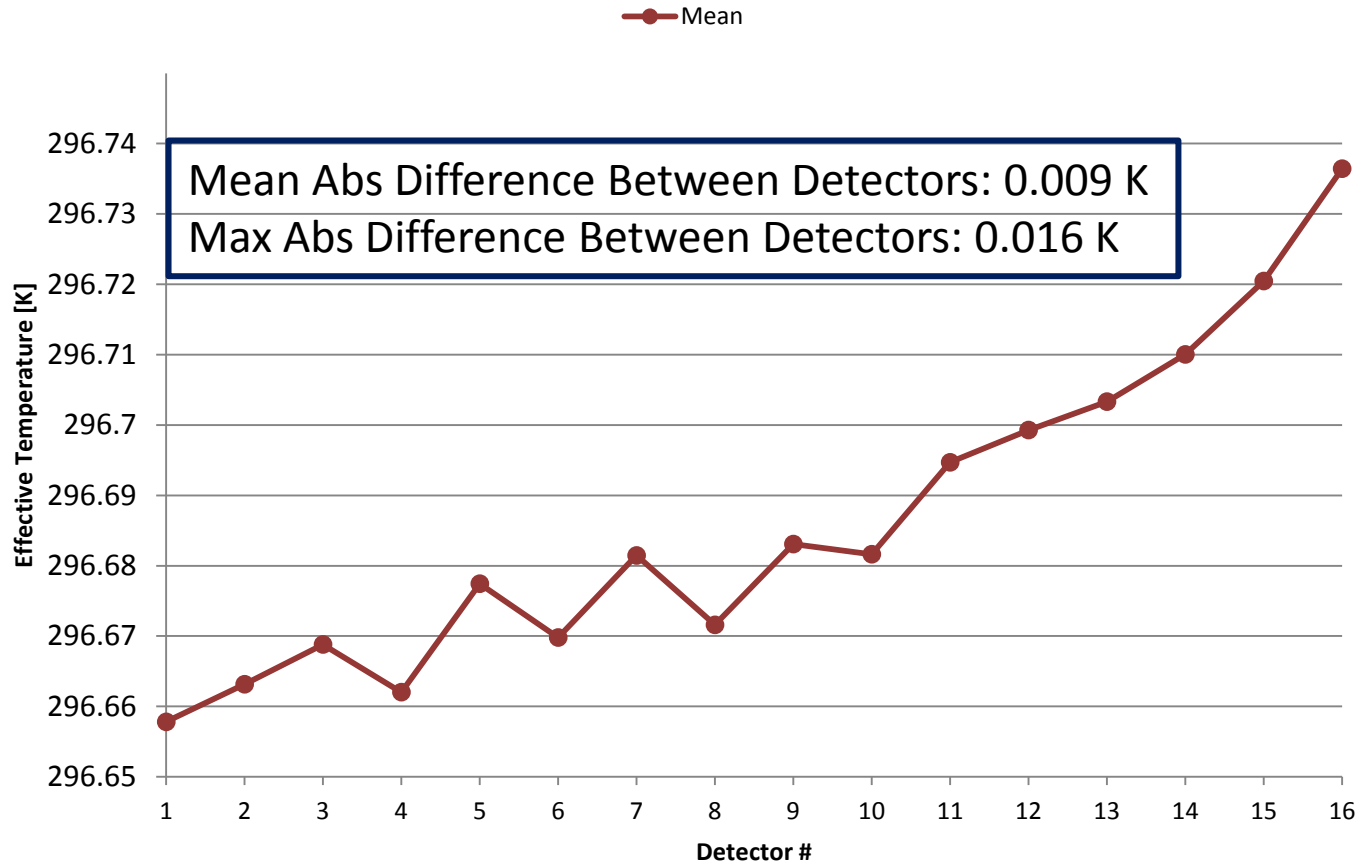
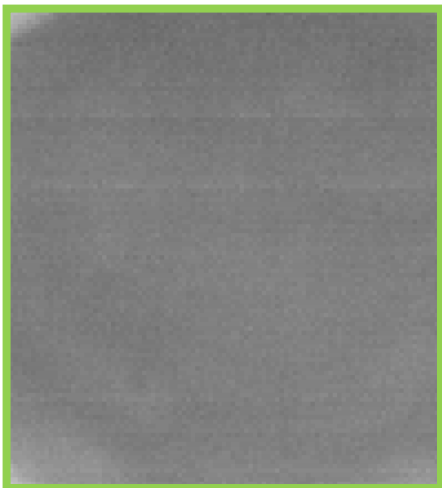
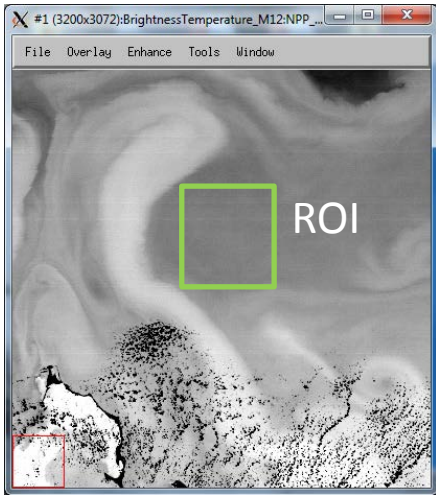
Detector-Level RSR - Band Avg. RSR (All Atms) at 56.063 deg OFF-NADIR



¹NEΔT values approximated using the interpolated values [Figure 6, Cao et al. 2013]

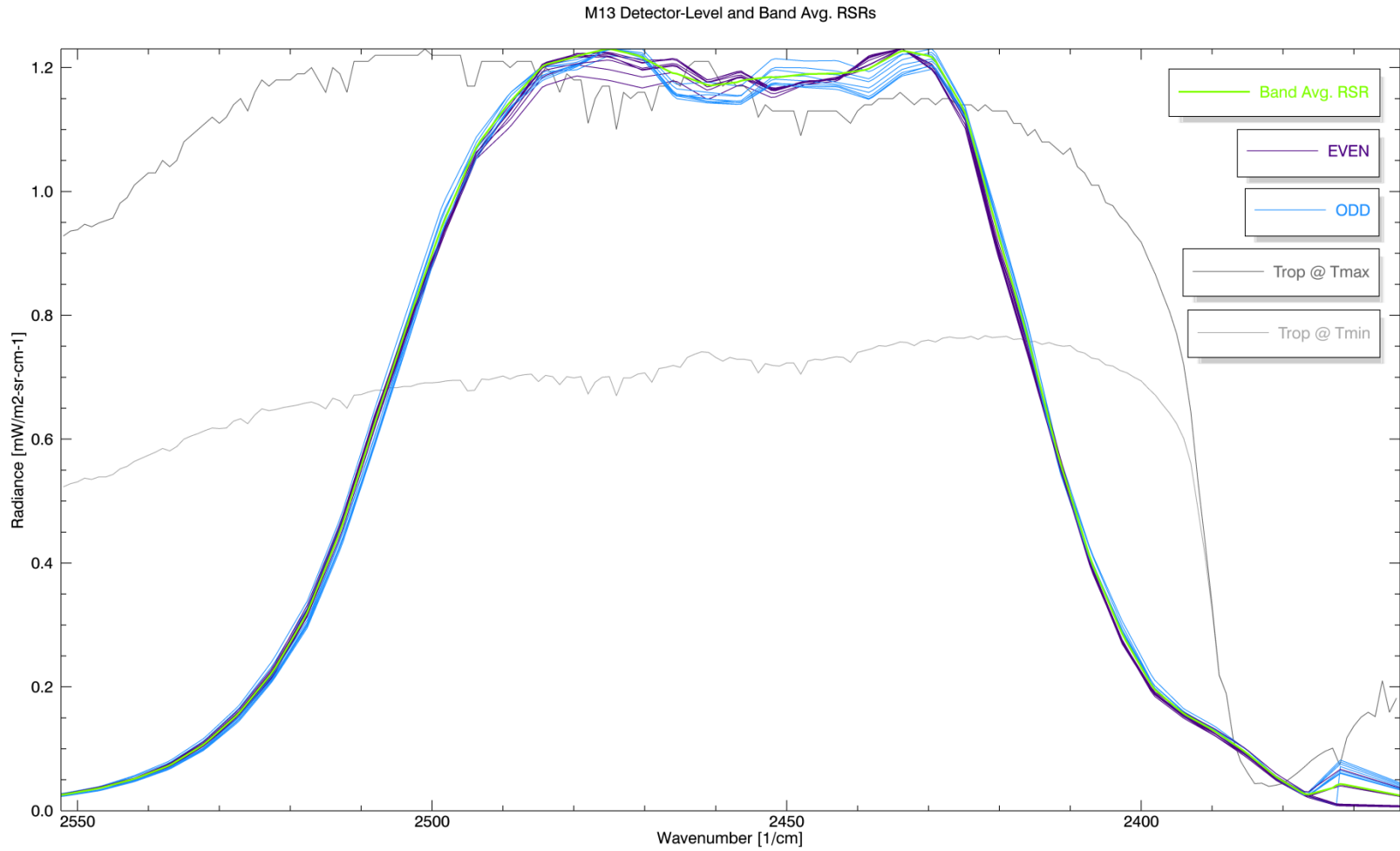
Date: May 6, 2014
Time: 06:35 UTC

Average of 6 Six Scans (91 pixels/detector) Over a "Uniform" Ocean ROI: M12



[NPP_VMAE_L1.A2014126.0635.P1_03002.2014126121715.hdf](https://npp.vmae.l1.a2014126.0635.p1_03002.2014126121715.hdf)

M13 Detector-Level RSRs



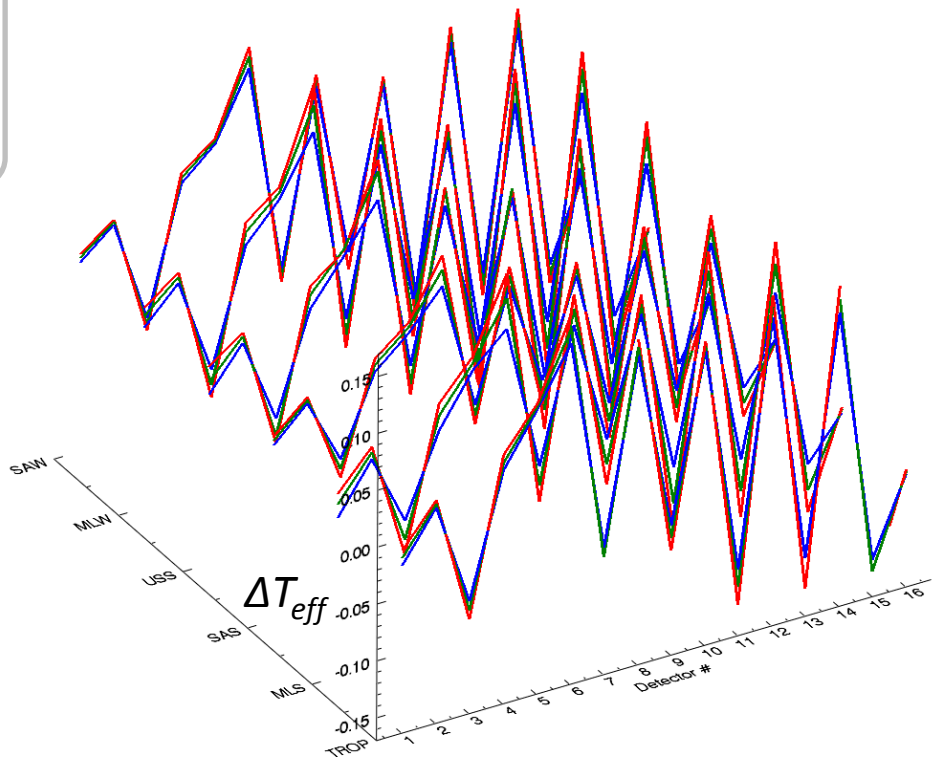
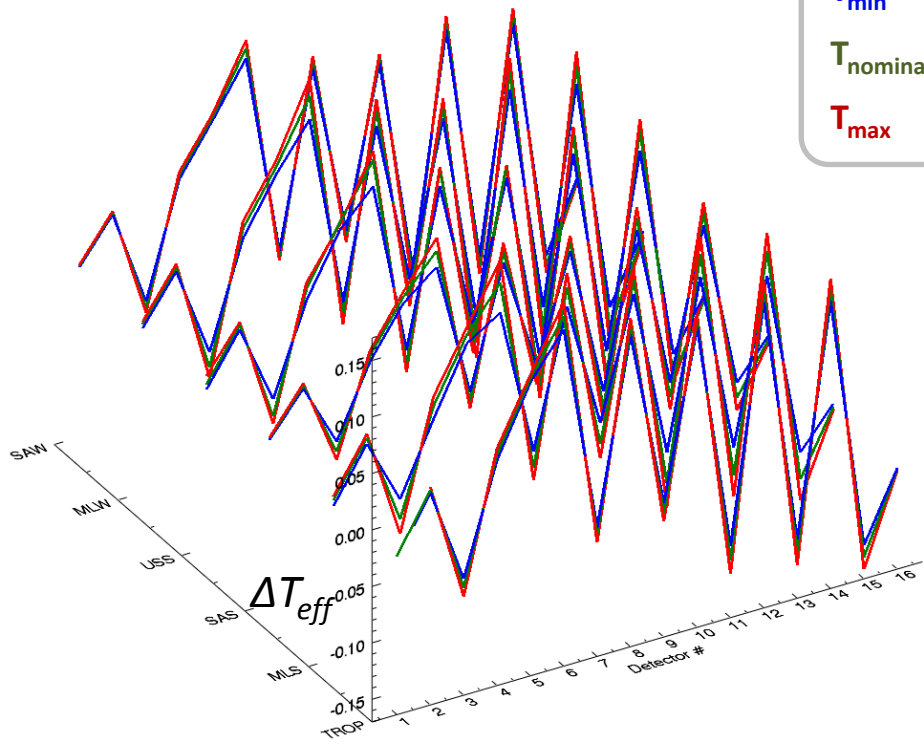
Strong Odd/Even Pattern

$$M13 (\Delta T_{eff} = T_{eff \text{ detector RSR}} - T_{eff \text{ band avg. RSR}})$$

NADIR

OFF-NADIR

T_{min}
 $T_{nominal}$
 T_{max}

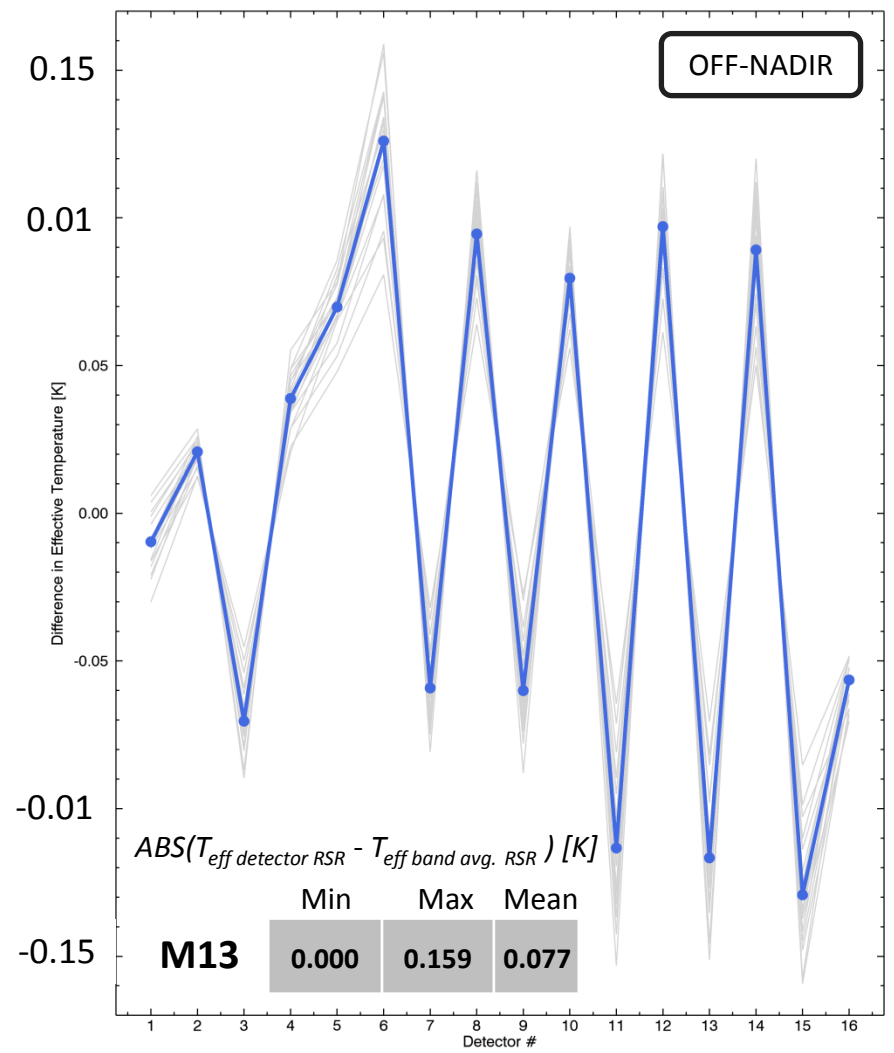
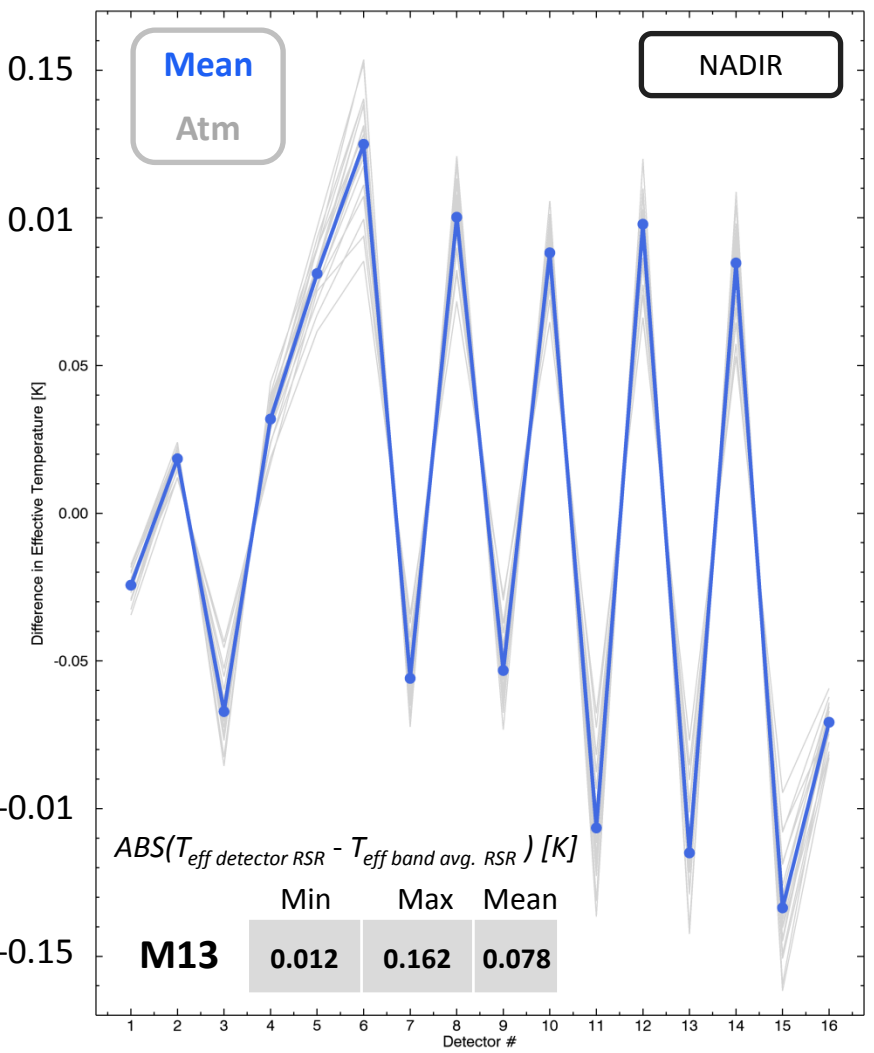


$$M13 (\Delta T_{eff} = T_{eff \text{ detector RSR}} - T_{eff \text{ band avg. RSR}})$$

NEAT (270 to 300 K) = ~0.2 to 0.1 K

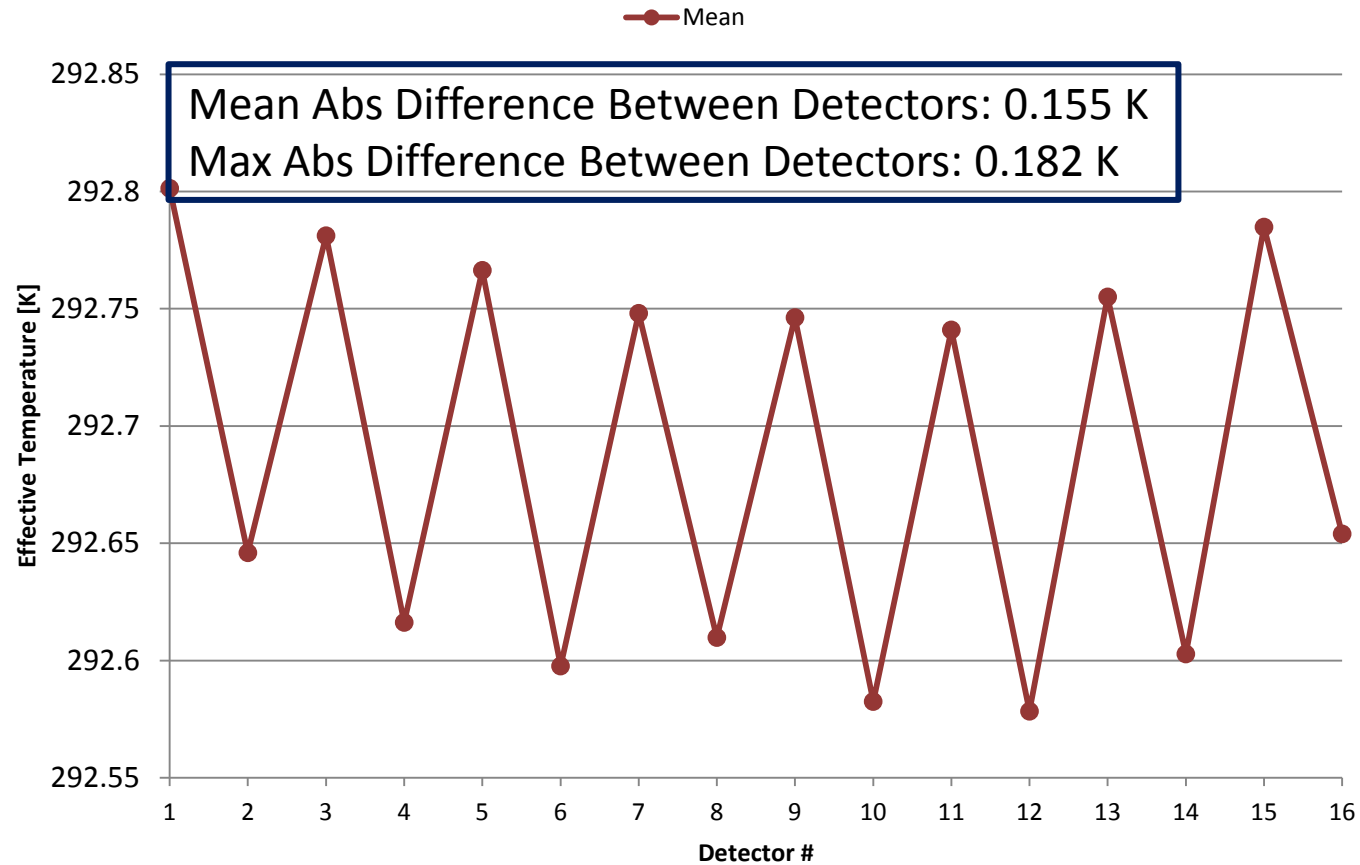
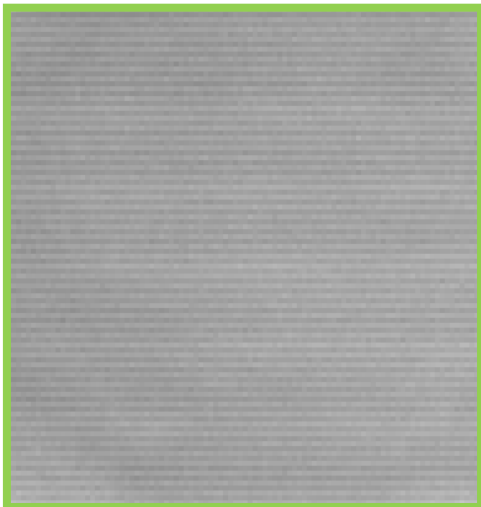
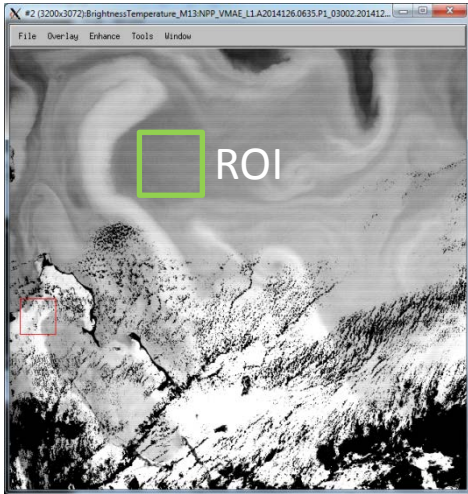
Detector-Level RSR - Band Avg. RSR (All Atms) at NADIR

Detector-Level RSR - Band Avg. RSR (All Atms) at 56.063 deg OFF-NADIR



Date: May 6, 2014
Time: 06:35 UTC

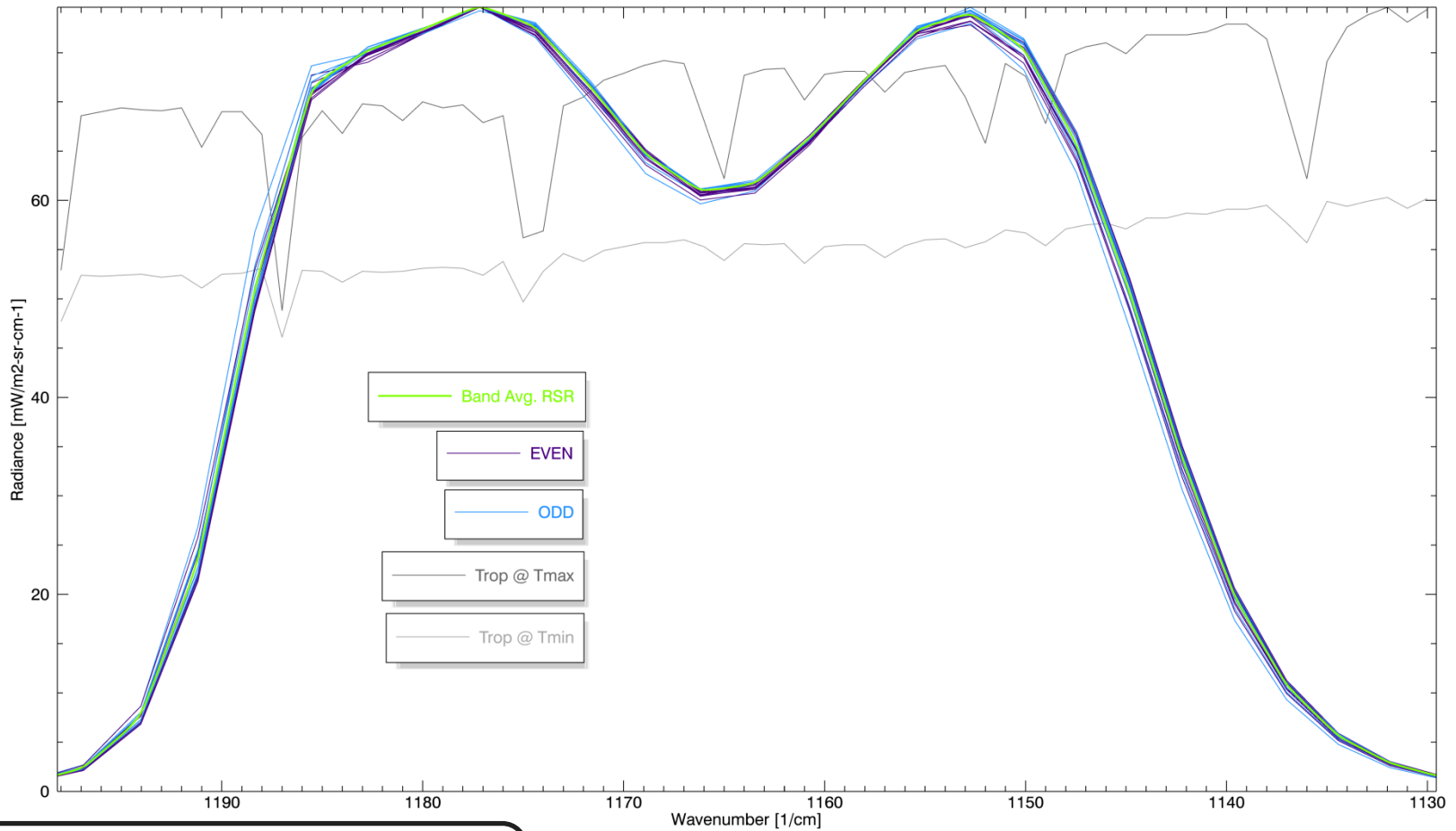
Average of 6 Six Scans (91 pixels/detector) Over a "Uniform" Ocean ROI: M13



[NPP_VMAE_L1.A2014126.0635.P1_03002.2014126121715.hdf](#)

M14 Detector-Level RSRs

M14 Detector-Level and Band Avg. RSRs



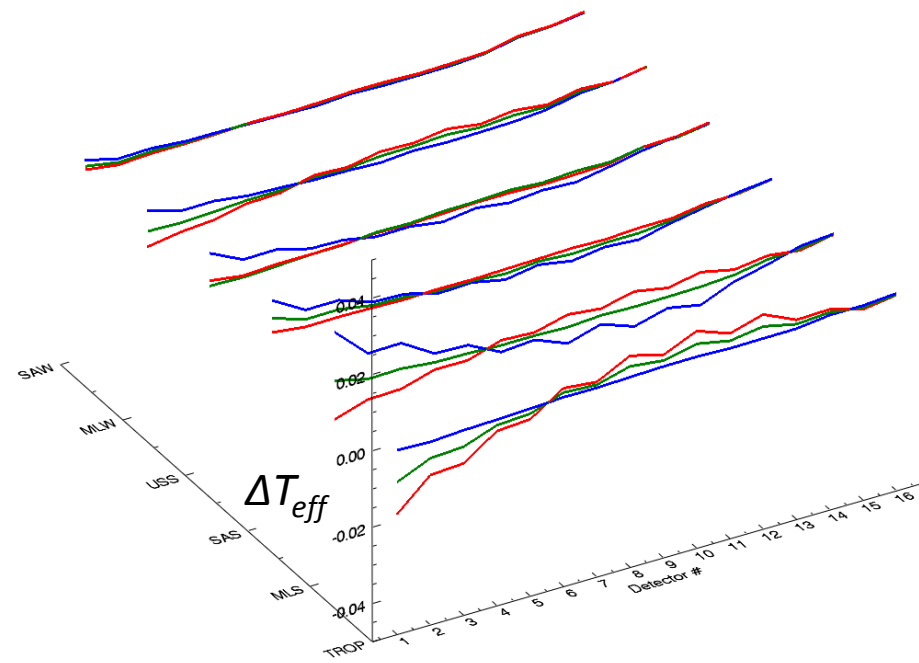
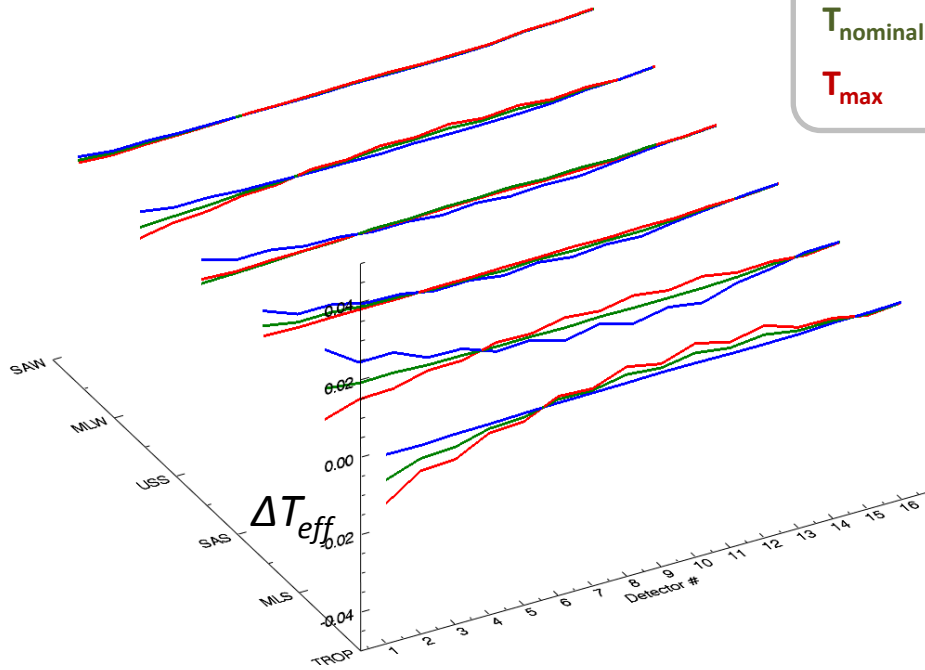
Good agreement between Detector-Level and Band Avg. RSRs

$$M14 (\Delta T_{eff} = T_{eff \text{ detector RSR}} - T_{eff \text{ band avg. RSR}})$$

NADIR

OFF-NADIR

T_{min}
 $T_{nominal}$
 T_{max}

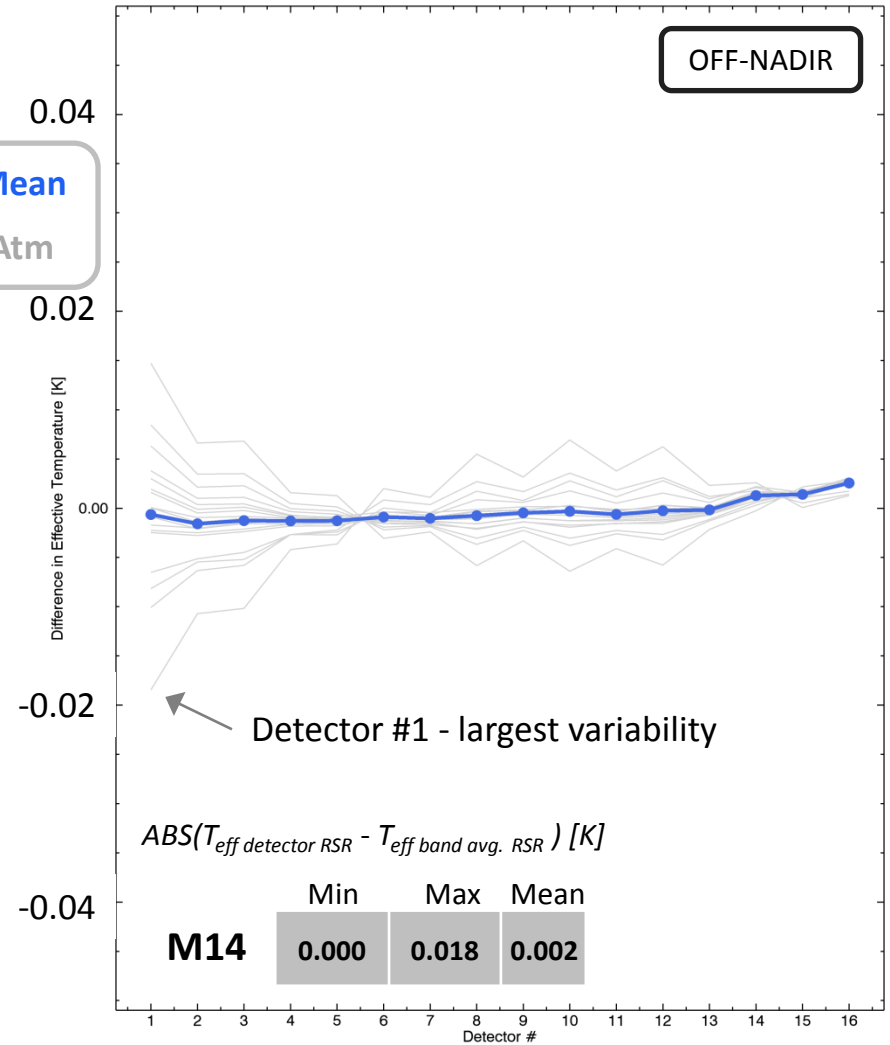
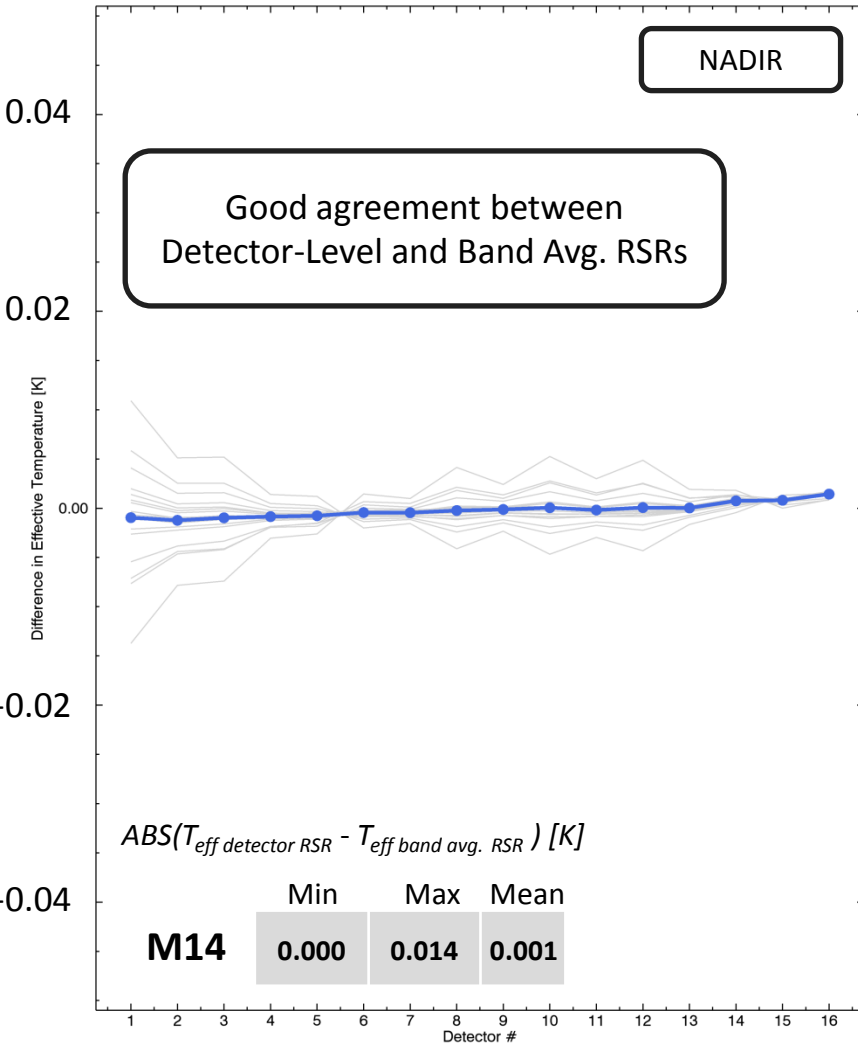


$$M14 (\Delta T_{eff} = T_{eff \text{ detector RSR}} - T_{eff \text{ band avg. RSR}})$$

$NE\Delta T (270 \text{ to } 300 \text{ K}) = \sim 0.06 \text{ to } 0.05 \text{ K}$

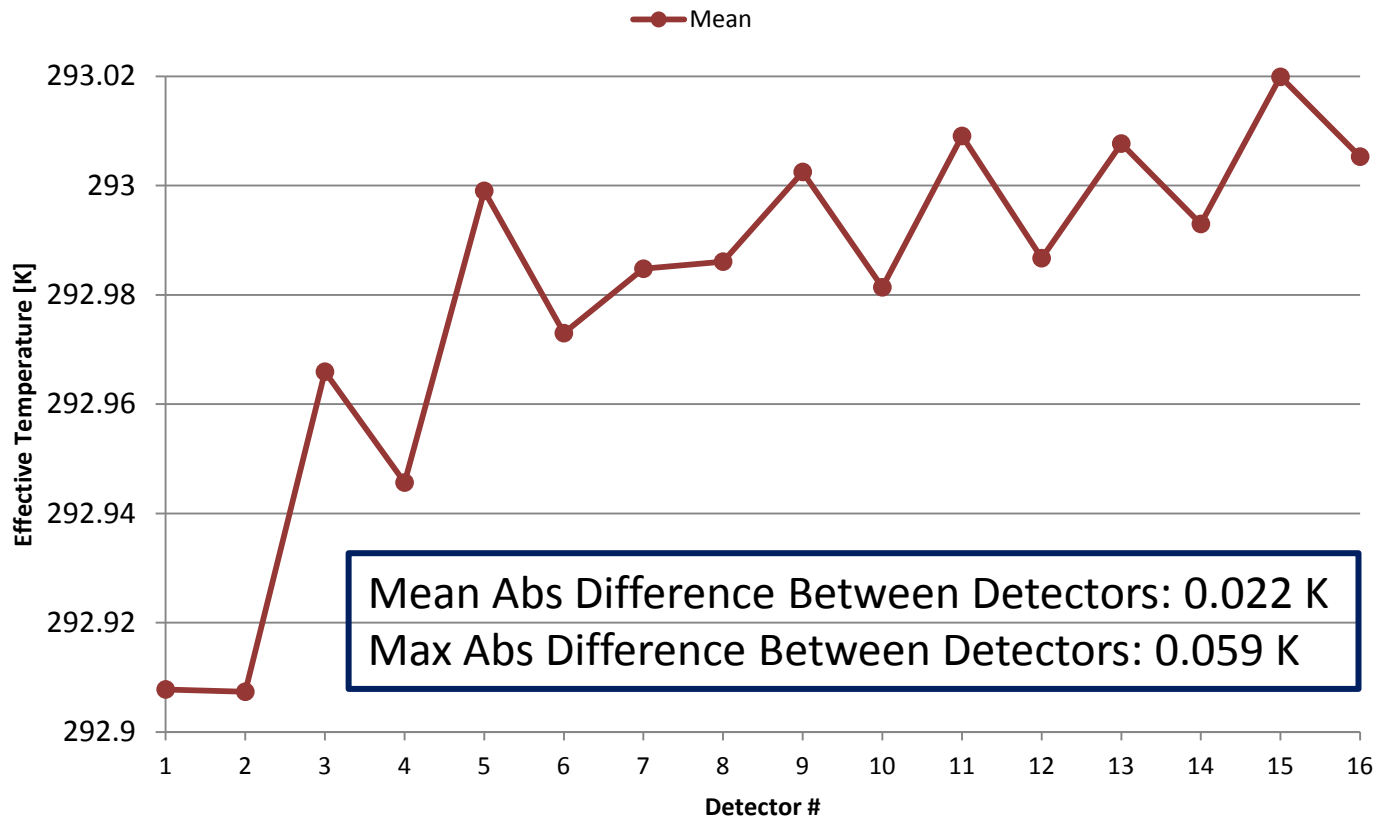
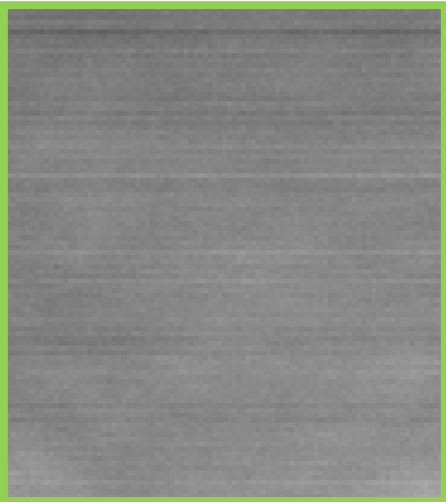
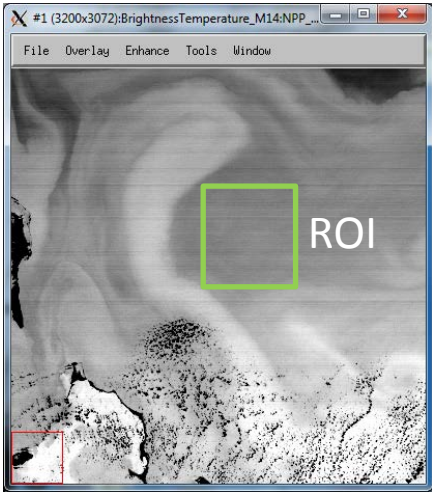
Detector-Level RSR - Band Avg. RSR (All Atms) at NADIR

Detector-Level RSR - Band Avg. RSR (All Atms) at 56.063 deg OFF-NADIR



Date: May 6, 2014
Time: 06:35 UTC

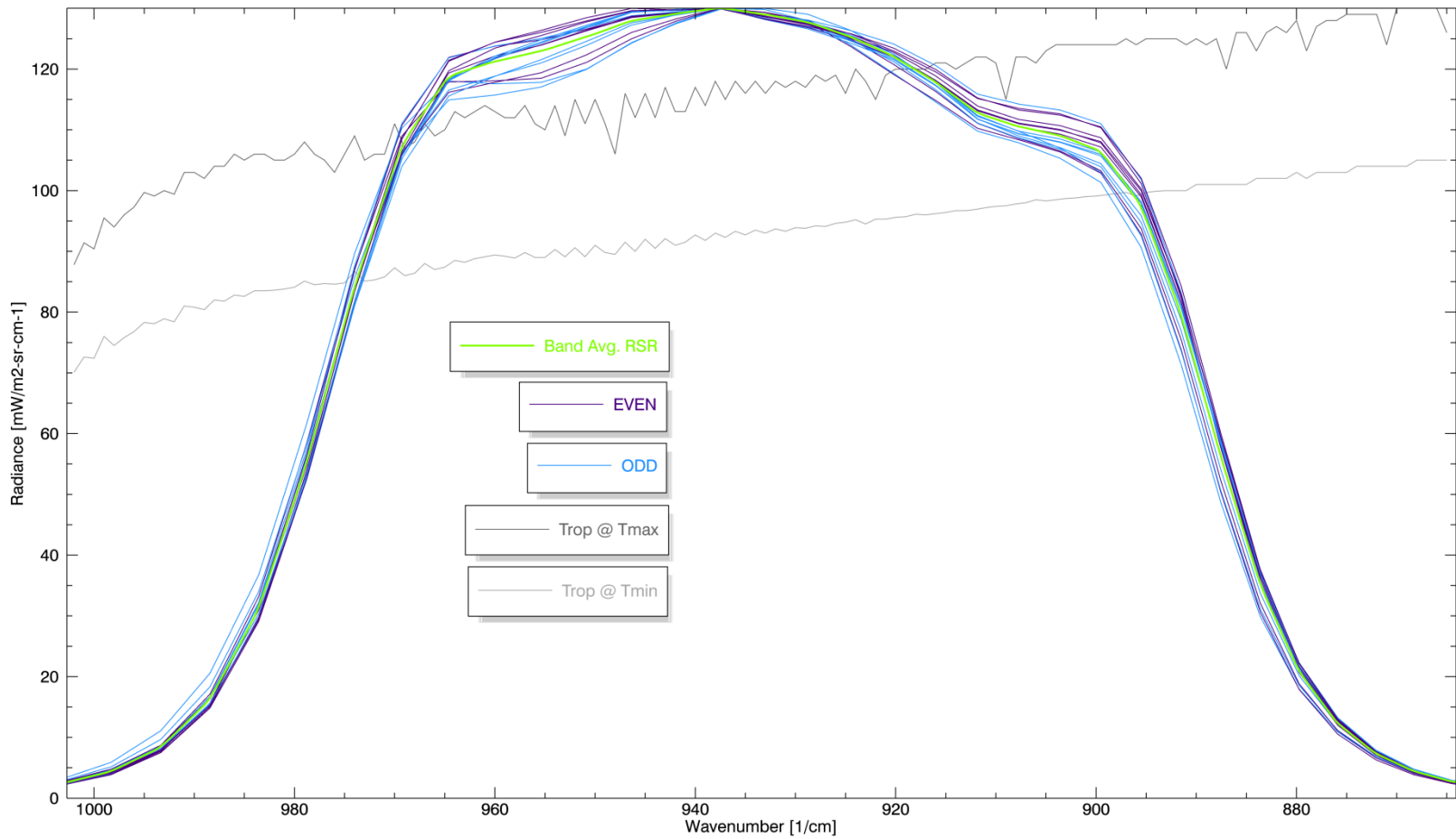
Average of 6 Six Scans (91 pixels/detector) Over a "Uniform" Ocean ROI: M14



[NPP_VMAE_L1.A2014126.0635.P1_03002.2014126121715.hdf](https://data.nasa.gov/data-repository/data-distribution-staging/JPSS/JPSS-0001/2014/05/06/0635/P1_03002.2014126121715.hdf)

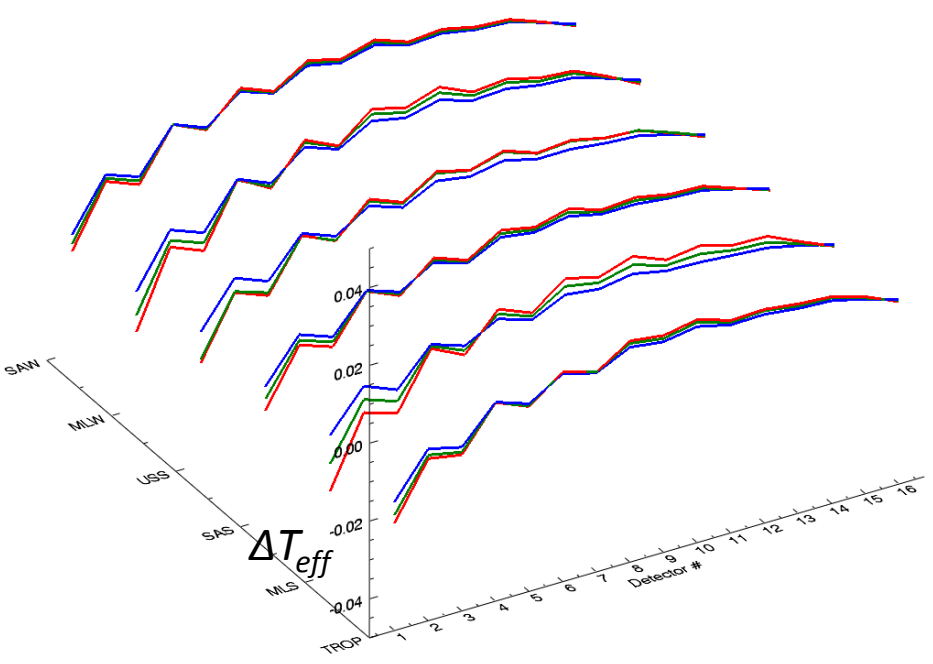
M15 Detector-Level RSRs

M15 Detector-Level and Band Avg. RSRs

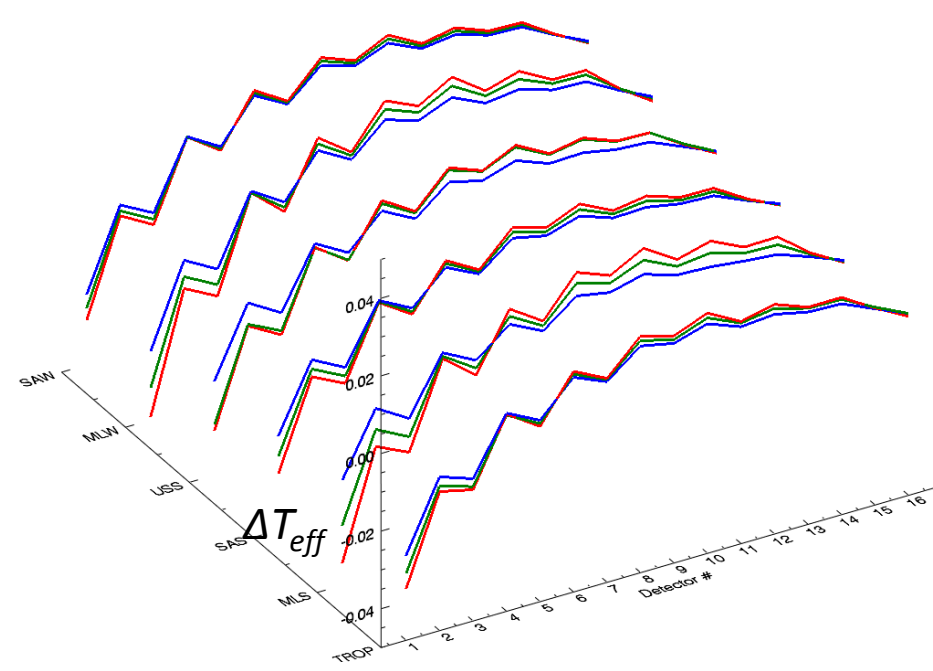


M15 ($\Delta T_{eff} = T_{eff\ detector\ RSR} - T_{eff\ band\ avg.\ RSR}$) as a Function of Atmosphere & Detector

NADIR



OFF-NADIR

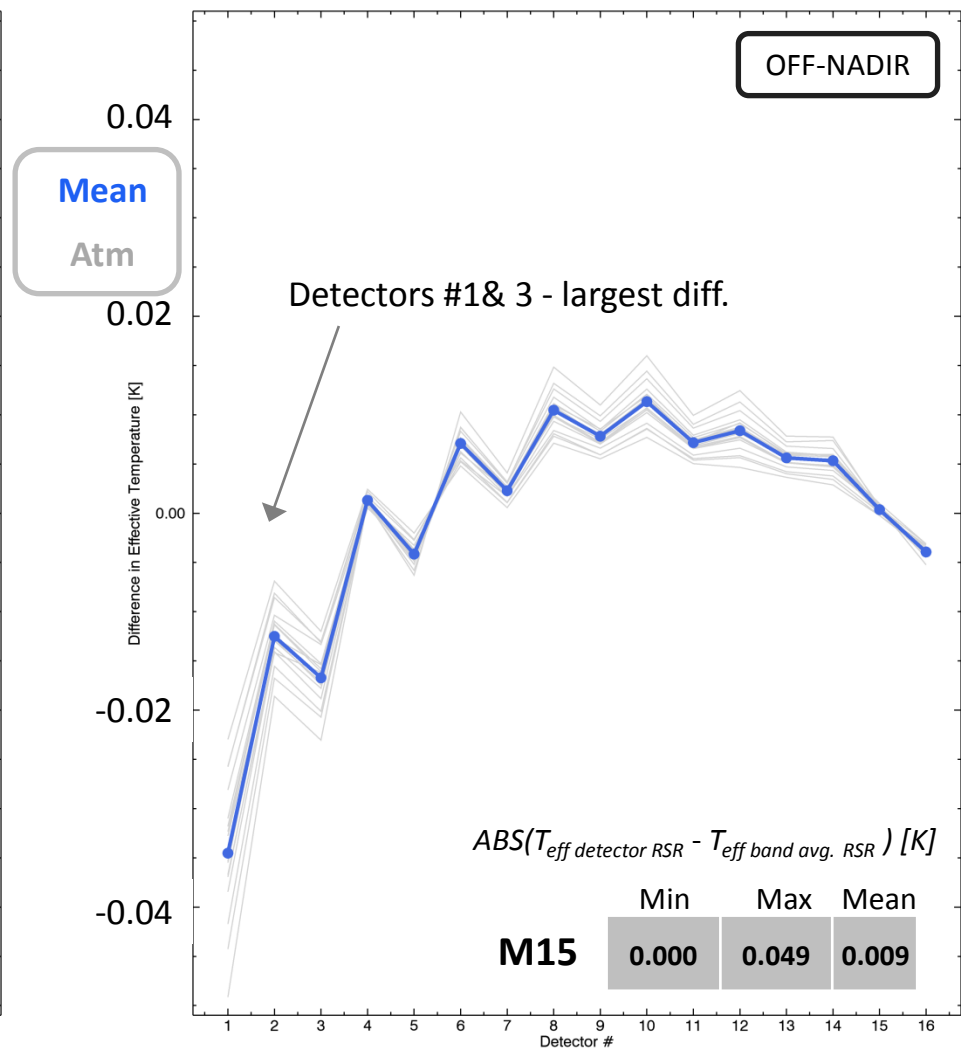
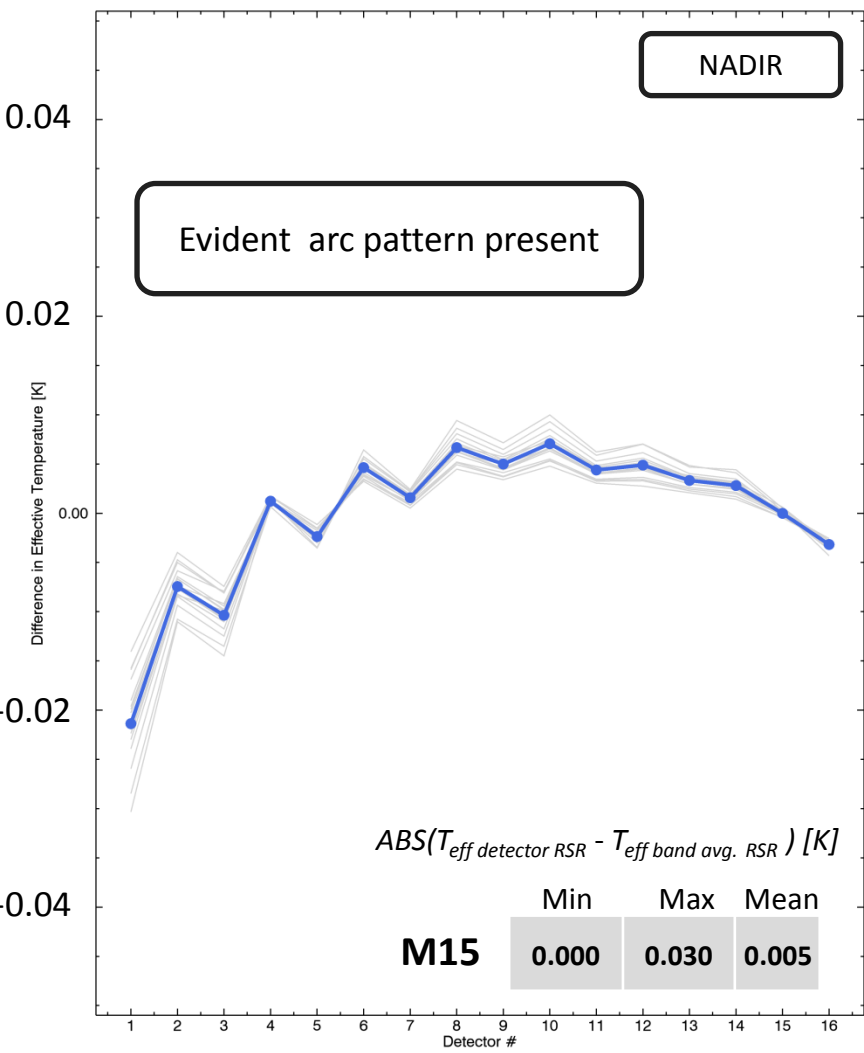


$$M15 (\Delta T_{eff} = T_{eff\ detector\ RSR} - T_{eff\ band\ avg.\ RSR})$$

$NE\Delta T (270\ to\ 300\ K) = \sim 0.03\ K$

Detector-Level RSR - Band Avg. RSR (All Atms) at NADIR

Detector-Level RSR - Band Avg. RSR (All Atms) at 56.063 deg OFF-NADIR

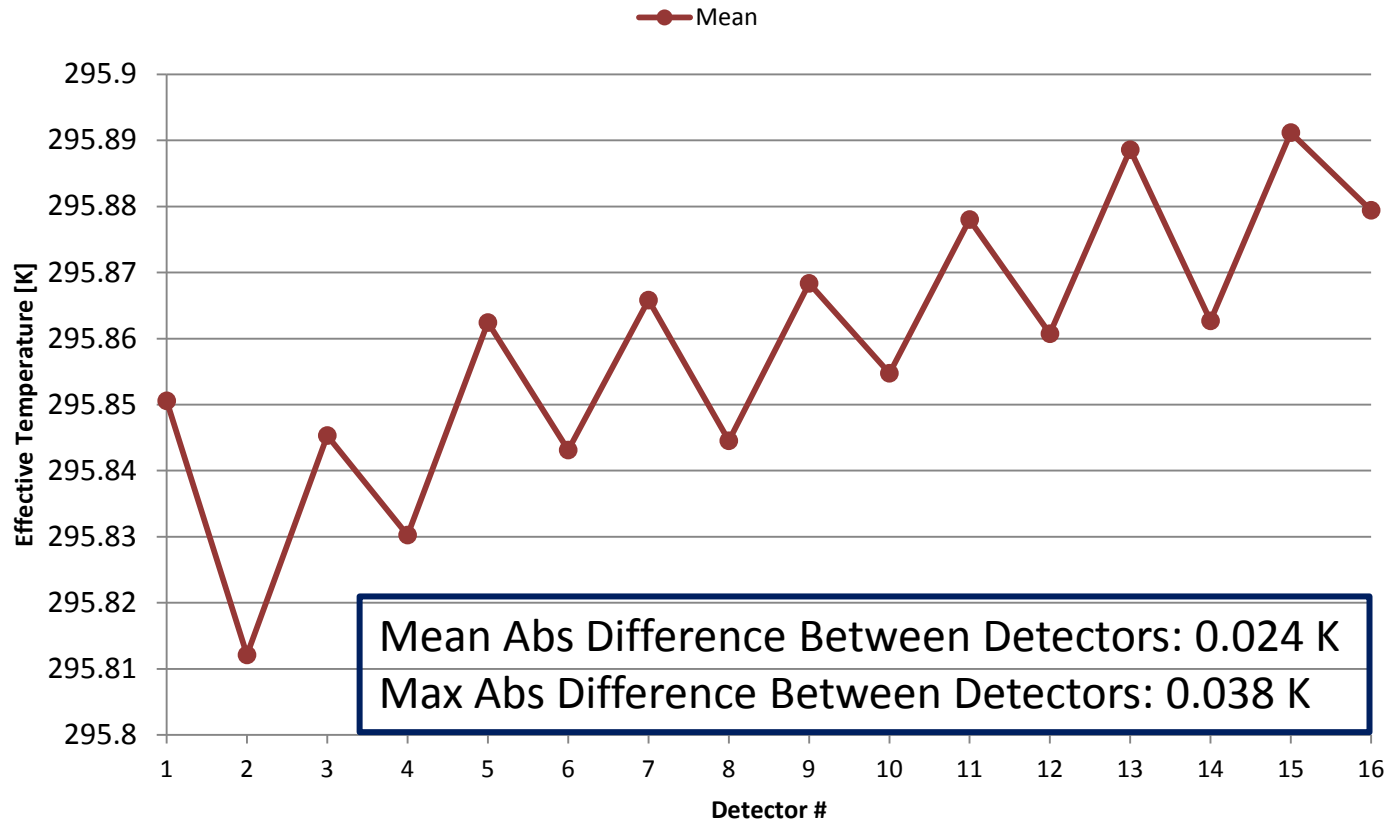
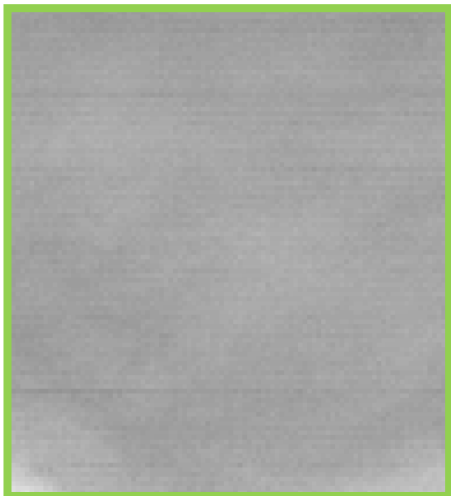
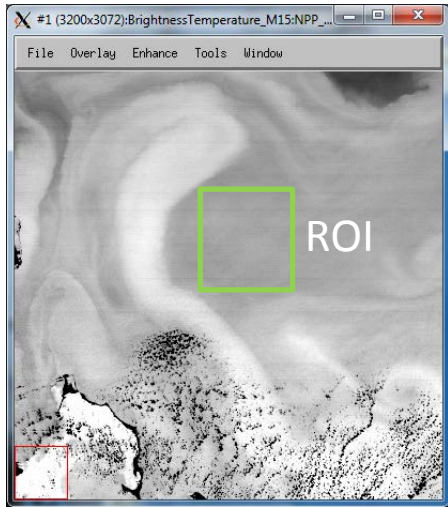


Example of Observed Phenomenology in Suomi NPP

VIIRS: M15

Date: May 6, 2014
Time: 06:35 UTC

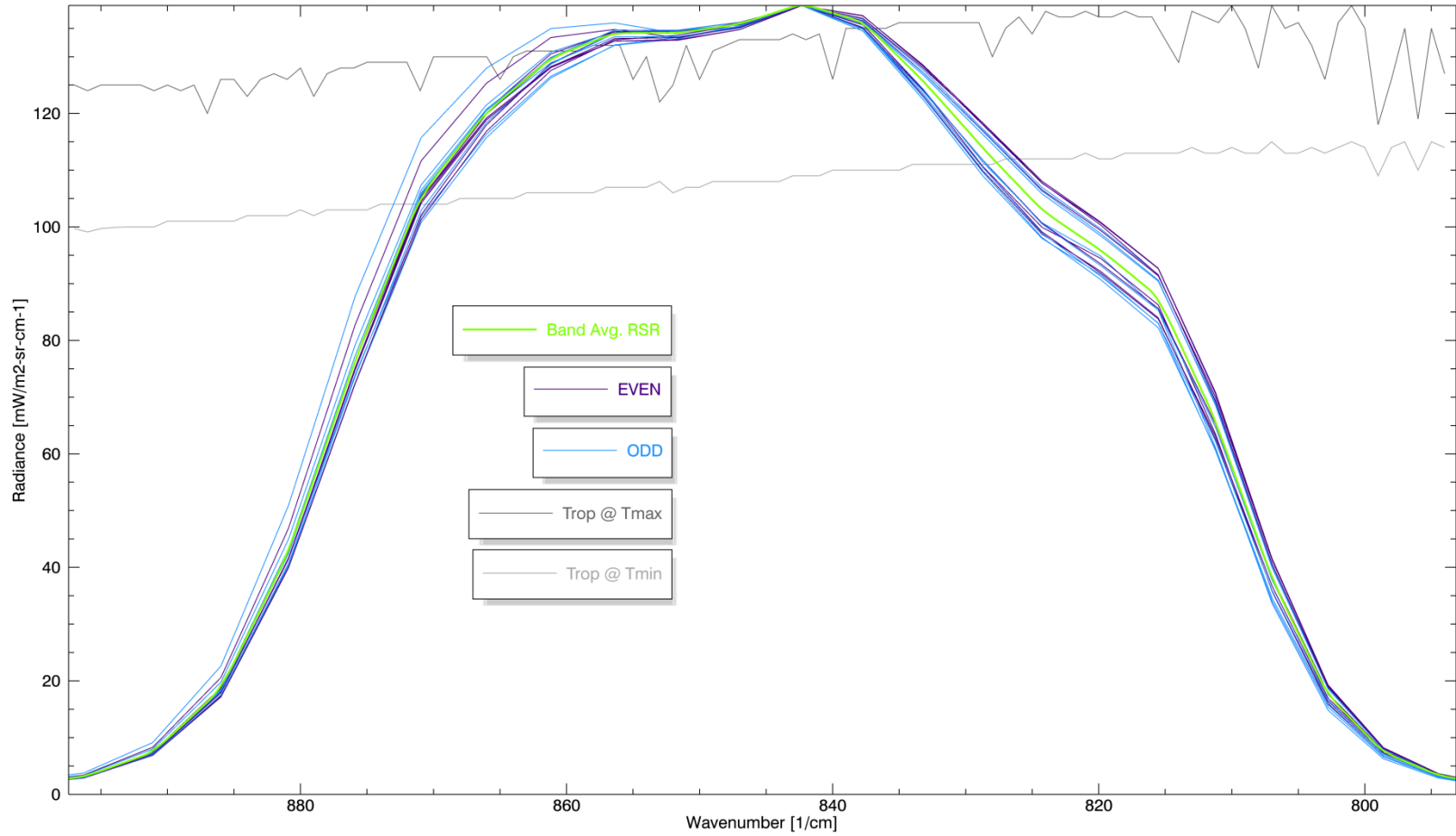
**Average of 6 Six Scans (91 pixels/detector) Over a
"Uniform" Ocean ROI: M15**



[NPP_VMAE_L1.A2014126.0635.P1_03002.2014126121715.hdf](https://npp.vmae.l1.a2014126.0635.p1_03002.2014126121715.hdf)

M16a Detector-Level RSRs

M16a Detector-Level and Band Avg. RSRs

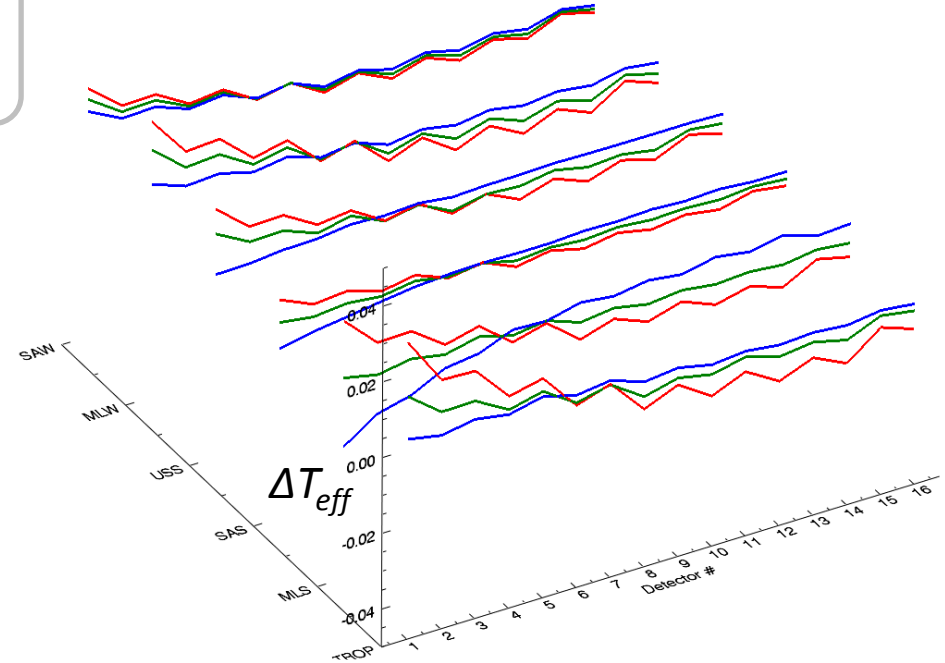
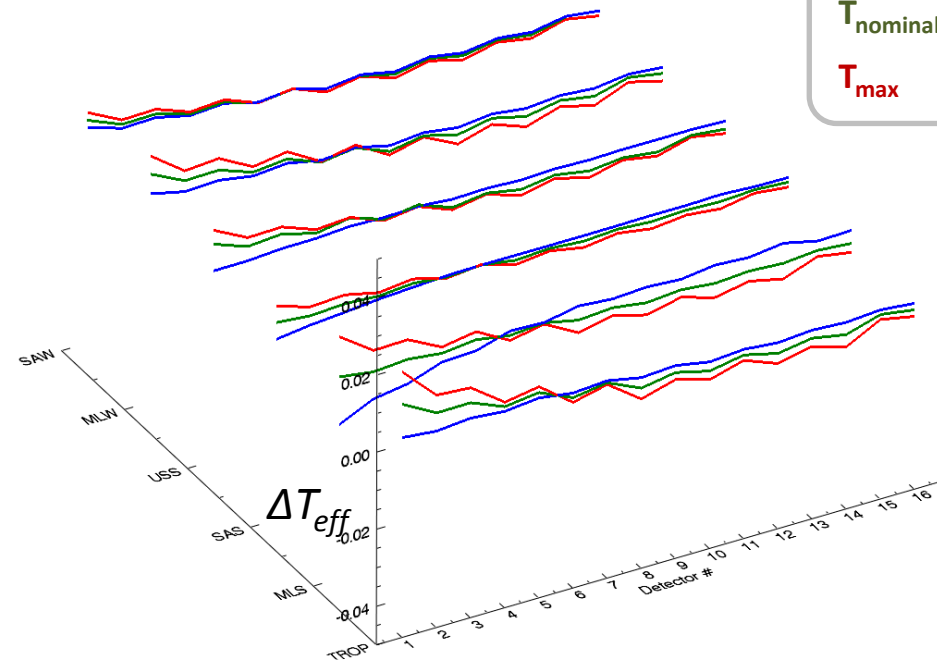


$$M16a (\Delta T_{eff} = T_{eff\ detector\ RSR} - T_{eff\ band\ avg.\ RSR})$$

NADIR

OFF-NADIR

T_{min}
 $T_{nominal}$
 T_{max}

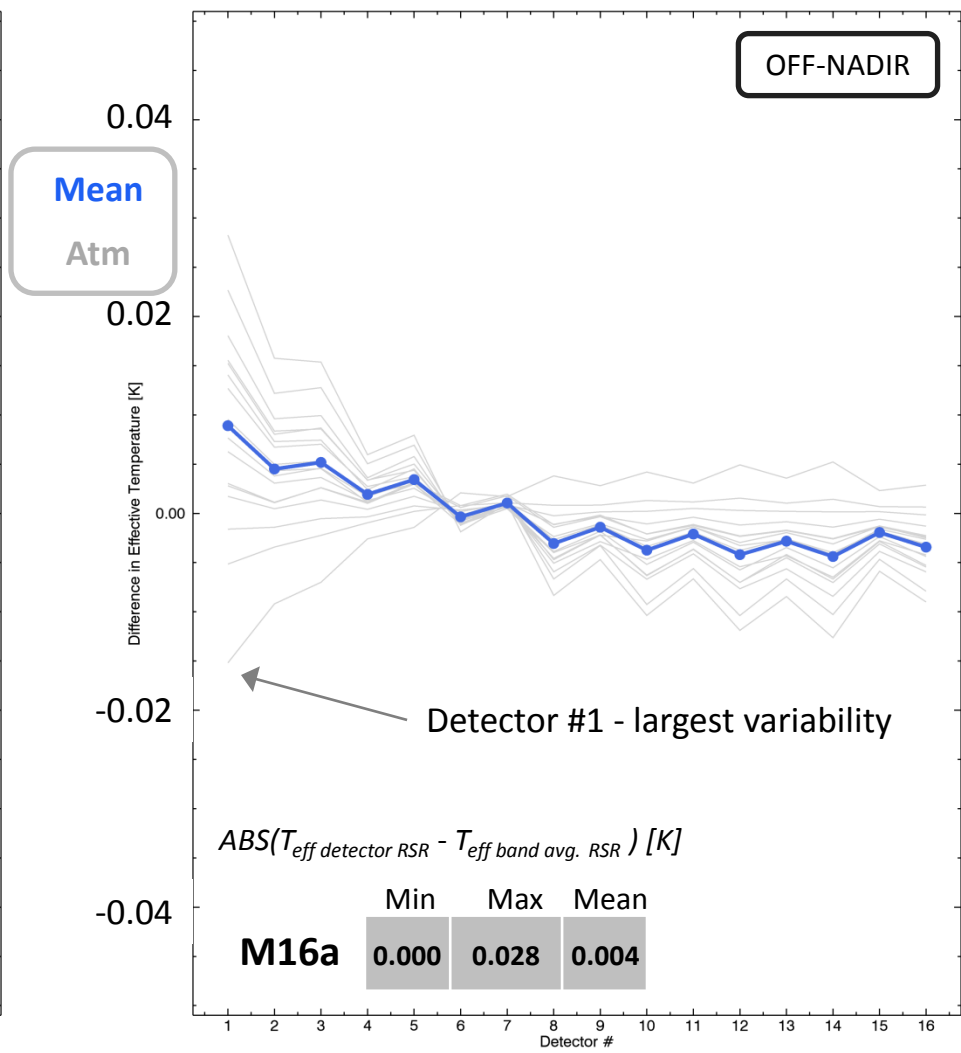
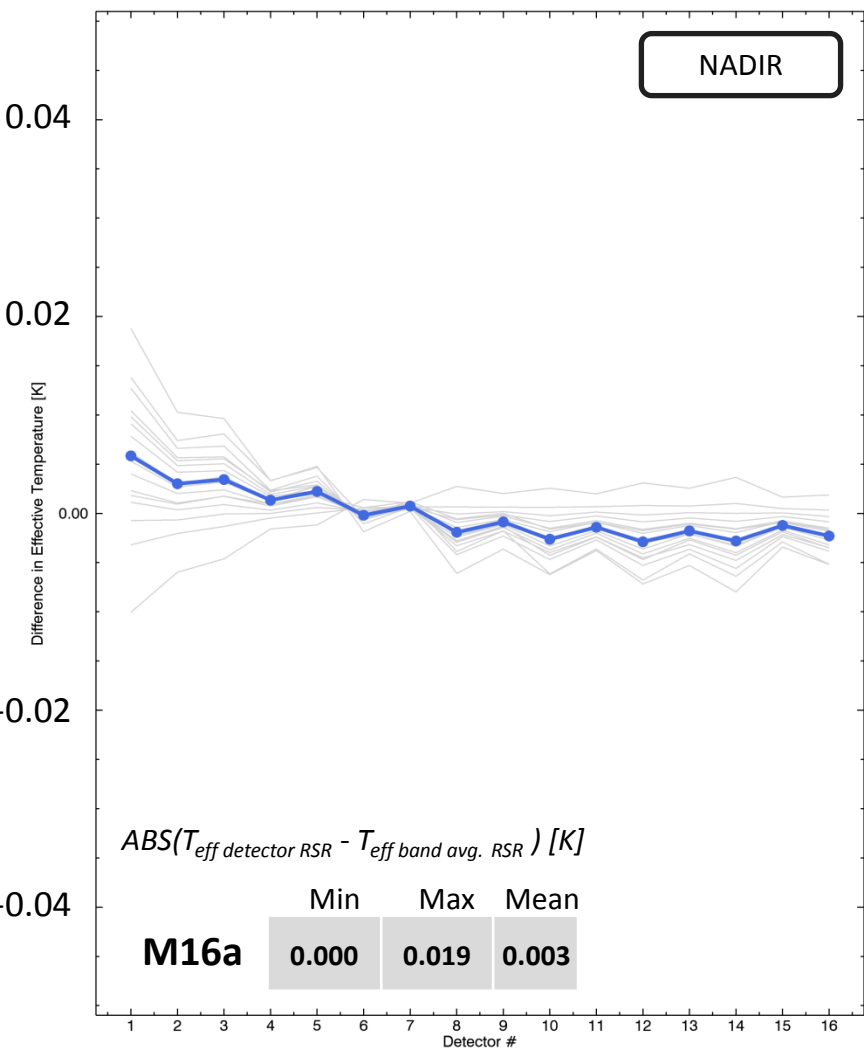


$$M16a (\Delta T_{eff} = T_{eff\ detector\ RSR} - T_{eff\ band\ avg.\ RSR})$$

$NE\Delta T (270\ to\ 300\ K) = \sim 0.03\ K$

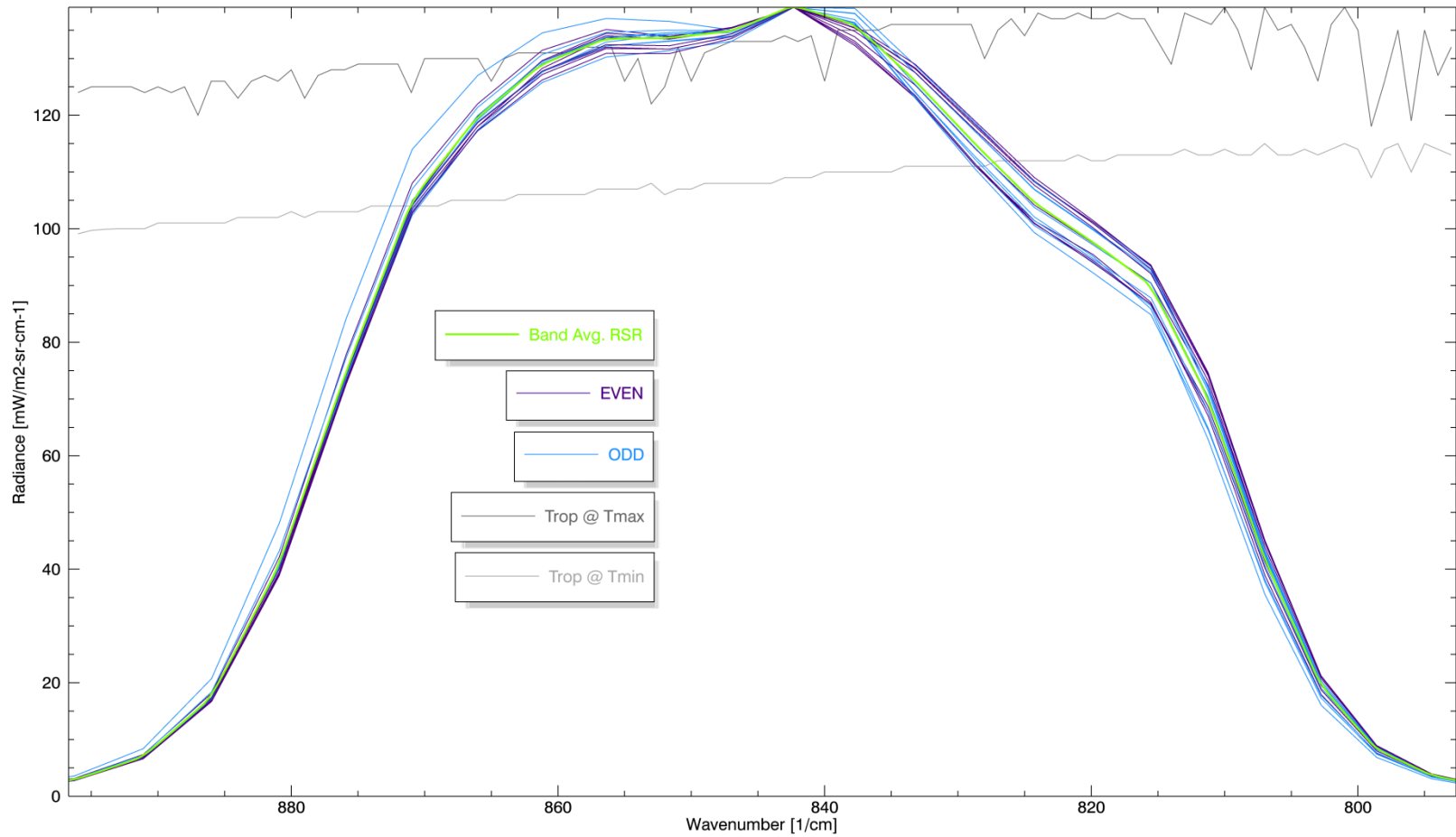
Detector-Level RSR - Band Avg. RSR (All Atms) at NADIR

Detector-Level RSR - Band Avg. RSR (All Atms) at 56.063 deg OFF-NADIR



M16b Detector-Level RSRs

M16b Detector-Level and Band Avg. RSRs

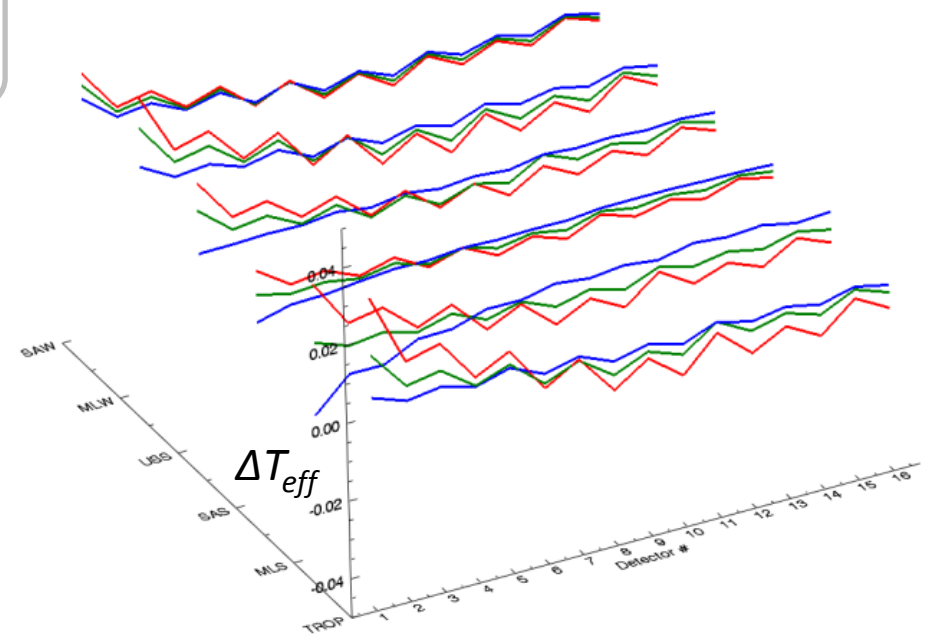
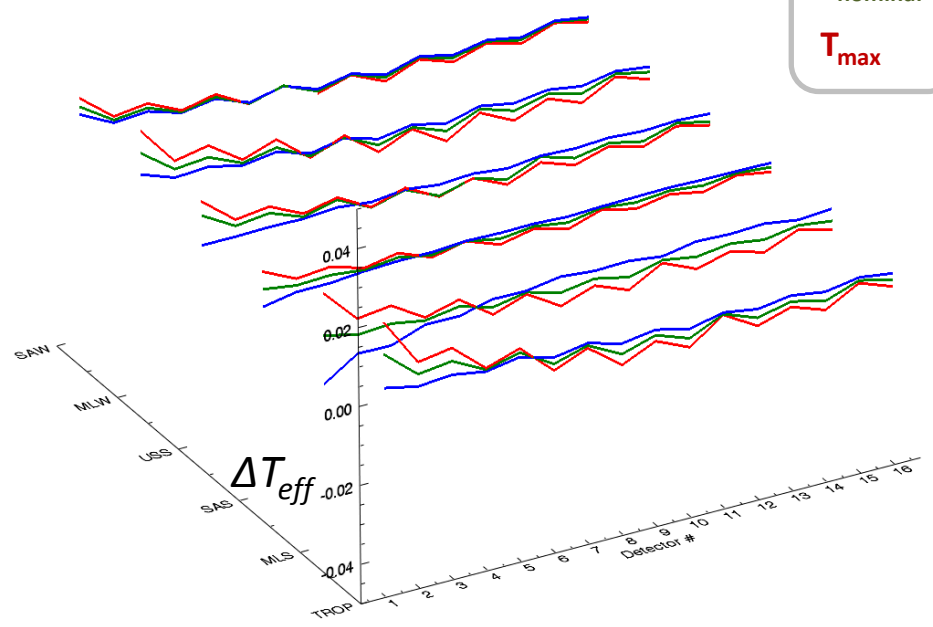


$$M16b (\Delta T_{eff} = T_{eff\ detector\ RSR} - T_{eff\ band\ avg.\ RSR})$$

NADIR

OFF-NADIR

T_{min}
 $T_{nominal}$
 T_{max}

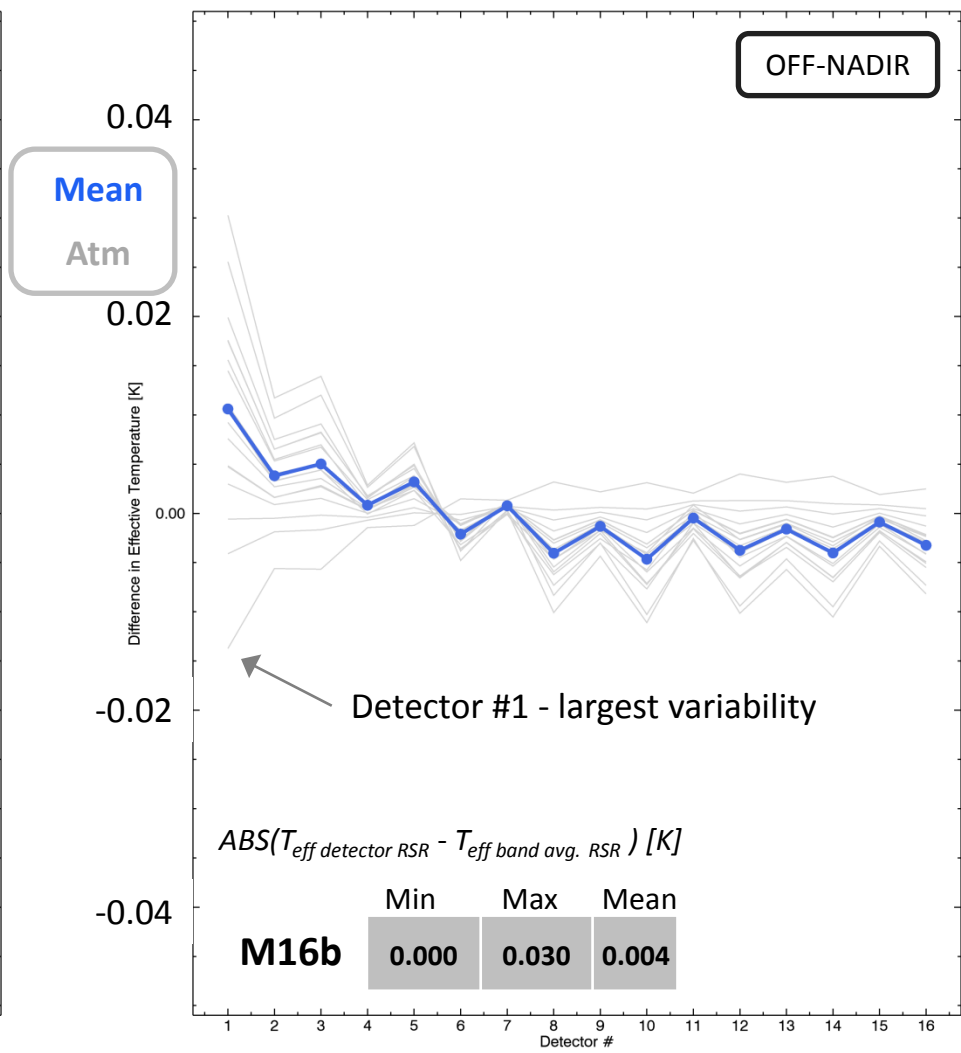
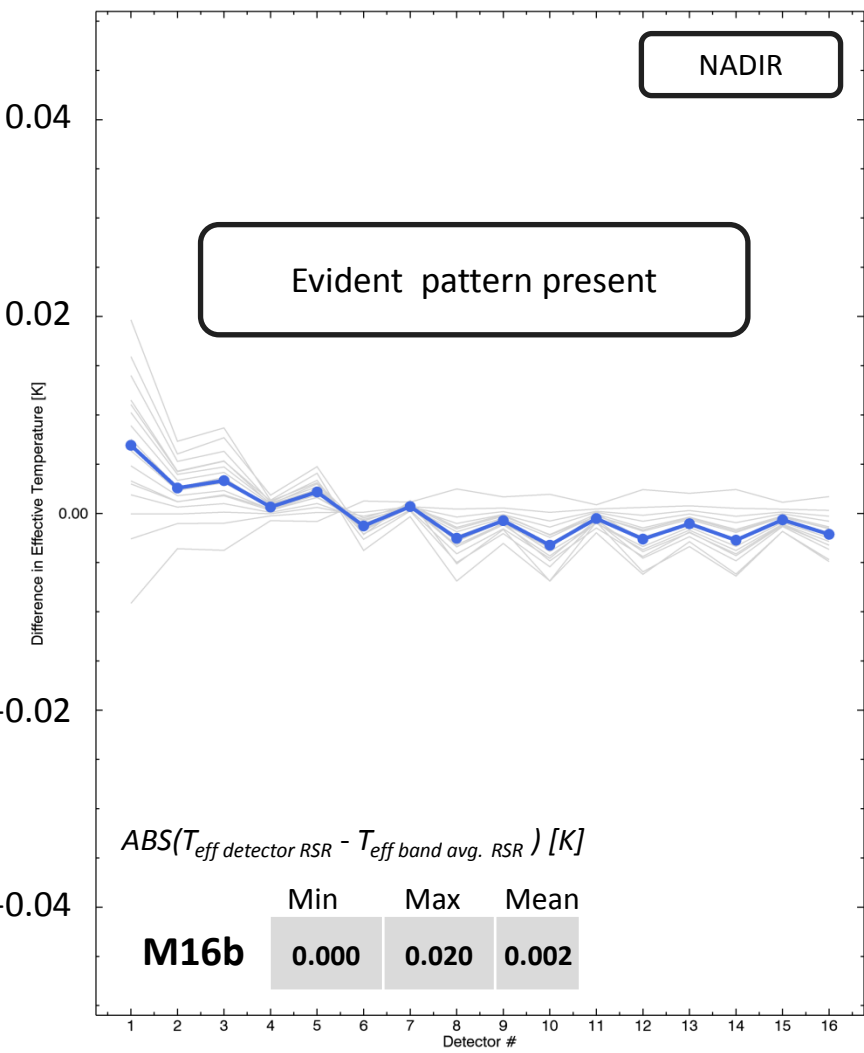


$$M16b (\Delta T_{eff} = T_{eff \text{ detector RSR}} - T_{eff \text{ band avg. RSR}})$$

$NE\Delta T (270 \text{ to } 300 \text{ K}) = \sim 0.03 \text{ K}$

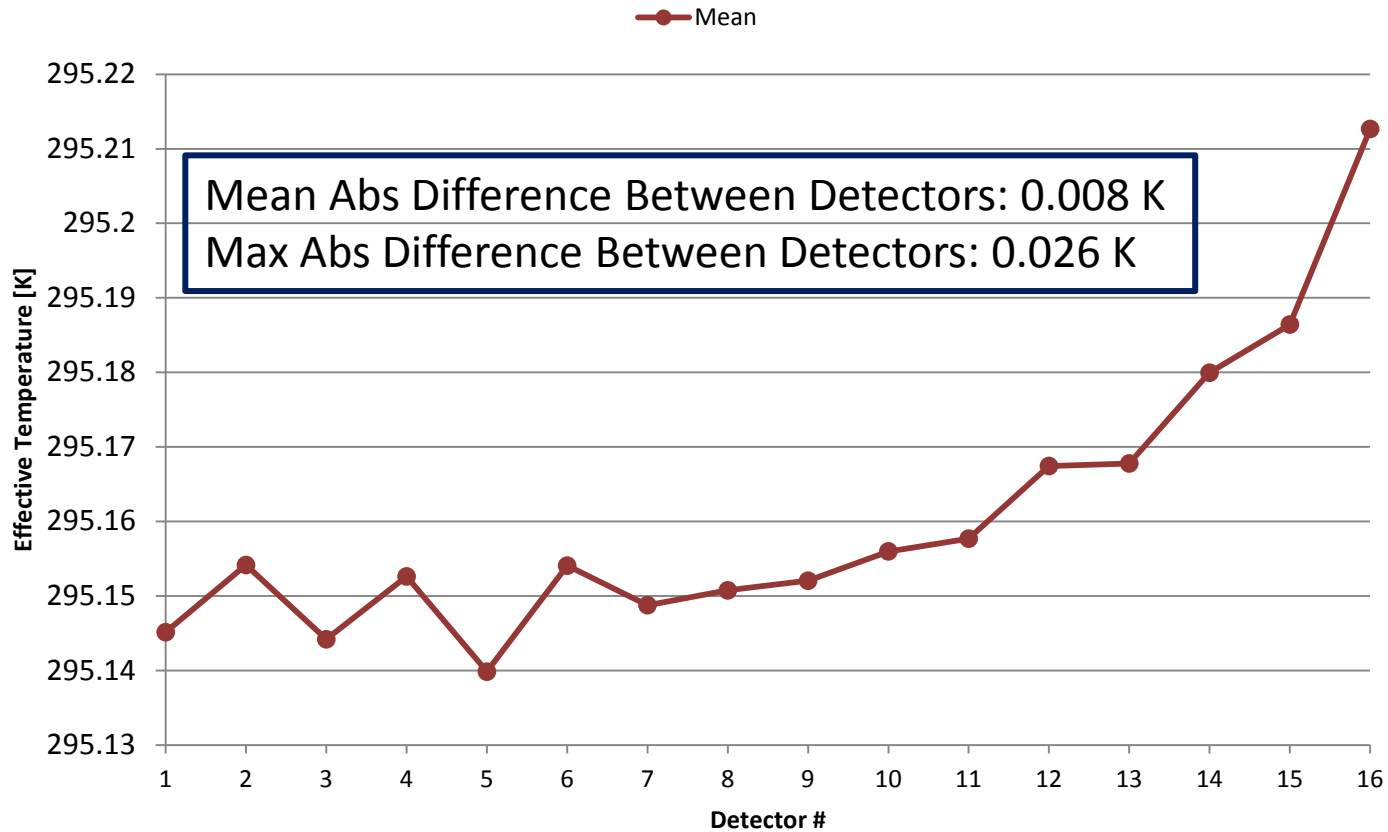
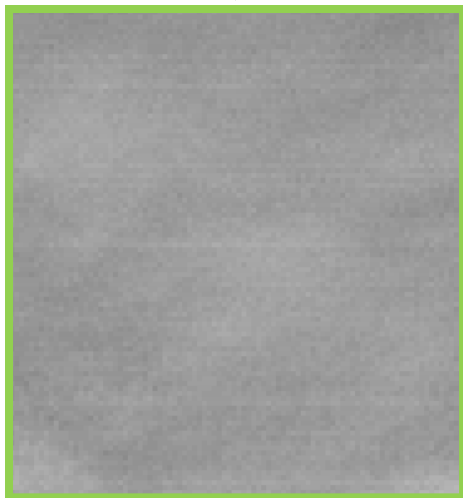
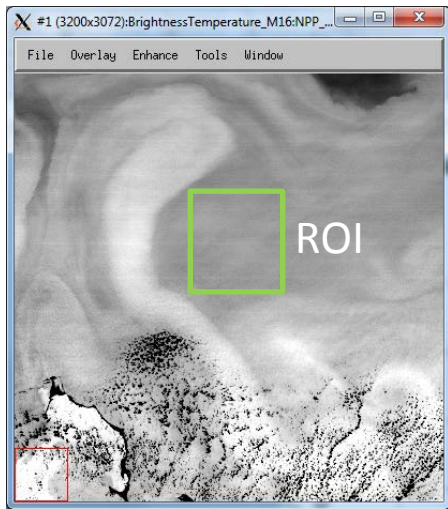
Detector-Level RSR - Band Avg. RSR (All Atms) at NADIR

Detector-Level RSR - Band Avg. RSR (All Atms) at 56.063 deg OFF-NADIR



Date: May 6, 2014
Time: 06:35 UTC

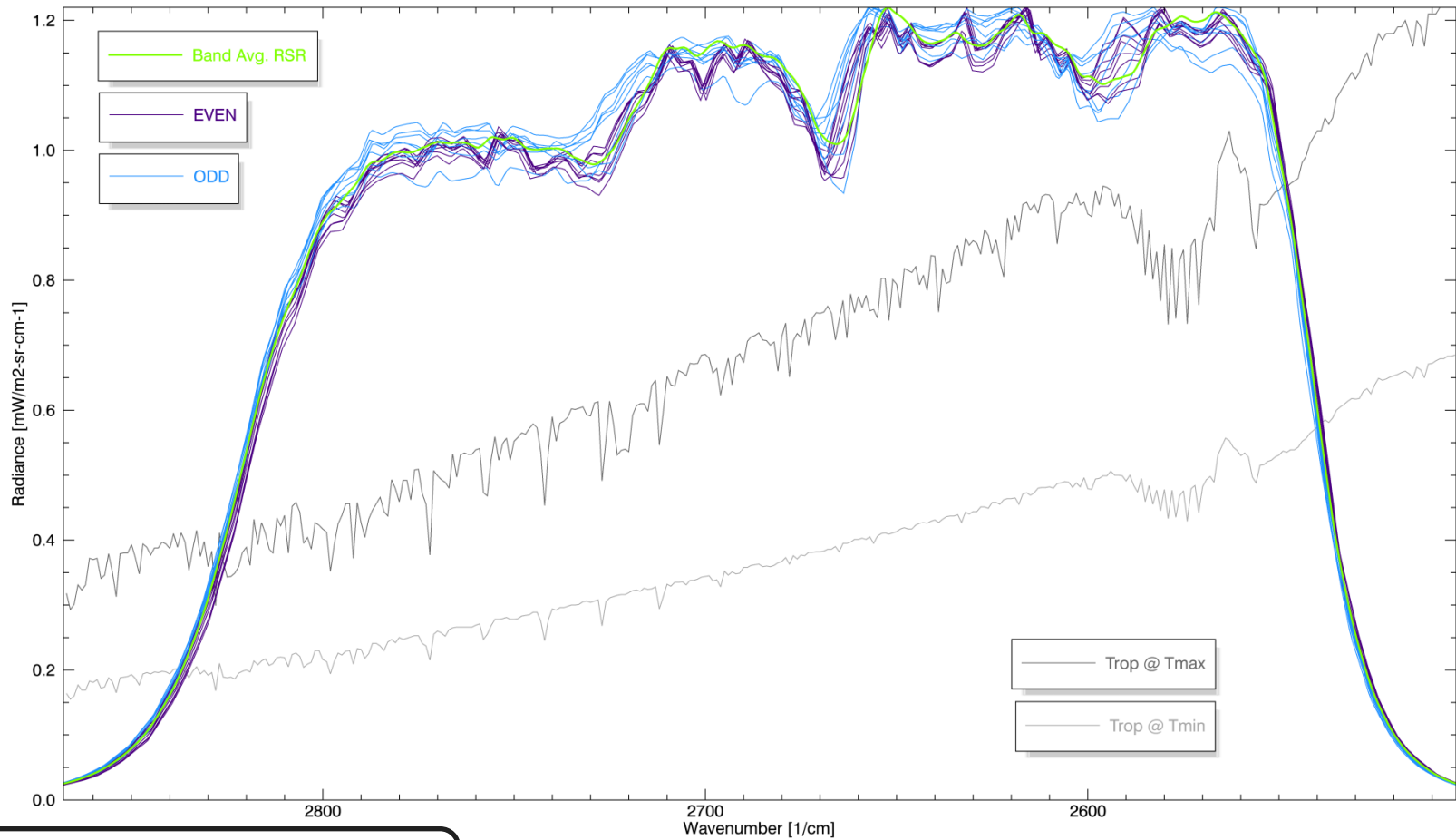
Average of 6 Six Scans (91 pixels/detector) Over a "Uniform" Ocean ROI: M16



[NPP_VMAE_L1.A2014126.0635.P1_03002.2014126121715.hdf](https://data.nasda.nasa.gov/data/JPSS1/SuomiNPP/2014/05/06/0635/P1_03002.2014126121715.hdf)

14 Detector-Level RSRs

14 Detector-Level and Band Avg. RSRs



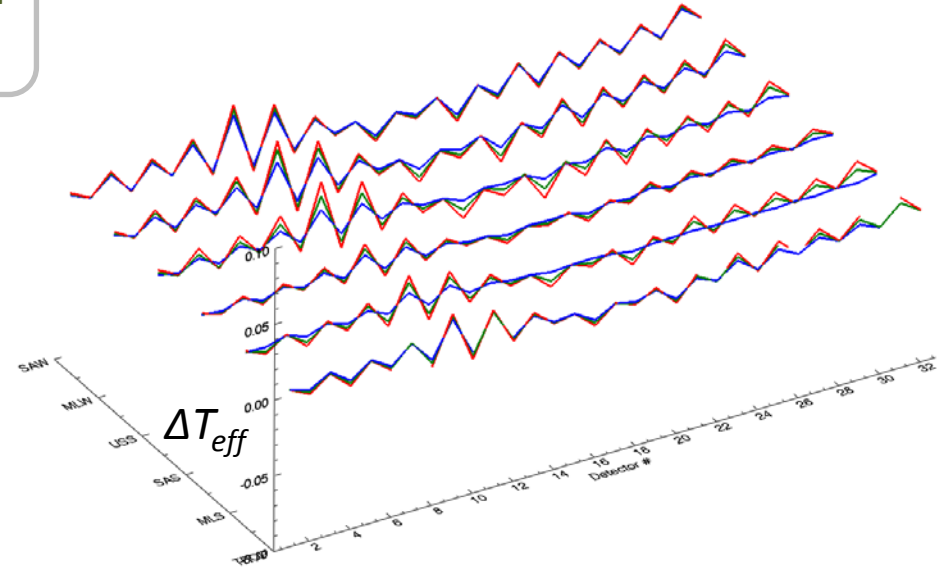
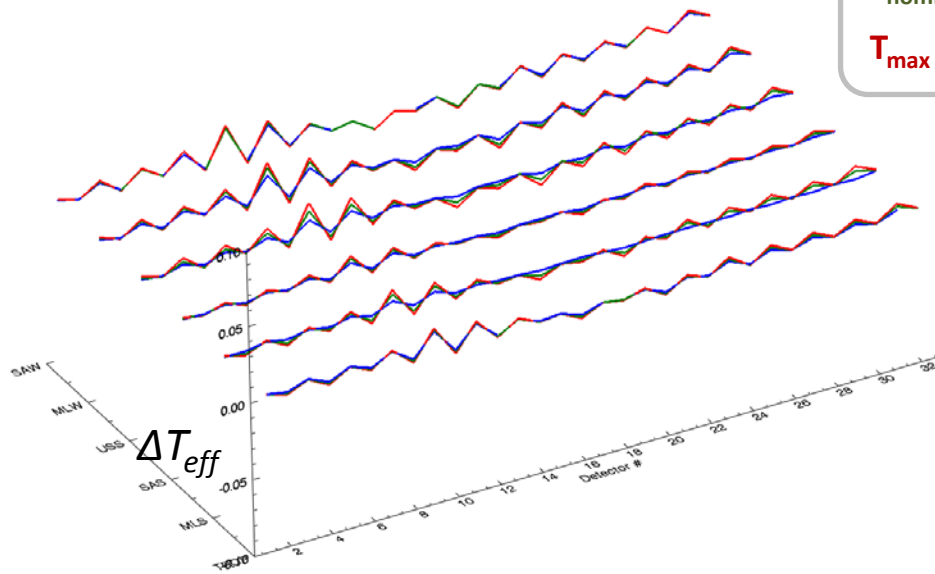
Strong odd/even pattern present

$$14 (\Delta T_{eff} = T_{eff \text{ detector RSR}} - T_{eff \text{ band avg. RSR}})$$

NADIR

T_{min}
 $T_{nominal}$
 T_{max}

OFF-NADIR

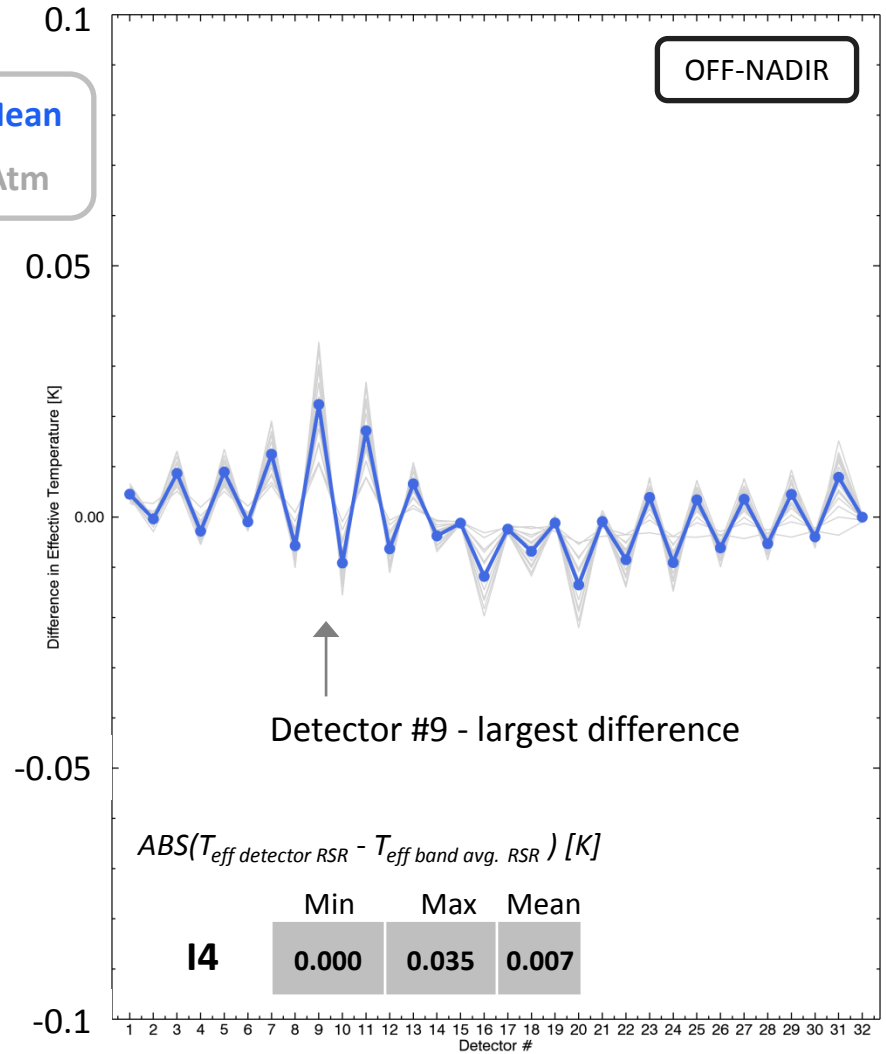
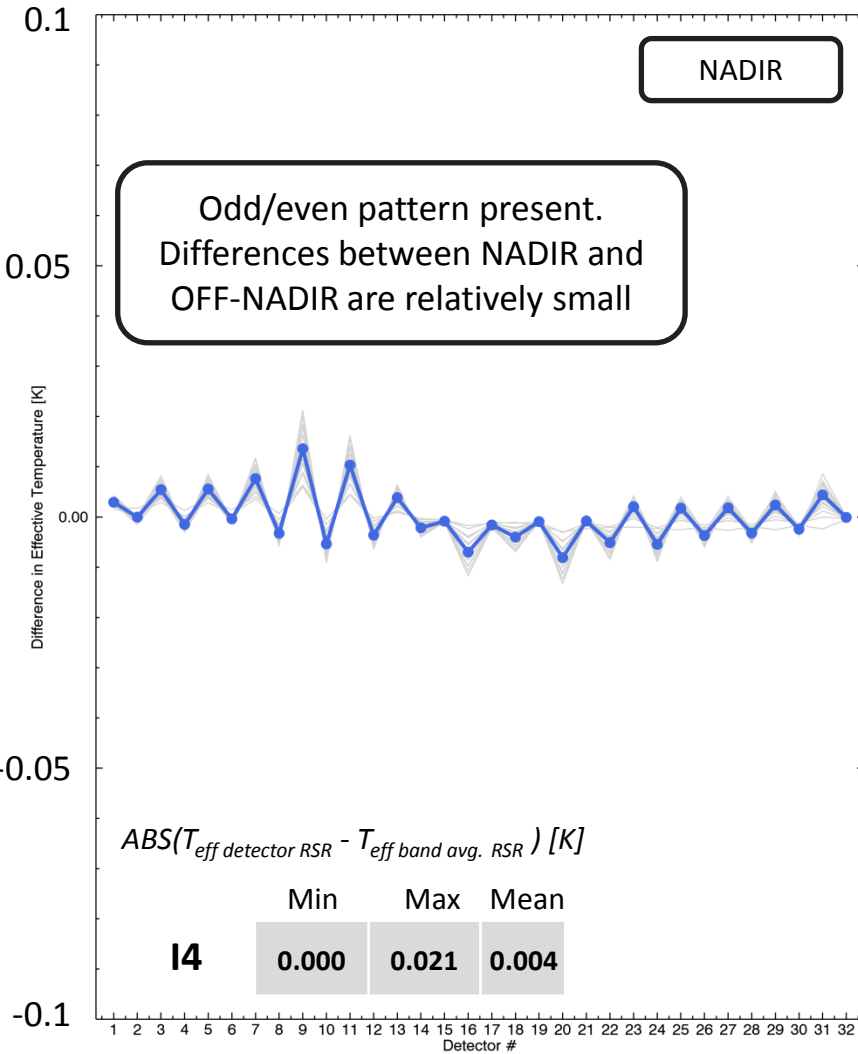


$$I4 (\Delta T_{eff} = T_{eff \text{ detector RSR}} - T_{eff \text{ band avg. RSR}})$$

$NE\Delta T (270 \text{ to } 300 \text{ K}) = \sim 0.35 \text{ to } 0.11 \text{ K}$

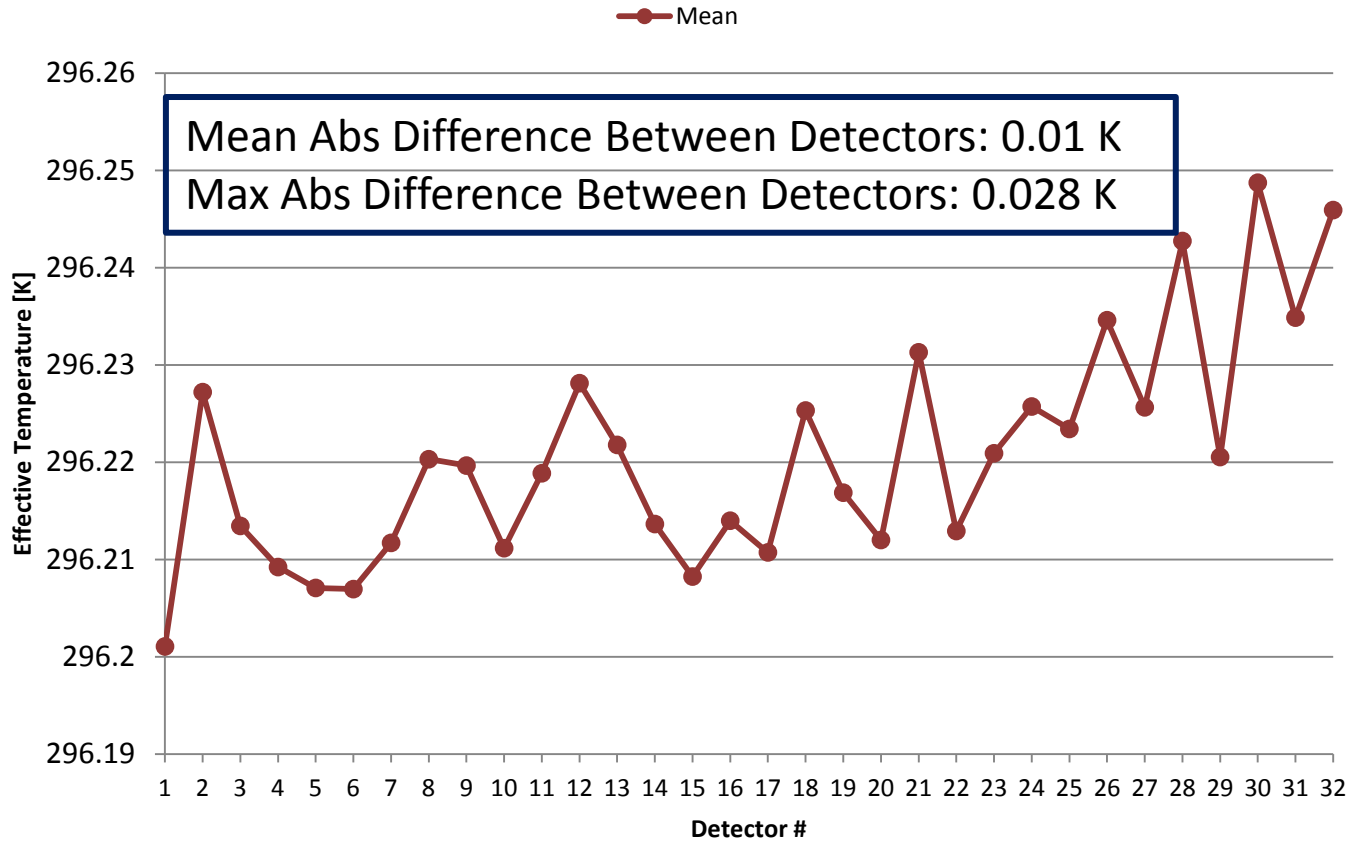
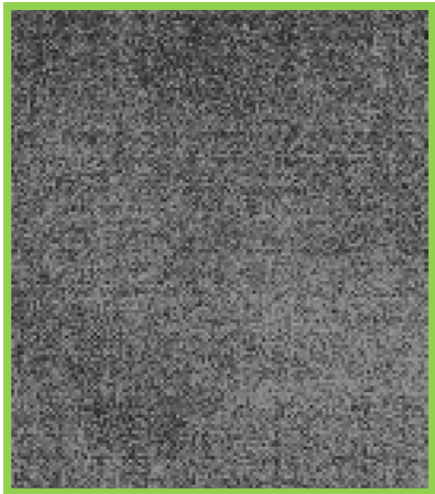
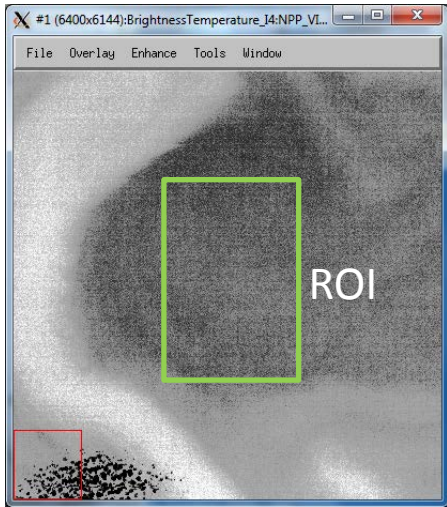
Detector-Level RSR - Band Avg. RSR (All Atms) at NADIR

Detector-Level RSR - Band Avg. RSR (All Atms) at 56.063 deg OFF-NADIR



Date: May 6, 2014
Time: 06:35 UTC

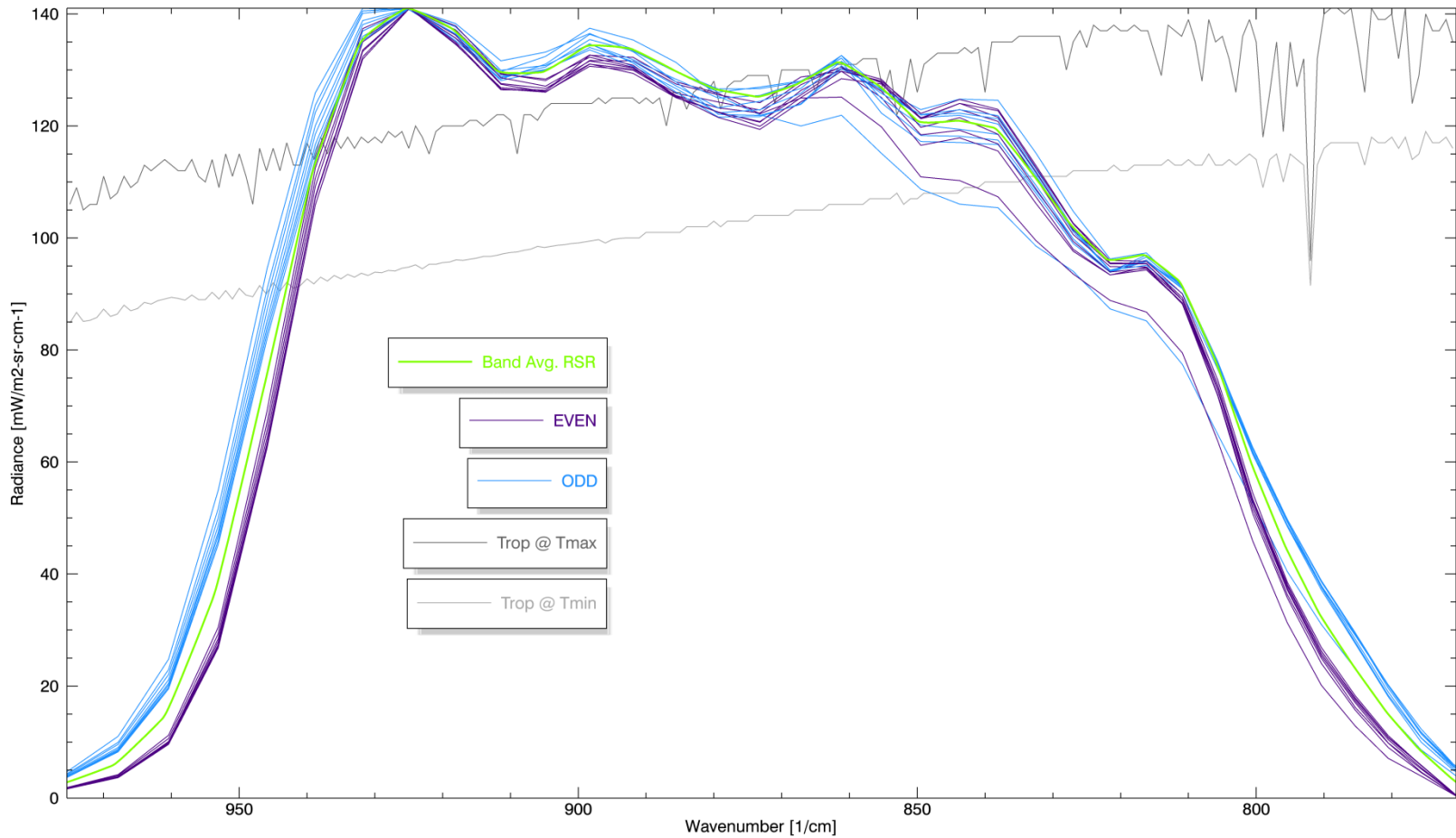
Average of 6 Six Scans (128 pixels/detector) Over a "Uniform" Ocean ROI: I4



[NPP_VMAE_L1.A2014126.0635.P1_03002.2014126121715.hdf](#)

15 Detector-Level RSRs

15 Detector-Level and Band Avg. RSRs



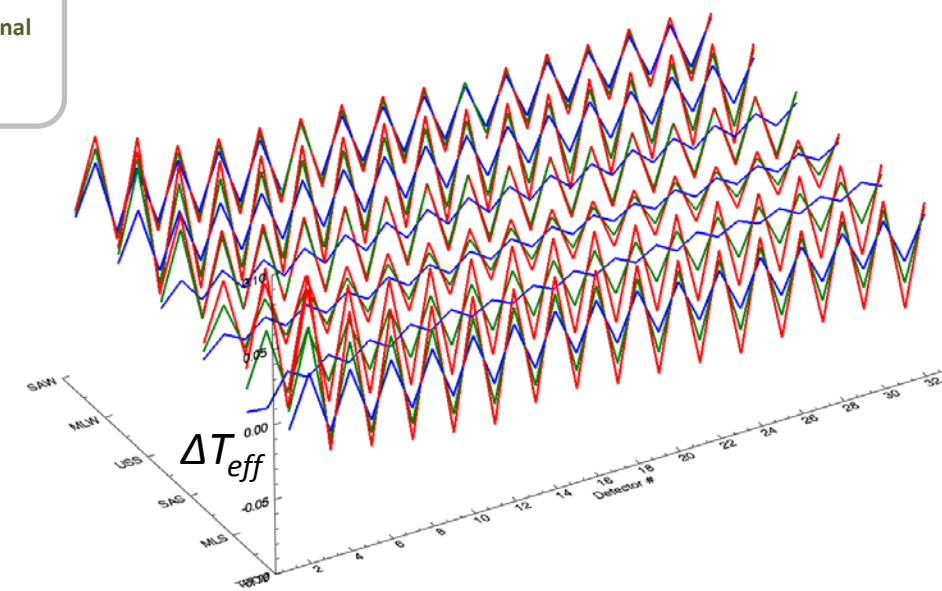
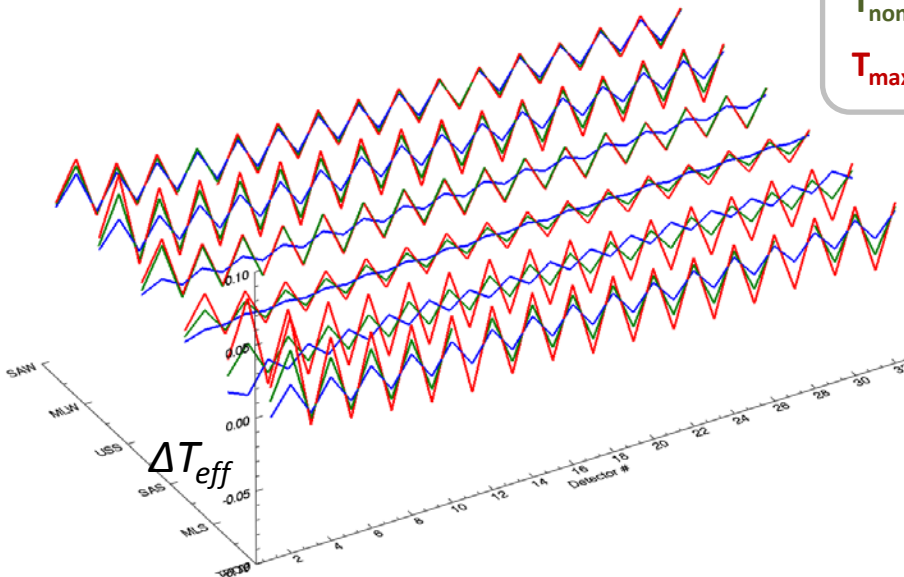
Strong odd/even pattern present

$$15 (\Delta T_{eff} = T_{eff \text{ detector RSR}} - T_{eff \text{ band avg. RSR}})$$

NADIR

OFF-NADIR

T_{min}
 $T_{nominal}$
 T_{max}

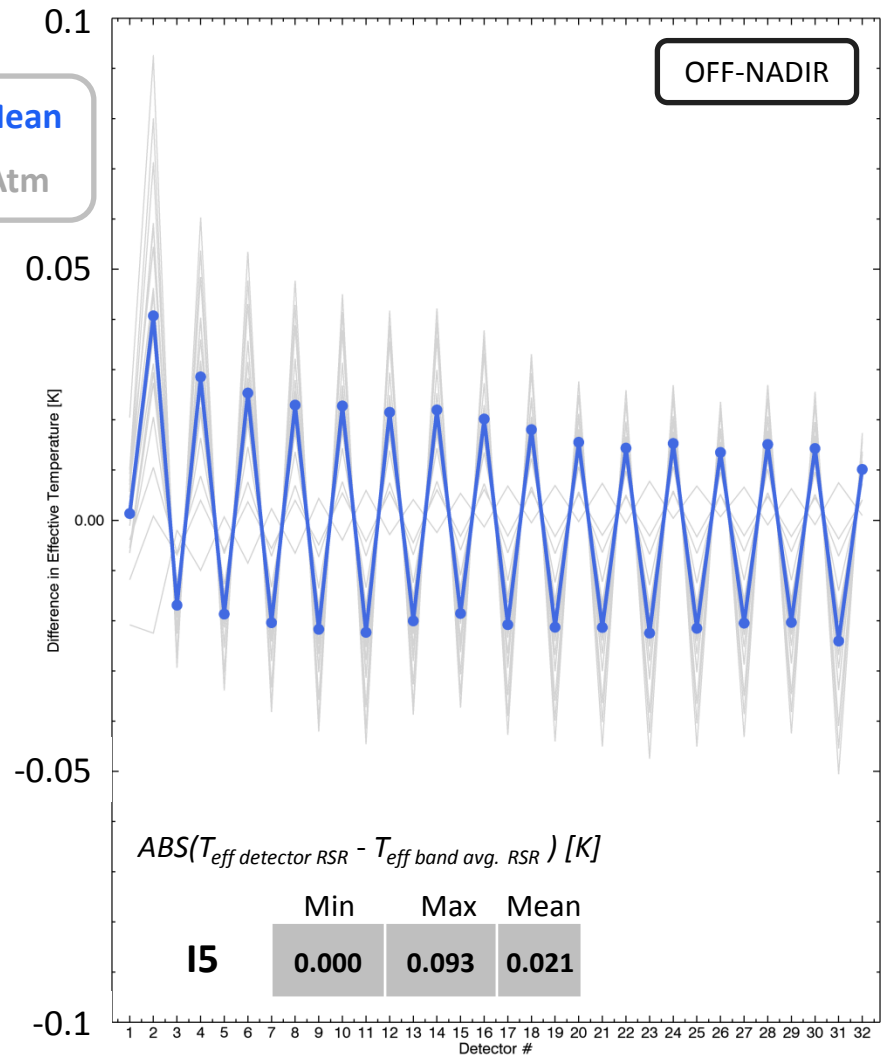
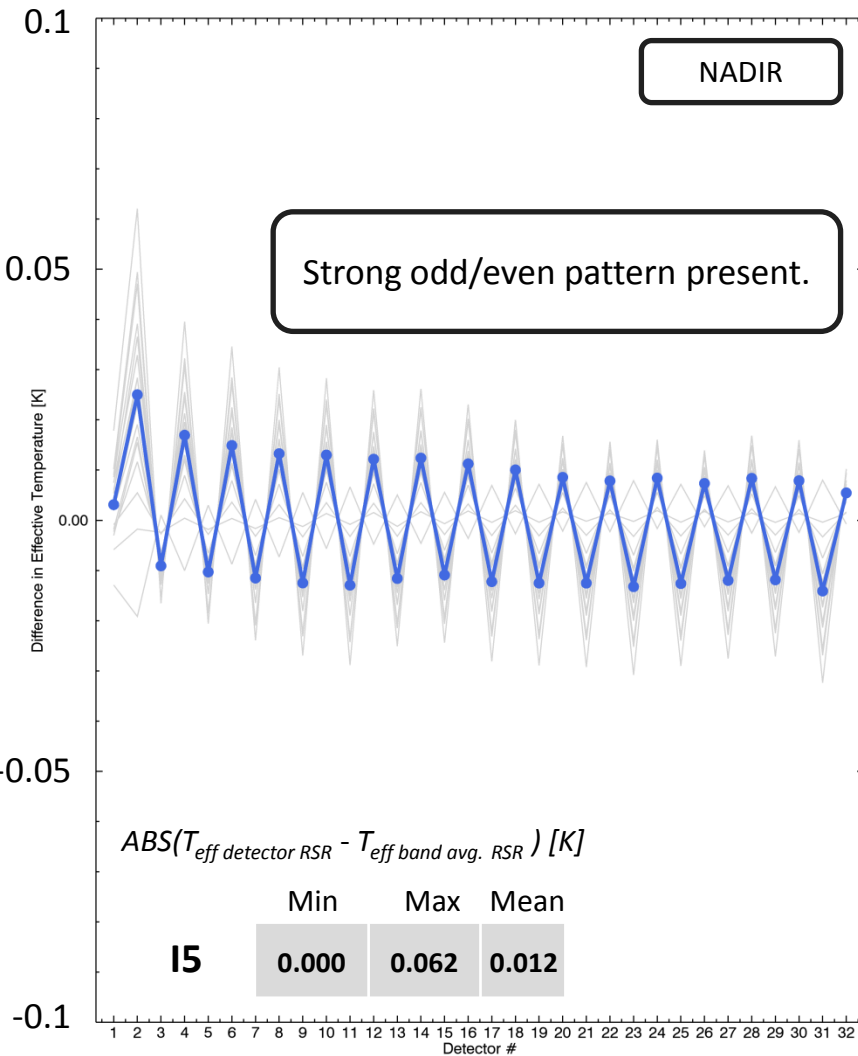


$$15 \left(\Delta T_{eff} = T_{eff \text{ detector RSR}} - T_{eff \text{ band avg. RSR}} \right)$$

$NE\Delta T$ (270 to 300 K) = ~0.2 to 0.15 K

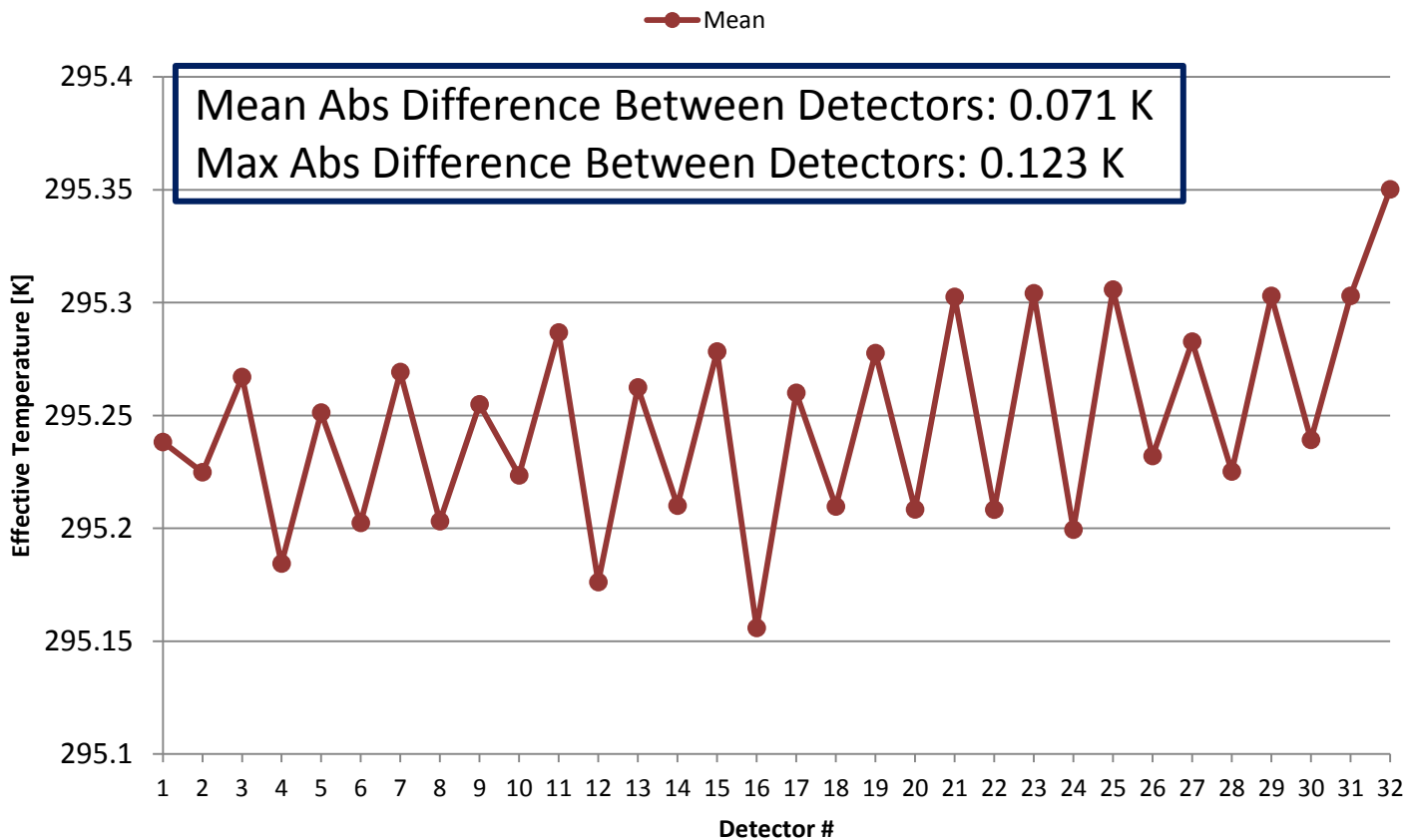
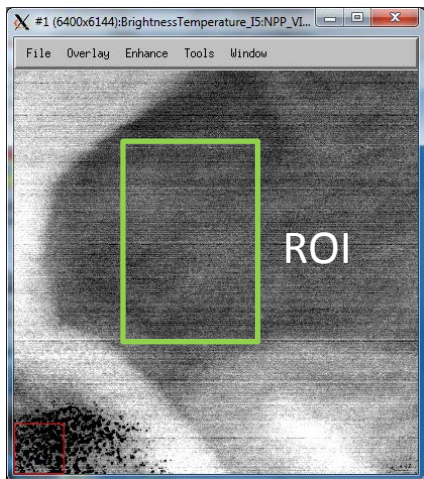
Detector-Level RSR - Band Avg. RSR (All Atms) at NADIR

Detector-Level RSR - Band Avg. RSR (All Atms) at 56.063 deg OFF-NADIR



Date: May 6, 2014
Time: 06:35 UTC

**Average of 6 Six Scans (128 pixels/detector) Over a
"Uniform" Ocean ROI: I5**



[NPP_VMAE_L1.A2014126.0635.P1_03002.2014126121715.hdf](#)

- » Band average processing meets specification although not optimal
- » Atmospheric effects can amplify differences between detectors
- » Detector-level processing is ideal
- » Detector-Level atmospheric dependencies were observed in all bands
 - M12 & M14 demonstrated the weakest atmospheric dependencies
 - M13 & I5 demonstrated the strongest atmospheric dependencies
 - Evident in observed data
- » Odd/Even pattern observed in most channels

Future work:

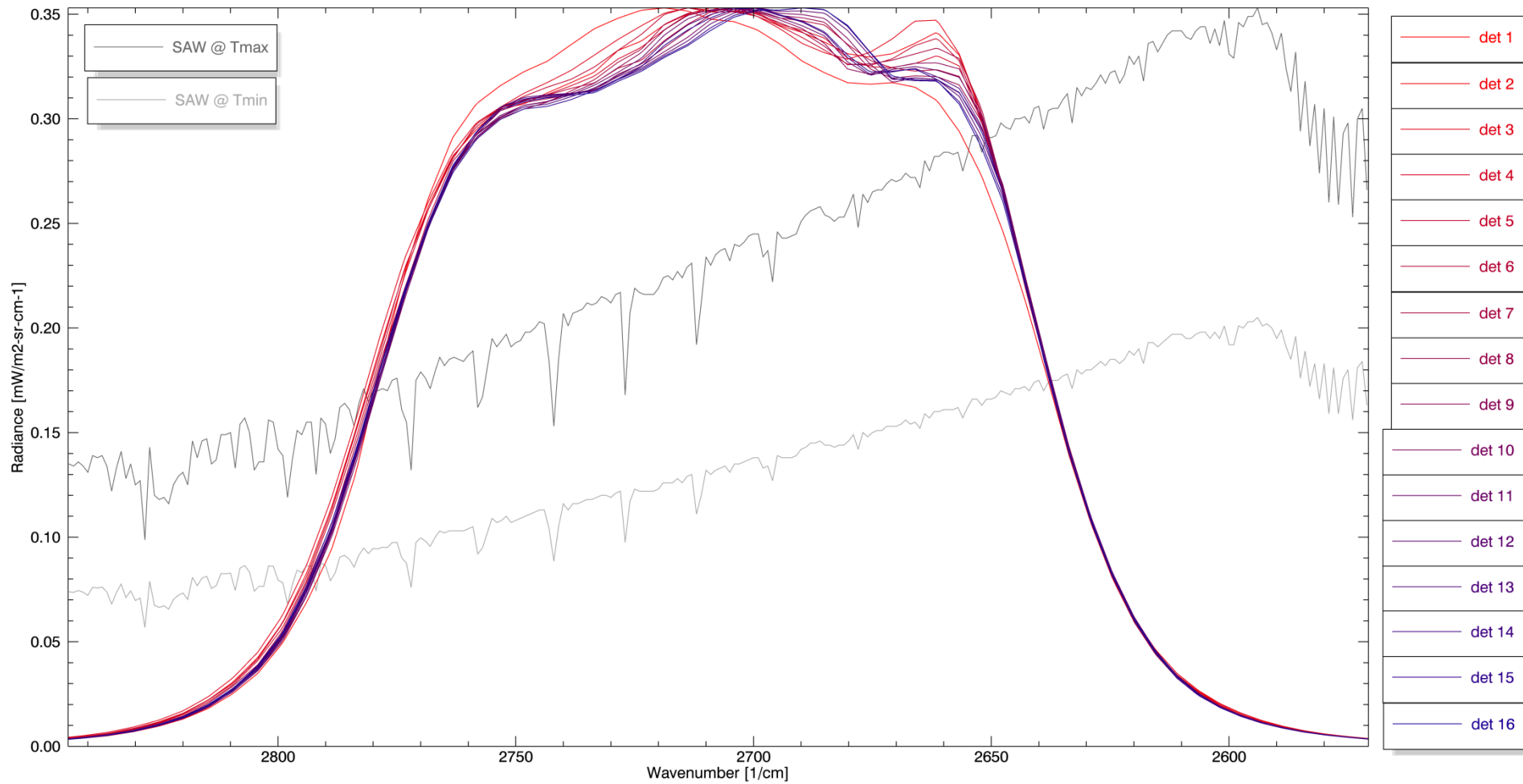
- » Discuss findings with EDR teams on possibilities of detector level processing
- » Further investigate image artifacts found in observed data

Band	NADIR [0°]			OFF-NADIR [56.063°]		
	$ABS(T_{eff\ detector\ RSR} - T_{eff\ band\ avg.\ RSR}) [K]$			$ABS(T_{eff\ detector\ RSR} - T_{eff\ band\ avg.\ RSR}) [K]$		
	Min	Max	Mean	Min	Max	Mean
M12	0.000	0.007	0.002	0.000	0.012	0.003
M13	0.012	0.162	0.078	0.000	0.159	0.077
M14	0.000	0.014	0.001	0.000	0.018	0.002
M15	0.000	0.030	0.005	0.000	0.049	0.009
M16a	0.000	0.019	0.003	0.000	0.028	0.004
M16b	0.000	0.020	0.002	0.000	0.030	0.004
I4	0.000	0.021	0.004	0.000	0.035	0.007
I5	0.000	0.062	0.012	0.000	0.093	0.021

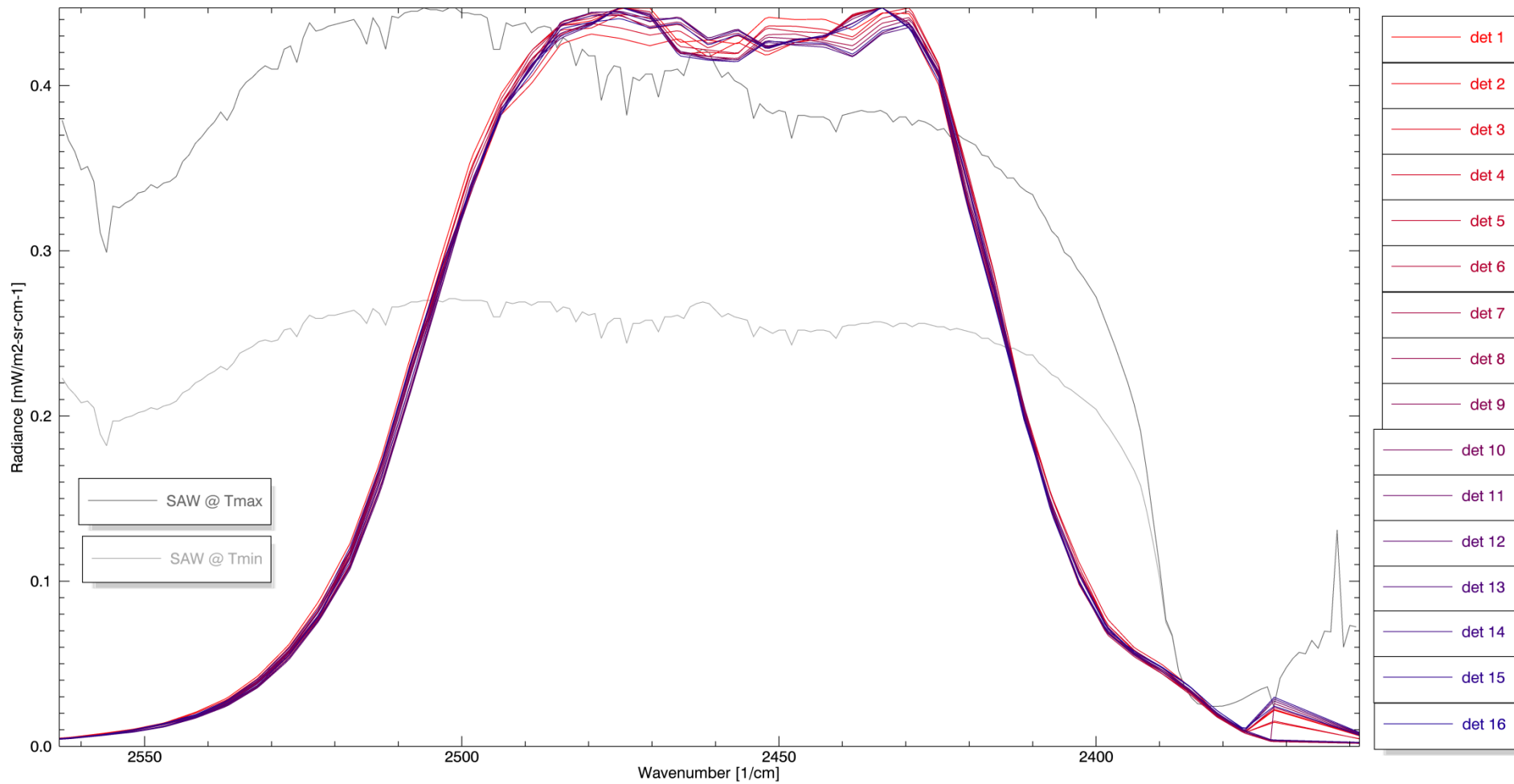


BACKUP

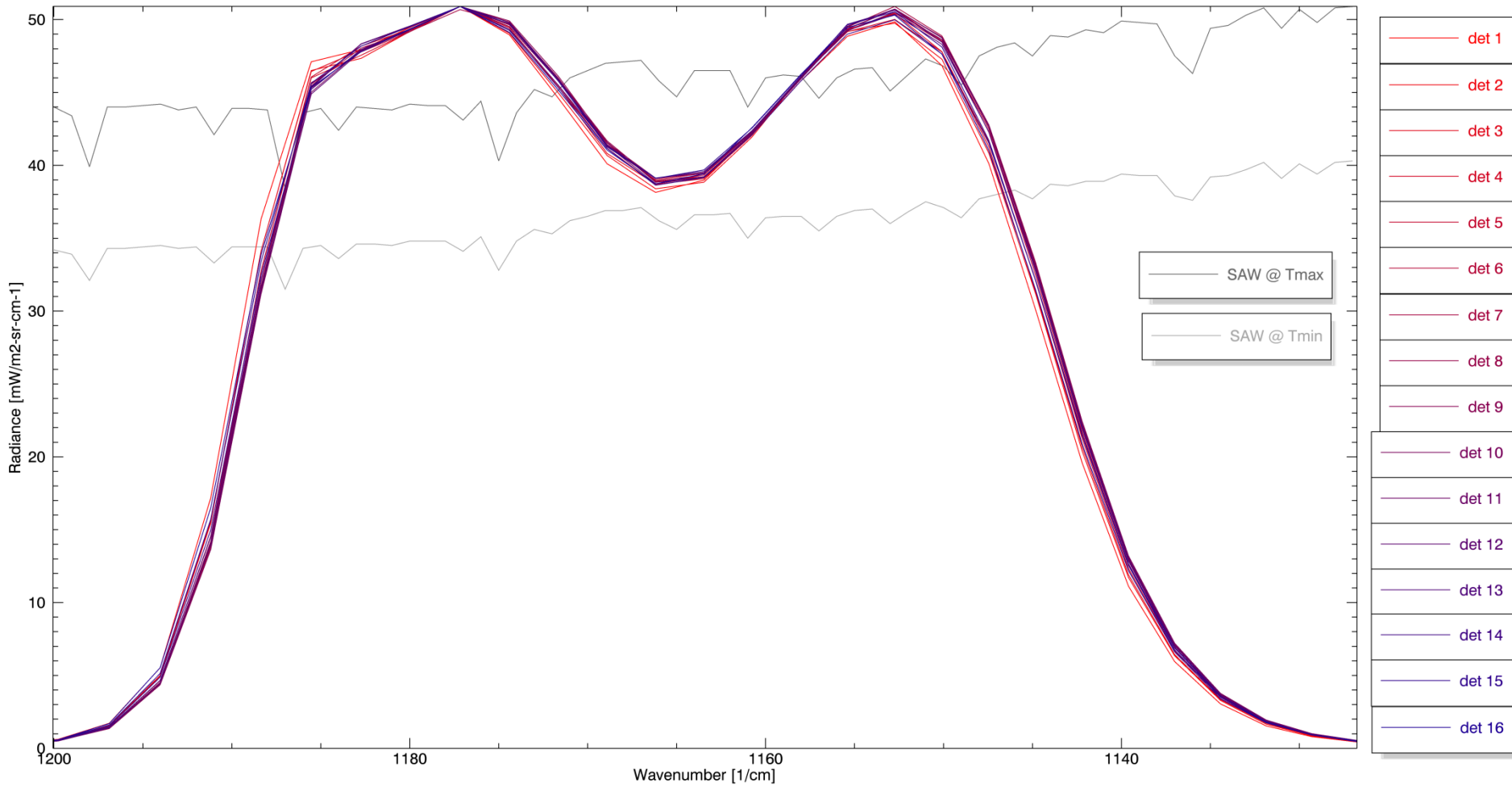
M12 Detector-Level RSRs



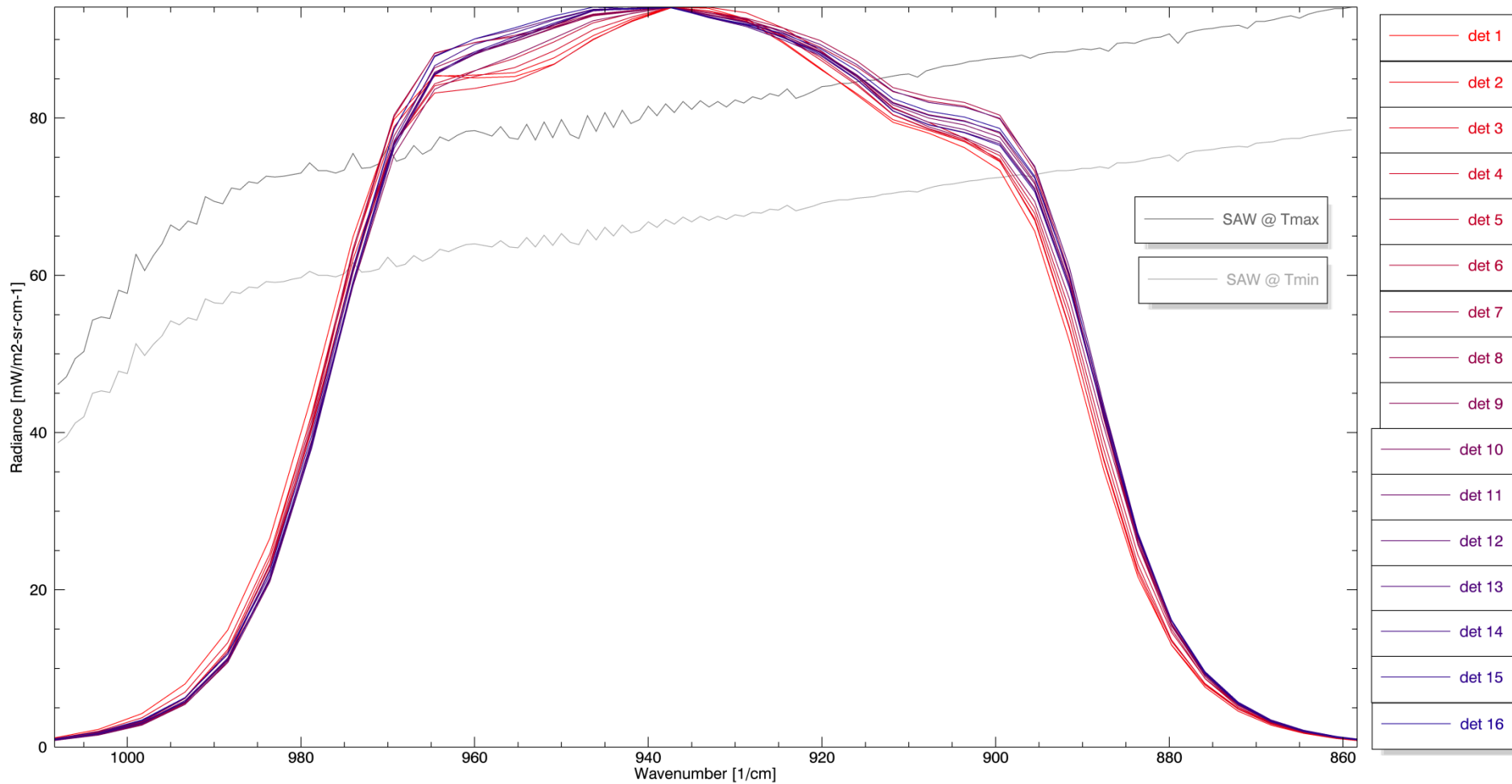
M13 Detector-Level RSRs



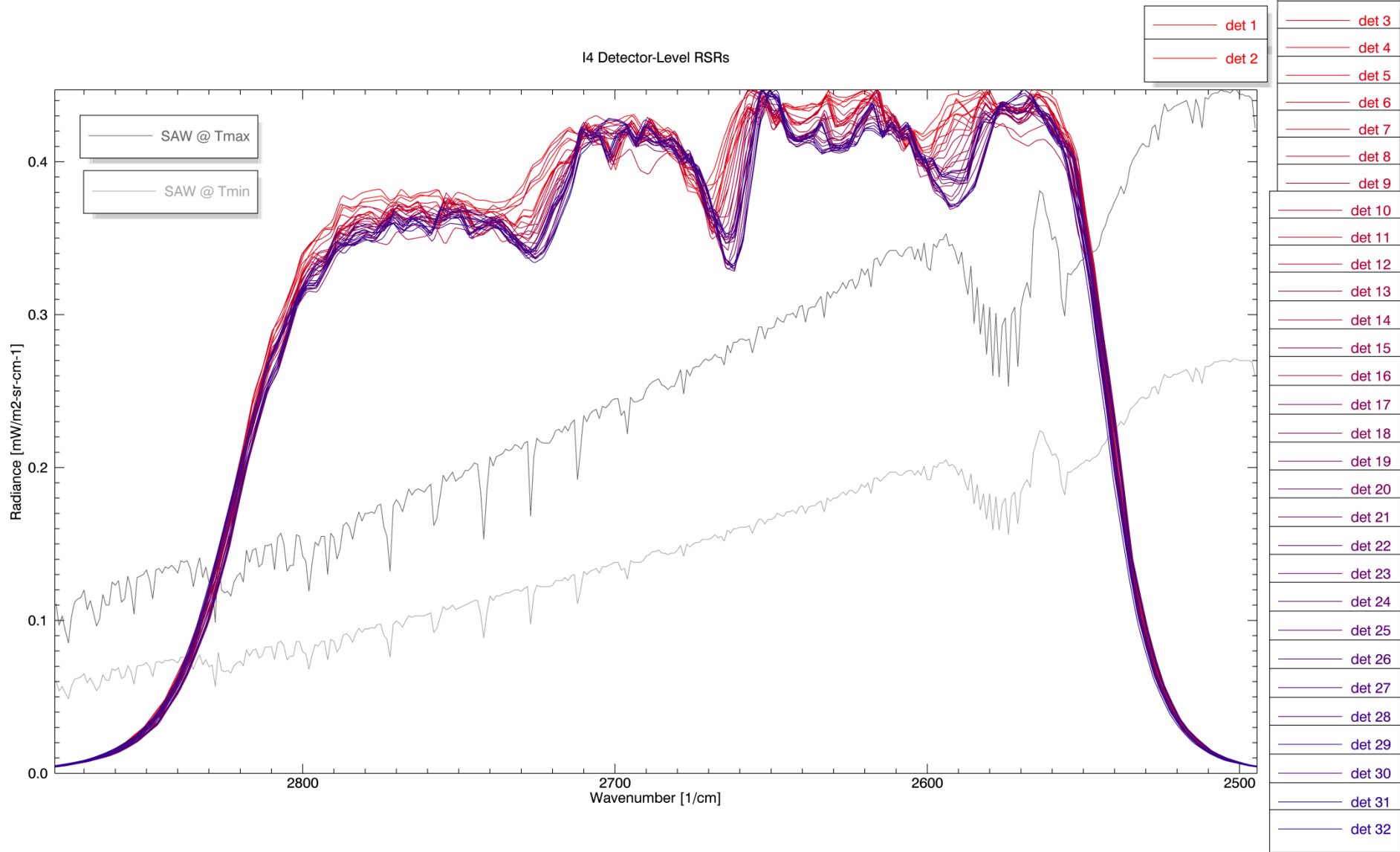
M14 Detector-Level RSRs

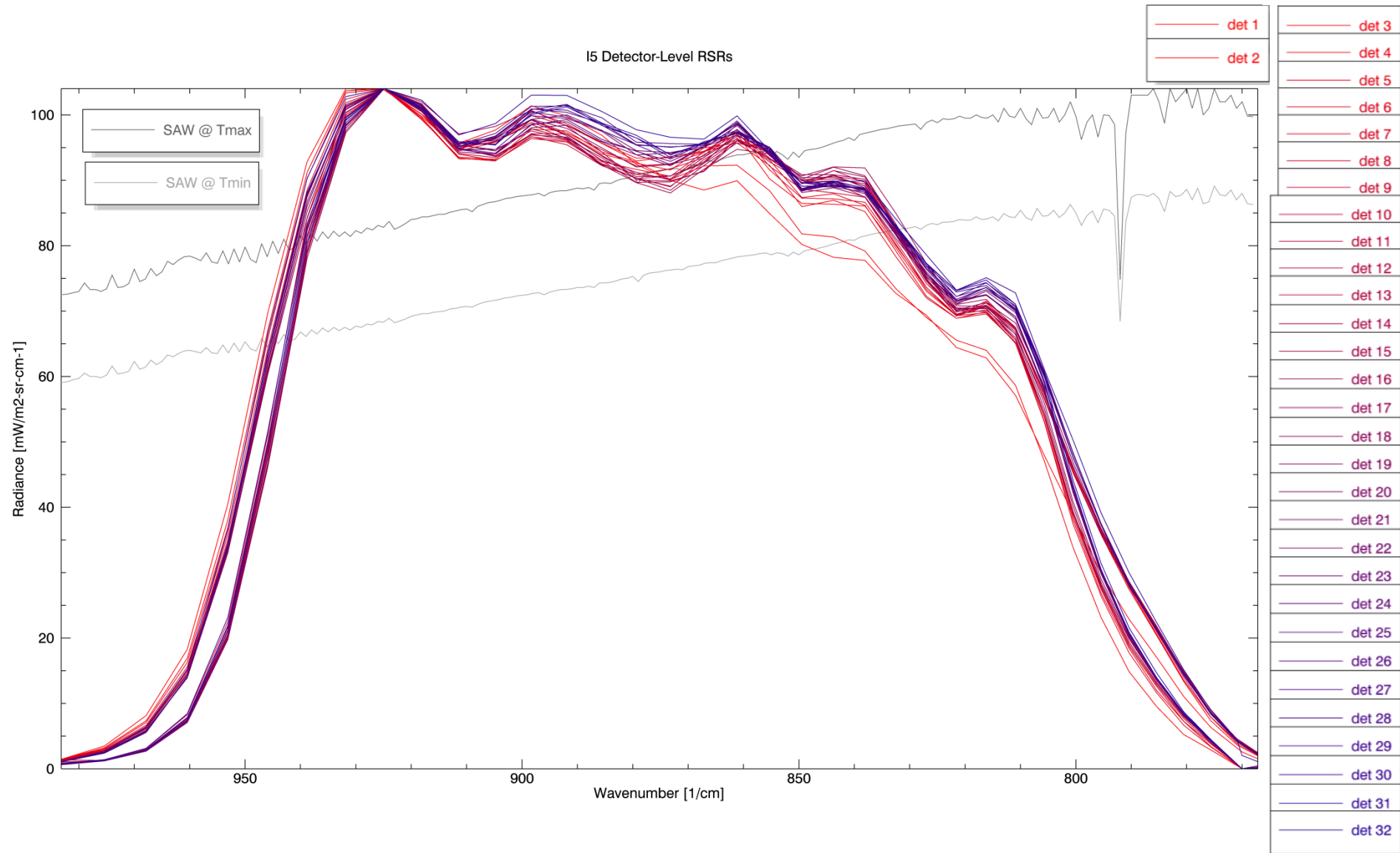


M15 Detector-Level RSRs



I4 Detector-Level RSRs





On-orbit radiometric characterization of Suomi NPP Day/Night Band (DNB)

THE VALUE OF PERFORMANCE.
NORTHROP GRUMMAN

JPSS Science Team Meeting, May 12-16, 2014

L. B. Liao, Stephanie Weiss, and

Calvin Liang

- General DNB characteristics
- Radiometric sensitivity
 - Dynamic Range and saturation issues
 - SNR
 - Impact of airglow on offset
- Radiometric Accuracy
 - Radiometric accuracy
 - Low gain stage (LGS) radiometric accuracy from direct lunar observation
 - High gain stage (HGS) radiometric accuracy from lunar illuminated ground scenes
 - Mid gain stage (MGS) radiometric accuracy inferred from calibration transfer uncertainty
 - Stray light, stray light correction and remaining stray light issues.
- Recommendations

DNB Characteristics: meeting most performance requirements

In backup

Covered in this talk

1. DNB Characteristics	Specification	Prelaunch Performance	On-orbit Performance
Spectral Passband center	700 ±14 nm	707 nm	Model estimate 694 nm ⁽¹⁾
Spectral Passband bandwidth	400 ±20 nm	379 nm	Model estimate 375 nm ⁽¹⁾
Horizontal Sampling Interval (HSI)	742 m (±5%)	742 m (±9%) scan 742 m (±7%) track	704-790 m (scan) 734-777 m (track)
Horizontal Spatial Resolution (HSR)	≤ 800 m	< 820 m, scan < 670 m, track	< 770 m, <52° < 750 m, <52°
Geolocation uncertainty (3σ) on ellipsoid	400 m nadir 1500 m edge	N/A	249 m (nadir) 1041 m (edge)
Dynamic Range	3x10 ⁻⁹ W·cm ⁻² ·sr ⁻¹ – 0.02 W·cm ⁻² ·sr ⁻¹	3x10 ⁻⁹ W·cm ⁻² ·sr ⁻¹ – 0.021 W·cm ⁻² ·sr ⁻¹	3x10 ⁻⁹ W·cm ⁻² ·sr ⁻¹ – 0.0209 W·cm ⁻² ·sr ⁻¹
SNR @ <53 deg	≥6 @ Lmin	>10 across scan	>9 across scan now
SNR @ ≥ 53 deg	≥5 @ Lmin		>8 projected EOL
Calibration Uncertainty LGS ⁽²⁾	5%/10% (0.5 Lmax/ transition to MGS)	3.5%	[4%,8%] (1 σ, ROLO); 8% [-4%,2%] (1 σ, Modis) 4%
Calibration Uncertainty MGS ⁽²⁾	10%/30% (upper/ lower transition)	7.8%	[-7.7%, 5.7%] (1 σ) ⁽⁴⁾ ; 7.7% [-9.6%, 7.6%] (1 σ) ^(4,5) 10%
Calibration Uncertainty HGS ⁽²⁾	30%/100% (transition from MGS/ Lmin)	11%	[-2.8%, 15%] ⁽³⁾ ; [-10%, 8.2%] ^(3,4) [0.8%, 18.6%] ; [-6.4%, 11.8%] ⁽⁴⁾ [-9.7%, 14.3%]; [-16.9%] 7.5% ^(4,5)
Stray light	10% of minimum radiance	N/A	>100% Lmin ~15%-205 Lmin after stray light correction

(1) Lei, N., Z. Wang, B. Guenther, X. Xiong, and J. Gleason (2012), Modeling the detector radiometric response gains of the Suomi NPP VIIRS reflective solar bands, *Proc. of SPIE*, **8533**, 853319.

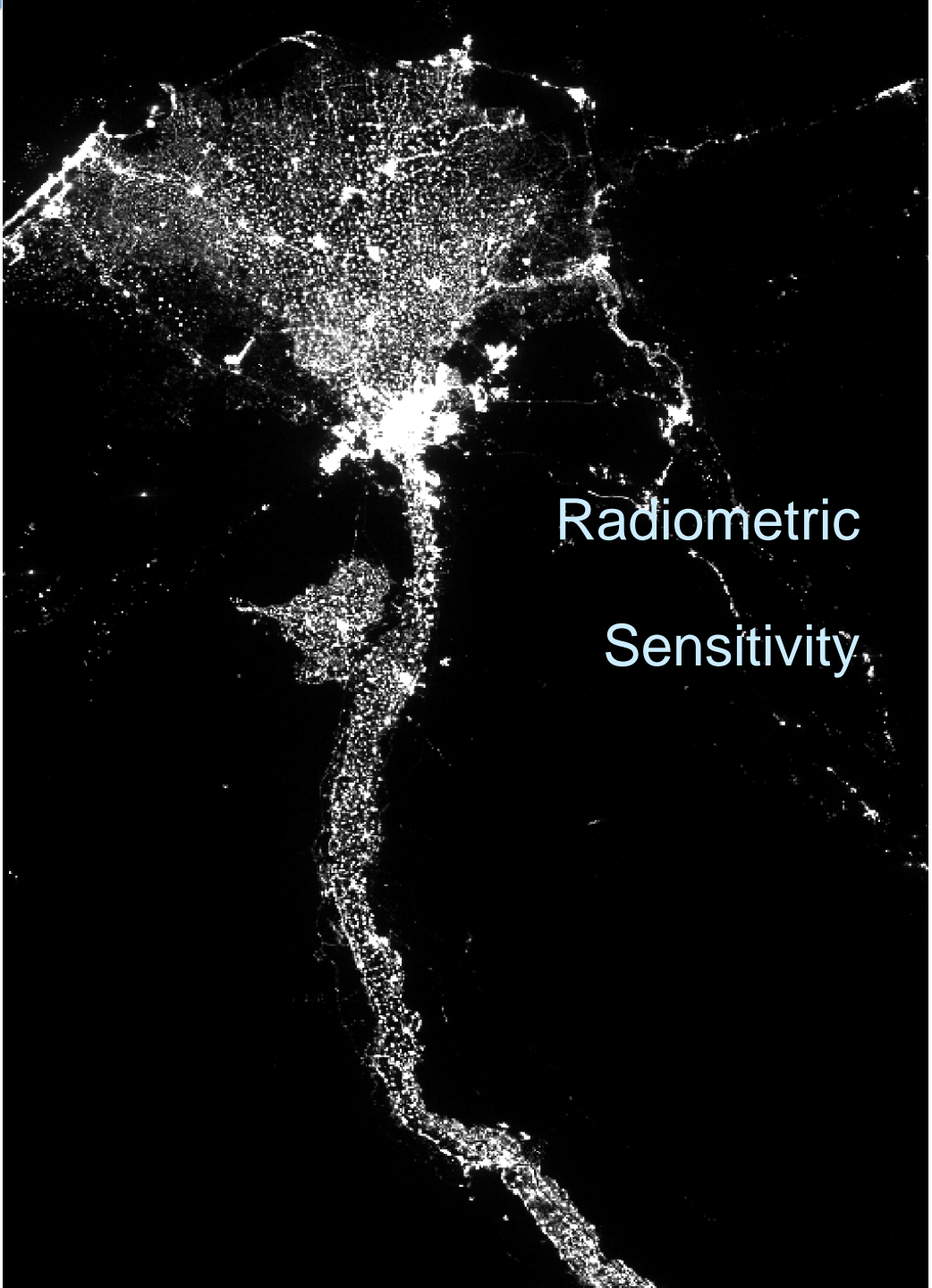
(2) Radiometric uncertainty assumes signal with sufficient SNR. For per measurement uncertainty RSS with 1/SNR.

(3) Before Nov 16, 2012

(4) Inferred comparison with Modis

(5) Includes large scan angle data

THE VALUE OF PERFORMANCE.
NORTHROP GRUMMAN

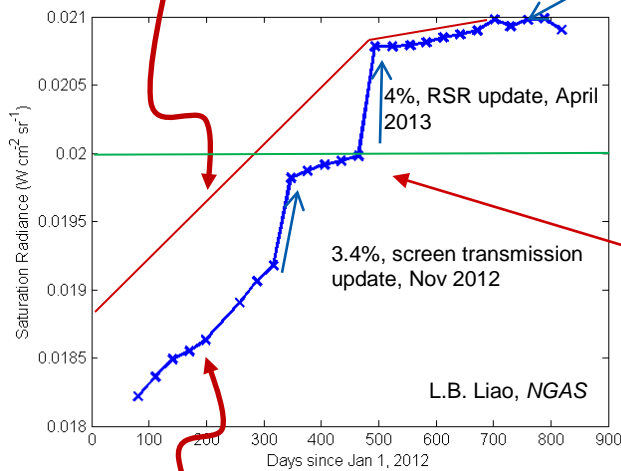


Radiometric
Sensitivity

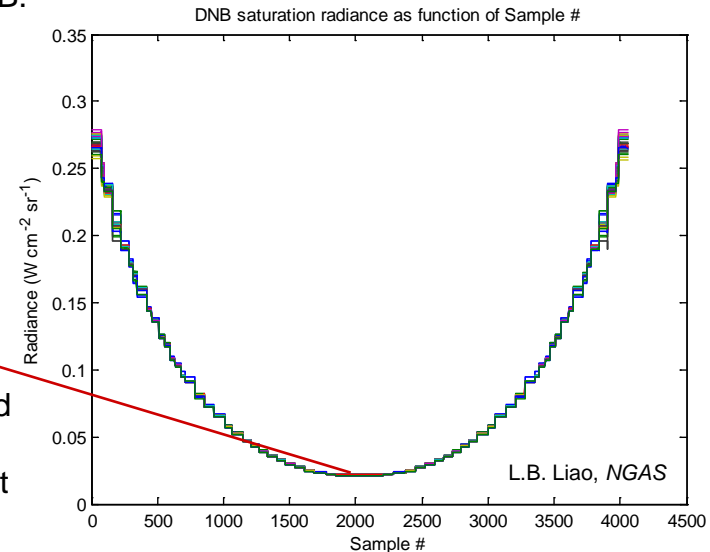
Dynamic Range

Approximate saturated radiance if correct RSR and screen transmission used at all times.

Saturation radiance rolling over, indicating degradation in gain coefficient has stopped for DNB.



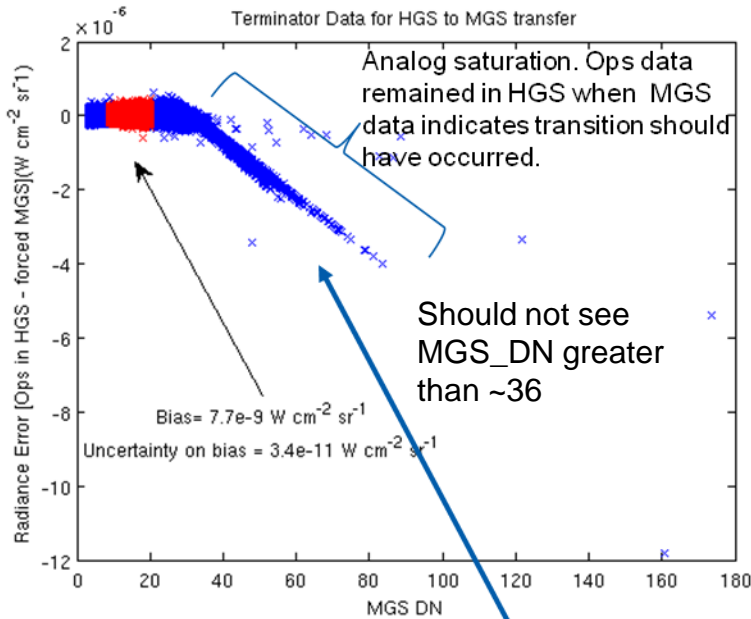
Saturation radiance defined by aggregation zone with lowest saturation radiance value.



Gentle upslope due to RTA throughput degradation.

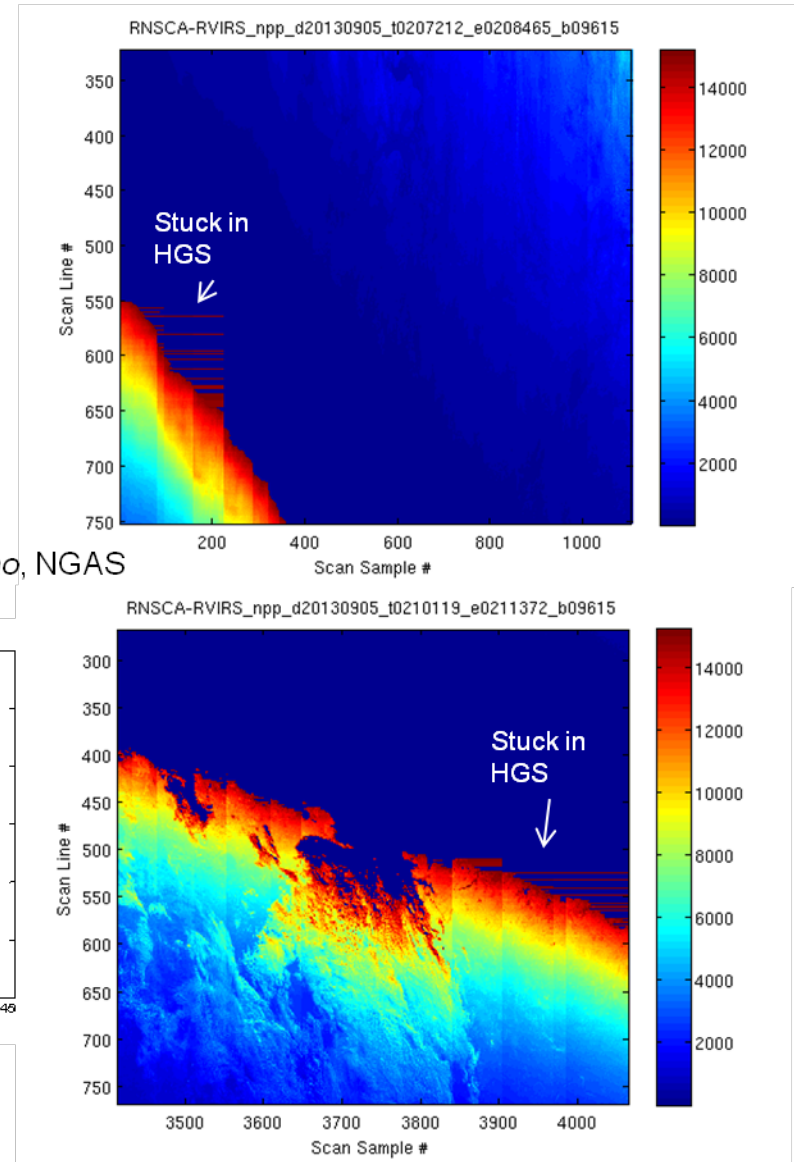
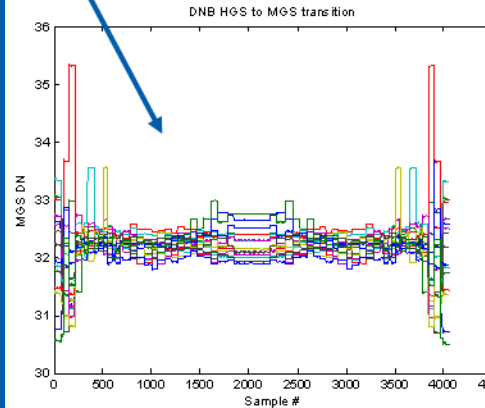
Due to aggregation scheme to keep a constant ground footprint, saturation radiance is a function of scan angle. As of May 2013, saturation radiance meets the requirement of $0.02 \text{ W}\cdot\text{cm}^{-2}\cdot\text{sr}^{-1}$.

Analog saturation (late transition, DR 4603) observed

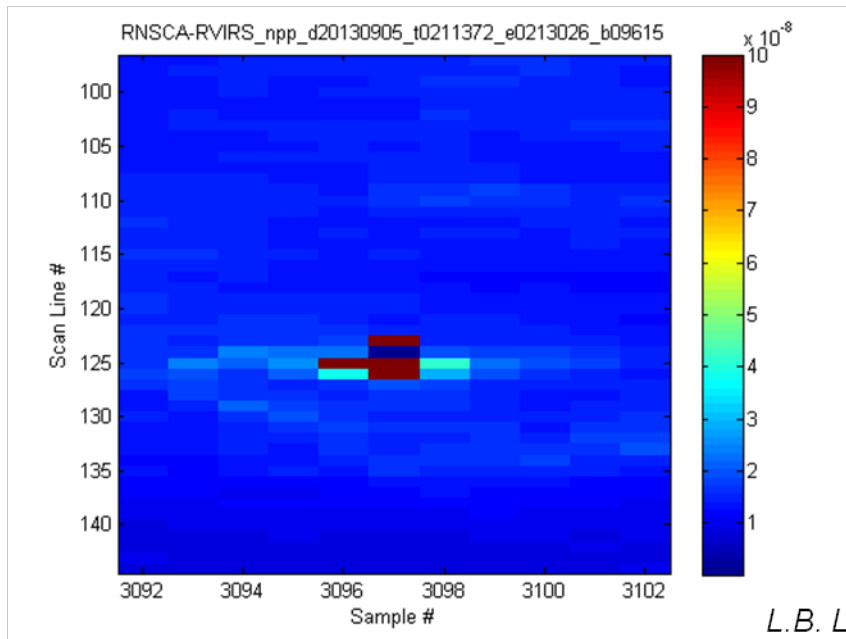


L.B. Liao, NGAS

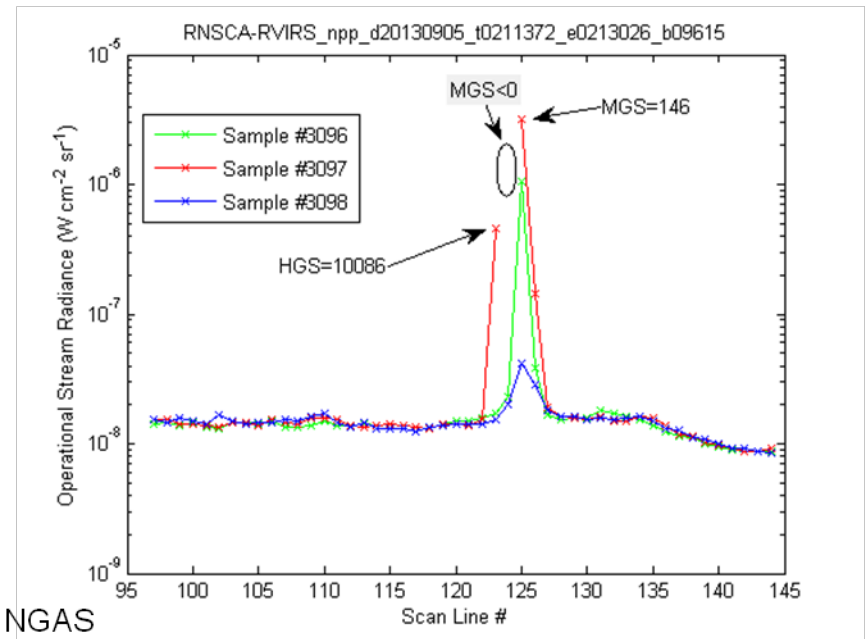
Analog saturation occurs mostly in aggregation zones 29-32. Some isolated pixels occur in other zones. If included in cross cal between stages, saturated pixels will bias c1 for higher sensitivity stages high. This results in higher retrieved radiance for all pixels in the affected aggregation zone. Furthermore, during normal ops, analog saturated pixels will retrieve lower radiance than actual radiance.



Early transition (DR 7364)

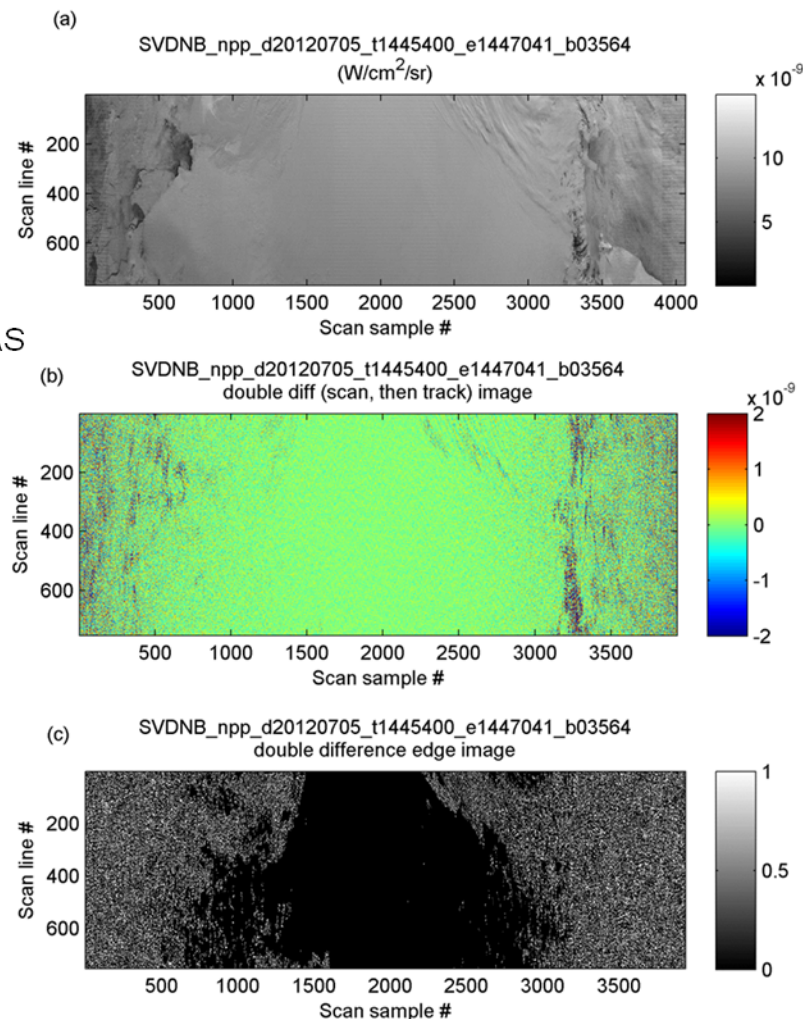
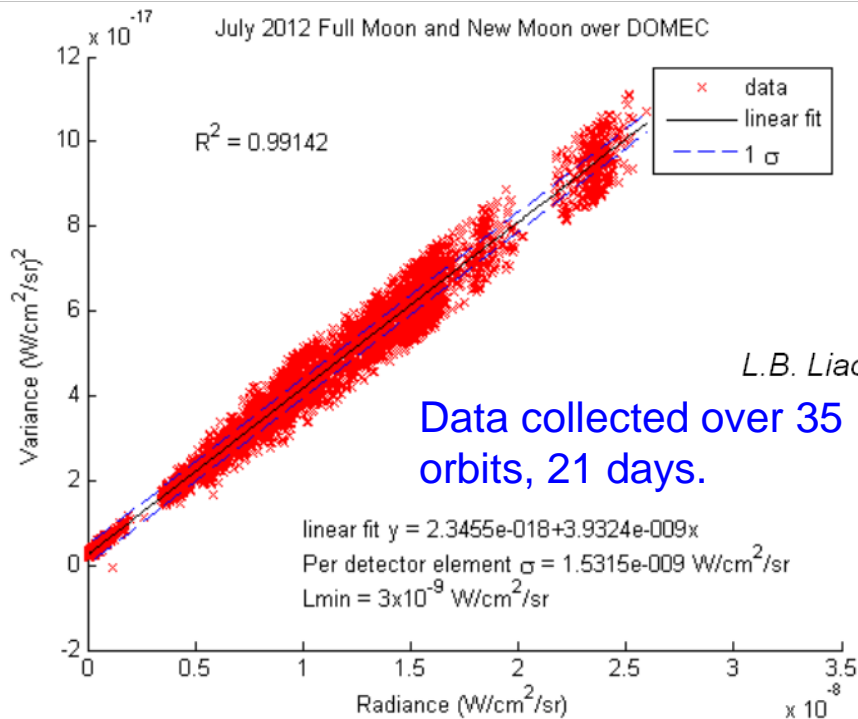


L.B. Liao, NGAS



Sudden negative or extremely low radiance pixels observed within a bright patch. This is due to early transition from HGS to MGS. In some instances, truncation of the data results in negative MGS_dn. Recall that base on digital saturation consideration, transition is supposed to occur around 20-30 dn's. This is a hardware issue that will impact future DNB units.

Scene based determination of SNR using photon transfer curve (PTC) (1/2)



$$N_{agg} \times Var(L) - \left(\frac{1}{N_{agg}} \right) \left(\frac{G_e}{G_L} \sigma_{e^-,T} \right)^2 = \left(\frac{G_e}{G_L} \sigma_{e^-,S} \right)^2 + \left(\frac{G_e}{G_L} \langle L \rangle \right)$$

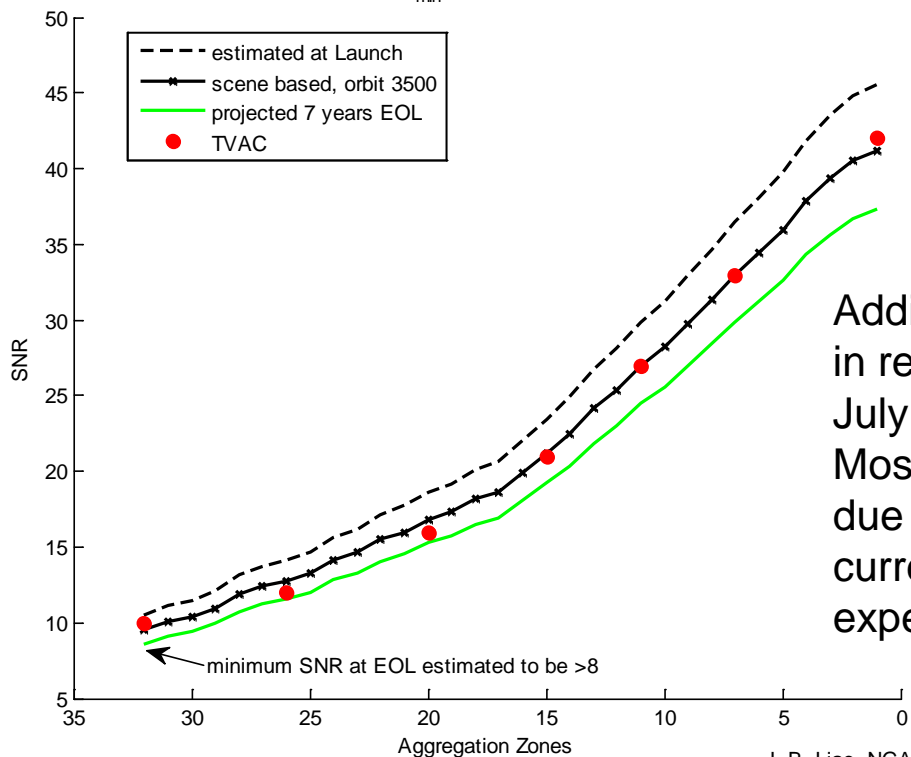
aggregated read-out noise
detector element dark current noise

In order for PTC to be valid, noise sources must add in quadrature and photon noise must obey Poisson distribution. Thus we must remove other sources of noise via signal processing and image processing.

Scene based determination of SNR using PTC (2/2)

$$SNR = \frac{\sqrt{Var(L)}}{\langle L \rangle} = \sqrt{\left(\frac{1}{N_{agg}^2} \left(\frac{G_e}{G_L} \sigma_{e^-,T} \right)^2 + \frac{1}{N_{agg}} \left(\frac{G_e}{G_L} \sigma_{e^-,S} \right)^2 + \frac{1}{N_{agg}} \left(\frac{G_e}{G_L} \langle L \rangle \right)^2} \right)}$$

SNR at L_{min} ($3 \times 10^{-9} \text{ W cm}^{-2} \text{ sr}^{-1}$)



Total readout noise.
Intercept of zero
radiance PTC.

Detector element
dark current noise.
Intercept of scene
based PTC and
slope of zero
radiance PTC.

Additional 10% degradation in response expected from July 2012 to EOL in 2017. Most degradation in SNR due to increase in dark current noise. We still expect SNR > 8 EOL.

L.B. Liao, NGAS

Once derived, PTC can be used to predict SNR at any time and any radiance (within the linear range), provided that one can derive the temporal evolution function of various noise sources other than the photon shot noise.

Zero signal PTC (from calibration views) can be used to derive dark current noise and readout noise

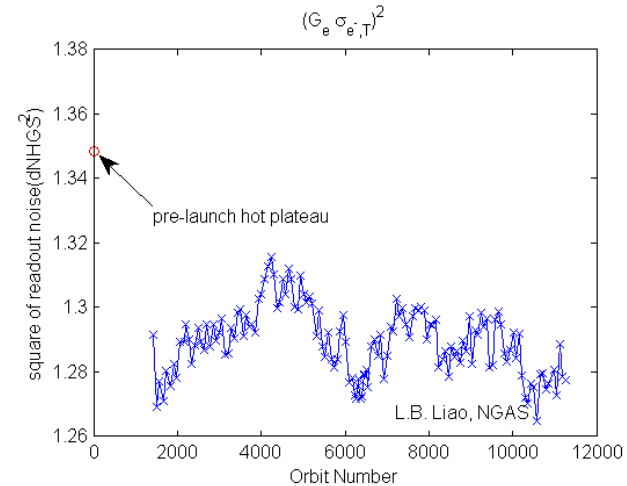
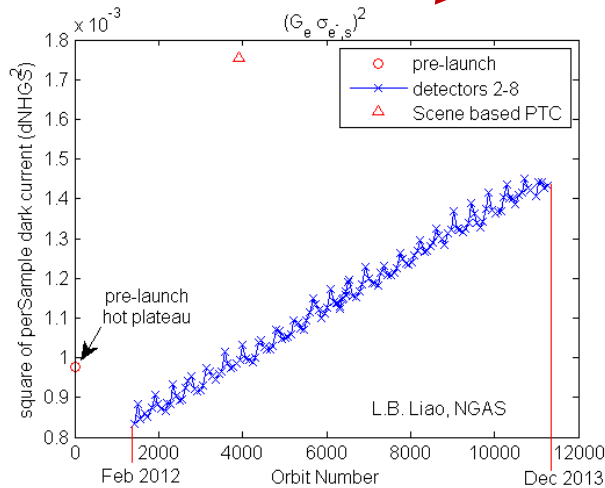
When observing a perfectly dark scene, the PTC for DNB can be written as,

$$Var(HGSdN_s) = N_{agg} \times \left(G_e \sigma_{e^-,S}\right)^2 + \left(G_e \sigma_{e^-,T}\right)^2$$

Plot of variance of HGSDN versus N_{agg} results in intercept of read out noise and slope of detector element dark current noise.

detector element dark current noise

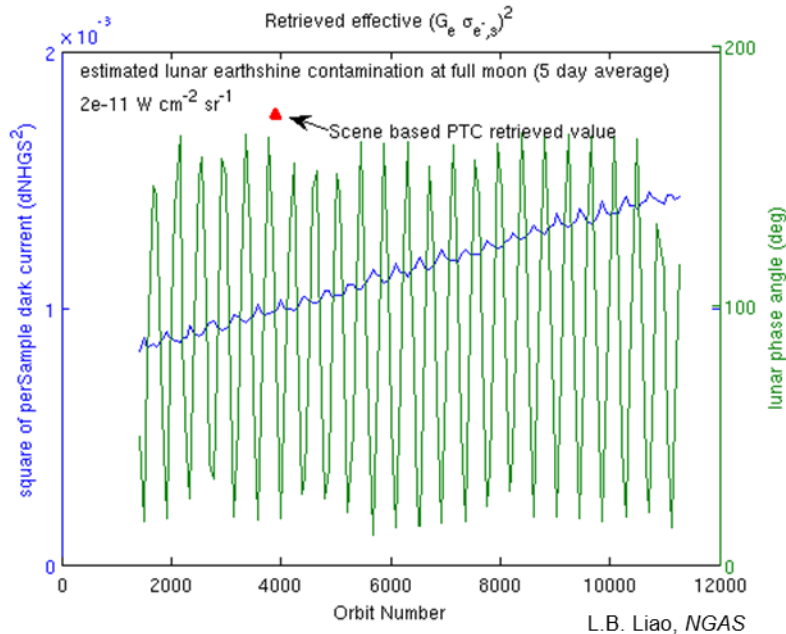
aggregated read-out noise



Dark current noise increasing with time (radiation exposure). We can use this time dependence to get EOL dark current noise. Interestingly, there is an oscillation which correlates with lunar phase variation.

Readout noise is relatively stable.

Variation in detector element dark current points to problem with radiometric offset



- Periodic structure in detector element dark current is correlated with lunar phase angle: peak at full moon and valley at new moon.
- This indicates that the signal from OBC Black Body is contaminated by lunar earthshine the magnitude of which is $2e-11 \text{ W cm}^{-2} \text{ sr}^{-1}$, approximately 1% of L_{\min} .
- The difference in value determined from two different PTC's indicates that the radiometric offset is $2.6e-10 \text{ cm}^{-2} \text{ sr}^{-1}$. That is the SDR 'zero radiance' is really $2.6e-10 \text{ cm}^{-2} \text{ sr}^{-1}$.

$$Var(HGSdN_s) = \underbrace{N_{agg} \times (G_e \sigma_{e^-,S})^2 + (G_e \sigma_{e^-,T})^2}_{\text{True dark}} + \underbrace{G_e G_L N_{agg} L}_{\text{Contribution from external signal}}$$

Slope of $Var(HGSdN_s)$ vs N_{agg} is $(G_e \sigma_{e^-,S})^2 + G_e G_L L$

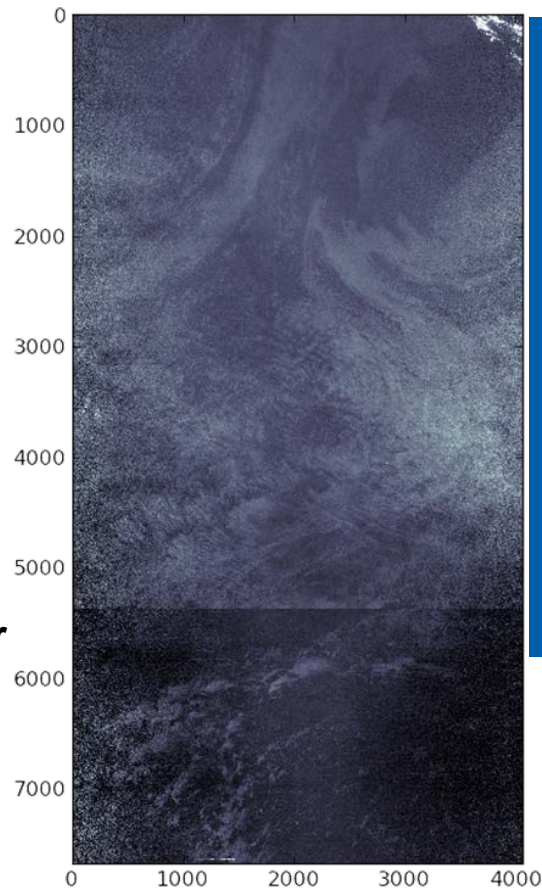
DNB offset is contaminated with airglow signal

- **DNB calibration is conceptually simple.**

- Linear calibration means $L = c1 * (DN - DN0) / RVS$.
- $c1$ for low gain stage (LGS) is derived from solar diffuser data.
- $c1$ for other gain stages (MGS and HGS) requires transfer from LGS using simultaneous observations around terminator region.
- $DN0$ unfortunately can not be determined from the calibration views due to offsets between calibration view and earth view that are expected to change with FPA temperature and possibly amount of radiation damage.

- **$DN0$ determined for each detector, mirror side and sample number monthly.**

- Assumes that new moon data over the ocean are completely dark.
- There are two parts to the offset: on-board offset which is applied on-board and the ground offset which applied by the IDPS to the transmitted HGSdN.
- Only the ground offset is updated monthly.



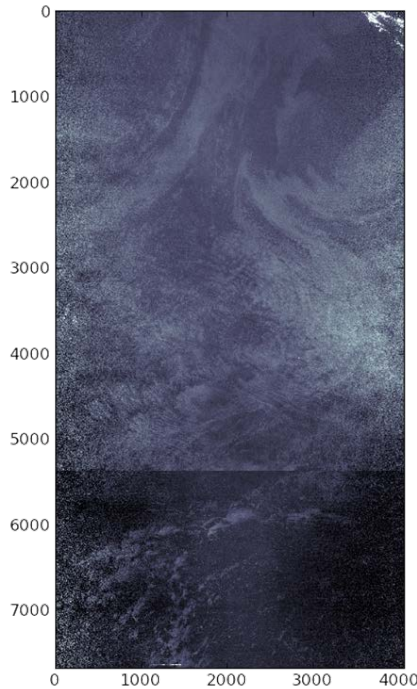
Calvin Liang, *NGAS*

- Granules used in $DN0$ calculation for April 21, 2012.

- Obviously not dark. Contains signal from airglow.

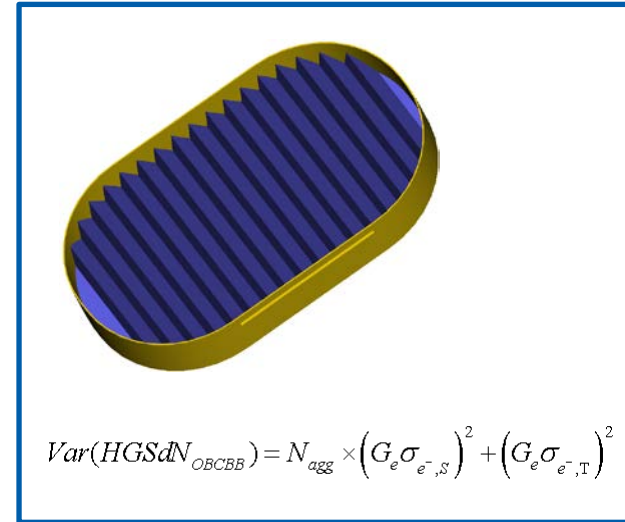
- How to calculate the magnitude of this signal if we don't know the offset?

Combined PTC approach derives photon signal from variance values, eliminating the need to know the offset

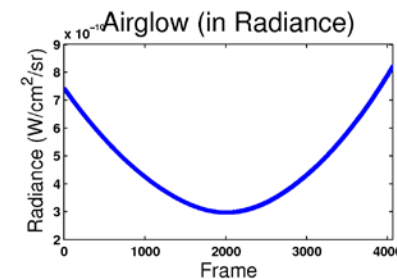
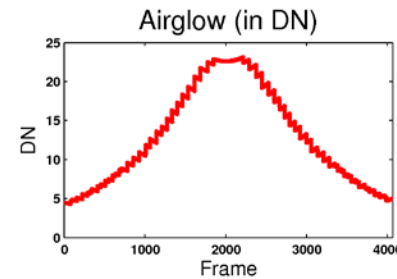
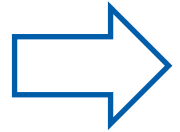


Calvin Liang, NGAS

$$Var(HGSdN_{EV}) = N_{agg} \times (G_e \sigma_{e^-,S})^2 + G_e \langle HGSdN_{EV} \rangle + (G_e \sigma_{e^-,T})^2$$

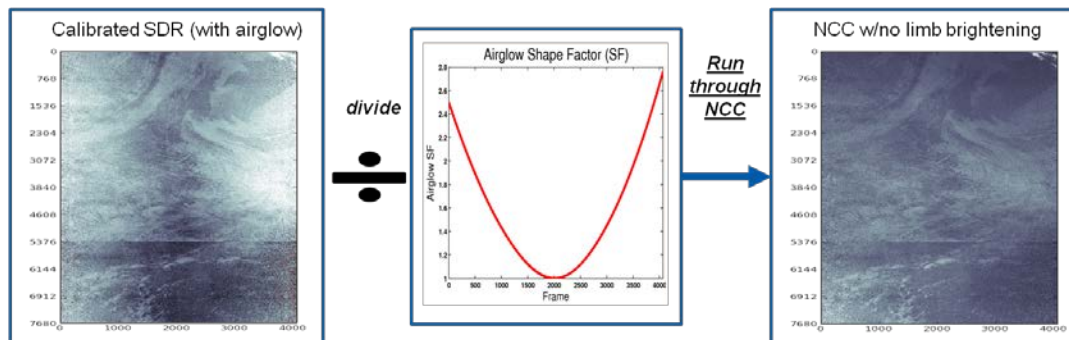
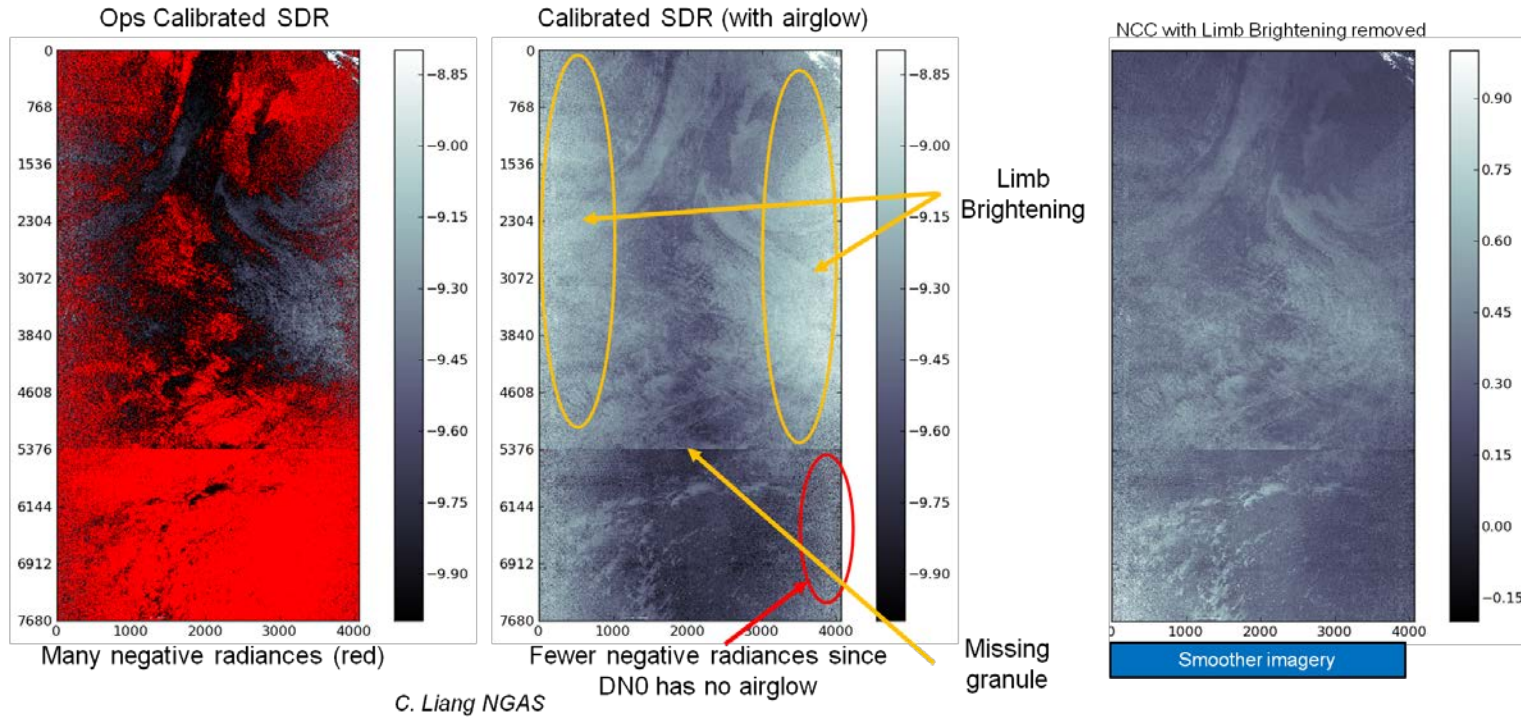


$$Var(HGSdN_{OBCBB}) = N_{agg} \times (G_e \sigma_{e^-,S})^2 + (G_e \sigma_{e^-,T})^2$$



$$HGSdN_{EV} = \frac{Var(HGSdN_{EV}) - Var(HGSdN_{OBCBB})}{G_e}$$

Airglow corrected SDR shows limb brightening which can be corrected for NCC with the derived airglow curve



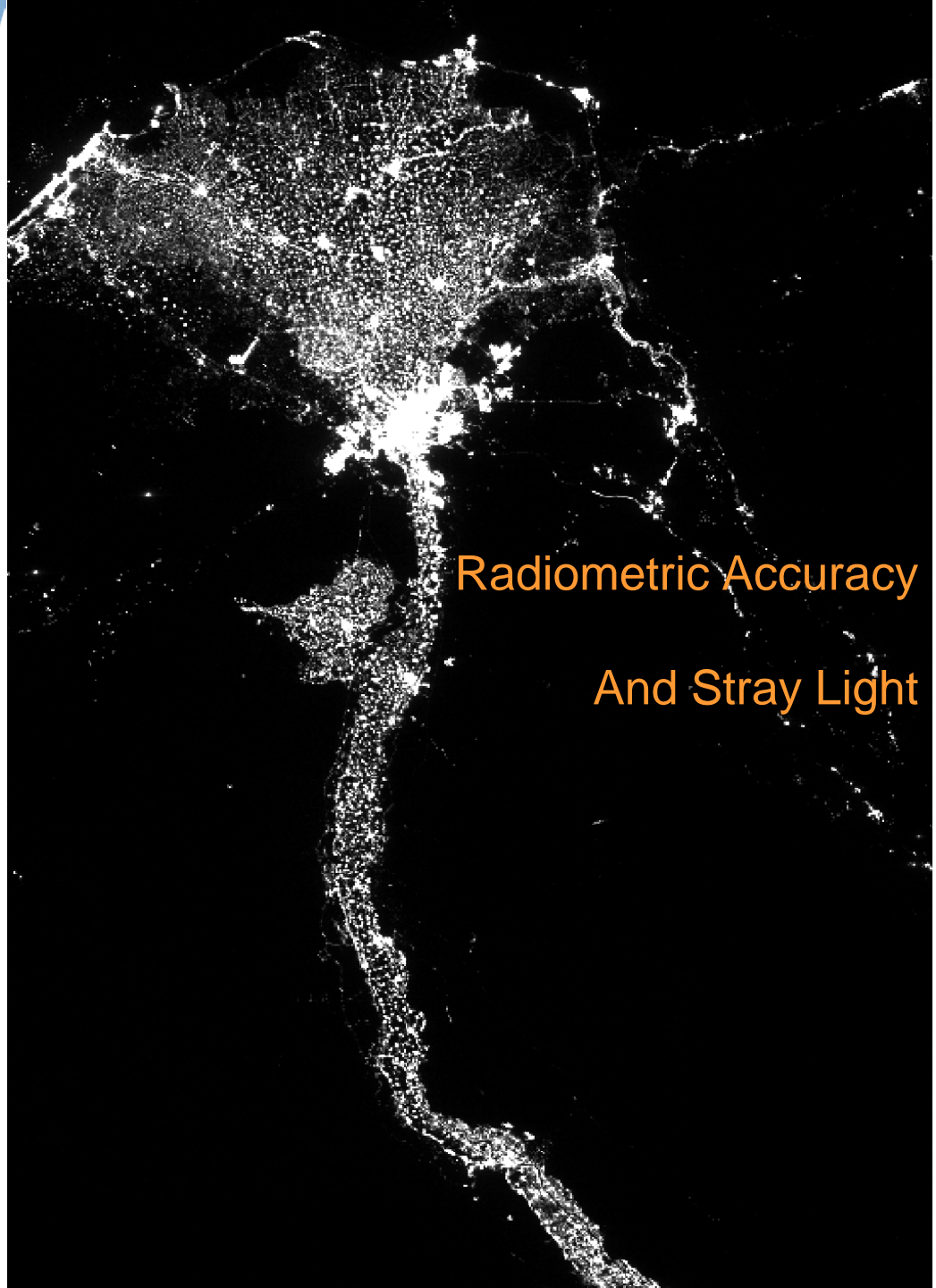
Example application from April 21, 2012

THE VALUE OF PERFORMANCE.

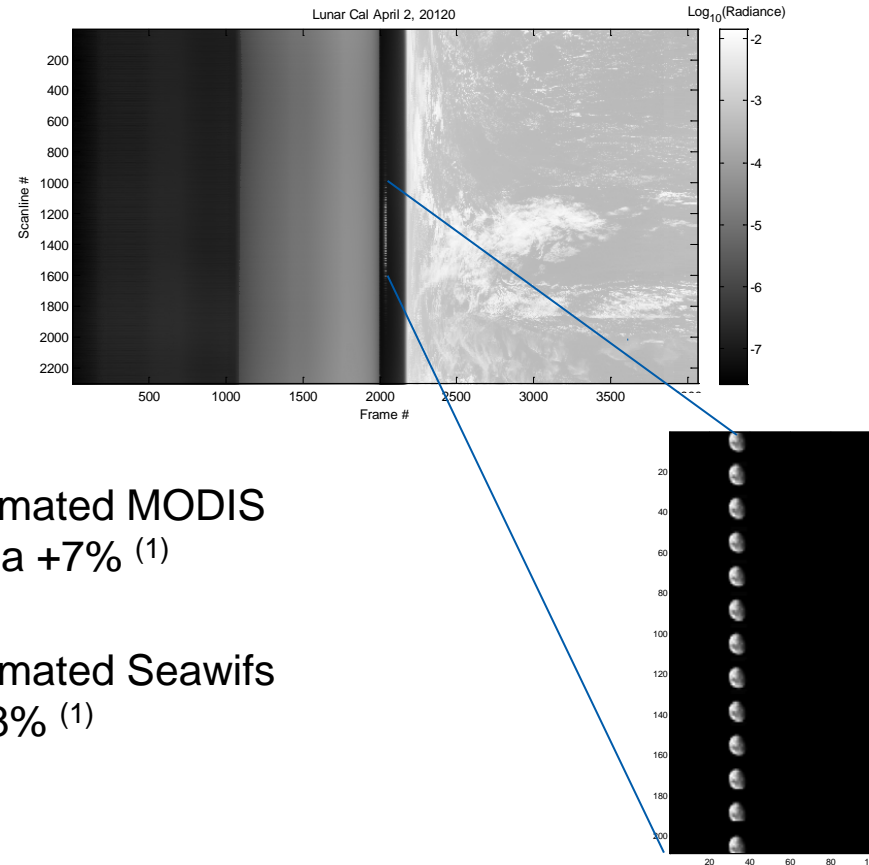
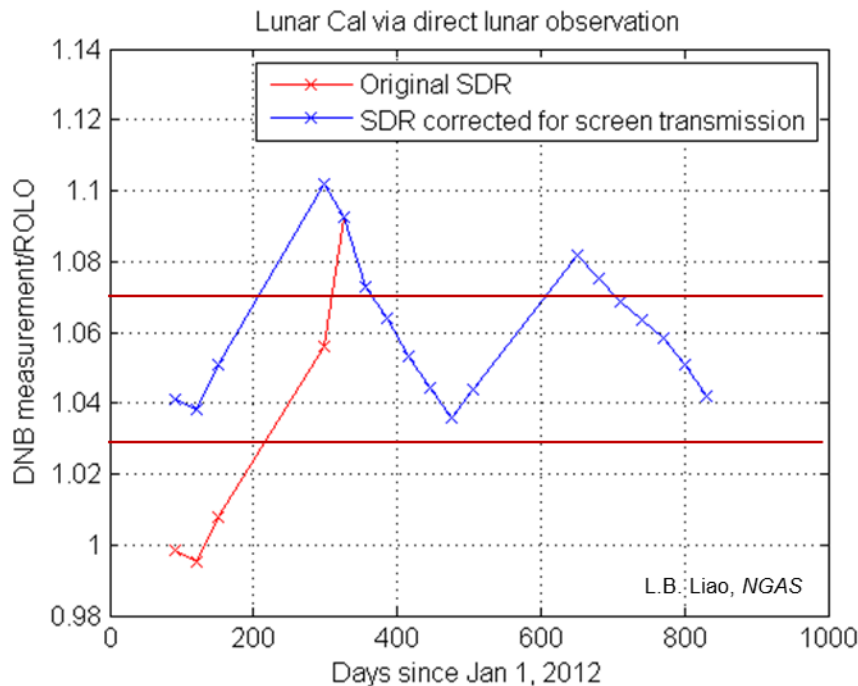
NORTHROP GRUMMAN

Radiometric Accuracy

And Stray Light



Lunar Cal for Low Gain Stage (LGS)

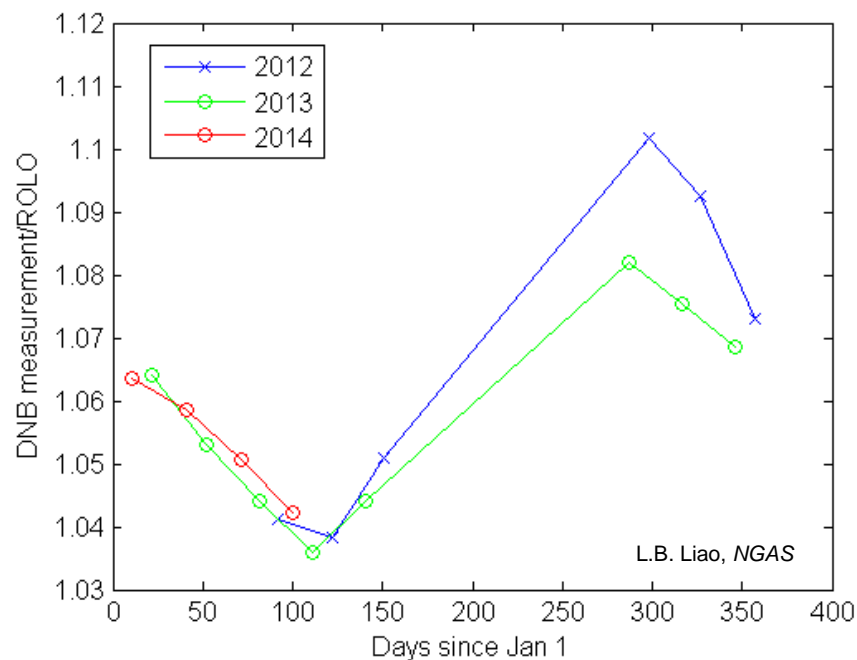


Estimated MODIS
Aqua +7% ⁽¹⁾

Estimated Seawifs
+2.8% ⁽¹⁾

Radiometric uncertainty relative to ROLO (lunar model from USGS) is $(6 \pm 2) \%$.
 Relative to MODIS, this would translate to $(-1\% \pm 3) \%$.
 For a given scene, this implies DNB retrieves slightly lower radiance than MODIS.

Lunar observations oscillates on an annual cycle

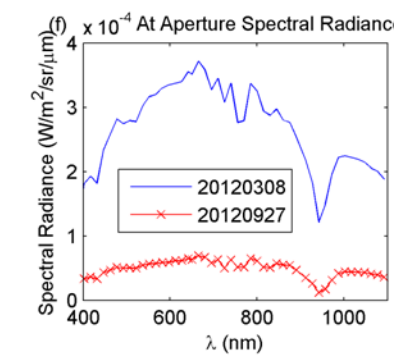
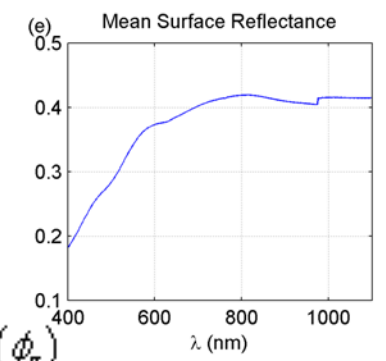
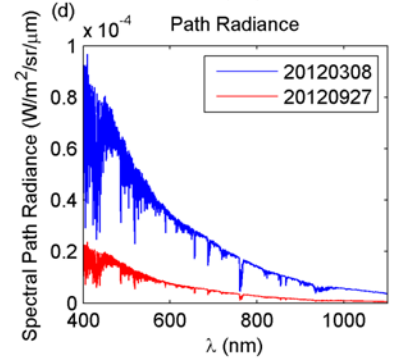
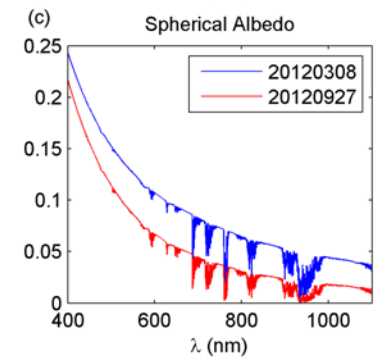
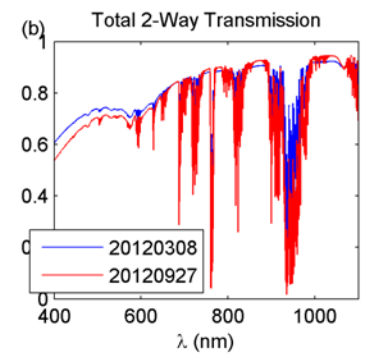
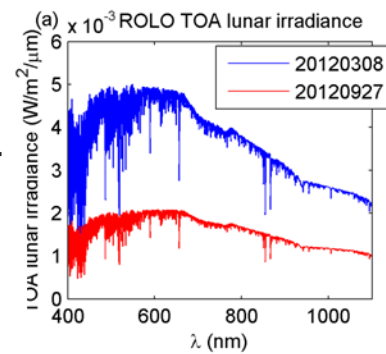
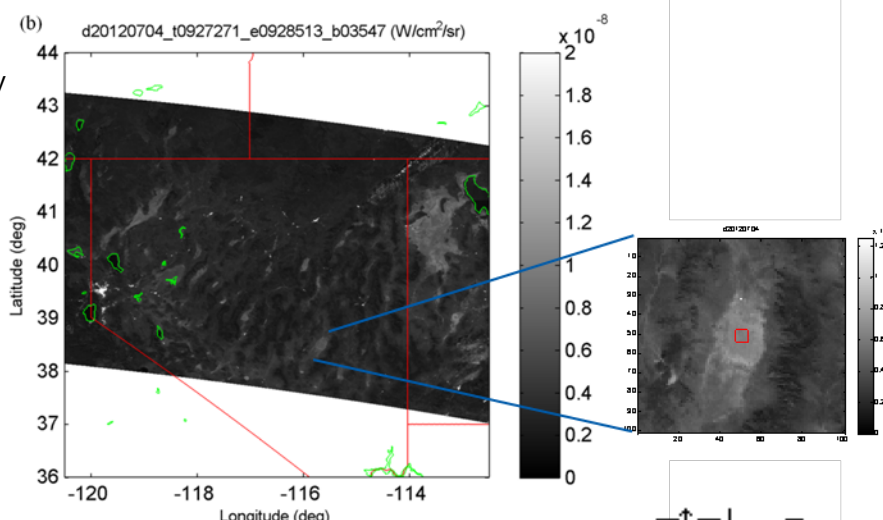
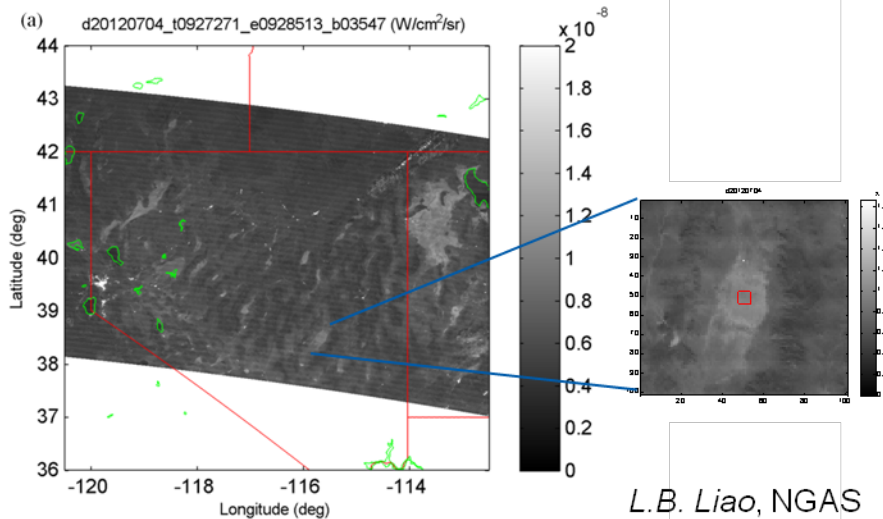


DNB observation of the moon is higher in radiance than predicted by ROLO. There is an average offset of approximately 6%. However, there is also an unexpected annual cycle in the observed radiance ratio of DNB observation measurement relative to ROLO prediction. The cycle appears to be repeatable but the peak value for 2013 was 2% lower than 2012. In fact, all late fall measurements (Oct –Dec) were lower in 2013 than 2012.

Vicarious Cal of High Gain Stage (HGS) data with lunar illuminated playa

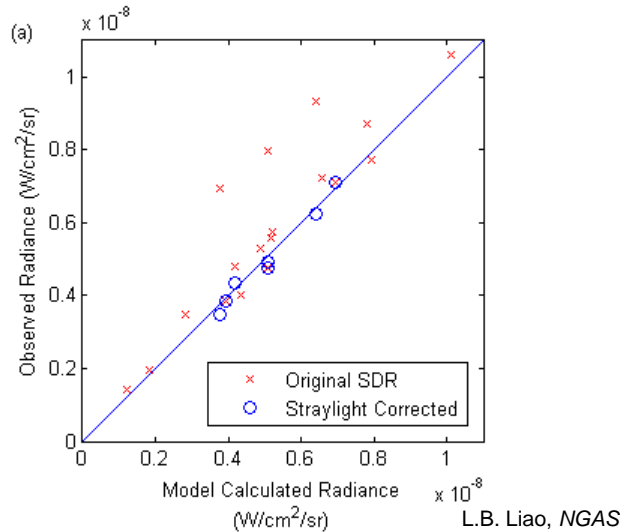
Before stray light removal

After stray light removal



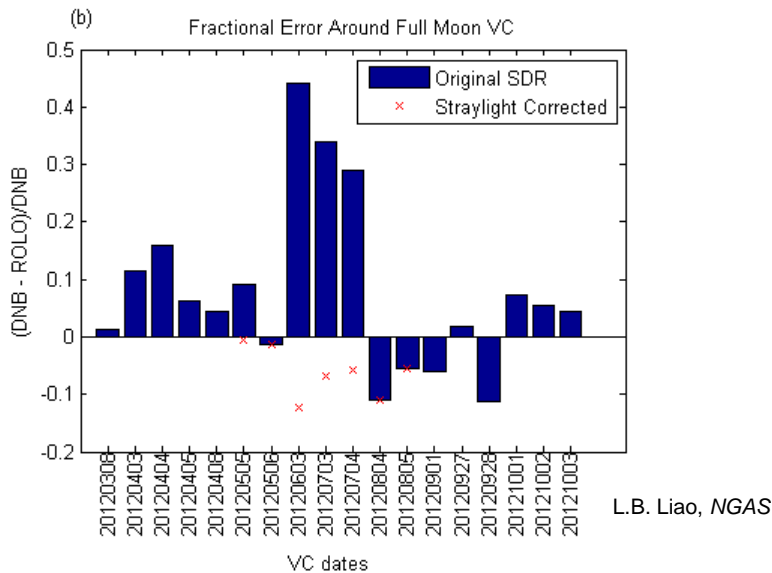
$$L = L_{path} + \frac{T^T T^\downarrow \rho_s E_L \cos(\phi_z)}{\pi \times (1 - A_{spherical} \rho_s)}$$

Results of 2012 HGS vicarious calibrations



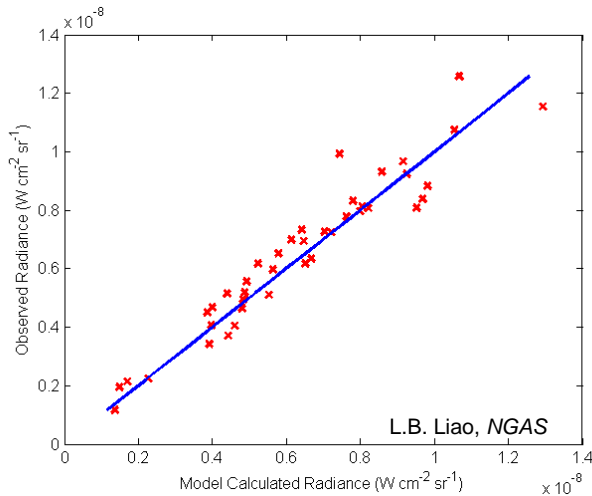
HGS Radiometric Uncertainty (1 σ)		
	Before Nov 16, 2012	After Nov 16, 2012
Relative to ROLO (DNB-ROLO)/DNB	6.1 \pm 8.9 %	9.7 \pm 8.9 %
Relative to MODIS (DNB-MODIS)/DNB	-0.9 \pm 9.1 %	2.7 \pm 9.1 %

Estimated calibration transfer uncertainty is 6.4% per transfer, implying MGS uncertainty of -1% \pm 6.7%. (MGS uncertainty is quoted with same sign as LGS)



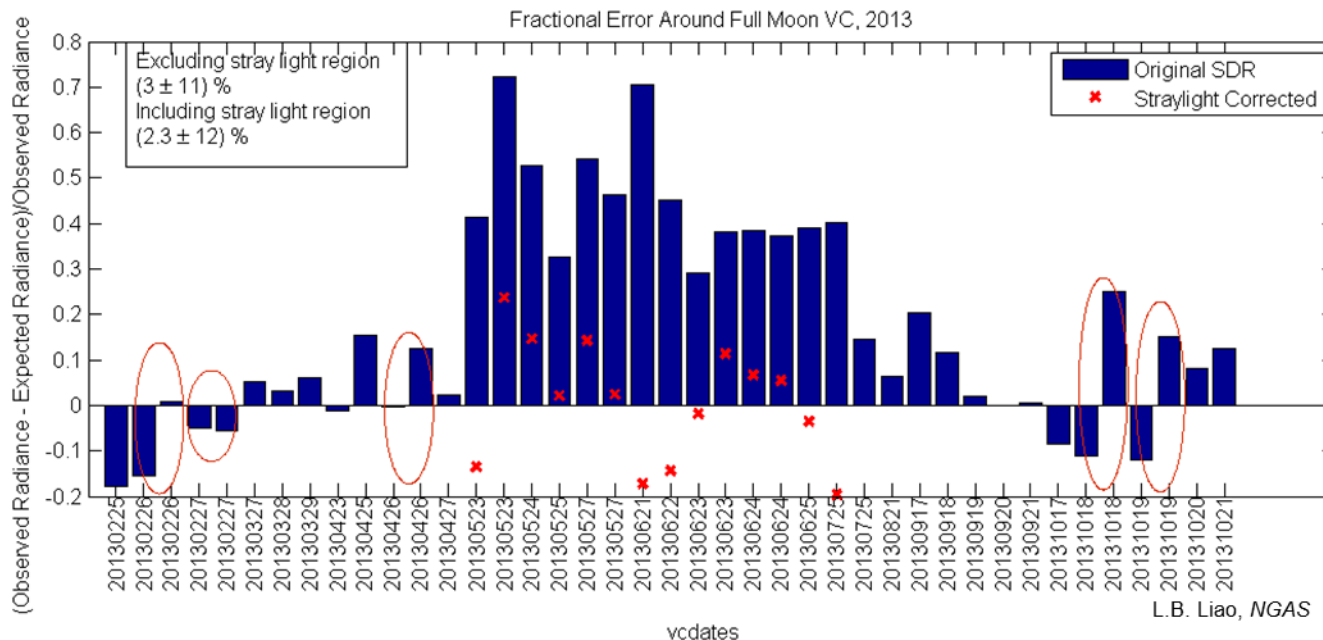
	Stray light contamination
Before Correction	2.4x10 ⁻⁹ W·cm ⁻² ·sr ⁻¹ (~100% L _{min})
After Correction	4.5x10 ⁻¹⁰ W·cm ⁻² ·sr ⁻¹ (~15% L _{min})

Results of 2013 HGS vicarious calibrations



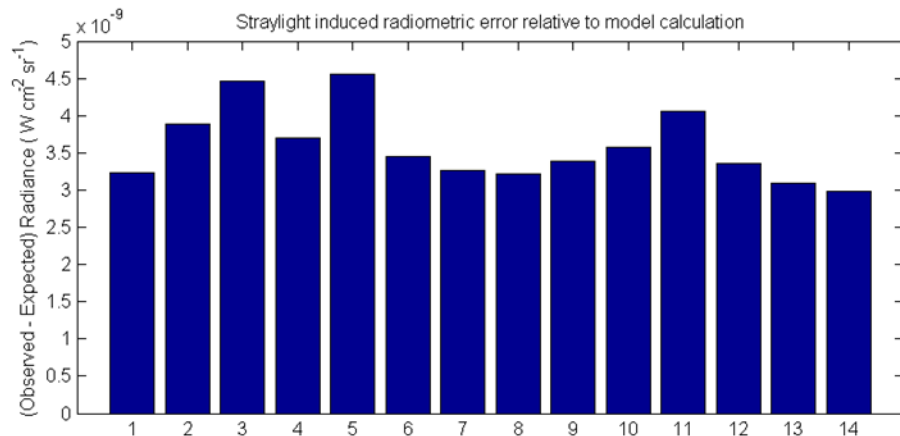
HGS Radiometric Uncertainty (1 σ)		
	2013	Expected, based on 2012 data
Relative to ROLO (DNB-ROLO)/DNB	$2.3 \pm 12 \%$	$9.7 \pm 8.9 \%$
Relative to MODIS (DNB-MODIS)/DNB	$-4.7 \pm 12.2 \%$	$2.7 \pm 9.1 \%$

Estimated calibration transfer uncertainty is 8.6% per transfer, implying MGS uncertainty of $-1\% \pm 8.6\%$. (MGS uncertainty is quoted with same sign as LGS)

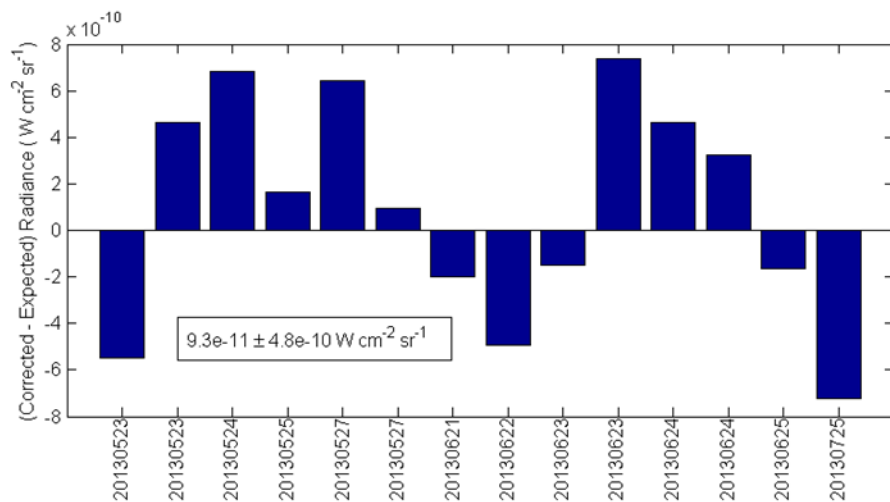


Additional scatter caused by inclusion of large angle data. Overlap observations indicate that retrieved radiance at start of scan is lower than retrieved radiance at end of scan.

Stray light correction improves the radiometric quality of the data from 2013 VC



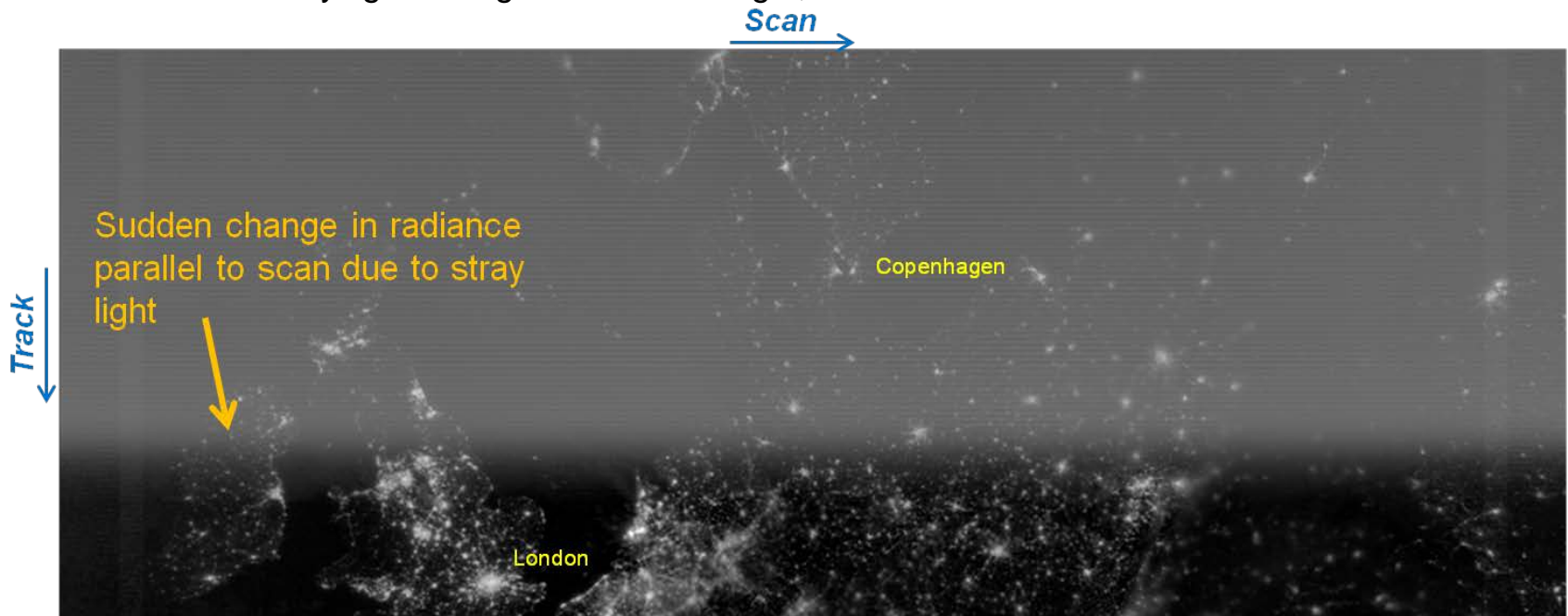
L.B. Liao, NGAS



	Stray light contamination
Before Correction	$4 \times 10^{-9} W \cdot cm^{-2} \cdot sr^{-1}$ (~100% L_{min})
After Correction	$6 \times 10^{-10} W \cdot cm^{-2} \cdot sr^{-1}$ (~20% L_{min})

DNB Stray Light Description

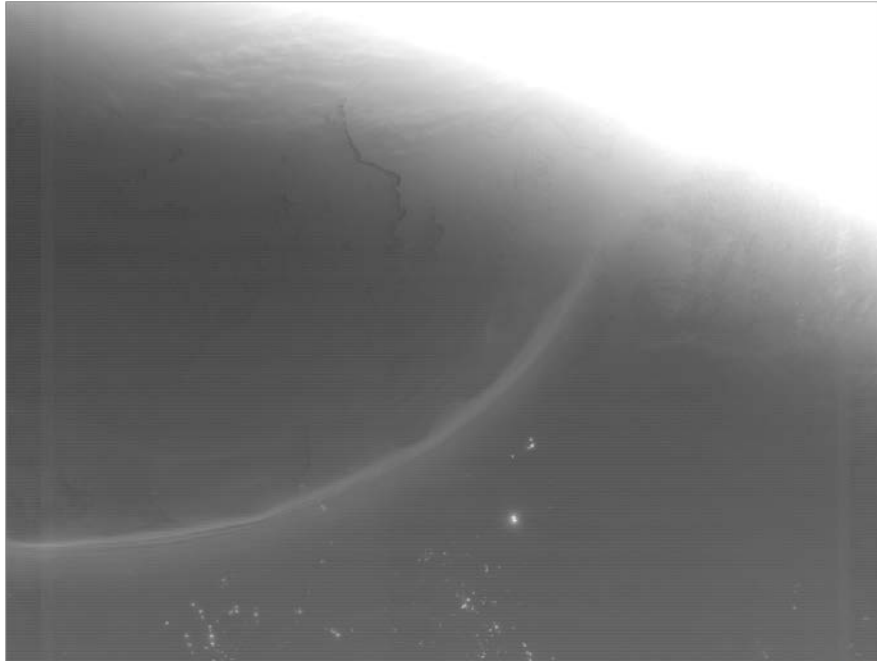
- Stray light appears on the night side of the terminator
 - Occurs for both the northern & southern terminator crossing
 - Ends when sun is eclipsed by the earth relative to the spacecraft, indicating it is caused by direct path from the sun.
 - Affects different segments of the orbit in the Northern and Southern hemispheres
 - Sun shining into EV port
 - Sun shining into both SD and EV ports (southern hemisphere only)
 - Stray light has detector dependence
 - Level of stray light changes with scan angle, but extends across the entire scan



d20120915_t0126328_e0129224

Northern Hemisphere (log scale)

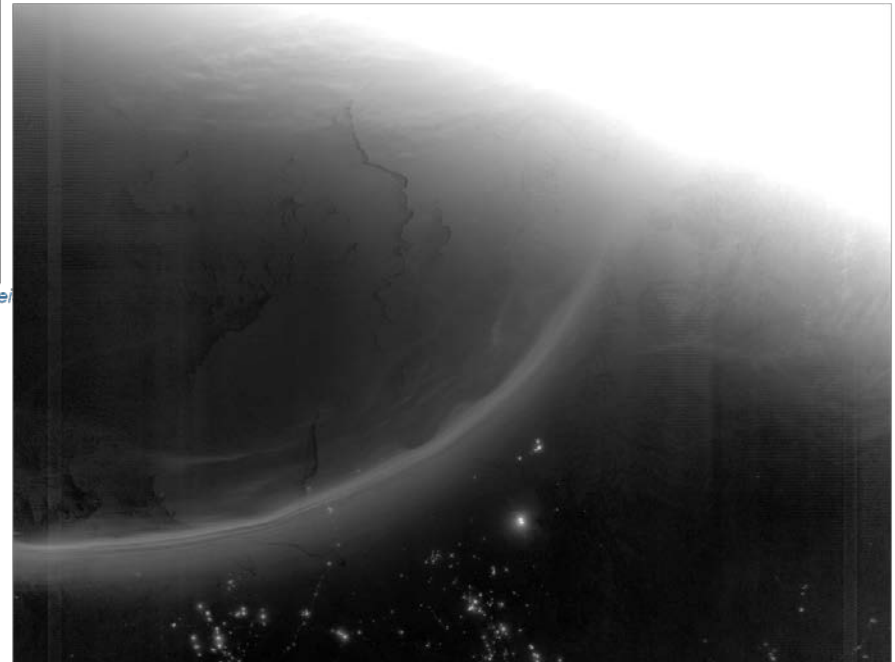
d20130310_t2138151_e2143537



S. Weiss

The stray light correction enhances the dynamic range of the scene and allows users to extract details that were previously washed out due to the stray light.

d20130310_t2138151_e2143537

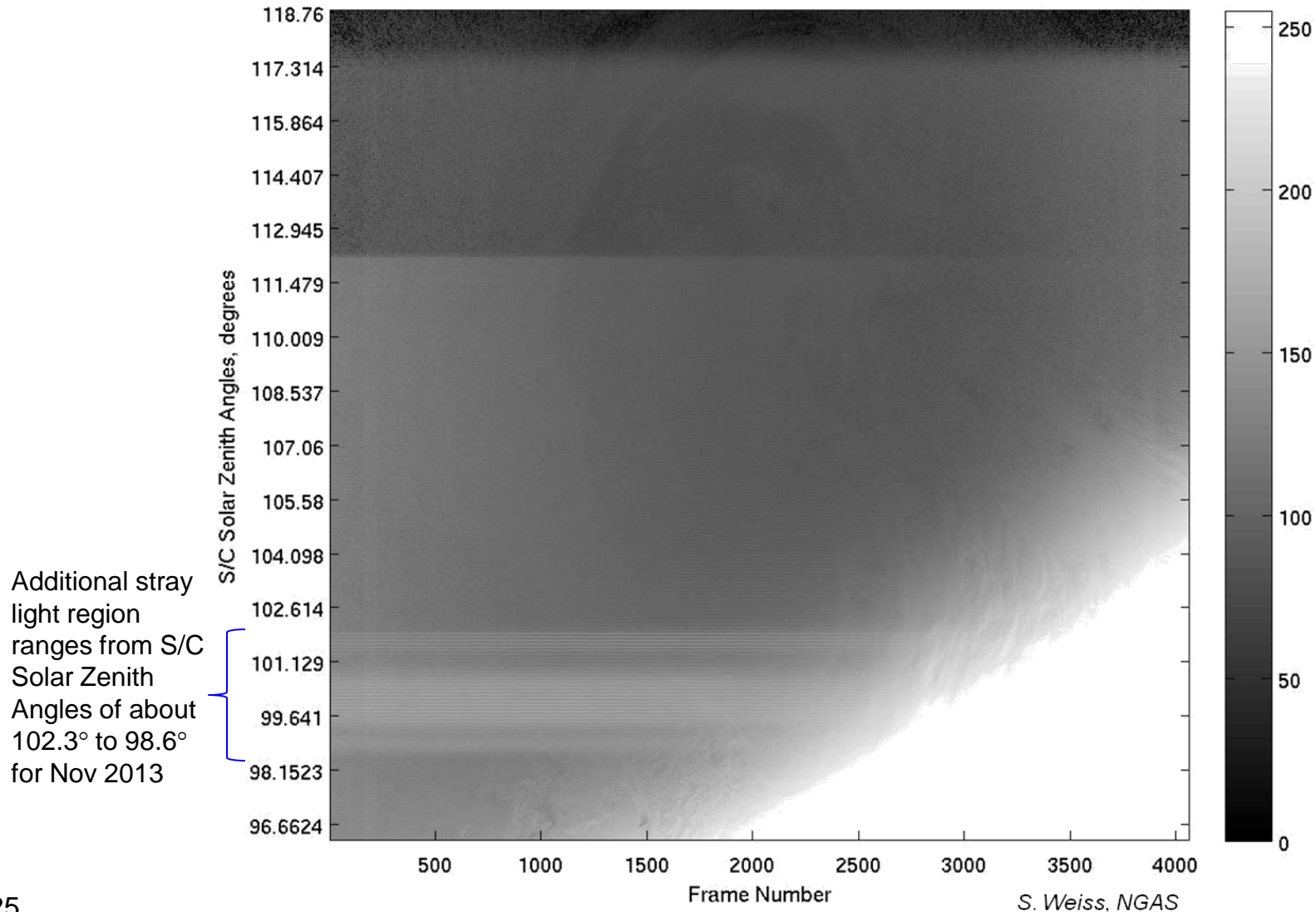


S. Weiss, NGAS

- Additional stray light region shows up from October through December in the southern hemisphere
 - Ranges from about ~102.4 to ~98.8 degrees, depending on the month
 - Has a dependence on S/C solar zenith angle and detector
- Existing stray light correction scheme does not correct for this additional stray light region
 - Pattern shifts between the months, making it difficult to model and correct

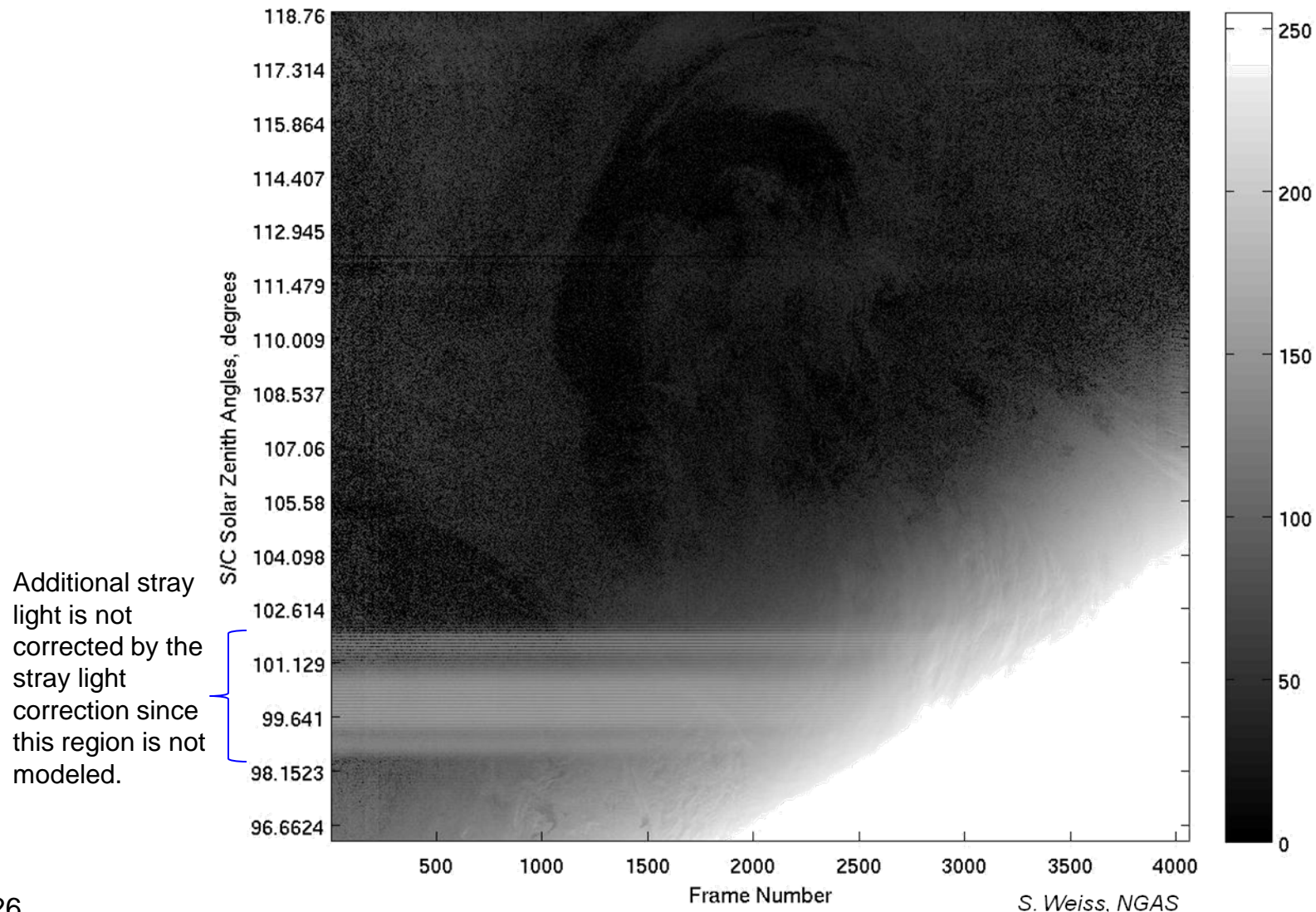
Uncorrected Radiances for Nov 2013 - Additional Stray Light Region Near Terminator

Log₁₀ Radiances, d20131103-t0237282-e0245594



Corrected Radiances for Nov 2013 - Additional Stray Light Region Not Corrected

Log₁₀ Radiances, d20131103-t0237282-e0245594

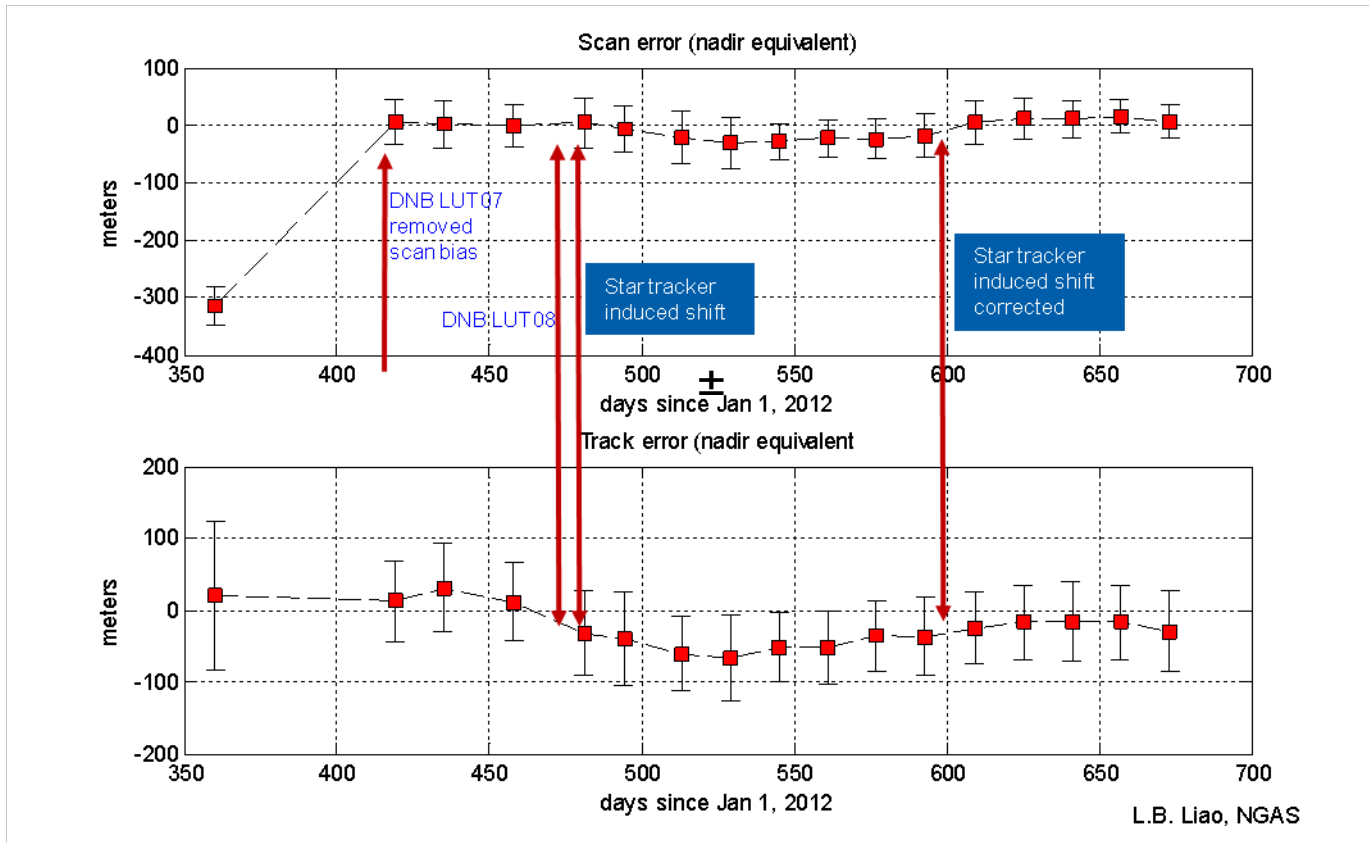


- **DNB is performing well on-orbit**
 - Exceeding most radiometric performance requirements
 - LGS radiometric uncertainty of 4%, MGS radiometric uncertainty of 10%, HGS radiometric uncertainty of 17%
 - Projected SNR >8 at end of life.
 - Minor decrease due to response degradation. Majority of SNR decrease due to increase in dark current noise.
 - Stray light correction enhances the contrast and radiometric accuracy of the scene and allows users to extract details that were previously washed out.
- **New technique using Photon Transfer Curve (PTC) was developed to retrieve noise and signal in the presence of unknown offset**
 - PTC allows for retrieval of various noise sources, depending on the source of input data. zero signal PTC can be used to monitor change in dark current noise and SNR throughout the life of the mission. (As well as monitoring possible change in electronic gain and read out noise all of which should be fed back to JPSS-1.)
 - Combining PTC data of both calibration and earthview allowed us to remove the airglow signal, which is ALWAYS present, from the DNB offset data. This allows us to produce more accurate radiance data and eliminates the large fraction of negative radiance data around new moon.
 - Periodic variation in retrieved effective dark current signal is due to presence of lunar earthshine.
 - Technique can be used to calculate earthshine contamination in calview ports and its implication for calibration of other RSB.
- **It has been shown that Combined PTC scheme has been demonstrated to retrieve accurate airglow signal for data from the time period near the pitch maneuver.**

- **Some performance issues and potential improvements:**
 - Analyze the additional small stray light region appearing from October to December in the southern hemisphere. The stray light pattern for this region changes from month to month and may be difficult to model and correct.
 - More vicarious calibration data to quantify residual radiometric error after DNB stray light removal.
 - Develop a scheme for flagging 'dark' pixels described in DR7364. Detailed analysis showing frequency of occurrence as function of detector # and aggregation zones will help JPSS-1 DNB build.
 - Develop a scheme for flagging analog saturation (DR 4603) and verify that these points are not included in cross calibration. If designed properly, this should not have occurred. JPSS-1 DNB build should optimize its gains for different stages so that this does not happen.
 - Use combined PTC scheme to validate the assumption that the offsets between earth view samples and black body view samples are constant.
 - Use combined PTC approach to estimate the contamination of SD and SV ports by earthshine.
 - Combined PTC can be used to remove limb brightening in NCC products once RSB_autocal is operational.

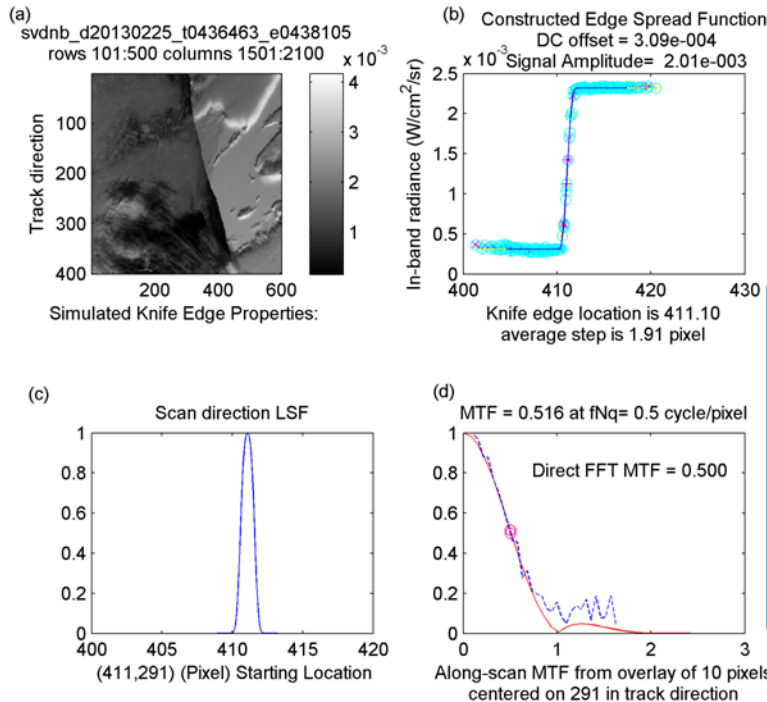
THE VALUE OF PERFORMANCE.
NORTHROP GRUMMAN

Back up



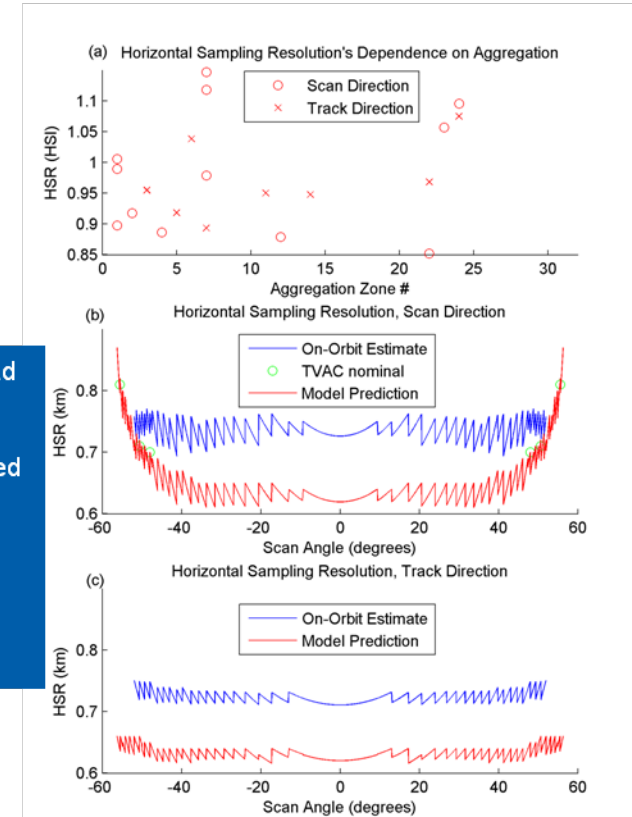
As of Nov 4, 2013, the DNB geolocation accuracy is,
 Scan : $8 \pm 33 \mu\text{rad}$; Track : $-35 \pm 68 \mu\text{rad}$

DNB spatial characteristics



Model based line spread function (LSF) construction using ice edge scenes was utilized to retrieve horizontal sampling resolution (HSR). Correction for edge slant was performed in Fourier space.

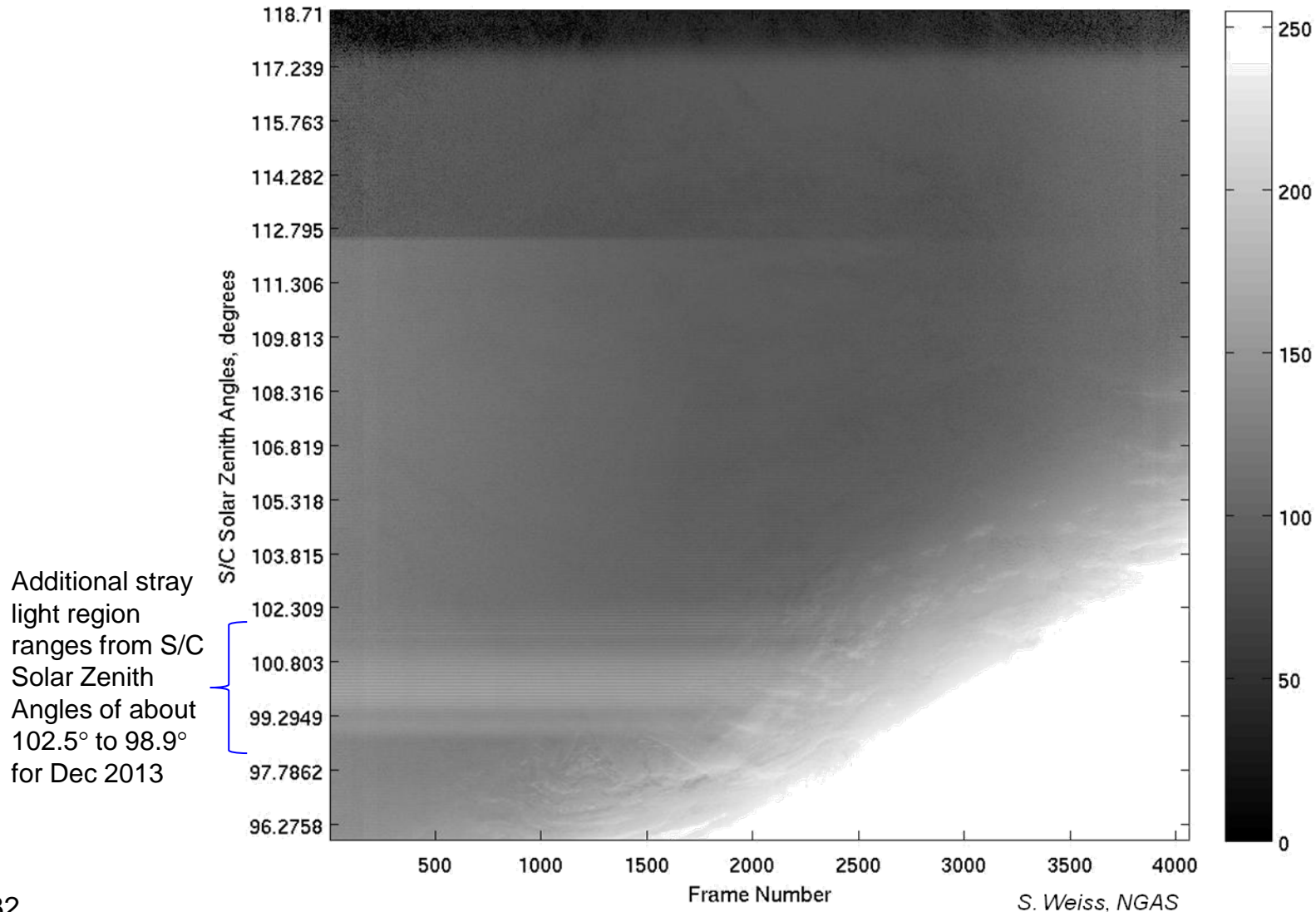
L.B. Liao, NGAS



DNB HSR is approximately a constant multiple of the horizontal sampling interval (HSI) for aggregation zones 1-24. This results in approximately constant HSR in units of ground distance, with saw tooth pattern that is inherent in the ground HSI. HSR meets the requirement of 800 meters upto scan angle of 52 degrees.

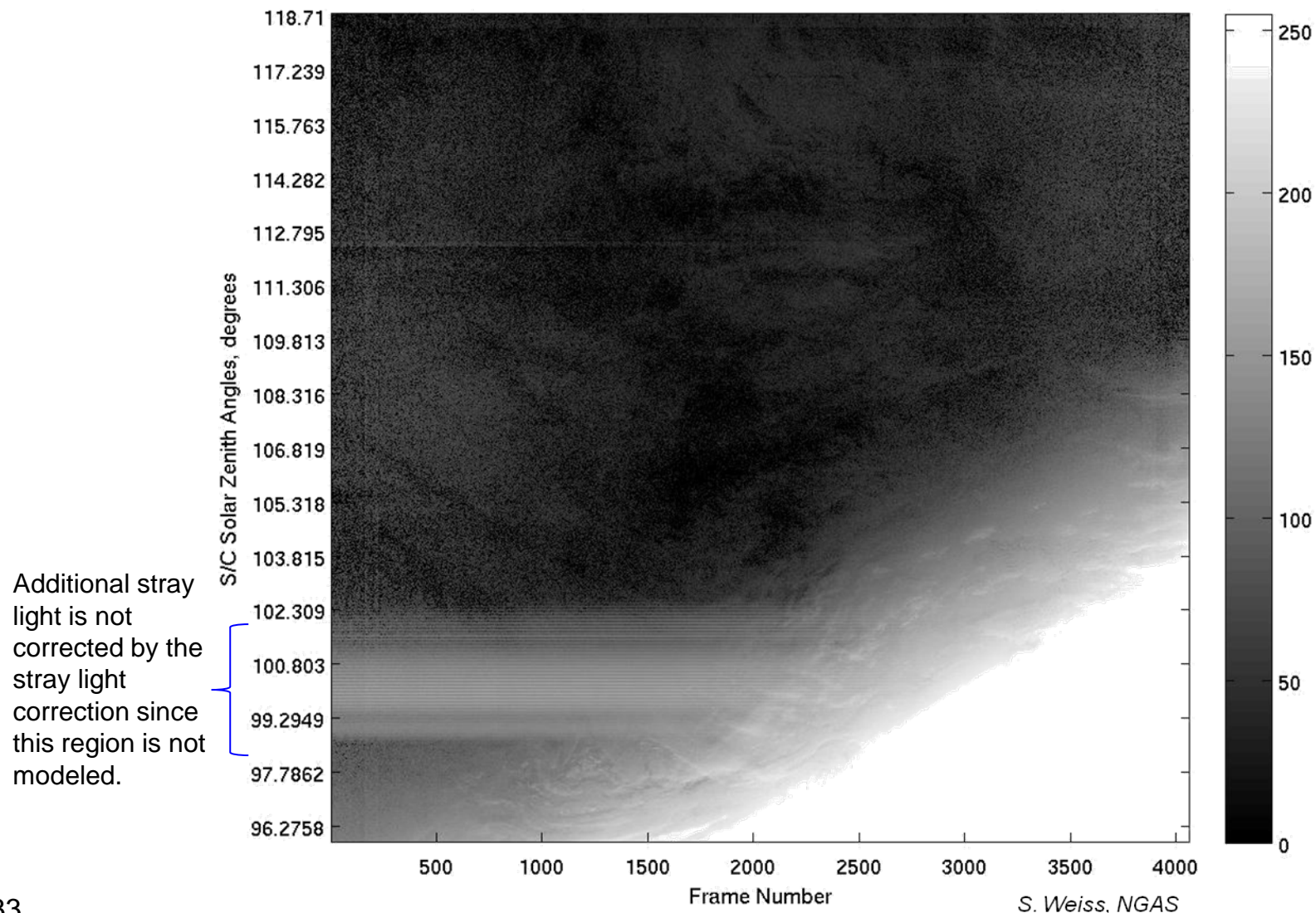
Uncorrected Radiances for Dec 2013 - Additional Stray Light Region Near Terminator

Log₁₀ Radiances, d20131203-t2149365-e2158077



Corrected Radiances for Dec 2013 - Additional Stray Light Region Not Corrected

Log₁₀ Radiances, d20131203-t2149365-e2158077



THE VALUE OF PERFORMANCE.

NORTHROP GRUMMAN



Visible Infrared Imaging Radiometer Suite

Vicarious Calibration of VIIRS Day Night Band

Xi Shao¹, Changyong Cao², Sirish Uprety³

1. Astronomy, UMD, 2. NOAA/NESDIS/STAR, 3. CIRA

Acknowledgement:

Bin Chang, Wenhui Wang, and Shi Qiu (NOAA/NESDIS/STAR)

Chris Elvidge and Michael Von Hendy (NOAA/NGDC)

Suomi NPP SDR Product Review
NOAA Center for Weather and Climate Prediction (NCWCP)
5830 University Research Park, College Park, Maryland
May 12-16, 2014

- Vicarious validation of VIIRS-Day Night Band (DNB) using DOME-C/Greenland under moon light
 - Event selection
 - Lunar irradiance model and TOA reflectance estimation
 - Validation and trending of DNB radiometric performance
- Preliminary radiometric calibration of DMSP-OLS using VIIRS-DNB through vicarious calibration
(In collaboration with Chris Elvidge and Michael Von Hendy of NOAA/NGDC)
- Future work

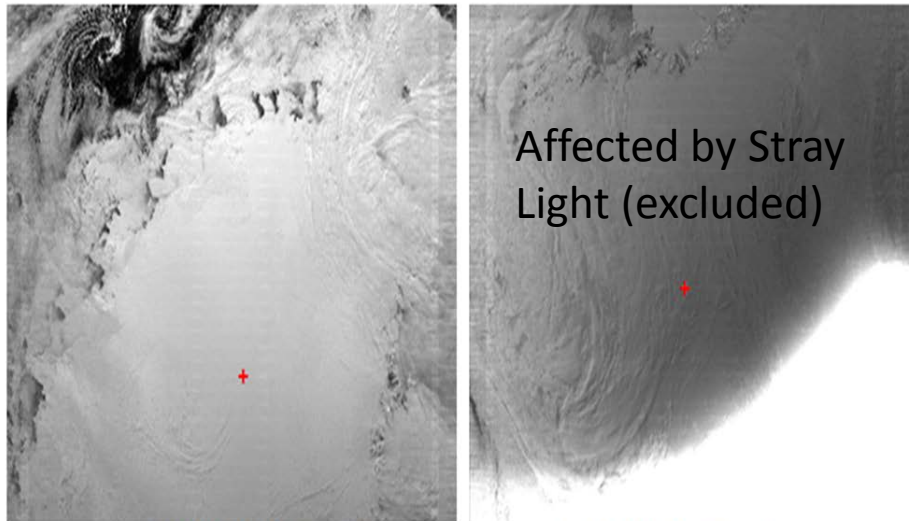
- The Day Night Band (DNB) of VIIRS provides imagery of clouds and other Earth features over illumination levels ranging from full sunlight to quarter moon.
- Three gain stages. The low gain stage (LGS) gain values are determined by the daytime onboard solar diffuser data.
- The medium and high gain stage values are determined by multiplying the LGS gains by the MGS/LGS and HGS/LGS gain ratios derived from data collected at solar terminator region, respectively.

Key DNB Radiometric Characteristics

	Specification	Prelaunch Performance	On-orbit performance
Spectral passband center	700±14 nm	707 nm	Model estimate: 694 nm
Spectral passband bandwidth	400±20 nm	379 nm	Model estimate: 375 nm
Dynamic Range (W/cm ² -sr)	3×10 ⁻⁹ to 0.02	3×10 ⁻⁹ to 0.021	3×10 ⁻⁹ to 0.0186
Calibration Uncertainty (HGS)	30%/100% (Transition from MGS/Lmin)	11%	15% (1σ) [2.8%, -15%]

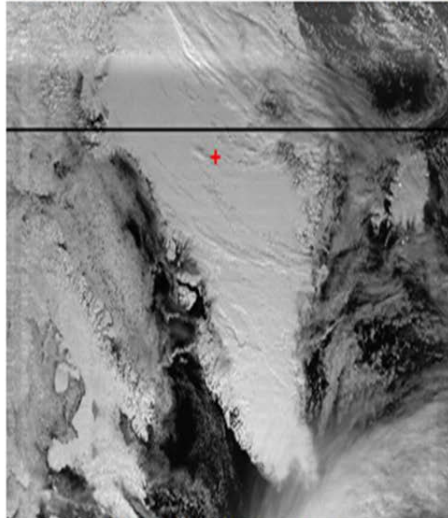
Adapted from Liao et al., 2013

VIIRS-DNB observations of Dome-C/Greenland under Lunar Illumination



(a) 7/4/2012 15:05 (Dome C)

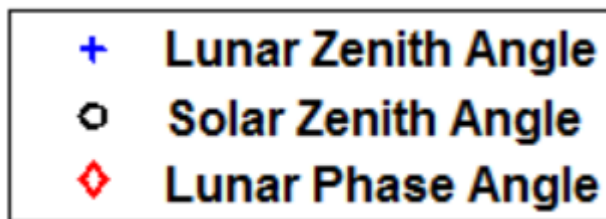
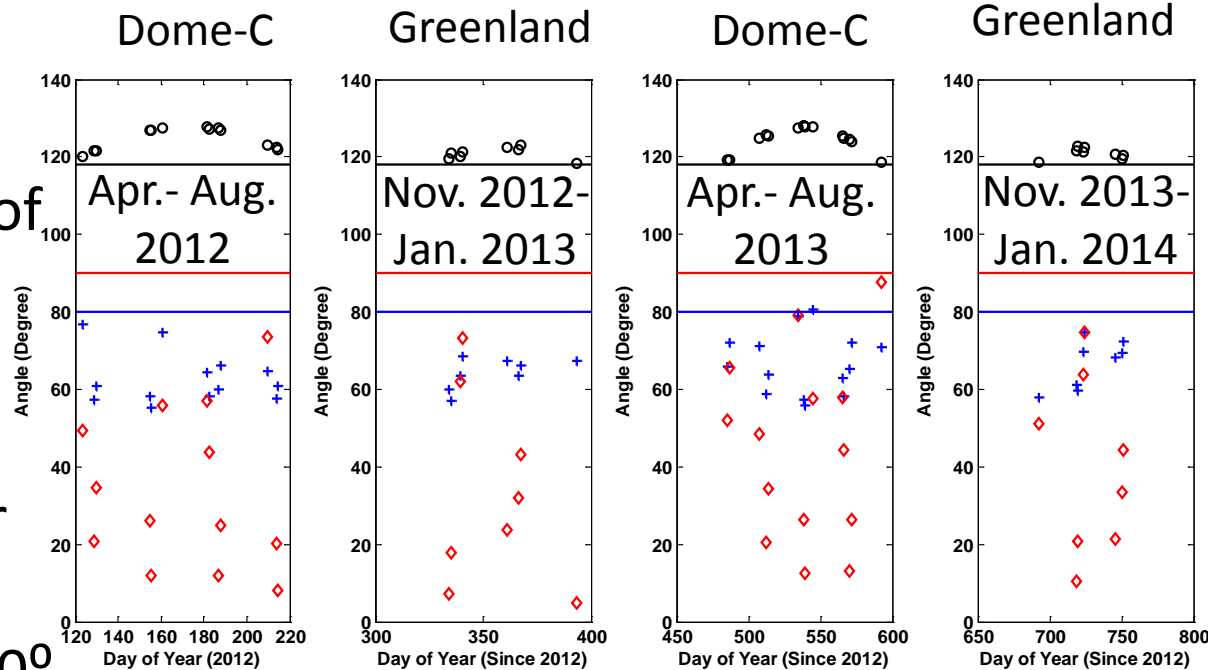
(b) 7/1/2012 7:42 (Dome C)



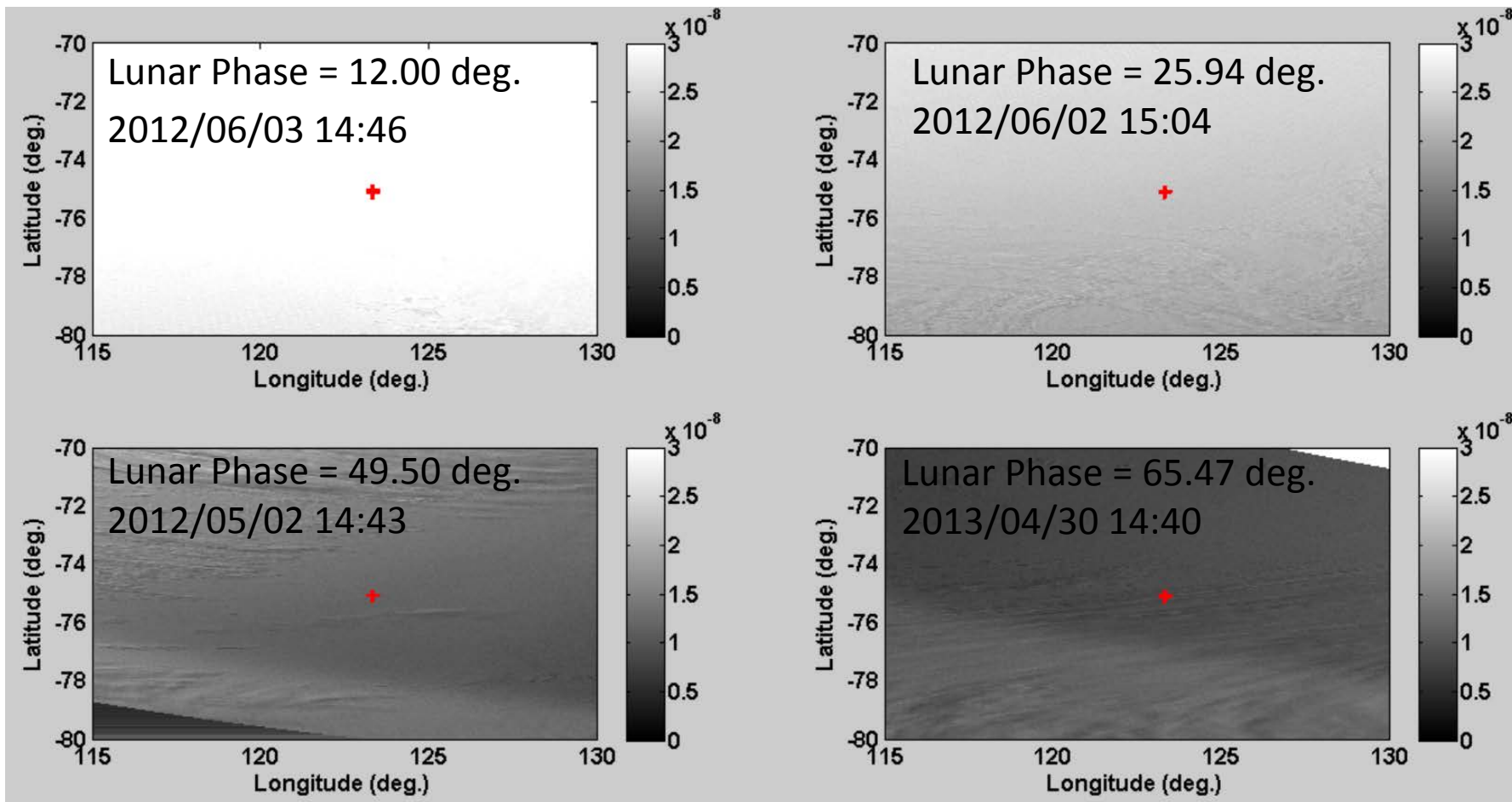
(c) 11/30/2012 6:01 (Greenland)

- Observations from perpetual night
 - Dome-C at Antarctic (Apr.-Aug.)
 - Greenland (Nov. – Jan.)
- Both sites
 - High reflectance
 - Stable atmosphere
 - Uniformity
- Dome-C
 - Radiometric calibration site for CEOS

- Suomi-NPP overpasses the ROI
- Solar zenith angle $>118.4^\circ$. No influence of stray light effects
- Lunar phase angle $< 90^\circ$, i.e. lunar phase is larger than the quarter moon.
- Lunar zenith angle $< 80^\circ$
- Both above conditions ensure that adequate lunar light illuminates the vicarious sites.

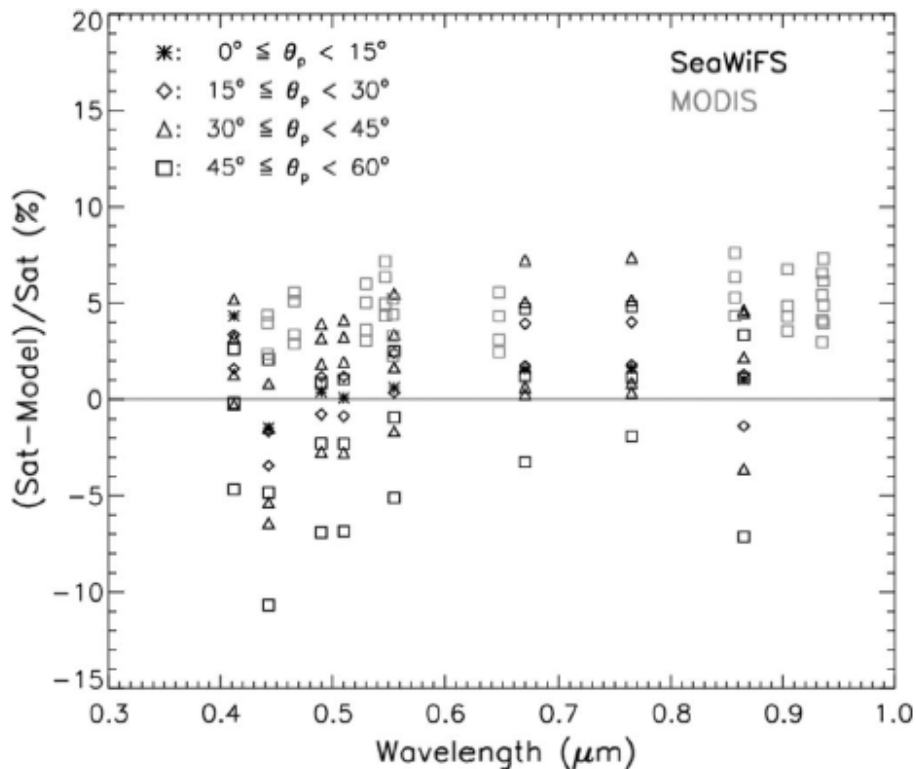


DNB observations of Dome-C at different lunar phases



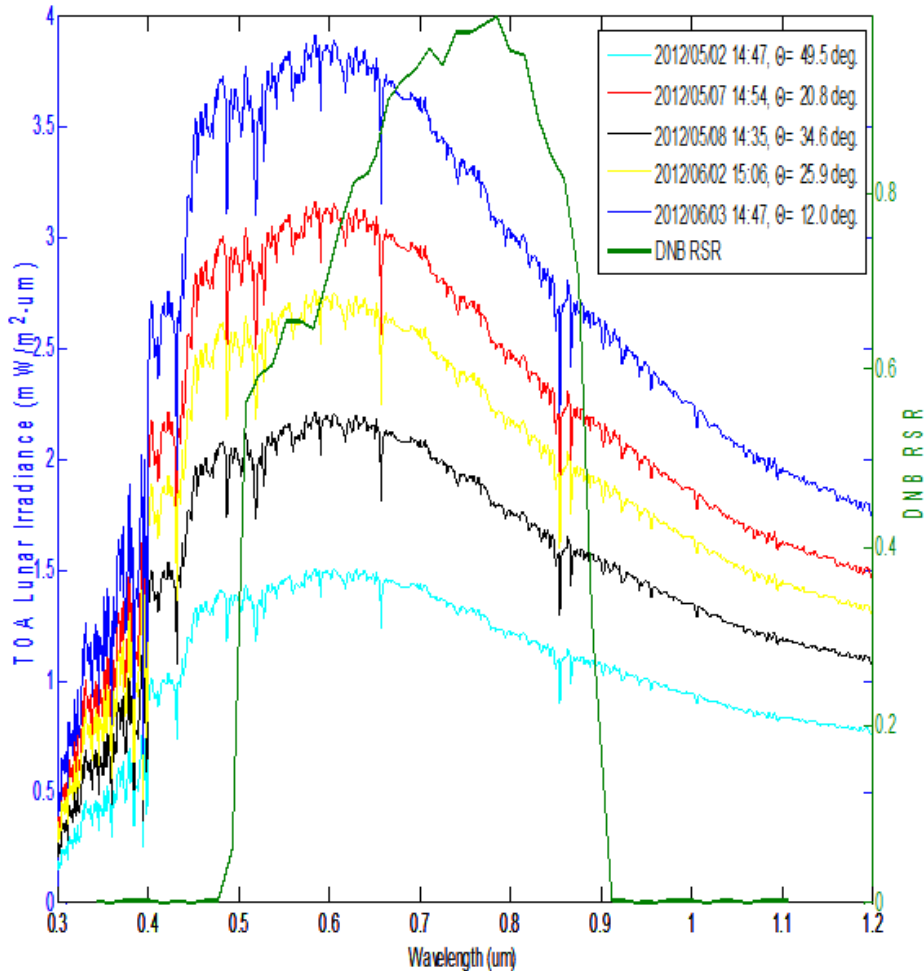
- To derive TOA reflectance at Dome-C/Greenland from DNB Observations
 - Lunar Irradiance Model
 - Reference reflectance at vicarious sites for comparison

Miller-Turner (2009) Model vs. SeaWiFS and Aqua MODIS

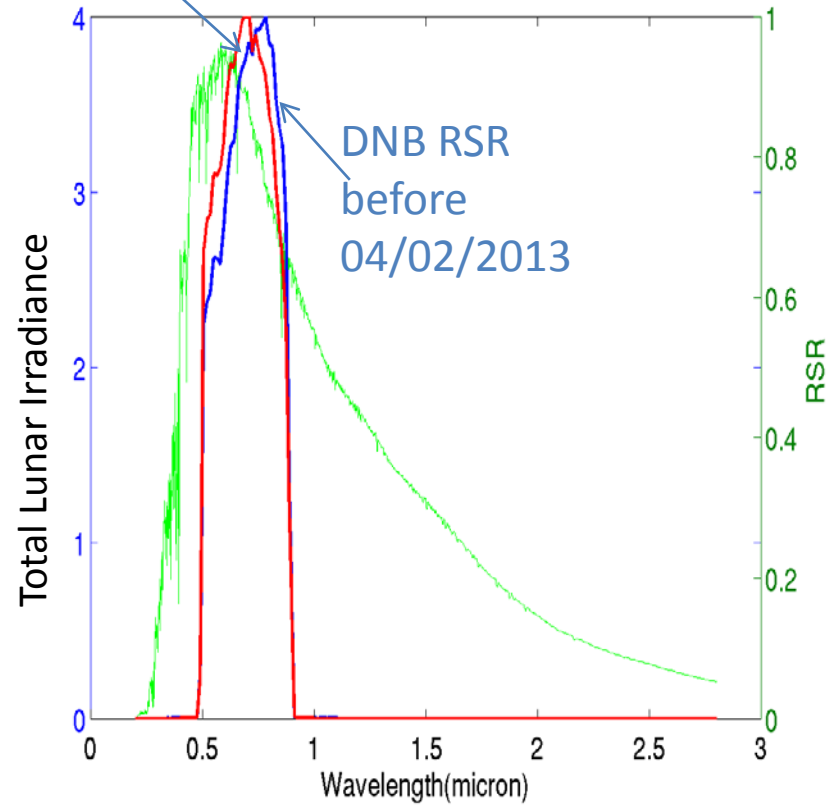


- Miller-Turner (2009) model
 - Developed in preparation for Suomi-NPP VIIRS DNB calibration
 - Quantify spectral irradiance of Moon
 - Incorporated state-of-the-art
 - Solar source observation
 - Lunar spectral albedo data
 - Account for Sun/Earth/Moon geometry and lunar phase
 - Covering **0.3-2.8 μm** spectra with 1-nm resolution.
 - Benchmarked against observation, and ROLO model
 - **Publically available**

Miller-Turner 2009 Lunar Irradiance Model



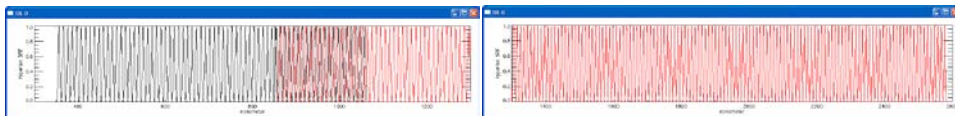
DNB RSR after
04/02/2013



Change in RSR causes ~3-4% increase in lunar radiance.

- Hyperion is on-board of the Earth Observing One (EO-1) Mission, launched in November, 2000.
- 242 spectral channels covering visible and SWIR (0.35 to 2.57 μm)
- Pushbroom sensor with two spectrometers. 256 pixels, 30 m on the ground, 7.65 km swath.

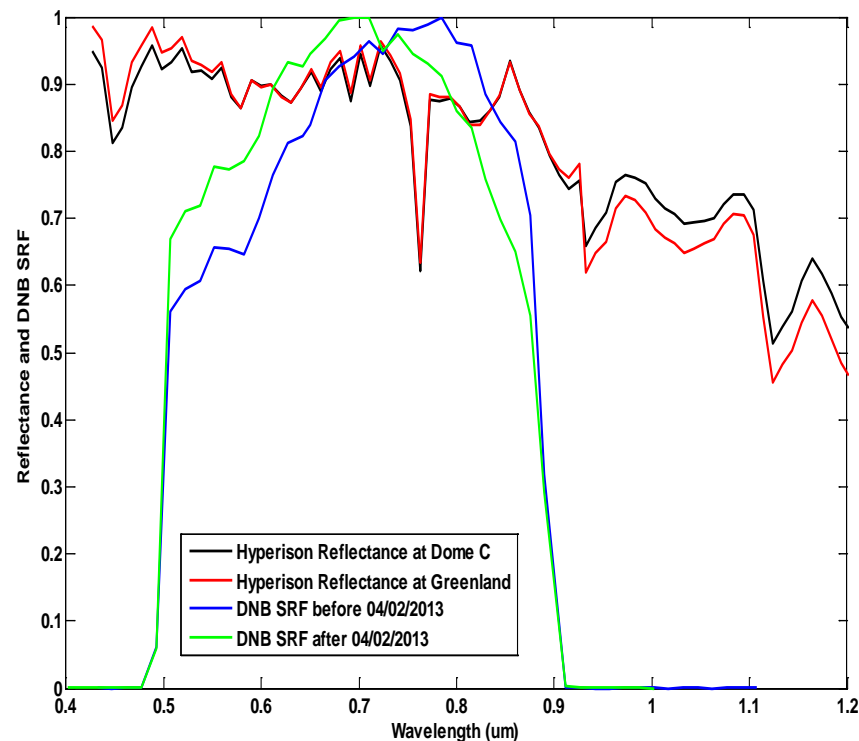
Spectral response functions for 242 channels of Hyperion



Visible bands

Near infrared bands

Characteristic Reflectance of Vicarious Sites from Hyperion



DNB RSR before 04/02/2013

$$\rho_{Dom\ C,Hyp} = 0.886 \quad \rho_{Greenland,Hyp} = 0.892$$

DNB RSR after 04/02/2013

$$\rho_{Dom\ C,Hyp} = 0.889 \quad \rho_{Greenland,Hyp} = 0.894$$

TOA lunar radiance above the ROI sites

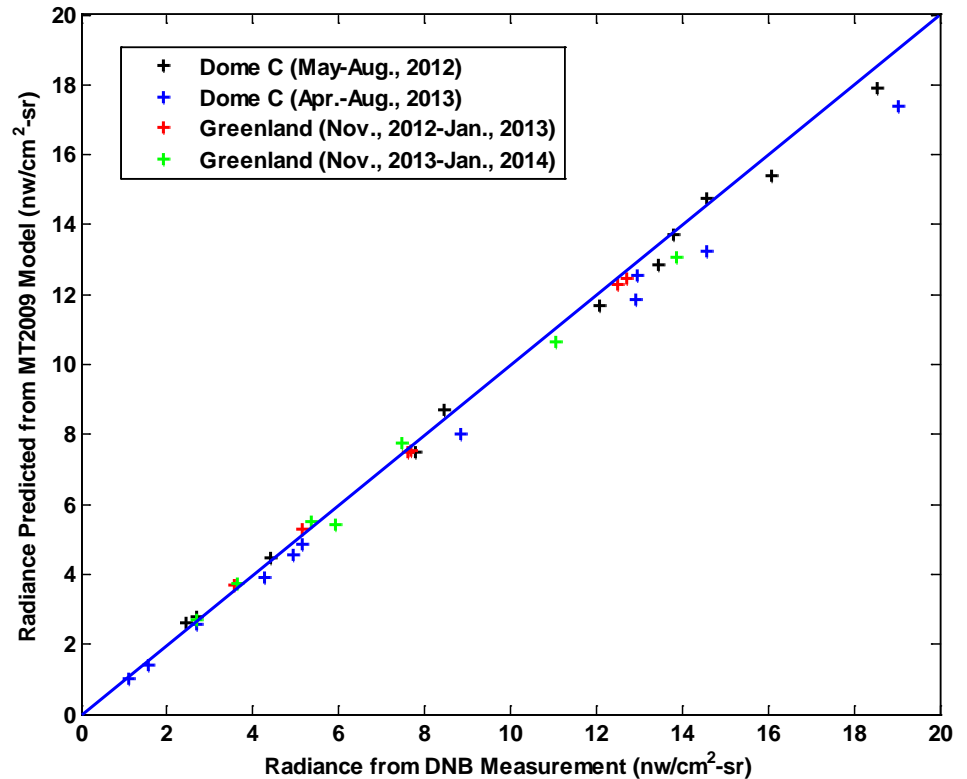
$$L_{MT2009} = \frac{E_m}{\pi} \cos(\theta_m)$$

E_m downwelling top-of-atmosphere (TOA) lunar radiance

$$E_m = \frac{\int_{\lambda_1}^{\lambda_2} I_{MT}(\lambda) SRF(\lambda) d\lambda}{\int_{\lambda_1}^{\lambda_2} SRF(\lambda) d\lambda}$$

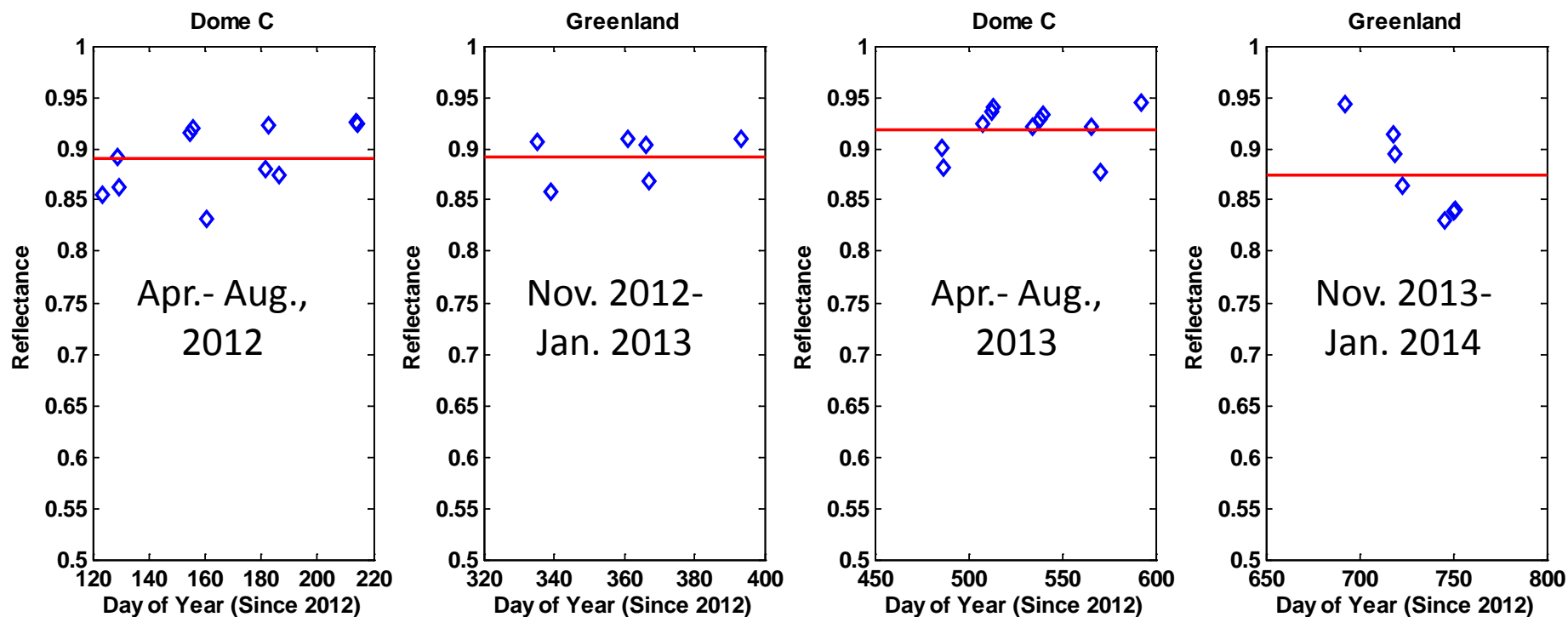
SRF is the spectral response function of DNB sensor.

$$\rho_{DNB} = L_{DNB} / L_{MT2009}$$



Total: 35 observations;
 $R^2 = 0.989$, $RMSE = 0.529$

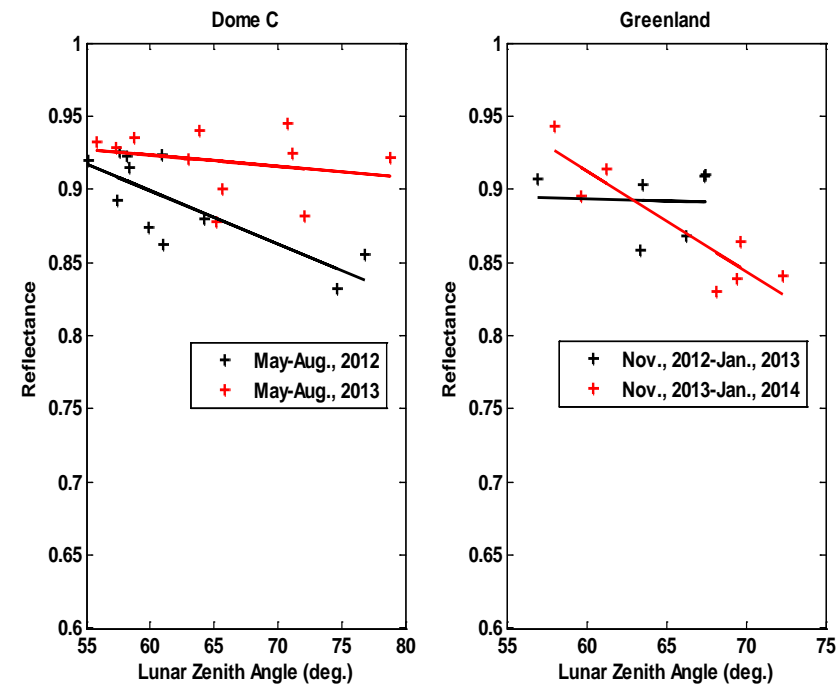
Trending of TOA Reflectance derived from DNB Observations



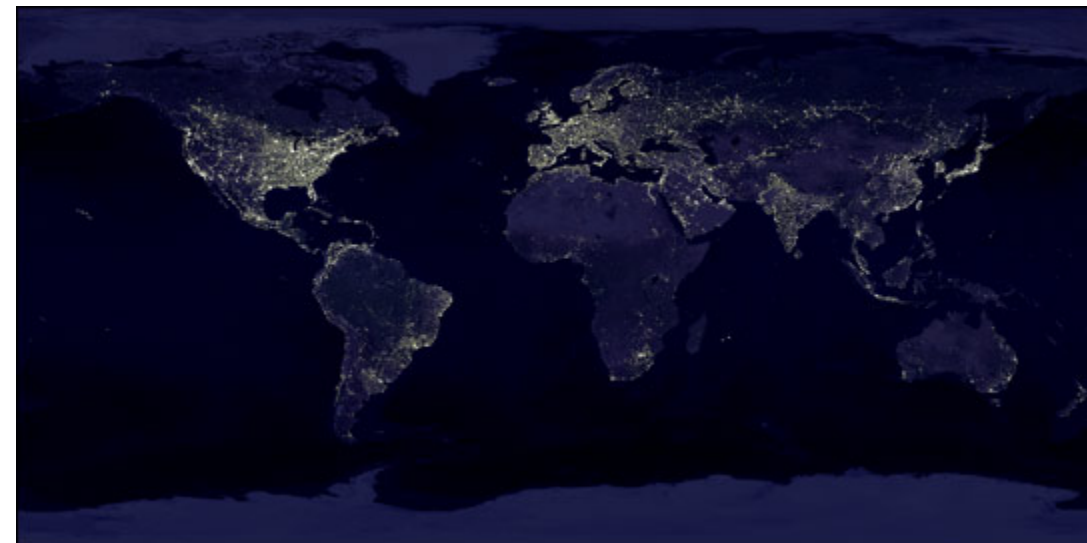
ρ_{Hyperion}	0.886	0.892	0.889	0.894
Mean ρ_{DNB}	0.891 ± 0.033	0.892 ± 0.023	0.919 ± 0.023	0.875 ± 0.043
Mean $\rho_{\text{DNB}} / \rho_{\text{Hyperion}}$	$1.006 \pm 3.7\%$	$1.0 \pm 2.6\%$	$1.034 \pm 2.6\%$	$0.979 \pm 4.8\%$
Range of $\rho_{\text{DNB}} / \rho_{\text{Hyperion}}^{-1}$	$[-6.1\%, 4.5\%]$	$[-3.8\%, 2.0\%]$	$[-1.3\%, 6.3\%]$	$[-7.6\%, 5.0\%]$

- DNB HGS radiometric variability (relative accuracy) $\sim 8\%$ is within the DNB specs (30%) and smaller than the 15% from post-launch performance analysis by Liao et al., 2013.
- Difference w.r.t. Liao et al., 2013 analysis
 - 2012-2014 vs. Mar.- Oct. 2012
 - Vicarious sites selection (Dome-C/Greenland vs. Railroad Valley Playa)
 - Events with stray light effects excluded in our analysis
 - Various lunar phases in our analysis vs. Near full moon in Liao et al., 2013
 - Different lunar irradiance model
- Residue variability in our analysis can be from lunar irradiance model, atmospheric absorption/scattering and its variability, BRDF of vicarious sites.

Reflectance vs. Lunar Zenith Angle




Preliminary radiometric calibration of DMSP-OLS using VIIRS-DNB through vicarious calibration



- Onboard series of DMSP-OLS (Defense Meteorological Satellite Program/Operational Linescan System) (F4-F19) satellites
- Collecting night low light imaging data for more than 40 years
- Various applications such as military surveillance, estimating population, monitoring social-economic development and power consumption, and providing weather and climate related data.

VIIRS-DNB vs. DMSP-OLS

Variable	DMSP-OLS	SNPP-VIIRS
Builder / Operator	U.S. Air Force	NASA – NOAA Joint Polar Satellite System (JPSS)
Orbit	Polar – 850 km altitude, 98.8 degree inclination, 102 minutes	Polar – 827 km altitude, 98.7 degree inclination, 102 minutes
Swath	3000 km 	3000 km
Nighttime overpass	~19:30	~01:30
Low light imaging bandpass	Panchromatic 0.5 to 0.9 um	Panchromatic 0.5 to 0.9 um
Additional spectral bands	Thermal infrared (10 um)	21 additional bands spanning 0.4 to 13 um.
Quantization	6 bit	14 bit
Saturation	Common in urban cores	No saturation
Calibration	None for low light imaging band.	Solar diffuser used to calibrate daytime DNB data. Calibration extended to low light imaging mode using data collected along solar terminator.
Elvidge et al., 2013		

- Perform vicarious calibration of DMSP-OLS using VIIRS-DNB
- Convert DN of DMSP-OLS into radiance unit

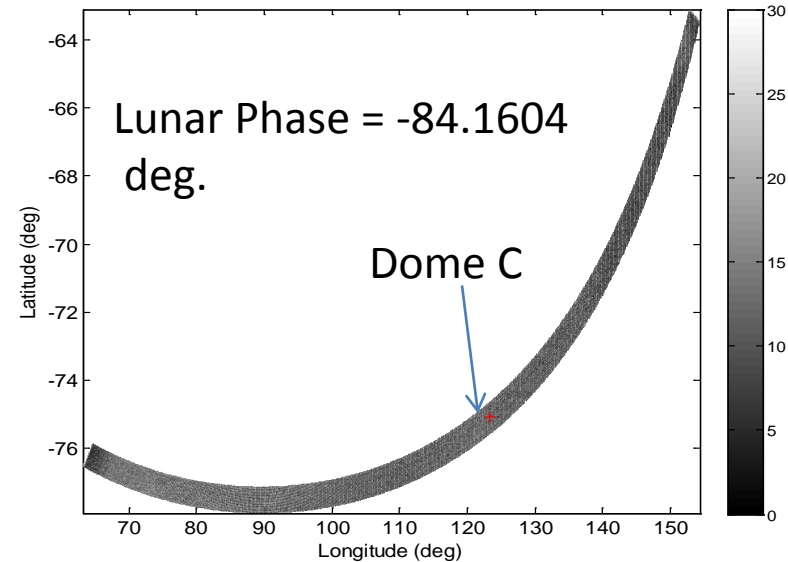
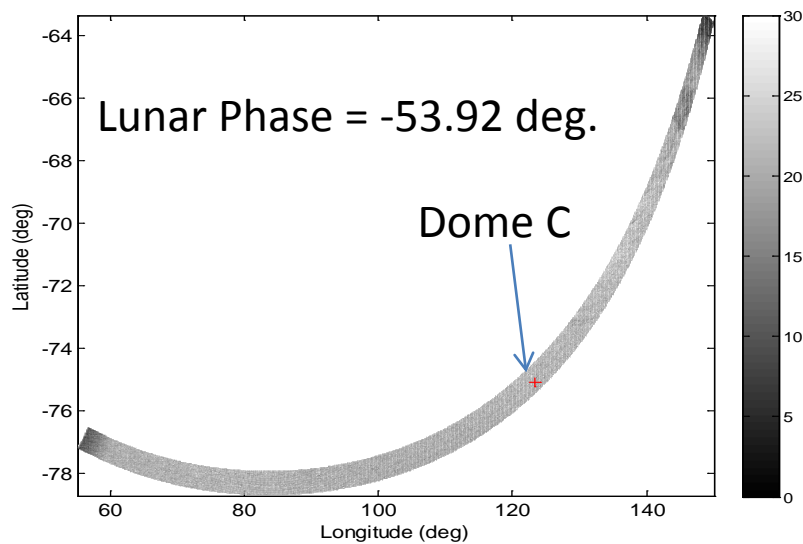
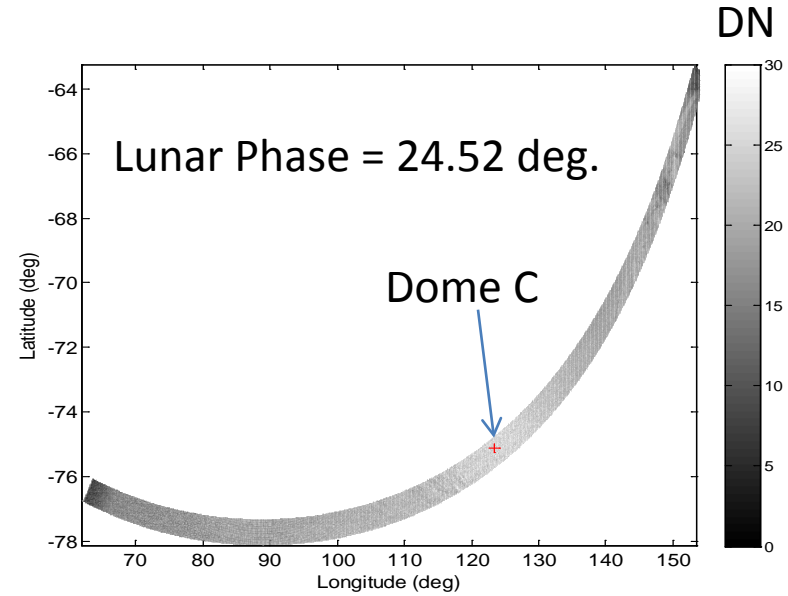
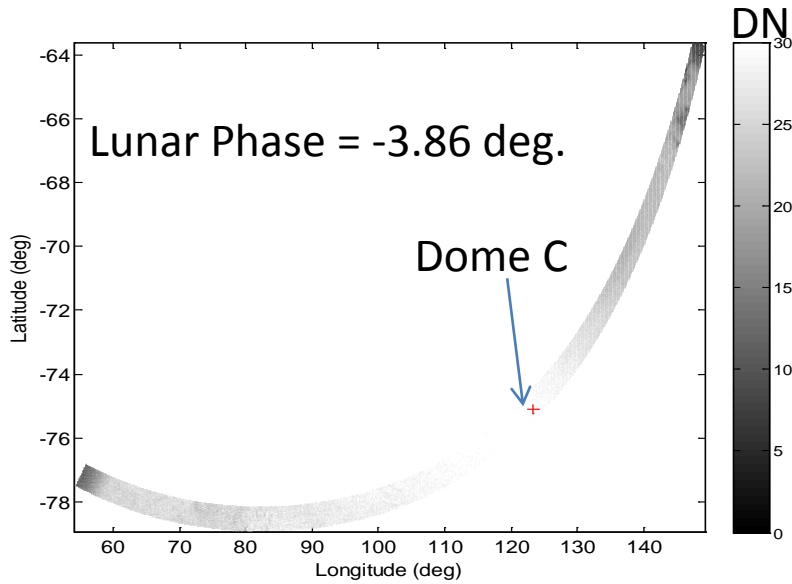


Screening Criteria

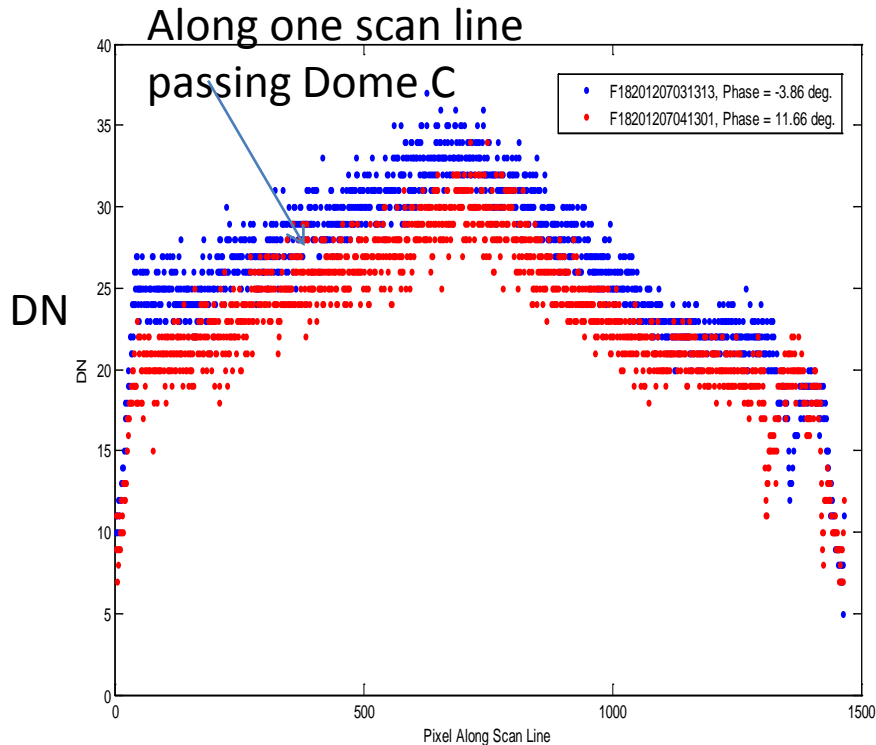
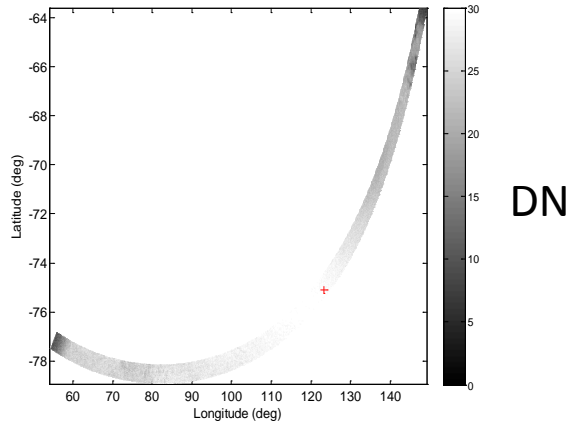


- ROI: Dome-C (Latitude: -75.1; Longitude: 123.25);
- DMSP-OLS overpasses the ROI, i.e. the nadir distance to DOME-C is < 300 km.
- Solar zenith angle $>118^\circ$. Overpass occurs at night and there are no influence of stray light effects
- Lunar phase angle is less than 90 degree, i.e. moon is larger than the quarter moon.
- Lunar zenith angle <80 degree
- Over all, 8 observations are selected from DMSP data from May to July, 2012.

DMSP-OLS F18 Observation of Dome C under moon light with different lunar phases

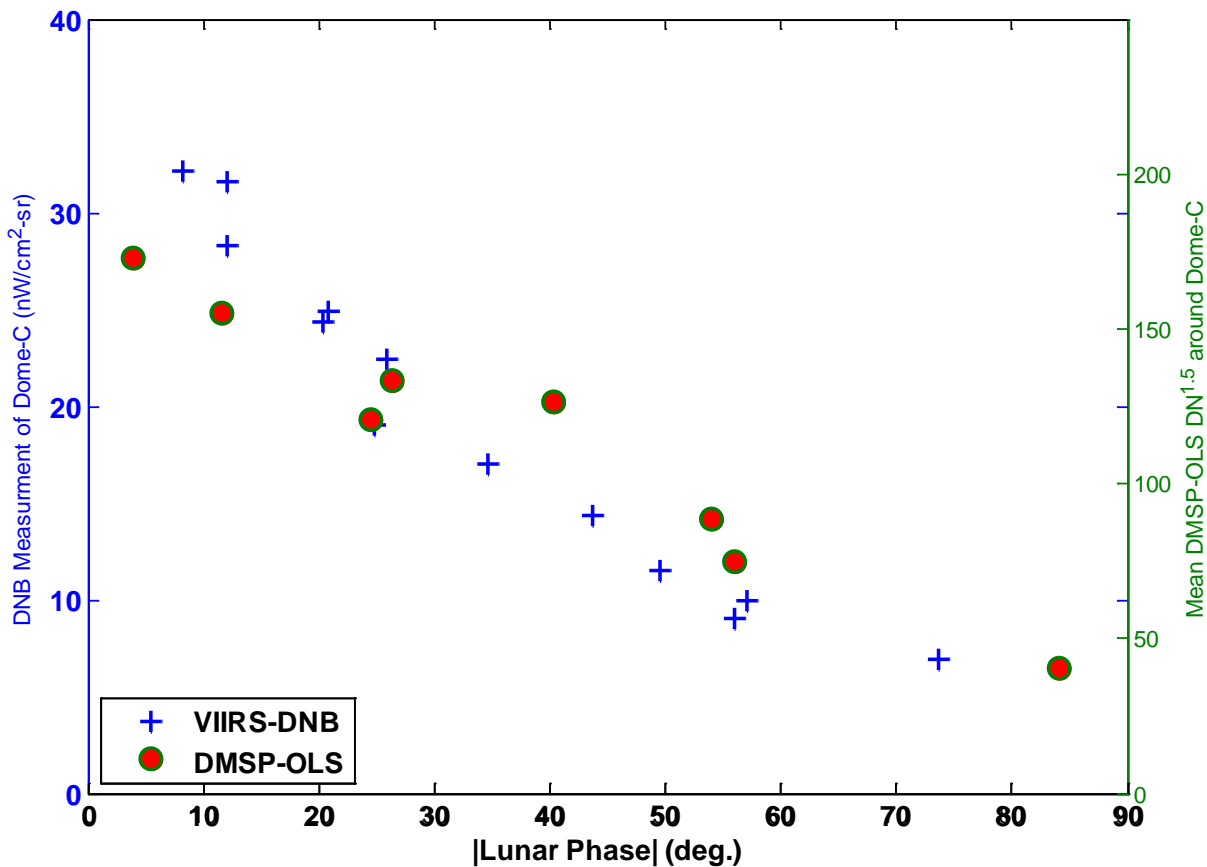


Deriving Mean DN^{1.5} at Region of Interest from DMSP-OLS data



- Strong scan-angle dependence of DMSP-OLS data
- We derive mean DN^{1.5} within 10 km around nadir of DMSP-OLS in the Dome-C region.
- Correct for Sun-Moon and Moon-Earth Distance.
- Arrange data w.r.t. lunar phase angle together with that from VIIRS-DNB during 2012.

Estimation of conversion coefficient of DMSP-OLS (DN^{1.5}) to Radiance Unit



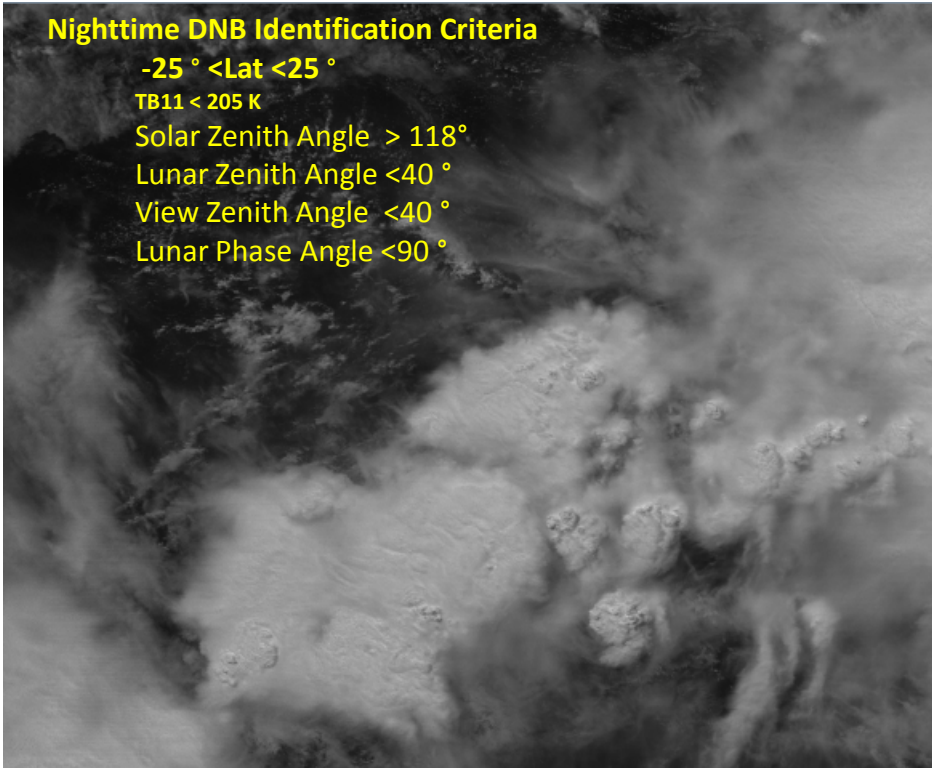
- DMSP-OLS Radiance = α DN^{1.5} (W/cm²-sr), $\alpha \sim 1.6 \times 10^{-10}$ (W/cm²-sr)
- Further analysis of 2013 data will be performed

DCC Under Moonlight

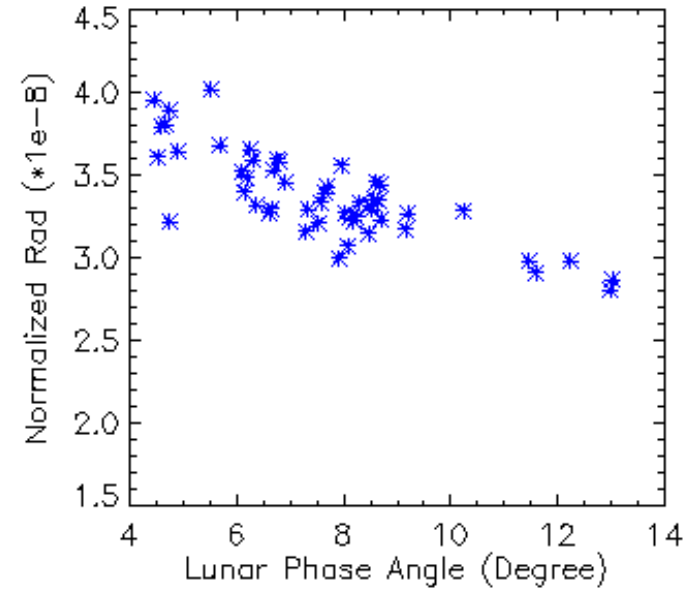
(Granule d20140116_t1432272_e1433514)

Nighttime DNB Identification Criteria

- 25° < Lat < 25°
- TB11 < 205 K
- Solar Zenith Angle > 118°
- Lunar Zenith Angle < 40°
- View Zenith Angle < 40°
- Lunar Phase Angle < 90°



Preliminary Analysis



Granule avg. nighttime DNB DCC radiance (adj. for lunar zenith angle effect) vs. Lunar Phase Angle

- Validated and performed trending of the radiometric performance of VIIRS-DNB with vicarious sites (Dome-C/Greenland) under moon light
- Performed preliminary radiometric calibration of DMSP-OLS using VIIRS-DNB through vicarious calibration
- Future work
 - Continue radiometric validation/calibration and trending of DNB using vicarious sites (Dome-C, Greenland and others) and DCC
 - Improve lunar irradiance model, characterization of BRDF of vicarious sites to reduce uncertainty
 - Study vicarious observations with stray light corrections being applied and assess the radiometric performance of DNB.
 - Cross-calibrate with DMSP-OLS.

Using VIIRS DNB SDRs to Generate Nighttime Lights Composites

May 13, 2014

Kimberly Baugh
Earth Observation Group (EOG)
University of Colorado - CIRES
NOAA National Geophysical Data Center
Kim.baugh@noaa.gov

Chris Elvidge - NOAA National Geophysical Data Center
Mikhail Zhizhin - CIRES - University of Colorado
Feng Chi Hsu - CIRES - University of Colorado

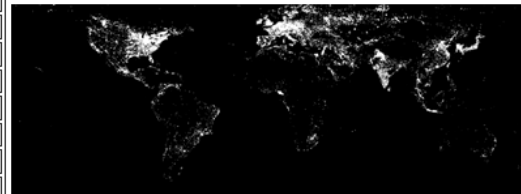
Nighttime Lights Composites

The EOG Group at NGDC has a long history of making global annual nighttime lights composites using DMSP-OLS data.

<http://www.ngdc.noaa.gov/eog/dmsp/downloadV4composites.html>

Average Visible, Stable Lights, & Cloud Free Coverages						
Year\Sat.	F10	F12	F14	F15	F16	F18
1992	F101992	-----	-----	-----	-----	-----
1993	F101993	-----	-----	-----	-----	-----
1994	F101994	F121994	-----	-----	-----	-----
1995	-----	F121995	-----	-----	-----	-----
1996	-----	F121996	-----	-----	-----	-----
1997	-----	F121997	F141997	-----	-----	-----
1998	-----	F121998	F141998	-----	-----	-----
1999	-----	F121999	F141999	-----	-----	-----
2000	-----	-----	F142000	F152000	-----	-----
2001	-----	-----	F142001	F152001	-----	-----
2002	-----	-----	F142002	F152002	-----	-----
2003	-----	-----	F142003	F152003	-----	-----
2004	-----	-----	-----	F152004	F162004	-----
2005	-----	-----	-----	F152005	F162005	-----
2006	-----	-----	-----	F152006	F162006	-----
2007	-----	-----	-----	F152007	F162007	-----
2008	-----	-----	-----	-----	F162008	-----
2009	-----	-----	-----	-----	F162009	-----
2010	-----	-----	-----	-----	-----	F182010
2011	-----	-----	-----	-----	-----	F182011
2012	-----	-----	-----	-----	-----	F182012

F15 2003 Nighttime Lights Composite



VIIRS Day-Night Band vs DMSP-OLS Spatial Resolution

- The VIIRS DNB footprint is 45 times smaller than the nighttime DMSP-OLS pixel footprint!

Nighttime DMSP OLS
5 km² footprint



VIIRS Day / Night Band
742 m² footprint

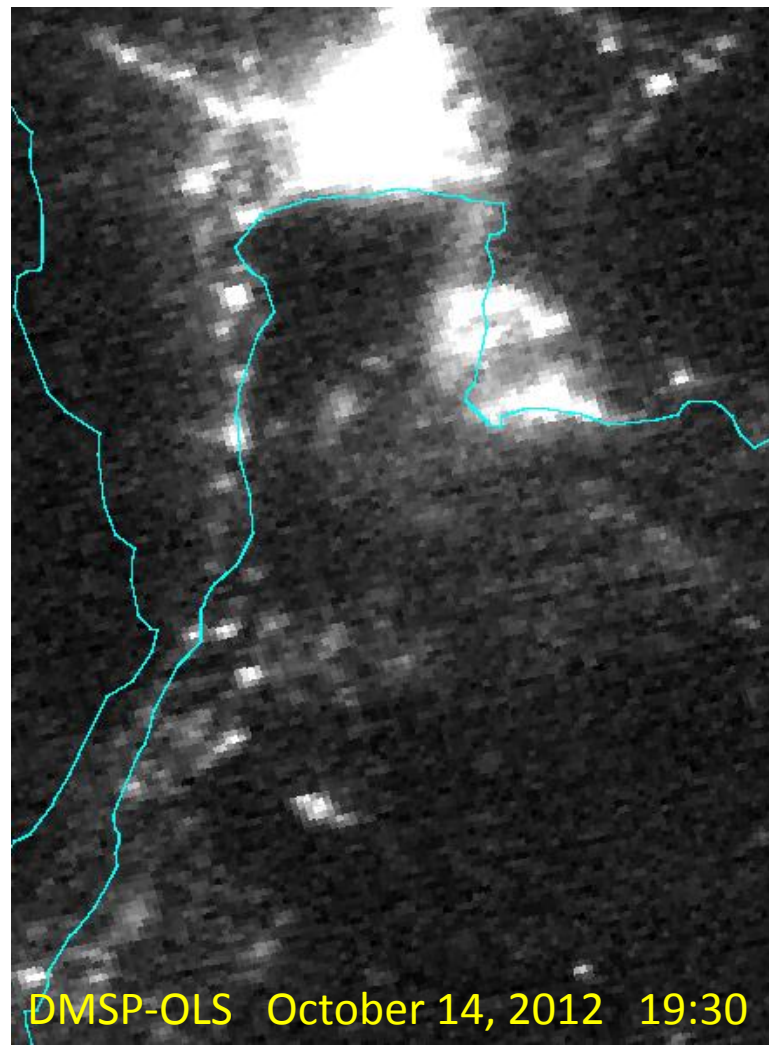
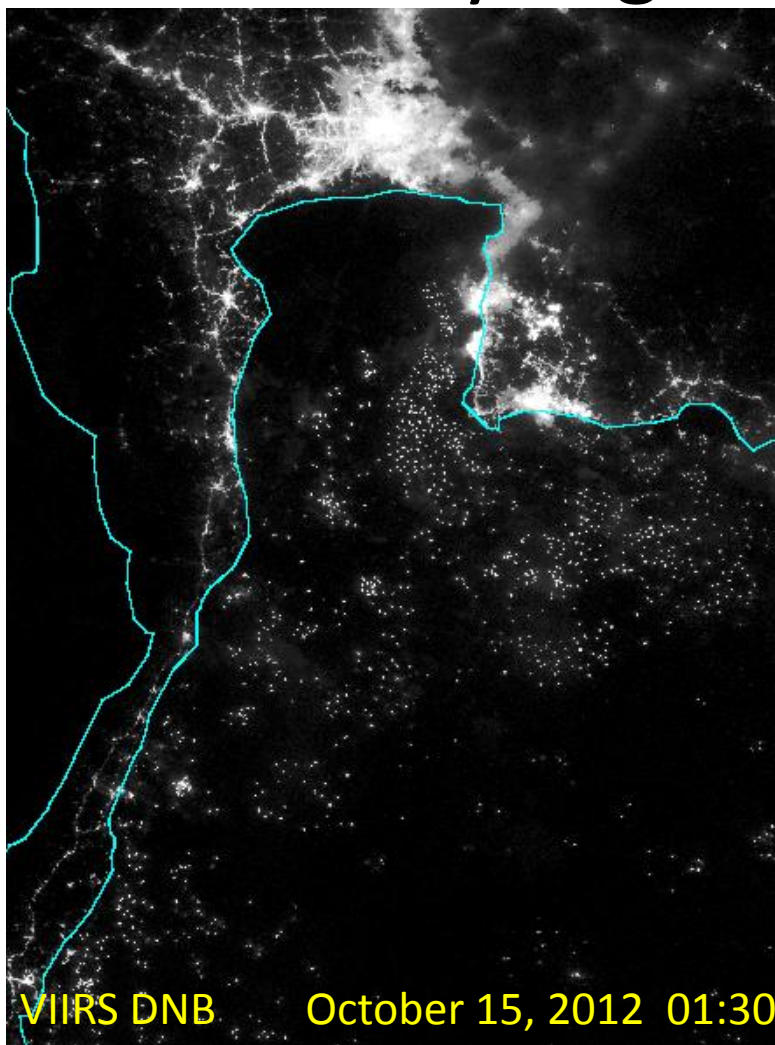


VIIRS Day-Night Band vs DMSP-OLS

- **Quantization:** DNB is 14 bit versus 6 bit for OLS.
- **Dynamic Range:** Due to limited dynamic range, OLS data saturate on bright lights in operational data collections.
- **Lower Detection Limits:** DNB can detect dimmer lighting than OLS.
- **Quantitative:** DNB is calibrated, the OLS visible band has no in-flight calibration.
- **Multispectral:** VIIRS has additional spectral bands to discriminate combustion sources from lights and to characterize the optical thickness of clouds.



VIIRS Day-Night Band vs DMSP-OLS



Note the lack of DNB saturation in Bangkok. Also the increased spatial resolution and lower detection limits allow DNB to distinguish small roads and more isolated fishing boats.

Using VIIRS DNB for Nighttime Lights Composites

- **Some DMSP-OLS algorithms could be reused**
 - Day/night/twilight flagging
 - Zero lunar illuminance flagging
 - Stray light region flagging
 - Cloud algorithm (used M15 in place of OLS thermal band)
- **Some algorithms needed makeovers**
 - Light filter (to separate background from signal)
 - Lightning detector (to work on 16-line scan)
 - Terrain correction for geolocation
- **New algorithms**
 - Blurry lights filter (to remove reliance on cloud mask)
 - Fire removal (taking advantage of other VIIRS spectral bands)



VIIRS DNB Composites – First Attempt

- First prototypes made in Dec 2012 for low-moon nights in April and Oct 2012.
- Average radiance values were constructed on a 15 arc-second grid for data determined to be:
 - Cloud-free
 - Zero lunar-illuminance
 - Out of “stray light” region
- Composites weren’t as “sharp” as expected. We suspected either the cloud algorithm and/or errors in geolocation.

VIIRS DNB Composites – First Attempt

- Investigation revealed a known DNB pointing error. NGDC received a table of estimated pointing errors from L. Liao at Northrup Grumman, which were then matched with GEO LUT filenames recorded as an attribute in the DNB h5 files.
- Adding pointing error adjustment to terrain correction software made huge improvement in composite feature sharpness.
- It was decided to try using the VIIRS Cloud Mask for the next attempt to see if additional blurriness was reduced.

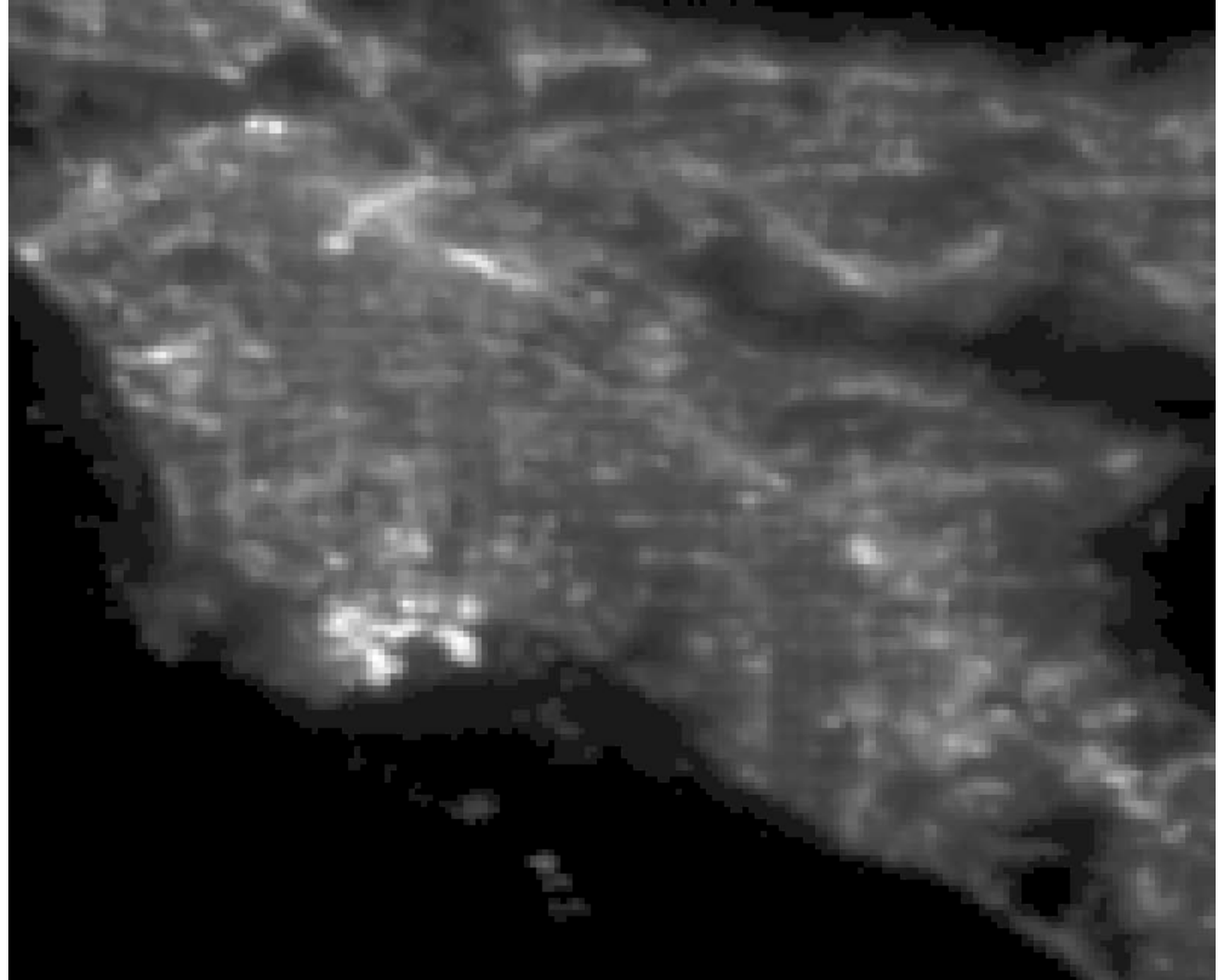


VIIRS DNB Composite (Oct 2012) Before Pointing Error Correction

Close-up of Los Angeles Basin.

Toggle with next slide.

Notice westward shift and increased spread of lighting features due to pointing error.



VIIRS DNB Composite (Jan 2013) After Pointing Error Correction

Close-up of Los Angeles Basin.

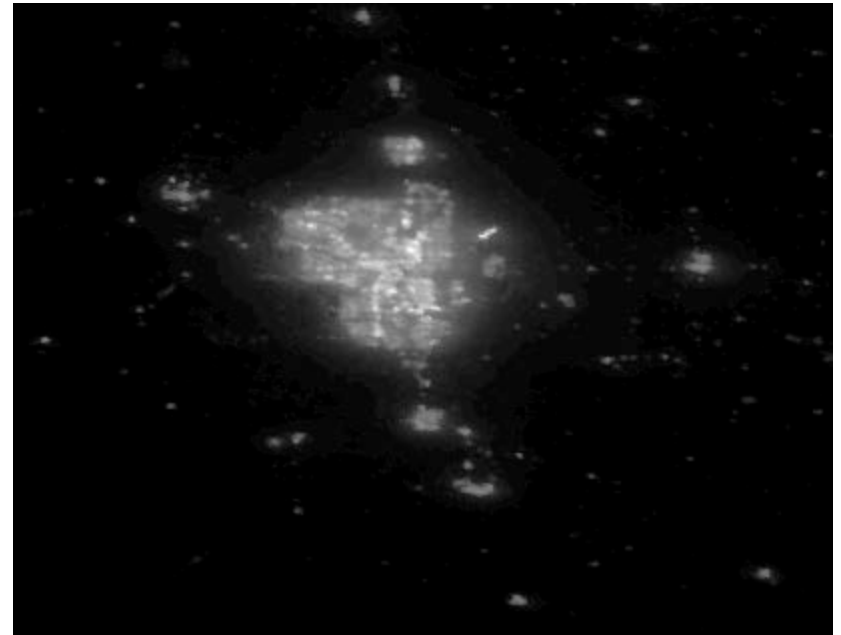
Toggle with prev slide.

Notice westward shift and increased spread of lighting features due to pointing error.



VIIRS DNB Composites – Second Attempt

- Second prototype made in April 2013 for all low-moon nights in Jan 2013.
- Composite still wasn't as “sharp” as expected in some regions of the world.
- The Jan 2013 composite used the VIIRS cloud-mask (VCM) to screen for clouds. Some clouds seem to be evading the cloud mask resulting in blurry lights.

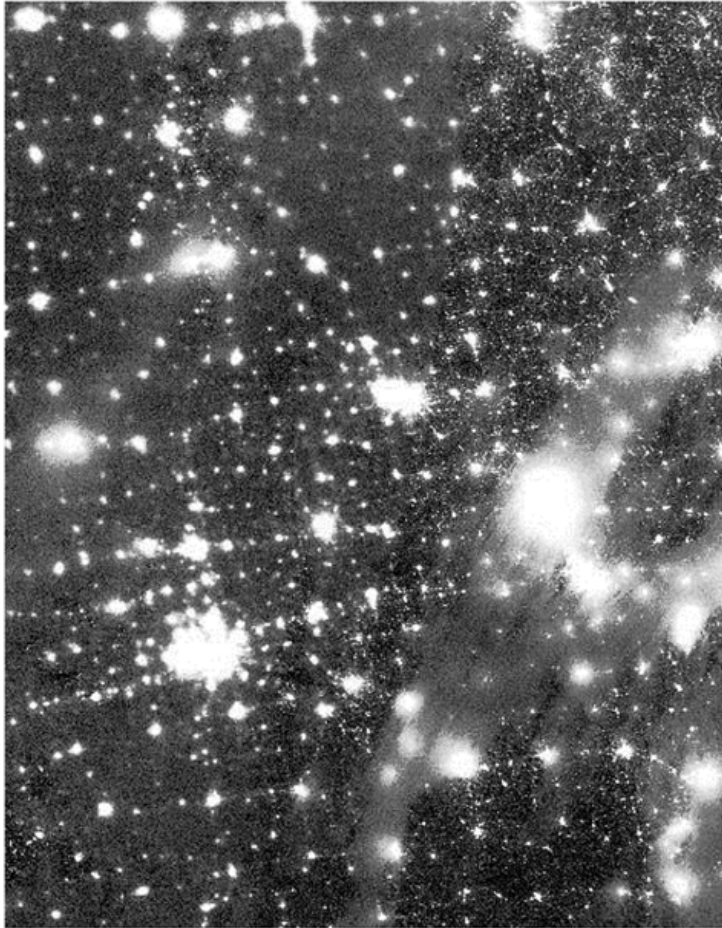


Calgary, Canada. Jan 2013 DNB Composite.

VIIRS DNB Composites – Current Run

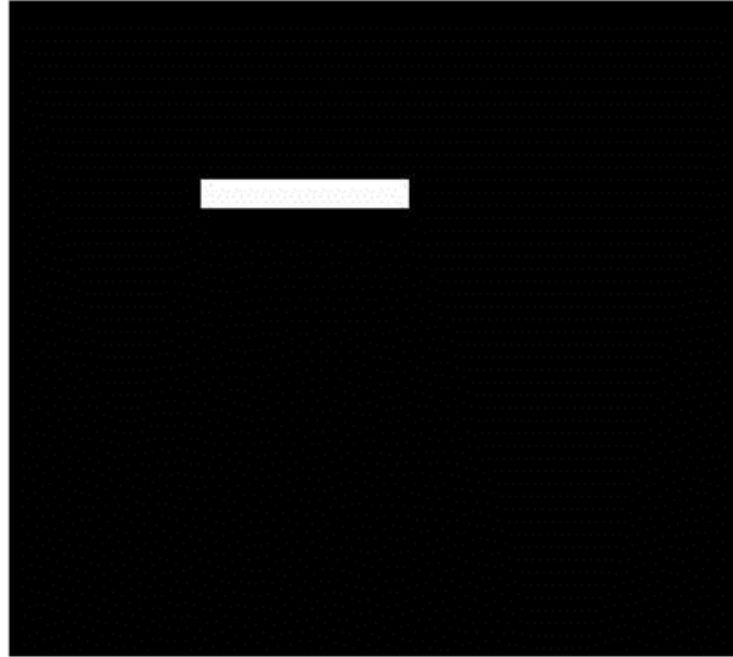
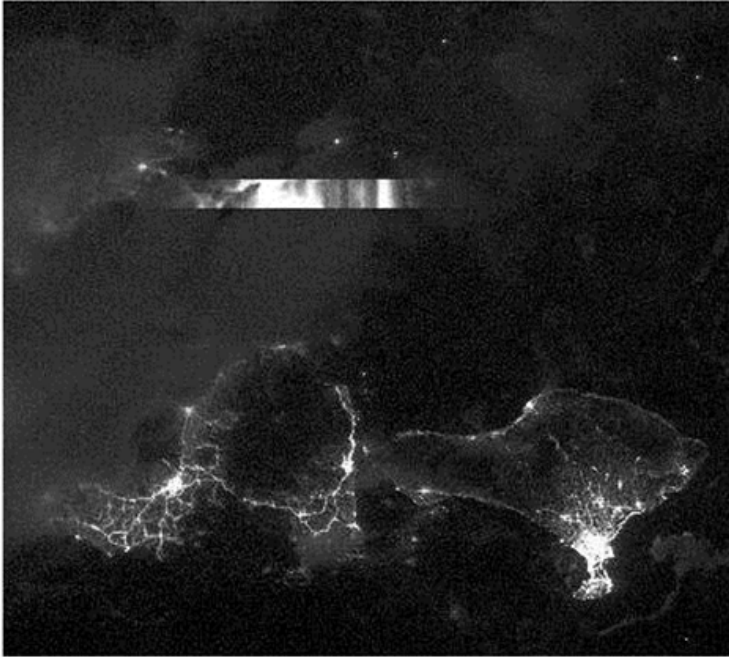
- Currently processing May 2014 data as it comes in.
- Additional algorithms being run are:
 - Blur Index (remove blurry lights without reliance on cloud mask)
 - Lightning filter
 - Light detection (separation of lights from background)

Blur Index



On the left is a DNB image showing areas with blur induced by clouds. On the right is the blur index image. Blurry areas are dark and sharp lights are bright. By applying a threshold on this index it will be possible to screen blurry areas from the composite.

Lightning Filter

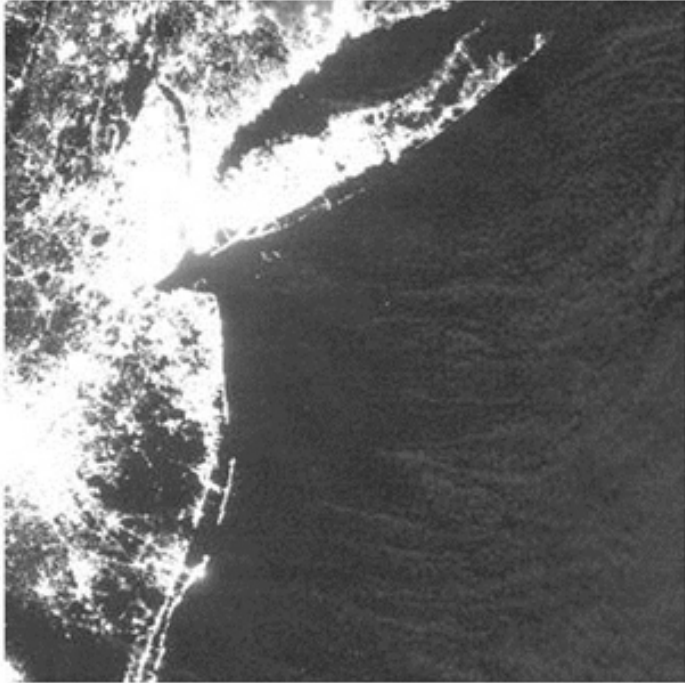


Example of lightning streaks detected by the DNB. The streaks are sixteen lines wide, arising from individual scans.

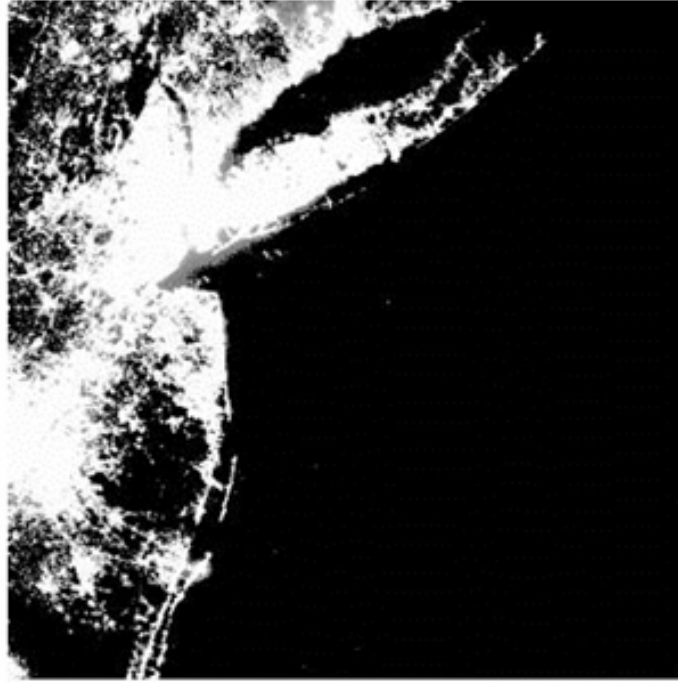
Removing reliance on a cloud-mask by using the blur index will make filtering for lightning signatures necessary for a clean DNB composite.

Light Detection

Raw DNB image



Background removed



A light detection algorithm is also being tested. It is designed for use on low lunar illumination DNB data.

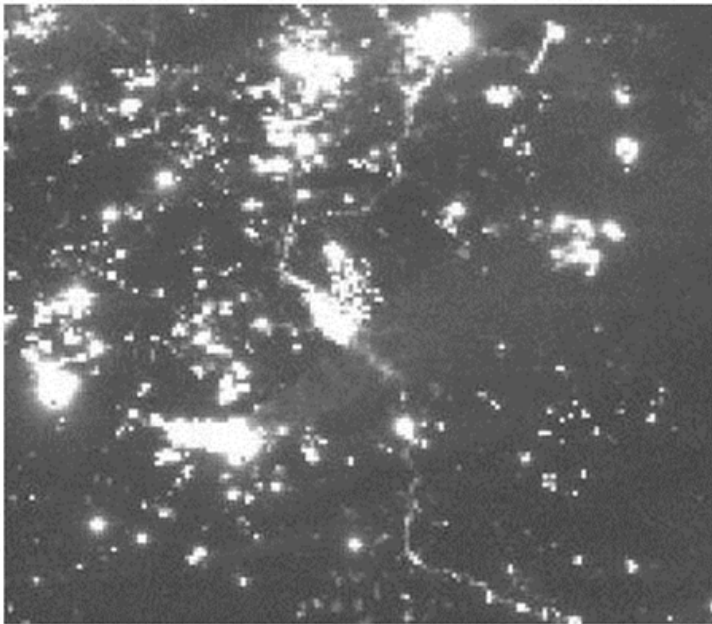
NGDC DNB Data Availability

- Monthly product generation started 5/1/14. The three preliminary products discussed are available at:
http://ngdc.noaa.gov/eog/viirs/download_monthly.html
- NGDC also generates nightly mosaics in png and Google Earth Super-overlay formats
http://ngdc.noaa.gov/eog/viirs/download_ut_mos.html

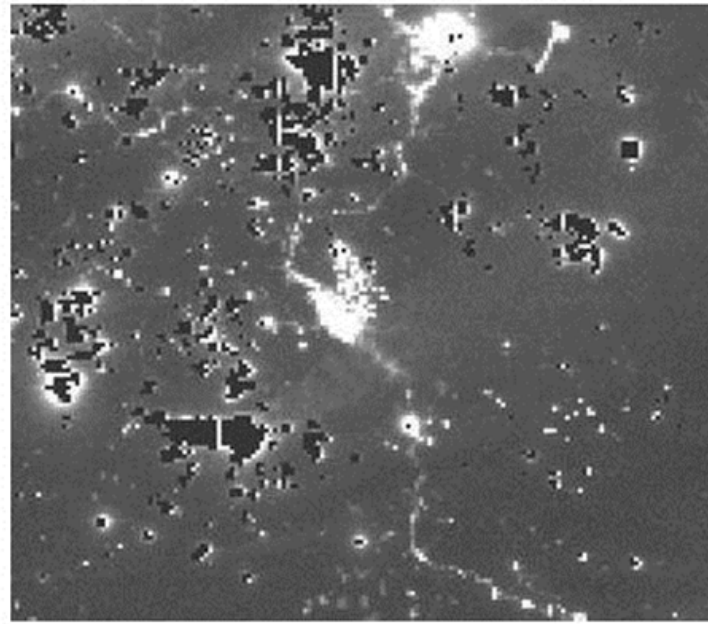
Next for VIIRS DNB Composites

- Still in algorithm development - R&D
 - Separating fires from lights using NGDC Nightfire product

Mixture of fires and towns



VNF fires masked out



The image on the left is the raw DNB. The image on the right shows the masking of biomass burning pixels from the Nightfire (VNF) data.



DNB Atmospheric Correction

In development – R&D

- The loss of signal in the DNB due to atmospheric absorption and scatter is both substantial and highly variable, in the range of 15 to 60%.
- We are working on an atmospheric correction for the DNB that uses MODTRAN to estimate the transmissivity of the atmosphere in the DNB.
- We parameterize MODTRAN using atmospheric profiles generated from ATMS data, which are collected simultaneous to the VIIRS.
- Specifically, we will use atmospheric pressure, temperature and relative humidity profiles generated from ATMS data using the MIIRS processing package (NOAA, 2013).
- The MODTRAN runs are computationally intensive, therefore the correction will only be run on pixels that are entering the monthly composites.



Stray light correction algorithm from Northrup Grumman



This algorithm was implemented at the IDPS in August 21, 2013. We will likely need to implement the algorithm at NGDC and apply it to archive data acquired prior to that.

Publications

- VIIRS Nightfire: Satellite pyrometry at night
<http://www.mdpi.com/2072-4292/5/9/4423>
- What is so great about nighttime VIIRS data for the detection and characterization of combustion sources?
DOI: <http://dx.doi.org/10.7125/APAN.35.5>
- Using the short-wave infrared for nocturnal detection of combustion sources in VIIRS data.
DOI: <http://dx.doi.org/10.7125/APAN.35.6>
- Why VIIRS data are superior to DMSP for mapping nighttime lights. DOI: <http://dx.doi.org/10.7125/APAN.35.7>
- Nighttime lights compositing using the VIIRS day-night band: Preliminary results DOI: <http://dx.doi.org/10.7125/APAN.35.8>



Suomi NPP VIIRS

Geolocation Performance & Improvements

NASA VIIRS Calibration Support Team (VCST)

Geometric Calibration Group

Robert E. Wolfe, NASA/GSFC Code 619

[Guoqing \(Gary\) Lin](#) & Zhangshi Yin, Innovim/GSFC

Mash Nishihama & Bin Tan, Sigma Space/GSFC

James C. Tilton, NASA/GSFC Code 606

JPSS 2014 Annual Science Team Meeting

College Park, Maryland

13 May 2014



Acknowledgements

- Thanks Carol Davidson & her Land PEATE Team for processing control point residuals and possible two line element (TLE) use from both IDPS and LPEATE forward-&re-processed VIIRS geolocation products, and testing Geo LUTs updates
- Thanks Geo JAMs -- Alice Isaacman (retired) and Robert Williamson & John Dellomo -- for helping us resolving DRs in the DPE/DPA at the GRAVITE
- Thanks NGAS Team for updating DNB Geo LUTs



Outline



- Geolocation Performance and Trends
- Geolocation Improvements
 - accomplished
 - to be accomplished (potentially)
- Conclusions

Residuals	Error IDPS	Error Land PEATE Re-processed
Track mean	-7 m	3 m
Scan mean	-5 m	3 m
Track RMSE	74 m	69 m
Scan RMSE	60 m	59 m
Data-days	796 (2.2 yrs)	831 (2.3 yrs)
Missing days	21	2
GCP matched w/ band I1	132	135

- **Nadir equivalent** accuracy (RMSE – Root Mean Square Error)

- Meet Spec: 133 m (1σ); within 20% I-HSI (375 m) = 75 m @ nadir

- Time period:

- IDPS: 23 Feb 2012 (VIIRS I/M-band LUT update) to 28 April 2014; excluding 18 days right after A/B side switch

- Land PEATE: 19 Jan 2012 to 28 April 2014



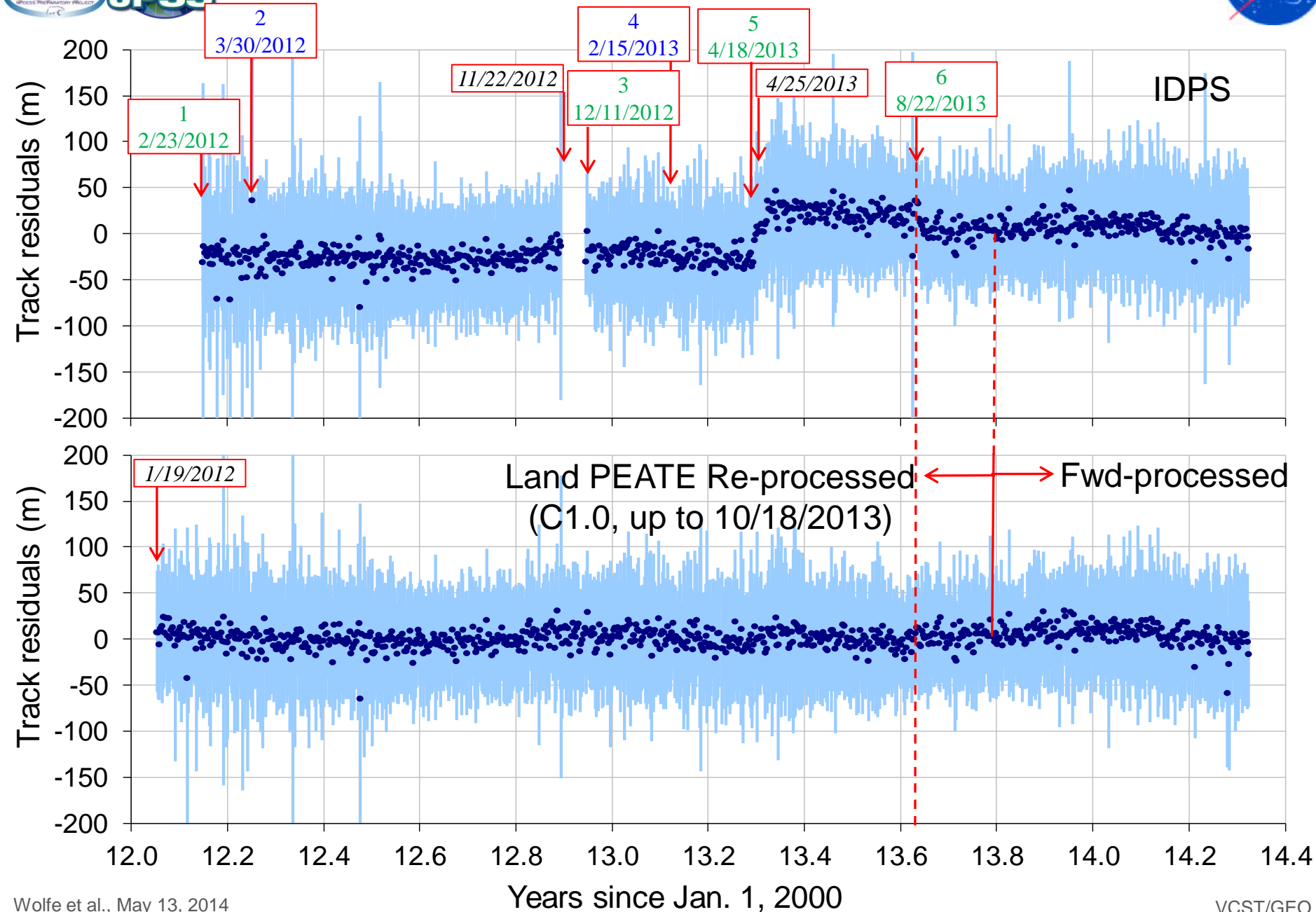
On-orbit Geolocation LUT Updates



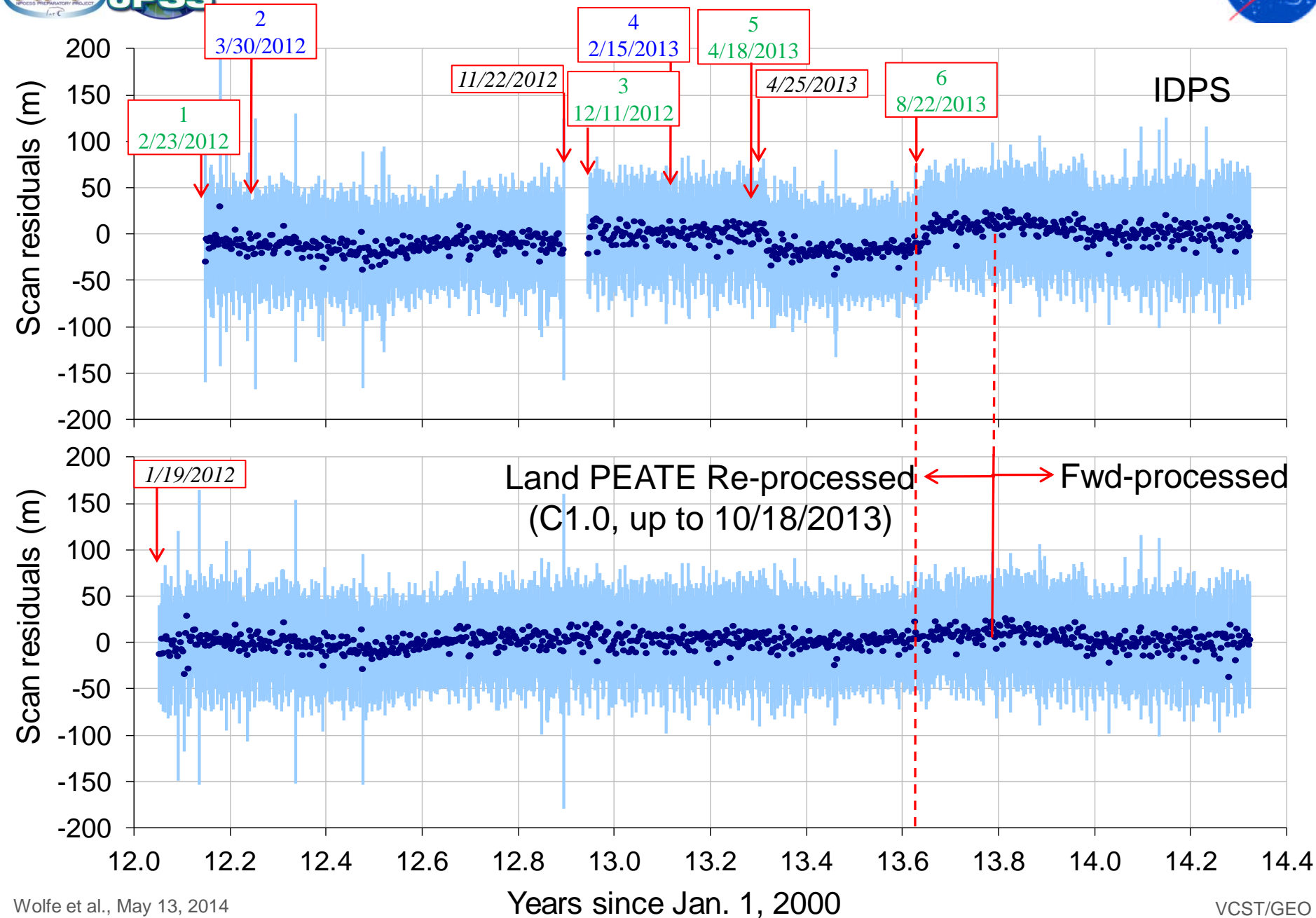
Update	Date	Description	Comments
a	1/19/2012	Cryo-radiator door open	All VIIRS band available, LPEATE re-process start date
1	2/23/2012	Initial mounting coef. update	Removed bias ~ 1.3 km
2	3/30/2012	Initial DNB FPA center update	Removed bias ~ 1 km
b	11/22/2012	Scan control electronics (SCE) was switched from B-side to A-Side	Caused bias ~ 300 m
3	12/11/2012	Correction after SCE was switched from B-Side to A-side	Removed bias ~ 300 m
4	2/15/2013	Second, fine DNB FPA center update	Removed DNB bias ~ 300 m
5	4/18/2013	Second, scan angle dependent, fine Geo LUT update	Fine tuned and removed scan dependent biases
c	4/25/2013	Star tracker maintenance/re-alignment	Caused bias ~ 25 m
6	8/22/2013	Correction to the star tracker re-alignment	Removed bias ~ 25 m

Key: All bands impacted DNB only External event

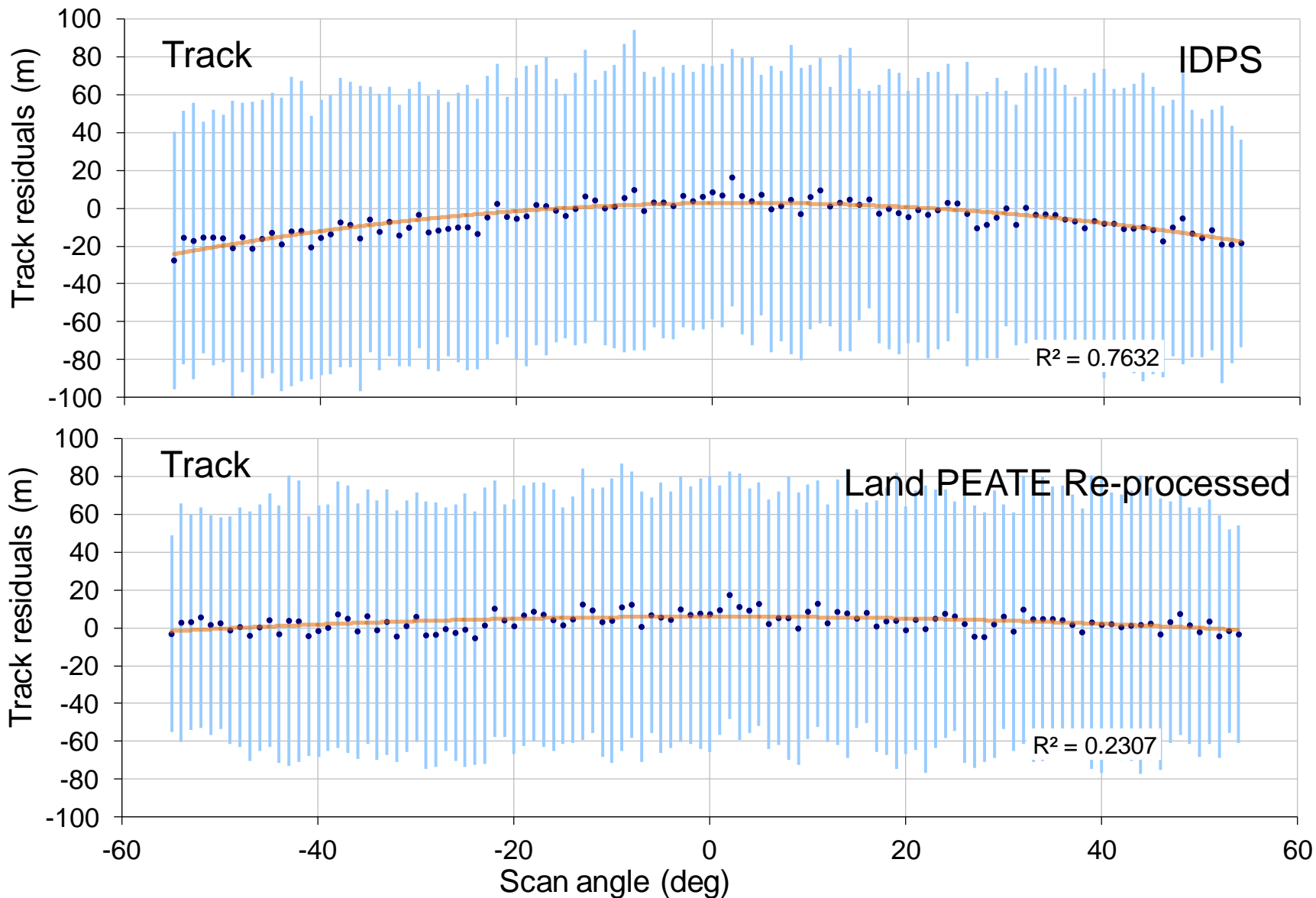
VIIRS Track Residual Trends



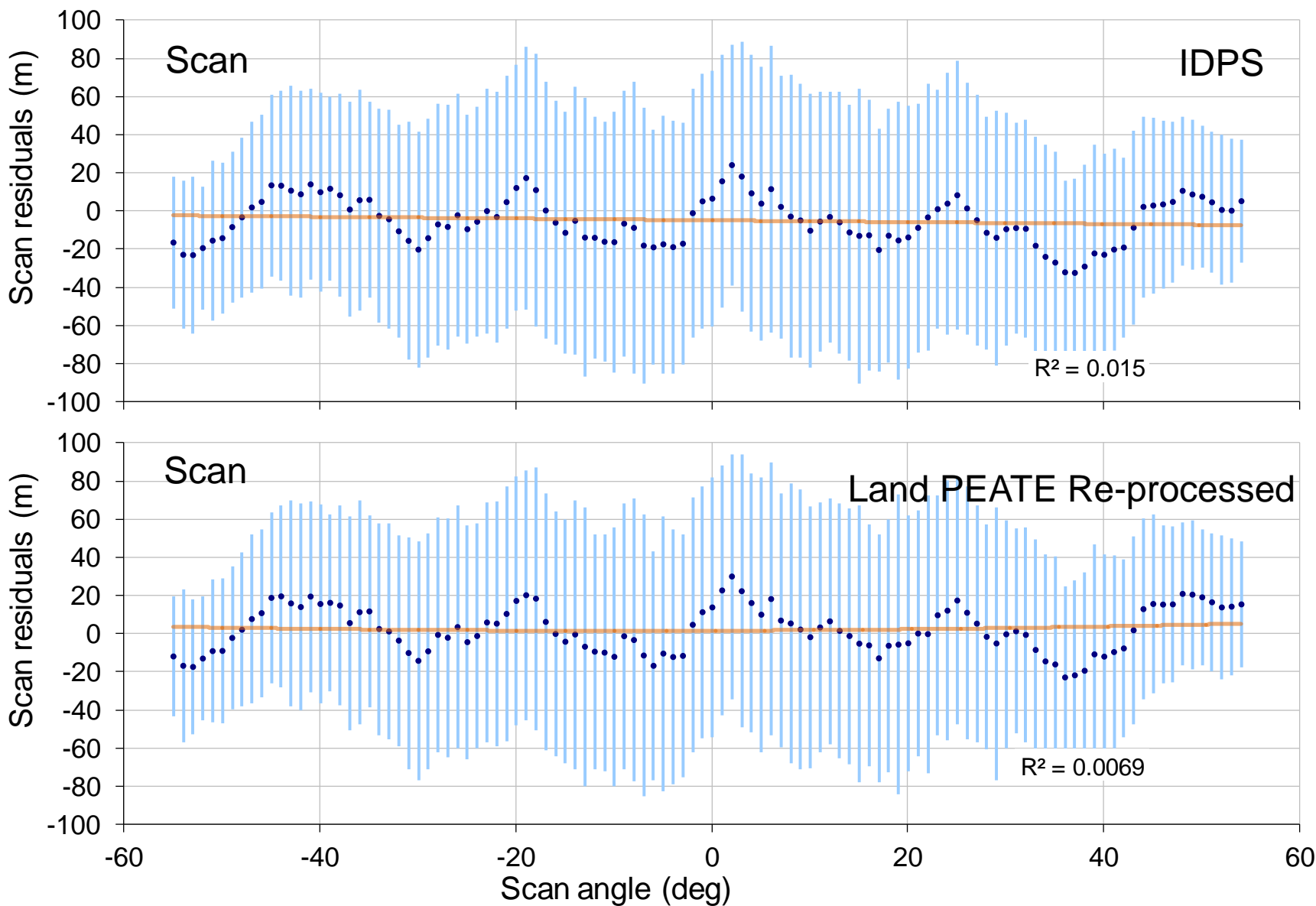
VIIRS Scan Residual Trends



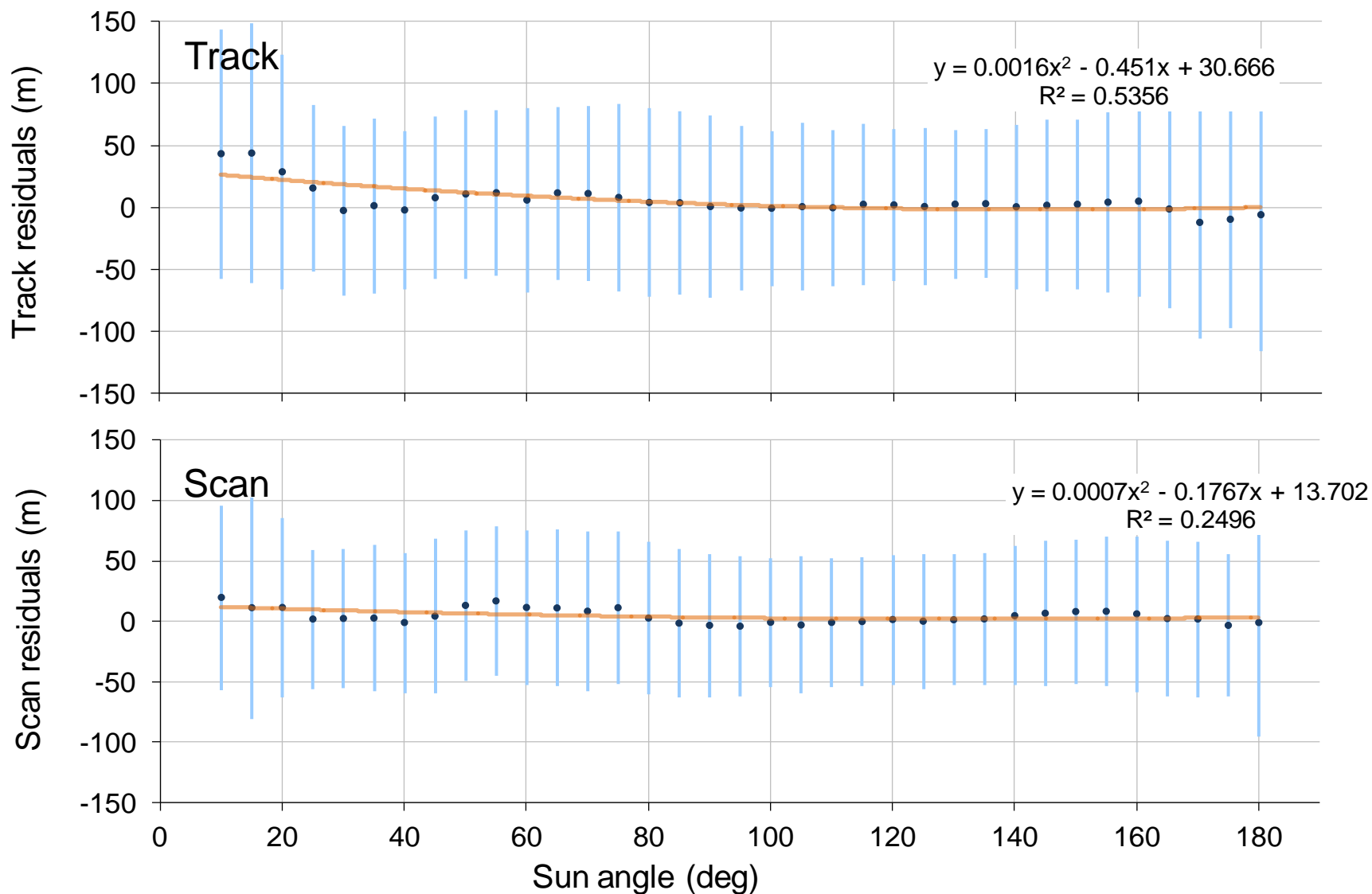
VIIRS Scan Angle Residuals



VIIRS Scan Angle Residuals



VIIRS Sun Angle Residuals

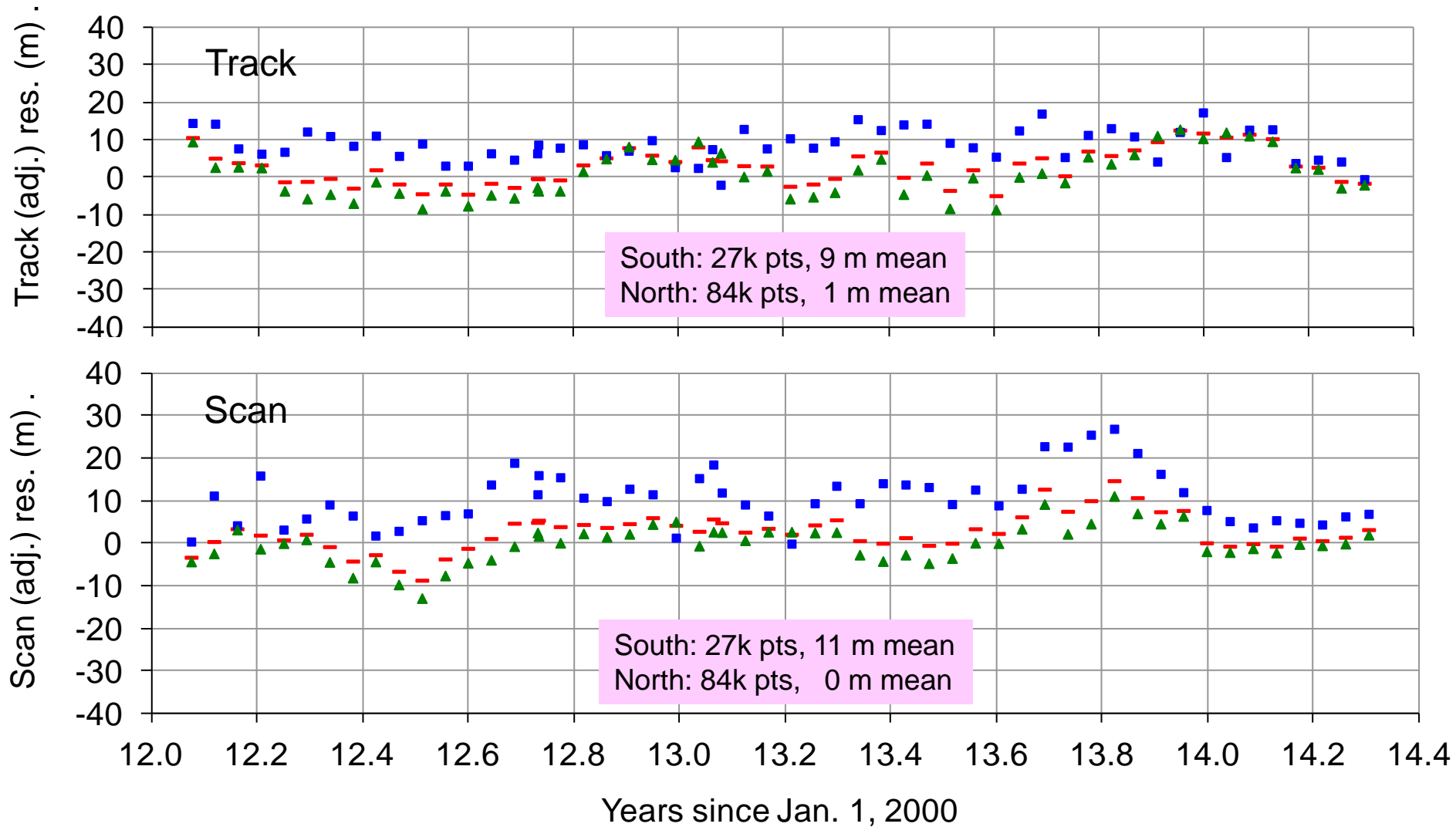


VIIRS Hemispheric Residuals

- 16-day Global

■ 16-day Southern Hemisphere

▲ 16-day Northern Hemisphere



Land PEATE Re-processed, no correction yet

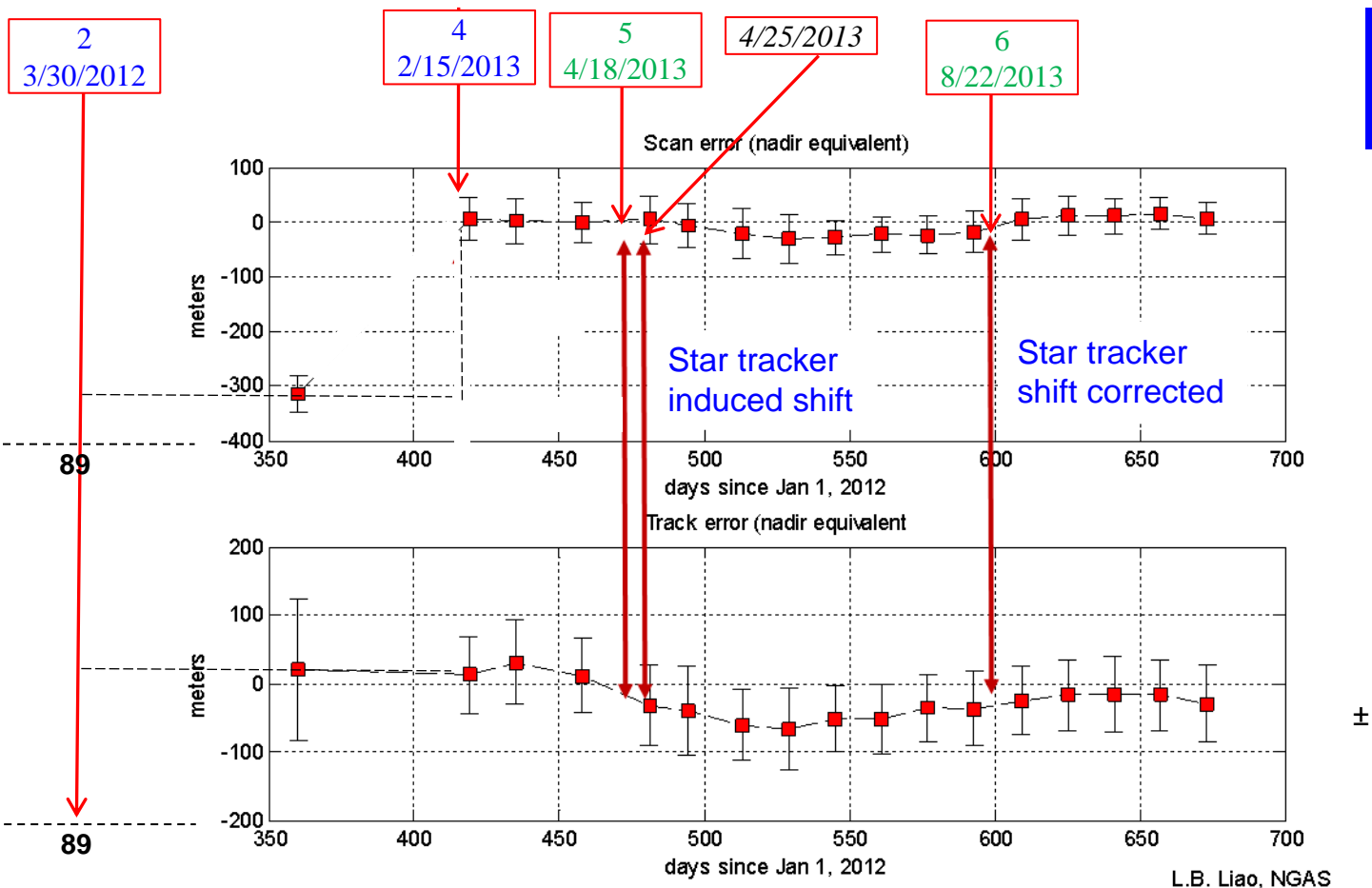


Improvements accomplished

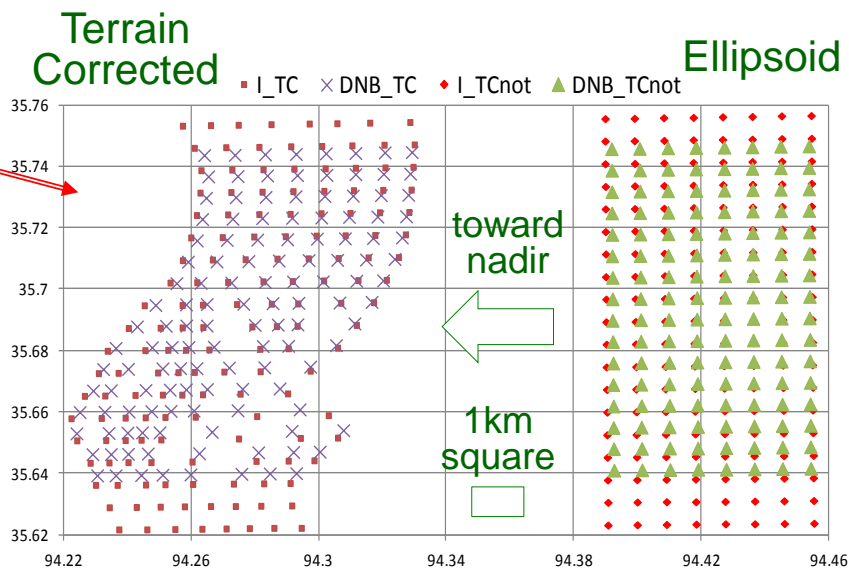
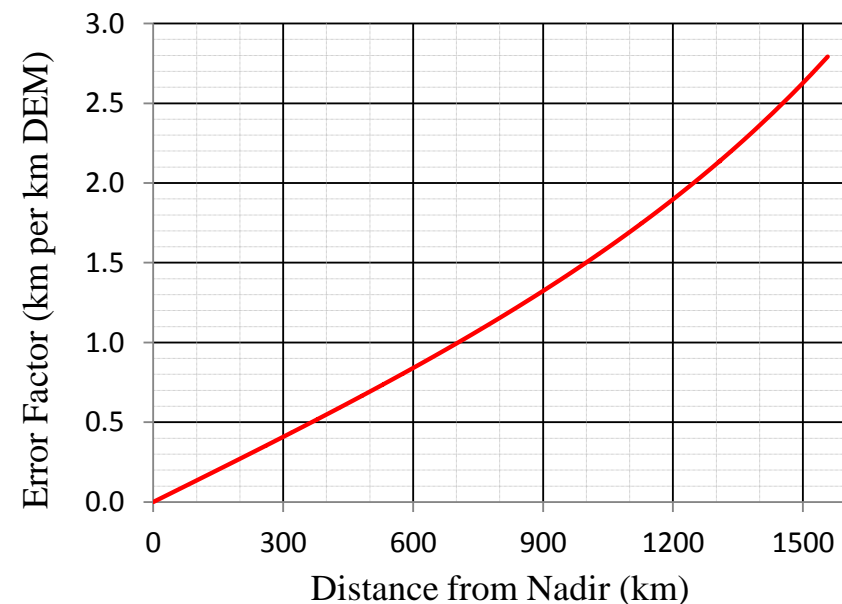
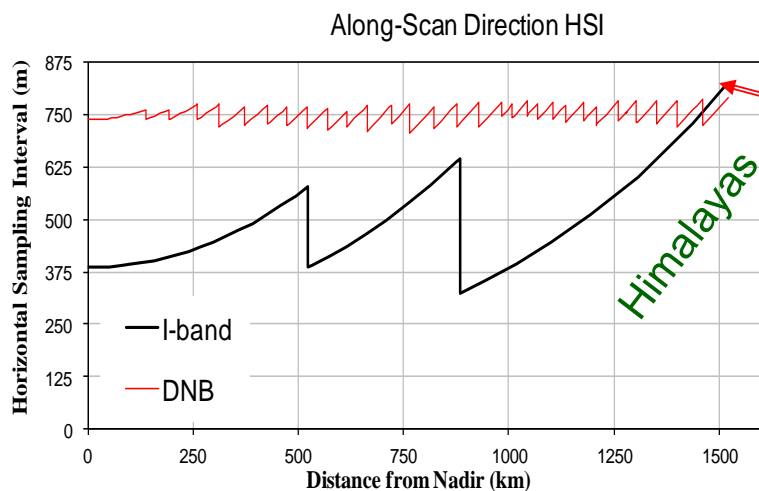
- Initial on-orbit and fine tuned I-/M-bands SDR/GEO LUTs (backup)
- Updated LUTs in responses to on-orbit changes (backup)
 - 1) Scan control electronics (SCE) side A (switched from side B in Nov 2012))
 - 2) Star tracker re-alignment in April 2013
- Worked DNB TC geolocation to be implemented in IDPS TTO 22 May 2014 (already in NASA Land PEATE since May 2013) (Chart 13&14)
- Reduced geolocation bias from (up to) 20 km to (up to) 1.5 km through a fix in calculation using backup TLE data (Chart 15)
- Corrected solar/lunar vector errors (~ 0.2 deg) in CmnGeo (Chart 16)
 - The correction will reduce RSB Cal bias $\sim 0.5\% \pm 0.25\%$, expected TTO Mx8.5?/6 August?/October 2014
- Trended (2.5 years) SC ephemeris -- understand altitude $\mu = 838.8$ km (Chart 17)

DNB Geolocation based on coastal areas GCP matching

Courtesy
of NGAS

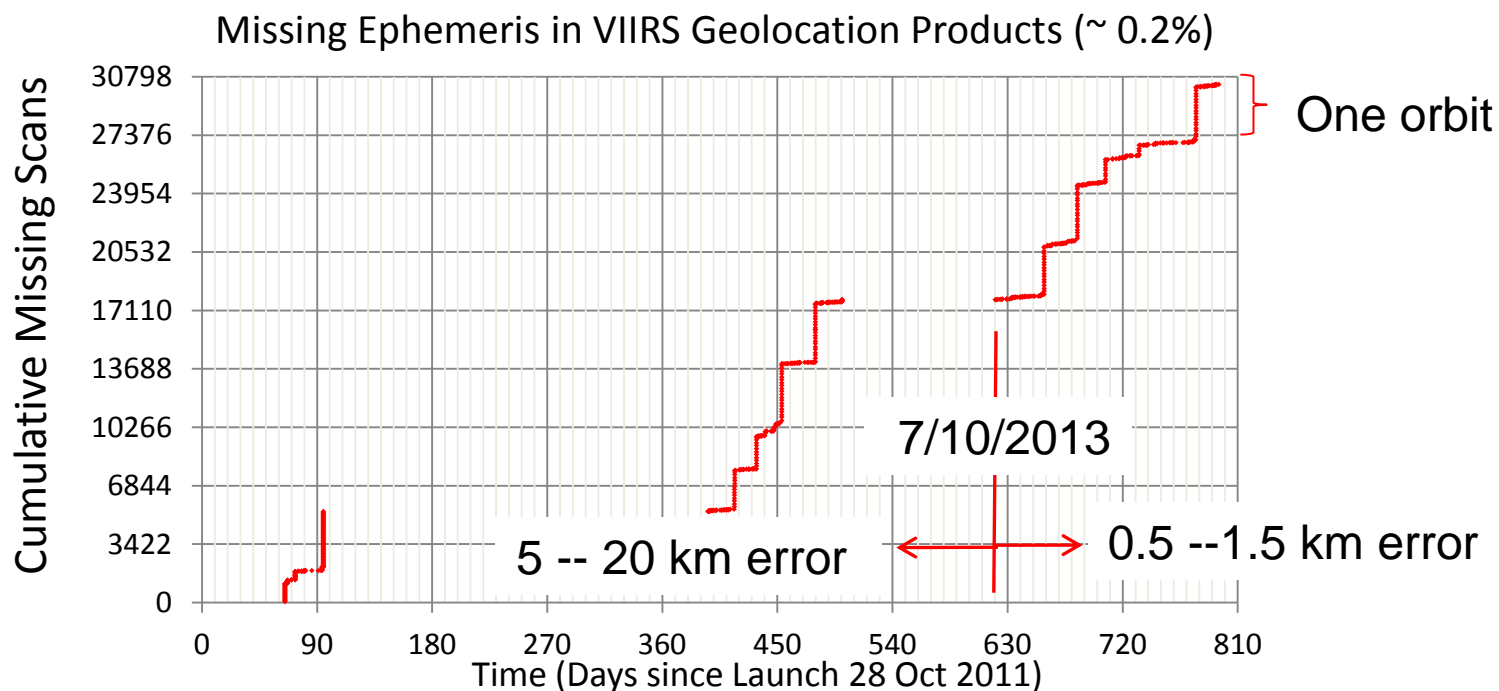


As of Nov 4, 2013, the DNB geolocation accuracy is
 Scan: $8 \pm 33 \mu\text{rad}$ Track: $-35 \pm 68 \mu\text{rad}$
Scan: $7 \pm 28 \text{ m}$ Track: $-29 \pm 57 \text{ m}$ over coastal areas
 (nadir equivalent with mean altitude of 838.8 km)



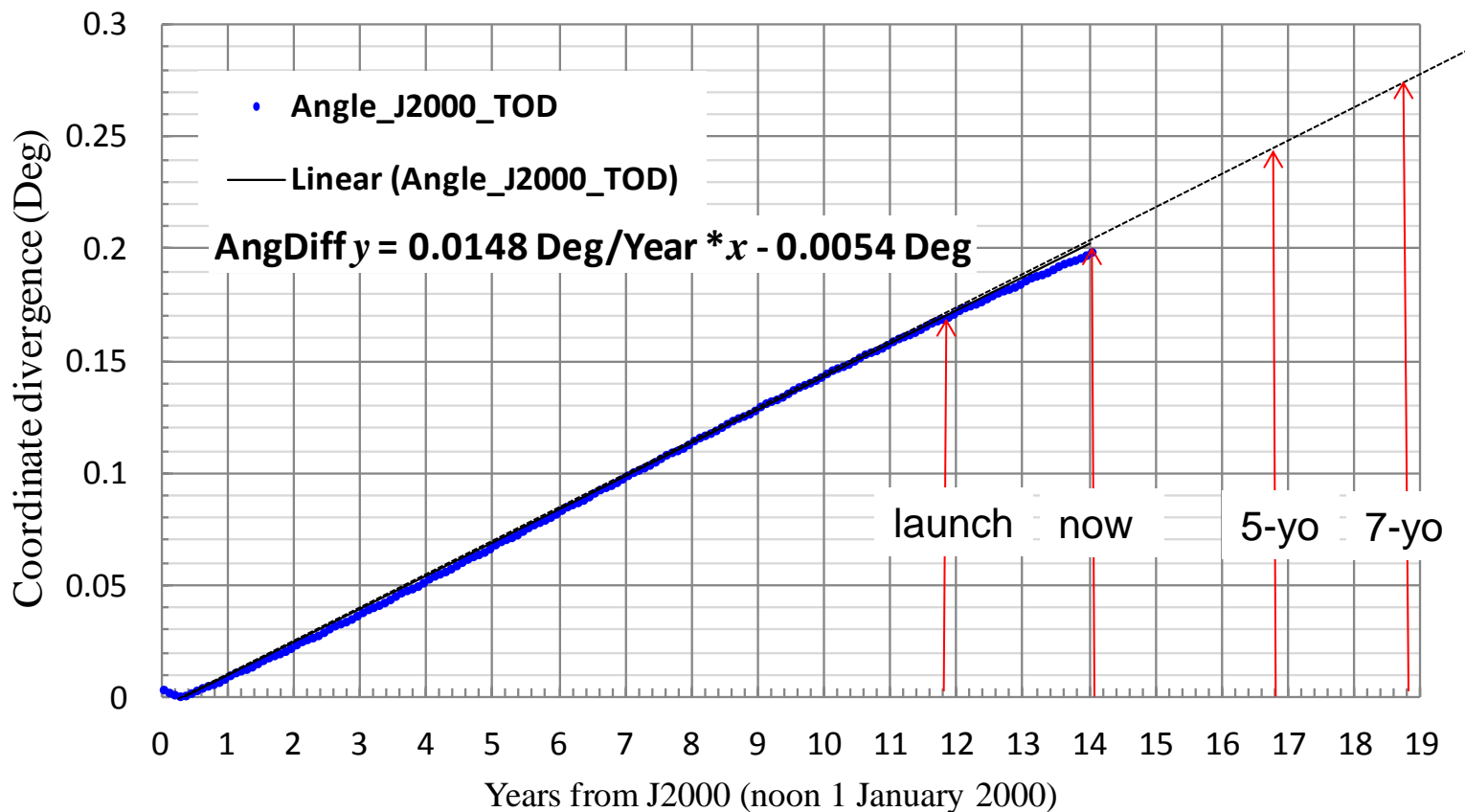
- The un-corrected DNB geolocation error depends on position off-nadir and terrain height
- DNB Geo LUTs updates based on coast areas (Thanks to NGAS)
- DNB TC geolocation products available from LPEATE since May 2013
- DNB TC geolocation products generated in IDPS Mx8.4 22 May 2014

TLE use and geolocation errors



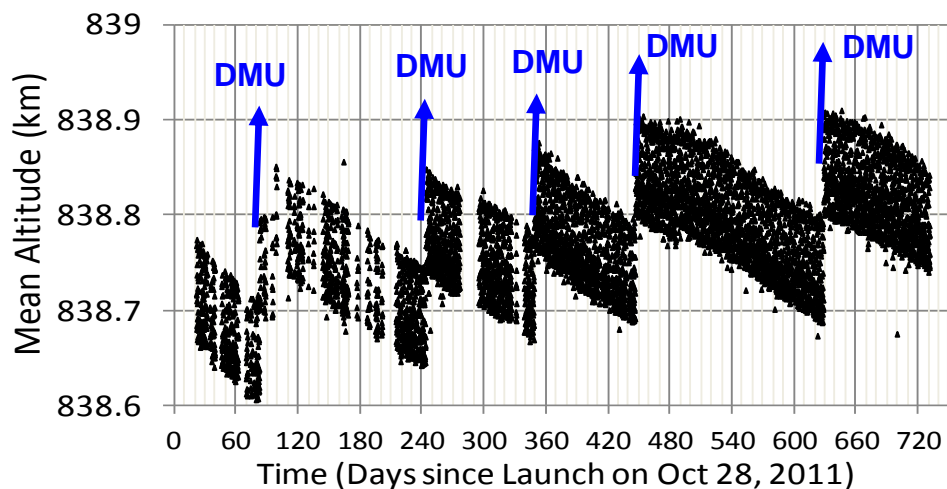
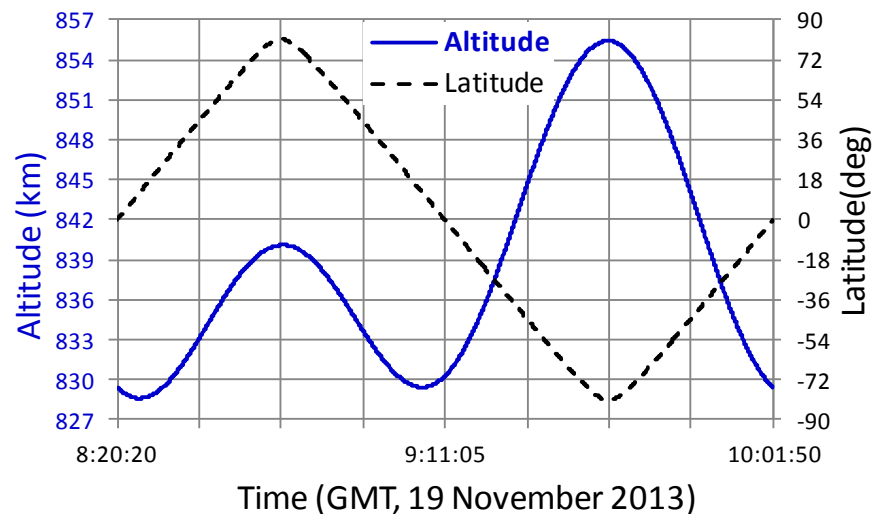
- TLE used in IDPS when SC diaries were delayed to and
- 314 days (periods 65-95, 395-501 & 620-795) of data checked
- 0.2% of scans used TLE backupdata =? Data availability loss
- Most of them occurred in whole-orbit chunks
- A CCR reduced geolocation bias from (up to) 20 km to (up to) 1.5 km on 10 July 2013
- SRS baselined: “SRS.01.08_280 The Common Ground System shall provide the spacecraft diary, when available from the Spacecraft, within 30 seconds of the instrument data for a given data product.” → geo error reduce to ~ 100m for SC diary gap < 30 seconds

Solar & Lunar Vector Correction



- Erroneous use of calls in the IDPS CmnGeo routines (J2000 and TOD)
- Combination of precession-nutation-polarWander pulls true vectors apart from the IDPS computed vectors at a rate of 0.015 deg/year from year 2000
- Correction in August/October 2014 timeframe will help VIIRS RSB calibration and ocean color products (& VIIRS TEB calibration by narrowing lunar intrusion into spaceView)

SNPP Altitude? $\mu = 838.8$ km



- Altitude (km)
 - Mean: 838.8 ± 0.2 Peak-to-Valley
 - Min: 828.5 ± 0.6 P-V; Max: 856 ± 0.6 P-V; Equator: 829.8 ± 1.0 P-V
- Drag make-up (DMU) maneuvers keeps altitude from falling and 16-day ground track repeatable (± 20 km P-V)
- Local time of ascending node (LTAN) drifts from 13:25:24 in Nov 2011 westward 66 km to 3:23:02 in Nov 2012 then back eastward 104 km to 13:26:46 in 4 Dec 2013, continues eastward
- Orbital period: 101.5 min ± 0.3 sec P-V
- Inclination angle drifts $98.65 \rightarrow 98.72$ deg (0.07 degrees more away from the poles) in 2 years, and continues to move away from the poles

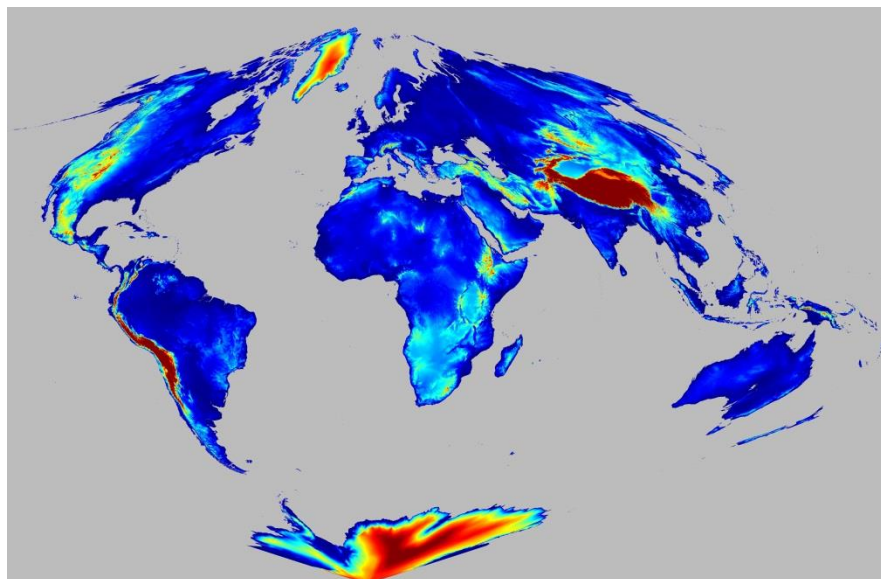


Potential Improvements

- Remove sun angle and hemispheric dependent geolocation biases (Charts 10&11)
- Update 1 km with 500m Digital Elevation Model (DEM) (such as those in MODIS Collection 6) (Charts 19&20)
- Insert 500m resolution Land/Water (L/W) mask (such as those in MODIS Collection 6) (Chart 21)
- Re-format geolocation output (Chart 22)
- Monitor on-orbit operations and response to possible events – another star tracker re-alignment is expected to happen

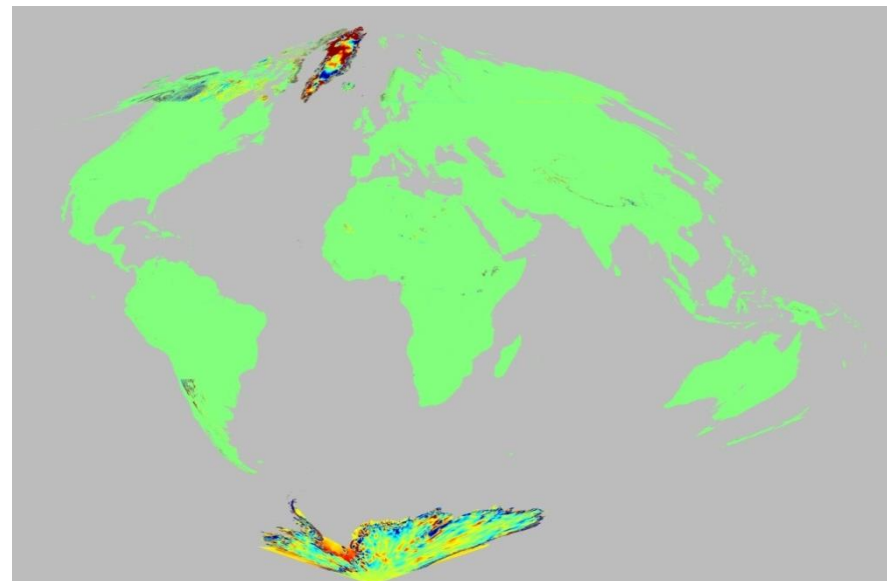
Old and new DEMs Analysis

500 m DEM used in MODIS C6



- MODIS C6 DEM, 1 km and 500 m resolution, from GMTED2010
<http://pubs.usgs.gov/of/2011/1073/pdf/of2011-1073.pdf>, since November 2011, with equal area sinusoidal projection
- MODIS C5 1 km DEM is used in **VIIRS, with polar stereographic projection**

DEM improvement, MODIS (C6-C5) height, 1 km cells



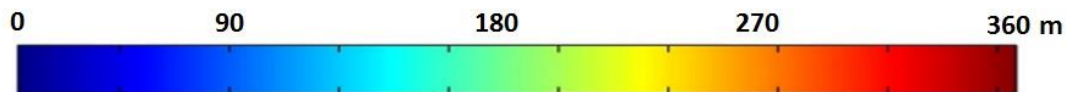
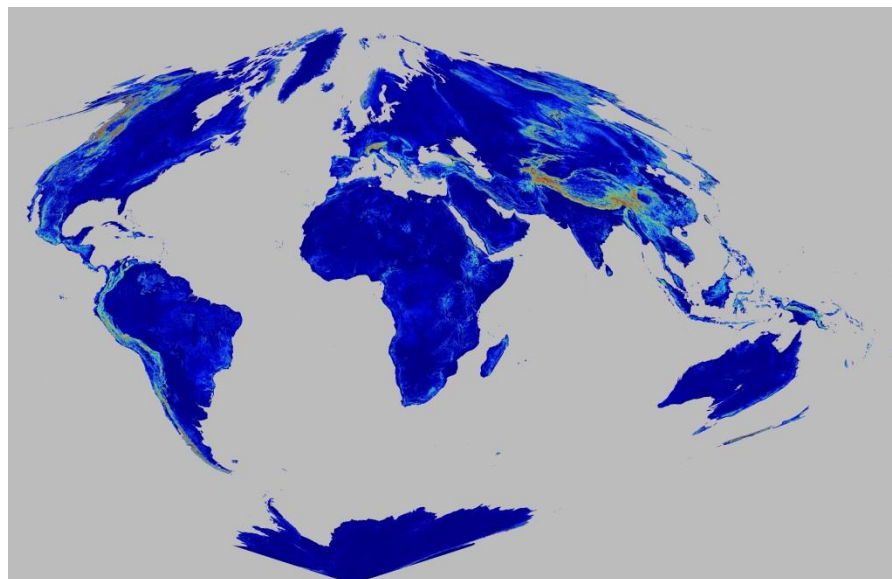
- 33.5% of land area has no change
- **13.7% of land area has a change ranges > 10 m**
- C6 DEM fixes some of the issues with C5 DEM in the non-polar regions
- **C6 DEM fixes extensive issues at the poles**

Within 60 deg latitudes

1. 40% of land area has no change
2. **2 % of land area has change > 10 m**

1 km vs. 500 m DEM

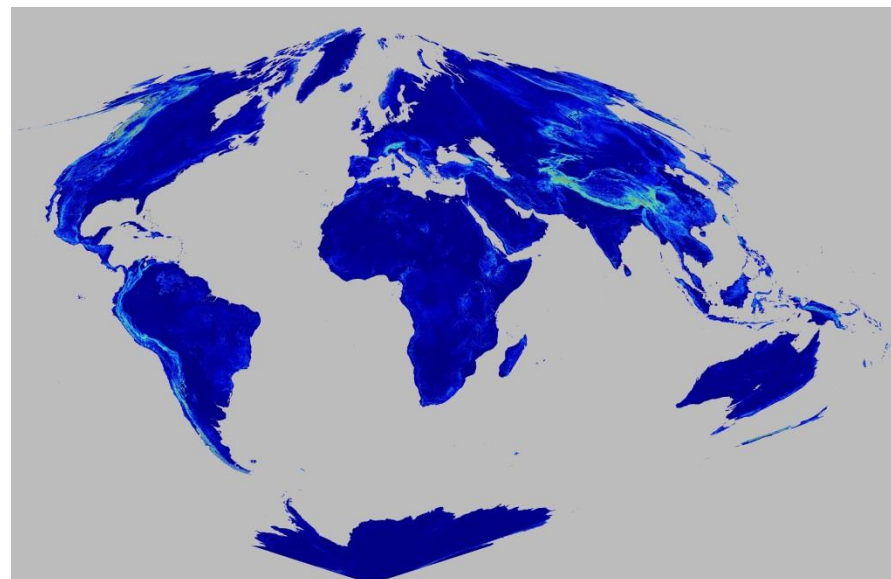
Variants of 500m DEMs within 1km grid



Variations of 500 m DEM within 1km grids

- **18% land area has a variant more than 50 m**
- **5.3% land area has a variant more than 150 m**

Maximum difference between 1km DEM and 500m DEMs within the 1km grid



Differences between 1 km and corresponding 500 m DEM

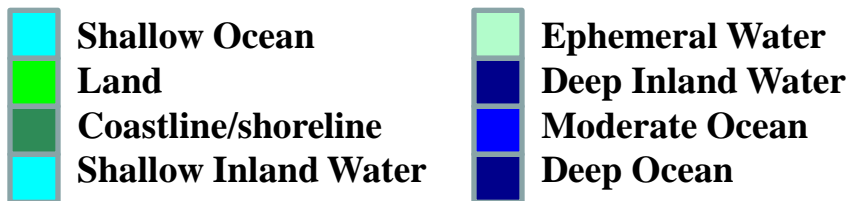
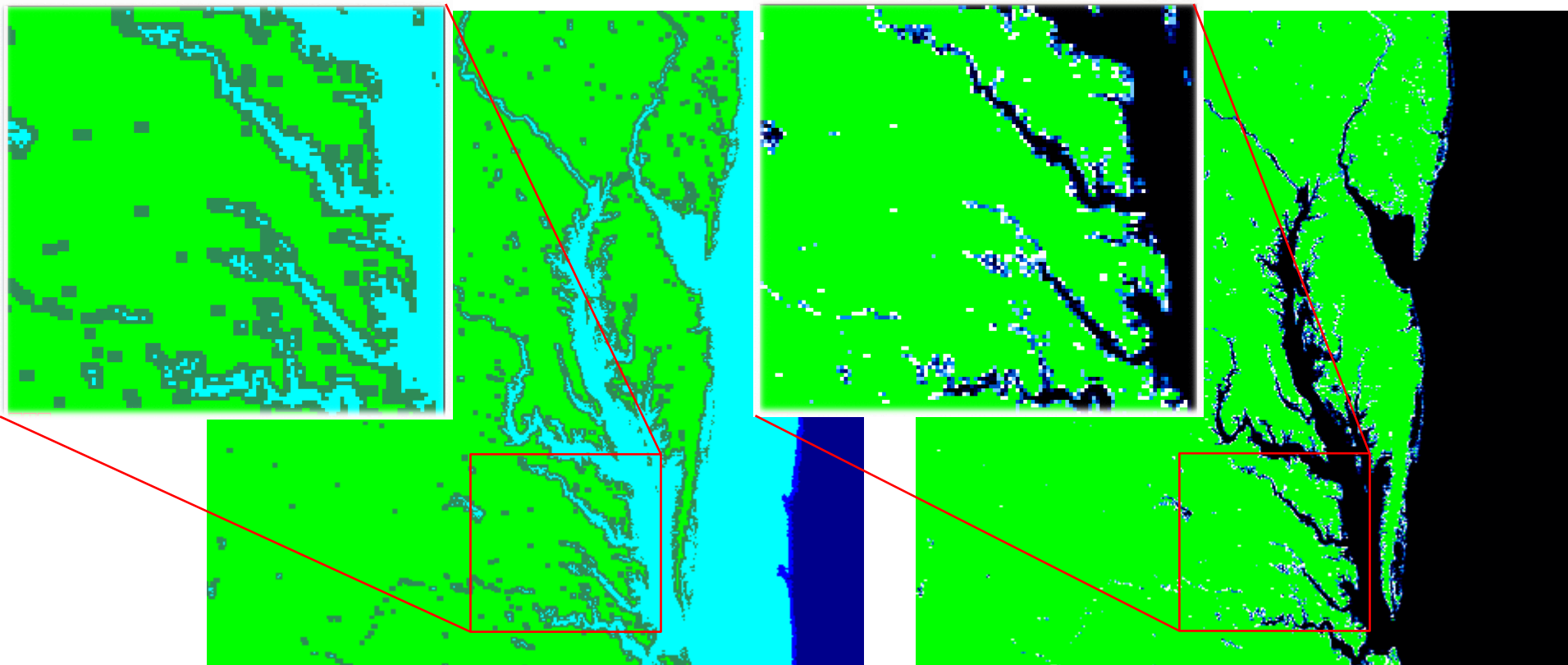
- **12% land area has a a diff of 50 m or more**
- **1.7% land area has a diff of 150 m or more**

New Land Water Mask in C6 MOD03

Spatial Subset from Terra Granule 16:20, Day 2003-193

Land Water Mask

Water Present





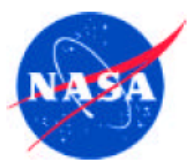
Experiment on DNB output format

- Combined DNB TC Geo and Cal data
- Reformat: ~~FLOAT32~~INT16 (solar/lunar/satellite zen/azi angles, height, sat-ground range) at pixel-level
- A whole day, 287 5-min granule files
- FLOAT32 → 100.97 GB
- INT16 → 36.77 GB
- 63.6% (35% from SciData, 29% from better HDF internal compression) savings in storage
- 63.6% savings in delivery time → 2.7 times faster in delivering the same data content

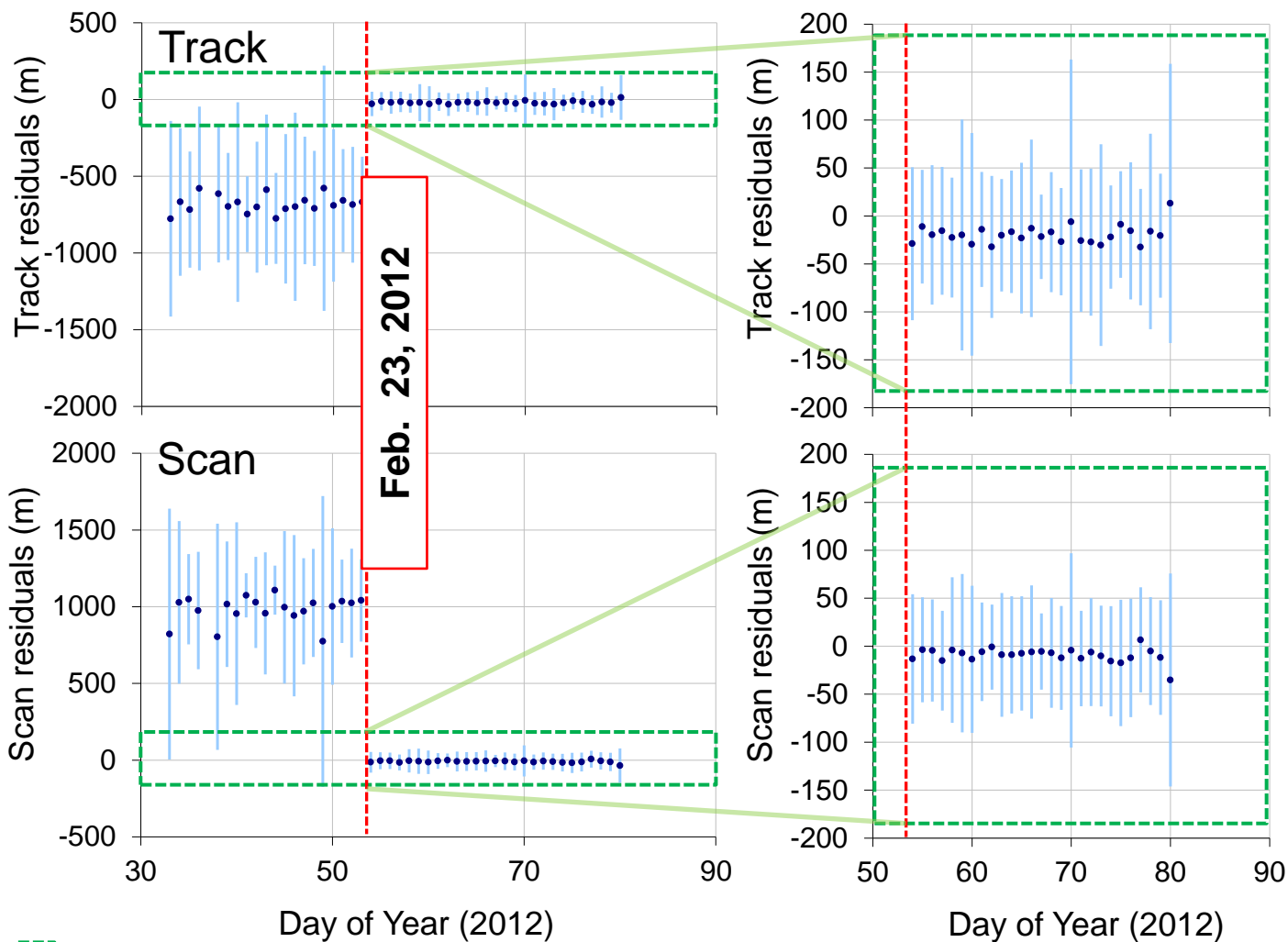


Conclusions

- VIIRS geolocation performance is excellent
- Geolocation mean errors for I-/M-bands are near 0 and uncertainties are ~ 70 m at nadir, much better than the specification (133 m 1σ)
 - Caveat: DNB terrain corrected geolocation product is expected in Mx8.4 on 22 May 2014
- LUTs updating, prompt responding to events and “discoveries”, incorporating experiences from other remote sensing instruments help improve VIIRS geolocation accuracies



Backup Slides



375 m

Nadir equivalent units;

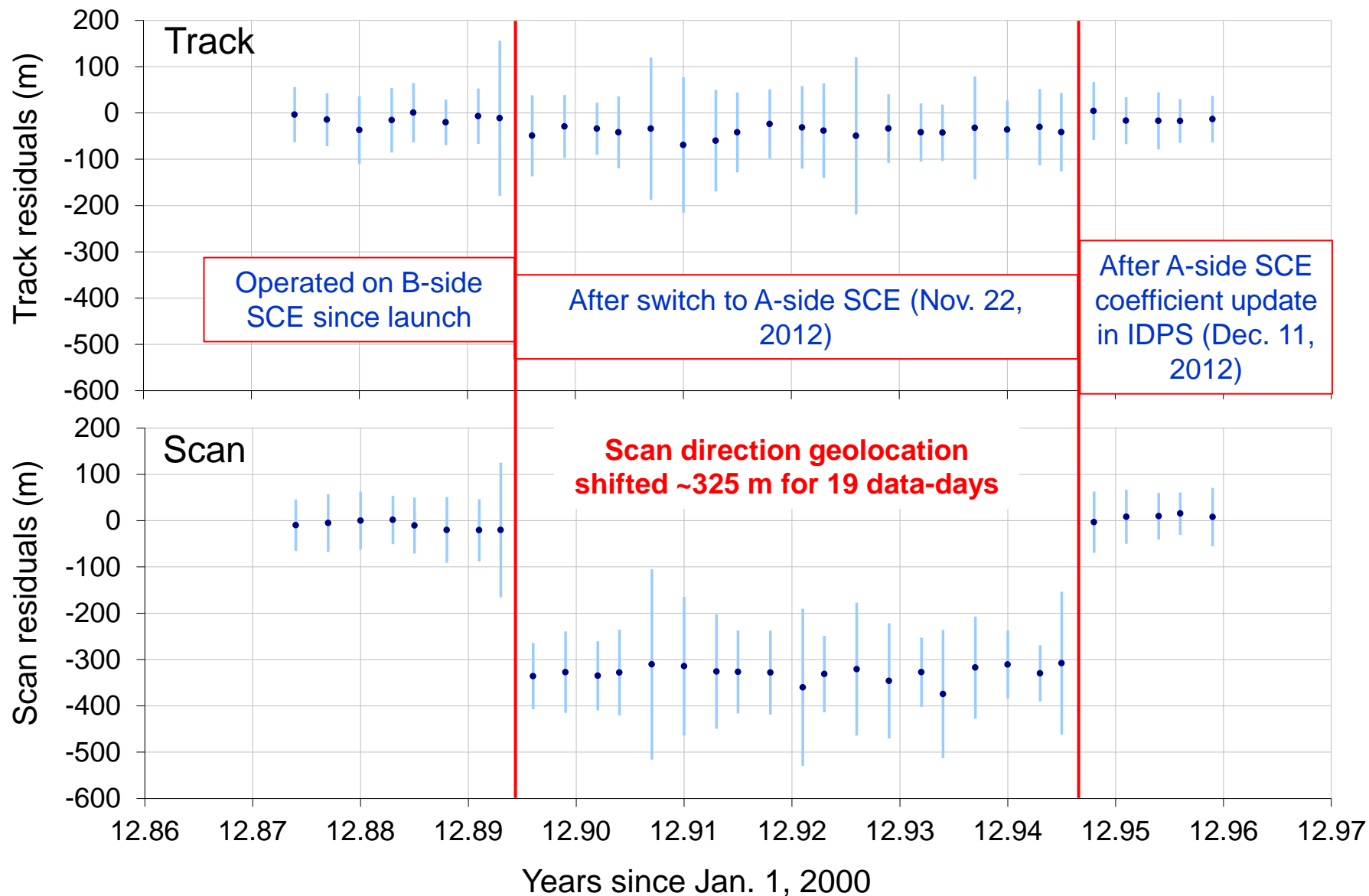
Biases removed: Track -755 m, Scan 1118 m

Error after
LUT update
(2/23/2012, doy 54)

	Bias (m)	RMSE (m)
Track	-21	80
Scan	-8	64

27 days with average of
142 matchups/day
(minus 12 outliers/day)

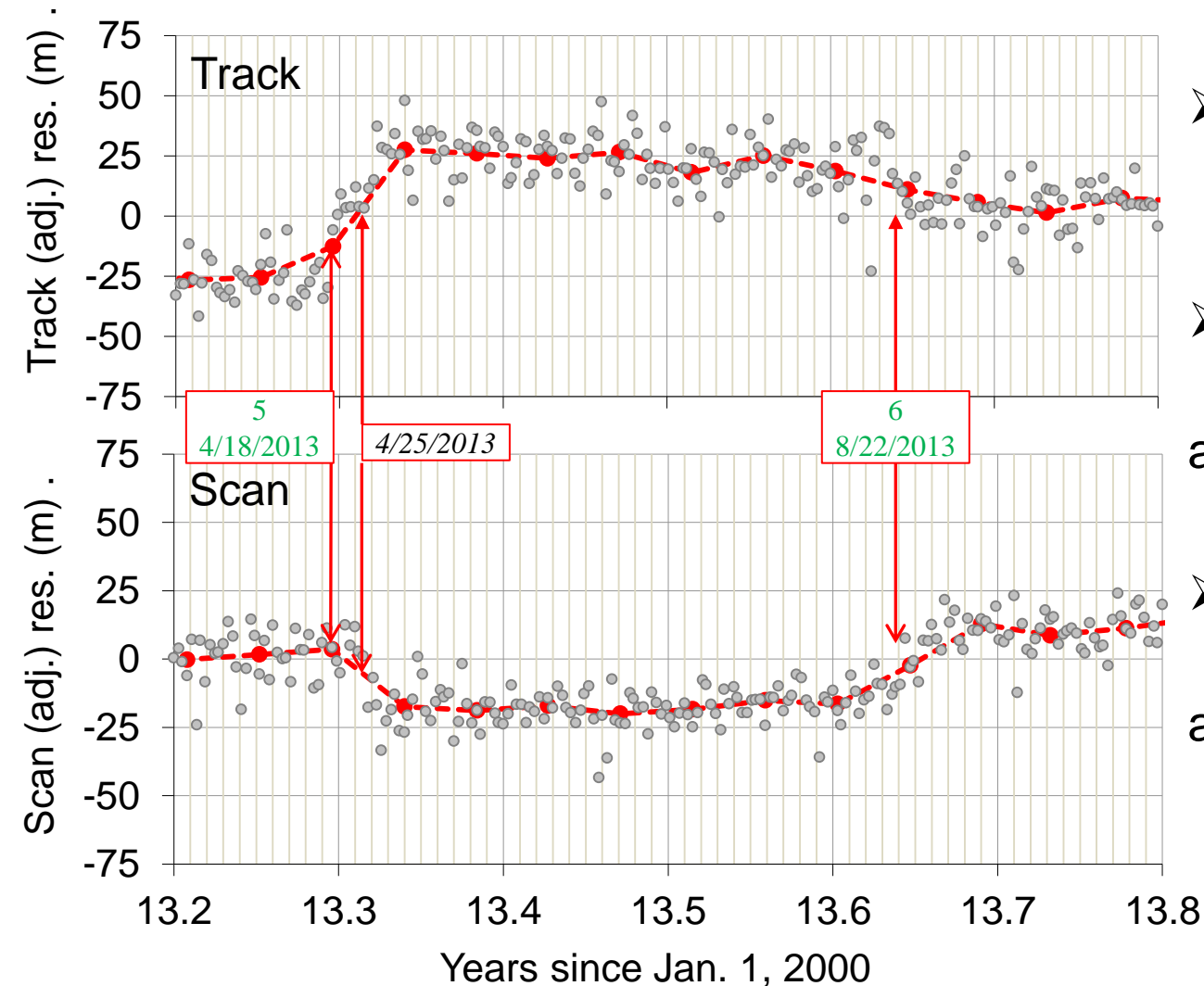
Scan Control Electronics (SCE) Side Switch, Geolocation Error and Correction



(Nadir equivalent units)

Star Tracker Re-alignment and Correction

● Daily -●- 16-day Global



- 4/18/2013:
Geo LUTs fine tuned
- 4/25/2013:
Star tracker re-alignment
- 8/22/2013
Error ~ 25 m found and corrected

Improving RSB Calibration for Ocean Color

Frank De Luccia, Kameron Rausch, David Moyer,
Scott Houchin, Jason Cardema, Evan Haas, Gabriel Moy,
Ye Hong, Tim Wilkinson, William Chen

2014 STAR JPSS Science Teams Annual Meeting
12-16 May 2014

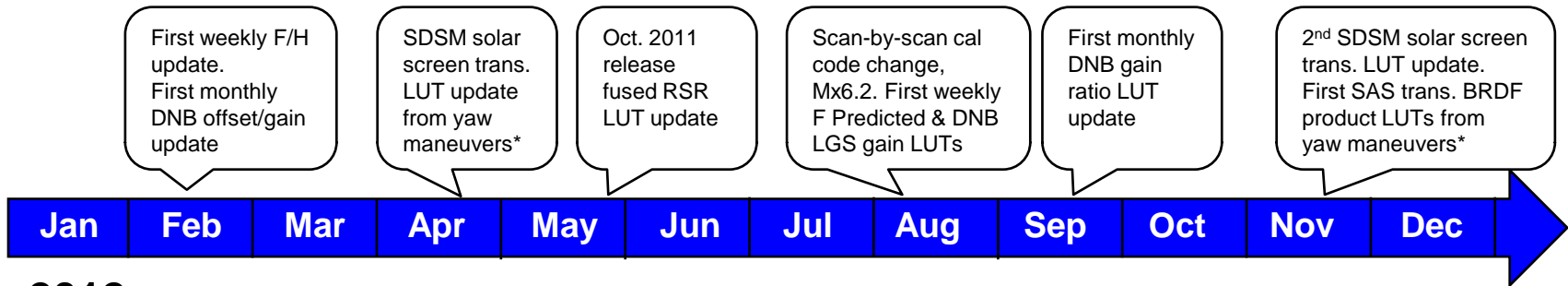
Topics

- SDR calibration operational methodology improvements
 - *Scan-by-scan F correction code change*
 - *Automated RSB calibration (RSBAutoCal) code change*
- SDR RSB radiometric model input parameter improvements
 - *C0 = 0 calibration coefficient LUT update*
 - *Screen transmission and solar diffuser reflectance LUT updates*
 - *Relative spectral response (RSR) LUT updates*
 - *Solar vector correction code change (in work)*
 - *Calibration coefficient LUT temperature dependence correction (in work)*
 - *Screen transmission and solar diffuser reflectance LUT update using mission data to date and solar vector correction (in work)*
- Top-of-atmosphere reflectance trending over MOBY site
- Summary

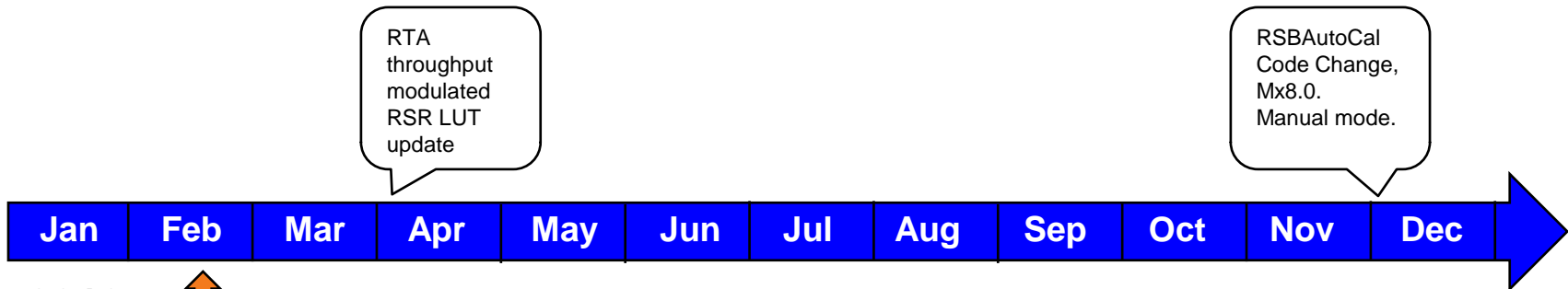
Introduction

- The VIIRS RSB calibration, like the TEB calibration, is physics based and limited principally by the fidelity of the underlying radiometric model and knowledge of the model parameters
- Improvements made thus far since launch, and those in work, increase model parameter accuracy and therefore data product accuracy
 - *Almost every parameter in the radiance and reflectance retrieval equations has been modified by LUT changes during cal/val*
 - *Underlying radiometric model has remained unchanged*
- Significant code changes have also been made to apply the calibration more frequently, thereby improving data product stability as well as accuracy
- These improvements affect all the RSB, including the VisNIR, and therefore benefit Ocean Color performance

RSB Calibration Improvement Timeline

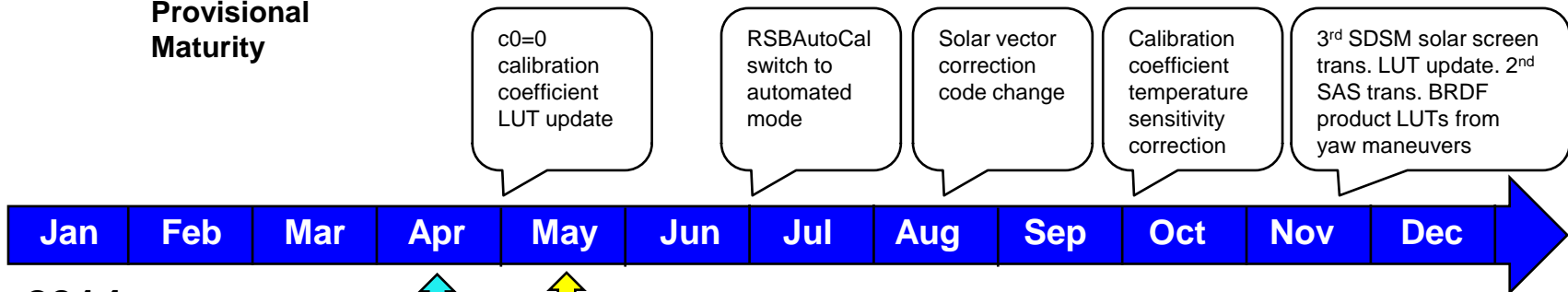


2012



2013

↑
Provisional Maturity



2014

↑ Validated Maturity
↑ Present

* LUT change for offline calibration codes only. No IDPS change.

SDR Calibration Operational Methodology Improvements

Regular Weekly and Monthly LUT Updates Maintain the RSB Calibration and Data Product Quality

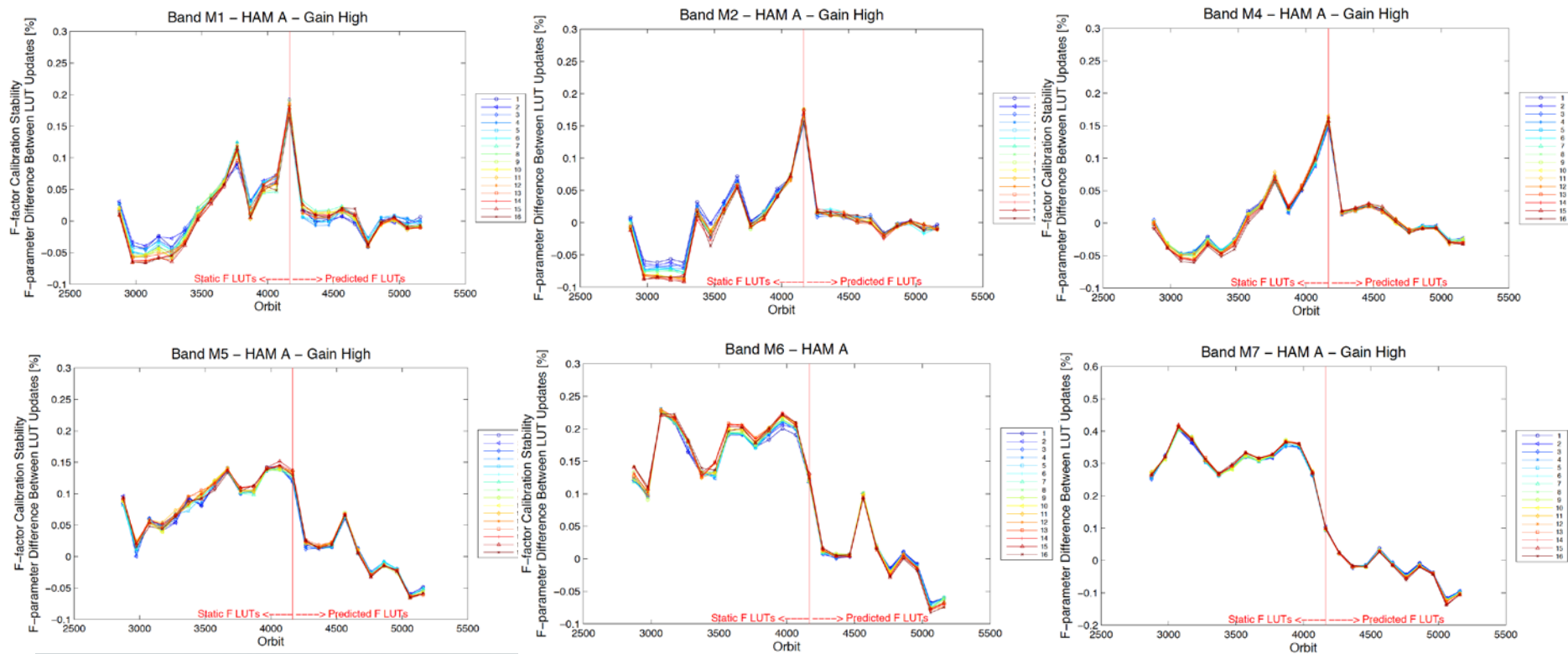
- Until the automated RSB calibration algorithm, RSBAutoCal, is switched to automated mode in IDPS, RSB calibration is being maintained by operational LUT updates.
- Every week two sets of updated LUTs derived from solar calibration are delivered to Data Products & Engineering Services (DPES) for functional testing by Tim Wilkinson, Aerospace
 - *F Predicted and DNB LGS Gain LUTs in Mx8.X for IDPS operations*
 - *F Predicted, DNB LGS Gain, and H LUTs in Mx7.2 for direct broadcast users*
- Every month updated DNB offset and gain ratio LUTs in Mx8.X derived from special data collects during new moon periods are delivered by William Chen, Aerospace
- These regular LUT updates are the backbone of RSB calibration to date, and ensuring their quality through IDPS code changes and changes in other LUTs is both challenging and essential to the quality of the SDR and downstream EDRs

Scan-by-Scan F Factor Correction Code Change

- In 2012 Aerospace developed modified SDR code to:
 - *Ingest F factor reference and trend data from LUTs for non-DNB bands*
 - *Ingest DNB LGS gains and trend data from LUTs for the DNB*
 - *Calculate F factors and DNB LGS gains “on the fly” on a scan-by-scan basis*
- Use of trend information and scan-by-scan updates was intended to improve improve the fidelity and continuity of the RSB calibration within the limits of the weekly manual LUT update process
- The scan-by-scan F correction code change, implemented in IDPS Mx6.2 on August 9, 2012, was successful in meeting its objectives
- The scan-by-scan F factor and DNB LGS gain correction continues to operate in the Mx8.X versions of the code that implement the automated RSB calibration algorithm (RSBAutoCal), whether in manual or automated mode

Scan-by-scan F Factor Correction Impacts on Data Product Radiometric Stability

- Metric plotted is F factor difference between updated LUT and the LUT it replaces at a common reference time
 - *Measures discontinuity in F factor when a LUT is replaced*



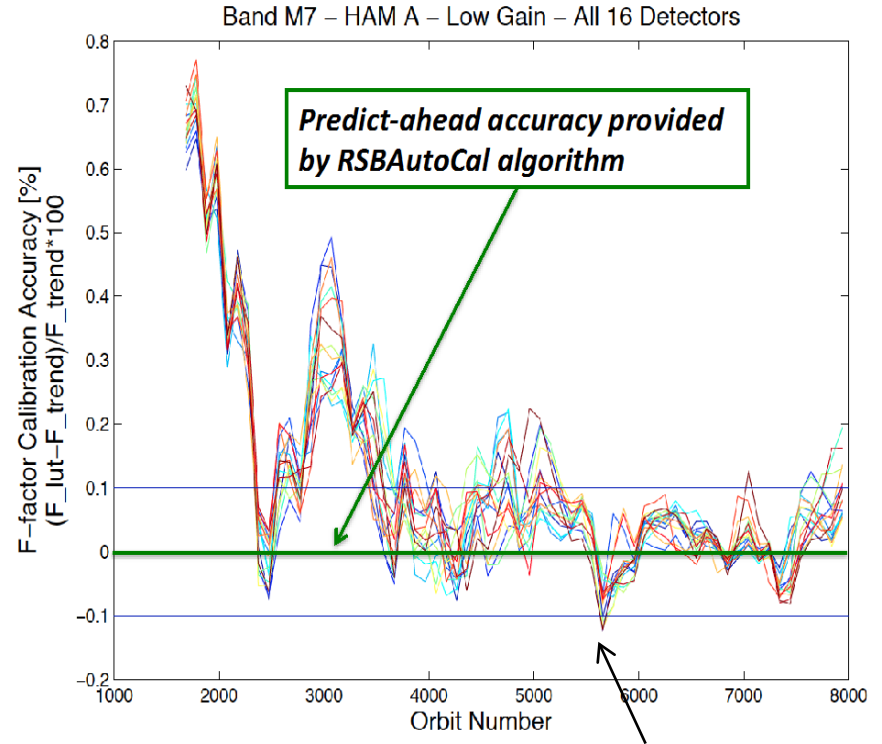
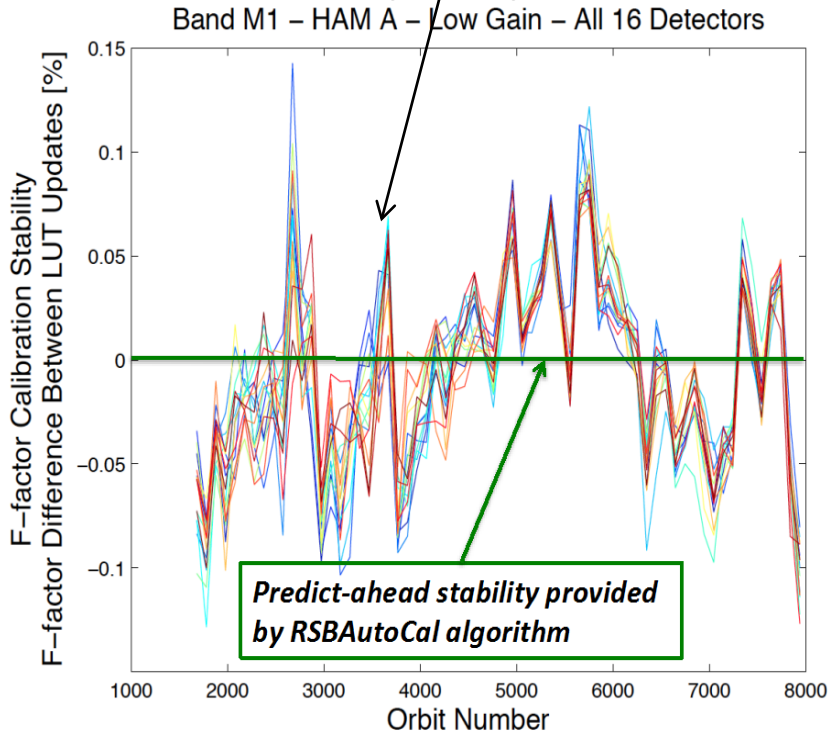
Continuity after code change was generally +/- 0.1%, even for bands affected by RTA throughput degradation

Automated RSB Calibration Code Change - RSBAutoCal

- In 2012/2013 Aerospace developed SDR code to fully automate RSB calibration
- F factors and DNB LGS gains and their time derivatives are calculated immediately after data acquisition from the SD each orbit and applied in the next orbit
 - *Eliminates discontinuities associated with weekly LUT updates*
 - *Eliminates predict-ahead accuracy error, difference between current best estimate F factors and LUT F factors and trends calculated based on calibration data 100-200 orbits old*
- Application of Robust Holt Winters filtering allows RSBAutoCal to maintain calibration during data outages and re-acquire new trends afterward, should they occur, without manual intervention
- RSBAutoCal inserted into IDPS operations with Mx8.0 in 11/2013
 - *Input LUTs recently adjusted to provide desired smoothing and outlier rejection*
 - *Under evaluation for transition from manual to automated mode*

RSBAutoCal Eliminates Calibration Discontinuities and Predict-Ahead Accuracy Errors

Discontinuities in F at instant of LUT replacement in operations each week are removed with RSBAutoCal algorithm (green line)



Time varying instantaneous difference between extrapolated F applied in operations and offline F without extrapolation is removed with RSBAutoCal algorithm (green line)

SDR RSB Radiometric Model Input Parameter Improvements

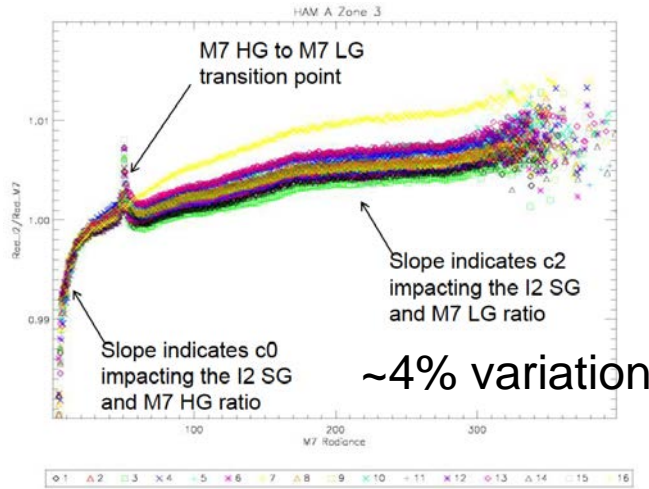
Calibration Coefficients Modified to $c_0 = 0$ and Refit c_2 version

- Aerospace analysis of pre-launch TVAC data applied $c_0 = 0$ constraint and demonstrated improved radiometric response characterization uncertainty and predicted calibrated response uniformity
 - *No theoretical basis for c_0 coefficient – disappears in radiance path differencing*
 - *Nonzero c_0 justified in TEB to absorb errors in self-emission parameters and radiometric model, essentially providing an on-orbit tuning parameter*
 - *C_0 values derived from TVAC test data analysis shown to be statistically indistinguishable from zero for many, but not all, RSB bands*
 - Any earth sector-calibration sector offsets significant enough to disturb calibration, if they exist at present, would require separate compensation
- $C_0 = 0$ coefficients shown to significantly reduce I2/M7 and I3/M10 differences on orbit
- $C_0 = 0$ cal coefficient IDPS LUT update implemented in May 2014
- NASA OCC team already performs calibration with both $c_0 = 0$ & $c_2 = 0$

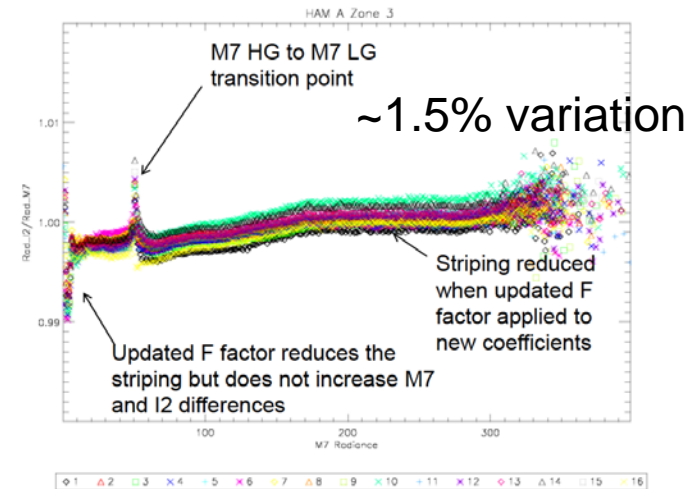
Modified $c_0 = 0$ Calibration Coefficients with Refit c_2 Improve Agreement Between Bands Under Same Filter

I2/M7
Ratio

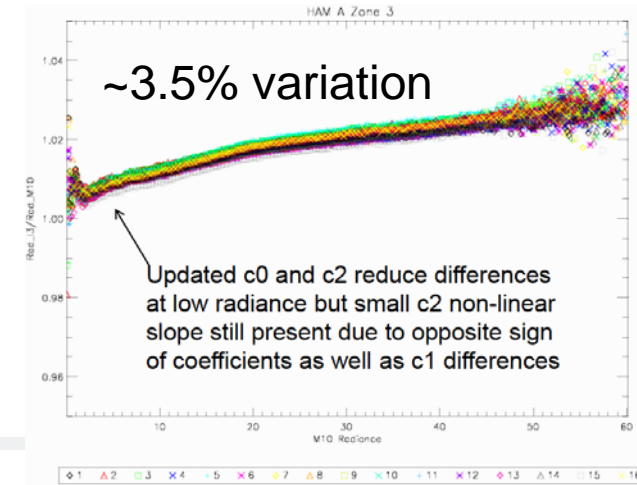
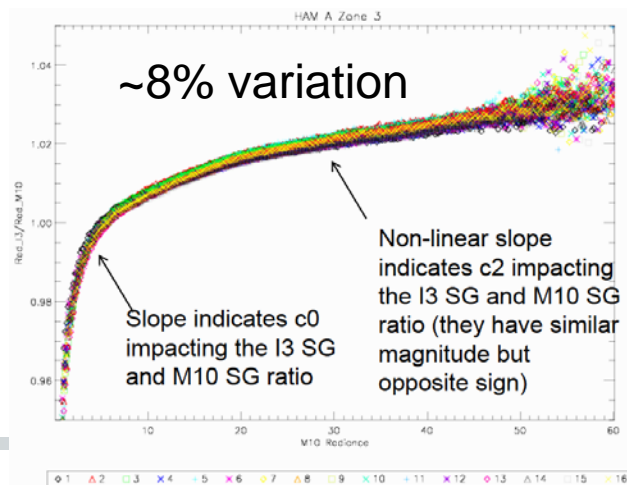
Baseline



$c_0 = 0$ & refit c_2



I3/M10
Ratio



Improved Screen Transmission and Solar Diffuser (SD) Bidirectional Reflectance Distribution Function (BRDF) LUTs

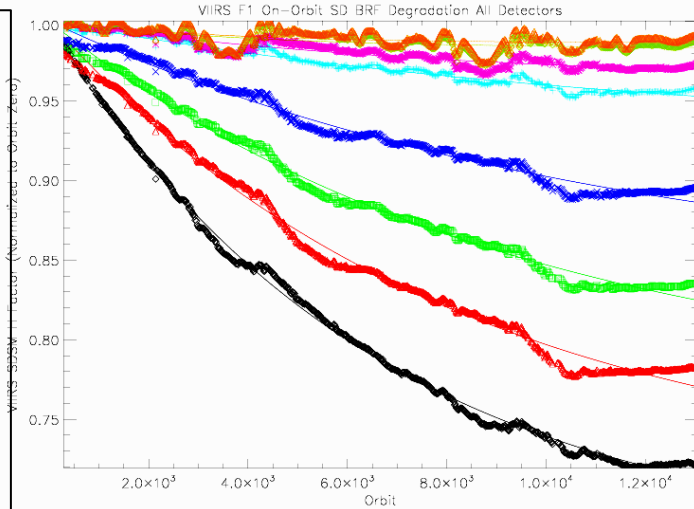
- SDSM solar screen transmission LUT derived by NASA VCST from yaw maneuver data incorporated in offline codes for operational IDPS F and H factor LUT calculation in April 2012
- New Solar Attenuation Screen (SAS) SD BRDF product LUTs, RTA view and SDSM view, derived by VCST from yaw maneuver data incorporated in offline F/H processing in November 2012, along with refined version of SDSM solar screen transmission LUT derived by Aerospace
 - *November 2012 version of LUTs went into IDPS operations with RSBAutoCal (manual mode) in Mx8.0 in November 2013*
- Improved SDSM screen transmission LUT decreased modulations and transmission errors in the H factor, resulting in improved calibration accuracy and stability
 - *Reduced H modulations reduce week-to-week differences in predicted F vs reference F in LUT updates*

Improved Screen Transmission and Solar Diffuser (SD) Bidirectional Reflectance Distribution Function (BRDF) LUTs (cont.)

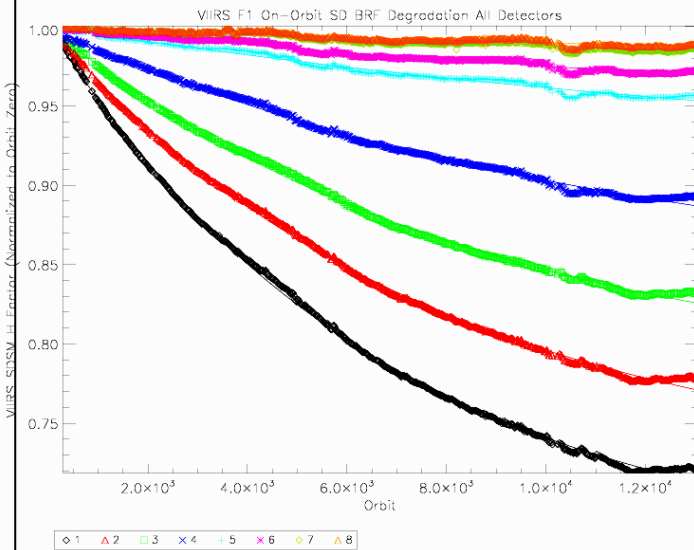
- Solar Attenuation Screen (SAS) SD BRDF product LUTs, RTA view and SDSM view, reduces spurious trend changes in calibration as solar azimuth varies over the year
- Update of all three operational LUTs in work and recommended for insertion in IDPS at time of solar vector correction code change in August 2014 or shortly thereafter

Improvement in H factor Behavior Due to Refined SDSM Solar Screen Transmission LUT

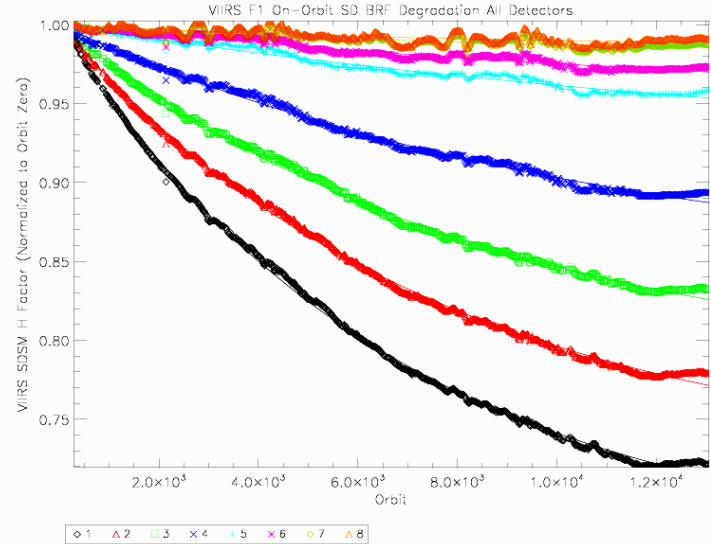
Pre-launch SDSM Solar Screen Transmission LUT



November 2012 SDSM Solar Screen Transmission LUT



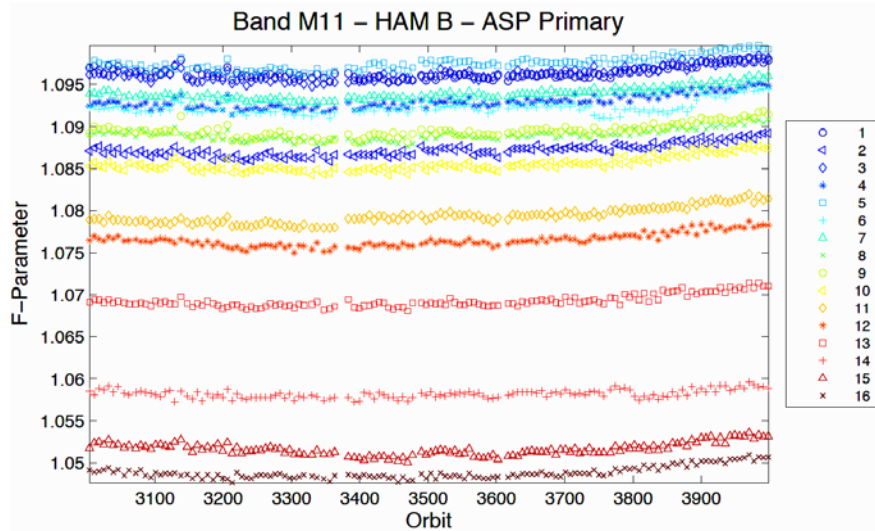
April 2012 SDSM Solar Screen Transmission LUT



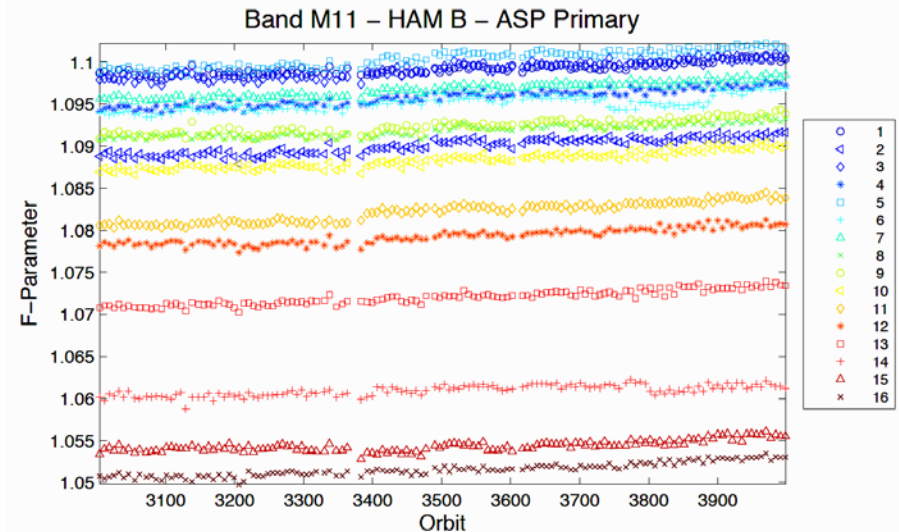
H factors using pre-launch SDSM screen transmission LUT contained errors causing “ripples” and biases in the H factor values (upper left).
 H factors after the NASA VCST LUT update using yaw data removes transmission biases and a majority of the “ripples” (upper right).
 The 2nd LUT update used the NASA VCST LUT and the first 9 months of H factor data to remove the remaining “ripples” in the H factors (lower left).

Reduction in Spurious F Trend Change due to Nov 2012 SAS Transmission SD BRDF Product LUTs (from NASA VCST yaw data analysis)

At-launch LUTs



November 2012 LUTs



- M11 chosen as example as it has no significant modulations to obscure impact of this LUT change. All bands similarly affected
- Concave upward behavior in F trend centered on orbit where solar azimuth reverses (around 3600) largely removed
- Slight linear upward trend remains

RSB Relative Spectral Response (RSR) LUT Updates

- Chris Moeller of the University of Wisconsin led data analysis efforts leading to both RSR LUT updates
- May 2012 update
 - *Replaced at-launch RSRs for bands M1-M7 with NG-generated October 2011 fused RSR incorporating government team best-estimate spacecraft-level RSRs*
 - *Water vapor correction applied to M9*
 - *Improved data filtering for all RSB*
 - *<0.1% quantitative impact on SDR radiances*
- April 2013 update – Modulated RSR
 - *RSRs updated to take into account RTA throughput degradation as of 1 February 2013*
 - *<0.2% quantitative impact on SDR radiances*
- Need for future RSR update will be evaluated based on progress of RTA throughput degradation

Planned and Proposed Improvements not yet Implemented

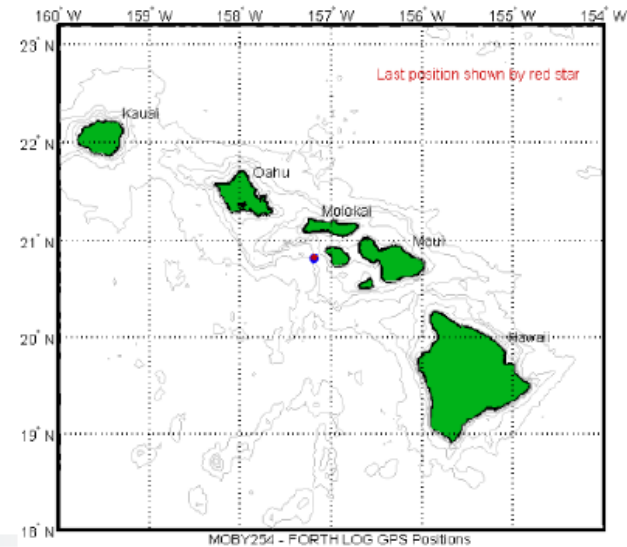
- Correction of solar vector error discovered by NASA GEO team
 - *Impacts F factors at 0.1% level according to VCST preliminary analysis*
- Correction of calibration coefficient temperature dependency errors/omissions in current Delta C LUT
 - *Impact on M6 is annually cyclic at nearly 0.1%*
- 3rd update of SDSM solar screen transmission LUT and 2nd update of SAS transmission SD BRDF product LUTs, RTA and SDSM views, based on 2.5+ years of mission data supplementing the yaw maneuver data
 - *Impacts in shorter wavelength bands approach 0.2%*

Impacts of all these improvements large enough to benefit OCC

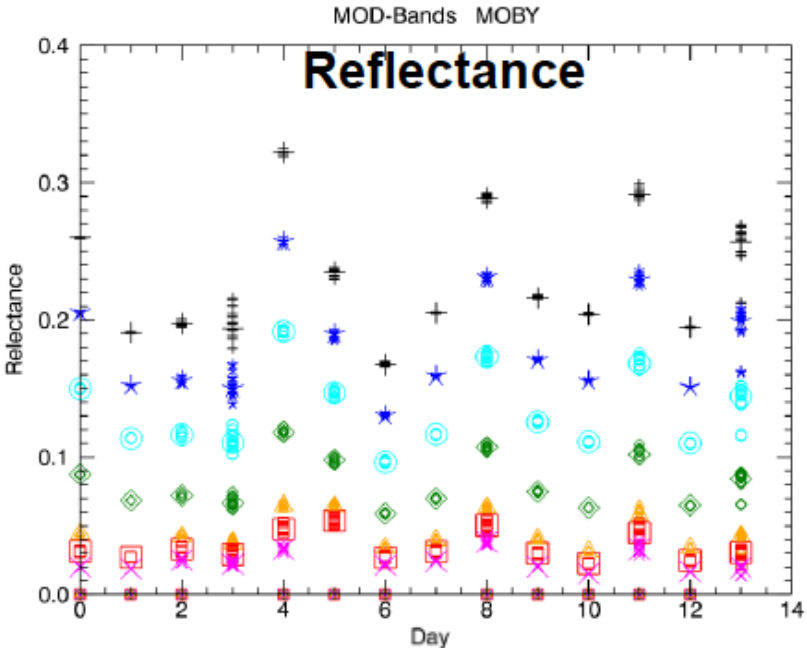
Trending SDR Reflectance Over MOBY Site

Data

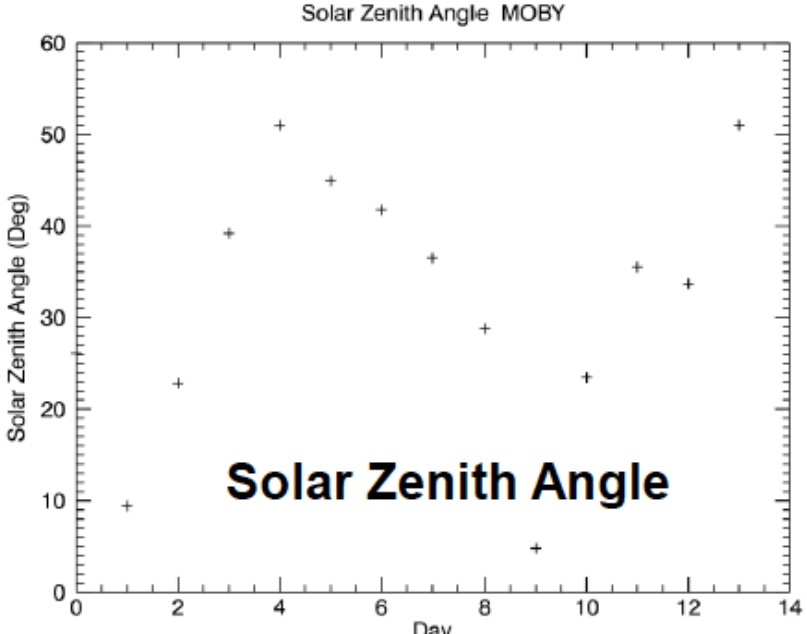
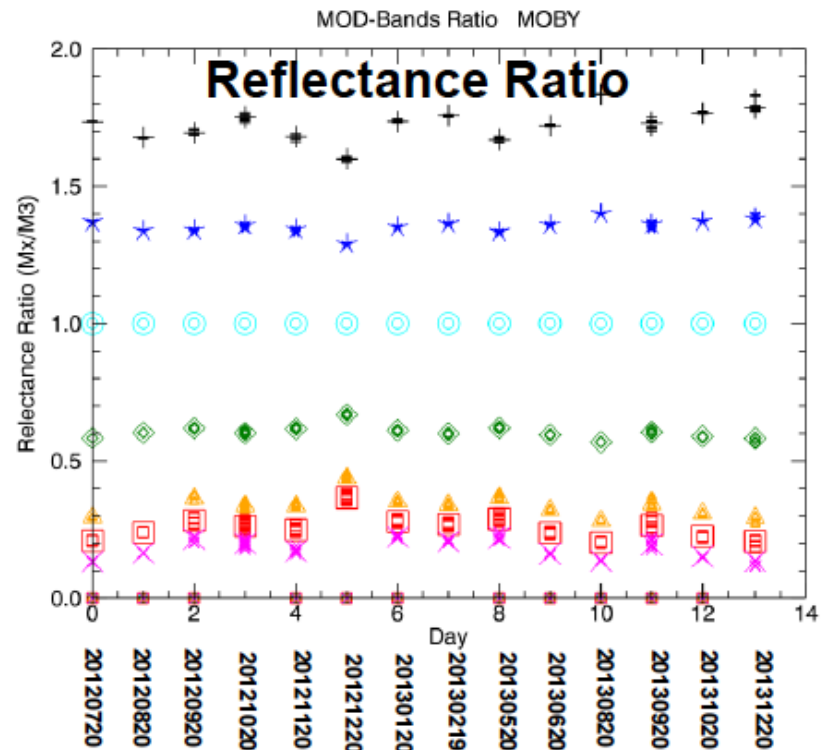
- VIIRS SDR over the MOBY site (see Figure below) were collected once a month from Feb 2012 to Dec 2013 (i.e. 23 Granules)
- Corresponding Cloud Mask (CM) IP data (available starting in May 2012) were also collected so that only *clear ocean* SDR data (and *no glint*) will be used for analyzing VIIRS reflectance stability
- 14 out of 23 granules passed the CM test
- Time series of reflectance for the 14 granules are displayed on the next slide



No Obvious TOA Reflectance Trend Change Over MOBY, 7/12–12/13



+ M01
 * M02
 M03
 M04
 M05
 M06
 x M07



- There are total 17 points for each day and each band (16 detectors (smaller symbols) plus the averaged one (larger symbol)).
- Screen criteria:
 - 1) Confidently clear
 - 2) No sun glint
 - 3) Sea water
 - 4) SZA < 75 deg
 - 5) Distance to MOBY site < 10 km



Summary

- Almost every parameter in the radiance and reflectance retrieval equations has been, or will be, improved in accuracy since launch
 - *An exception is Response vs Scan (RVS), which warrants further study*
- In our physics based RSB calibration these parameter accuracy improvements and the resulting SDR data product improvements necessarily benefit OCC and all other EDRs derived from the RSB
- The Scan-by-Scan F Correction and RSBAutoCal code changes apply the solar calibration immediately and smoothly after calibration data acquisition, taking into account trend information
 - *Result is significantly improved radiometric stability and accuracy relative to the soon-to-be-obsolete manual LUT update process*
- Preliminary radiometric stability studies over the Moby site show no obvious trend changes in reflectance for correlation with trend changes reported by the OCC team



Ocean Color EDR Feedback

Impacts of Recent VIIRS F-table Trends on Ocean Color Products

Menghua Wang

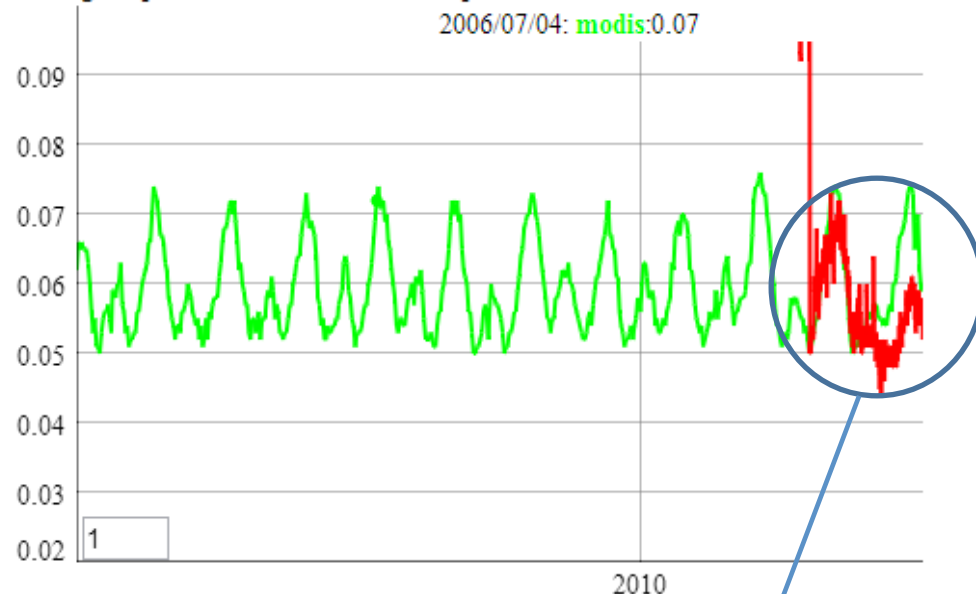
VIIRS Ocean Color Team

13 May 2014

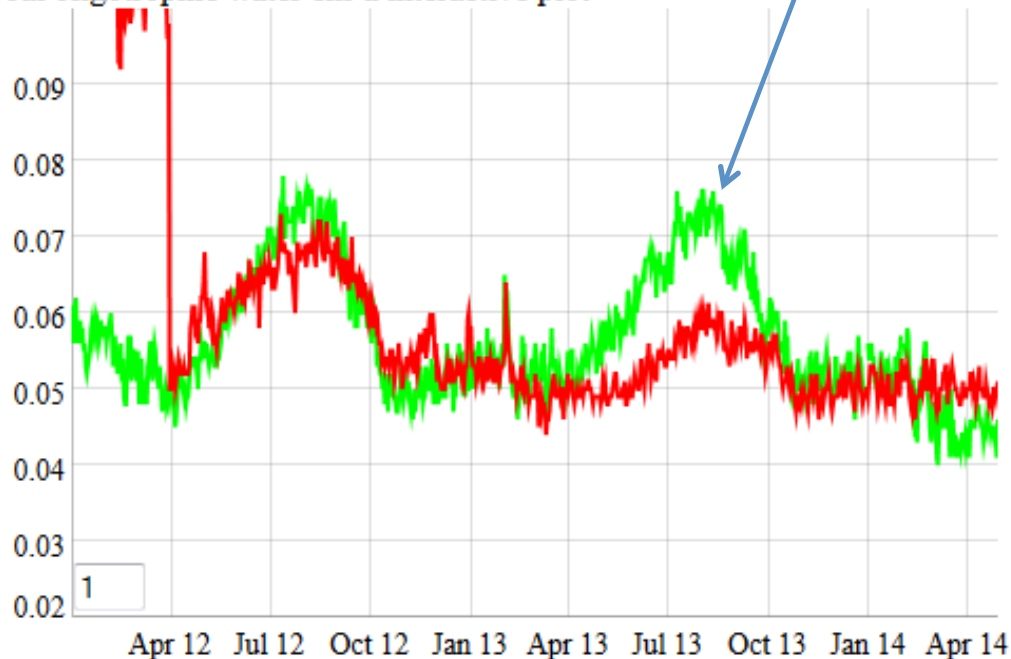


The Existing VIIRS Calibration Issue

Global oligotrophic water chl-a interactive plot



Global oligotrophic water chl-a interactive plot



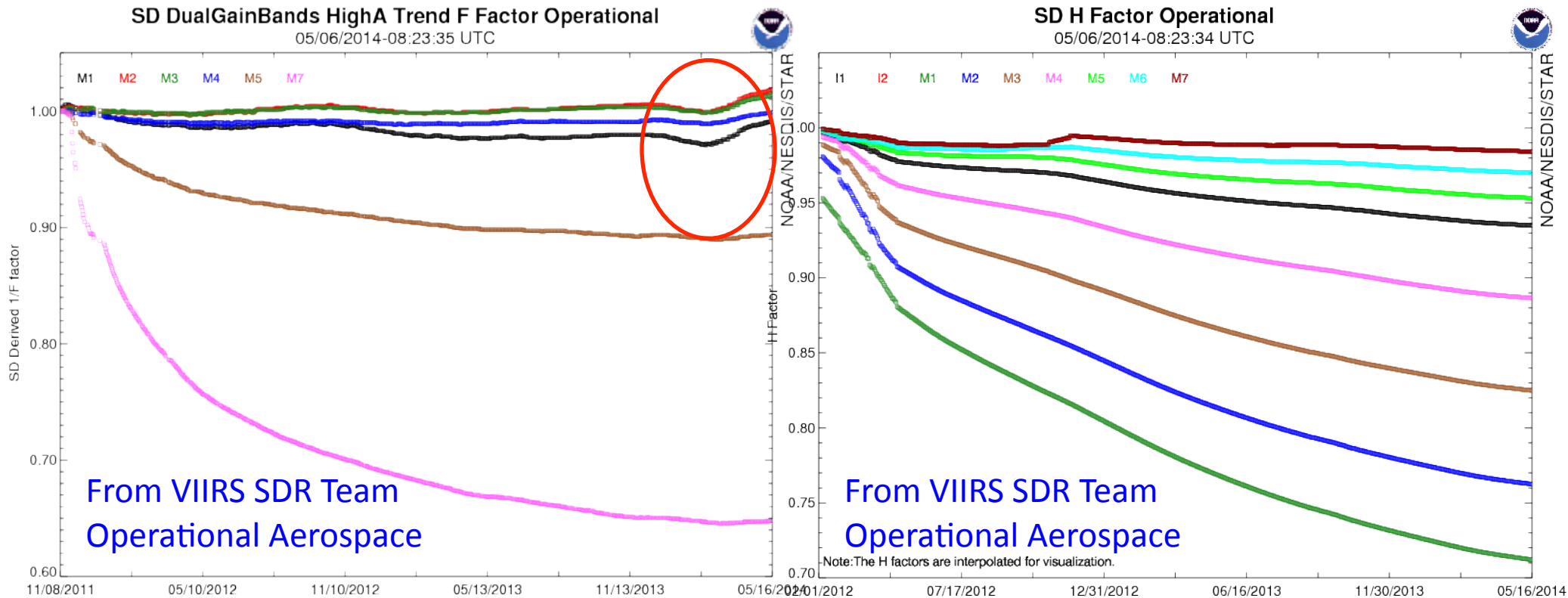
MODIS-Aqua global oligotrophic water Chl-a from 2002 to 2013 (green), overplotted with VIIRS data from 2012 to 2013 (red)

— MODIS-Aqua

— VIIRS (NOAA-MSL12)

- VIIRS and MODIS-Aqua match each other quite well in 2012.
- They have noticeable difference in 2013 (biased low from VIIRS).
- Since MODIS-Aqua has a reasonable Chl-a annual repeatability, It is confirmed that VIIRS SDR has calibration issues, in particular, for the M4 (551 nm) band (**biased low**), at least for 2013.

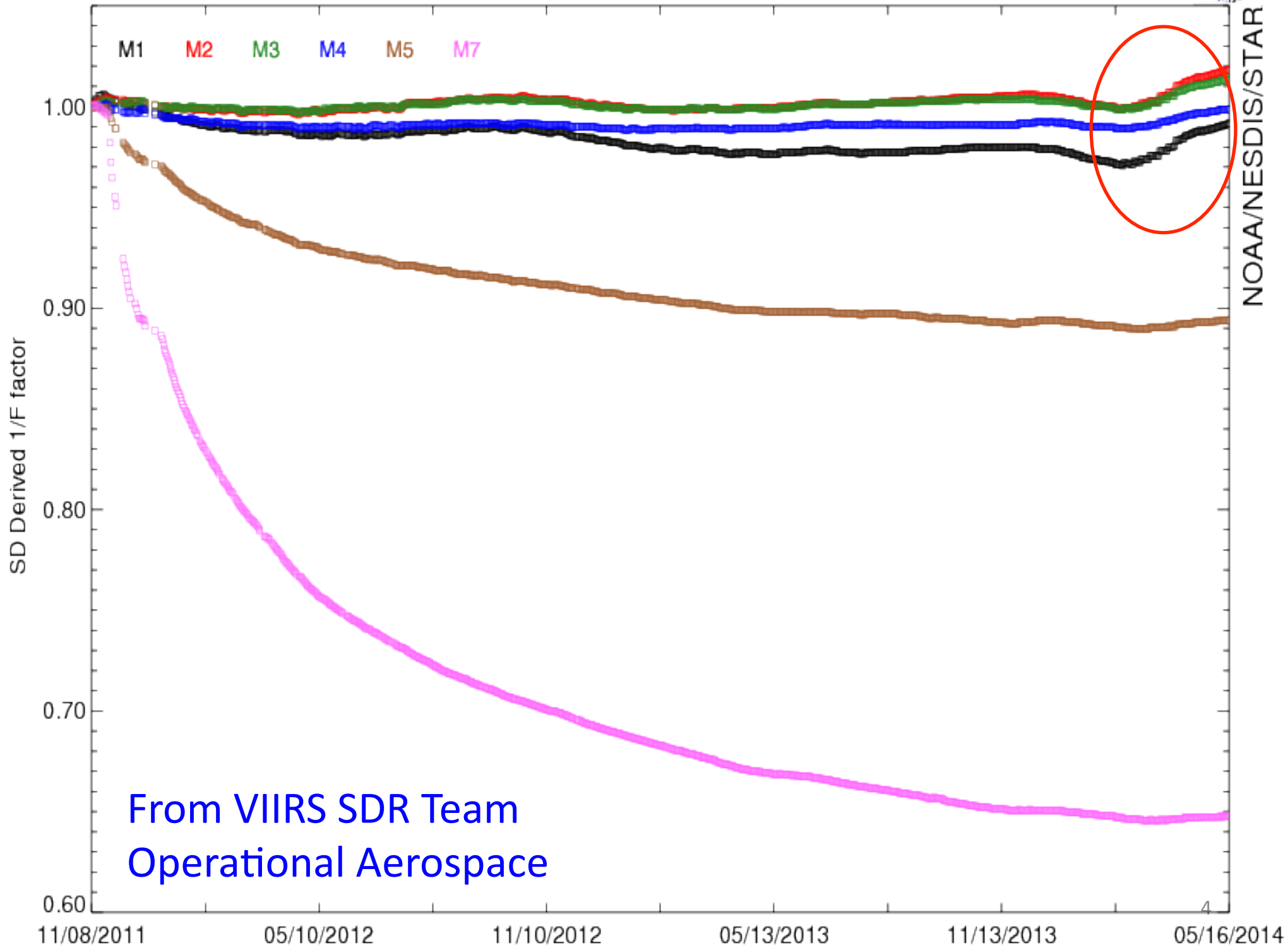
Recent Operational RSB H&F Factors Trends



- Recent F-factors (1/F) show significant trend change which suggests that degradation has stopped or even reversed.
- F-lookup tables for M1-M4 show significant increase of ~1-2% since early February. F factors for M1 and M2 increased ~2% in 3 months.
- Thus, calibration gains are decreased by ~2% for M1 and M2.

SD DualGainBands HighA Trend F Factor Operational

05/06/2014-08:23:35 UTC



NOAA/NESDIS/STAR

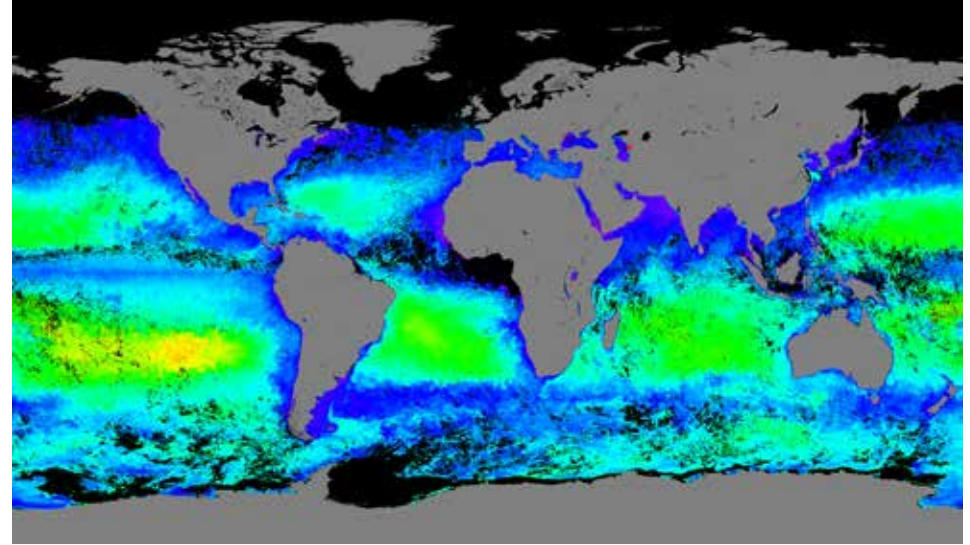
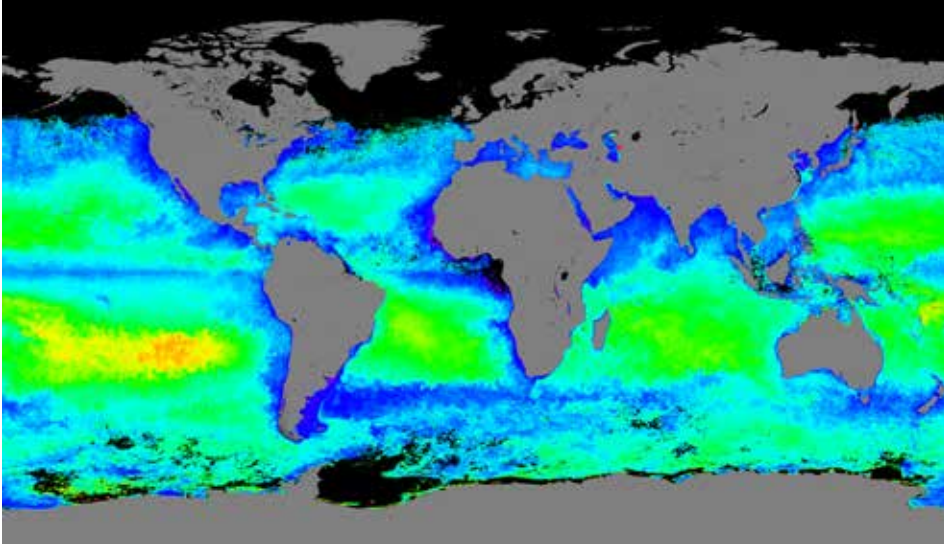
From VIIRS SDR Team
Operational Aerospace

Global OC nLw since February 2014

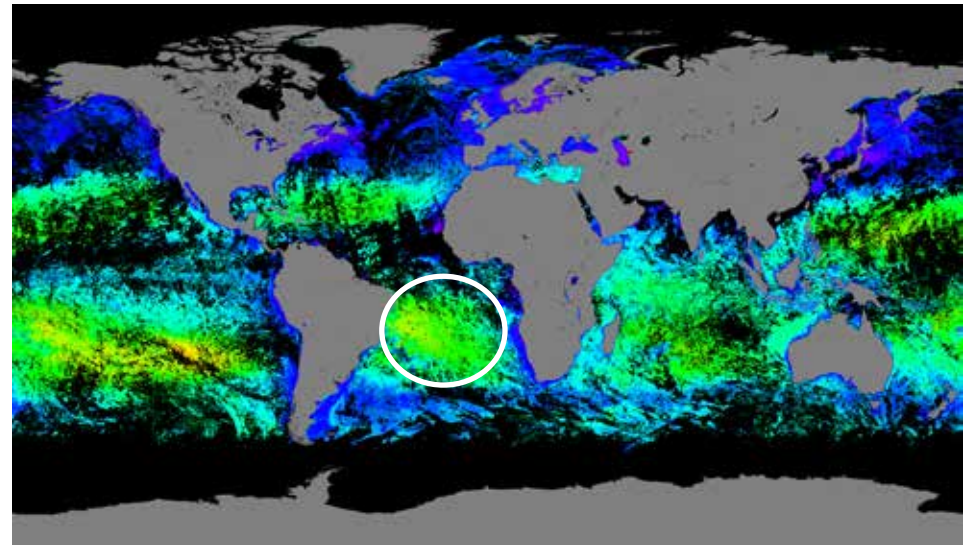
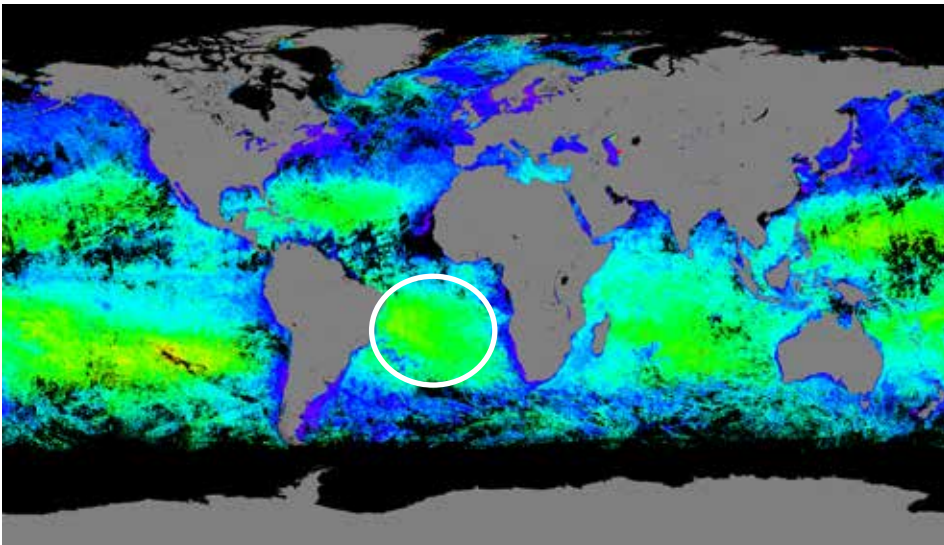
VIIRS nLw(410)

MODIS nLw(412)

January 2014



3rd Week of April 2014



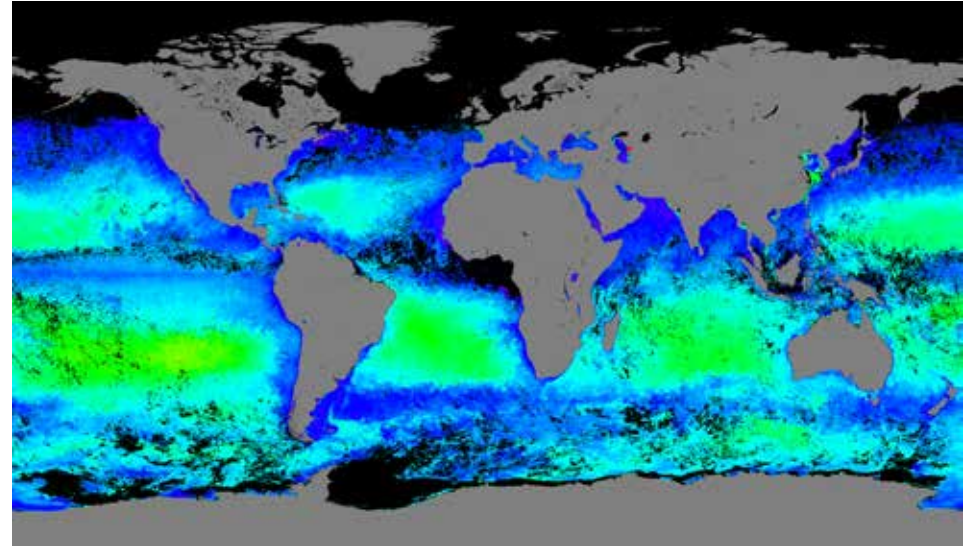
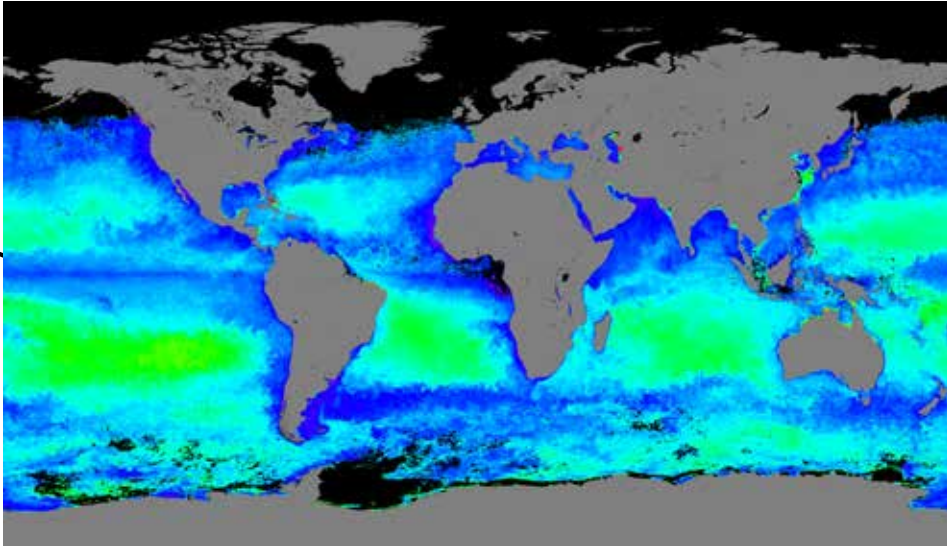
VIIRS data were generated using **NOAA-MSL12**

Global OC nLw since February 2014

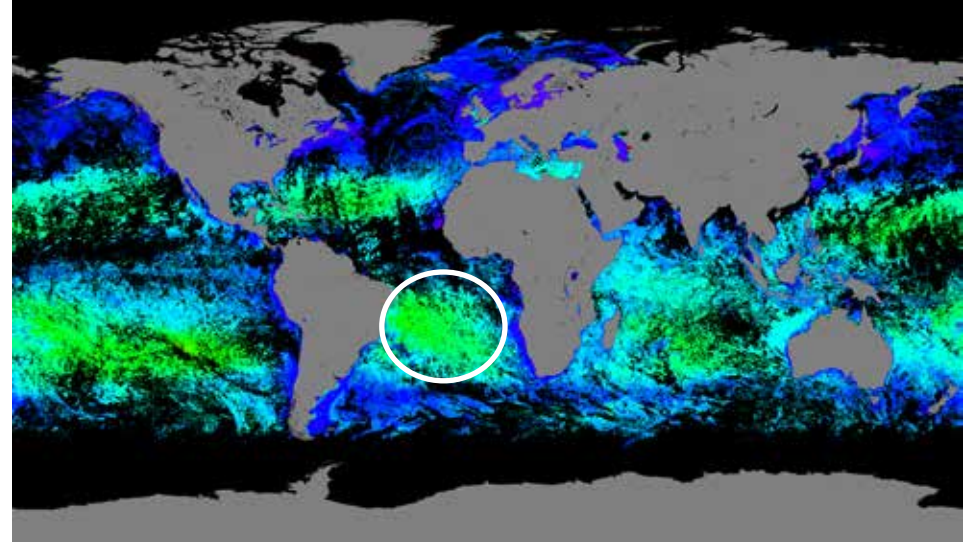
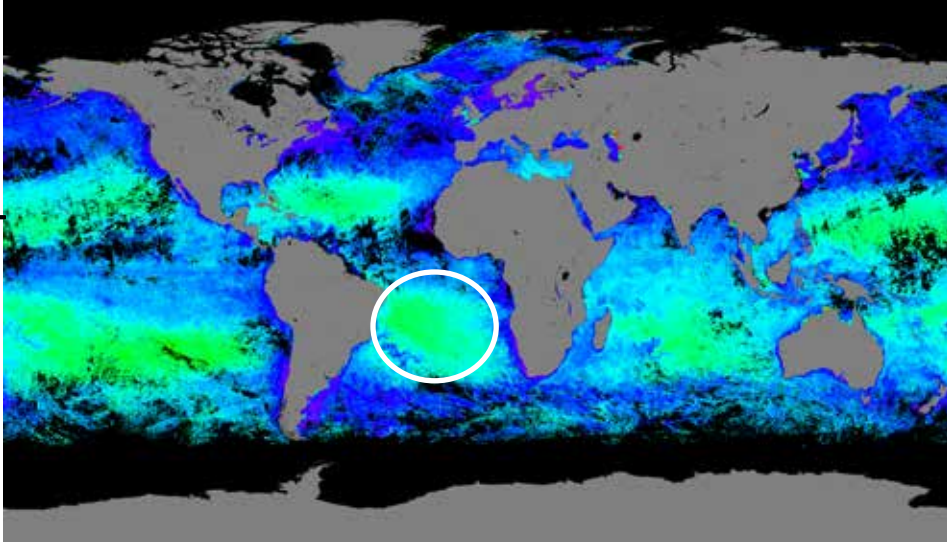
VIIRS nLw(443)

MODIS nLw(443)

January 2014



3rd Week of April 2014



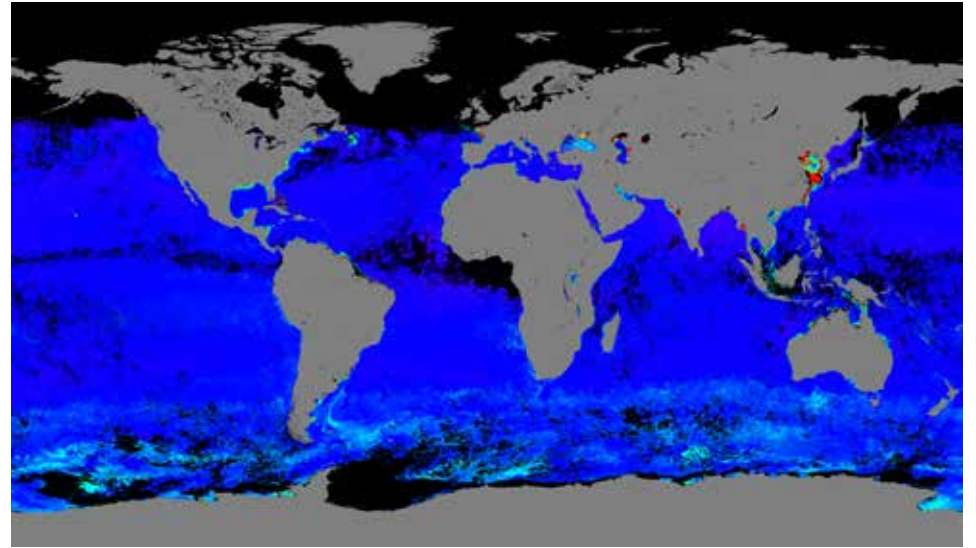
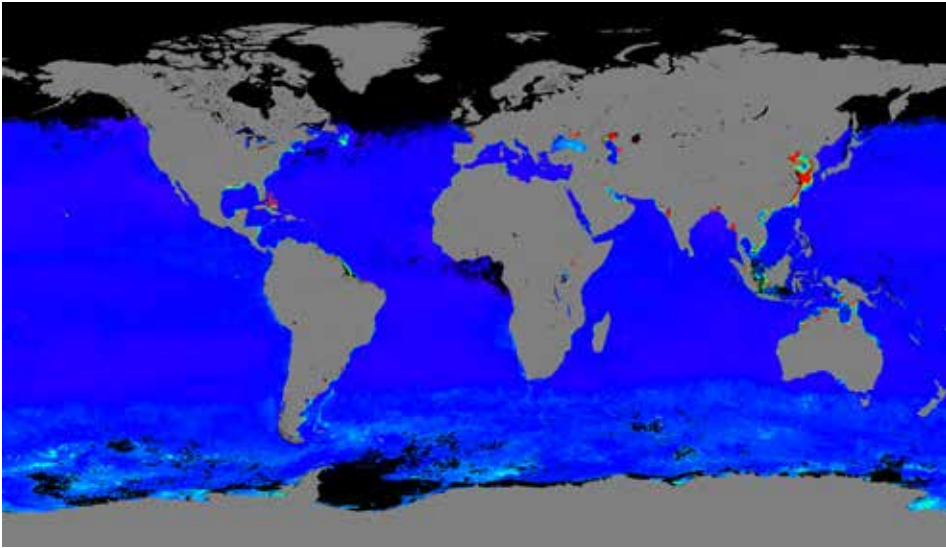
VIIRS data were generated using **NOAA-MSL12**

Global OC nL_w since February 2014

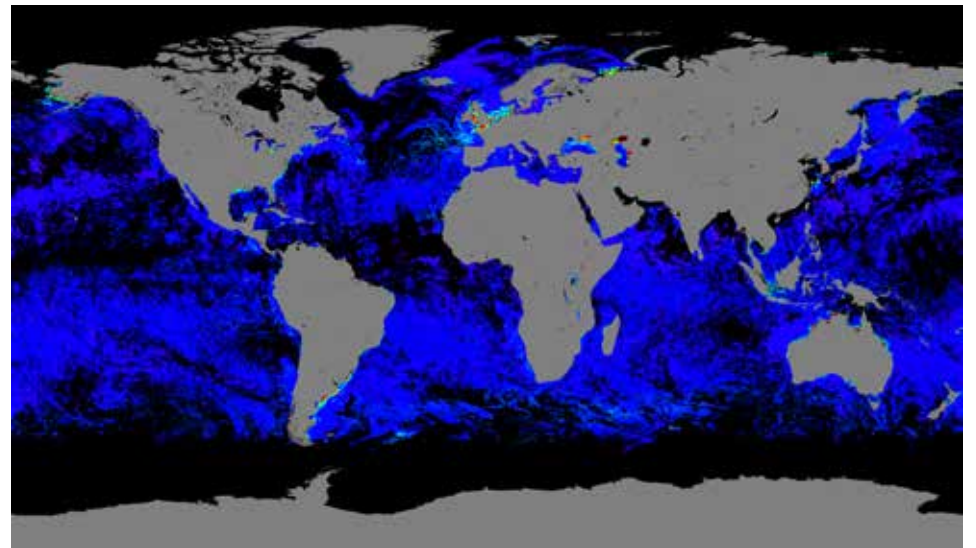
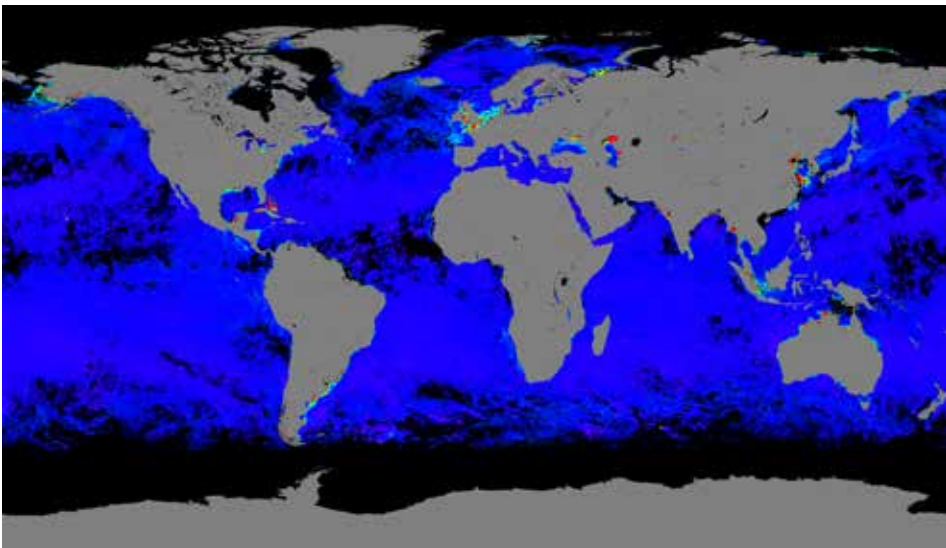
VIIRS $nL_w(551)$

MODIS $nL_w(551)$

January 2014

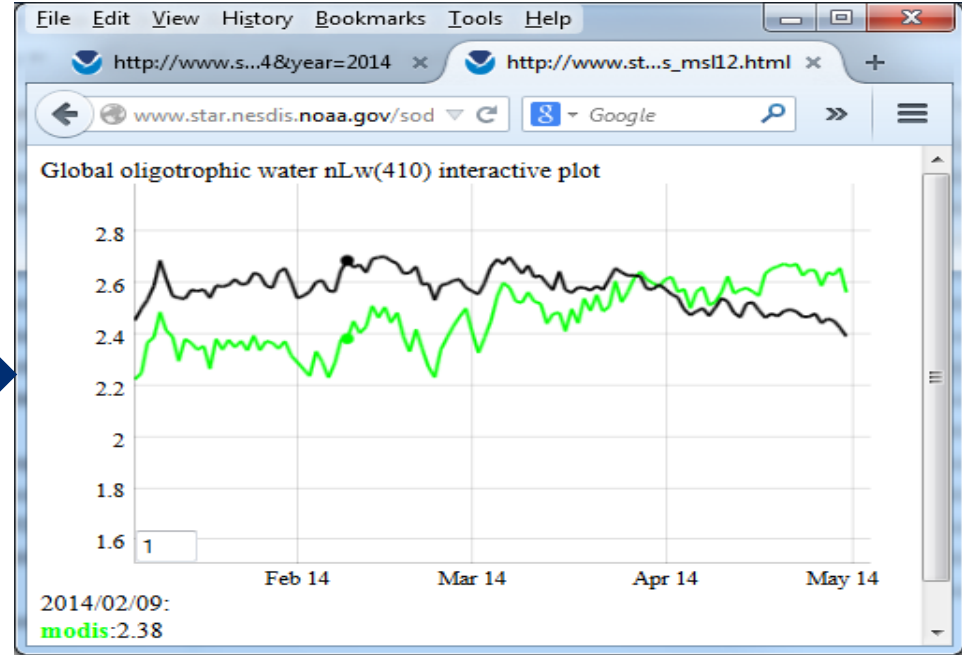
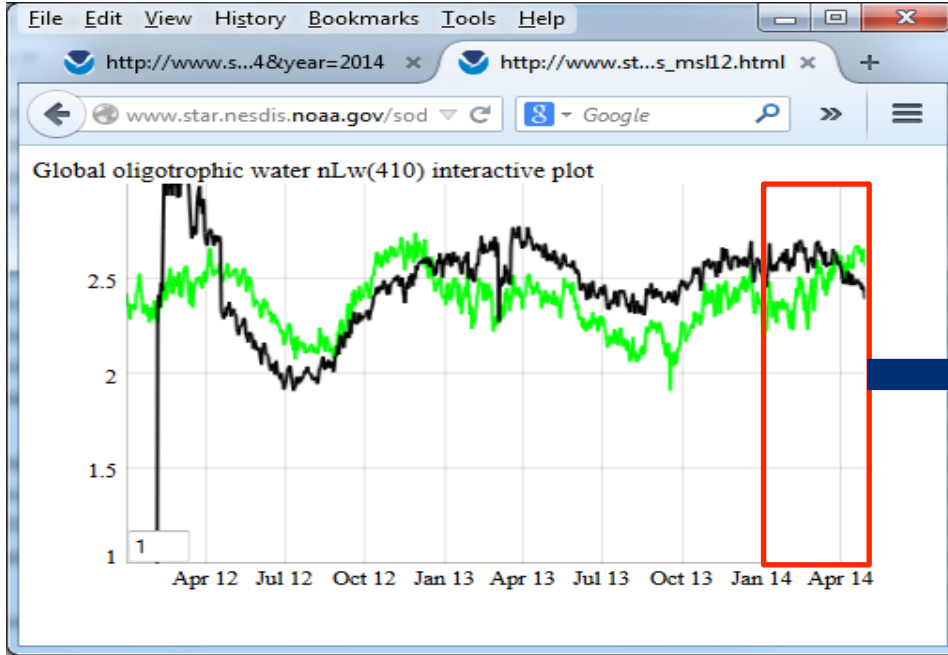


3rd Week of April 2014

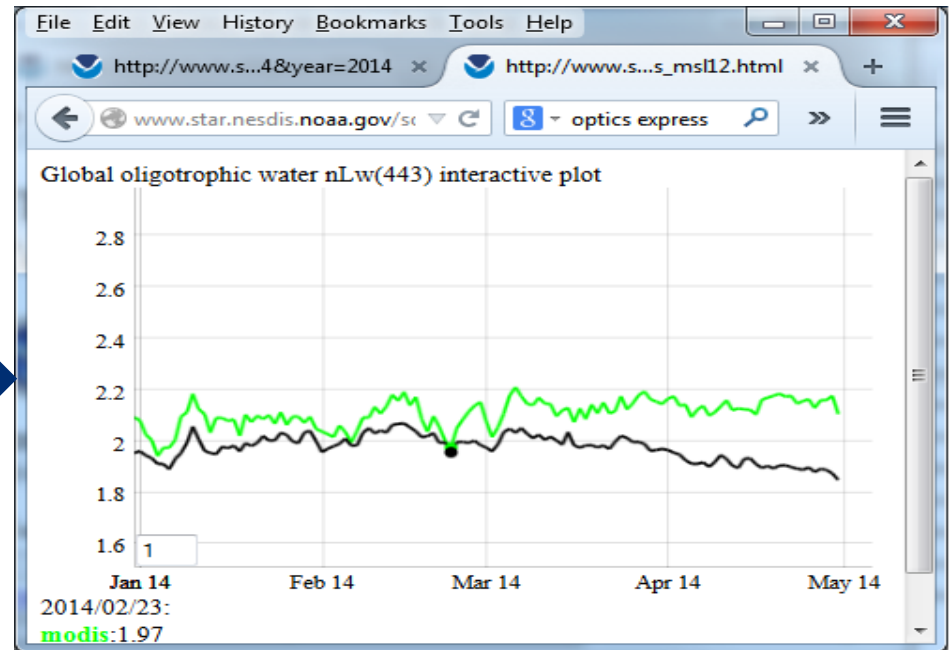
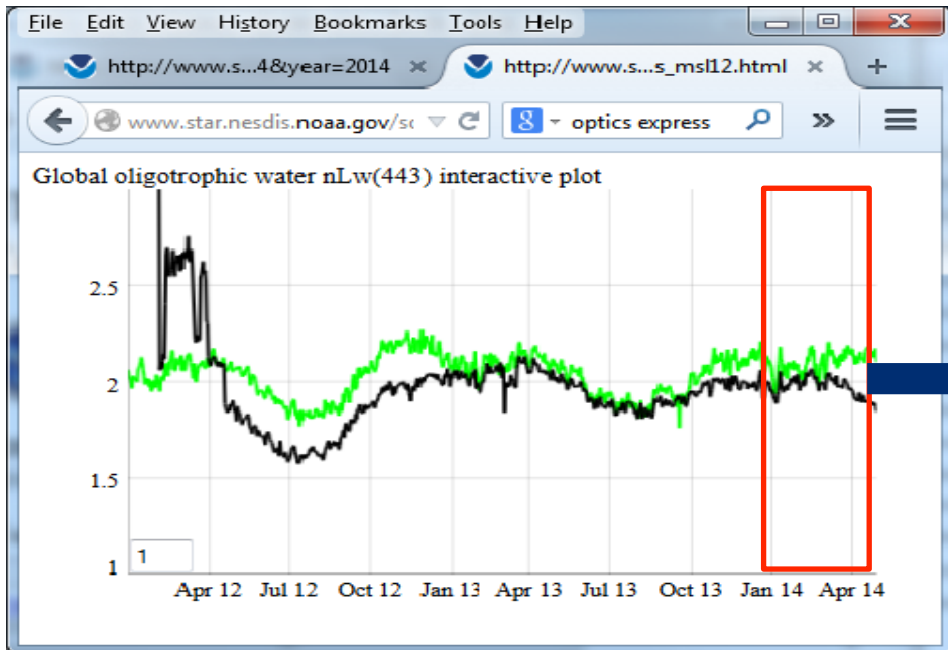


Quantitative Evaluation for Global Oligotrophic Waters

VIIRS vs. MODIS nLw(412)

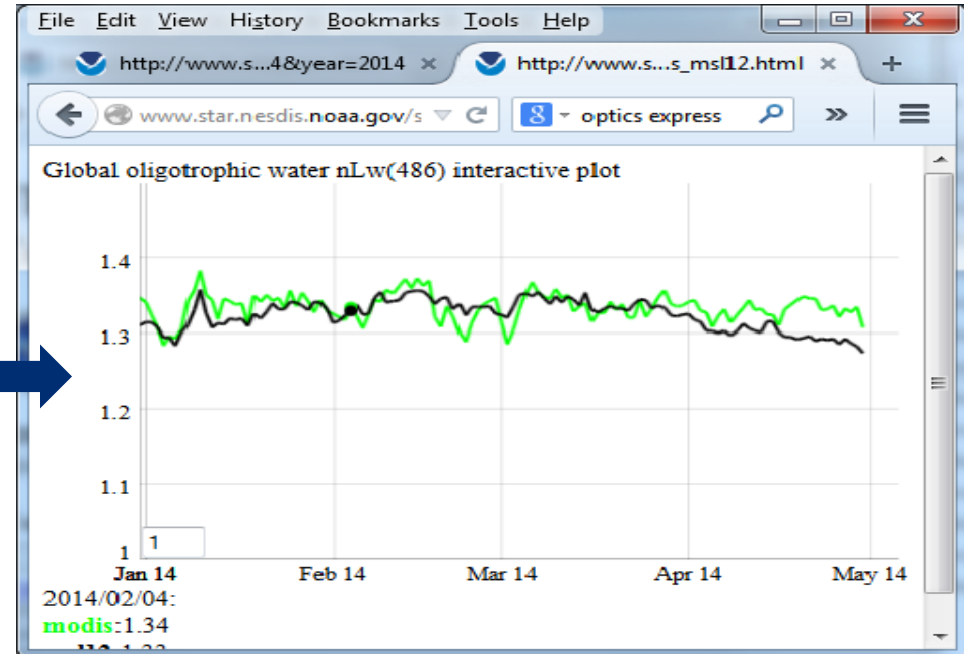
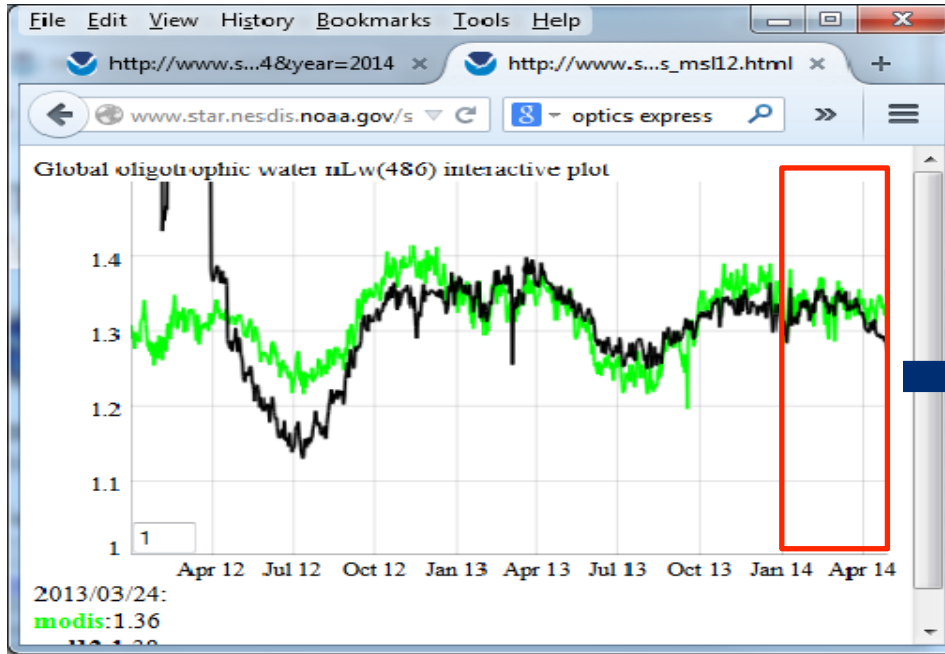


VIIRS vs. MODIS nLw(443)

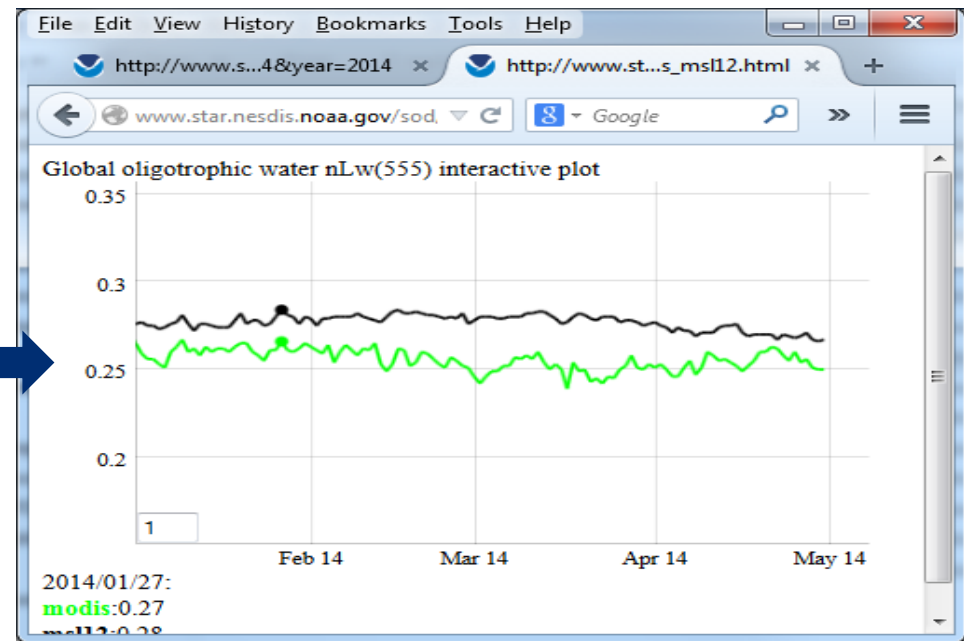
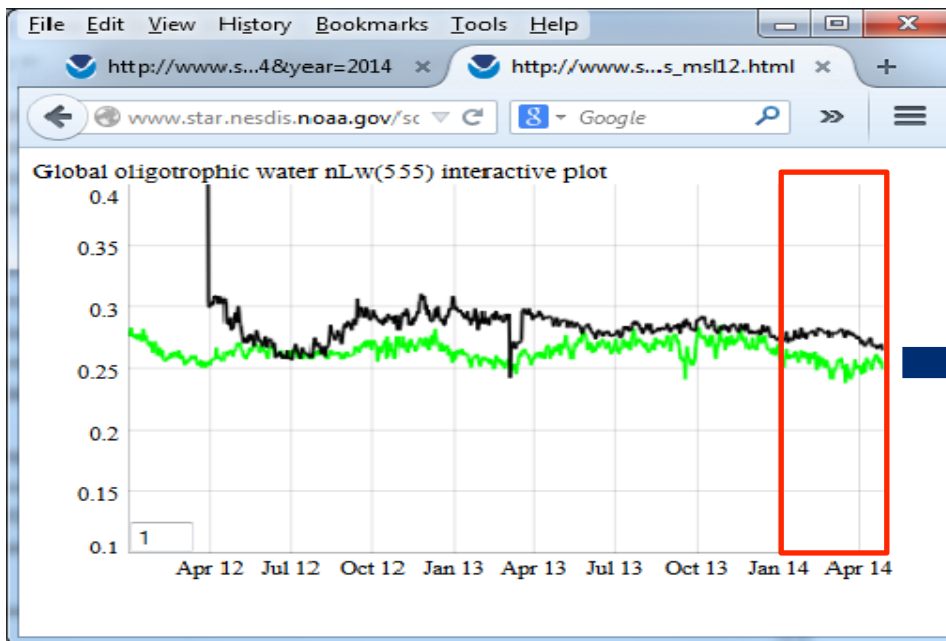


Quantitative Evaluation for Global Oligotrophic Waters

VIIRS vs. MODIS nLw(488)

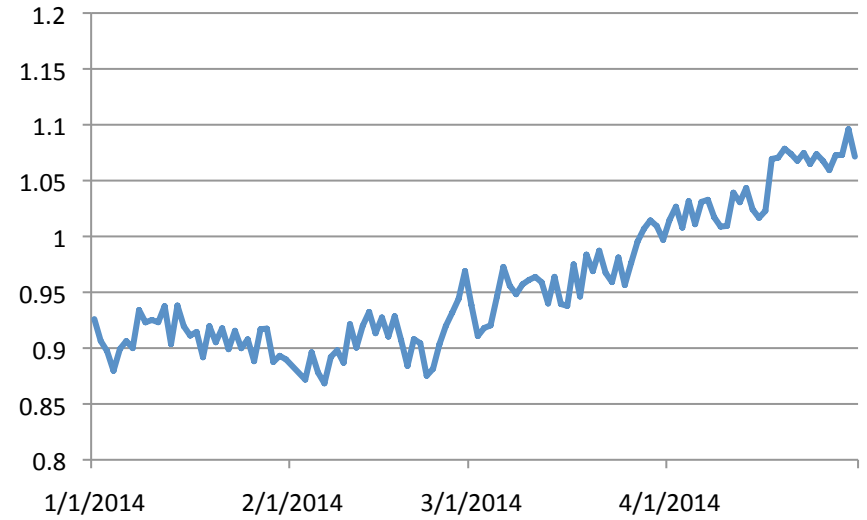
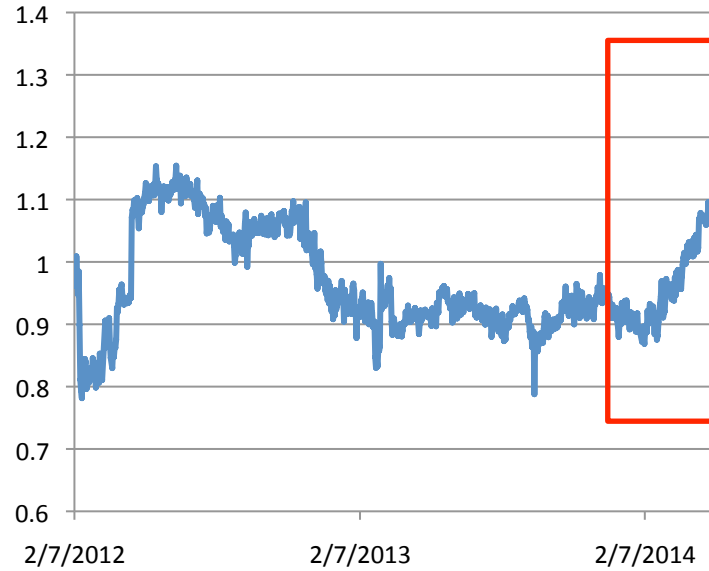


VIIRS vs. MODIS nLw(551)

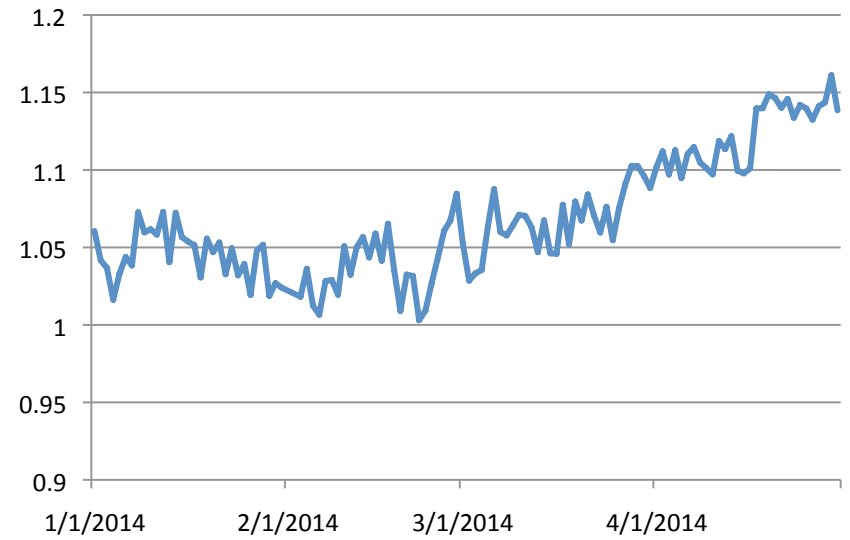
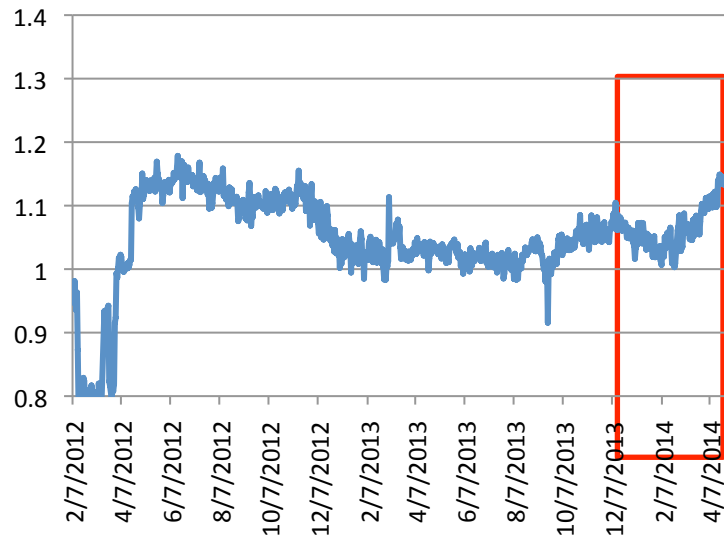


nLw Ratio (MODIS/VIIRS) for Global Oligotrophic Waters

MODIS/VIIRS nLw(412)

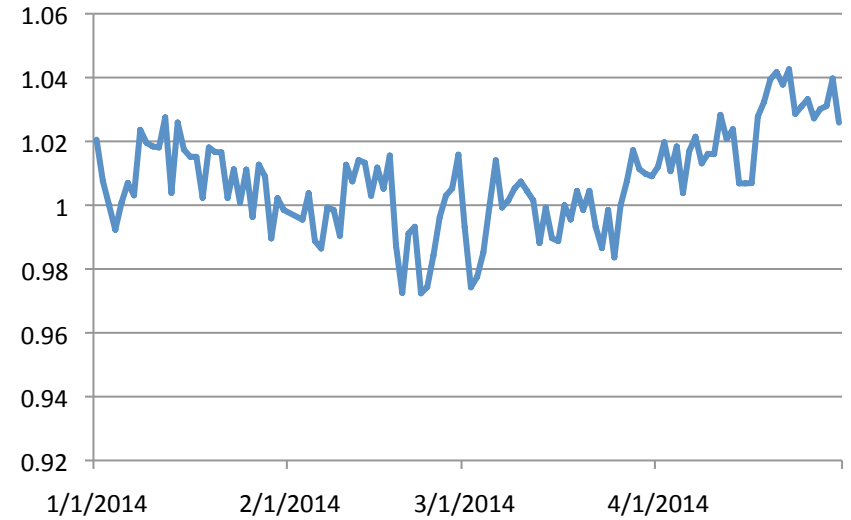
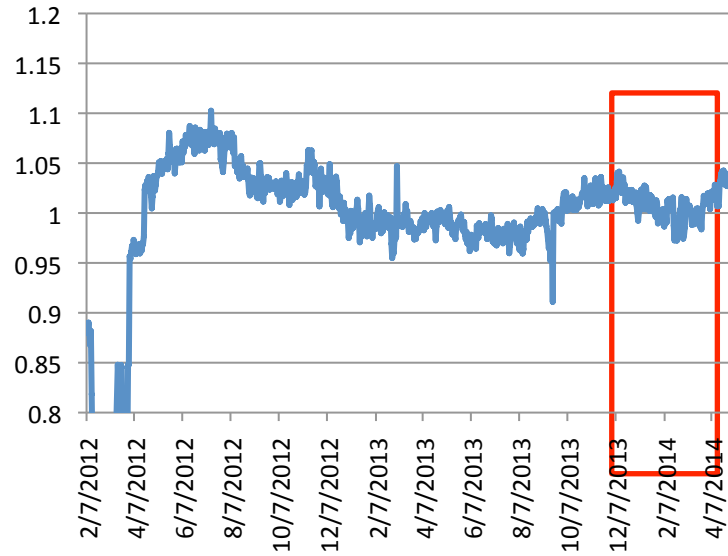


MODIS/VIIRS nLw(443)

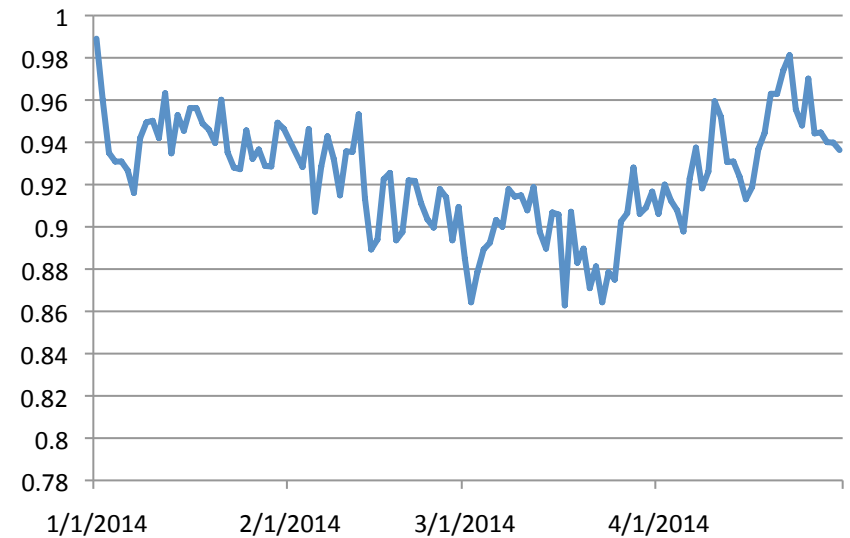
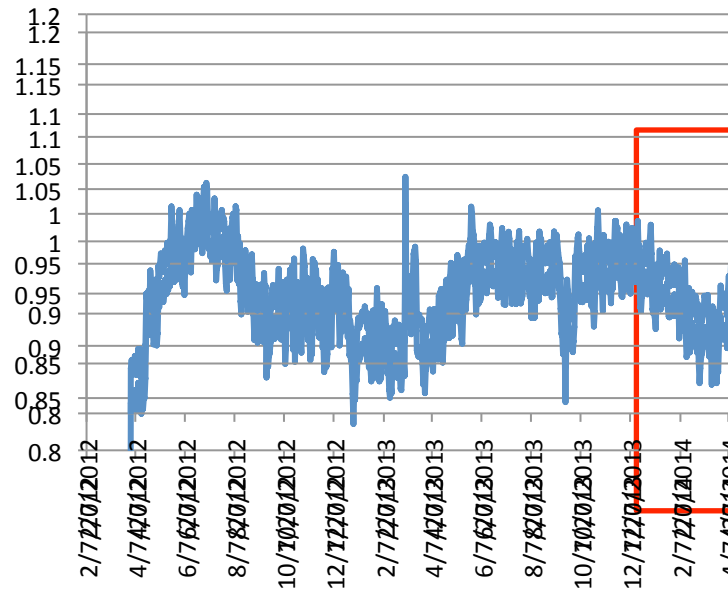


nLw Ratio (MODIS/VIIRS) for Global Oligotrophic Waters

MODIS/VIIRS nLw(488)

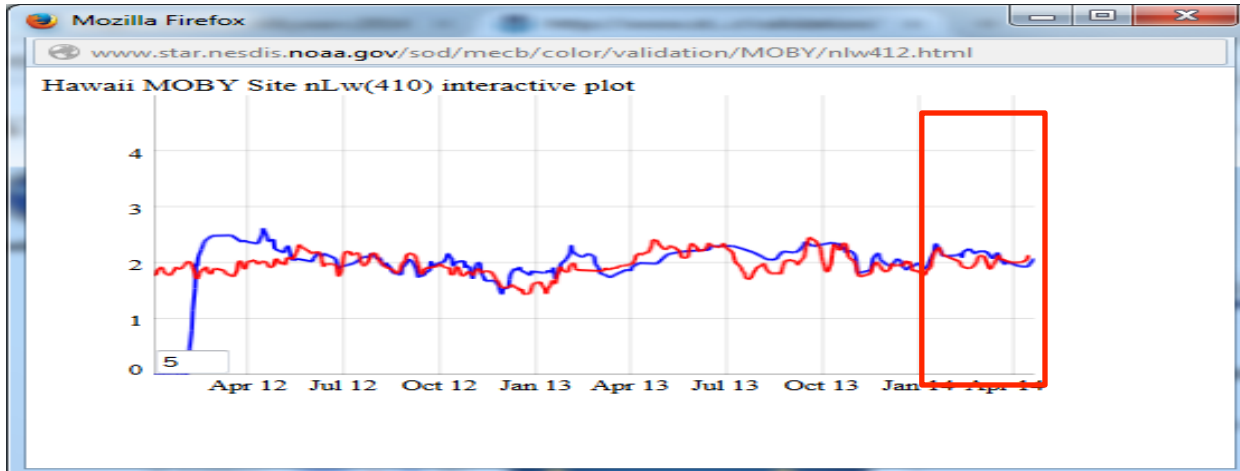


MODIS/VIIRS nLw(551)

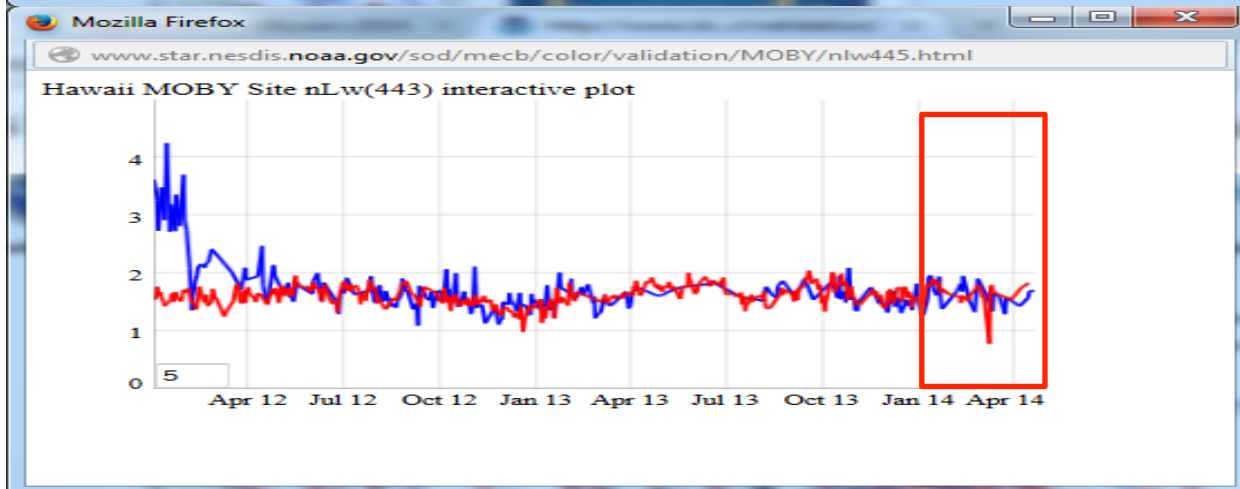


Compare with MOBY In Situ Data

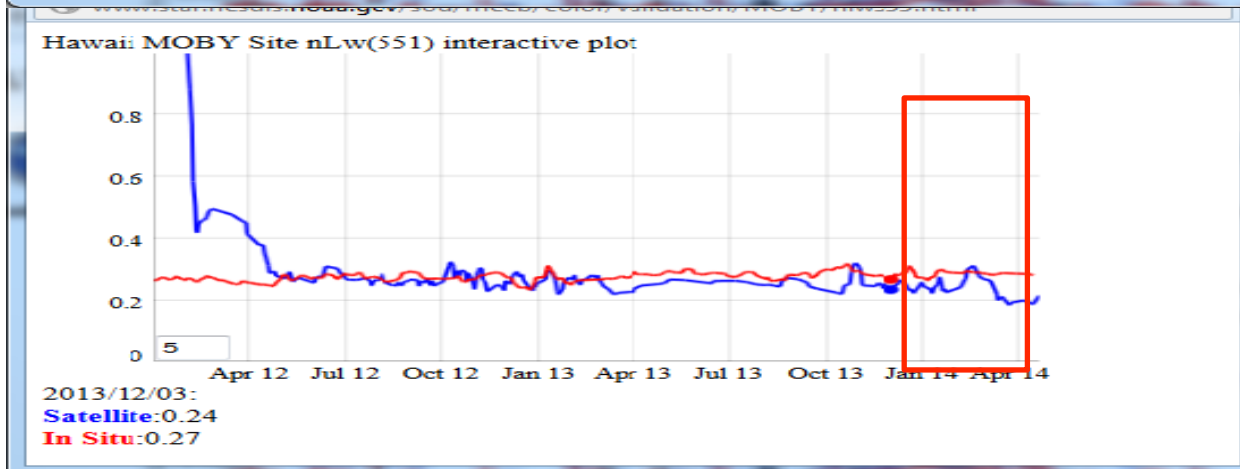
VIIRS nLw(410)



VIIRS nLw(443)

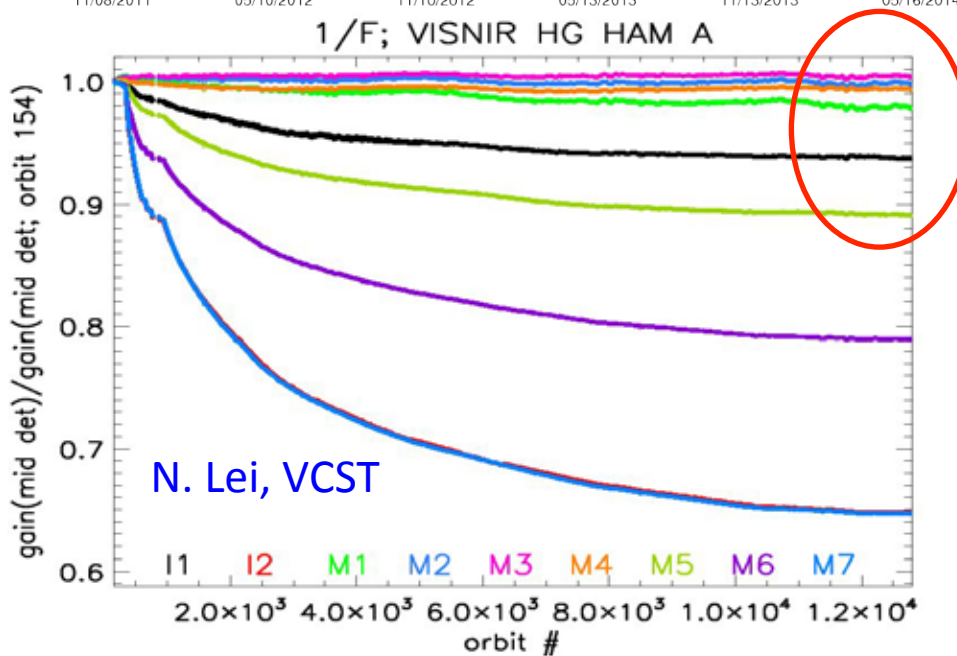
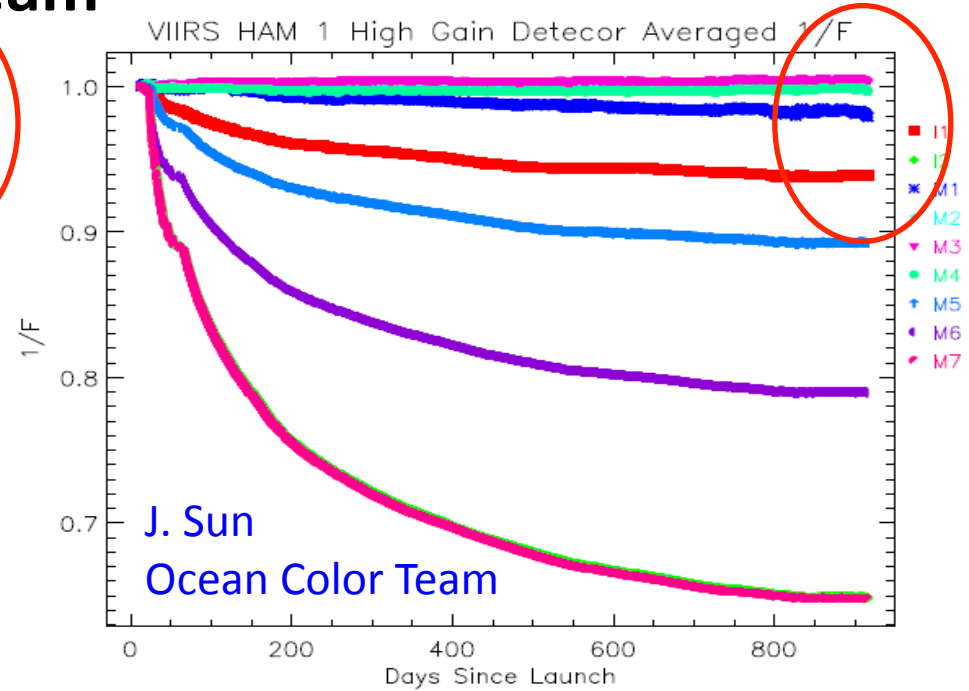
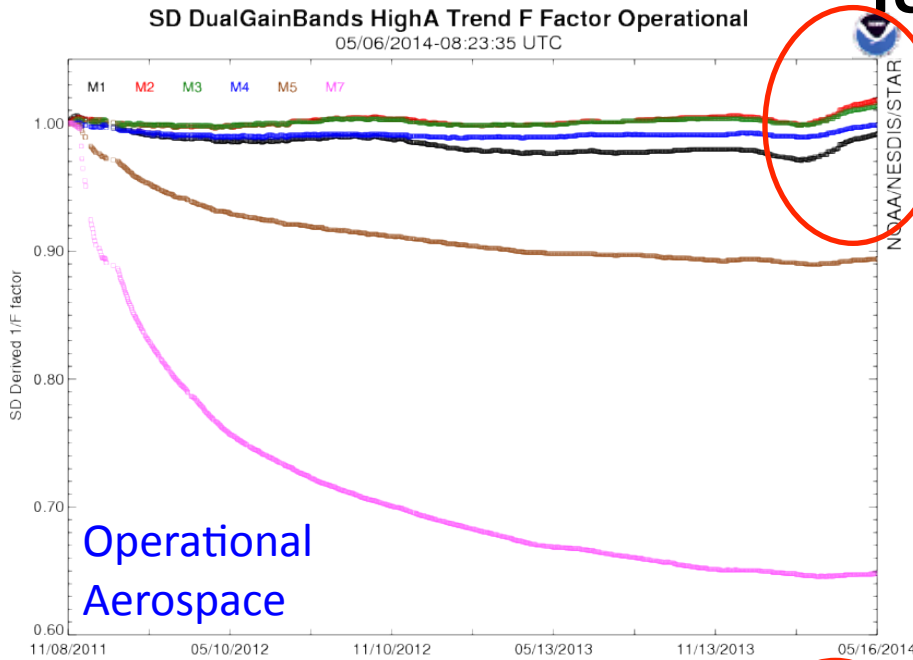


VIIRS nLw(551)



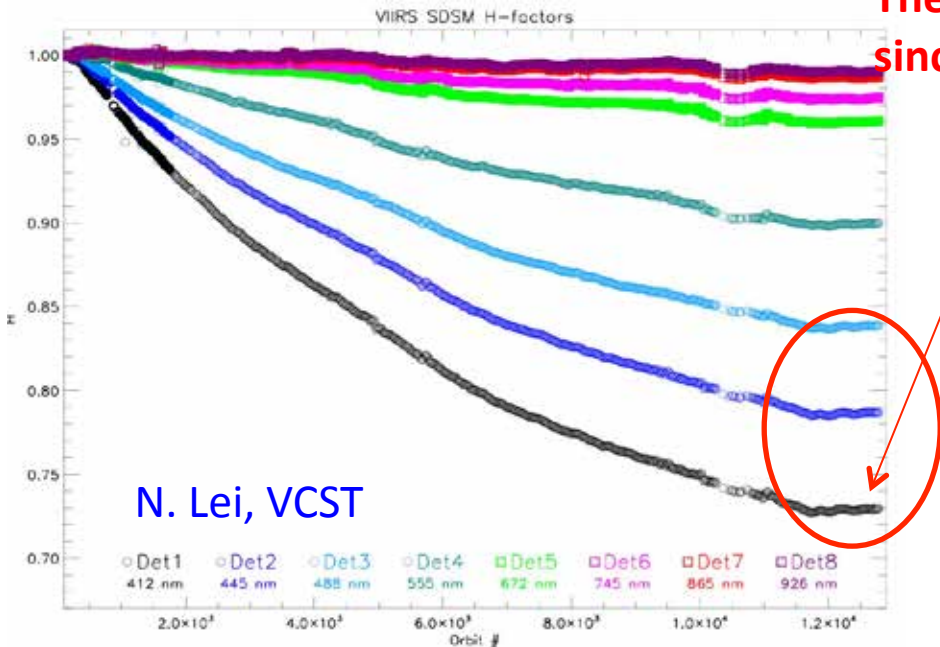
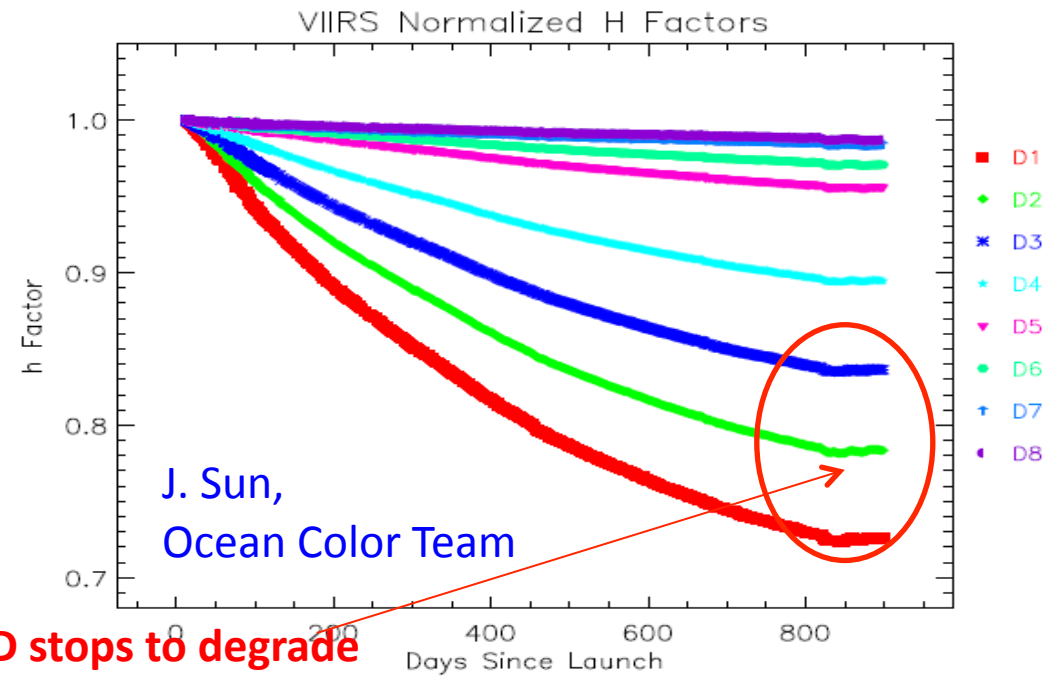
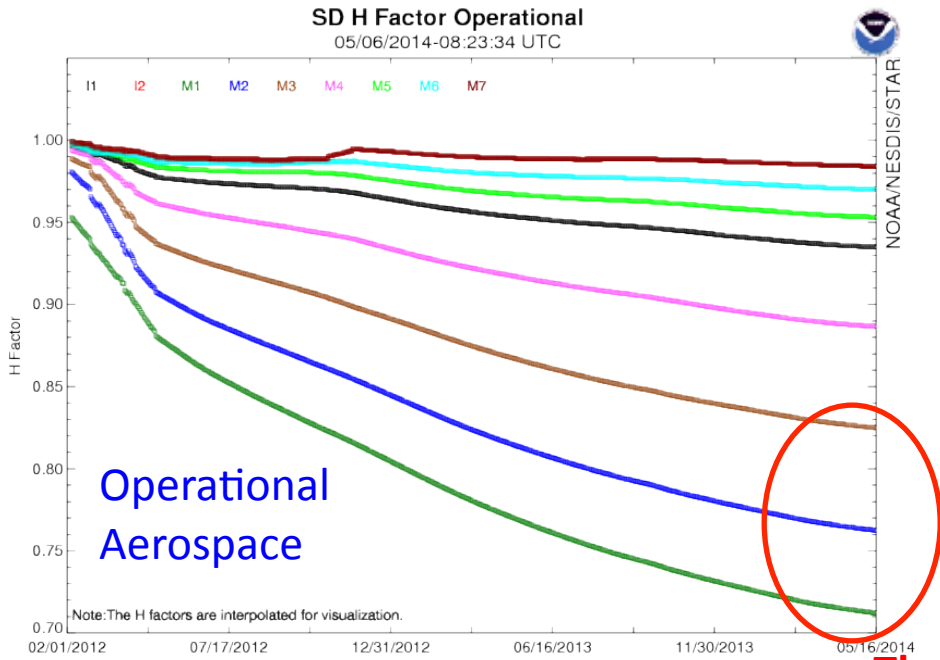
F factors from Operational, VCST, and Ocean Color EDR

Team



- The recently F-factors (1/F) increase (Cal. gains decrease) in short wavelength bands observed in operational F-LUTs is not seen in F factors derived by Ocean Color Team and VCST.
- The artificial F-factors increase lead to the EV radiance/reflectance decrease and significantly impacted VIIRS ocean ocean products, leading to biased low nLw values and missing values due to $nLw < 0$.

H factors from Operational, VCST, and Ocean Color EDR Team



The SD stops to degrade since Feb. 2014

- The operational H-LUTs do not reflect the recent SD degradation rate change.
- The artifacts in SD degradation in the operational H-LUTs induced the artifacts in gain decrease or increase of the F-factors in the operational F-LUTs.
- The artifact of increase in the F-factors then induces the EV radiance/reflectance decrease.

Summary

- Following the reverse trends of VIIRS SDR F-LUTs, global VIIRS nLw data show decreasing trends from February to May. Using MODIS-Aqua as reference, nLw(410) (M1) and nLw(443) (M2) drifted lower ~**15-20%** as of early May 2014, and nLw(488) (M3) decreased ~**8-10%** for global oligotrophic waters. There also may be some effect to nLw(551) (M4).
- We do not see above nLw trends at MOBY site between February and May, this can be attributed to the lack of the MOBY in-situ data in this period.
- The recently operational F factors increase trends (Cal gains decrease) in short wavelength bands is not seen in F factors derived by VCST and VIIRS Ocean Color Team.
- Operational H-LUTs do not reflect the recent SD degradation rate change. Artificial SD degradation in the operational H-LUTs induced the artificial gain decrease (or increase of the F-factors) in the operational F-LUTs, and consequently leads to biased-low ocean color nLw retrievals since February 2014. The impact to OC products is quite significant. **The correct F-LUTs should be used now.**